

William Murphy · Jonathan Black
Garth Hastings *Editors*

Handbook of Biomaterial Properties

Second Edition

 Springer

Handbook of Biomaterial Properties

William Murphy • Jonathan Black
Garth Hastings
Editors

Handbook of Biomaterial Properties

Second Edition

 Springer

Editors

William Murphy
Department of Biomedical Engineering
University of Wisconsin
Madison, WI, USA

Jonathan Black
Principal: IMN Biomaterials
King of Prussia, PA, USA

Department of Orthopedics and
Rehabilitation
University of Wisconsin
Madison, WI, USA

Garth Hastings
Staffordshire University (Emeritus)
Lyme, Staffordshire, UK

ISBN 978-1-4939-3303-7 ISBN 978-1-4939-3305-1 (eBook)
DOI 10.1007/978-1-4939-3305-1

Library of Congress Control Number: 2016933771

© Springer Science+Business Media New York 2016

This work is subject to copyright. All rights are reserved by the Publisher, whether the whole or part of the material is concerned, specifically the rights of translation, reprinting, reuse of illustrations, recitation, broadcasting, reproduction on microfilms or in any other physical way, and transmission or information storage and retrieval, electronic adaptation, computer software, or by similar or dissimilar methodology now known or hereafter developed.

The use of general descriptive names, registered names, trademarks, service marks, etc. in this publication does not imply, even in the absence of a specific statement, that such names are exempt from the relevant protective laws and regulations and therefore free for general use.

The publisher, the authors and the editors are safe to assume that the advice and information in this book are believed to be true and accurate at the date of publication. Neither the publisher nor the authors or the editors give a warranty, express or implied, with respect to the material contained herein or for any errors or omissions that may have been made.

Printed on acid-free paper

This Springer imprint is published by Springer Nature
The registered company is Springer Science+Business Media LLC New York

Foreword

Progress in the development of surgical implant materials has been hindered by the lack of basic information on the nature of the tissues, organs and systems being repaired or replaced. Materials' properties of living systems, whose study has been conducted largely under the rubric of tissue mechanics, has tended to be more descriptive than quantitative. In the early days of the modern surgical implant era, this deficiency was not critical. However, as implants continue to improve and both longer service life and higher reliability are sought, the inability to predict the behavior of implanted manufactured materials has revealed the relative lack of knowledge of the materials properties of the supporting or host system, either in health or disease. Such a situation is unacceptable in more conventional engineering practice: the success of new designs for aeronautical and marine applications depends exquisitely upon a detailed, disciplined and quantitative knowledge of service environments, including the properties of materials which will be encountered and interacted with. Thus the knowledge of the myriad physical properties of ocean ice makes possible the design and development of icebreakers without the need for trial and error. In contrast, the development period for a new surgical implant, incorporating new materials, may well exceed a decade and even then only short term performance predictions can be made.

Is it possible to construct an adequate data base of materials properties of both manufactured materials and biological tissues and fluids such that *in vitro* simulations can be used to validate future implant designs before *in vivo* service? While there are no apparent intellectual barriers to attaining such a goal, it clearly lies in the distant future, given the complexity of possible interactions between manufactured materials and living systems.

However, a great body of data has accumulated concerning the materials aspects of both implantable materials and natural tissues and fluids. Unfortunately, these data are broadly distributed in many forms of publication and have been gained from experimental observations of varying degrees of accuracy and precision. This is a situation very similar to that in general engineering in the early phases of the Industrial Revolution. The response then was the publication of engineering handbooks, drawing together, first in general publication and later in specialty versions,

the known and accepted data of the time. In this spirit, we offer this 2nd Edition of the *Handbook of Biomaterial Properties*

Biomaterials, as manufactured for use in implants, do not exist usefully out of context with their applications. Thus, a material satisfactory in one application can be wholly unsuccessful in another. In this spirit, the Editors have given direction to the experts responsible for each part of this *Handbook* to consider not merely the intrinsic and interactive properties of biomaterials but also their appropriate (and in some cases inappropriate) applications as well as their historical context. The experts have in some cases added significant content specific to each class of material. For example, content is included on not just bulk properties but also surface modifications of titanium, which has become quite important in orthopedic implant design. It is hoped that the results will prove valuable, although in different ways, to the student, the researcher, the engineer and the practicing physician who uses implants.

A handbook like this necessarily becomes incomplete immediately upon publication, since it will be seen to contain errors of both omission and commission. Such has been the case with previous engineering handbooks: the problem can only be dealt with by providing new, revised editions. This 2nd Edition provides updated insights, data, citations, and topic areas not found in the 1st Edition. The Editors would appreciate any contributions and/or criticisms which the users of this handbook may make and promise to take account of them in future revisions.

Introduction

It is a feature of any developing science and its accompanying technology that information relating to different aspects is scattered throughout the relevant, and sometimes not so relevant literature. As the subject becomes more mature, a body of information can be categorized and brought together for the use of practitioners. In providing this *Handbook of Biomaterial Properties* the Editors believe that the latter stage has been reached in several parts of the vast field of biomaterials science and engineering. This 2nd Edition of the *Handbook* provides an updated body of information for a subset of chapters, as well as new chapters that represent biomaterials fields that have matured in the intervening time between the 1st and 2nd Editions.

Many of the properties of the synthetic materials have been available for some time, for example those of the various metallic alloys used in clinical practice have been specified in various International, European and National Standards and can be found by searching. In the case of polymeric materials, while the information is in commercial product literature and various proprietary handbooks, it is diverse by the nature of the wide range of materials commercially available and the search for it can be time consuming. The situation is much the same for ceramic and composite materials: there the challenge is finding the appropriate properties for the specific compositions and grades in use as biomaterials.

However, when information is sought for on materials properties of human tissues, the problem is more acute as such data are even more scattered and the methods for determination are not always stated or clearly defined. For the established worker this presents a major task. For the new researcher it may make establishing a project area a needlessly time consuming activity. The biomaterials bulletin boards (on the Internet) frequently display requests for help in finding characterization methods and/or reliable properties of natural materials, and sometimes the information is actually not available. Even when it is available, the original source of it is not always generally known.

In approaching their task, the Editors have tried to bring together into one source book the information that is available. To do this they have asked for the help of many colleagues worldwide to be contributors to the *Handbook*. It has not been possible to cover all the areas the Editors had hoped. Some topics could not be covered,

or the information was judged to be too fragmentary or unreliable to make it worth including. This is inevitably the sort of project that will continue to be incomplete; however, new information will be provided as more experiments are done and as methods for measurement and analysis improve. The aim has been to make this *Handbook* a ready reference which will be consulted regularly by every technician, engineering and research worker in the fields of biomaterials and medical devices.

We have tried, not always successfully, to keep the textual content to a minimum, and emphasize tabular presentation of data. However, in some cases it has been decided to include more text in order to establish the background of materials properties and use, and to point to critical features in processing or production which would guide the worker looking for new applications or new materials. For example, in polymer processing, the need to dry materials thoroughly before fabrication may not be understood by those less well versed in production techniques. In another example, the relationship of synthetic biomaterials to vocal fold or corneal tissue repair may not be obvious by those outside of this specialized area, so text is included to clarify the connection of these natural biomaterials to synthetic biomaterials used as devices.

It is hoped that the *Handbook* will be used and useful, not perfect but a valuable contribution to a field that we believe has matured sufficiently to merit such a publication. The fields embodied in the 1st Edition of The Handbook have now further matured to justify this updated 2nd Edition - inevitable technological improvement in materials design and characterization have led to updated data, and tissue engineering applications have created a need for reference data in new tissue areas (e.g. ligament, cornea, vocal fold). The *Handbook* is divided into synthetic and natural materials and the treatment is different in each part. More background was felt to be needed for many of the synthetic materials, since processing and structural variations have a profound effect on properties and performance. Biological performance of these materials depends on a range of chemical, physical and engineering properties and the physical form can also influence *in vivo* behavior. We have not attempted to deal with issues of biological performance, or biocompatibility, but have dealt with those other features of the materials which were felt to be relevant to them as potential biomaterials. Only materials having apparent clinical applications have been included.

The biological materials have more dynamic properties since, *in vivo*, they respond to physiological stimuli and may develop modified properties accordingly. The treatment of their properties has been limited to those determined by well characterized methods for human tissues, with a few exceptions where data and other species are deemed to be applicable and reliable. Those properties determined almost totally *in vitro* may not be directly predictive of the performance of the living materials *in vivo*, but are a guide to the medical device designer who wishes to determine a device design specification. Such a designer often finds it hard to realize the complexity of the task of dealing with a non-engineering system. What really are the parameters needed in order to design an effectively functioning joint endoprosthesis or a heart valve? Do tissue properties measure post explantation assist? Is individual patient lifestyle an important factor? There is immediately a degree of

uncertainty in such design processes, and total reliability in performance cannot be given a prospective guarantee. However, the more we learn about the materials and systems of the human body and their interaction with synthetic biomaterials, the closer we may perhaps become to the ideal ‘menotic’ or forgotten implant which remains in ‘menosis’—close and settled union from the Greek $\mu\epsilon\nu\omega$ —with the tissues in which it has been placed.

Two final comments:

First, although the Editors and contributors frequently refer to synthetic and, in some cases, processed natural materials as ‘biomaterial,’ nothing herein should be taken as either an implied or explicit warrantee of the usefulness, safety or efficacy of any material or any grade or variation of any material in any medical device or surgical implant. Such determinations are an intrinsic part of the design, development, manufacture and clinical evaluation process for any device. Rather, the materials listed here should be considered, on the basis of their intrinsic properties and, in many cases, prior use, to be *candidates* to search as biomaterials: possibly to become parts of successful devices to evaluate, direct, supplement, or replace the functions of living tissues.

Second, the Editors earlier refer to absences of topics and of data for particular synthetic or natural materials. While this may be viewed, perhaps by reviewers and users alike, as a shortcoming of the *Handbook*, we view it as a virtue for two reasons:

- Where reliable data are available but were overlooked in this edition, we hope that potential contributors will come forward to volunteer their help for hoped for subsequent editions.
- Where reliable data are not available, we hope that their absence will prove both a guide and a stimulus for future investigators in biomaterials science and engineering.

Indeed, this 2nd edition of the *Handbook* provides new data and citations in more than 10 chapters, new contributors, and also includes new chapters in areas that have more recently matured (e.g. the vocal fold). We are hopeful that this new Edition adds value to the 1st Edition, and that future Editions will address inevitable “shortcomings” in this Edition

The Editors, of course, welcome any comments and constructive criticism.

Madison, WI, USA
King of Prussia, PA, USA
Lyme, Staffordshire, UK

William Murphy
Jonathan Black
Garth Hastings

Contents

<i>Foreword</i>	v
<i>Introduction</i>	vii
<i>Contributors</i>	xv
PART I	
A1 Cortical Bone	3
<i>J. Currey</i>	
A2 Cancellous Bone	15
<i>Christopher J. Hernandez</i>	
A3 Dentin and Enamel	23
<i>K.E. Healy</i>	
B1 Cartilage	37
<i>J.R. Parsons</i>	
B2 Fibrocartilage	45
<i>V.M. Gharpuray</i>	
B3 Ligament and Tendon	55
<i>Connie S. Chamberlain and Ray Vanderby</i>	
B4 Skin and Muscle	63
<i>A.F.T. Mak and M. Zhang</i>	
B5 Brain Tissues	67
<i>S.S. Margulies and D. F. Meaney</i>	
B6 Arteries, Veins and Lymphatic Vessels	77
<i>X. Deng and R. Guidoin</i>	

B7	The Intraocular Lens	103
	<i>Traian V. Chirila and Shuko Suzuki</i>	
C1	Blood and Related Fluids	115
	<i>V. Turitto and S.M. Slack</i>	
C2	The Vitreous Humor	125
	<i>Traian V. Chirila and Ye Hong</i>	
C3	The Cornea	135
	<i>Traian V. Chirila and Shuko Suzuki</i>	
PART II		
1a	Metallic Biomaterials: Introduction	151
	<i>H. Breme, V. Biehl, Nina Reger, and Ellen Gawalt</i>	
1b	Metallic Biomaterials: Cobalt-Chromium Alloys	159
	<i>Gopinath Mani</i>	
1c	Metallic Biomaterials: Titanium and Titanium Alloys	167
	<i>H. Breme, V. Biehl, Nina Reger, and Ellen Gawalt</i>	
1d	Dental Restoration Materials	191
	<i>Jonathan Black and Garth Hastings</i>	
2	Composite Materials	205
	<i>L. Ambrosio, G. Carotenuto, and L. Nicolais</i>	
3	Thermoplastic Polymers In Biomedical Applications: Structures, Properties and Processing	261
	<i>S.H. Teoh, Z.G. Tang, and Garth W. Hastings</i>	
4	Biomedical elastomers	291
	<i>J.W. Boretos and S.J. Boretos</i>	
5	Oxide Bioceramics: Inert Ceramic Materials in Medicine and Dentistry	339
	<i>J. Li and G.W. Hastings</i>	
6	Ceramic Materials Testing and Fracture Mechanics	353
	<i>Garth Hastings, Ishbel Gair, and D. Daily</i>	
7	Properties of Bioactive Glasses and Glass-ceramics	447
	<i>L.L. Hench and T. Kokubo</i>	
8	Wear	455
	<i>M. LaBerge and J.D. Desjardins</i>	
9	Degradation/resorption in Bioactive Ceramics in Orthopaedics	495
	<i>H. Oonishi and H. Oomamiuda</i>	

Contents	xiii
10 Corrosion of Metallic Implants	509
<i>M.A. Barbosa</i>	
11 Carbons	549
<i>A.D. Haubold, R.B. More, and J.C. Bokros</i>	
PART III	
1 General Concepts of Biocompatibility	563
<i>D.F. Williams</i>	
2 Soft Tissue Response	571
<i>J.M. Anderson</i>	
3 Hard Tissue Response	581
<i>T.O. Albrektsson</i>	
4 Immune Response	593
<i>K. Merritt</i>	
5 Cancer	607
<i>M. Rock</i>	
6 Blood–material Interactions	621
<i>S.R. Hanson</i>	
7 Soft Tissue Response to Silicones	631
<i>S.E. Gabriel</i>	
8 Vocal Folds	645
<i>Joel Gaston and Susan L. Thibeault</i>	
Erratum	E1
Index	659

Contributors

T.O. Albrektsson Handicap Research, Institute for Surgical Sciences, University of Gothenburg, Gothenburg, Sweden

L. Ambrosio Department of Materials and Production Engineering, University of Naples Federico II Institute of Composite Materials Technology CNR, Piazzale Technio, Naples, Italy

J.M. Anderson Department of Pathology Case Western Reserve University, University Hospitals of Cleveland, Cleveland, OH, USA

M.A. Barbosa INEB-Ma do Campo Alegre, Porto, Portugal

V. Biehl Lehrstuhl für Metallische Werkstoffe, Universität des Saarlandes, Saarbrücken, Germany

Jonathan Black Principal: IMN Biomaterials, King of Prussia, PA, USA

J.C. Bokros Medical Carbon Research Institute, Austin, TX, USA

J.W. Boretos Consultants for Biomaterials, Rockville, Maryland, USA

S.J. Boretos Consultants for Biomaterials, Rockville, Maryland, USA

J. Breme Lehrstuhl für Metallische Werkstoffe, Universität des Saarlandes, Saarbrücken, Germany

G. Carotenuto Department of Materials and Production Engineering, University of Naples Federico II Institute of Composite Materials Technology CNR, Piazzale Technio, Naples, Italy

Connie S. Chamberlain Department of Orthopedics and Rehabilitation, Wisconsin Institute for Medical Research, University of Wisconsin-Madison, Madison, WI, USA

Traian V. Chirila Queensland Eye Institute, South Brisbane, QLD, Australia

J. Currey Department of Biology, York University, York, YO1 5DD, UK

X. Deng Laboratoire de Chirurgie Exp Agriculture Services, Université Laval, Québec, G1K 7P4, Canada

J.D. DesJardins Department of Bioengineering, Rhodes Clemson University, Clemson, SC, USA

S.E. Gabriel Division of Rheumatology, Mayo Clinic, Rochester, MN, USA

Ishbel Gair Technical Consultant, Lucideon Ltd, Staffordshire, UK

Joel Gaston Department of Biomedical Engineering, University of Wisconsin—Madison, Madison, WI, USA

Ellen Gawalt Department of Chemistry and Biochemistry, Bayer School of Natural and Environmental Sciences, Mellon, Pittsburgh, PA, USA

V.M. Gharpuray Department of Bioengineering, Clemson University, Clemson, SC, USA

R. Guidoin Laboratoire de Chirurgie Exp Agriculture Services, Université Laval, Québec, Canada

S.R. Hanson Division of Hematology/Oncology, Emory University, AJ, Atlanta, GA, USA

Garth Hastings Staffordshire University (Emeritus), Lyme, Staffordshire, UK

A.D. Haubold Medical Carbon Research Institute, Austin, TX, USA

K.E. Healy Department of Biological Materials, Northwestern University, Chicago, IL, USA

L.L. Hench Division of Material Chemistry Faculty of Engineering, Imperial College Department of Materials, Kyoto University, Sakyo-ku Kyoto, Japan, London, UK

Christopher J. Hernandez Sibley School of Mechanical and Aerospace Engineering, Cornell University, Ithaca, NY, USA

Meinig School of Biomedical Engineering, Cornell University, Ithaca, NY, USA

Ye Hong Cooper Vision, Pleasanton, CA, USA

T.M. Keaveny Department of Mechanical Engineering Etcheverry Hall, University of California at Berkeley, Berkeley, CA94720, USA

T. Kokubo Division of Material Chemistry Faculty of Engineering, Imperial College Department of Materials, Kyoto University, Sakyo-ku Kyoto, Japan, London, UK

M. LaBerge Department of Bioengineering, Rhodes Clemson University, Clemson, SC, USA

R.E. Levine Musculoskeletal Research Centre, University of Pittsburgh, Pittsburgh, PA, USA

J. Li Centre for Oral Biology, Karolinska Institute, Huddinge, Sweden

A.F.T. Mak Rehabilitation Engineering Centre Hong Kong Polytechnic, Hunghom, Kowloon, Hong Kong

Gopinath Mani Department of Biomedical Engineering, University of South Dakota, Sioux Falls, SD, USA

S.S. Margulies Department of Bioengineering, University of Pennsylvania, Philadelphia, PA, USA

D.F. Meaney Department of Bioengineering, University of Pennsylvania, Philadelphia, PA, USA

K. Merritt Stoneridge Dr., Gaithersburg, MD, USA

R.B. More Medical Carbon Research Institute, Austin, TX, USA

L. Nicolais Department of Materials and Production Engineering, University of Naples Federico II Institute of Composite Materials Technology CNR, Piazzale Technio, Naples, Italy

H. Oomamiuda Department of Orthopaedic Surgery Artificial Joint Section and Biomaterial Research Laboratory, Osaka-Minami National Hospital, Osaja, Japan

H. Oonishi Department of Orthopaedic Surgery, Artificial Joint Section and Biomaterial Research Laboratory, Osaka-Minami National Hospital, Osaka, Japan

J.R. Parsons Orthopaedics-UMDNJ, 185 South Orange A venue University Heights, Newark, NJ, USA

Nina Reger Department of Chemistry and Biochemistry, Bayer School of Natural and Environmental Sciences, Mellon, Pittsburgh, PA, USA

M. Rock Department of Orthopaedics, Mayo Clinic, Rochester, MN, USA

S.M. Slack Department of Biomedical Engineering, University of Memphis, Memphis, TN, USA

Shuko Suzuki Queensland Eye Institute, South Brisbane, Queensland, Australia

Z.G. Tang BIOMAT Centre, National University of Singapore, Singapore, Singapore

S.H. Teoh Institute of Materials Research & Engineering – IMRE, National University of Singapore, Singapore, Singapore

Susan L. Thibeault Department of Surgery, University of Wisconsin–Madison, Madison, WI, USA

Department of Biomedical Engineering, University of Wisconsin–Madison, Madison, WI, USA

Department of Communication Sciences and Disorders, University of Wisconsin–Madison, Madison, WI, USA

V. Turitto Department of Biomedical Engineering, University of Memphis, Memphis, TN, USA

Ray Vanderby Jr. Department of Orthopedics and Rehabilitation, Wisconsin Institute for Medical Research, University of Wisconsin-Madison, Madison, WI, USA

Department of Biomedical Engineering, Wisconsin Institute for Medical Research, University of Wisconsin-Madison, Madison, WI, USA

D.F. Williams Department of Clinical Engineering, Royal Liverpool University Hospital, UK

S.L. -Y. Woo Musculoskeletal Research Center, University of Pittsburgh, Pittsburgh, PA, USA

M. Zhang Rehabilitation Engineering Centre, Hong Kong, Polytechnic, Hungam, Kowloon, Hong Kong

Part I

Chapter A1

Cortical Bone

J. Currey

A1.1 Composition

A1.1.1 Overall

The main constituents are the mineral hydroxyapatite, the fibrous protein collagen, and water. There is some non-collagenous organic material.

Highly mineralized bone (petrosal bones of some non-human mammals) has little organic material (8% in the horse petrosal to 3% in the tympanic bulla) [3]. (Almost certainly human ear bones will be somewhere near or in this region, though they seem not to have been studied.)

A1.1.2 Organic

The main organic component is collagen. Most is Type I, but there are small amounts of Type III and Type VI, found in restricted locations [4]. Slowly heated collagen shrinks at a particular temperature, giving an indication of the stability of the molecules. Bone collagen in men has a shrinkage temperature of about 61.5°–63.5°C up to the age of about 60, but about 60°C over that age. Bone from women showed much greater variability [5]. About 10% of the bone organic material is non-collagenous, mainly non-collagenous protein, NCP. The main ones are listed below. They have supposed functions that change rapidly.

- Osteocalcin (OC), or bone Gla protein (BGP)
- Osteonectin (ON), or SPARC
- Osteopontin (OPN) or secreted phosphoprotein I (SPPI)

J. Currey (✉)

Department of Biology, York University, York YO1 5DD, UK

Table A1.1 Composition of Cortical Bone

	Water	Organic	Ash	Source
Mass %	12.0	28.1	59.9	[1]
Volume %	23.9	38.4	37.7	[1]
Volume %	15.5	41.8	39.9	[2]

Table A1.2 Density of Cortical Bone

Wet bone	1990 kg m ⁻³ [1]
----------	-----------------------------

- Bone sialoprotein (BSP)

The relative amounts of these proteins can vary greatly. Ninomiya *et al.* [6] report far more osteocalcin (31 times) in cortical bone than in trabecular bone, and far more osteonectin (29 times) in trabecular bone than in cortical bone.

A1.1.3 Mineral

The mineral has a plate-like habit, the crystals being extremely small, about 4 nm by 50 nm by 50 nm. The mineral is a variant of hydroxyapatite, itself a variant of calcium phosphate: $\text{Ca}_{10}(\text{PO}_4)_6(\text{OH})_2$ [7]. The crystals are impure. In particular there is about 4–6% of carbonate replacing the phosphate groups, making the mineral technically a carbonate apatite, *dahllite*, and various other substitutions take place [8].

A1.1.4 Cement line

The cement line round Haversian systems (secondary osteons) contains less calcium and phosphorus, and more sulphur than nearby parts of bone. This may indicate the presence of more sulphated mucosubstances, making the cement line viscous [9].

A1.2 Physical Properties

A1.2.1 Density

A1.2.2 Electromechanical behavior

Strained bone develops electrical potential differences. These used to be attributed to piezoelectric effects. However, the size of the piezoelectric effects is small compared with those produced by streaming potentials [10]. Furthermore, there were

various anomalies with the potentials generated, which did not always accord with theory. The consensus now is that ‘SGPs’ (stress-generated potentials) are overwhelmingly caused by streaming potentials [10, 11]. Scott and Korostoff [12] determined, amongst other things, the relaxation time constants of the stress generated potentials, which varied greatly as a function of the conductivity and viscosity of the permeating fluid. As an example of their findings: a step-imposed loading moment which produced a peak strain of 4×10^{-4} induced an SGP of 1.8 mV, yielding a value of the SGP/strain ratio of 4500 mV. The SGP decayed rapidly at constant strain, reaching zero within about one second. For more detail, the complex original paper must be consulted.

A1.2.3 Other Physical Properties

Behari [10] gives a useful general review of many ‘solid state’ properties of bone, both human and non-human, many of which are not dealt with here. These properties include the Hall effect, photo-electric effects, electron paramagnetic resonance effects and so on.

A1.3 Mechanical Properties

A1.3.1 General

There is a great range for values in the literature for many reasons. Amongst these are:

(a) Different treatment of specimens Drying bone and then re-wetting it produces some small differences [13], as does formalin fixation [14]. Testing bone dry produces results quite different from those in wet bone; dry bone is stiffer, stronger, and considerably more brittle. Very small samples produce values for stiffness and strength less than those from larger samples [15, 16]. High strain rates generally produce a higher modulus of elasticity, a higher strength [17], and a greater strain to failure than specimens tested at low strain rate.

(b) Different age and health of donors Age may affect intrinsic properties. Osteoporotic bone may differ from ‘normal’ bone in ways other than the fact that it is more porous; there is evidence that the collagen is different from that in similar-aged non-osteoporotic subjects [18]. Bone from osteogenesis imperfecta patients has a higher proportion of Type III and Type V collagen compared with Type I collagen, than bone from normal subjects [19]. Bone collagen from osteopetrotic subjects is in general older than that from normal subjects, and has correspondingly different properties [5].

(c) Differences between bones, and sites in the bones The ear bones (ossicles) and portions of the temporal bones (petrosals) are highly mineralized, and will undoubtedly be stiffer and more brittle than others (though they seem not to have been investigated in humans). Long bones differ along their length and around their circumference. The distal femur is less highly mineralized and weaker in tensile and compressive static loading, and at any level the posterior part is similarly less mineralized and weaker [20].

The values reported below should be considered paradigmatic, that is, to be valid for a well-performed test on bone obtained from a middle aged person with no disease. Other values are reported in such a way as to make it clear how some property is a function of other features of the specimen.

A1.3.2 Stiffness

(a) General There are two ways of testing bone: mechanically by relating stresses to strains; ultrasonically, by subjecting the bone to ultrasound and measuring the velocity of the sound. From a knowledge of the density one can then obtain a stiffness matrix. If this is inverted it becomes a compliance matrix, the reciprocal of the individual terms of which are equivalent to the so-called technical moduli derived by mechanical testing [21]. Reilly and Burstein [22] give mechanical values, and Ashman *et al.* [23] give ultrasonic measurements. Reilly and Burstein [22] assumed transverse isotropy (that is, symmetry around the longitudinal axis of the bone), while Ashman *et al.* [23] assumed orthotropy (that is, that the values for stiffness could be different in the longitudinal, radial and tangential directions).

Reilly and Burstein [22] give values for Young's modulus at a number of intermediate angular orientations, but they do not form a very uniform set.

(b) Tensile modulus versus compressive modulus Reilly *et al.* [24] tested femoral specimens specifically to determine whether the value for Young's modulus was different in tension and compression. A paired Student's 't' test showed no significant difference between the compressive and tensile moduli at the 95% confidence level. Calculations on their data show the the 95% confidence interval ranged from compression modulus 1.72 GPa higher to tension modulus 0.27 GPa higher. The load-deformation traces showed no change of slope going from compression into tension and vice versa.

(c) Very small specimens The bending modulus of very small specimens was 6.62 GPa [5].

(d) Locational variations: Metaphysis versus diaphysis Young's modulus has been determined in three-point bending for extremely small plates (7 mm by 5 mm by (about) 0.3 mm) from the femoral metaphyseal shell and from the diaphysis of the same bones [16].

Table A1.3 Mechanical Properties

	Femur Tension [23]	Femur Tension [22]	Femur Compression [22]
Elastic moduli (GPa):			
E_1	12.0	12.8	11.7
E_2	13.4	12.8	11.7
E_3	20.0	17.7	18.2
Shear moduli* (GPa):			
G_{12}	4.5	–	–
G_{13}	5.6	3.3	–
G_{23}	6.2	3.3	–
Poisson's ratios:			
ν_{12}	0.38	0.53	0.63
ν_{13}	0.22	–	–
ν_{23}	0.24	–	–
ν_{21}	0.42	0.53	0.63
ν_{31}	0.37	0.41	0.38
ν_{32}	0.35	0.41	0.38

Subscript 1: radial direction relative to the long axis of the bone, 2: tangential direction, 3: longitudinal direction.

* Shear values are included under tension for convenience.

Table A1.4 Locational Variations in Modulus

Location	Longitudinal (GPa)	Transverse (GPa)	Source
Metaphysis	9.6	5.5	[16]
Diaphysis	12.5	6.0	[16]

The differences between these values and those reported by Reilly and Burstein [22] are probably attributable not to the difference in testing mode, since bending and tension tests from the same bone generally give similar values for Young's modulus, but to the very small size of the specimen, and to the rather low density of the specimens.

(e) Compression; effect of mineral The compressive behavior of cubes, relating the properties to the density of the specimens gives, using ρ_a (fat-free mass divided by anatomical volume, g cm^{-3}) as the explanatory variable:

Young's modulus (GPa) = $3.3\rho_a^{2.4}$ for compact bone [25].

The higher values of ρ_a were of the order of 1.8 g cm^{-3} ($=1800 \text{ kg m}^{-3}$); this equation [25] predicts a value of 13.5 GPa for such a specimen. Multiple regression analysis showed that the dependence of Young's modulus on density was caused by

Table A1.5 Moduli of Osteons

Modulus (GPa)	Longitudinal Osteons	'Alternate' Osteons	Source
Tension	11.7	5.5	[26]
Compression	6.3	7.4	[27]
Bending	2.3	2.6	[28]
Torsional*	22.7	16.8	[29]

* Values for an 80-year-old man excluded.

the effect of porosity on density, and that, in these specimens, the effect of mineral content was insignificant.

(f) Single secondary osteons Ascenzi and co-workers [26–29] distinguish two types of secondary osteon: 'longitudinal' osteons, whose collagen fibres have a basically longitudinal orientation, and 'alternate' osteons, whose fibres have markedly different courses in neighboring lamellae. (This difference is a contentious issue.)

N.B.: These studies of Ascenzi and co-workers [26–29] are widely quoted, so beware of some apparent anomalies (apart from changes in nomenclature between papers). The bending modulus is remarkably low compared with the tension and compression moduli. The torsional (shear) modulus is remarkably high, compared both with the shear modulus values obtained by others (above), and with the tension and compression values. Torsional moduli are expected, on theoretical grounds, to be less than the tension and compression moduli. Furthermore, the large differences between the tension and compression moduli have not been reported elsewhere.]

(g) Strain rate effects Calculations [30], incorporating data from non-human as well as human material, predict that Young's modulus is very modestly dependent upon strain rate:

$$E = 21402(\text{strain rate } (s^{-1}))^{0.050} \text{ MPa}$$

[N.B. statements about strain rate effects in bone are suspect unless it is clear that the workers have taken machine compliance into account!]

(h) Viscoelastic-damage properties Viscoelastic time constant (the value τ (s) in the equation):

$$\epsilon(t) = \beta_1 \exp[t_o - t / \tau] + \beta_2$$

where the betas are parameters, t is time (s), t_o is time at which the specimen is held at a constant stress below the creep threshold: 6.1 s [31]. For reference, its value in bovine bone: 3.6 s.

Table A1.6 Strength of Cortical Bone [22]

Mode	Orientation	Breaking Strength (MPa)	Yield Stress (MPa)	Ultimate Strain
Tension	Longitudinal	133	114	0.031
	Tangential	52	–	0.007
Compression	Longitudinal	205	–	–
	Tangential	130	–	–
	Shear	67	–	–

Table A1.7 Locational Variations in Strength

Location	Longitudinal (MPa)	Transverse (MPa)	Source
Metaphysis	101	50	[16]
Diaphysis	129	47	[16]

Table A1.8 Strength of Osteons

Strength (MPa)	Longitudinal Osteons	'Alternate' Osteons	Source
Tension	120	102	[26]
Compression	110	134	[27]
Bending	390	348	[28]
Torsional*	202	167	[29]

* Values for an 80 year old man excluded.

A1.3.3 Strength

(a) Overall

(b) Combined loading Cezayirlioglu *et al.* [32] tested human bone under combined axial and torsional loading. The results are too complex to tabulate, but should be consulted by readers interested in complex loading phenomena.

(c) Metaphysis versus diaphysis Same specimens as reported for modulus above (Table A1.4) [16]. 'Tensile' strength calculated from the bending moment, using a 'rupture factor' to take account of the non-uniform distribution of strain in the specimen.

(d) Effect of mineral Keller [25], using the same specimens as above, provides the following relationship:

$$\text{Strength} = 43.9\rho_a^{2.0} (\text{MPa})$$

[N.B.: The effect of mineralization, as opposed to density, is possibly of importance here; the original paper must be consulted.]

(e) Single secondary osteons The same nomenclature applies as for moduli of osteons (Table A1.5).

[N.B. The bending strengths and torsional strengths seem very high, even bearing in mind that no allowance has been made in bending for non-elastic effects.]

(f) Strain rate effects Bone will bear a higher stress if it is loaded at a higher strain (or stress) rate. Carter and Caler [17] found an empirical relationship that failure stress (σ_f (MPa)) was a function of either stress rate ($\dot{\sigma}$) or strain rate ($\dot{\epsilon}$):

$$\sigma_f = 87(\dot{\sigma})^{0.053}$$

$$\sigma_f = 87(\dot{\epsilon})^{0.055}$$

N.B. These relationships imply an increase of 44% in the failure stress if the stress rate is increased one thousandfold. This relationship has been found to be roughly the same in other, non-human, mammals.

(g) Creep Creep threshold (the stress below which no creep occurs): 73 MPa [31]. The equivalent value for bovine bone is 117 MPa [31]. Specimens in tension or compression were held at particular stresses [33]. The time (seconds) to failure is given as a function of normalized stress (stress/Young's modulus (MPa/MPa)):

$$\text{Tension: } \text{Time to failure} = 1.45 \times 10^{-36} (\text{normalized stress})^{-15.8}$$

$$\text{Compression: } \text{Time to failure} = 4.07 \times 10^{-37} (\text{normalized stress})^{-17.8}$$

(h) Fatigue Some workers report the log of the number of cycles as a function of the applied stress levels, some report the log cycle number as a function of log stress levels, and some report log stress levels as a function of log cycle number. [The last seems wrong, since the applied stress can hardly be a function of the number of cycles the specimen is going to bear, but it is frequently used in fatigue studies. It is not possible simply to reverse the dependent and independent axes because the equations are derived from regressions with associated uncertainty.] The variation between the results for different testing modes is considerable.

Carter *et al.* [34] report on the effect of Young's modulus of elasticity and porosity in their specimens. They find that Young's modulus is positively associated with fatigue life, and porosity is negatively associated:

Table A1.9 Effect of Remodeling [35]

Property	Primary Osteons	Haversian Osteons
Tensile Strength (MPa)	162	133
Ultimate Strain	0.026	0.022
Young's modulus (GPa)	19.7	18.0

$$\begin{aligned} \log N_f &= -2.05 \log \Delta\sigma_o && (S.E. 0.599) \\ \log N_f &= -4.82 \log \Delta\sigma_o + 0.186 E && (S.E. 0.387) \\ \log N_f &= -2.63 \log \Delta\sigma_o - 0.061 P && (S.E. 0.513) \\ \log N_f &= -4.73 \log \Delta\sigma_o + 0.160 E - 0.029 P && (S.E. 0.363) \end{aligned}$$

where N_f : number of cycles to failure; $\Delta\sigma_o$: initial stress range (these experiments were carried out under strain control, so stress range decreased as damage spread and the specimens became more compliant); E : Young's modulus (GPa); P : porosity (%). Incorporating Young's modulus into the equation has a marked effect in reducing the standard error; porosity has a much less strong effect.

[N.B. Many workers normalize their data in an effort to reduce the effect that variations in Young's modulus have in increasing the scatter of the results.]

Choi and Goldstein [15] provide alternate, somewhat higher values.

(i) Effect of remodeling Vincentelli and Grigorov [35] examined the effect of Haversian remodelling on the tibia. The specimens they reported were almost entirely primary or Haversian, with few specimens having a scattering of secondary osteons. [Unfortunately they probably (it is not clear) allowed their specimens to dry out, so it is not sure that bone *in vivo* would show the same behavior. However, their results are similar to those found in nonhuman specimens.]

Additional Reading

Cowin, S.C. (ed.) (1989) *Bone Mechanics* Boca Raton: CRC Press.

A more rigorous, less chatty and less biologically, oriented approach than the following books by Currey and by Martin and Burr. The chapters on mechanics (2, 6 and 7), written by Cowin himself, are particularly authoritative.

Currey, J.D. (1984) *The Mechanical Adaptation of Bones* Princeton: University Press.

Out of print, new edition in preparation. Tries to deal with all aspects of mechanical properties of bone as a material and of whole bones. Not overly technical. Written from a general biological perspective, thus, does not concentrate on human material.

Martin, R.B. and Burr, D.B. (1989) *Structure, Function and Adaptation of Compact Bone* New York: Raven Press.

There are not many values of mechanical properties here, but the treatment of the biology of bone, and of fatigue of bone tissue, is excellent and the discussion of remodeling, although now somewhat out of date, is a very good introduction to this intellectually taxing topic.

Nigg, B.M. and Herzog, W. (eds)(1994) *Biomechanics of the Musculoskeletal System* John Wiley: Chichester.

Deals with many aspects of biomechanics, including locomotion, with an emphasis on human material. There is a full treatment of the measurement of many biomechanical properties.

References

1. Gong, J.K., Arnold, J.S. and Cohn, S.H. (1964) Composition of trabecular and cortical bone. *Anat. Rec.*, **149**, 325–331.
2. Biltz, R.M. and Pellegrino, E.D. (1969) The chemical anatomy of bone I. A comparative study of bone composition in sixteen vertebrates. *J. Bone Joint Surg.*, **51A**, 456–466.
3. Lees, S. and Escoubes, M. (1987) Vapor pressure isotherms, composition and density of hyperdense bones of horse, whale and porpoise. *Con. Tiss. Res.*, **16**, 305–322.
4. Keene, D.R., Sakai, L.Y. and Burgeson, R.E. (1991) Human bone contains type III collagen, type VI collagen, and fibrillin: Type III collagen is present on specific fibers that may mediate attachment of tendons, ligaments, and periosteum to calcified bone cortex. *J. Histochem. Cytochem.*, **39**, 59–69.
5. Danielsen, C.C., Mosekilde, Li., Bollerslev, J. *et al.* (1994) Thermal stability of cortical bone collagen in relation to age in normal individuals and in individuals with osteopetrosis. *Bone*, **15**, 91–96.
6. Ninomiya, J.T., Tracy, R.P., Calore, J.D., *et al.* (1990) Heterogeneity of human bone. *J. Bone Min. Res.*, **5**, 933–938.
7. Lowenstam, H.A. and Weiner, S. (1989) *On Biomineralization*, Oxford University Press, New York.
8. McConnell, D. (1962) The crystal structure of bone. *Clin. Orthop. Rel. Res.*, **23**, 253–68.
9. Burr, D.B., Schaffler, M.B. and Frederickson, R.G. (1988) Composition of the cement line and its possible mechanical role as a local interface in human compact bone. *J. Biomech.*, **21**, 939–945.
10. Behari, J. (1991) Solid state bone behavior. *Prog. Biophys. Mol. Biol.*, **56**, 1–41.
11. Martin, R.B. and Burr, D.B. (1989) *Structure, Function, and Adaptation of Compact Bone*, Raven Press, New York.
12. Scott, G.C. and Korostoff, E. (1990) Oscillatory and step response electromechanical phenomena in human and bovine bone. *J. Biomech.*, **23**, 127–143.
13. Currey, J.D. (1988) The effects of drying and re-wetting on some mechanical properties of cortical bone. *J. Biomech.*, **21**, 439–441.
14. Sedlin, E.D. (1967) A rheological model for cortical bone. *Acta Orthop. Scand.*, (Suppl. 83), 1–78.
15. Choi, K. and Goldstein, S.A. (1992) A comparison of the fatigue behavior of human trabecular and cortical bone tissue. *J. Biomech.*, **25**, 1371–1381.
16. Lotz, J.C., Gerhart, T.N. and Hayes, W.C. (1991) Mechanical properties of metaphyseal bone in the proximal femur. *J. Biomech.*, **24**, 317–329.

17. Carter, D.R. and Caler, W.E. (1985) A cumulative damage model for bone fracture. *J. Orthop. Res.*, **3**, 84–90.
18. Bailey, A.J., Wotton, S.F., Sims, T.J. *et al.* (1993) Biochemical changes in the collagen of human osteoporotic bone matrix. *Con. Tiss. Res.*, **29**, 119–132.
19. Bateman, J.F., Chan, D., Mascara, T. *et al.* (1986) Collagen defects in lethal perinatal osteogenesis imperfecta. *Biochem. J.*, **240**, 699–708.
20. Saito, S. (1983) (Distribution of the X-ray density, compressive and tensile breaking strength in the human femoral shaft) Die Verteilung von Dichte, Druck und Festigkeit im menschlichen Femurschaft. *Anat. Anzeiger Jena*, **154**, 365–376.
21. Cowin, S.C. (1989) *Bone Mechanics*, CRC Press, Boca Raton.
22. Reilly, D.T. and Burstein, A.H. (1975) The elastic and ultimate properties of compact bone tissue. *J. Biomech.*, **8**, 393–405.
23. Ashman, R.B., Cowin, S.C., Van Buskirk, W.C. (1984) A continuous wave technique for the measurement of the elastic properties of cortical bone. *J. Biomech.*, **17**, 349–361.
24. Reilly, D.T. and Burstein, A.H. (1974) The mechanical properties of cortical bone. *J. Bone Joint Surg.*, **56A**, 1001–1022
25. Keller, T.S. (1994) Predicting the compressive mechanical behavior of bone. *J. Biomech.*, **27**, 1159–1168.
26. Ascenzi, A. and Bonucci, E. (1967) The tensile properties of single osteons. *Anat. Rec.*, **158**, 375–386.
27. Ascenzi, A. and Bonucci, E. (1968) The compressive properties of single osteons. *Anat. Rec.*, **161**, 377–391.
28. Ascenzi, A., Baschieri, P., and Benvenuti, A. (1990) The bending properties of single osteons. *J. Biomech.*, **23**, 763–771.
29. Ascenzi, A., Baschieri, P., and Benvenuti, A. (1994) The torsional properties of single selected osteons. *J. Biomech.*, **27**, 875–884.
30. Carter, D.R. and Caler, W.E. (1983) Cycle-dependent and time-dependent bone fracture with repeated loading. *J. Biomech. Eng.*, **105**, 166–170.
31. Fondrk, M., Bahniuk, E., Davy, D.T. *et al.* (1988) Some viscoplastic characteristics of bovine and human cortical bone. *J. Biomech.*, **21**, 623–630.
32. Cezayirlioglu, H., Bahniuk, E., Davy, D.T. *et al.* (1985) Anisotropic yield behavior of bone under combined axial force and torque. *J. Biomech.*, **18**, 61–69.
33. Caler, W.E. and Carter, D.R. (1989) Bone creep-fatigue damage accumulation *J. Biomech.*, **22**, 625–635.
34. Carter, D.R., Caler, W.E., Spengler, D.M. *et al.* (1981) Uniaxial fatigue of human bone. The influence of tissue physical characteristics. *J. Biomech.*, **14**, 461–70.
35. Vincentelli, R., and Grigorov, M. (1985) The effect of haversian remodeling on the tensile properties of human cortical bone. *J. Biomech.*, **18**, 201–207.

Chapter A2

Cancellous Bone

Christopher J. Hernandez

A2.1 Microstructure

Cancellous bone (also referred to as trabecular bone or spongy bone) is a porous cellular solid consisting of platelike and rodlike struts called trabeculae. The size and arrangement of trabeculae vary among species and within regions of the skeleton and change with age. Average trabecular thickness can be as great as 300 μm but, in elderly human tissue, ranges from 100 to 200 μm [1]. The orientation of trabeculae within cancellous bone varies, resulting in considerable specimen-to-specimen heterogeneity. At the continuum level (specimens 3–5 mm in smallest dimension) the density of cancellous bone is measured as the mass of the specimen (wet after removing the marrow) divided by specimen volume and is referred to as the “apparent density.” The apparent density of human cancellous bone typically ranges from 0.05 to 1.1 g/cm^3 . The apparent density of cancellous bone is not to be confused with the “tissue density” which expresses the density of individual trabeculae. The volume fraction of human cancellous bone (expressed in the bone literature as BV/TV) ranges from 5 % to 60 %. The surface-to-volume ratio of human cancellous bone (BS/TV) is related to bone volume fraction in the following manner [2]:

$$\frac{\text{BS}}{\text{TV}} = 8.84 \left(\frac{\text{BV}}{\text{TV}} \right)^{0.70}$$

C.J. Hernandez (✉)
Sibley School of Mechanical and Aerospace Engineering, Cornell University,
219 Upson Hall, Ithaca, NY 14853, USA

Meinig School of Biomedical Engineering, Cornell University, 219 Upson Hall,
Ithaca, NY 14853, USA
e-mail: cjh275@cornell.edu

A2.2 Tissue Composition and Ultrastructure

At the tissue level cancellous bone is a ceramic polymer composite with composition similar to that of cortical bone. By mass, bone tissue is 65 % mineral (primarily an impure hydroxyapatite), 25 % organic (primarily type I collagen but also including non-collagenous proteins), and 10 % water. By volume bone tissue is 36 % mineral, 55 % organic, and 9 % water [3]. These proportions vary with age of the individual as well as length of time the tissue has been present in the body (the “tissue age”) and differ among species. In general tissue density is highly conserved and shows a small range within a species (1.6–2.0 g/cm³ in humans) [3, 4]. Heterogeneity within bone tissue is present, however, and is caused primarily by bone remodeling. Bone remodeling is a process in which bone cells remove and replace bone tissue at discrete locations on bone surfaces. Structures known as cement lines mark the boundaries of previous remodeling activity within trabeculae and divide more recently remodeled (younger) tissue from non-remodeled (older) regions of the tissue that are typically stiffer and more mineralized. The large surface-to-volume ratio of cancellous bone (as compared to cortical bone) enables greater turnover of bone tissue during remodeling, reducing the proportion of older tissue, possibly explaining why cancellous bone has been reported to have 10–14 % lower tissue density than cortical bone [5].

A2.3 Mechanical Properties

The mechanical properties of cancellous bone at the continuum scale (specimens 3–5 mm in smallest dimension) are reported here. Mechanical properties of cancellous bone can vary among species and among anatomical sites within individuals. Mechanical properties can also be altered with aging and in the presence of disease states.

A2.3.1 *Elastic Modulus and Strength*

The stiffness and strength of cancellous bone are determined primarily by apparent density [6, 7]. When loaded in uniaxial compression or tension cancellous bone displays a slightly nonlinear stress-strain curve [8] and yield is commonly determined using the 0.2 % offset criteria. Cancellous bone is anisotropic due to both microstructure and tissue anisotropy.

The Young’s modulus and shear modulus of cancellous bone are determined primarily by tissue apparent density (Table A2.1) and can vary over tenfold among regions of the skeleton within the same individual. Hence, there is no one value for an elastic modulus of cancellous bone and cancellous bone mechanical properties must therefore be estimated from apparent density. Empirically derived power law

Table A2.1 Mechanical properties of cancellous bone are strongly influenced by density. Regression models relating cancellous bone mechanical properties to apparent density (wet) are provided. Mechanical properties are reported on axis (in the direction of primary trabecular orientation). Results are provided as mean \pm SD and (95 % CI) when available. Regression equations were achieved using linear regression on log-transformed data

Mechanical property	n	Age	Apparent density (g/cm ³)	Y=A × X ^b		r ²
				A	B	
Young's modulus (MPa) ^a	142	67 ± 15 (61–68)	0.27 (0.09–0.75)	8920 (7540–10,550)	1.83 (1.72–1.94)	0.88
Shear modulus (MPa) ^b	42	Bovine	NR ^b	2.09	1.90	0.84
σ_y (MPa, tension) ^a	52	65 ± 14 (61–68)	0.29 (0.25–0.34)	31.35 (23.81–41.29)	1.67 (1.58–1.77)	0.86
σ_z (MPa, compression) ^a	68	65 ± 14 (61–68)	0.27 ± 0.17 (0.24–0.32)	51.15 (41.53–62.99)	1.85 (1.72–1.99)	0.91
σ_{ult} (MPa tension) ^c	22	54 ± 11 (27–82)	0.19 ± 0.04 (0.09–0.29)	13.3	1.07	0.47
σ_{ult} (MPa compression) ^c	22	54 ± 11 (27–82)	0.17 ± 0.04 (0.07–0.27)	33.2	1.53	0.68
τ_{ult} (MPa) ^b	15	Bovine	NR ^b	72.74	1.86	0.64
K_{\perp} (MPa/m ^{1/2} , crack oriented ⊥ to trabeculae) ^d	166	82 ± 6.8 (65–99)	Range: 0.25–1.10 g/cm ³	0.67	1.58	0.62
K_{\parallel} (MPa/m ^{1/2} , crack oriented ∥ to trabecular orientation) ^d	169	82 ± 6.8 (65–99)	Range: 0.25–1.10 g/cm ³	0.54	1.60	0.56

NR not reported

^aRegression models include cancellous bone from vertebrae, proximal tibia, and proximal femur. More predictive regression models for each anatomical region are available [9, 10]

^bDetermined in the bovine proximal tibia through torsion testing [11]

^cVertebral trabecular bone [12]

^dSpecimens from human femoral head and equine vertebrae were pooled. Measures of K_{IC} were not achieved due to elastic-plastic behavior associated with trabecular bending/torsion [13]

models are useful for general prediction of specimen Young's modulus and shear modulus, although linear regressions are appropriate when the range in apparent density is small (for example, if only one region of the skeleton is considered). The Poisson's ratio of cancellous bone is difficult to measure and poorly understood and is typically estimated (common estimates range from 0.1 to 0.3). Cancellous bone strength is strongly correlated with Young's modulus. The ultimate strength of cancellous bone is strongly correlated with yield strength (in vertebral cancellous bone ultimate strength is 20 % greater than yield strength [14]). Yield strain and ultimate strain are not correlated with apparent density. Yield strain of cancellous bone within a region of the skeleton shows little interindividual variability, but differences among skeletal sites have been noted. Compressive yield strains of human cancellous bone have been reported to range from 0.70 to 0.85 (across different regions of the skeleton). Yield strains in tension are always lower than those in compression (reported to range from 0.60 to 0.70). Ultimate strain is more variable for unknown reasons.

Trabecular alignment and microstructure have been shown to influence mechanical properties of cancellous bone. Trabecular alignment is the primary cause of cancellous bone anisotropy. When loading is applied at 90° to the primary trabecular orientation, cancellous bone Young's modulus is 40–60 % smaller and the ultimate strength is 30–45 % smaller [15]. Interestingly yield strain in the transverse directions is not different from that on axis. The effects of trabecular alignment on Young's modulus can be described using a fabric tensor and a quadratic Tsai-Wu criteria has been used successfully to describe a multiaxial failure envelope for cancellous bone [16]. More complicated multiaxial failure criteria have been used to address some shortcomings of the Tsai-Wu criteria [17, 18].

Tissue material properties also influence cancellous bone Young's modulus and strength. Compressive Young's modulus and strength of bone (cancellous and cortical bone pooled) is related to bone volume fraction (BV/TV) and the tissue degree of mineralization (α , inorganic mass/bone mass) in the following manner [19]:

$$E(\text{GPa}) = 84 \left(\frac{\text{BV}}{\text{TV}} \right)^{2.58} \alpha^{2.74}$$

$$\sigma_{\text{ult}}(\text{MPa}) = 794 \left(\frac{\text{BV}}{\text{TV}} \right)^{1.92} \alpha^{2.79}.$$

The regression exponents applied to tissue degree of mineralization are greater than those on bone volume fraction, demonstrating that bone strength is more sensitive to variation in tissue degree of mineralization than to variation in bone volume fraction.

A2.3.2 Viscoelastic and Fatigue Properties

Cancellous bone displays viscoelastic properties. The strain rate has only a small effect on the Young's modulus and strength of cancellous bone under uniaxial loading; Young's modulus and strength are related to strain rate to the power of 0.06 [6]. Hydraulic stiffening of the marrow does not influence Young's modulus and strength

until strain rates exceed 1 s^{-1} [6]. Creep deformation in cancellous bone follows the pattern of a rapid primary phase, slow secondary phase, and rapid tertiary phase [20]. The creep rate of bovine cancellous bone is related to normalized stress (σ/E_0 , where E_0 is the initial Young's modulus) as follows [20]:

$$\frac{d\varepsilon_c}{dt} = 2.21 \times 10^{33} \left(\frac{\sigma}{E_0} \right)^{17.65}.$$

Human vertebral cancellous bone submitted to low-magnitude, compressive creep loading ($\sigma/E_0 = 1500 \mu\varepsilon$ or less) has been shown to have nonlinear viscoelastic properties such that residual strains persist up to ten times longer than the period of constant loading [21].

Under fatigue loading cancellous bone displays an S-N curve such that the number of cycles to failure (N_f) is related to normalized stress (σ/E_0) as follows [22]:

$$N_f = 4.57 \times 10^{-18} (\sigma / E_0)^{-8.54}.$$

A2.3.3 *Fracture Toughness*

Relatively little is known regarding resistance to crack growth in cancellous bone. Resistance to crack growth in cancellous bone specimens has been assessed with linear elastic fracture mechanics approaches (Table A2.1), but care must be taken in interpreting the quantitative values because large deformations in trabeculae at the crack tip prevent assessment of K_{IC} (see [13] for a discussion of the utility of linear elastic fracture mechanics in continuum specimens of cancellous bone).

A2.3.4 *Post-Yield and Damage Behavior*

Tissue damage in cancellous bone impairs mechanical performance during subsequent loading. Reductions in Young's modulus have been observed in specimens of cancellous bone submitted to as little as 0.4 % apparent strain (well below yield strain) [23]. Loading in compression causes reductions in Young's modulus [24–26] and strength [24, 25] that are related to the maximum applied strain experienced by the specimen. Tissue damage in the form of microscopic and sub-microscopic cracks is also related to the maximum applied strain and subsequent reductions in Young's modulus and strength. Relatively small amounts of microscopic tissue damage (less than that characterized as “naturally occurring”) have been associated with 50–60 % reductions in strength and the use of over 90 % of cancellous bone fatigue life [24, 26]. Hence, microscopic tissue damage accumulated in cancellous bone in vivo may contribute to bone failure. Microscopic tissue damage is generated more rapidly following changes in loading mode (between compression and shear for example) [27]. Despite the presence of microscopic damage, residual strains

following loading are typically small; upon removal of load cancellous bone recovers as much as 70–94 % of the applied strain [24, 25, 28].

A2.4 Tissue-Level Mechanical Properties

The mechanical properties of cancellous bone tissue (the constituents of individual trabeculae) remain poorly understood. Mechanical testing of individual trabeculae is challenging and requires many assumptions that may limit the accuracy of the results. The Young's modulus of individual trabeculae typically averages 3–6 GPa [29]. In contrast, the Young's modulus of human cancellous bone tissue assessed through nanoindentation is, on average, 10–18 GPa [30–32], and is similar to the range to tissue-level Young's moduli estimated using finite element models of cancellous bone microstructure [33]. Relatively little is known regarding tissue-level anisotropy, tissue-level viscoelasticity, fatigue, and fracture toughness.

Additional Reading

Cowin S. *Bone Mechanics Handbook*. In. 2 ed. Boca Raton: CRC Press; 2001.

This book provides a complete review of bone mechanical properties and interactions with bone cell biology.

Currey JD. *Bones: Structure and Mechanics*. Princeton, NJ, USA: Princeton University Press; 2002.

This is a review that includes thorough discussion of non-human bone mechanical properties and function.

References

1. Liu XS, Sajda P, Saha PK, Wehrli FW, Bevill G, Keaveny TM, Guo XE (2008) Complete volumetric decomposition of individual trabecular plates and rods and its morphological correlations with anisotropic elastic moduli in human trabecular bone. *J Bone Miner Res* 23:223–235
2. Fyhrie DP, Fazzalari NL, Goulet R, Goldstein SA (1993) Direct calculation of the surface-to-volume ratio for human cancellous bone. *J Biomech* 26:955–967
3. Robinson RA (1975) Physicochemical structure of bone. *Clin Orthop* 53:263–315
4. Galante J, Rostoker W, Ray RD (1970) Physical properties of trabecular bone. *Calcif Tissue Res* 5:236–246
5. Gong JK, Arnold JS, Cohn SH (1964) Composition of trabecular and cortical bone. *Anat Rec* 149:325–332
6. Carter DR, Hayes WC (1977) The compressive behavior of bone as a two-phase porous structure. *J Bone Joint Surg* 59-A:954–962
7. Keaveny TM, Morgan EF, Niebur GL, Yeh OC (2001) Biomechanics of trabecular bone. *Annu Rev Biomed Eng* 3:307–333
8. Morgan EF, Yeh OC, Chang WC, Keaveny TM (2001) Nonlinear behavior of trabecular bone at small strains. *J Biomech Eng* 123:1–9

9. Morgan EF, Bayraktar HH, Keaveny TM (2003) Trabecular bone modulus-density relationships depend on anatomic site. *J Biomech* 36:897–904
10. Morgan EF, Keaveny TM (2001) Dependence of yield strain of human trabecular bone on anatomic site. *J Biomech* 34:569–577
11. Garrison JG, Gargac JA, Niebur GL (2011) Shear strength and toughness of trabecular bone are more sensitive to density than damage. *J Biomech* 44:2747–2754
12. Kopperdahl DL, Keaveny TM (1998) Yield strain behavior of trabecular bone. *J Biomech* 31:601–608
13. Cook RB, Zioupos P (2009) The fracture toughness of cancellous bone. *J Biomech* 42:2054–2060
14. Crawford RP, Cann CE, Keaveny TM (2003) Finite element models predict in vitro vertebral body compressive strength better than quantitative computed tomography. *Bone* 33:744–750
15. Goulet RW, Goldstein SA, Ciarelli MJ, Kuhn JL, Brown MB, Feldkamp LA (1994) The relationship between the structural and orthogonal compressive properties of trabecular bone. *J Biomech* 27:375–389
16. Cowin SC (1985) The relationship between the elasticity tensor and the fabric tensor. *Mech Mater* 4:137–147
17. Bayraktar HH, Gupta A, Kwon RY, Papadopoulos P, Keaveny TM (2004) The modified super-ellipsoid yield criterion for human trabecular bone. *J Biomech Eng* 126:677–684
18. Wolfram U, Gross T, Pahr DH, Schwiedrzik J, Wilke HJ, Zysset PK (2012) Fabric-based Tsai-Wu yield criteria for vertebral trabecular bone in stress and strain space. *J Mech Behav Biomed Mater* 15:218–228
19. Hernandez CJ, Beaupre GS, Keller TS, Carter DR (2001) The influence of bone volume fraction and ash fraction on bone strength and modulus. *Bone* 29:74–78
20. Bowman SM, Keaveny TM, Gibson LJ, Hayes WC, McMahon TA (1994) Compressive creep behavior of bovine trabecular bone. *J Biomech* 27:301–310
21. Yamamoto E, Paul Crawford R, Chan DD, Keaveny TM (2006) Development of residual strains in human vertebral trabecular bone after prolonged static and cyclic loading at low load levels. *J Biomech* 39:1812–1818
22. Haddock SM, Yeh OC, Mummaneni PV, Rosenberg WS, Keaveny TM (2004) Similarity in the fatigue behavior of trabecular bone across site and species. *J Biomech* 37:181–187
23. Morgan EF, Yeh OC, Keaveny TM (2005) Damage in trabecular bone at small strains. *Eur J Morphol* 42:13–21
24. Hernandez CJ, Lambers FM, Widjaja J, Chapa C, Rinnac CM (2014) Quantitative relationships between microdamage and cancellous bone strength and stiffness. *Bone* 66:205–213
25. Keaveny TM, Wachtel EF, Kopperdahl DL (1999) Mechanical behavior of human trabecular bone after overloading. *J Orthop Res* 17:346–353
26. Lambers FM, Bouman AR, Rinnac CM, Hernandez CJ (2013) Microdamage caused by fatigue loading in human cancellous bone: relationship to reductions in bone biomechanical performance. *PLoS One* 8, e83662
27. Wang X, Niebur GL (2006) Microdamage propagation in trabecular bone due to changes in loading mode. *J Biomech* 39:781–790
28. Fyhrie DP, Schaffler MB (1994) Failure mechanisms in human vertebral cancellous bone. *Bone* 15:105–109
29. Guo XE (2001) Mechanical properties of cortical bone and cancellous tissue. In: Cowin SC (ed) *Bone Mechanics Handbook*. CRC Press, Boca Raton, pp 10.11–10.23
30. Kim G, Cole JH, Boskey AL, Baker SP, van der Meulen MC (2014) Reduced tissue-level stiffness and mineralization in osteoporotic cancellous bone. *Calcif Tissue Int* 95:125–131
31. Norman J, Shapter JG, Short K, Smith LJ, Fazzalari NL (2008) Micromechanical properties of human trabecular bone: a hierarchical investigation using nanoindentation. *J Biomed Mater Res A* 87:196–202
32. Rho JY, Roy ME, Tsui TY, Pharr GM (1999) Elastic properties of microstructural components of human bone tissue as measured by nanoindentation. *J Biomed Mater Res* 45:48–54
33. Bayraktar HH, Morgan EF, Niebur GL, Morris GE, Wong EK, Keaveny TM (2004) Comparison of the elastic and yield properties of human femoral trabecular and cortical bone tissue. *J Biomech* 37:27–35

Chapter A3

Dentin and Enamel

K.E. Healy

A3.1 Introduction

A3.1.1 *Structure of human dentition:*

The permanent adult human dentition normally consists of 32 teeth, of which 16 are located in the mandible and 16 in the maxilla. There are 4 incisors, 2 canines, 4 premolars and 6 molars for the upper and lower dentition. The incisors are used for cutting food, the canines for tearing, the premolars for grasping, and the molars for grinding (i.e., masticating). There is a generic heterogeneous structure for these teeth, where enamel forms an exterior layer over the underlying dentin. From the cervix to the apex of the root, the exterior of the dentin is covered by cementum to which the periodontal ligament attaches the tooth to alveolar bone. Dental enamel is dense, highly mineralized, hard, and brittle. It contains prism-like structures that span from the enamel surface to the junction of enamel and dentin, the dentino-enamel junction (DEJ). The prisms are comprised of hydroxyapatite crystallites and contain very little organic matrix. These properties make dental enamel an excellent material for cutting and masticating food (i.e., processes that involve friction and wear). In contrast, dentin is not as hard as enamel, but it is tougher. Dentin is a heterogeneous material and can be thought of as a composite structure containing four major components: dentin matrix; dentinal tubules; mineral (i.e., carbonate containing hydroxyapatite); and, dentinal fluid. The dentinal tubules (~45 000 per mm²) are formed during development of the dentin matrix and are distributed

K.E. Healy (✉)

Department of Biological Materials, Northwestern University,
311 E. Chicago Ave., Chicago, IL 60611-3008, USA

throughout the dentin matrix in a somewhat uniform manner. The dentin matrix mineralizes in an anisotropic fashion, where a highly mineralized tissue, peritubular dentin, surrounds the dentinal tubules. The mineralized tissue between the dentinal tubules and peritubular dentin is referred to as intertubular dentin. Histological examination has revealed that intertubular dentin is less mineralized than peritubular dentin. Furthermore, the matrix and mineral content of root dentin is different from coronal dentin. A good review of the structure of teeth can be found in Waters [1].

A3.2 Composition

Table A3.1 Basic Constituents of Human Dentin and Enamel*

	Enamel		Dentin	
	Weight %	Volume %	Weight %	Volume %
Mineral (density, 3000 kg m ⁻³)	96	90	70	50
Organic (density, 1400 kg m ⁻³)	1	2	20	30
Water (density, 1000 kg m ⁻³)	3	8	10	20

* Adapted from [1–3].

Table A3.2 Major Elemental Composition of Surface and Bulk Dental Enamel

	Enamel Mean wt% (range or standard deviation, ±)	Dentin Mean wt% (range or standard deviation, ±)	Source, Comments
Ca	37.4 ± 1.0	–	[4]#
	37.1 ± 0.2 (26.7–47.9)	26.9 ± 0.2 (21.8–31.3)	[5]#
	36.3 ± 0.1 (27.7–42.0)	27.6 ± 0.1 (24.7–31.5)	[5]‡
P	17.8 ± 0.2	13.5 ± 0.1	[5]●, age >25yrs
	17.68 ± 0.2		[6]□
Na	0.72 ± 0.008 (0.42–1.03)	0.72 ± 0.008 (0.26–0.87)	[5]#
	0.72 ± 0.008 (0.49–0.88)	0.64 ± 0.001 (0.55–0.75)	[5]‡
Cl	0.28 ± 0.01	0.05 ± 0.004	[5]#, age >25yrs
	0.32 ± 0.01	0.072 ± 0.022	[7]#
K	0.026 ± 0.001	0.02 ± 0.001	[5]‡, age <25yrs
Mg	0.39 ± 0.02 (0.13–0.77)	0.74 ± 0.02 (0.25–0.94)	[5]#
	0.39 ± 0.004 (0.24–0.48)	0.76 ± 0.004 (0.58–0.89)	[5]‡
CO ₃	3.2 (2.4–4.2)	4.6 (4–5)	[2,3]†

Neutron activated gamma-ray spectrometric analysis.

‡ Atomic absorption spectrophotometry.

● Colorimetric assay.

† Average compiled from the literature.

* Neutron activated gamma-ray spectrometric analysis (Na, Cl, Al, Mn, Ca, and P), atomic absorption spectrophotometry (K, Mg, Zn, Cu, and Fe), or a fluoride-specific electrode (F).

□ Atomic absorption spectrophotometry (Ca), and colorimetric method (P).

Table A3.3 Trace Elemental Composition of Surface and Bulk Dental Enamel

	At.#	Surface Enamel		Whole Enamel		Source, comments
		Mean (range) $\mu\text{g/g}$	Median $\mu\text{g/g}$	Mean (range) $\mu\text{g/g}$	Median $\mu\text{g/g}$	
S	16			281 (530–130)	270	[8]†,[9]‡
F	9	752 (1948–25)	666	293 (730–95)	200	[8]†,[9]‡
				123.8 \pm 7.9		[10]◇
Zn	30	893 (5400–61)	576	199 (400–91)	190	[8]†,[9]‡
				276 \pm 106		[4]#
				263.42 \pm 14.8		[10]◇
Mg	12	745 (3600–115)	576	1,670 (3,000–470)	1,550	[8]†,[9]‡
Al	13	343 (2304–16)	202	12.5 (70–1.5)	5.6	[8]†,[9]‡
Sr	38	204 (7632–9)	36	81 (280–26)	56	[8]†,[9]‡
				93.5 \pm 21.9		[4]#
				111.19 \pm 9.86		[10]◇
Fe	26	138 (1404–18)	68	4.4 (21–0.8)	2.6	[8]†,[9]‡
				2.77		[7]*
Si	14	70 (504–1.3)	40			[8]†,[9]‡
Mn	25	59 (468–2.6)	33	0.28 (0.64–0.08)	0.26	[8]†,[9]‡
				0.54 \pm 0.08		[4]#
				0.59 \pm 0.04		[10]◇
Ag	47	32 (396–0.2)	2	0.35 (1.3–0.03)	0.16	[8]†,[9]‡
				0.56 \pm 0.29		[10]◇
Pb	82	24 (79–1.2)	18	3.6 (6.5–1.3)	3.6	[8]†,[9]‡
Ni	28	23 (270–0.4)	9			[8]†,[9]‡
Ba	56	22 (432–0.8)	7	4.2 (13–0.8)	3.4	[8]†,[9]‡
Se	34	18 (72–2.9)	16	0.27 (0.5–0.12)	0.22	[8]†,[9]‡
Li	3	14 (58–0.3)	10	1.13 (3.4–0.23)	0.93	[8]†,[9]‡
Sb	51	8 (90–0)	3	0.13 (0.34–0.02)	0.11	[8]†,[9]‡
Ga	31	6 (32–0)	5			[8]†,[9]‡
Sn	50	9.3 (72–0.9)	5.8	0.21 (0.92–0.03)	0.14	[8]†,[9]‡
Ge	32	7.6 (39.6–0.5)	4.0			[8]†,[9]‡
B	5	5.3 (13.0–0.8)	3.6	5.0 (39–0.5)	2.4	[8]†,[9]‡
Cu	29			4.20 (81–0.1)	0.45	[8]†,[9]‡
				0.26 \pm 0.11		[4]#
				1.38		[7]*
Br	35	3.1 (14.0–0.4)	4.1	1.12 (2.6–0.32)	0.93	[8]†,[9]‡
				4.6 \pm 1.1		[4]#
Cd	48	2.7 (7.6–0.6)	1.8	0.51 (2.4–0.03)	0.22	[8]†,[9]‡
Y	39	1.8 (9.3–0)	0.9	0.007 (0.17–<0.01)	<0.01	[8]†,[9]‡
Ti	22	1.6 (24.5–0.1)	0.6	0.19 (4.4–<0.1)	<0.1	[8]†,[9]‡
V	23	1.4 (14.4–0.1)	0.5	0.017 (0.03–0.01)	0.02	[8]†,[9]‡
La	57	1.4 (7.2–0)	0.8			[8]†,[9]‡
Be	4	1.3 (6.1–0)	1.2			[8]†,[9]‡
Cr	24	1.1 (4.7–0.2)	0.7	3.2 (18–0.1)	1.5	[8]†,[9]‡

Table A3.3 (continued)

	At.#	Surface Enamel		Whole Enamel		Source, comments
		Mean (range) $\mu\text{g/g}$	Median $\mu\text{g/g}$	Mean (range) $\mu\text{g/g}$	Median $\mu\text{g/g}$	
				1.02 \pm 0.51		[10]◇
Rb	37	0.6 (4.0–0.1)	0.4	0.39 (0.87–0.17)	0.32	[8]†,[9]‡
Zr	40	0.6 (1.9–0)	0.3	0.1 (0.57–<0.02)	O.Q7	[8]†,[9]‡
Ce	58	0.6 (6.1–0)	0	0.07 (1.9–0.02)	0.07	[8]†,[9]‡
W	74			0.24 \pm 0.12		[8]†,[9]‡
Co	27	0.2 (2.7–0)	0.1			[8]†,[9]‡
				0.13 \pm 0.13		[10]◇
Pr	59	0.2 (4.7–0)	0	0.027 (0.07–<0.01)	0.03	[8]†,[9]‡
Cs	55	0.1 (1.9–0)	0	0.04 (0.1–<0.02)	0.04	[8]†,[9]‡
Mo	42	0.1 (0.5–0.04)	0.04	7.2 (39–0.7)	6.3	[8]†,[9]‡
I	53	0.05 (4.7–0)	0.05	0.036 (0.07–0.01)	0.03	[8]†,[9]‡
Bi	83	0.001 (0.04–0)	0	0.006 (0.07–<0.02)	0.02	[8]†,[9]‡
Nd	60	0.045 (0.09–<0.02)	0.05			[8]†,[9]‡
Nb	41			0.28 (0.76–<0.1)	0.24	[8]†,[9]‡
Au	79			0.02 \pm 0.01		[4]#

‡ Whole enamel from premolars of young patients (age<20 yrs), determined by spark source mass spectroscopy.

† Surface enamel (depth of analysis $42 \pm 8.5 \mu\text{m}$) from premolars of young patients (age<20yrs), determined by spark source mass spectroscopy.

Bulk enamel from premolars of 14–16 yrs male and female patients, selected population of Stockholm Sweden, determined by neutron activated gamma-ray spectrometric analysis. Standard deviation, \pm .

◇ Neutron activated gamma-ray spectrometric analysis.

* Neutron activated gamma-ray spectrometric analysis (Na, Cl, Al, Mn, Ca, and P), atomic absorption spectrophotometry (K, Mg, Zn, Cu, and Fe), or a fluoride-specific electrode (F).

Table A3.4 Significant Differences in Trace Element Composition of Whole Human Enamel for High and Low Caries Populationst†

	At.#	High Caries (Mean \pm SE), $\mu\text{g/g}$	Low Caries (Mean \pm SE), $\mu\text{g/g}$	Source
F	9	82.1 \pm 7.99	125.7 \pm 11.23	[11]
Sr	38	104.1 \pm 9.14	184.0 \pm 14.68	[11]
Mn	25	1.57 \pm 0.24	0.87 \pm 0.15	[12]
Zr	40	0.27 \pm 0.1	0.16 \pm 0.09	[11]
Cu	26	0.71 \pm 0.2	0.17 \pm 0.04	[12]

† Determined by spark source mass spectroscopy

Table A3.5 Ca/P Molar Ratio of Human Enamel and Dentin

Enamel Ca/P molar ratio	Dentin Ca/P molar ratio	Source, comments
1.58		[4]#
1.61	1.54	[5]†, ●, age >25 yrs
1.58	1.58	[5]*, ●, age >25 yrs
1.65		[3]**
1.64		[6]□
	1.61	[14]**

Neutron activated gamma-ray spectrometric analysis.

† Ca determined by neutron activated gamma-ray spectrometric analysis

* Ca determined by atomic absorption spectrophotometry

● P determined by colorimetric assay.

** Determined by energy dispersive X-ray analysis.

□ Determined by atomic absorption spectrophotometry (Ca), and by the colorimetric method (P).

Table A3.6 Crystallite Size and Lattice Parameters of the Apatite in Human Enamel and Dentin*

	a-axis (nm)	c-axis (nm)	Width (nm)	Thickness (nm)	Source, Comments
Enamel					
	0.9445	0.6885			[2]#
	0.9440	0.6872			[15]†
	0.9441	0.6880	68.4 ± 3.4	26.3 ± 2.2	[6]†, ● ± S.D.
	0.9446	0.6886			[16]†
			68.3 ± 13.4	26.3 ± 2.19	[17]‡, ● ± S.E.
Dentin					
	0.9434 ±	0.6868 ±	[18]‡		
	0.0007	0.0009	29.6 ± 3.7	3.2 ± 0.5	[19]●, intertubular dentin
			36.55 ± 1.45	10.33 ± 7.91	[20]●, mixed carious and sound dentin

* Asymmetric hexagonal crystal with the thickness of the crystal less than the width.

† X-ray diffraction method of determination.

● High resolution transmission electron microscopy.

Data from [2], average compiled from the literature.

Table A3.7 Elastic Moduli and Viscoelastic Properties of Human Dentin and Enamel

	Incisors	Canine	Pre-molars	Molars	Source, Comments
E: Dentin					
				11.0 (5.8)	[21]t, †, ‡
	13 (4)	14 (6)	14 (0.7)	12 (2)	[22]Crown, c, †
	9.7 (2)	12 (3)	9.0 (2)	7.6 (3)	[22]Root, c, †
				10.16	[23]b, ll
				10.87	[23] b,dehyd., ll
				9.49	[23] b, re-hyd, ll
E: Enamel					
				84.3 (8.9)	[24]Cusp, c, ll
				77.9 (4.8)	[24]Side, c, ll
		48 (6)		46 (5)	[22]Cusp, c, ‡
		33 (2)		32 (4)	[22]Axial (side), c, ^
				9.7 (3)	[22]Axial (side), c, ll
				12 (3)	[22]Occlusal, c, ll
E _r (∞): Dentin					
				12	[25]c, constant strain, hydrated, ^, ‡
H ₁ (t): Dentin					
				0.38	[25] c, constant
				(0.136)	strain, hydrated, ^, ‡

E: modulus of elasticity (GPa); E_r (∞): relaxed modulus (GPa); H₁(t): distribution of relaxation times (GPa); c: compression; t: tension; b: three-point bending.

ll Applied load approximately parallel to either the long axis of the enamel rods or dentinal tubules.

^ Applied load approximately perpendicular to either the long axis of the enamel rods or dentinal tubules.

† Applied load with respect to either the long axis of the enamel rods or dentinal tubules was variable.

‡ Type of tooth unknown or various teeth used for measurement; data are tabulated under molar.

Note: standard deviations are given in parentheses.

Table A3.8 Mechanical Properties of Human Enamel

	Incisors	Canine	Pre-molars	Molars	Source, comments
Stress at				353 (83)	[24]Cusp, c, ll
Proportional				336 (61)	[24]Axial(side), c, ll
Limit (MPa)		194 (19)		224 (26)	[22]Cusp, c, †
		183 (12)		186.2 (17)	[22]Axial (side), c, ^
				70.3 (22)	[22]Axial (side), c, ll
				98.6 (26)	[22]Occlusal, c, ll
		91.0 (10)			[22]Incisal edge, c, †
Tensile Strength (MPa)				10 (2.6)	[26]†
Compressive				384 (92)	[24]Cusp, c, ll
Strength (MPa)				372 (56)	[24]Axial (side), c, ll
		288 (48)		261 (41)	[22]Cusp, c, †
		253(35)		239 (30)	[22]Axial (side), c, ^

(continued)

Table A3.8 (continued)

	Incisors	Canine	Pre-molars	Molars	Source, comments
				94.5 (32)	[22]Axial (side), c, ll
				127 (30)	[22]Occlusal, c, ll
		220 (13)			[22]Incisal edge, c, †

c: compression; hyd: hydrated; dehyd: dehydrated; re-hyd: re-hydrated.

ll Fracture or applied load approximately parallel to the long axis of the enamel rods.

^ Fracture or applied load approximately perpendicular to the long axis of the enamel rods.

† Applied load with respect to either the long axis of the enamel rods or dentinal tubules was variable.

‡ Type of tooth unknown or various teeth used for measurement; data are tabulated under molar.

Note: standard deviations are given in parentheses.

Table A3.9 Mechanical Properties of Human Dentin

	Incisors	Canine	Pre-molars	Molars	Comments
Stress at				167 (20.0)	[24]c
Proportional	124 (26)	140 (15)	146 (17)	148 (21)	[22]c
Limit (MPa)	86 (24)	112 (34)	110 (38)	108 (39)	[22]c
				110.5 (22.6)	[23]b, hyd., ll
				167.3 (37.5)	[23]b, dehyd, ll
				103.1 (16.8)	[23]b, re-hyd, ll
				158 (32)	[17]
				154 (23)	[17]
Tensile				52 (10)	[26]hyd, †, ‡
Strength				37.3 (13.6)	[23]hyd, ll
(MPa)				34.5 (11.1)	[23]dehyd, ll
				37.3 (9.0)	[23]re-hyd, ll
				39.3 (7.4)	[21]hyd, †, ‡
Compressive				297 (24.8)	[24]Crown
Strength	232 (21)	276 (72)	248 (10)	305 (59)	[22] Crown
(MPa)	233 (66)	217 (26)	231 (38)	250 (60)	[22]Root
				295 (21)	[23]Crown, ‡
				251 (30)	[23]Crown, ‡
Shear Strength				134 (4.5)	[27]Oil, Cervical
(MPa)					root, ^, ‡
Flexural				165.6 (36.1)	[23]hyd, ll
Strength				167.3 (37.5)	[23]dehyd, ll
(MPa)				162.5 (25.4)	[23]re-hyd, ll

hyd: hydrated; dehyd: dehydrated; re-hyd: re-hydrated

ll Applied load approximately parallel to the long axis of the dentinal tubules

* Applied load approximately perpendicular to the long axis of the dentinal tubules;

‡ Type of tooth unknown or various teeth used for measurement; data are tabulated under molar;

† Applied load with respect to either the long axis of the dentinal tubules was variable.

‡ 95% confidence intervals.

Note: standard deviations are given in parentheses.

Table A3.10 Toughness, Fracture Toughness, and Work of Fracture of Human Dentin and Enamel

	Incisors	Canine	Pre-molars	Molars	Source, comments
Fracture Toughness, Kc (MNm ^{-3/2})					[28]*
Enamel	0.97(0.09)	1.00(0.23)			Maxillary, cervical, †
	1.27(0.09)			0.7(0.08)	Mandibular, cervical, †
Toughness (MJm ⁻³) Dentin				62.7 (6.2)†	[27] Root, shear, oil storage, ^, ‡
				2.4 (1.1)	[17]Tension, crown, hydr.,
Work of Fracture (10 ² Jm ⁻²) Dentine			2.7 (1.6)		[29],^
			5.5 (1.7)		[29]
Enamel			1.9(0.56)		[29], ^
			0.13(.065)		[29]

|| Applied load approximately parallel to either the long axis of the enamel rods or dentinal tubules.

^ Applied load approximately perpendicular to either the long axis of the enamel rods or dentinal tubules.

† Applied load with respect to either the long axis of the enamel rods or dentinal tubules was variable.

‡ Type of tooth unknown or various teeth used for measurement; data are tabulated under molar.

* Microindentation method used. Load was 500 g with a Vickers' indenter.

Note: standard deviations are given in parentheses.

Table A3.11 Hardness of Fracture of Human Dentin and Enamel (see notes for units)

	Incisor	Pre-molar	Molar	Source, comments
Enamel	365 (35)			[30] >90% incisors, ®, †
			393 (50)	[30] ‡, molars and premolars, ®, †
			385 (5.8)	[31] ⊗ † ‡
		367 (17)		[32] ‖, ⊗, incisors, premolars
		327 (34)		[32] ^, ⊗, incisors, premolars
Dentin				
			25–81.7	[33] Δ, ‖, [34] ^a
			97.8	[33] a, calculated for zero tubule density
			44.5–80.9	[14] ◇, ‖, [34] ^a
			100	[14] a, calculated for zero tubule density
			75 (0.8)	[31] ⊗, †, ‡

^a Inverse correlation between hardness and dentinal tubule density.
 ‖ Applied load approximately parallel to either the long axis of the enamel rods or dentinal tubules.
 ^ Applied load approximately perpendicular to either the long axis of the enamel rods or dentinal tubules.
 † Applied load with respect to either the long axis of the enamel rods or dentinal tubules was variable.
 ‡ Type of tooth unknown or various teeth used for measurement; data are tabulated under molar.
 * Microindentation method used. Load was 500 g with a Vickers' indenter.
 ® Knoop hardness test using 500 g load.
 ⊗ Knoop microhardness test using 50 g load.
 Δ Knoop microhardness test using 100 g load.
 ◇ Micromdentation method used. Load was 50 g with a Vickers' indenter.

Table A3.12 Permeability^a of Human Dentin

Periphery (µl cm ⁻² min ⁻¹)	Center (µl cm ⁻² min ⁻¹)	Source, comments
36.4 (13.1) ‡	14.3 (7.0) †	[33], unerupted third molars,

^a Fluid filtration rate.
 ‡ Sound human dentin, average of 4 samples, 4 readings per sample.
 † Sound human dentin, average of 4 samples, 1 reading per sample.

Table A3.13 Wettability of Human Enamel

Liquid	Surface Tension, γ_{LV} (dynes/cm)	Contact Angle, θ (deg)		Source Comments
		In situ enamel	Ground enamel	
<i>Polar</i>				
Water	72.4 [35]	25.4 [36]†		
	72.8	36		[37]
	72.6		40.0 (0.1)	[38]* n=330
Glycerol	63.7 [35]	44.7 [36]†		
	63.4	55		[37]
	63.4		45.6(0.2)	[38]* n=50
Formamide	58.5 [35]	28.0 [35]†		
	58.2	24		[36]
	58.2		37.6 (0.1)	[37]* n=50
Thiodiglycol	53.5 [34]	30.8 [36]†		
	54.0	43		[37]
	54.0		27.6 (0.2)	[38]* n=60
<i>Non-polar</i>				
Methylene iodide	51.7 [35]	48.6 [36]†		
	50.8	50		[37]
	50.8		38.1 (0.1)	[38] n=50
S-Tetrabromoethane	49.8 [35]	38.3 [36]†		
	47.5	40		[38]
1- Bromonaphthalene	44.6	34		[38]*, n=50
	44.6		16.1 (0.1)	
<i>o</i> -Dibromobenzene	42.0	22		[37]
Propylene carbonate	41.8 [35]	31.8 [36]†		
1-Methyl-naphthalene	38.7	20		[36]
Dicyclohexyl	32.7 [35]	12.2-spread		[37]
	33.0	7		[36]†
n-Hexadecane	27.6 [35]	spreading		[37]
	27.7	spreading		[36]†

* Plane ground enamel surfaces, measurements from 46 erupted and unerupted teeth, mixed location (molars, premolars, incisors). Parentheses: standard error

† *in situ* contact angle measurements on human enamel, average of mean values for 4 teeth (maxillary or mandibular incisors).

Table A3.14 Wettability of Human Dentin [38]

Liquid	Surface Tension, γ_{LV} (dynes/cm)	Ground Dentin Contact Angle, θ (deg)	Comments
<i>Polar</i>			
Water	72.6	45.3 (0.2)	*, n=100
Glycerol	63.4	44.6 (0.1)	*, n=50
Formamide	58.2	37.6 (0.2)	*, n=50
Thiodiglycol	54.0	33.6 (0.3)	*, n=50
<i>Non-polar</i>			
Methylene iodide	50.8	36.7 (0.3)	*, n=50
1-bromo-naphthalene	49.8	16.8 (0.2)	*, n=50

* Plane ground dentin surfaces, measurements from 46 erupted and unerupted teeth, mixed location (molars, premolars, incisors). Parentheses: standard error.

Table A3.15 Critical Surface Tensions (γ_c) of Human Enamel and Dentin

	Critical Surface Tension, γ_c (dynes cm ⁻¹)	Source, Comments
Enamel Ground surface	46.1 (40.0–55.6) ^a	[38]*, calculated from polar and non-polar liquids
In situ enamel, γ_c^d	45.3 \pm 70.2 ^b	[39] Δ , calculated from polar liquids,
In situ enamel, γ_c^d	32.9 \pm 4.7	[38] Δ , calculated from non-polar liquids
In situ enamel, γ_c^d	32	[37] \dagger , calculated from non-polar liquids
Dentin	45.1 (40.7–51.1) ^a	[38]*, calculated from polar and non-polar liquids

^a Range of values from different test liquids.

^b Standard deviation.

* Plane ground dentin surfaces, measurements from 46 erupted and unerupted teeth, mixed location (molars, premolars, incisors). Parentheses: standard error.

Δ In situ measurements from 76 test subjects: 29 female and 47 male. Measurements made on teeth with intact pellicle (i.e., biofilm). γ_c^p only calculated from glycerol and thiodiglycol.

\dagger Average of 4 teeth from 2 subjects. γ_c^d calculated from non-polar liquids.

A3.3 Final Comments

The quality of data presented can be inferred from the standard deviations or standard error associated with the mean values. In some cases the error can be attributed to either small sample populations or specimen preparation. Where possible, either the number of specimens used or the number of replications of a measurement was reported. The reader should use this information as a guideline of the quality of data. When data are reported for small sample populations, then these data were usually the only source for a given physical property. In review of the literature, specimen preparation appears to have had the most influence on the precision and accuracy of data. Sample collection and storage conditions (e.g., dehydration, cross-linking agents, exogenous contamination) need to be taken into consideration when

utilizing the information tabulated. Additional sources of error are dependent on the analytical technique or test method used to make the measurement. It is more difficult to discern the influence of the instrumentation on the reliability of the measurements. However, confidence of the accuracy was judged based on the use of adequate control samples with known physical properties (e.g., correction of mechanical data). In light of these comments, data in the literature were deemed most accurate and appropriate for this handbook when the following conditions were met: the sample population was large; non-destructive specimen preparation and storage conditions were used; and, multiple replications of measurements on a single sample were performed.

There are significant omissions in the data available in the literature. Most notable, is the lack of quantitative analysis of the organic phase of dentin and enamel, and determination of the viscoelastic properties of dentin. The lack of data is attributed to the technical difficulty required to make such measurements and the heterogeneous nature of the dentin, which imparts large variations in these data depending on anatomical location. Other significance absences are the lack of electrical and thermal properties. Finally, vacancies in the tables provided demonstrate omissions in available data.

Additional Reading

Carter, J.M., Sorensen, S.E., Johnson, R.R., Teitelbaum, R.L. and Levine, M.S. (1983) Punch Shear Testing of Extracted Vital and Endodontically Treated Teeth. *J. Biomechanics* **16(10)**, 841–848.

Utilized a miniature punch shear apparatus to determine shear strength and toughness perpendicular to the direction of dentinal tubules. Dentin harvested from the cemento-enamel junction to one-third the distance to the root apex. Strengths: novel measurements, precise measurements, defined specimen location, defined orientation of testing. Limitations: tooth type not defined for ‘constrained’ tests, teeth stored in mineral oil prior to testing.

Driessens, F.C.M., and Verbeeck, R.M.H. (1990a) The Mineral in Tooth Enamel and Dental Caries. In *Biominerals*, F.C.M and Verbeeck, R.M.H. (eds), CRC Press, Boca Raton, Florida, pp. 105–161.

Driessens, F.C.M., and Verbeeck, R.M.H. (1990b) Dentin, Its Mineral and Caries, In *Biominerals*, F.C.M and Verbeeck, R.M.H. (eds), CRC Press, Boca Raton, Florida, pp. 163–178.

An authoritative text on biominerals with an excellent review of the properties of enamel and dentin. An excellent supplement to this handbook.

Glantz, P-O. (1969) On Wettability and Adhesiveness. *Odontologisk Revy*, **20** **supp.** **17**, 1–132.

Comprehensive assessment of the wettability of human enamel and dentin. Strengths include using multiple probe liquids on numerous teeth.

Korostoff, E., Pollack, S.R., and Duncanson, M.G. (1975) Viscoelastic Properties of Human Dentin. *J. Biomedical Materials Res.*, **9**, 661–674.

Measured some viscoelastic properties of human radicular dentin under constant strain. Linear viscoelastic theory applied. Strengths: unique examination of viscoelastic properties, defined orientation of dentinal tubules, storage conditions and testing environment well controlled. Limitations: large scatter in $H_1(t)$, mixed data for different teeth.

Marshall, G.W. (1993) Dentin: Microstructure and Characterization. *Quintessence International*, **24(9)**, 606–616.

A Review of the microstructure and characterization of dentin.

Waters, N.E. (1980) Some Mechanical and Physical Properties of Teeth. *Symposia of the Society for Experimental Biology*, **34**, 99–135.

Concise review of mechanical and physical properties of teeth. Good paper for anatomy of enamel and dentin.

References

1. Waters, N.E. (1980) Some mechanical and physical properties of teeth. *Symp. Soc. Exp. Biol.*, **34**, 99–135
2. Driessens, F.C.M. and Verbeek R.M.H. (1990) The mineral in tooth enamel and dental caries. In: *Biomaterials*, F.C.M. and Verbeek, R.M.H. (eds), CRC Press, Boca Raton, Florida, pp. 105–161
3. Driessens, F.C.M. and Verbeek, R.M.H. (1990) Dentin, its mineral and caries, In: *Biomaterials*, Driessens, F.C.M. and Verbeek, R.M.H. (eds), CRC Press, Boca Raton, Florida, pp 163–178
4. Söremark, R. and Samsahl, K. (1961) Gamma-ray spectrometric analysis of elements in normal human enamel. *Arch. Oral Bio., Special Suppl.*, **6**, 275–283.
5. Derise, N.L., Ritchey, S.J. and Furr, A.K. (1974) Mineral composition of normal human enamel and dentin and the relation of composition to dental caries: I Macrominerals and comparison of methods of analyses. *J. Dental Res.*, **53(4)**, 847–852
6. LeGeros, R.Z., Silverstone, L.M., Daculsi, G. *et al.* (1983) *In vitro* caries-like lesion formation in F-containing tooth enamel. *J. Dental Res.*, **62(2)**, 138–144
7. Lakomaa, E-L. and Rytömaa, I. (1977) Mineral composition of enamel and dentin of primary and permanent teeth in Finland. *Scand. J. Dent. Res.*, **85**, 89–95.
8. Cutress, T.W. (1979) A preliminary study of the microelement composition of the outer layer of dental enamel. *Caries Res.*, **13**, 73–79.
9. Losee, F.L., Cutress, T.W. and Brown, R (1974) Natural elements of the periodic table in human dental enamel. *Caries Res.*, **8**, 123–134.
10. Retief, D.H., Cleaton-Jones, P.E., Turkstra, J. *et al.* (1971) The quantitative analysis of sixteen elements in normal human enamel and dentine by neutron activation analysis and high-resolution gamma-spectrometry. *Arch. Oral Bio.*, **16**, 1257–1267.
11. Curzon, M.E.J. and Losee, F.L. (1977) Dental caries and trace element composition of whole human enamel: Eastern United States. *J. Amer. Dental Assoc.*, **94**, 1146–1150.
12. Curzon, M.E.J. and Losee, F.L. (1978) Dental caries and trace element composition of whole human enamel: Western United States. *J. Amer. Dental Assoc.*, **96**, 819–822.
13. Kodaka, T., Debari, K., Yamada, M. *et al.* (1992) Correlation between microhardness and mineral content in sound human enamel. *Caries Res.*, **26**, 139–141.
14. Panighi, M. and G'Sell, C. (1992) Influence of calcium concentration on the dentin wettability of an adhesive. *J. Biomed. Mater. Res.*, **26**, 1081–1089.

15. Holcomb, D.W. and Young, R.A. (1980) Thermal decomposition of human tooth enamel. *Calcif Tiss. Intern.*, **31**, 189–201
16. Sakae, T. (1988) X-Ray diffraction and thermal studies of crystals from the outer and inner layers of human dental enamel. *Archs. Oral Bio.*, **33(10)**, 707–713.
17. Huang, T.-J.G., Schilder, H. and Nathanson, D. (1992) Effects of moisture content and endodontic treatment on some mechanical properties of human dentin. *J. Endodontics*, **18(5)**, 209–215
18. Kerebel, B., Daculsi, G. and Kerebel, L.M. (1979) Ultrastructure studies of enamel crystallites. *J. Dental Res.*, **58(B)**, 844–851.
19. Jervøe, P. and Madsen, H.E.L. (1974) Calcium phosphates with apatite structure. I. Precipitation at different temperatures. *Acta Chem. Scand.*, **A28**, 477–481.
20. Daculsi, G., Kerebel, B. and Verbaere, A (1978). (Méthode de mesure descristaux d'apatite de la dentine humaine en microscopie électronique en transmission de Haute Résolution)(Fr.) (Method of measurement of apatite crystals in human dentin by high resolution transmission electron microscopy), *Comptes Rendu Acad. Sci. Paris, Sér. D.*, **286**, 1439.
21. Voegel, J.C. and Frank, R.M. (1977) Ultrastructural study of apatite crystal dissolution in human dentine and bone. *Jour. Bioi. Buccale*, **5**, 181–194.
22. Lehman, M.L. (1963) Tensile strength of human dentin. *J. Dent. Res.*, **46(1)**, 197–201
23. Stanford, J.W., Weigel, K.V., Paffenbarger, G.C. *et al.* (1960) Compressive properties of hard tooth tissues and some restorative materials. *J. American Dental Assoc.*, **60**, 746–756.
24. Jameson, M.W., Hood, J.A.A. and Tidmarsh, B.G. (1993) The effects of dehydration and rehydration on some mechanical properties of human dentine. *J. Biomech.*, **26(9)**, 1055–1065.
25. Craig, R.G., Peyton, F.A. and Johnson, D.W. (1961) Compressive properties of enamel, dental cements, and gold. *J. Dent. Res.*, **40(5)**, 936–945.
26. Korostoff, E., Pollack, S.R. and Duncanson, M.G. (1975) Viscoelastic properties of human dentin. *J. Biomed. Mater. Res.*, **9**, 661–674.
27. Bowen, R.L. and Rodriguez, M.S. (1962) Tensile strength and modulus of elasticity of Tooth Structure and Several Restorative Materials. *J. American Dental Assoc.*, **64**, 378–387.
28. Carter, J.M., Sorensen, S.E., Johnson, R.R., *et al.* (1983) Punch shear testing of extracted vital and endodontically treated teeth. *J. Biomech.*, **16(10)**, 841–848.
29. Hassan, R., Caputo, A.A. and Bunshah, R.F. (1981) Fracture toughness of human enamel. *J. Dent. Res.*, **60(4)**, 820–827.
30. Rasmussen, S.T., Patchin, R.E., Scott, D.B. *et al.* (1976) Fracture properties of human enamel and dentin. *J. Dent. Res.*, **55(1)**, 154–164.
31. Caldwell, R.C., Muntz, M.L., Gilmore, R.W. *et al.* (1957) Microhardness studies of intact surface enamel. *J. Dent. Res.*, **36(5)**, 732–738.
32. Remizov, S.M., Prujansky, L.Y. and Matveevsky, R.M. (1991) Wear resistance and microhardness of human teeth. *Proc. Inst. Mech. Eng., Part H: J. Eng. in Med.*, **205(3)**, 201–202.
33. Davidson, C.L., Hoekstra, I.S. and Arends, J. (1974) Microhardness of sound, decalcified and etched tooth enamel related to the calcium content. *Caries Res.*, **8**, 135–144.
34. Pashley, D.H., Andringa, H.J., Derkson, G.D. *et al.* (1987) Regional variability in the permeability of human dentin. *Arch. Oral Biol.*, **32(7)**, 519–523.
35. Pashley, D.H., Okabe, A. and Parham, P. (1985) The Relationship between dentin microhardness and tubule density. *Endod. Dent. Traumatol.*, **1**, 176–179.
36. Baier, R.E. and Zisman, W.A. (1975) Wetting properties of collagen and gelatin surfaces, in 'Applied Chemistry at Protein Interfaces', vol. 145, Advances in Chemistry series (ed. R.F. Gould), American Chemical Society, Washington DC, pp. 155–174.
37. Jendresen, M.D., Baier, R.E. and Glantz, P.-O. (1984) Contact angles in a biological setting: Measurements in the human oral cavity. *J. Coli. Interface Sci.*, **100(1)**, 233–238.
38. Baier, R.E. (1973) Occurrence, nature, and extent of cohesive and adhesive forces in dental integuments. in: *Surface Chemistry and Dental Integument's*. Lasslo, A. and Quintana, R.P. (eds), Thomas, Springfield, IL pp. 337–391.
39. Glantz, P.-O. (1969) On wettability and adhesiveness. *Odontologisk Revy*, **20 suppl. 17**, 1–132.
40. Jendresen, M.D. and Glantz, P.-O. (1980) Clinical adhesiveness of the tooth surface. *Acta Odontol. Scand.*, **38**, 379–383.

Chapter B1

Cartilage

J.R. Parsons

B1.1 Introduction

B1.1.1 Articular cartilage

Articular or hyaline cartilage forms the bearing surfaces of the movable joints of the body. Hyaline cartilage also exists in tissues of the larynx, tracheal tube rings, rib and costal cartilage, nasal septum and in the growth plates of long bones. As a bearing surface, this tough, resilient tissue displays exceptional mechanical and tribologic properties due exclusively to the unique interaction of the constituents of the tissue extracellular matrix. Usually, the phenotypic cells (chondrocytes) of cartilage make up less than 10% of the total volume of the tissue and have not been considered to contribute to the mechanical properties of the tissue. The extracellular matrix consists of a tight collagen fiber network which contains and constrains a highly hydrophilic gel of aggregated proteoglycan macromolecules. Collagen accounts for approximately 50% of the dry weight of the tissue, the remainder being proteoglycans and cellular material. In the fully hydrated state, water contributes 60% to 80% of the wet weight of the tissue. Mechanically, intact normal articular cartilage behaves as a linear viscoelastic solid. This behavior is the result of viscous drag of fluid through the tissue in concert with the intrinsic properties of the extracellular matrix. Further, fluid exudation across the cartilage surface in response to physiologic loading is thought to play a significant role in the lubrication of joints. The importance of articular cartilage as a bearing surface has led to extensive mechanical and tribologic studies of this tissue.

J.R. Parsons (✉)
Orthopaedics-UMDNJ 185 South Orange Avenue
University Heights, Newark, NJ 07103-2714, USA

B1.1.2 Fibrocartilage

Fibrocartilage contains a higher dry weight percentage of collagen and less proteoglycan than does articular cartilage. Consequently, in the hydrated state, fibrocartilage contains less water. Fibrocartilage is generally considered to be tougher and somewhat less resilient than articular cartilage. In humans, fibrocartilage is found in the meniscus of the knee joint, the annulus fibrosus of the intervertebral disc and in the temporomandibular joint. The mechanical behavior of fibrocartilage has not been studied to the extent of articular cartilage; however, it is not as satisfactory a load bearing material.

B1.1.3 Elastic cartilage

Elastic cartilage is more elastic and resilient in nature than is either hyaline or fibrocartilage. This is the result of lower collagen content coupled with the presence of elastin fibers. Elastic cartilage is found in the human epiglottis, external ear structures and eustachian tube. As elastic cartilage is not a major structural component of the musculoskeletal system, the mechanical properties of this tissue have been largely ignored.

B1.2 Composition

Table B1.1 Cartilage Composition

	Water (wt%)	Organic (wt%)	Source
Articular Cartilage	60–80	20–40	[1]
Type II Collagen	—	15–20	
Other collagen	—	<2	
Proteoglycan	—	10	
Fibrocartilage	74	26	[2]
Type I Collagen	—	20	
Other collagen	—	<1	
Proteoglycan		<1	

B1.3 Mechanical Properties of Articular Cartilage

B1.3.1 Compression (Table B1.2)

Compressive cartilage properties have often been examined using creep indentation, confined compression or free/unconfined compression methods. Indentation techniques permit in situ testing without the necessity of special specimen preparation as with tensile testing. However, the extraction of intrinsic mechanical

Table B1.2 Compressive Properties of Articular Cartilage

Location	Value (MPa)	Source
	<i>Un relaxed (initial):</i>	
	Creep modulus (indentation):	
Femoral head	1.9–14.4	[7]
	Young’s modulus (indentation):	
Patella	2.25	[8]
	Young’s Modulus (confined compression):	
Tibial plateau	5.1–7.9*	[9]
	11.6*	[6]
	Bulk Modulus (confined compression):	
Tibial plateau	31–56	[9]
	25*	[6]
	Young’s Modulus (unconfined compression):	
Various	8.4–15.3	[7]
	<i>Relaxed (equilibrium):</i>	
	Aggregate modulus (Indentation):	
Patella	0.3–0.6	[4]
	0.3–1.5	[10]
Femoral condyle	0.4–1.0	[10]
	0.5–0.7	[11]
Carpo-metacarpal joint	0.4–0.8	[12]
	Young’s modulus (confined compression):	
Patella	0.7	[8]
Tibial plateau	0.7*	[6]
	Bulk modulus (confined compression):	
Tibial plateau	9.1*	[6]

* Calculated from other measurements.

parameters from creep indentation data is analytically complex [3, 4]. Confined compression or unconfined compression tests require preparation of cylindrical cored specimens of tissue and underlying bone. With unconfined compression, the free draining tissue edges and low aspect ratio, layered nature of the test specimen may introduce error. Compression of a laterally confined specimen by a porous plunger produces uniaxial deformation and fluid flow. Confined compression creep data has been analyzed to yield an aggregate equilibrium compressive modulus and permeability coefficient [5] and uniaxial creep compliance [6].

B1.3.2 Tensile (Table B1.3)

Tensile properties for human articular have been determined by cutting standard tensile specimens from the cartilage surface and performing constant strain rate, creep or stress relaxation tensile tests. Test results are strongly influenced by

Table B1.3 Tensile Properties of Articular Cartilage

Location	Value (MPa)*	Source
	<i>Relaxed (equilibrium):</i>	
	Young's modulus:	[13]
Femoral condyle,		
Surface zone	10.5	
Subsurface zone	5.5	
Middle zone	3.7	
	<i>Un relaxed (100%/min):</i>	
	Young's modulus:	[7]
Femoral condyle,		
Surface zone	200–400	
Middle zone	40–175	
	Strength:	[7]
Femoral condyle,		
Surface zone	20–35	
Middle zone	11–25	

* All measurements parallel to collagen direction.

Table B1.4 Shear Properties of Articular Cartilage

Location	Value (MPa)	Source
	<i>Relaxed (equilibrium):</i>	
	Shear modulus:	
Patella,		
Middle zone	0.25	[14]
Tibial plateau	2.6	[6]
	<i>Unrelaxed (initial):</i>	
	Shear modulus:	
Tibial plateau	4.1	[6]
	5.1–7.9	[9]

collagen volume fraction and orientation and are largely insensitive to proteoglycan content [7] Collagen volume fraction and orientation is highest in the cartilage surface layer. Collagen content and orientation diminishes in subsequent lower layers.

B1.3.3 Shear (Table B1.4)

Shear properties for articular cartilage have been determined through torsional creep, stress relaxation and torsional dynamic tests of excised cartilage disks. Creep and dynamic shearing of rectangular cartilage specimens between plates has been conducted on animal tissue (usually bovine) but not human tissue. When torsional shear strains remain small, the observed shear properties are flow independent. That is, under small strain conditions, fluid flow is negligible and viscoelastic behavior can be attributed strictly to the collagen/proteoglycan extracellular matrix.

B1.3.4 Poisson's ratio

Poisson's ratio has been calculated directly from tensile tests ($\nu = 0.37\text{--}0.50$) [10] and indirectly from torsional shear and confined compression creep data ($\nu = 0.37\text{--}0.47$) [6, 9]. More recently, the relationship between Poisson's ratio, ν , aggregate modulus, H_a , and permeability, k , have been established for cartilage indentation testing based on biphasic (fluid and porous solid) constitutive theory [15]. Using a complex numerical solution and curve fitting scheme, Poisson's ratio can be extracted from indentation data, resulting in values of $\nu = 0.00\text{--}0.30$ [11, 12, 16]. However, care must be exercised in interpreting such indirect measures of Poisson's ratio as unexpected results can arise; e.g. $\nu = 0.0$.

B1.3.5 Permeability

The porous solid matrix of articular cartilage permits the movement of interstitial water in response to a pressure gradient. Flow of water through and across the tissue is largely responsible for the viscoelastic character of cartilage. Flow is related to tissue permeability through the hydraulic permeability coefficient, k , as defined by Darcy's law. The permeability coefficient has been measured in flow chambers where a known pressure gradient produces flow across a cartilage layer of known thickness and area ($k = 4.0\text{--}17.0 \times 10^{-16}\text{m}^4/\text{Ns}$) [7]. However, such experiments have demonstrated significant decreases in permeability coefficient with increasing pressure gradient, increasing compressive tissue strain and with increasing proteoglycan content. Evoking biphasic constitutive theory with numerical solutions and/or curve fitting routines permits an indirect determination of the permeability coefficient from confined compression creep data and creep indentation data ($k = 5.2\text{--}21.7 \times 10^{-16}\text{m}^4/\text{Ns}$) [11, 12].

B1.3.6 Articular cartilage tribologic properties

Healthy articular cartilage has remarkable tribologic properties. Under high load conditions the tissue displays extremely low frictional coefficients and virtually undetectable wear. The dynamic coefficient of friction, μ_d , has been measured in whole joints using Stanton pendulum or other pendulum techniques where the joint forms the pendulum pivot ($\mu_d = 0.015\text{--}0.04$) [17–19]. The coefficients of friction of cartilage plugs bearing on other materials has been determined for human and animal tissue but these sorts of experiments have little relevance for actual in situ cartilage behavior and are not reported here.

The lubrication of articular cartilage remains a subject of continuing debate and no one lubrication mechanism can be clearly identified. Both fluid film and boundary lubrication are thought to play primary roles in joint lubrication and the dominance of one or the other probably depends on loading and velocity conditions. Further as cartilage is a relatively soft viscoelastic material, elasto-hydrodynamics

may discourage fluid film breakdown and thus promote hydrodynamic lubrication. Exudation of fluid across the cartilage surface in response to an advancing load has also been suggested to aid lubrication.

No reliable wear tests have been performed on human articular cartilage bearing surfaces under physiologic conditions.

B1.4 Fibrocartilage Mechanical Properties

Human fibrocartilage tensile mechanical properties have been determined by cutting standard tensile specimens either from the knee meniscus or from single or multiple lamella from the annulus fibrosus and performing constant strain rate tensile tests. Test results are strongly influenced by collagen volume fraction and orientation and are largely insensitive to proteoglycan content. Annulus fibrosus has also been tested in confined compression, permitting derivation of an aggregate compressive modulus and permeability. Data are reported in Section B2.

B1.5 Elastic Cartilage Mechanical Properties

No reliable data are available for human tissue.

Additional Reading

Freeman, MAR (ed.) (1979) *Adult Articular Cartilage*, 2nd ed., Pitman Medical Publishing Co, Kent, UK.

Although now somewhat out of date, this classic text forms the basis for current thinking on cartilage biochemistry, physiochemistry, biomechanics and tribology. The volume of original data, found nowhere else, is truly impressive.

Mow V.C., Holmes, M.H. and Lai, W.M. (1984): Fluid transport and mechanical properties of articular cartilage. A review. *J. Biomech.*, 17:377–394.

This survey article provides an historical perspective of cartilage mechanics research and leads the reader through the modern biphasic theory of cartilage mechanics at the material level. References provided are particularly useful in developing a bibliography of the important classic studies in this field.

Mow, V.C. and Ratcliffe, A (eds)(1993): *Structure and Function of Articular Cartilage*, CRC Press, Boca Raton.

This up-to-date monograph is perhaps the best current work on the subject. Details from many of the references in this section (below) can be found in the section on cartilage biomechanics.

References

1. Maroudas, A. (1979) Physiochemical properties of articular cartilage. in *Adult Articular Cartilage*, 2nd ed., M.A.R. Freeman (ed.), Pitman Medical Publishing Co, Kent, UK, pp. 215–290.
2. Fithian, D.C., Kelly, M.A. and Mow, V.C. (1990) Material properties and structure-function relationships in the menisci. *Clin. Orthop. Rel. Res.*, **252**, 19–31.
3. Mak, A., Lai, W.M. and Mow, V.C. (1987) Biphasic indentation of articular cartilage: Part I, Theoretical analysis. *J. Biomech.*, **20**, 703–714.
4. Mow, V., Gibbs, M.C. and Lai, W.M., *et al.* (1989) Biphasic indentation of articular cartilage: Part II, A numerical algorithm and experimental study. *J. Biomech.*, **22**, 853–861.
5. Mow, V., Kuei, S.C. and Lai, W.M. (1980) Biphasic creep and stress relaxation of articular cartilage in compression: Theory and experiments. *J. Biomech. Eng.*, **102**, 73–84.
6. Hayes, W. and Mockros, L.F. (1971) Viscoelastic properties of human articular cartilage. *J. Appl. Physiol.*, **31**, 562–568.
7. Kempson, G. (1979) Mechanical properties of articular cartilage. In *Adult Articular Cartilage*, 2nd ed., Freeman M.A.R., Editor, Pitman Medical Publishing Co. Ltd., Kent, England, pp. 333–414.
8. Sokoloff, L. (1966) Elasticity of aging cartilage. *Fed. Proc.*, **25**, 1089–1095.
9. Hori, R. and Mockros, L.F. (1976) Indentation tests of human articular cartilage. *J. Biomech.*, **9**, 259–268.
10. Armstrong, C. and Mow, V.C. (1982) Variations in the intrinsic mechanical properties of human articular cartilage with age, degeneration and water content. *J. Bone Joint Surg.*, **64A**, 88–94.
11. Athanasiou, K., Rosenwasser, M.P., and Buckwalter, J.A., *et al.* (1991) Interspecies comparison of in situ intrinsic mechanical properties of distal femoral cartilage. *J. Orthop. Res.*, **9**, 330–340.
12. Ateshian, G., Gardner, J.R., Saed-Nejad, F. *et al.* (1993) Material properties and biochemical composition of thumb carpometacarpal joint cartilage. *Trans. Orthop. Res. Soc.*, **18**, 323.
13. Akizuki, S., Mow, V.C. and Muller, F., *et al.* (1986) Tensile properties of human knee joint cartilage: Part I, Influence of ionic concentrations, weight bearing and fibrillation on the tensile modulus. *J. Orthop. Res.*, **4**, 379–392.
14. Zhu, W., Lai, W.M. and Mow, V.C. (1986) Intrinsic quasilinear viscoelastic behavior of the extracellular matrix of cartilage. *Trans. Orthop. Res. Soc.*, **11**, 407.
15. Mak, A. (1986) The apparent viscoelastic behavior of articular cartilage- The contributions from the intrinsic matrix viscoelasticity and interstitial fluid flows. *J. Biomech. Eng.*, **108**, 123–130.
16. Akizuki, S., Mow, V.C., Lai, W.M., *et al.* (1986) Topographical variation of the biphasic indentation properties of human tibial plateau cartilage. *Trans. Orthop. Res. Soc.*, **11**, 406.
17. Charnley, J. (1960) The lubrication of animal joints in relation to surgical reconstructions by arthroplasty. *Ann. Rheum. Dis.*, **19**, 10–19.
18. Little, J., Freeman, M.A.R., and Swanson, S.V. (1969) Experience on friction in the human joint. In *Lubrication and Wear in Joints*, Wright V., Editor, Sector Publishing, London, UK., pp. 110–114.
19. Unsworth, A., Dawson, D. and Wright, V. (1975) Some new evidence on human joint lubrication. *Ann. Rheum. Dis.*, **34**, 277–285.

Chapter B2

Fibrocartilage

V.M. Gharpuray

B2.1 Introduction

The human menisci and intervertebral discs perform several important mechanical functions in the human body. The ability to perform these functions and consequently their intrinsic biomechanical properties are dependent on the interaction of the constituents of these structures. Both the menisci and intervertebral discs have a fibrocartilaginous structure that consists of two distinct phases: a fluid phase consisting of mainly water and dissolved electrolytes, and a solid phase composed of highly oriented collagen fibers, cells, proteoglycans and other proteins. As with all other biological materials, both menisci and discs exhibit non-linear viscoelastic and anisotropic properties. The non-linear stiffness or elasticity of the structure is imparted by the collagen fibers and to a lesser extent by osmotic pressures within the tissue which are generated by the degree of hydration [1, 2]. The viscoelastic or energy dissipation properties are a result of fluid flow within and through the structures and also of molecular relaxation effects from the motion of long chains of collagen and proteoglycans [3]. Anisotropy is a consequence of the orientation and concentration of collagen fibers within the proteoglycan gel.

B2.2 Structure and Composition

A normal adult human knee contains two menisci – the lateral and the medial, whose average lengths are 38 and 45 mm, and average volumes are 2.9 and 3.45 cm³ respectively [4]. At the femoral articulating surface of each meniscus, for a depth of

V.M. Gharpuray (✉)
Department of Bioengineering 401 Rhodes Eng. Res. Ctr., Clemson University,
Clemson, SC 29634-0905, USA

approximately 100 μm , fine collagen fibrils (mainly Type II) are randomly oriented to form a woven mesh [5, 6]. Beneath this surface layer, larger rope-like bundles (approximately 100 μm in diameter) of Type I collagen are arranged predominantly in the circumferential direction. In the posterior half of the medial meniscus however, the fibers are not as highly oriented [6, 7]. A few radial fibers may also be seen interspersed within the circumferential fibers [6–8]. At the tibial surface is another articulating layer, in which the principal orientation of the fibers is radial.

Collagen and other proteins make up the organic content of the meniscus, while dissolved electrolytes make up the inorganic content (which is negligibly small). The collagen is primarily Type I (98%) with small amounts of Type II, III and Type V [9], and comprises up to 25% of the wet weight and 90% of the dry weight in human material (Table B2.1). 10% of the dry weight and up to 2% of the wet weight are due to non-collagenous proteins, which consist predominantly of proteoglycans, and smaller amounts of structural glycoproteins, cell membrane bound receptors and intercalated membrane glycoproteins. These proportions do not appear to vary with location in the menisci [10].

There are 23, approximately cylindrical, intervertebral discs in the human spine that account for 20–30% of its overall length [13]. The cross sectional shape varies with level: roughly elliptical, rounded triangular and kidney shaped in the cervical, thoracic and lumbar regions respectively [14]. The cross sectional shape is sometimes quantified by a shape index (S) defined by $S = 4\pi A/C^2$ where A = cross sectional area, and C = circumference of the cross section (Table B2.2). Most discs are wedge-shaped in sagittal section with the anterior height greater than the posterior height. The cross sectional area increases with level such that lumbar discs are larger than cervical discs.

The intervertebral disc contains two distinct regions, the nucleus pulposus and the annulus fibrosus. The nucleus occupies about 50% of the volume of the disc, and contains mostly water and small amounts of randomly oriented collagen fibers, cells and non-collagenous proteins [19]. The annulus is a tough ring-like structure that surrounds the nucleus. Highly oriented collagen fibers (primarily Types I and II) form a laminate structure in the annulus, with approximately 20–25 laminae oriented alternately at approximately $+(60-70)^\circ$ and $-(60-70)^\circ$ to the spinal axis [14, 20, 21]). Type IX collagen is believed to cross link the Types I and II fibers, and provide some resistance to circumferential tears. Collagen content and fiber orientation is highest in the outermost layers, and both decrease as the nucleus is approached from the periphery of the disc (Table B2.3) The water content in the disc varies with position in the disc: it is highest in the nucleus and lowest in the outermost layers of the annulus [22, 23]. It has also been shown that the water content varies with circumferential position [4], and is higher in the posterior of the disc. The nucleus

Table B2.1 Composition of the menisci

Wet weight			Dry weight	
Water	Collagen	NCP*	Collagen	NCP
60–70% ^a	15–25% ^a	1–2% ^a	70–90% ^{a,b}	8–20% ^{b,c,‡}

* NCP = non-collagenous proteins; ‡ 21.9% in neonates decreasing to 8.1 % between 30–70 years. a: [8];b: [11];c: [12].

Table B2.2 Shape and size of the adult intervertebral disc

Disc Level	Shape Index (S ^a)	Posterior/ Anterior Height ^a	Cross Sectional Area (mm ²)	Height (mm)
L5-S1	0.885	0.35		
L4-L5	0.897	0.51	1714 ^b	11–12 ^{b,c}
L3-L4	0.866	0.55	1662 ^b	10.4 ^b
L2-L3	0.866	0.61	1859 ^b	9.75 ^b
L1-L2	0.825	0.68	1640 ^b	8.83 ^b
T12-L1	0.844	0.75		
T11-T12	0.856	0.80		
T10-T11	0.885	1.11		
T9-T10	0.879	0.74		
T8-T9	0.919	0.88		4–6 ^c
T7-T8	0.878	0.81		
T6-T7	0.898	0.84		
T5-T6	0.935	1.07		
T4-T5	0.868	0.97		
T3-T4	0.836	0.72		
T2-T3	0.870	0.74		
T1-T2	0.815	0.76		
C7-T1	0.785	0.62	1292 [*]	6.00 ^d
C6-C7	0.708	0.82	1152 [*]	5.67 ^d
C5-C6	0.828	0.44	949 [*]	5.50 ^d
C4-C5	0.825	0.47	892 [*]	5.25 ^d
C3-C4	0.870	0.50	827 [*]	5.00 ^d
C2-C3	0.893	0.56	732 [*]	4.75 ^d

* Computed from data in (18). a: (13);b: (15,16);c: (17);d: (18).

Table B2.3 Composition of the intervertebral disc in young adults

Tissue	Water Content %	Collagen Content %
Nucleus Pulposus	85–95 ^a	2–5 ^b
Annulus Fibrosus	85 (innermost layer)	5 (innermost layer)
	65 (outermost layer)	21 (outermost layer)

a: [23]; b: [24].

loses water and becomes more fibrous and desiccated with age, causing the boundary between the annulus and the nucleus to become less clear [19, 23].

B2.3 Hydraulic Permeability and Drag Coefficients

Experimental data suggest that water is capable of flowing through both meniscal and discal tissues, and is dependent on a material property of the tissue called hydraulic permeability [25], which may be modeled by Darcy’s Law as:

$$Q = k \frac{A\Delta P}{h} \quad (\text{B2.1})$$

where k = hydraulic permeability coefficient of the tissue; Q = volume rate of fluid flow; A = area across which fluid flow occurs; h = thickness of the tissue; and ΔP = pressure gradient across the thickness h that causes fluid flow.

The diffusive drag coefficient K is related to the permeability coefficient by

$$K = \frac{(\Phi f)^2}{k} \quad (\text{B2.2})$$

where Φf is the porosity of the tissue and is defined as the ratio of interstitial fluid volume to total tissue volume.

For human meniscal (annulus) tissue, k , the permeability is $2.5 \times 10^{-16} \text{ m}^4/\text{Ns}$ [22], about one third of that reported for bovine tissue: $8.1 \times 10^{-16} \text{ m}^4/\text{Ns}$ [26]. There is no significant variation in the permeability coefficient with location of the specimen. The porosity (Φf) of both tissues is approximately 0.75, and therefore the drag coefficient, K , is very high and ranges from 10^{14} to 10^{15} N/s/m^4 .

B2.4 Elastic Properties

Under quasi-static loading, or in conditions under which ‘short-term’ loading responses are expected to occur [27], both meniscal and discal tissues may be modeled as linear elastic and orthotropic. Under a constant load rate, the non-linear behavior may be described by an exponential stress-strain relationship given by

$$\sigma = A[e^{B\epsilon} - 1] \quad (\text{B2.3})$$

where A and B are constants for the given material. The constant B is proportional to the tangent modulus (i.e., $d\sigma/d\epsilon$), and sometimes a third constant C is defined as $C = A*B$, and is the tangent modulus as $\sigma \rightarrow 0$ [8].

The macroscopic tensile strength of the entire meniscus was studied by Mathur *et al.* [4] by gripping the horns of the meniscus, and stretching it to failure. The results suggested that the medial meniscus was significantly weaker than the lateral meniscus (ultimate loads of 247 N and 329 N respectively), and that the mode of failure was not by transverse cracking, but predominantly by oblique (medial) or spiral (lateral) tearing.

Strength and modulus of the meniscus vary with different locations and with different orientations of the specimen due to structural and compositional changes (Table B2.4). For loading parallel to the fibers, it appears that the meniscus may be stronger in the anterior location, and that the lateral meniscus may be stronger than the medial meniscus. This may be explained in part by the fact that the fiber orientation is more random in the posterior part of the medial meniscus.

Table B2.4 Tensile strength of meniscal tissue (MPa)^{a,*}

			Location		
Meniscus	Orientation†	Anterior	Central	Posterior	
Lateral	Parallel	10.37	6.31	6.87	
	Perpendicular	0.80	0.88	0.54	
Medial	Parallel	—	3.36	5.86	
	Perpendicular	—	0.85	1.23	

a: Averaged from data in [6].

* Tissues were fixed in formalin before testing.

† Either parallel or perpendicular to the circumferential direction.

Table B2.5 Non-linear parameters and tensile modulus of menisci

Meniscus	Location	A	B	C	Tensile modulus ^a (MPa)
Medial	Anterior	1.6	28.4	42.4	159.6
	Central	0.9	27.3	23.7	93.2
	Posterior	1.4	20.1	25.2	110.2
Lateral	Anterior	1.4	28.8	30.2	159.1
	Central	2.1	31.9	55.7	228.8
	Posterior	3.2	27.5	67.5	294.1

a: Slope of the stress-strain curve in the linear portion after the toe region.

A similar trend is seen in the tensile modulus of meniscal specimens oriented parallel to the circumferential direction (Table B.2.5), and if a power law is used as the constitutive equation (equation B2.3), the coefficients A and C show an identical pattern [7, 10, 28].

The properties of intervertebral discs are more complex than those of the menisci, since properties vary with disc level, and discs must withstand loads and moments in three orthogonal directions. (Table B2.6).

As with the meniscus, strength and modulus of discal tissue vary with location and orientation of the specimen (Table B2.7). Lin *et al.* [15, 16] have however shown that elastic moduli of annular specimens are independent of disc level.

B2.5 Viscoelastic Behavior

Finally, the rate dependent properties are usually modeled by a three-parameter solid which consists of a spring (m_2) and a dashpot (h) in parallel connected to another spring (m_1) in series. Viscoelastic properties may also be expressed in terms of the dynamic modulus G^* . A sinusoidal displacement of the form $u = u_o e^{i\omega t}$ is applied to the specimen (this is usually a torsional strain), and the resulting force response $F = F_o e^{i\omega t + \delta}$ is measured. Here ω = circular frequency, $i = \sqrt{-1}$ and δ is

Table B2.6 Mechanical properties of the intervertebral disc

		Stiffness (N/mm or Nm/rad)			
Loading mode	Level	Strength (N)	Initial ^a	Average ^b	Finale
Compression	L5-S1	5574 ^d	1448 ^d		3511 ^d
	L4-L5	5128 ^d	306 ^d , 413 ^c		2405 ^d , 721 ^c
	L3-L4	5351 ^d	1352 ^d		2756 ^d
	L2-L3	4905 ^d	439 ^d , 461 ^c		3160 ^d , 997 ^c
	L1-L2				
Flexion	Lumbar		46 ^f		8451 ^f
Extension	Lumbar		74 ^f		
Lateral bending	Lumbar		64 ^f		704 ^f
Axial torsion	Lumbar		157 ^f		604 ^f
Compression	Lumbar			800 ^g	
Posterior shear	Lumbar		102 ^g		148 ^g
Anterior shear	Lumbar		91 ^g		123 ^g
Lateral shear	Lumbar		113 ^g		169 ^g

a: Slope of the toe region of the load displacement curve.

b: Average slope of the load displacement curve.

c: Slope of the load displacement curve excluding the toe region.

d: [29]; e: [30]; f: [31]; g: [32].

Table B2.7 Mechanical properties of the annulus fibrosus

		Layer Location			
Property	Specimen orientation	Average	Inner	Middle	Outer
Tensile Modulus	Horizontal	3.54 ^c			
	Parallel to fibers	3.41			410 ^a
	Perpendicular to lamellae				0.16 ^b
Ultimate stress	Horizontal				
	Parallel to fibers				110 ^a
	Perpendicular to lamellae				0.187 ^b

a: MPa, Specimen 2×2.5 mm cross section, 6.5 mm length [33].

b: MPa, Specimen 7.5×2.5 mm cross section, 4.5 mm length [33].

c: N/mm, Specimen 2×1.5 mm cross section, 15–25 mm length [34].

the phase angle shift between the applied displacement and the measured force. The dynamic modulus is than obtained as

$$G^* = \frac{F}{u} = \frac{F_0}{u_0} e^{j\delta} = G' + iG'' \quad (\text{B2.4})$$

where G' and G'' are the loss and storage moduli respectively. In some cases, it may be more convenient to express viscoelastic properties in terms of the magnitude of the dynamic shear modulus and the phase angle shift as

Table B2.8 Viscoelastic properties of meniscal tissue

Specimen orientation	G* (MPa)	δ (degrees)
Circumferential	36.8	16.7
Axial	29.8	19.4
Radial	21.4	20.8

Table B2.9 Viscoelastic properties of the intervertebral disc* [36, 37]

m ₁ (MPa)	m ₂ (MPa)	h (GPa.s)
10–13	13–40	65–280

* Ranges.

$$|G|^* = \sqrt{(G'{}^2 + G''{}^2)}; \delta = \tan^{-1}\left(\frac{G''}{G'}\right) \tag{B2.5}$$

The anisotropic viscoelastic properties in shear of the meniscus have been determined by subjecting discs of meniscal tissue to sinusoidal torsional loading [35] (Table B2.8). The specimens were cut in the three directions of orthotropicsymmetry, i.e. circumferential, axial and radial. A definite correlation is seen with the orientation of the fibers and both the magnitude of the dynamic modulus |G*| and the phase angle δ.

The viscoelastic properties of the human intervertebral disc have been modeled [36, 37] using the three-parameter solid. The parameters were obtained by fitting experimentally obtained creep curves to analytical equations using linear regression (Table B2.9).

B2.6 Discussion

Since it is nearly impossible to carry out meaningful experiments *in vivo* on the human disc or meniscus, the properties reported above have been obtained from cadaveric tissue. Test specimens were obtained from autopsy material (10–48 hours after death), and were either tested immediately or stored frozen for varying periods of time before testing. Statistical analyses of these data show high standard deviations and errors may be a consequence of aging and degeneration, diurnal changes or surgical interventions) cause a subsequent change in mechanical properties. Further, it has been well documented that the mechanical properties of collagenous tissues change with storage medium, storage temperature, time after death and ‘preconditioning’ state [38, 39]. Both the disc and the meniscus contain highly oriented collagen fibers, and location and orientation of the test specimen can cause significant changes in the test results. Additional factors such as sex, diet, and level of activity also play a relatively minor role in this variation.

Additional Reading

Ghosh, P. (ed.) (1988) *The Biology of the Intervertebral Disc*, Vol I and II, CRC Press, Boca Raton.

One of the most comprehensive texts available about the intervertebral disc. It is written from the biological perspective, and contains exhaustive information about each component of the disc. Volume I includes chapters on disc structure and development, vasculature, innervation, collagen and non-collagenous proteins. Volume II contains information on nutrition and metabolism, mechanics, pathology and disease states.

Mow, V.C., Arnoczky, S.P. and Jackson, D.W. (1992) *Knee Meniscus: Basic and Clinical Foundations*. Raven Press, New York.

This monograph is designed to serve as a comprehensive reference for clinicians and researchers interested in the meniscus. It includes chapters on gross anatomy, structure and function of the menisci and their mechanical behavior, pathological disorders, clinical and surgical methods of treatment and meniscal disorders.

Mow, V.C. and Hayes, W.C. (1991) *Basic Orthopaedic Biomechanics*, Raven Press, New York.

This book is aimed at teaching senior engineering students or orthopaedic residents the fundamental principles of biomechanics of the musculoskeletal system. The book contains several chapters on the mechanics of joints, and the properties and functions of joint tissues. The chapter devoted to articular cartilage and the meniscus includes a review of collagen-proteoglycan interactions, and how these directly affect the mechanical behavior of the tissue. The biphasic and the triphasic theories for the viscoelastic properties are also discussed.

White, A.A. and Panjabi, M.M., (1990) *Clinical Biomechanics of the Spine*, J.B. Lippincott Company, Philadelphia.

An excellent reference book for an engineer or a physician interested in the spine. Each topic is written from the viewpoint of a biomechanician and the topics covered include kinetics and kinematics of vertebral joints, pathological disorders of the spine and their surgical management. Chapter 1 contains an introductory section on the intervertebral disc that describes its structure, function and biomechanics.

References

1. Armstrong, C.G. and Mow, V.C. (1982) Variations in the intrinsic mechanical properties of human articular cartilage with age, degeneration and water content. *J. Bone Joint Surg.*, **64A**, 88–94.
2. Mow, V.C., Holmes, M.H. and Lai, W.M. (1984) Fluid transport and mechanical properties of articular cartilage: A review. *J. Biomech.*, **102**, 73–84.
3. Hayes, W.C. and Bodine, A.J. (1978) Flow independent viscoelastic properties of articular cartilage matrix. *J. Biomech.*, **11**, 407–419.
4. Mathur, P.D., McDonald, J.R. and Ghormley, R.K. (1949) A study of the tensile strength of the menisci of the knee. *J. Bone Joint Surg.*, **32A**, 650–654.
5. Aspden, R.M., Yarker, Y.E. and Hukins, D.W.L. (1985) Collagen Orientations in the meniscus of the knee joint. *J. Anat.*, **140**, 371–380.
6. Bullough, P.G., Munuera, L., Murphy, J. and Weinstein, A.M. (1970) The strength of the menisci of the knee as it relates to their fine structure. *J. Bone Joint Surg.*, **52B**, 564–570.

- 7 Fithian, D.C., Kelly, M.A. and Mow, V.C. (1990) Material properties and structure-function relationships in the menisci. *Clin. Orthop. Rel. Res.*, **252**, 19–31.
- 8 Mow, V.C., Zhu, W. and Ratcliffe, A. (1991) Structure and function of articular cartilage and meniscus, in *Basic Orthopaedic Biomechanics*, (eds V.C. Mow and W.C. Hayes), Raven Press, New York, pp. 143–198.
- 9 Eyre, D.R. and Wu, J.J. (1983) Collagen of fibrocartilage: A distinctive molecular phenotype in bovine meniscus. *F. E. B. S. Letters*, **158**, 265–270.
- 10 Fithian, D.C., Zhu, W.B., Ratcliffe, A., Kelly, M.A. and Mow, V.C. (1989b) Exponential law representation of tensile properties of human meniscus. *Proceedings of the Institute of Mechanical Engineers. The Changing Role of Orthopaedics*, Mechanical Engineering Publications Limited, London. pp. 85–90
- 11 Ghosh, P. and Taylor, T.K.F. (1987) The knee joint meniscus: A fibrocartilage of some distinction. *Clin. Orthop. Rel. Res.*, **224**, 52–63.
- 12 Ingman, A.M., Ghosh, P. and Taylor, T.K.F. (1974) Variation of collagenous and non-collagenous proteins of human knee joint menisci with age and degeneration. *Gerontology*, **20**, 212–223.
- 13 Pooni, J.S., Hukins, D.W.L., Harris, P.F., Hilton, R.C. and Davies, K.E. (1986) Comparison of the structure of human intervertebral discs in the cervical, thoracic and lumbar regions of the spine. *Surg. Radiol. Anat.*, **8**, 175–182.
- 14 Hirsch, C., Inglemark, B.-H. and Miller, M. (1963) The anatomical basis of back pain. *Acta Orthop. Scand.*, **33**, 2–17.
- 15 Lin, H.S., Liu, Y.K. and Adams, K.H. (1978) Mechanical response of the lumbar intervertebral joint under physiological (complex) loading. *J. Bone Joint Surg.*, **60A**, 41–55.
- 16 Lin, H.S., Liu, Y.K., Ray, G. and Nikravesh, P. (1978) System identification for material properties of the intervertebral joint. *J. Biomech.*, **11**, 1–14.
- 17 Taylor, J.R. (1975) Growth of human intervertebral discs and vertebral bodies. *J. Anat.*, **120**, 49–68.
- 18 Panjabi, M.M., Summers, D.J., Pelker, R.R., Videman, T., Friedlander, G.E. and Southwick, W.O. (1986) Three-dimensional load-displacement curves due to forces on the cervical spine. *J. Ortho. Res.*, **4**, 152–161.
- 19 Inoue, H. (1981) Three-dimensional architecture of lumbar intervertebral discs. *Spine*, **6**, 139–146.
- 20 Panagiotacopoulos, N.D., Knauss, W.G. and Bloch, R. (1979) On the mechanical properties of human intervertebral disc materials. *Biorheology*, **16**, 317–330.
- 21 Marchand, F. and Ahmed, A.M. (1988) Investigation of the laminate structure of lumbar disc annulus fibrosus. *Trans. Orthop. Res. Soc.*, **13**, 271.
- 22 Best B.A., Guilak, F., Setton, L.A., Zhu, W., Saed-Nejad, F., Ratcliffe, A., Weidenbaum, M. and Mow, V.C. (1994) Compressive mechanical properties of the human annulus fibrosus and their relationship to biochemical composition. *Spine*, **19**, 212–221.
- 23 Gower, W.E. and Pedrini, V. (1969) Age-related variations in protein-polysaccharide from human nucleus pulposus, annulus fibrosus and costal cartilage. *J. Bone Joint Surg.*, **51A**, 1154–1162.
- 24 Lyons, G., Eisenstein, S.M. and Sweet, M.B.E. (1981) Biochemical changes in intervertebral disc degeneration, *Biophysics Acta*, **673**, 443.
- 25 Lai, W.M. and Mow, V.C. (1980) Drag-induced compression of articular cartilage during a permeation experiment. *Biorheology*, **17**, 111–123.
- 26 Proctor, C.S., Schmidt, M.B., Whipple, R.R., Kelly, M.A. and Mow, V.C. (1989) Material Properties of the normal medial bovine meniscus. *J. Ortho. Res.*, **7**, 771–782.
- 27 Eberhardt, A.W., Keer, L.M., Lewis, J.L. and Vithoontien, V. (1990) An analytical model of joint contact. *J. Biomech. Eng.*, **112**, 407–413.
- 28 Fithian D.C., Schmidt, M.B., Ratcliffe, A. and Mow, V.C. (1989a) Human meniscus tensile properties: Regional variation and biochemical correlation. *Trans. Orthop. Res. Soc.*, **14**, 205.

- 29 Brown, T., Hansen, R.J. and Torra, A.J. (1957) Some mechanical tests on the lumbosacral spine with particular reference to the intervertebral discs. *J. Bone Joint Surg.*, **39A**, 1135–1164.
- 30 Hirsch, C. and Nachemson, A. (1954) New observations on the mechanical behavior of the lumbar discs. *Acta Orthop. Scand.*, **23**, 254–283.
- 31 Schultz, A.B., Warwick, D.N., Berkson, M.H. and Nachemson, A.L. (1979) Mechanical properties of human lumbar spine motion segments Part I. *J. Biomech. Eng.*, **101**, 46–52.
- 32 Berkson, M.H., Nachemson, A. and Schultz, A.B. (1979) Mechanical properties of human lumbar spine motion segments Part I. *J. Biomech. Eng.*, **101**, 53–57.
- 33 Marchand, F. and Ahmed, A.M. (1989) Mechanical properties and failure mechanisms of the lumbar disc annulus. *Trans. Orthop. Res. Soc.*, **14**, 355.
- 34 Galante, J.O. (1967) Tensile properties of the human lumbar annulus fibrosus. *Acta Orthop. Scand.*, (Suppl. 100), 1–91.
- 35 Chern, K.Y., Zhu, W.B. and Mow, V.C. (1989) Anisotropic viscoelastic shear properties of meniscus. *Adv. Bioeng.*, **BED-15**, 105–106.
- 36 Burns, M.L. *et al.* (1984) Analysis of compressive creep behavior of the vertebral unit subjected to uniform axial loading using exact parametric solution equations of Kelvin solid models Part I. *J. Biomech.*, **17**, 113–130.
- 37 Kazarian, L.E. and Kaleps, I. (1979) Mechanical and physical properties of the human intervertebral joint. Technical Report AMRL-TR-79-3, Aerospace Medical Research Laboratory, Wright Patterson Air Force Base, OH
- 38 Black, J. (1976) Dead or alive: The problem of *in vitro* tissue mechanics. *J. Biomed. Mats. Res.*, **10**, 377–389.
- 39 Black, J. (1984) Tissue properties: Relation of *in vitro* studies to *in vivo* behavior, in *Natural and Living Biomaterials*, Ed. G.W. Hastings and P. Ducheyne, CRC Press, Boca Raton, pp. 5–26.

Chapter B3

Ligament and Tendon

Connie S. Chamberlain and Ray Vanderby Jr.

B3.1 Structure

Ligaments and tendons (T/L) are a hierarchical structure of dense, parallel connective tissue bands that are hypovascular and hypocellular and span a joint connecting bone to bone and bone to muscle, respectively. T/Ls are initially assembled from cross-linked tropocollagen molecules aggregated progressively into microfibrils, subfibrils, fibrils, and fibers (Fig. B3.1). Collagen fibers, which display a waviness or crimp pattern in an unloaded state, are contained in fiber bundles, called fascicles. The entire T/L is then organized into a collection of fascicles and surrounded by a more vascular connective tissue called the epiligament/epitenon. The paratenon surrounds the epiligament/epitenon and facilitates gliding along contiguous structures. Altogether, this hierarchical structure provides the T/L with high tensile force and resilience while preventing damage and separation of the fibers under mechanical stress.

C.S. Chamberlain (✉)

Department of Orthopedics and Rehabilitation, Wisconsin Institute for Medical Research,
University of Wisconsin-Madison, 1111 Highland Avenue, Madison, WI 53705, USA
e-mail: Chamberlain@ortho.wisc.edu

R. Vanderby Jr.

Department of Orthopedics and Rehabilitation, Wisconsin Institute for Medical Research,
University of Wisconsin-Madison, 1111 Highland Avenue, Madison, WI 53705, USA

Department of Biomedical Engineering, Wisconsin Institute for Medical Research, University
of Wisconsin-Madison, 1111 Highland Avenue, Madison, WI 53705, USA

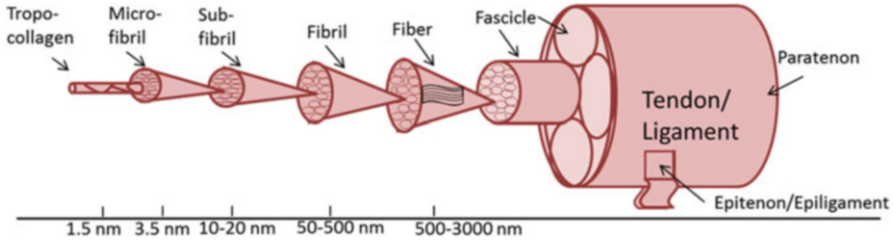
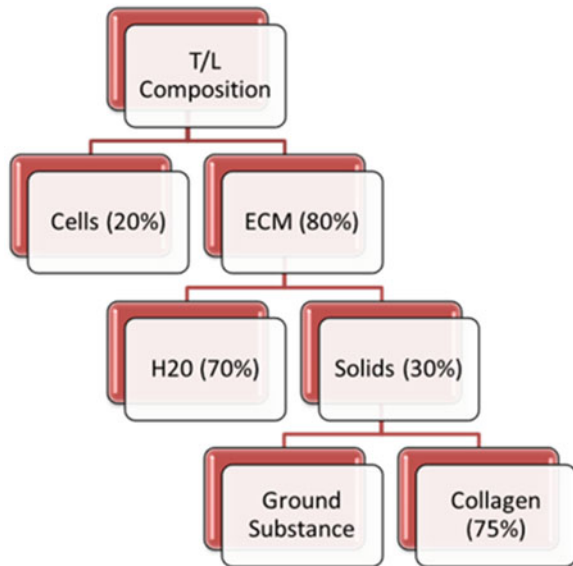


Fig. B3.1 Hierarchical structure of the tendon/ligament. The tropocollagen cross-linked molecules are arranged in microfibrils, subfibrils, fibrils, fibers, and fascicles. The fascicles are surrounded by the epitenon/epiligament and paratenon

Fig. B3.2 Composition of the T/L



B3.2 Composition

Ligaments and tendons consist of few cells and abundant extracellular matrix. The cellular component, primarily consisting of fibroblasts/tenocytes, comprises 20 % of the total tissue volume whereas the ECM accounts for the remaining 80 % (Fig. B3.2) [1, 2]. Approximately 70 % of the ECM consists of water, which contributes to modulating cellular function and viscoelastic (i.e., time dependent) behavior. The remaining 30 % of the ECM is comprised of solids, such as collagen and ground substance. The ground substance (non-fibrous component of the matrix) primarily comprises hyaluronan, glycoproteins, and proteoglycans and modulates tissue metabolism, provides shock absorption, decreases internal friction, and binds water. The fibrous component, comprising 75–80 % of T/L dry weight, provides

strength and a support framework and consists primarily of type I collagen. Lesser amounts of types III, VI, V, XI, and XIV collagens are also present.

B3.3 Normal T/L Function

The ligament primarily serves a mechanical function to passively stabilize and guide joints through a normal range of motion. It offers virtually no resistance to normal joint motion but stiffens to become a “check rein” against non-physiologic joint motions that could damage articular structures. Tendons with muscles move or stabilize articular joints. T/Ls must therefore exhibit nonlinear mechanical behavior that is relatively compliant under low loads and quickly stiffens under higher loads. This passive elastic behavior is accompanied by a time-dependent (or viscous) behavior (e.g., if we stretch and “warm up” before exercise our joints move with less resistance).

The mechanical behavior of a T/L provides a clear understanding of its normal function as well as injury mechanisms. The strength of a T/L under a uniformly distributed load is largely determined by the cross-sectional size of the tissue and the rate of loading. For instance, T/Ls exhibit increased strength and stiffness with increased rate of loading. Structural properties of T/Ls are typically gathered via tensile tests at a constant rate of deformation and displayed on a force-elongation curve (Fig. B3.3a). From the force-elongation data, a nominal stress-strain relationship is determined to provide mean mechanical properties of the tissue (i.e., normalized structural properties; Fig. B3.3b). Here nominal stress (σ) is the force (F) divided by the original cross-sectional area of the ligament (A_0) and nominal strain (ϵ) is the

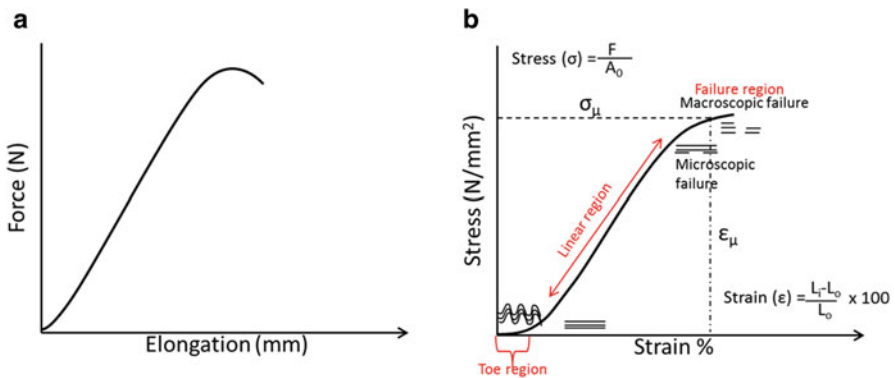


Fig. B3.3 Example of force-elongation (a) and stress-strain (b) curves of the ligament tested to failure. (b) Stress-strain curve of a ligament contains the three primary regions (in red), including the toe, linear, and failure regions. The toe region indicates a nonlinear increase in load as the tissue elongates. The linear region indicates the area of greatest stiffness whereas the failure region indicates that the collagen fibers have disrupted and failed. F =force; A_0 =ligament cross-sectional area; L_1 =instantaneous length after loading; L_0 =original length

stretched ligament length (L_i) minus its original length (L_o) and divided by its original length (L_o). Often this result is multiplied by 100 to be expressed as a percent. The calculated stress-strain curve further identifies the commonly reported elastic modulus (slope of the linear region), ultimate tensile strength (σ_u), and strain (ϵ_u).

The resulting stress-strain or force-elongation curves separate the tissue behavior into three regions, called the toe, linear, and failure regions (Fig. B3.3b). Within the toe region, collagen fibers of unstressed T/L are composed in a sinusoidal (“crimp”) pattern. The mechanism causing collagen fiber crimp is not well understood but the crimped fibers provide minimal resistance to movement over an initial range of strains. The crimp region is very compliant. As the T/L becomes loaded, the fibers straighten and the crimp pattern is lost [3, 4]. As loading continues, T/L stiffness increases and greater force is required to produce an equivalent increment of strain. Once the strain increases to 1.5–4 % [5], a nearly linear stiffness is observed (i.e., the linear region). As strain is further increased beyond the linear range (8–10 % strain), fiber disruption and ultimately complete and irreversible failure occur [4, 6]. Irreversible damage begins approximately half way through the linear region, after which the original length (L_o) can no longer be recovered with unloading, and fibrillar damage is observed with electron microscopy [7]. Once entering the linear region, ultimate failure occurs after a predictable increment of strain (~9.3 %) [8].

Viscoelastic behavior of T/Ls aids and protects joint function. Viscoelasticity adds time dependence to the above elastic phenomena. It manifests itself by allowing easier joint motion after stretching, by increasing the T/L strength to resist impact forces, and by absorbing some of the energy in dynamic loadings [5]. These behaviors can be quantified via creep and relaxation testing. If a T/L is held at a constant deformation (or strain), it exhibits relaxation which means that the load (or stress) decreases over time (Fig. B3.4a). T/L also exhibits creep where deformation

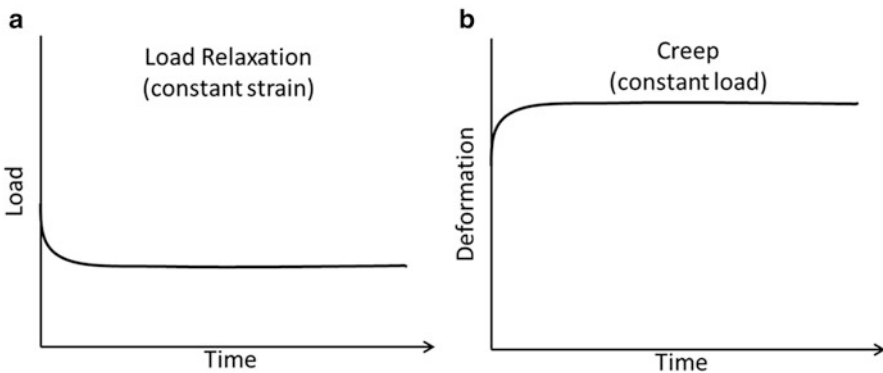


Fig. B3.4 Viscoelastic properties of ligaments are demonstrated by load relaxation (a) and creep (b). Load relaxation is demonstrated by loading the ligament (below the linear region) and maintaining constant strain over an extended period. Load decreases rapidly the first 6–8 h, and then continues at a low rate (a). Creep takes place when the ligament is loaded (below the linear region) at a constant level over time. As a result, deformation increases quickly at first and then continues at a low rate

(or strain) increases over time under constant tensile force (Fig. B3.4b). As a T/L is subjected to increased rate of loading, the linear portion of the stress-strain curve becomes steeper, indicating greater stiffness and a greater tissue load before reaching the failure strain.

In vitro ligament and tendon testing is often conducted as a composite of bone-ligament-bone and muscle-tendon-bone, respectively, because bone blocks are easy to grip and this minimizes gripping artifacts in the tissue. However, the maximum load, stiffness, and elongation values can then represent the average properties of a composite and may vary depending on the material behavior of the bone and enthesis, as well as the size, shape, and orientation of the sample [9]. Mechanical properties of the human ligaments and tendons from various joints are included in Table B3.1.

Table B3.1 Mechanical properties of the lower and upper limb ligaments and tendons

Tissue	Modulus (MPa)	UTS (MPa)	Strain at UTS (%)	Source
<i>Knee ligament</i>				
Anterior cruciate	65–541	13–46	9–44	[10, 11]
Posterior cruciate	109–248	24–36	10–29	[12, 13]
<i>Knee tendon</i>				
Patellar	143–660	24–69	14–27	[10, 14–17]
<i>Ankle ligament</i>				
Lateral collateral	216–512	24–46	13–17	[18]
Medial collateral	54–321	16–34	10–33	[18, 19]
<i>Ankle tendon</i>				
Achilles	65	24–61	24–59	[20]
Palmaris longus	2310±620	91±15	NA	[19]
<i>Other</i>				
Semintendinous	362±22	89±5	52±3	[10]
Gracilis	613±41	112±4	34±2	[10]
<i>Shoulder ligament</i>				
Inferior glenohumoral	30–42	5–6	8–15	[21, 22]
Capsule	32–67	8–21	NA	[22]
<i>Spine ligament</i>				
Posterior longitudinal	NA	21–28	11–44	[23]
Ligamentum flavum	NA	1–15	21–102	[23]
Anterior longitudinal	286–724	8–37	10–57	[23, 24]
Supraspinal	NA	9–16	39–115	[23]
Interspinal	NA	2–9	39–120	[23]
<i>Forearm ligament</i>				
Carpal joint	23–119	NA	NA	[25]
Palmar radioulnar	39±18	5.7±1.7	51±24	[26]
Dorsal radioulnar	52±33	8±5	61±29	[26]

Tissues separated into bundles or tested in multiple studies are listed as a range of values. Data determined by one bundle or one study are expressed at mean±S.E.M.

B3.4 Injured T/L Function

T/L injury results from sudden, prolonged, or excessive forces that exceed the elastic or recoverable limits of the tissue. When subfailure damage occurs, the tissue does not recover its original length (L_0) after removal of the deforming load. Ligaments incapable of returning to their original length after elongation are considered lax and no longer provide the same passive restraints to joint motion and the same proprioception. If tendon length changes, optimal muscle strength occurs at different joint positions. Once the ultimate strain is exceeded, the collagen fibers reach a point of failure and all will rupture. The functional recovery of T/Ls after injury is a slow and incomplete process. After 2 years of healing, MCLs only reached 80 % of their control values for strength [8]. During the remodeling phase of healing, viscoelastic properties are significantly compromised, and scars tend to stress-relax and maintain load less efficiently than normal ligament [27–29]. Remodeling ligament scars also creep twice the amount as normal ligaments during cyclic and static loads [30]. This would increase joint laxity and decrease proprioception after healing. Long-term biomechanical recovery of ligament is dependent on a number of factors, including the size of the initial gap, proximity of the torn ligament ends, and joint movement during healing. Tendon's functional recovery is also dependent on length, but the bigger concern is scarring down during healing to restrict joint motion. Tendon movement is necessary early to prevent adhesions but load must be very low because of mechanical compromise. Many strategies have attempted to recapitulate original properties after healing, including surgical repair, physical therapy protocols, grafting, gene therapy, and tissue engineering, but thus far, healing does not regenerate the native tissue. This issue continues as a focus for future investigations.

B3.5 Conclusions

Ligament and tendon injuries are a frequent occurrence with significant morbidity. Appropriate clinical management requires an understanding of damaged T/L mechanical function and its capacity for self-repair. The composition and hierarchical organization of these tissues facilitate its important function. One-dimensional, elastic properties such as the ultimate tensile strength, modulus, and strain are commonly gathered and pertinent for comparing normal and compromised tissue and evaluating the efficacy of different healing treatments. In addition, viscoelastic properties provide metrics to further characterize tissue behavior [31]. These are typically one-dimensional, mean behaviors of normal or healing tissues. Defects, scarring, and tissue flaws are really three-dimensional, localized phenomena. Alternative methods are needed that locally characterize these regions of compromise both in vitro and in vivo. Recently, ultrasound-based methods (example [32]) have been explored as a possible approach to measure local tendon stress and

strain in a dynamic, time-dependent manner. Such data would further enhance our knowledge of T/L behavior and provide a tool to evaluate new treatment strategies.

References

1. Frank CB (2004) Ligament structure, physiology and function. *J Musculoskelet Neuronal Interact* 4(2):199–201
2. Nordin M, Lorenz T, Campello M (2001) Biomechanics of tendons and ligaments. In: Nordin M, Frankel VH (eds) *Basic biomechanics of the musculoskeletal system*. Lippincott Williams & Wilkins, Philadelphia, PA, pp 102–125
3. Hirsch G (1974) Tensile properties during tendon healing. A comparative study of intact and sutured rabbit peroneus brevis tendons. *Acta Orthop Scand Suppl* 153:1–145
4. Woo SLY, An KN, Arnoczky DVM, Fithian D, Myers B (1994) Anatomy, biology, and biomechanics, of the tendon, ligament, and meniscus. In: Simon SR (ed) *Orthopaedic basic science*. AAOS, Rosemont, IL, p 52
5. Viidik A (1973) Functional properties of collagenous tissues. *Int Rev Connect Tissue Res* 6:127–215
6. Sharma P, Maffulli N (2006) Biology of tendon injury: healing, modeling and remodeling. *J Musculoskelet Neuronal Interact* 6(2):181–190
7. Provenzano PP, Alejandro-Osorio AL, Valhmu WB et al (2005) Intrinsic fibroblast-mediated remodeling of damaged collagenous matrices in vivo. *Matrix Biol* 23(8):543–555
8. LaCroix AS, Duenwald-Kuehl SE, Lakes RS et al (2013) Relationship between tendon stiffness and failure: a metaanalysis. *J Appl Physiol* 115(1):43–51
9. Woo SLY, Hollis JM, Adams DJ et al (1991) Tensile properties of the human femur-anterior cruciate ligament-tibia complex—the effects of specimen age and orientation. *Am J Sports Med* 19(3):217–225
10. Butler DL, Grood ES, Noyes FR et al (1984) Effects of structure and strain-measurement technique on the material properties of young human tendons and fascia. *J Biomech* 17(8):579–596
11. Noyes FR, Grood ES (1976) The strength of the anterior cruciate ligament in humans and Rhesus monkeys. *J Bone Joint Surg Am* 58(8):1074–1082
12. Race A, Amis AA (1994) The mechanical properties of the two bundles of the human posterior cruciate ligament. *J Biomech* 27(1):13–24
13. Prietto MP, Bain JR, Stonebrook SN et al (1988) Tensile strength of the human posterior cruciate ligament (PCL). *Transactions of the Orthopaedic Research Society* 13:195
14. Bechtold JE, Eastlund DT, Butts MK et al (1994) The effects of freeze-drying and ethylene oxide sterilization on the mechanical properties of human patellar tendon. *Am J Sports Med* 22(4):562–566
15. Blevins FT, Hecker AT, Bigler GT et al (1994) The effects of donor age and strain rate on the biomechanical properties of bone-patellar tendon-bone allografts. *Am J Sports Med* 22(3):328–333
16. Butler DL, Kay MD, Stouffer DC (1986) Comparison of material properties in fascicle-bone units from human patellar tendon and knee ligaments. *J Biomech* 19(6):425–432
17. Johnson GA, Tramaglini DM, Levine RE et al (1994) Tensile and viscoelastic properties of human patellar tendon. *J Orthop Res* 12(6):796–803
18. Siegler S, Block J, Schneck CD (1988) The mechanical characteristics of the collateral ligaments of the human ankle joint. *Foot Ankle* 8(5):234–242
19. Regan WD, Korinek SL, Morrey BF et al (1991) Biomechanical study of ligaments around the elbow joint. *Clin Orthop Relat Res* 271:170–179

20. Paulos LE, Cawley PW, France EP (1991) Impact biomechanics of lateral knee bracing. The anterior cruciate ligament. *Am J Sports Med* 19(4):337–342
21. Bigliani LU, Pollock RG, Soslowky LJ et al (1992) Tensile properties of the inferior glenohumeral ligament. *J Orthop Res* 10(2):187–197
22. Itoi E, Grabowski JJ, Morrey BF et al (1993) Capsular properties of the shoulder. *Tohoku J Exp Med* 171(3):203–210
23. Pintar FA, Yoganandan N, Myers T et al (1992) Biomechanical properties of human lumbar spine ligaments. *J Biomech* 25(11):1351–1356
24. Neumann P, Keller TS, Ekstrom L et al (1992) Mechanical properties of the human lumbar anterior longitudinal ligament. *J Biomech* 25(10):1185–1194
25. Savelberg HH, Kooloos JG, Huiskes R et al (1992) Stiffness of the ligaments of the human wrist joint. *J Biomech* 25(4):369–376
26. Schuind F, An KN, Berglund L et al (1991) The distal radioulnar ligaments: a biomechanical study. *J Hand Surg Am* 16(6):1106–1114
27. Woo SLY, Inoue M, McGurkburleson E et al (1987) Treatment of the medial collateral ligament injury. 2. Structure and function of canine knees in response to differing treatment regimens. *Am J Sports Med* 15(1):22–29
28. Clayton ML, Miles JS, Abdulla M (1968) Experimental investigations of ligamentous healing. *Clin Orthop Relat Res* 61:146–153
29. Chimich D, Frank C, Shrive N et al (1991) The effects of initial end contact on medial collateral ligament healing—a morphological and biomechanical study in a rabbit model. *J Orthop Res* 9(1):37–47
30. Thornton GM, Leask GP, Shrive NG et al (2000) Early medial collateral ligament scars have inferior creep behaviour. *J Orthop Res* 18(2):238–246
31. Duenwald SE, Vanderby R Jr, Lakes RS (2009) Viscoelastic relaxation and recovery of tendon. *Ann Biomed Eng* 37(6):1131–1140
32. Duenwald S, Kobayashi H, Frisch K et al (2011) Ultrasound echo is related to stress and strain in tendon. *J Biomech* 44(3):424–429

Chapter B4

Skin and Muscle

A.F.T. Mak and M. Zhang

B4.1 Introduction

Early studies [11] of the material properties of human skin and muscle are largely suspect due to problems of inappropriate tissue handling, preservation and specimen preparation. Recent efforts have focused on methods which can determine properties *in situ* in living individuals or on very freshly excised tissues. Among the *in vivo* testing methodologies, indentation has proven to be the most popular, although it sums up the contributions of various tissue layers [1, 3, 4, 6, 7, 9]. The load-displacement curve obtained during indentation depends in decreasing degree upon each of the tissues beneath the indenter. The derived properties, in addition, can be expected to vary with anatomical site, subject age and external environmental conditions (temperature, relative humidity, etc.). Additional results have been obtained *in vivo* through the use of Doppler ultrasound techniques [2, 5].

B4.2 In-Vivo Mechanical Properties

B4.2.1 Doppler Results

Krouskop *et al.* [5, 8] applied Doppler ultrasound techniques to measure the point-to-point biomechanical property of the human skin and subcutaneous musculatures. Tests of the forearms and legs suggested that the elastic moduli are strongly dependent on the contraction status of the muscles. A 16-fold increase (from 6.2 kPa

Data are provided from indentation and ultrasound measurement techniques only.

A.F.T. Mak (✉) • M. Zhang

Rehabilitation Engineering Centre, Hong Kong Polytechnic, Hunghom, Kowloon, Hong Kong

Table B4.1 Apparent Elastic Moduli of Relaxed Above Knee Tissues [5]*

Anatomical Location	Elastic Modulus (kPa)(std dev.)
Anterior	57.9 (31.1)
Lateral	53.2 (30.5)
Posterior	141.4 (79.1)
Medial	72.3 (45.5)
Superficial	117.6 (63.0)
Underlying	59.1 (74.0)

* Determined by Doppler ultrasonic techniques.

to 109 kPa) in the modulus was reported at a 10% strain as muscle contraction changed from minimal to maximum. Malinauskas *et al.* [5] used the same technique to examine the stump tissues of above-knee amputees and found that the average modulus was significantly higher in posterior tissues than in other locations (Table B4.1). They found, additionally, that superficial tissues were stiffer than deeper structures. Note that the ages and sex of the subjects of these two studies [2, 5] were not reported.

B4.2.2 Indentation results

Ziegert and Lewis [9] measured the *in vivo* indentation properties of the soft tissues covering the anterior-medial tibiae. A preload of 22.4 N was used with indentors of 6 to 25 mm in diameter. The observed load displacement relationships were essentially linearly elastic. The structural stiffness was noted to vary by up to 70% between sites in one individual and up to 300% between individuals. Unfortunately, the thicknesses of overlying tissues were not determined at the different sites for the individuals studied.

Lanir *et al.* [3] measured the *in vivo* indentation behavior of human forehead skin with pressures up to 5 kPa. The observed behavior was linearly elastic and calculated stiffnesses were 4 to 12 kPa.

Bader and Bowker [1] studied the *in vivo* indentation properties of soft tissues on the anterior aspects of human forearms and thighs by applying constant pressures of 11.7 and 7 kPa respectively. Tissue thickness was measured by using a skinfold caliper and Poisson's ratio was assumed to be 0.3. With these data, the stiffness of forearm and thigh tissue were calculated to be, respectively, 1.99 and 1.51 kPa.

Vannah and Chlidress [7] applied similar techniques to measure the human calf, but confined the limb within a shell. They noted that stress relaxation occurred within one second of load application and no preconditioning effect was noted. Torres-Morenos *et al.* [6] performed a similar study, working through ports in quadrilateral sockets of three above-knee amputees. However, they found the mechanical properties of the tissues to be significantly non-linear, with site and rate dependencies, as well as being strongly influenced by muscular activity.

Mak *et al.* [4] (Table B4.2) measured the *in-vivo* indentation properties of the below knee tissues of young adults (N=6) between the ages of 25 and 35.

Table B4.2 Initial and Relaxed Elastic Moduli of Tissues Around Proximal Human Tibiae [4]*

Anatomical Location	Initial Elastic Modulus (E_{in}) (kPa)(std dev.)	Relaxed Elastic Modulus (E_{eq}) (kPa)(std dev.)
Medial		
Relaxed	102.6 (8.6)	99.8 (9.2)
Contracted	147.3** (15.8)	142.9** (16.7)
Con./Relax.	1.44	1.43
Lateral†		
Relaxed	132.9 (7.2)	130.1 (7.9)
Contracted	194.3** (24.7)	188.4** (23.0)
Con./Relax.	1.46	1.45

* By indentation; ** Different from relaxed ($p < 0.001$); † Between tibia and fibula.

A 4 mm diameter indenter was used, with a final indentation of about 5 mm. The fixed indentation was then maintained for 2–3 seconds to observe the difference between initial and relaxed (equilibrium) properties. The tests were done with the knee in 20° of flexion and were repeated with and without muscular contraction. The Poisson's ratio was assumed to be 0.5 for initial measurements and 0.45 for relaxed (equilibrium) measurements.

Additional Reading

Bader, D.L. and Bowker, P. (1983) Mechanical characteristics of skin and underlying tissues *in vivo*. *Biomaterials*, **4**, 305–8

This paper describes an indentation experiment to investigate *in vivo* the bulk mechanical properties of the composite of skin and underlying tissues on the anterior aspects of human forearms and thighs by applying constant pressures. Significant variations in tissue stiffness with sex, age and body site were also demonstrated.

Malinauskas, M., Krouskop, T.A. and Barry, P.A. (1989) Noninvasive measurement of the stiffness of tissue in the above-knee amputation limb. *J. Rehab. Res. Dev.*, **26**(3), 45–52

The paper reports a noninvasive technique to measure the mechanical properties of the bulk soft tissues by a pulsed ultrasonic Doppler system. An ultrasonic transducer was used to measure internal displacement resulting from external acoustical perturbations. Measurements were made at four sites of 8 aboveknee residual limbs. The Young's moduli were found in a range of 53–141 kPa. Superficial tissue had a significantly higher modulus than the tissue beneath.

The repeatability test indicated an acceptable repeatability. An improved device can possibly be a useful tool in prosthetic fitting and CAD socket design.

Rab, G.T. (1994) Muscle, in *Human Walking* (2nd ed.) (eds J. Rose, J.C. Gamble), Williams & Wilkins, Baltimore, pp. 101–122.

A concise description of the active properties of muscle tissue, with direct application to the development of forces within the human gait cycle.

Reynolds, D. and Lord, L. (1992) Interface load for computer-aided design of below-knee prosthetic sockets. *Med. & Biol. Eng. & Comput.*, **30**, 419–426.

The authors investigated the bulk tissue behaviour of the below-knee amputee's residual limb. An assessment of Young's modulus was made by matching the indentation experimental curves with the curves produced by the finite element modelling of the indentation into a layer of tissue with idealized mechanical properties. *In vivo* tests, conducted at four sites of a below-knee amputee's limb (patella tendon, popliteal, and anterolateral regions) found the local moduli to be 145, 50, 50 and 120 kPa respectively. The effect of muscle tension on the measured indentation response was also investigated. The results showed that the stiffness increased with muscle contraction.

References

1. Bader D.L. Bowker, P. (1983) Mechanical characteristics of skin and underlying tissues *in vivo*. *Biomaterials* **4**:305–8
2. Krouskop, T.A, Dougherty, D.R and Vonson, F.S. (1987) A pulsed Doppler ultrasonic system for making noninvasive measurements of the mechanical properties of soft tissue. *I. Rehab. Res. Dev.*, **24**(1), 1–8.
3. Lanir, Y., Dikstein, S., Hartzstark, A., *et al.* (1990) In-vivo indentation of human skin. *Trans. ASME (J. Biomech. Eng.)*, **112**, 63–69.
4. Mak, A.F.T., Liu, G.H.W. and Lee, S.Y. (1994) Biomechanical assessment of below-knee residual limb tissue, *J. Rehab. Res. Dev.*, **31**, 188–198.
5. Malinauskas, M., Krouskop, T.A and Barry, P.A (4) (1989) Noninvasive measurement of the stiffness of tissue in the above-knee amputation limb. *I.Rehab. Res. Dev.*, **26**(3), 45–52.
6. Torres-Morenos, R., Solomonidis, S.E. and Jones, D. (1992) Geometric and mechanical characteristics of the above-knee residual limb. *Proc. 7th. World Cong. Int. Soc. Prosthetics Orthotics*, pp. 149.
7. Vannah, W.M. and Chlidress, D.S. (1988) An investigation of the three dimensional mechanical response of bulk muscular tissue: Experimental methods and results, in *Computational Methods in Bioengineering* (eds R.L. Spilker and B.R Simon), Amer. Soc. Mech. Eng., New York, pp. 493–503
8. Yamada, H. (1970) (ed. F.G. Evans) *Strength of Biological Tissues*, Williams & Wilkins, Baltimore.
9. Ziegert, J.C. and Lewis, J.L. (1978) In-vivo mechanical properties of soft tissue covering bony prominence, *Trans ASME (J. Biomech. Eng.)*, **100**, 194–201.

Chapter B5

Brain Tissues

S.S. Margulies and D.F. Meaney

B5.1 Introduction

The brain is organized into the cerebrum, brain stem, and cerebellum. The cerebrum consists of two cerebral hemispheres, basal ganglia, and the diencephalon. The hemispheres contain the cerebral cortex and underlying white matter, and are associated with higher order functioning, including memory, cognition, and fine motor control. The basal ganglia, contained within the hemispheres, controls gross motor function. The diencephalon is much smaller than the cerebrum, contains the thalamus and hypothalamus, and is associated with relaying sensory information and controlling the autonomic nervous system. The brainstem contains the mesencephalon, pons and the medulla oblongata. The smallest segment of the brain, the mesencephalon, is located below the diencephalon and is thought to play a role in consciousness. Muscle activation, tone and equilibrium is controlled in the pons and cerebellum located below the mesencephalon, and respiratory and cardiac processes are governed by the medulla oblongata, located directly beneath the pons.

The brain contains grey matter and white matter substances that are easily distinguished upon gross examination. Grey matter contains a densely packed network of neural cell bodies and associated glial cells, whereas white matter contains myelinated axonal tracts, relatively few neuronal cell bodies, and a supporting environment of glial cells. The entire brain is surrounded by cerebrospinal fluid contained within an extensive ventricular system that occupies approximately one-tenth of the total brain volume. The ventricular system supports the brain as well as the spinal cord, and provides nutrients to and removes waste products from the central nervous system.

S.S. Margulies (✉)
Department of Bioengineering, University of Pennsylvania,
105D Hayden Hall, Philadelphia, PA 19104-6392, USA

D.F. Meaney
Department of Bioengineering, 105E Hayden Hall, University of Pennsylvania,
Philadelphia, PA 19104-6392, USA

Understanding the response of the complex brain structure to thermal, electrical, or mechanical stimuli necessitates a thorough investigation of the physical properties of each brain component. This task is still in its infancy, and therefore the material cited in this chapter is accompanied by several caveats. First, most properties cited are for whole brain. However, where available, properties of the white matter, gray matter, cerebrum, cerebellum, and brainstem are noted. Second, extensive studies have been conducted on brain tissue from a broad range of species. To provide the reader with information most similar to human tissue, only primate data (nonhuman and human) have been included. Exceptions occur only when there is no primate data available, and are noted. Finally, because the brain is a highly perfused organ and its properties may differ between *in vivo* and *in vitro* conditions, and with the post mortem time period before testing. To facilitate comparison between tests, information regarding *in vivo/in vitro* conditions, post mortem time, and test procedure is included with the data.

B5.2 Composition

Table B5.1 Brain Tissue Composition

	Water (wt%)	Ash (wt%)	Lipid (wt%)	Protein (wt%)
Whole brain	76.3–78.5 (77.4)	1.4–2 (1.5)	9–17	8–12
Grey matter	83–86	1.5	5.3	8–12
White matter	68–77	1.4	18	11–12

Approximate overall ranges given. Values in parentheses indicate averages.
Source: [1–3].

B5.2.1 Mass [2]

Adult male whole brain (20–30 yr): 1400 g
(cerebrum 1200 g, cerebellum, 150 g)
Adult female whole brain (20–30 yr): 1200 g
Adult male whole brain (90 yr): 1161 g

B5.2.2 Dimensions and shape [2]

The adult brain with the brain stem is approximately half an ellipsoid.

Diameter:	Vertical	Transverse	Anteroposterior
Male:	13 cm	14 cm	16.5 cm
Female:	12.5 cm	13 cm	15.5 cm

B5.2.3 Density (adult) in kg/m³

Brain	1030–1041	[2]
Grey matter	1039	[1, 3]
White matter	1043	[1, 3]

B5.3 Mechanical Properties**B5.3.1 Bulk modulus**

Excised brain samples: 2.1×10^6 kPa (independent of frequency) [4].

B5.3.2 Poisson's ratio

Using the relationship $\nu = (3K - E)/6K$

where K is the bulk modulus and E is the elastic modulus, and considering that K is 4–5 orders of magnitude larger than E, brain is approximated as an incompressible material ($\nu = 0.5$) [5].

B5.3.3 Elastic and shear moduli

See Table B5.2.

B5.3.4 Creep modulus

See Table B5.3.

B5.4 Electrical Properties

(no primate data available)

B5.4.1 Electrical conductivity temperature coefficient [14]

Cow and pig whole brain ($\Delta\sigma/\sigma)/\Delta T = 3.2$ °C⁻¹.

Table B5.2 Elastic Modulus and Shear Modulus of Normal Brain at 37°C (typical values, not averages)

Testing technique	Species (post mortuum time)	Frequency (Hz)	Analysis format	Results (kPa)	G_1 (kPa)	G_2 (kPa)	Source
Free vibration	Rhesus monkey (15 min)	31	$E^* = E_1 + i E_2$	$E_1 = 91.2$ $E_2 = 53.9$	30.3	18.0	[6]
Free vibration	Human (6–12 hr)	34	$E^* = E_1 + i E_2$	$E_1 = 66.8$ $E_2 = 26.3$	22.3	8.7	[6]
Harmonic shear	Human white matter (10–62 hr)	9–10	$G^* = G_1 + i G_2$	Min: $G^* = 0.75 + i 0.3$ Max $G^* = 1.41 + i 0.6$	0.75–1.41	0.3–0.6	[7]
Driving point impedance	Rhesus (in vivo)	80	Theoretical approx of data $G^* = G_1 + i G_2$	$G_1 = 19.6$ $G_2 = 11.2$	19.6	11.2	[7, 8]
Quasi-static expansion of balloon within tissue	Rhesus monkey live (in vivo) dead (5–45 min) fixed (formaldehyde)	0	Static elastic Modulus, E_1	$E_1 = 10-60$ live and dead $E_1 = 40-120$ fixed	10–60		[9]
Sudden acceleration of a cylinder filled with tissue	Human	(acceleration duration \approx 17.5 ms.)	compare tissue displacement with that of a Voigt solid cylinder	Shear modulus $G = 1.17-2.19$ kPa (average = 1.7) Kinematic viscosity $\nu = 14-124$ cm ² /s (average = 89)	1.7		[10] (Tissue temp unknown)

Harmonic shear	Human (<3 hr)	5-350 5 15 35 85 105 225 350	$G^* = G_1 + i G_2$	G_1 7.6 8.4 11.7 19.3 21.4 29.0 33.9	G_2 2.8 3.5 5.2 13.4 18.0 45.9 81.4	2.76-81.4	[11]
Harmonic shear	Human (<3 hr) Grey matter Axis 1 Axis 2 Axis 3 average	2-10	$G^* = G_1 + i G_2$	G_1 10.6 6.3 4.1 7.0	G_2 1.5 1.5 1.4 1.5	1.5	[11]
	white matter Axis 1 Axis 2 Axis 3 average	2-10		7.7 7.0 7.3 7.3	2.6 3.2 3.5 3.1	7.0 3.1	

* Assumed tissue is incompressible ($\nu = 0.5$), therefore $G^* = E^*/3$.

Table B5.3 Creep Modulus of Normal Brain at 37°C (typical values, not averages)

Testing technique*	Species	Model	Results	Source
Compression	Rhesus monkey (15 min)	$J(t) = C_1 + C_2 \ln(t)$	$C_1 = 2.97 \text{ kPa}^{-1}$ $C_2 = 0.18 \text{ kPa}^{-1}$ $t > 0.1 \text{ s}$	[6]
Compression	Human (6–12 hr)	$J(t) = C_1 - C_2 \ln(t)$	$C_1 = 2.45 \text{ kPa}^{-1}$ $C_2 = 0.18 \text{ kPa}^{-1}$ $t > 0.1 \text{ s}$	[6]
Compression	Human (6–12 hr)	Nonlinear solid $\epsilon(t) = \frac{\sigma_0 e^{-\mu t}}{k_2} + \left(\frac{\sigma_0}{k_1} + \frac{(k_2^2 + 4\sigma_0 k_3)^{1/2}}{2k_3} - \frac{k_2}{2k_3} \right) \cdot (1 - e^{-\mu t})$ Where $\mu = \frac{K_2}{C_1}$	$K_1 = 25.77 \text{ kPa}$ $K_2 = 20.46 \text{ kPa}$ $K_3 = 104.04 \text{ kPa}$ $C_1 = 651.8 \text{ kPa s}$ $\sigma_0 = 3.44, 4.82, 6.89 \text{ kPa}$	[12]
Compression	Human (6–12 hr)	Nonlinear fluid $\epsilon(t) = \frac{\sigma_0}{K_2} + \frac{C_1 C_2}{2K_1 C_3} - \frac{C_1 (C_2^2 + 4\sigma_0 C_3)^{1/2}}{2K_1 C_3} + \frac{1}{2C_3} [(C_2^2 + 4\sigma_0 C_3)^{1/2} - C_2]$ $\left(t + \frac{C_1}{K_1} e^{-\mu t} \right) + \frac{\sigma_0}{K_1} \left[1 + \frac{C_1}{C_2} (1 - e^{-\mu t}) \right]$	$K_1 = 74.41 \text{ kPa}$ $K_2 = 20.67 \text{ kPa}$ $C_1 = 1266.38 \text{ kPa}$ $C_2 = 36599.7 \text{ kPa s}$ $C_3 = 1.38 \text{ kPa S}^2$ $\sigma_0 = 3.44, 4.82, 6.89 \text{ kPa}$	[12]

<p>Compression</p>	<p>Human (6–12 hr)</p>	<p>Hyperelastic with material dissipation</p> $\frac{\sigma_{11}}{2C_1} = \left[\lambda^2 - \frac{1}{\lambda} \right] \left[1 + \frac{C_2}{C_1 \lambda} \right] + \frac{B_1 \lambda}{C_1 \lambda^3}$ <p>$[\lambda^2 - 6\lambda^3 + 1]$</p>	<p>$C_1 = 6.89 \text{ kPa}$ $C_2 = 17.23 \text{ kPa}$ $B_1 = 0.55 \text{ kPa S}^2$ $\lambda = \text{stretch ratio}$ $\kappa = \text{stretch rate}$</p>	<p>[12]</p>
<p>Fluid infusion</p>	<p>Cat</p>	<p>Poroelectric</p> $\frac{\partial \mathbf{e}}{\partial t} = \kappa (2G + \lambda) \nabla^2 \mathbf{e}$ <p>G = shear modulus $\lambda = \text{Lame constant}$ K = permeability</p>	<p><i>Grey matter</i> $G = 2 \text{ kPa}$ $\lambda = 90 \text{ kPa}$ $\kappa = 7.5 \times 10^{-9} \text{ kPa-m}^2/\text{s}$</p> <p><i>White matter</i> $G = 0.9 \text{ kPa}$ $\lambda = 40 \text{ kPa}$ $\kappa = 5 \times 10^{-9} \text{ kPa-m}^2/\text{s}$</p>	<p>[13]</p>

* All tests consisted of a load applied rapidly and then held constant.

Table B5.4 Electrical conductivity of brain tissues

	Temp (°C)	Conductivity (s) (mS/cm)	Species	Source
Whole brain	37	1.7	cow, pig	[14]
Cerebrum	39	1.38–1.92	rabbit	[15]
Cerebellum	39	1.17–1.64	rabbit	[15]
Cortex	body	3.1	rabbit	[16]
Cortex	37	4.5	cat	[17]
White matter	body	1.0	rabbit	[18]
White matter	37	2.9	cat	[17]

B5.5 Thermal Properties

Table B5.5 Thermal properties of normal, unperfused human brain tissue

	Temp (°C)	Conductivity, (W/m°K)	Diffusivity, (cm ² /s × 10 ³)	Specific heat, (J/g °K)	Source
Whole brain	5–20	0.528	1.38 ± 0.11	–	[19]
Whole brain	37	0.503–0.576	–	–	[20]
Cortex	37	0.515	1.47	–	[21]
	5–20	0.565	1.43 ± 0.09	3.68	[19]
White matter	5–20	0.565	1.34 ± 0.10	3.60	[19]

Values A–B indicate approximate range, values A ± B indicate mean ± standard deviation.

B5.6 Diffusion Properties

5.6.1 Sucrose (feline brain) [22]

D ~ 3.2–3.8 × 10⁻⁶ cm²/sec matter
 ~ 1.3–1.9 × 10⁻⁶ cm²/sec white matter

B5.6.2 Small ions [23]

D ~ 8.6 × 10⁻⁶ cm²/sec

5.6.3 Large molecules (>150 angstrom): [23]

Hindered diffusion occurs

B5.7 Comments

The list of primate brain tissue properties presented in this chapter highlights the numerous areas where data are either unavailable or largely incomplete. With a renewal of interest in modeling the normal and pathological response of the brain to various stimuli, it is possible that some of the missing tissue property data will be generated in the near future. Investigators should be cautioned, however, that because brain tissue properties vary with environmental factors, measurements made under unphysiologic conditions may differ from those of living tissue. As an example, the brain is highly vascularized, and the role of blood flow, volume, and pressure on tissue behavior remains to be determined.

The caution exercised by the experimentalist in generating new data should be matched by sound skepticism on the part of the investigators who are developing analytical or computational models of brain functional and structural response. Although the ability to calculate detailed responses has improved greatly in the past decade, these sophisticated models are limited by the available experimental data used to develop and validate the models. To create a realistic representation of normal or pathological response of the brain, it is essential that the model parameters be based on measured tissue properties and that any conclusions drawn from the models be validated with measured response data. Therefore, it is clear that future experimental studies are needed to determine the properties and response of living primate brain tissue.

Additional Reading

Cooney, D.O. (1976) *Biomedical Engineering Principles: An introduction to fluid, heat and mass transfer processes*, Marcel Dekker, New York.

Provides more detailed examples in bioheat transfer and pharmacokinetics which may be useful in modeling heat and mass transfer in the brain parenchyma.

Fung, Y.C. (1993) *Biomechanics: Mechanical properties of living tissues*, 2nd ed., Springer-Verlag, New York.

Fung, Y.C. (1990) *Biomechanics: Motion, flow, stress and growth*, Springer-Verlag, New York.

Fung, Y.C. (1965) *Foundations of Solid Mechanics*, Prentice Hall, Englewood Cliffs.

These works describe both basic principles of mechanics and their specific applications in biomechanics. A review of the constitutive property relationships for biological tissues included throughout these texts may be particularly helpful for applying the material-property information listed previously.

Lih, M.L. (1975) *Transport Phenomena in Medicine and Biology*, John Wiley & Sons, New York.

A concise review of the principles used in modeling the transport phenomena in several biological systems including examples of heat and mass transfer.

Nolte, J. (1988) *The Human Brain*, 2nd. ed., C.V. Mosby, St Louis

Provides a more detailed review of the structure and function of the different brain regions.

References

1. Duck, F.A. (1990) *Physical Properties of Tissue*, Academic Press, New York.
2. ICRP (1975) *Report of the Task Group on Reference Man*, ICRP Publication 23, International Commission on Radiological Protection, Pergamon Press, Oxford, pp. 212–215; 280–281.
3. Woodard, H.Q. and White, D.R. (1986) The composition of body tissues. *Brit. J. Radiol.*, **59**, 1209–1219.
4. McElhaney, J.H., Roberts, V.L. and Hilyard, J.F. (1976) *Handbook of Human Tolerance*, Japanese Automobile Research Institute, Tokyo, pp. 151.
5. Fung, Y.C. (1993) *Biomechanics: Mechanical properties of living tissues*, 2nd ed., Springer-Verlag, New York.
6. Galford, J.E. and McElhaney, J.H. (1970) A viscoelastic study of scalp, brain, and dura. *J. Biomech.*, **3**, 211–221.
7. Fallenstein, G.T., Hulce, V.D. and Melvin, J.W. (1969) Dynamic mechanical properties of human brain tissue. *J. Biomech.*, **2**, 217–226.
8. Wang, H.C. and Wineman, A.S. (1972) A mathematical model for the determination of viscoelastic behavior of brain in vivo - I: Oscillatory response. *J. Biomech.*, **5**, 431–446.
9. Metz, H., McElhaney, J. and Ommaya, A.K. (1970) A comparison of the elasticity of live, dead, and fixed brain tissue. *J. Biomech.*, **3**, 453–458.
10. Ljung, C. (1975) A model for brain deformation due to rotation of the skull. *J. Biomech.*, **8**, 263–274.
11. Shuck, L.Z. and Advani, S.H. (1972) Rheological response of human brain tissue in shear. *J. Basic Eng., Trans ASME*, **94**, 905–911.
12. Pamidi, M. and Advani, S. (1978) Nonlinear constitutive relations for human brain tissue. *J. Biomech. Eng.*, **100**, 44–48.
13. Basser, P. (1992) Interstitial pressure, volume and flow during infusion into brain tissue. *Microvascular Res.*, **44**, 143–165.
14. Osswald, K. (1937), (Measurement of the conductivity and dielectric constants of biological tissues and liquids by microwave) (Ger.) Messung der Leitfähigkeit und Dielektrizitätskonstante biologischer gewebe und Flüssigkeiten bei kurzen Wellen. *Hochfrequenz Tech. Elektroakustik*, **49**, 40–49.
15. Crile, G.W., Hosmer, H.R. and Rowland, A.F. (1922) The electrical conductivity of animal tissues under normal and pathological conditions. *Am. J. Physiol.*, **60**, 59–106.
16. Ranck, J.B. and Be Merit, S.L. (1963) Specific impedance of rabbit cerebral cortex. *Exp. Neurol.*, **7** 144–152.
17. Freygang, W.H. and Landaw, W.M. (1955) Some relations between resistivity and electrical activity in the cerebral cortex of the cat. *J. Cell. Comp. Physiol.*, **45**, 377–392.
18. van Harreveld, A., Murphy, T. and Nobel, K.W. (1963) Specific impedance of rabbit's cortical tissue. *Am. J. Physiol.*, **205**, 203–207.
19. Cooper, T.E. and Trezek, G.J. (1972) A probe technique for determining thermal conductivity of tissue. *J. Heat Transfer; Trans. ASME*, **94**, 133–140.
20. Bowman, H.F. (1981) Heat transfer and thermal dosimetry. *J. Microwave Power*, **16**, 121–133.
21. Valvano, J.W., Cochran, J.R. and Diller, K.R. (1985) Thermal conductivity and diffusivity of biomaterial measured with self-heating thermistors. *Int. J. Thermophys.*, **6**, 301–311.
22. Rosenberg, G.A., Kyner, W.T. and Estrada, E. (1980) Bulk flow of brain interstitial fluid under normal and hypermolar conditions. *Am. J. Physiol.*, **238**, f42–f49.
23. Nicholson, C. (1985) Diffusion of a substance in brain tissue with arbitrary volume fraction and tortuosity. *Brain Research*, **33** 325–329.

Chapter B6

Arteries, Veins and Lymphatic Vessels

X. Deng and R. Guidoin

B6.1 Introduction

Blood and lymphatic vessels are soft tissues with densities which exhibit nonlinear stress-strain relationships [1]. The walls of blood and lymphatic vessels show not only elastic [2, 3] or pseudoelastic [4] behavior, but also possess distinctive inelastic character [5, 6] as well, including viscosity, creep, stress relaxation and pressure diameter hysteresis. The mechanical properties of these vessels depend largely on the constituents of their walls, especially the collagen, elastin, and vascular smooth muscle content. In general, the walls of blood and lymphatic vessels are anisotropic. Moreover, their properties are affected by age and disease state. This section presents the data concerning the characteristic dimensions of arterial tree and venous system; the constituents and mechanical properties of the vessel walls. Water permeability or hydraulic conductivity of blood vessel walls have been also included, because this transport property of blood vessel wall is believed to be important both in nourishing the vessel walls and in affecting development of atherosclerosis [7–9].

The data are collected primarily from human tissue but animal results are also included in places for completeness. Among the three kinds of vessels, the arte-

X. Deng (✉) • R. Guidoin
Laboratoire de Chirurgie Exp Agriculture Services,
Room 1701 Services Building Université Laval, Québec G1K 7P4, Canada

rial wall has been extensively investigated while studies of lymphatic vessels are very rare.

B6.2 Morphometry of the Arterial Tree and Venous System

Detailed measurements of the number and size of blood vessels in the living body are very difficult to perform, so reliable information is scarce. Moreover, data collected on vessels in one tissue or organ are not applicable to another. Thus one should be cautious in using morphometric data; only the data for large vessels are reliable.

The aorta is tapered, but most other arteries can be considered to have a constant diameter between branches. The rate of taper varies from individual to individual, presumably, between species. However, in the dog, the change of aortic cross sectional area can be described by the exponential equation:

$$A = A_0 e^{(-\beta x / R_0)} \quad (\text{B6.1})$$

Table B6.1 Morphometric and Related Properties of the Human Systemic Circulation*

Vessel	Diameter (mm)	Wall thickness (mm)	Length (cm)	Blood velocity (cm/sec)	Reynolds number
Ascending aorta	32	1.6	5–5.5	63	3600–5800
Arch of aorta	25–30		4–5		
Thoracic aorta	20	1.2	16	27	1200–1500
Abdominal aorta	17–20	0.9	15		
Femoral artery	8	0.5	32		
Carotid artery	9	0.75	18		
Radial artery	4	0.35	23		
Large artery	2–6			20–50	110–850
Capillaries	0.005–0.01			0.05–0.1	0.0007–0.003
Large veins	5–10			15–20	210–570
Vena cava	20			11–16	630–900

* Source [11–17]. Note: The Reynolds numbers were calculated assuming a value for the viscosity of the blood of 0.035 poise.

Table B6.2 Morphometries of the Pulmonary Arterial System*

Zone	Number of branches	Diameter (mm)	Length (mm)
Proximal	1.000	30.000	90.50
	3.000	14.830	32.00
	8.000	8.060	10.90
	2.000 x 10	5.820	20.70
	6.600 x 10	3.650	17.90
	2.030 x 10 ²	2.090	10.50
	6.750 x 10 ²	1.330	6.60
	2.290 x 10 ³	0.850	4.69
Intermediate	5.861 x 10 ³	0.525	3.16
	1.756 x 10 ⁴	0.351	2.10
	5.255 x 10 ⁴	0.224	1.38
	1.574 x 10 ⁵	0.138	0.91
Distal	4.713 x 10 ⁵	0.086	0.65
	1.411 x 10 ⁶	0.054	0.44
	4.226 x 10 ⁶	0.034	0.29
	1.266 x 10 ⁷	0.021	0.20
	3.000 x 10 ⁸	0.013	0.13

* Source: Adapted from [18].

Note: The data were obtained from a 32-year-old woman who had been free of respiratory disease and died of uremia. For the purpose of description, the pulmonary arterial tree was divided into three zones.

where A is the cross sectional area of the aorta, A_0 and R_0 are the respective cross sectional area and radius at the upstream site, x is the distance from the upstream site, and β a taper factor, which varies between 0.02 and 0.05 [10]. In man, the taper is found not to be as smooth as implied by the above equation; thus values of β are unavailable.

Morphometric and related data are given in Tables [B6.1](#), [B6.2](#) and [B6.3](#).

B6.3 Constituents of the Arterial Wall

B6.3.1 Normal arterial wall

The main constituents of normal human arterial tissues from young adult subjects (20–39 years) are listed in Table [B6.4](#) [20]. The major part of the dry matter in the arterial wall consists of proteins such as elastin and collagen. Because the importance of elastin and collagen in the mechanical properties of arterial wall, the composition of media and adventitial layers in terms of collagen, elastin, smooth muscle and ground substance is listed in Table [B6.5](#) for three different arterial tissues [1].

Table B6.3 Morphometric and Related Properties of the Canine Systemic Circulation*†

Site	Ascending aorta	Descending aorta	Abdominal aorta	Femoral artery	Carotid artery	Arteriole	Capillary	Venule	Vena cava, inferior	Pulmonary artery, main
Internal diameter, d_i (cm)	1.5 (1.0–2.4)	1.3 (0.8–1.8)	0.9 (0.5–1.2)	0.4 (0.2–0.8)	0.5 (0.2–0.8)	5×10^{-3} ($1-8 \times 10^{-3}$)	6×10^{-4} ($4-8 \times 10^{-4}$)	4×10^{-3} ($1-7.5 \times 10^{-3}$)	1.0 (0.6–1.5)	1.7 (1.0–2.0)
Wall thickness, h (cm)	0.065 (0.05–0.08)	–	0.05 (0.04–0.06)	0.04 (0.02–0.06)	0.03 (0.02–0.04)	2×10^{-3}	1×10^{-4}	2×10^{-4}	0.015 (0.01–0.02)	0.02 (0.01–0.03)
h/d_i	0.07 (0.055–0.084)	–	0.06 (0.04–0.09)	0.07 (0.055–0.11)	0.08 (0.055–0.095)	0.4	0.17	0.05	0.015	0.01
<i>In vivo</i> length (cm)	5	20	15	10	15 (10–20)	0.15 (0.1–0.2)	0.06 (0.02–0.1)	0.15 (0.1–0.2)	30 (20–40)	3.5 (3–4)
Cross-section area (cm ²)	2	1.3	0.6	0.2	0.2	2×10^{-5}	3×10^{-7}	2×10^{-5}	0.8	2.3
Total vascular cross-section at each level (cm ²)	2	2	2	3	3	125	600	570	3.0	2.3
Blood velocity (peak) (ms ⁻¹)	0.2 (0.4–2.9)	1.05 (0.25–2.5)	0.55 (0.5–0.6)	1.0 (1.0–1.2)	–	0.75	0.07	0.35	0.25 (0.15–0.4)	0.7
Blood velocity (mean) (ms ⁻¹)	0.2 (0.1–0.4)	0.2 (0.1–0.4)	0.15 (0.08–0.2)	0.1 (0.1–0.15)	–	$(5-10 \times 10^{-3})$	$2-17 \times 10^{-4}$	$2-5 \times 10^{-3}$	–	0.15 (0.06–0.28)
Peak Reynolds number, Re	4500	3400	1250	1000	–	0.09	0.001	0.035	700	3000

* Source: Adapted from [19].

† Normal values for canine cardiovascular parameters. An approximate average value, and then the range, is given where possible. All values are for the dog except those for arteriole, capillary, and venule, which have only been measured in smaller mammals.

Table B6.4 Composition of Normal Arterial Tissue*

	Components	Aorta (human)	Femoral artery (human)	Brachial artery (human)
Organic	Dry matter	28.0†	25.3	26.3
	Nitrogen	4.1	3.5	–
	Total lipids	1.680	–	–
	Cholesterol	0.290	0.135	0.185
Inorganic	Total ash	0.730	0.675	0.670
	Calcium	0.070	0.147	0.144
	Total PO ₄	0.375	–	–

* Source: Adapted from [20].

† Values are expressed in percentage of wet tissue weight.

Table B6.5 Composition of Human Arteries at *In Vivo* blood Pressure

	Thoracic aorta	Plantar artery	Pulmonary artery
<i>Media</i>			
Smooth muscle	33.5 ± 10.4†	60.5 ± 6.5	46.4 ± 7.7
Ground substance	5.6 ± 6.7	26.4 ± 6.4	17.2 ± 8.6
Elastin	24.3 ± 7.7	1.3 ± 1.1	9.0 ± 3.2
Collagen	36.8 ± 10.2	11.9 ± 8.4	27.4 ± 13.2
<i>Adventitia</i>			
Collagen	77.7 ± 14.1	63.9 ± 9.7	63.0 ± 8.5
Ground substance	10.6 ± 10.4	24.7 ± 2.6	25.1 ± 8.3
Fibroblasts	9.4 ± 11.0	11.4 ± 2.6	10.4 ± 6.1
Elastin	2.4 ± 3.2	0	1.5 ± 1.5

* Source: Adapted from [1].

† (Mean ± S.D.)

The collagen in adventitia and media is mostly Type III, some Type I, and a trace of Type V while the collagen of the basal lamina is Type IV [1].

Table B6.6 lists the constituents of additional arteries (canine), and the the ratio of collagen to elastin [21].

Composition changes of arterial tissues with age

The composition of normal human arterial tissues is altered with age in many aspects. Table B6.7 lists the observed changes in human aorta, pulmonary and femoral arteries [20]. There is a tendency that both the dry matter and nitrogen content of arterial tissues decreases with age. However, the relative quantity of collagen [22] and elastin [23, 24] in the arterial wall remains almost unchanged with age. Below the age of 39, the wall of human thoracic aorta has $32.1 \pm 5.5\%$ elastin, between the age 40–69, the wall contains $34.4 \pm 9.3\%$, and from 70–89, the elastin content is 36.5 ± 10.1 [24].

Table B6.6 Arterial Wall Constituents, and Ratio of Collagen to Elastin*

Artery	n [†]	Percentage of wet tissue			Percentage of dry defatted tissue			C	
		H ₂ O	Extracted fat+H ₂ O		Collagen	Elastin	Collagen+ elastin	E	
Coronary	9	63.2 ± 1.0 [‡]	71.5 ± 1.4		47.9 ± 2.6	15.6 ± 0.7	63.5 ± 2.7	3.12 ± 0.21	
Aorta, ascending	9	73.8 ± 0.6	74.0 ± 0.5		19.6 ± 1.2	41.1 ± 2.1	60.7 ± 2.2	0.49 ± 0.04	
Carotid	6	71.1 ± 0.1	71.2 ± 0.1		50.7 ± 2.1	20.1 ± 1.0	70.8 ± 2.5	2.55 ± 0.13	
Aorta, abdominal	10	70.4 ± 0.4	70.8 ± 0.3		45.5 ± 1.7	30.1 ± 1.7	75.6 ± 1.8	1.58 ± 0.15	
Cranial mesenteric, proximal	10	70.8 ± 0.5	71.6 ± 0.4		38.1 ± 1.7	26.5 ± 1.7	64.6 ± 1.8	1.51 ± 0.15	
Cranial mesenteric, distal	9	71.4 ± 0.4	72.0 ± 0.4		37.4 ± 1.4	22.4 ± 1.5	59.8 ± 1.6	1.72 ± 0.11	
Cranial mesenteric, branches	10	69.5 ± 0.6	73.1 ± 0.7		36.1 ± 1.5	21.8 ± 0.9	57.9 ± 1.7	1.69 ± 0.10	
Renal	9	70.4 ± 0.7	70.8 ± 0.7		42.6 ± 1.6	18.7 ± 1.8	61.3 ± 2.1	2.46 ± 0.27	
Femoral	10	68.0 ± 0.3	68.1 ± 0.3		44.5 ± 1.4	24.5 ± 1.6	69.0 ± 2.1	1.89 ± 0.14	

* Source: [21] by permission.

[†] Number of specimens.[‡] Specimens slightly dehydrated owing to unavoidably long dissection. Mean ± standard deviation. All percentage values refer to w/w.

Table B6.7 Variation of Normal Human Arterial Tissue Composition with Age*

Aorta										
Age group (years)	Dry matter	Nitrogen	Total lipids	Cholesterol	Total ash	Calcium	Total PO ₄	Acid soluble PO ₄	Potassium	
10-19	29.5†	4.38	1.23	0.15	—	0.03	0.25	0.16	0.055	
30-39	28.5	4.03	1.75	0.28	0.81	0.09	0.40	0.29	0.040	
50-59	28.0	3.67	1.90	0.48	1.55	0.21	0.54	0.41	0.039	
70-79	28.0	3.38	—	0.71	2.80	0.39	—	—	0.033	
Pulmonary artery						Femoral artery				
Age group (years)	Dry matter	Nitrogen	Cholesterol	Calcium	Potassium	Dry Matter	Nitrogen	Cholesterol	Total ash	Calcium
10-19	26.5	3.91	0.12	0.025	0.033	26.9	3.84	0.11	0.59	0.14
30-39	25.7	3.71	0.17	0.028	0.031	24.4	3.30	0.15	0.71	0.18
50-59	24.9	3.45	0.22	0.027	0.026	22.8	2.83	0.23	1.15	0.40
70-79	23.0	3.25	—	0.060	0.025	25.3	2.90	0.55	3.17	1.07

* Source: Adapted from [20]; see for additional age group values.

† Values expressed in percentage of wet tissue weight.

Table B6.8 Effect of Hypertension on Composition of Arteries*

Group	N‡	dry wt (mg)	Elastin (E)		Collagen (C)		E and C (% total wt)
			Wt(mg)	(% total wt)	WT(mg)	(% total wt)	
III C†	2	5.25	1.76	33.5	0.69	13.1	46.6
		5.58	2.20	39.0	0.83	14.3	53.3
III H†	2	7.00	2.86	41.6	1.44	20.6	62.2
		6.50	2.78	42.8	1.06	16.3	59.1
IIC	2	4.96	2.23	44.9	0.72	14.5	59.4
		5.26	2.14	40.6	0.68	12.8	53.4
IIH	2	8.12	2.94	36.2	1.68	20.7	56.9
		7.50	2.70	36.0	1.52	20.3	56.3
IC	2	4.36	1.91	43.8	1.12	25.7	69.5
		5.56	2.09	37.6	1.24	22.3	59.9
IH	2	8.88	3.08	34.7	2.08	23.4	58.1
		10.89	3.50	32.1	2.33	21.4	53.5
		P<0.01#	P<0.001	P>0.2	P<0.01	P=0.2	P>0.8

* Source[25] by permission: †: N = number of animals (rats); C = normotensive; H - hypertensive. #: Normotensive vs. hypertensive

Table B6.9 Effect of Atherosclerosis on Comparison of Arteries*

Site	H ₂ O (g/kg wet wt)	Collagen (% dry wt)	Elastin (% dry wt)	Collegen + Elastin (% dry wt)	Collegen Elastin
Carotid Control (n = 11)	740±3†	50.6±0.8	28.0±0.3	78.6±0.8	1.81±0.04
Diet (n = 7)	764±7##	49.8±1.6	33.1±1.3##	84.2±1.9##	1.61±0.07#
Iliac Control (n = 16)	742±3	46.2±0.6	33.0±0.7	79.2±1.1	1.41±0.03
Diet (n = 5)	724±6##	37.8±2.0	25.1±1.2##	66.0±2.3##	1.49±0.02#

* Source: (26) by permission; canine subjects.

† means ± SE.

Significantly different, P < 0.01; # Significantly different, P < 0.05.

Changes in elastin and collagen content due to hypertension

Experimental observation by Wolinsky [25] showed that the absolute amounts of both elastin and collagen contents increased in hypertensive rats; however, the percentage of these elements remained essentially constant (Table B6.8)

Table B6.10 Composition of Normal Human Venous Tissue*

	Femoral vein	Vena cava, inferior
Dry matter	28.0†	26.1
Nitrogen	4.08	–
Cholesterol	0.076	0.083
Total ash	0.590	–
Calcium	0.058	0.012
Potassium	–	0.065

* Source: adapted from [27].

† Percentage of wet tissue weight.

Changes in elastin and collagen content due to atherosclerosis

Table B6.9 lists the changes in elastin and collagen contents of canine carotid and iliac arteries due to dietary atherosclerosis [26]. In the iliac site the ratio of collagen to elastin was increased, while the ratio in the carotid site was decreased.

B6.4 Constituents of the venous wall

B6.4.1 Normal venous wall

The main constituents of normal human venous tissue are listed in Table B6.10.

Table B6.11 Composition of Normal Human Venous Tissue*

Femoral vein					
Age group	Dry matter	Nitrogen	Cholesterol	Total ash	Calcium
0–9	31.1 †	4.63	0.058	0.525	0.051
20–29	27.4	3.88	0.071	0.586	0.053
40–49	24.7	3.34	0.064	0.542	0.065
60–69	23.2	3.06	0.087	0.555	0.075
70–79	21.8	2.92	0.087	0.600	0.083
<i>Vena cava, inferior</i>					
Age group	Dry matter	Nitrogen	Cholesterol	Calcium	Potassium
0–9	30.9	–	–	–	–
20–29	26.8	–	0.082	0.011	0.072
40–49	24.5	–	0.091	0.011	0.053
60–69	21.7	–	0.097	0.010	0.048
70–79	22.7	–	0.097	0.011	0.048

* Source: [27] by permission.; see source for additional age groups.

† Percentage of wet tissue weight.

Table B6.12 Mechanical Properties of Layers of the Vascular Wall*

Material	Young’s modulus (dynes/cm ²)	Relative extensibility ^a (cm)	Maximum extension (%)	Tensile strength (dynes/cm ²)
Elastin	3 to 6 × 10 ⁶	10	100–220	3.6 × 10 ⁶ to 4.4 × 10 ⁷
Collagen	1 × 10 ⁹ to 2.9 × 10 ¹⁰	0.03	5.50	5 × 10 ⁷ to 5 × 10 ⁹
Smooth muscle				
Relaxed	6 × 10 ⁴	–	300	–
Contracted	1 × 10 ⁵ to 12.7 × 10 ⁶	2.3	300	–

* Source: Adapted from [28]; Fiber 10 em in length, 1 mm² cross section, sustaining a load of 30 g.

B6.4.2 Changes with age in composition of normal venous tissues

The changes with age in the composition of normal venous vessels are listed in Table B6.11.

B6.5 Mechanical Properties of Arteries

The blood vessel wall consists of three layers: the intima, media, and adventitia. The intima contains mainly the endothelial cells that contribute little to the strength of the blood vessels. The media and the adventitia contain smooth muscle cells, elastin and collagen. Elastin is the most ‘linearly’ elastic biosolid material known. Unlike elastin, collagen does not obey Hooke’s Law. However, collagen is the main load carrying element of blood vessels. Table B6.12 lists the mechanical properties of tissues composing the blood vessel wall.

B6.5.1 Static mechanical properties of arteries

Studies of arterial wall mechanics have clearly established the anisotropic nature of arteries [1, 29, 30]. *In vivo* pressurized arteries are deformed simultaneously in all directions. But, experimental studies [31] have demonstrated that arteries deform orthotropically. Therefore, arterial deformations may be examined in three orthogonal directions, namely, the longitudinal, circumferential, and radial directions. There are nine elastic parameters: the three elastic moduli, E_θ , E_z and E_r ; and six Poisson’s ratios, $\sigma_{r\theta}$, $\sigma_{\theta r}$, $\sigma_{z\theta}$, $\sigma_{\theta z}$, σ_{rz} and σ_{zr} . As far as hemodynamics is concerned however, among the three elastic moduli the circumferential one is most important.

The circumferential elastic modulus is termed the incremental modulus and determined by the following equation (B6.2):

$$E_\theta = \frac{\Delta p_i 2(1 - \sigma^2) R_0 R_i^2}{\Delta R_0 (R_0^2 - R_i^2)} \quad (\text{B6.2})$$

Table B6.13 Elastic Modulus of Human Arteries*

Arterial segment	$E_\theta (\times 10^6 \text{ dynes/cm}^2)$
Thoracic aorta	4.0–10
Abdominal aorta	4.0–15
Iliac artery	8.0–40
Femoral artery	12–40
Carotid artery	3.0–8.0

* Source: Adapted from [33,34]; young subjects (≤ 30 years) at a transmural pressure of 100 mmHg.

Note: The circumferential elastic moduli were calculated assuming that the arterial walls have a Poisson’s ratio (the ratio of transverse to longitudinal strain) of 0.5.

Table B6.14 Hydrodynamic Properties of the Aorta*

Thoracic aorta			
Age (yrs)	Z_o (mmHgS cm ³)	V_p (m/s)	E_o^\dagger (10 ⁶ N/m ²)
30–39	0.13	5.8	0.56
40–49	0.17	7.4	0.8
50–59	0.19	9.0	1.13
60–69	0.19	10.0	1.25
70–79	0.22	12.4	1.87
80–89	0.22	13.6	2.2
Abdominal aorta			
Age (yrs)	Z_o (mmHgS cm ³)	V_p (m/s)	E_o^\dagger (10 ⁶ N/m ²)
30–39	0.31	7.9	0.8
40–49	0.53	10.5	1.22
50–59	0.53	11.4	1.3
60–69	0.51	12.0	1.5
70–79	0.68	14.5	1.75

* Adapted from [35] by permission;

† Poisson's ratio of arterial wall assumed to be 0.5.

where Δp_i is the transmural pressure increment, R_o and R_i are the respective external and internal diameter of the vessel, ΔR_o is the change in the external diameter due to Δp_i , and σ the Poisson's ratio (the ratio of transverse strain to longitudinal strain). The detailed technique for measuring the circumferential incremental elastic modulus of the arteries was described by Bergel [32].

Table B6.13 presents the circumferential incremental elastic modulus of human arterial walls from young adults (≤ 35 years) at a transmural pressure of 100 mmHg.

Experimental data by Bader [34] demonstrated that the circumferential elastic modulus of human thoracic aorta increased almost linearly with age. Table B6.14 gives the variation with age in the elastic moduli for human thoracic and abdominal aorta at a pressure of 100 mmHg.

It should be mentioned that all the circumferential elastic moduli given in Table B6.14 are based on the assumption of a Poisson's ratio of 0.5. This is not strictly true when large strains are considered [36]. Patel *et al.* [37] measured Poisson's ratios for the aorta in living dogs at a transmural pressure of about 110 mmHg, as well as the circumferential, longitudinal and radial incremental elastic moduli and determined that individual values vary between 0.29 and 0.71.

B6.5.2 Compliance, pressure cross-sectional area relationship, and retraction

By measuring the static elastic properties of human thoracic and abdominal aortas *in vitro*, Langewouters *et al.* [35] proposed the following empirical relationship between the cross-sectional area of the lumen (A) and the pressure in the vessel (p):

$$A(p) = A_m \left\{ \frac{1}{2} + \frac{1}{\pi} \tan^{-1} \left(\frac{p - p_0}{p_1} \right) \right\} \quad (\text{B6.3})$$

in which A_m , P_0 and p_1 are three independent parameters that are defined in Equation (B6.4) below.

Another important mechanical property of blood vessels is the compliance. Langewouters *et al.* [35] defined the ‘static’ compliance as the derivative of equation (B6.3) with respect to pressure

$$C(p) = \frac{C_m}{1 + \left(\frac{p - p_0}{p_1} \right)^2}; C_m = \frac{A_m}{\pi p_1} \quad (\text{B6.4})$$

where C_m and A_m are the maximum compliance and the maximum cross-sectional area of the vessel, respectively; P_0 is the pressure at which aortic compliance reaches its maximum; and p_1 is the half-width pressure, i.e. at $p_0 \pm p_1$, aortic compliance is equal to $C_m/2$. According to Langewouters *et al.* [35], the ‘static’ compliance values of human thoracic aorta at 100 mmHg range from 1.9 to $17 \times 10^{-3} \text{ cm}^2/\text{mmHg}$; and 0.6 to $4.4 \times 10^{-3} \text{ cm}^2/\text{mmHg}$ for abdominal aorta.

Table B6.15 lists the relative wall thickness and the retraction on excision for a variety of blood vessels. The retraction of a vessel is the amount by which a segment of vessel shortens on removal from the body, expressed as a percentage of the length of the segment *in situ*. The relative wall thickness is the ratio of wall thickness to mean diameter of the vessel.

B6.5.3 Tensile properties of human arteries

Table B6.16 presents typical data for the tensile properties of arterial tissues from Yamada [43]. The test specimens of tissues were strips each with a reduced middle region 10 mm length, 2–3 mm in width, and a length to width ratio of 3:1. In the tables:

1. Tensile breaking load per unit width (g/mm) = ultimate tensile strength (g/mm^2) x thickness (mm)
2. Ultimate tensile strength (g/mm^2) = $\frac{\text{tensile breaking load (g)}}{\text{cross-section area of the test section}}$

Table B6.15 Relative Wall Thickness and Retraction on Excision of Various blood Vessels*

<i>Vessel</i>	<i>Species</i>	$\gamma \times \%$	<i>Retraction %</i>	<i>Source</i>
Thoracic aorta	Dog	10.5	32	[2]
Abdominal aorta	Dog	10.5	34	[2]
Femoral artery	Dog	11.5	42	[2]
Carotid artery	Dog	13.2	35	[2]
Iliac artery	Dog	–	40	[2]
Carotid artery	Dog	13.6	–	[38]
Carotid artery	Cat	14.5	–	[38]
Carotid artery	Rabbit	11.2	–	[38]
Carotid sinus	Dog	20.0	–	[38]
Carotid sinus	Cat	16.0	–	[38]
Carotid sinus	Rabbit	12.0	–	[38]
Thoracic aorta	Dog	14.0	–	[39]
Abdominal aorta	Dog	12.0	–	[39]
Femoral artery	Dog	13.0	–	[39]
Pulmonary artery	Man	2.0	–	[40]
Abdominal vena cava	Dog	2.3	30	[41]
Thoracic aorta	Man	6–9	25–15	[33]†
Abdominal aorta	Man	8–13	30–17	[33]†
Femoral artery	Man	12–19	40–25	[33]†
Carotid artery	Man	2–15	25–18	[33]†

Source: Adapted from [42].

† Measurement from [33] of young (<35) and old (>35) subjects respectively.

Table B6.16 Tensile Properties of Human Coronary Arterial Tissue* (Longitudinal Direction)

<i>Age (yrs)</i>	<i>Tensile Breaking Load/Unit width (g/mm)</i>	<i>Ultimate Tensile Strength (g/mm²)</i>	<i>Ultimate Elongation (%)</i>
10–19	85±3.1	140±3.0	99±2.4
20–39	82±1.8	114±9.3	78±1.6
40–59	82±1.8	104±4.7	68±3.5
60–79	79±2.9	104±4.7	4.5±3.8
Adult (average)	81	107	64

* Adapted from [43].

$$3. \text{ Ultimate percentage elongation}(\%) = \frac{\text{breaking elongation (mm)}}{\text{original length of the specimen (mm)}} \times 100$$

Table B6.16 lists the tensile data for human coronary arterial tissue in the longitudinal direction.

Other arteries have similar properties [43]. Yamada [43] provides the tensile properties of animal tissues in various tables.

B6.5.4 Dynamic mechanical properties of arteries

The most direct way to study arterial viscoelasticity is to determine the response of the test tissue to oscillatory stresses. If the arterial wall is conceived to be represented by a simple Kelvin-Voigt model consisting of a spring and a dashpot in parallel, the dynamic elastic component and the viscous component of a vessel can be expressed as

$$\begin{aligned} E_D &= \mathbf{E} \cos \phi \\ \eta\omega &= \mathbf{E} \sin \phi \end{aligned} \tag{B6.5}$$

where \mathbf{E} is the complex dynamic elastic modulus that is identical to the incremental elastic modulus under static stresses; ϕ is the phase lag of the strain behind the stress (in the case of circumferential direction, it is the phase lag of diameter behind the pressure); E_D is the dynamic elastic modulus of the vessel; and $\eta\omega$ is the viscous retarding modulus (η is the viscous constant and w the angular frequency). For measuring the circumferential dynamic mechanical properties, the test vessel is usually subjected to an oscillatory pressure. The pressure oscillations are in a sinusoidal form. In circumferential direction, \mathbf{E} can be calculated from equation (B6.2) with the recorded diameter of the blood vessel and the oscillatory pressure [44].

Table B6.17 lists the dynamic mechanical properties of different arteries at a frequency of 2.0 Hz at a mean pressure of 100 mmHg. In this table, E_p is the circumferential pressure-strain modulus defined as

Table B6.17 Circumferential Dynamic Mechanical Properties of Different Human Arteries*

Vessel	E_p (dynes-cm ⁻² x 10 ⁻⁶)	Φ (radians)	V_p (m/s)	Source
Ascending aorta	0.8	–	6.0	[29]
Carotid	6.2	–	17	[29]
Carotid	0.4	–	4.6 ⁺	[45]
Thoracic aorta	0.6–1.0	0.12	6–9 ⁺	[33] ⁺⁺
Abdominal aorta	0.7–1.5	0.1	6–8 ⁺	[33] ⁺⁺
Femoral	2.5–7.0	0.15	13–18	[33] ⁺⁺
Carotid	2.5–3.0	0.1	–	[33] ⁺⁺
Pulmonary artery	0.1–0.16	–	2.3–2.9	[29]

* Adapted from [42].

Elastic modulus and pulse-wave velocity values collected from the literature. Those values for the PWV marked thus: + were measured, the others have been calculated from dynamic elasticity measurements; ++ measurements for young (<35) and old (>35) subjects respectively. Φ = phase difference between wall stress and strain at 2 Hz. E_p is defined in eq (B6.6). The mean pressure was 100 mmHg.

$$E_p = \Delta P_i R_o / \Delta R_o \tag{B6.6}$$

in which ΔP_i is the pressure increment, R_o is the external diameter of the vessel and ΔR_o the external diameter change. E_p is essentially a reciprocal of the compliance of an artery and differs from elastic modulus in that it defines the stiffness of the total artery. Nevertheless, it is an indication of E_D .

Another important parameter listed in Table B6.17 is the pulse-wave velocity V_p (PWV) that can be calculated from the Moens-Korteweg equation:

$$V_p^2 = Eh/2R_p \tag{B6.7}$$

where E = elastic modulus of the wall, h = wall thickness, R = mean radius of the vessel, ρ = density of blood.

There is general understanding that the dynamic elastic modulus is not strongly frequency dependent above 2–4 Hz and that it increases from the static value at quite low frequencies. Bergel [42] provides additional values for canine vessels.

B6.5.5 Creep and stress relaxation

When a subject is suddenly strained and then the strain is maintained constant afterward, the corresponding stresses induced in the subject decrease with time, this phenomenon is called stress relaxation. If the subject is suddenly stressed and then the stress is maintained afterwards, the subject continues to deform, this phenomenon is called creep. Creep and stress relaxation are another two important phenomena in the arterial viscoelasticity. Langewouters *et al.* [46] studied the creep responses of human thoracic and abdominal aortic segments. The pressure in the segments was changed in steps of 20 mmHg between 20 and 180 mmHg. Aortic

Table B6.18 Creep Constants of Human Thoracic and Abdominal Aortas*

Parameter	Thoracic aorta (n = 35)			Abdominal aorta (n = 16)		
	Range	Mean	S.D.	Range	Mean	S.D.
α_1	0.05–0.13	0.076	0.017	0.05–0.12	0.078	0.017
α_2	0.03–0.15	0.102	0.028	0.07–0.15	0.101	0.025
t_1 (S)	0.31–1.43	0.73	0.29	0.33–0.81	0.61	0.12
t_2 (S)	5.9–23.5	14.0	4.1	4.6–17.7	12.1	3.4
$C \left(\frac{10^{-3} \text{ cm}^2}{\text{mmHg}} \right)$	1.5–12.3	5.1	2.5	0.5–3.3	1.5	0.78
Age	30–78	63	14	30–78	58	15

* Adapted from [46] by permission.

α_1, α_2 , creep fractions; t_1, t_2 , time constants; C , compliance; S.D., standard deviation.

creep curves at each pressure level were described individually by a constant plus biexponential creep model (C-model, [47])

$$A_i^c = \Delta A \left[1 - \alpha_1 \exp\left(\frac{-t_i}{\tau_1}\right) - \alpha_2 \exp\left(\frac{-t_i}{\tau_2}\right) \right] \tag{B6.8}$$

where A = aortic cross-sectional area; A_i^c = sample value of aortic creep response at time t_i ; δA = change in aortic area upon a 20 mmHg pressure step; t = time; i = sample number; α_1, α_2 = creep fraction; τ_1, τ_2 = time constant. Table B6.18 lists the creep fractions and time constants for all aortic segments [46].

Stress relaxation relations for human arteries are not available; however, Tanaka and Fung [48] studied the stress relaxation spectrum of the canine aorta. They expressed the stress history with respect to a step change in strain in the form:

$$T(t, l) = G(t) \cdot T^{(e)}(l), G(0) = 1 \tag{B6.9}$$

where $G(t)$ is the normalized relaxation function of time; $T^{(e)}(l)$ is a function of strain l , called elastic response. This is the tensile stress instantaneously generated in the aortic tissue when a step elongation, l , is imposed on the specimen.

If the relaxation function is written as:

$$G(t) = \frac{1}{A} \left[1 + \int_0^\infty s(\tau) e^{-t/\tau} d\tau \right] \tag{B6.10}$$

in which

$$A = \left[1 + \int_0^\infty s(\tau) d\tau \right]$$

is a normalized factor, then the spectrum $S(t)$ is expected to be a continuous function of relaxation time t . A special form of $S(t)$ is proposed

$$\begin{aligned} S(t) &= c / t \text{ for } t_1 \leq t \leq t_2 \\ &= 0 \text{ for } t_1 < t_1, t > t_2 \end{aligned} \tag{B6.11}$$

Values for segments of the canine aorta are given in [48].

Table B6.19 Comparison of elastic Moduli between Venous and arterial Segments*

Pressure (cm H ₂ O)	Extension ratio		Incremental venous elastic modulus		Carotid artery Incremental modulus	
	λ_0	λ_z	E_0 (dynes/cm ² x 10 ⁶)	E_z (dynes/cm ² x 10 ⁶)	E_0 (dynes/cm ² x 10 ⁶)	E_z (dynes/cm ² x 10 ⁶)
<i>Canine Jugular Vein</i>						
10	1.457	1.481	15 ± 3*	1.2 ± 0.18†	7.62	5.16
25	1.463	1.530	47 ± 6†	4.4 ± 0.35†	8.39	7.15
50	1.472	1.597	88 ± 7†	11.8 ± 2.1	9.51	10.69
75	1.478	1.646	98 ± 7†	46 ± 13*	10.37	13.97
100	1.482	1.675	117 ± 10†	67 ± 25	10.92	16.24
125	1.484	1.686	134 ± 24†	89 ± 32	11.16	17.17
150	1.484	1.686	171 ± 9†	113 ± 13†	11.16	17.17
<i>Human Saphenous Vein</i>						
10	1.357	1.169	0.27 ± 0.12†	1.61 ± 0.32*	5.30	0.017
25	1.417	1.206	0.65 ± 0.13†	2.03 ± 0.39*	5.82	0.328
50	1.500	1.266	1.89 ± 0.41†	2.75 ± 0.78	6.00	0.735
75	1.561	1.325	9.85 ± 1.6	3.18 ± 0.76	9.66	1.80
100	1.602	1.381	15.0 ± 2.6	3.56 ± 0.58	12.77	3.15
125	1.621	1.430	20.4 ± 1.6*	3.98 ± 0.96	14.79	4.59
150	1.621	1.470	25.1 ± 7.5	4.75 ± 1.2	15.51	5.93

* Adapted from [50] by permission.

* p < 0.05 for the comparison between the venous and carotid moduli.

† P < 0.01 for the comparison between the venous and carotid moduli.

B6.6 Mechanical Properties of veins

B6.6.1 Static mechanical properties of veins

The structure of the venous walls is basically similar to that of the arterial walls. The main difference is that they contain less muscle and elastic tissue than the arterial walls, which raises the static elastic modulus two to fourfold [49]. Because the venous walls are much thinner than the arterial wall, they are easily collapsible when they are subject to external compressions.

Table B6.19 lists the static incremental elastic moduli of the canine jugular vein and human saphenous vein. For the purpose of comparison, the static increment elastic modulus of the canine carotid artery segments are also presented in the table. This comparison is of interest because in some arterial reconstructive surgeries, a vein is used as a substitute for an artery.

Sobin [51] obtained data on the mechanical properties of human vena cava from autopsy material. The data may be expressed by the following equation:

Table B6.20 Tensile Properties of Human Venous Tissue*

Vein	Direction	Age group			
		20–39 yr	40–50 yr	60–69 yr	adult average
<i>Tensile Breaking Load per Unit Width (g/mm)</i>					
Inferior vena cava	L	102.0	87.0	68.0	89.0
	T	245.0	224.0	224.0	232.0
Femoral	L	159.0	149.0	149.0	153.0
	T	211.0	217.0	224.0	216.0
Popliteal	L	116.0	116.0	116.0	116.0
	T	180.0	197.0	158.0	182.0
<i>Ultimate Tensile Strength (kg/mm²)</i>					
Inferior vena cava	L	0.15	0.11	0.08	0.12
	T	0.36	0.28	0.27	0.31
Femoral	L	0.24	0.21	0.20	0.22
	T	0.32	0.31	0.29	0.31
Popliteal	L	0.20	0.17	0.15	0.18
	T	0.31	0.29	0.20	0.27
<i>Ultimate Percentage Elongation</i>					
Inferior vena cava	L	98.0	77.0	70.0	84.0
	T	58.0	47.0	44.0	51.0
Femoral	L	97.0	72.0	72.0	82.0
	T	79.0	67.0	56.0	70.0
Popliteal	L	112.0	97.0	81.0	100.0
	T	77.0	77.0	77.0	77.0

* Adapted from [43].L = longitudinal; T = transverse.

$$\begin{aligned}
 T &= \alpha EC\lambda[a(E^2 - E^{*2})] \\
 E &= (\lambda^2 - 1) / 2 \\
 T^* &= \alpha CE^* \lambda^*
 \end{aligned}
 \tag{B6.12}$$

where λ . is the ratio of the changed length of the specimen divided by the reference length of the specimen, C and a are material constants, and E^* is the strain that corresponds to a selected value of stress S^* . The product of the constant αC is similar to the elastic modulus, provided that the modulus is defined as the ratio, S^*/E^* , where $S^* = T^*/\lambda^*$. Fung [1] provides typical values of these constants obtained experimentally; however, no universal constants have been discovered.

B6.6.2 Tensile properties of veins

The tensile properties of human venous tissues are presented in Table B6.20. For the testing method and definitions of the terms in the table, please refer to Section B6.5 on *Mechanical properties of arteries*.

Table B6.21 Water Permeability of Iliac Vessels*

<i>Vessel</i>	<i>Pressure (mmHg)</i>	<i>Filtration rate (cm/sec x 10⁶)</i>
Iliac artery	0–20	0
	25–80	2.58
	100	4.08
	200	6.42
Iliac vein	0–20	6.94
	21–40	9.72
	41–60	11.67
	61–80	12.22
	81–100	12.78

* Adapted from [56].

B6.7 Mechanical Characteristics of Lymphatic Vessels

The problem concerning the ontogenesis of the lymphatic vessels is still not completely solved. However, most of the evidence indicates that the large lymphatic vessels are derived from the veins [52]. Therefore, lymphatics can be considered modified veins. According to the reports by Ohhashi *et al.* [53, 54], the circumferential elastic modulus of the bovine mesenteric lymphatics ranged from 4.2×10^4 to 2.7×10^5 dynes/cm² at a pressure range from 0 to about 20 mmHg, and the elastic modulus of canine thoracic duct is about 2.0×10^5 dynes/cm². These values are less than those of veins obtained by Bergel [55]. Therefore, the lymphatics are more distensible than the veins.

B6.8 Transport Properties of blood Vessels

Under transmural pressures, fluid or plasma will flow across the walls of blood vessels. On one hand, convective fluid motion through the blood vessel wall plays a very important role in nourishing the vessel walls, on the other hand, it is involved in atherogenesis by promoting the transport of macromolecules such as lipoproteins into the arterial wall [55–58], possibly through leaky endothelial cell junctions in regions of high endothelial cell turnover [59]. Table B6.21 lists the filtration properties of excised, presumably normal, human iliac blood vessels.

B6.9 Effect of Age, Hypertension and Atherosclerosis on blood Vessels

B6.9.1 Age

Two well known changes accompany aging of the cardiovascular system are dilation of thoracic aorta [60] and increased thickness of arterial wall [61]. Arterial walls become less distensible with aging [34, 62, 63]. Both dry matter and nitrogen content of artery tissue show a tendency to decrease with age in large and medium sized arteries [20]. But the relative quantity of collagen [22] and elastin [23, 24] in the arterial wall remains essentially unchanged. With aging the arterial wall becomes progressively stiffer. Bader [34] found that the circumferential elastic modulus of human thoracic aorta increased linearly with age. At 100 mmHg, the static circumferential modulus of ‘young’ (<35 years) human thoracic aorta averaged 7.5×10^6 dynes/cm² and for the ‘old’ (>35 years) the average was 16.6×10^6 dynes/cm² [33]. Young peripheral arteries tend to have a greater viscosity ($\eta\omega$) than the older ones [33]. Despite the overall increase in stiffness, the arterial wall itself is considerably weaker than the younger/older one [43].

B6.9.2 Hypertension

Several studies have shown that the water content of human, rat and dog arteries is increased in hypertension, and this increased water content may be associated with an increased wall thickness [64, 65]. Due to the limitations in studying samples from human subjects, animal models (mainly rats) have been employed. Mallov [66] found that the aorta from hypertensive rats had more smooth muscle than normal aorta. Greenwald and Berry [67] reported increased elastin and decreased collagen content in the aorta from spontaneous hypertensive rats when compared with the normal aorta. Wolinsky [25] observed an increase in the absolute amounts of both medial elastin and collagen contents in hypertensive rats. However, the relative percentage of these elements remained essentially constant. Experimental studies [67–69] showed an increase in vessel stiffness with the development of hypertension. This increase in vessel stiffness results in a smaller vessel diameter for a given distending pressure, i.e. a decrease in the distensibility [70].

B6.9.3 Atherosclerosis

It is generally accepted that substantial changes in the arterial wall occur with atherosclerosis in man. In human atherosclerotic arteries, it appears that there may be an absolute increase in collagen and a decrease in muscle fibers when compared

with normal arteries [28]. In canine iliac artery the ratio of collagen to elastin was found to be increased, while the ratio in carotid was decreased [26]. The elastic moduli of the diseased aorta and common iliac arteries are several times higher than those reported [33] for normal arteries. The most popular model used to study the effect of atherosclerosis on arterial wall properties is the rabbit subject to a high cholesterol diet. Cox and Detweiler [26] have shown that in the iliac arteries from high cholesterol fed greyhounds, collagen and elastin contents are decreased, but the ratio of collagen to elastin is increased. In carotid arteries from the treated animals, the elastin content is increased and the collagen to elastin ratio is decreased. Their results also show that the elastic modulus of the iliacs from the cholesterol fed animals is higher than that of the normal iliacs while the treated carotids are unchanged. By using a rabbit model, Pynadath and Mukherjee [71] found that cholesterol feeding had no effect on the longitudinal dynamic elastic modulus of the aorta, but the circumferential one was affected significantly. After six weeks of feeding, the circumferential dynamic elastic modulus increased from the normal value of 2.7×10^6 dynes/cm² to 4.0×10^6 dynes/cm². This increase showed a remarkable correlation with the cholesterol content in the aortas. Although animal models shed some light on the effects of cholesterol feeding, since atherosclerotic changes in the arterial wall are so closely related to aging, it is difficult to separate the effect of atherosclerosis from those of aging. The effects of atherosclerosis on the mechanical properties of the arterial wall remain unclear. Confusion with the effects of aging and other forms of arteriosclerosis such as medial calcification make interpretation of the results difficult.

B6.10 Final Comments

Mechanical properties of the arteries from human and various animals have been extensively studied. However, literature on lymphatic vessels is very scarce. The data on the circumferential elastic modulus of the lymphatic vessels obtained by Ohhashi *et al.* [53, 54] seem to be too low considering that the lymphatics are originating from the veins.

The overall viscoelastic properties of a large blood vessel such as the aorta are known to be nonlinear [2, 44] and anisotropic [37]. But due to the fact that the blood vessel wall is incompressible [72] and deforms orthotropically [31], the mechanical properties of blood vessels can be described mainly by six coefficients: an elastic and a viscous moduli in the longitudinal, circumferential and radial directions. Among them, only the moduli in the circumferential and longitudinal directions have been studied widely. Much fewer data in the radial direction can be found in literature. In calculation of the circumferential elastic moduli, it was usually assumed that the Poisson's ratio was 0.5 that is not strictly true when large strains are considered [36]. In fact, the measured data [37, 73] show that the Poisson's ratio is about 0.3, not 0.5 as would be predicted for an isotropic material. But the Poisson's

ratio was almost constant with respect to circumferential strain and pressure in both relaxed and constricted canine carotid arteries [73].

To our best knowledge, water diffusion properties of blood vessels have been studied extensively, but their electrical and thermal properties are still unknown.

Acknowledgement This work was supported by the Medical Research Council of Canada (Grant MT-7879). The assistance of Y. Marois, M. King and Y. Douville in preparation of this material is gratefully acknowledged.

Additional Reading

Canfield, T.R. and Dorbin, P.B. (1987) Static properties of blood vessels, in *Handbook of Bioengineering* (eds R. Skalak and S. Chien), McGraw-Hill Book Company, New York, pp. 16.1–16.28.

The authors discuss the mechanical behavior of arteries and the mathematical method required for quantification of such data. The discussion is entirely concerned with the elastic or pseudoelastic behavior of blood vessels. It should be emphasized that the arterial wall also exhibits inelastic properties, such as viscosity, creep, stress & relaxation and pressure-diameter hysteresis. Very few data on mechanical properties of blood vessels are presented.

Dorbin, P.B. (1983) Vascular mechanics, in *Handbook of Physiology, Vol. 3 The Cardiovascular System*, (eds J.T. Shepherd and F. Abboud), Amer. Physiol. Soc., Washington, DC, Section 2, pp. 65–102.

This chapter reviews the essential concepts of vascular mechanics and its methods of quantification. Some of the important controversies are discussed, and further research areas are pointed out. Detailed information is provided on the structural and mechanical changes of arteries with age. The effect of vascular disorders such as arterosclerosis and hypertension on the mechanical behavior of blood vessels is discussed as well. Extensive additional literature sources are provided.

Schneck, D.J. (1995) An outline of cardiovascular structure and function, in *The Biomedical Engineering Handbook*, (ed. J.D. Bronzino), CRC Press, Boca Raton, pp. 3–14.

The cardiovascular system is described as a highway network, which includes a pumping station (the heart), a working fluid (blood), a complex branching configuration of distributing and collecting pipes and channels (the blood vessels), and a sophisticated means for both intrinsic (inherent) and extrinsic (autonomic and endocrine) control. Data on both the arterial and venous systems are tabulated. However, no detailed sources are provided for the data listed. This is a very suitable reference for biomedical engineers.

Hargen, A.R. and Villavicenco, J.L. (1995) Mechanics of tissue/lymphatic support, in *The Biomedical Engineering Handbook*, (ed. J.D. Bronzino), CRC Press, Boca Raton, pp. 493–504.

From an engineering point of view, the authors discuss the lymphatic system as a drainage system for fluids and waste products from tissues. Basic concepts of lymphatic transport along with clinical disorders are discussed, although briefly. Extensive additional sources are cited.

References

1. Fung, Y.C. (1993) *Biomechanics, Mechanical Properties of Living Tissues*, 2nd edn, Springer-Verlag, New York, pp. 321–391.
2. Bergel, D.H. (1961) The static elastic properties of the arterial wall. *J. Physiol.*, **156**, 445–457.
3. Patel, D.J. and Vaishnav, R.N. (1972) The rheology of large blood vessels, *Cardiovascular Fluid Dynamics*, D.H. Bergel (ed.), Academic Press, New York, Vol. 2, pp. 1–64.
4. Fung, Y.C., Fronek, K. and Patitucci, P. (1979) Pseudoelasticity of arteries and the choice of its mathematical expression. *Am. J. Physiol.*, **237**, H620–H631.
5. Remington, J.W. (1955) Hysteresis loop behavior of the aorta and other extensible tissues. *Am. J. Physiol.*, **180**, 83–95.
6. Alexander, R.S. (1971) Contribution of plastoelasticity to the tone of the cat portal vein. *Circ. Res.*, **28**, 461–469.
7. Anitschkov, N. (1933) Experimental arteriosclerosis in animals, in *Arteriosclerosis*, E.V. Cowdry, Editor, Macmillan, New York, pp. 298–299.
8. Wilens, S.L. and McCluskey, R.T. (1954) The permeability of excised arteries and other tissues to serum lipid. *Circ. Res.*, **2**, 175–182.
9. Baldwin, A.L., Wilson, L.M. and Simon, B.R. (1992) Effect of pressure on aortic hydraulic conductance. *Arteria. Thromb.*, **12**, 163–171.
10. Fung, Y.C. (1984) *Biodynamics, Circulation*, Springer-Verlag, New York, p. 77.
11. Brecher, G.A. (1956) *Venous Return*, Grune & Stratton, New York, pp. 30–67.
12. Helps, E.P.W. and McDonald, D.A. (1954) Observation on laminar flow in veins. *J. Physiol.*, **124**, 631–639.
13. Spencer, M.P. and Denison, A.B. (1963) Pulsatile blood flow in the vascular system, in *Handbook of Physiology*, Section 2, Circulation, W.F. Hamilton and P. Dow, Editors, Am. Physiol. Soc., Washington, pp. 839–864.
14. Fry, D.L. and Greefield, J.C. Jr. (1964) The mathematical approach to hemodynamics, with particular reference to Womersley's theory, in *Pulsatile blood Flow*, Attinger, E.O. (ed), McGraw-Hill, New York, pp. 85–99.
15. Maggio, E. (1965) *Microhemocirculation, Observable Variables and Their Biological Control*, C.C. Thomas, Springfield.
16. Whitmore, R.L. (1968) *Rheology of the Circulation*, Pergamon Press, Oxford, pp. 99–108.
17. Morse, D.E. (1979) The normal aorta: embryology, anatomy, and histology of the aorta, in *The Aorta*, J. Lindsay, Jr. and J.W. Hurst, Editors, Grune & Stratton, New York, pp. 15–37.
18. Singhal, S., Henderson, R., Horsfield, K. *et al.* (1973) Morphometry of human pulmonary arterial tree. *Circ. Res.*, **33**, 190–197.
19. Fung, Y.C. (1984) *Biodynamics, Circulation*, Springer-Verlag, New York, pp. 77–165.
20. Kirk, J.E. (1962) Arterial and arteriolar system, biochemistry, in *Blood Vessels and Lymphatics*, D.I. Abramson, Editor, Academic Press Inc., London, pp. 82–95.
21. Fischer, G.M. and Llaurodo, J.G. (1966) Collagen and elastin content in canine arteries selected from functionally different vascular beds. *Circ. Res.*, **19**, 394–399.
22. Kanabrocki, E.L., Fels, I.G. and Kaplan, E. (1960) Calcium, cholesterol and collagen levels in human aorta. *J. Gerontol.*, **15**, 383–387.
23. Lansing, A., Alex, M. and Rosenthal, T.B. (1950) Calcium and elastin in human arteriosclerosis. *J. Gerontol.*, **5**, 112–119.

24. Kraemer, D.M. and Miller, H. (1953) Elastin content of the abdominal fraction of human aortae. *Arch. Pathol.*, **55**, 70–72.
25. Wolinsky, H. (1970) Response of the rat aortic media to hypertension. Morphological and chemical studies. *Circ. Res.*, **26**, 507–523.
26. Cox, R.H. and Detweiler, D.K. (1979) Arterial wall properties and dietary atherosclerosis in the racing greyhound. *Am. J. Physiol.*, **5**, H790–H797.
27. Kirk, J.E. (1962) Venous system, biochemistry, in *Blood Vessels and Lymphatics*, D.I. Abramson, Editor, Academic Press Inc., London, pp. 211–213.
28. Strandness, D.E. and Sumner, D.S. (eds) (1975) *Hemodynamics for Surgeons*, Grune & Stratton, New York, New York, pp. 161–205.
29. Patel, D.J., Greenfield, J.C. and Fry, D.L. (1964) *In vivo* pressure-length-radius relationships of certain vessels in man and dogs, in *Pulsatile blood Flow*, E.O. Attinger, Editor, McGraw-Hill, New York, pp. 293–302.
30. Cox, R.H. (1975) Anisotropic properties of the canine carotid artery *in vitro*. *J. Biomech.*, **8**, 293–300.
31. Patel, D.J. and Fry, D.L. (1969) The elastic symmetry of arterial segments in dogs. *Circ. Res.*, **24**, 1–8.
32. Bergel, D.H. (1958) A photo-electric method for the determination of the elasto-viscous behavior of the arterial wall. *J. Physiol.*, **141**, 22–23.
33. Learoyd, B.M. and Taylor, M.G. (1966) Alteration with age in the viscoelastic properties of human arterial walls. *Circ. Res.*, **18**, 278–292.
34. Bader, H. (1967) Dependence of wall stress in the human thoracic aorta on age and pressure. *Circ. Res.*, **20**, 354–361.
35. Langewouters, G.J., Wesseling, K.H. and Goedhard, W.J.A. (1984) The static elastic properties of 45 human thoracic and 20 abdominal aortas *in vitro* and the parameters of a new model. *J. Biomech.*, **17**, 425–435.
36. Bergel, D.H. (1960) *The Visco-elastic Properties of the Arterial Wall*. PhD thesis, University of London.
37. Patel, D.J., Janicki, J.S. and Carew, T.E. (1969) Static anisotropic elastic properties of the aorta in living dogs. *Circ. Res.*, **25**, 765–779.
38. Rees, P.M. and Jepson, P. (1970) Measurement of arterial geometry and wall composition in the carotid sinus baroreceptor area. *Circ. Res.*, **26**, 461–467.
39. Gow, B.S. and Taylor, M.G. (1968) Measurement of viscoelastic properties of arteries in the living dog. *Circ. Res.*, **23**, 111–122.
40. Reid, L. (1968) Structural and functional reappraisal of the pulmonary artery system, in *Scientific Basis of Medicine, Annual Reviews*, Vol. 8, pp. 289–307.
41. Yates, W.G. (1969) Experimental studies of the variations in the mechanical properties of the canine abdominal vena cava, in SUDAAR Report 393, Stanford University, California.
42. Bergel, D.H. (1972) The properties of blood vessels, in *Biomechanics, Its Functions and Objectives*, Y.C. Fung, Editor, Prentice-Hall, Englewood Cliffs, N.J., p. 110 and p. 131.
43. Yamada, H. (1970) *Strength of Biological Materials*, F.G. Evans, Editor, Williams and Wilkins, Baltimore, pp. 106–277.
44. Bergel, D.H. (1961) The dynamic elastic properties of arterial wall. *J. Physiol.*, **156**, 458–469.
45. Arndt, J.O., Klauske, J. and Mersch, F. (1968) The diameter of the intact carotid artery in man and its change with pulse pressure. *Pfulger's Arch.*, **30**, 230–240.
46. Langewouters, G.J., Wesseling, K.H. and Goedhard, W.J.A. (1985) The pressure dependent dynamic elasticity of 35 thoracic and 16 abdominal human aortas *in vitro* described by a five component model. *J. Biomech.*, **18**, 613–620.
47. Langewouters, G.J. (1982) *Visco-Elasticity of the Human Aorta in vitro in Relation to Pressure and Age*. PhD thesis, Free University, Amsterdam, The Netherland.
48. Tanaka, T.T. and Fung, Y.C. (1974) Elastic and inelastic properties of the canine aorta and their variation along the aortic trees. *J. Biomech.*, **7**, 357–370.

49. Attinger, E.O. (1967) Modelling of pressure-flow relations in arteries and veins (Abstract). *Biorheology*, **4**, 84.
50. Wesley, R.L.R., Vaishnav, R.N., Fuchs, J.C.A. *et al.* (1975) Static linear and nonlinear elastic properties of normal and arterIALIZED venous tissue in dog and man. *Circ. Res.*, **37**, 509–520.
51. Sobin, P. (1977) *Mechanical Properties of Human Veins*. M.S. thesis, University of California, San Diego, California.
52. Susznyák, I., Földi, M. and Szabó, G. (1967) *Lymphatics and Lymph Circulation: Physiology and Pathology*, Pergamon Press, London, pp. 33–50.
53. Ohhashi, T., Azuma, T. and Sakaguchi, M. (1980) Active and passive mechanical characteristics of bovine mesenteric lymphatics. *Am. J. Physiol.*, **239**, H88–H95.
54. Ohhashi, T. (1987) Comparison of viscoelastic properties of walls and functional characteristics of valves in lymphatic and venous vessels. *Lymphatic*, **20**, 219–223.
55. Bergel, D.H. (1964) Arterial viscoelasticity, in *Pulsatile blood Flow*, E.O. Attinger, Editor, McGraw-Hill, New York, pp. 275–292.
56. Wilens, S.L. and McCluskey, R.T. (1952) The comparative filtration properties of excised arteries and veins. *Am. J. Med. Sci.*, **224**, 540–547.
57. Tedgui, A. and Lever, M.J. (1985) The interaction of convection and diffusion in the transport of ¹³¹I-albumin within the media of rabbit thoracic aorta. *Circ. Res.*, **57**, 856–863.
58. Tedgui, A. and Lever, M.J. (1987) Effect of pressure and intimal damage on ¹³¹I-albumin and ¹⁴C-sucrose spaces in aorta. *Am. J. Physiol.*, **253**, H1530–H1539.
59. Weinbaum, S., Tzeghai, G., Ganatos, P. *et al.* (1985) Effect of cell turnover and leaky junctions on arterial macromolecular transport. *Am. J. Physiol.*, **248**, H945–H960.
60. Bazett, H.C., Cotton, F.S., Laplace, L.B. *et al.* (1935) The calculation of cardiac output and effective peripheral resistance from blood pressure measurements with an appendix on the size of the aorta in man. *Am. J. Physiol.*, **113**, 312–334.
61. Anderson, J.R. (1980), *Muir's Textbook of Pathology*, Arnold, London, pp. 360–395.
62. Nakashima, T. and Tanikawa, J. (1971) A study of human aortic distensibility with relation to atherosclerosis and aging. *Angiology*, **22**, 477–490.
63. Mozersky, D.J., Summer, D.S., Hokanson, D.E. *et al.* (1972) Transcutaneous measurement of the elastic properties of the human femoral artery. *Circulation*, **46**, 948–955.
64. Tobian, L. (1960) Interrelationship of electrolytes, juxtaglomerular cells and hypertension. *Physiol. Rev.*, **40**, 280–312.
65. Peterson, L.H. (1963) Systems behavior, feed-back loops and high blood pressure research. *Circ. Res.*, **12**, 585–596.
66. Mallov, S. (1959) Comparative reactivities of aortic strips for hypertensive and normotensive rats to epinephrine and levarterenol. *Circ. Res.*, **7**, 196–201
67. Greenwald, S.E. and Berry, C.L. (1978) Static mechanical properties and chemical composition of the aorta of spontaneously hypertensive rats, a comparison with the effects of induced hypertension. *Cardiovas. Res.*, **12**, 364–372.
68. Feigl, E.O., Peterson, L.H. and Jones, A.W. (1963) Mechanical and chemical properties of arteries in experimental hypertension. *J. Clin. Invest.*, **42**, 1640–1647.
69. Bandick, N. and Sparks, H. (1970) Viscoelastic properties of the aortas of hypertensive rats. *Proc. Soc. Exp. Biol. Med.*, **134**, 56–60.
70. Greene, M.A., Friedlander, R., Boltax, A.J. *et al.* (1966) Distensibility of arteries in human hypertension. *Proc. Roy. Soc. Exp. Biol.*, **121**, 580–585.
71. Pynadath, T.I. and Mukherjee, D.P. (1977) Dynamic mechanical properties of atherosclerotic aorta: A correlation between the cholesterol ester content and the viscoelastic properties of atherosclerotic aorta. *Atherosclerosis*, **26**, 311–318.
72. Carew, T.E.R., Vaishnav, R.N. and Patel, D.J. (1968) Compressibility of the arterial wall. *Circ. Res.*, **23**, 61–68.
73. Dobrin, P.B. and Doyle, J.M. (1970) Vascular smooth muscle and the anisotropy of dog carotid artery. *Circ. Res.*, **27**, 105–119.

Chapter B7

The Intraocular Lens

Traian V. Chirila and Shuko Suzuki

B7.1 Introduction

Although the existence of the intraocular crystalline lens in the eye was recognized by the scholars of the Hellenistic period (about 2000 years ago), the actual role of the lens in vision was properly understood much later. Truly scientific approaches to the lens measurements and properties began to be applied only in the nineteenth century [1]. For instance, a simple property—the weight of the human intraocular lens—was first reported in 1883 [2].

The intraocular crystalline lens is positioned between the aqueous humor and vitreous body of the eye. It is usually referred to as “the lens,” which is rather convenient considering that the term “intraocular lens” (with the acronym IOL) is nowadays used exclusively to designate an artificial device implanted after surgical removal of a cataractous (opaque) natural lens.

The lens refracts the light which enters the eye through the pupil and focuses it on the retina. Its main functions are the following: (1) provides refractive power to the optical system of the eye; (2) provides the accommodation necessary for normal vision; (3) maintains its own transparency; and (4) absorbs UV radiation and blue light, both deleterious to the subsequent ocular segments. These functions are all important, but the lens’ contribution to the process of accommodation is crucial for normal vision. Ocular accommodation is the ability of the eye to adjust the focal length from far to near through changes in the shape of the lens. The consequence of losing this ability with age is known as presbyopia, and is one of the major causes of the need for visual correction in the middle-aged humans. Although the existing theories attempting to explain presbyopia are still debated [3, 4], many investigators believe that this condition is related to changes within the lens, especially its age-

T.V. Chirila (✉) • S. Suzuki

Queensland Eye Institute, 140 Melbourne Street, South Brisbane, QLD 4101, Australia

e-mail: traian.chirila@qei.org.au

induced stiffening. As a result, the stiffness of the human lens has been extensively investigated, and serves as an important parameter in the modeling of the accommodation and presbyopia. The topic has been critically appraised and supplemented with improved experimental techniques in a recent study [5].

The lens is a biconvex body similar to a flattened globe. For descriptive purposes, it has two poles (anterior and posterior), an equator, and therefore two diameters (polar diameter, or thickness of the lens, and equatorial diameter).

The lens is composed of epithelial cells which become anuclear and elongated as they are displaced further toward the center. Because of the enormous length finally attained by these cells, they are referred to as lens fibers. The lens is surrounded by a transparent acellular capsule of variable thickness. A proper epithelium underlies the capsule along the anterior side and equator, but not under the posterior capsule. The superficial layers of cells and fibers constitute the lens cortex, while the lens nucleus is situated in the center. The fibers are continuously formed throughout life and the new fibers cover the old ones which are displaced toward the nucleus.

B7.2 Compendium of Physicochemical Characteristics of the Human Lens

Currently, there are significantly more compositional and physical property data available on animal lenses than on the human lens. The spread of the data measured for the human lens, compiled here from various sources, results from large variations in methodologies from one research group to another, and in the individual characteristics of the tissue from one human donor to another. Even the determination of a straightforward property like the water content has led to variable results (Tables B7.1 and B7.2), likely due both to nonuniform distribution of the water in the lens and to the variability of methods employed for measurements. While data on the inorganic content of the human lens (Table B7.3) are generally in agreement, there was a larger variation in reporting the organic content. This is presumably due to the greater sensitivity of the organic metabolism to age and disease. The most reliable results are included in Table B7.4.

Tables B7.5, B7.6, B7.7, and B7.8 provide some key dimensional properties of the lens, while Tables B7.9 and B7.10 are focused on perhaps its most important feature, the optical properties.

Mechanical characteristics of the lens required sophisticated procedures for their measurement and the data are likely difficult to reproduce. The currently available mechanical properties of the human lens are summarized in Tables B7.11, B7.12, B7.13, B7.14, B7.15, B7.16, B7.17, and B7.18. Although the lens was traditionally regarded as an elastic material, most investigators agree now that it is in fact a viscoelastic solid. The first rheological measurements on human lenses were reported

Table B7.1 Water content of the normal human lens

Method	Value (%)	Source
n.a.	65 ^a	[6]
Vacuum dehydration	68.6 ± 4.3 ^b ; 63.4 ± 2.9 ^c	[7]
Microsectioning	52.5–66.2 ^{c,d} ; 72.5–90 ^{d,e}	[8]
Raman microspectroscopy	69 ± 4 ^b ; 65 ± 4 ^c	[9]
Freeze drying	68 ^c ; 80 ^e ; 75 ^f	[10]
Raman microspectroscopy	58.0 ± 4.7 (<70 year) ^c	[11]
	63.0 ± 2.8 (>70 year) ^c	
	85.3 ± 9.4 ^e	
	80.9 ± 8.3 ^f	

± Standard deviation

^aWhole lens

^bCortex

^cNucleus

^dAge 62–68 years

^eOutermost anterior cortex

^fOutermost posterior cortex

Table B7.2 Water content of cataractous human lenses

Method	Value (%)	Source
Drying	67.6 ^a ; 75.4 ^b	[12]
Freeze-drying	79 ^{c,d} ; 83.5 ^{c,e} ; 78 ^{d,f} ; 87.5 ^{e,f} ; 68 ^{d,e,g}	[11]
Drying	63.8 (<60 year); 67.7 (>80 year)	[13]

^aNo sclerosis, average age 64.7 years

^bAdvanced sclerosis, average age 70.8 years

^cOutermost anterior cortex

^dPrimary nuclear cataract

^eSubcapsular cataract

^fOutermost posterior cortex

^gNucleus

by Itoi et al. [30], who found an apparent elastic modulus of 10–100 kPa and a loss tangent (phase shift) of 0.3–0.4. More recent studies using rheometry [31] confirmed the increase of stiffness with age and its variation with the distance from the center of the lens. We have to mention, however, that the magnitude of the values reported for the viscoelastic parameters of the human lens varies from one laboratory to another. Table B7.19 comprises the most recent results determined by rheometry.

Table B7.3 Inorganic ion content of the normal adult human lens

Ion	Representative value	Source
Sodium	91 mg/100 g wet wt	[6]
Potassium	170 mg/100 g wet wt	[6]
Calcium	1.4 mg/100 g wet wt	[6]
Magnesium	0.29 mg/100 g wet wt	[6]
	6.2 µg/g dry wt	[14]
Zinc	21 µg/g dry wt	[6]
	25 µg/g dry wt	[14]
Copper	<1 µg/g dry wt	[6]
	0.6 µg/g dry wt	[14]
Manganese	0.2 µg/g dry wt	[14]
Iron	0.4 µg/g dry wt	[14]
Rubidium	6.8 µg/g dry wt	[14]
Chloride	35.3 mg/100 g wet wt	[6]
Phosphate	25 mg/100 g wet wt	[15]
Sulfate	24 mg/100 g wet wt	[15]
pH	7.3–7.7	[16]

Table B7.4 Organic content of the human lens^a

Component	Representative value	Source
Proteins	30 % of lens (young); 35 % of lens (old)	[17]
Ascorbic acid	30	[14]
Glutathione ^b	170 (normal lens)	[18]
	52 (cataractous lens)	[18]
	46–150	[14]
	200–450	[15]
Taurine	10	[14]
	6.7	[15]
Alanine	11.9	[14]
Glycine	5.9	[14]
Glutamic acid	50	[14]
Serine	5.9	[14]
Urea	28.2	[14]
Inositol	462	[15]
Cholesterol	1.4 mg/lens	[14]
Phospholipids: cortex	600–725 ^c	[14]
Phospholipids: nucleus	450–650 ^c	[14]

^aExpressed as mg per 100 g wet weight of lens, unless otherwise specified

^bThere is a large variation in the reported data on glutathione content

^cVariation with age

Table B7.5 Dimensional variation with age of the human lens [14]

Dimension	Value (mm)
Polar diameter (lens thickness)	3.5–5
Equatorial diameter	6.5–9
Anterior radius of curvature	8–14
Posterior radius of curvature	4.5–7.5

Table B7.6 Dimensional variation with age of the equatorial diameter and thickness of the human lens [19]

Age (years)	Equatorial diameter (mm)	Thickness (mm)
22	8.90	3.77
31	9.22	3.60
41	9.16	3.62
50	9.37	3.78
62	8.99	4.22
83	8.77	5.31

Table B7.7 Thickness of a 35-year-old human lens capsule [14]

Location	Value (µm)
Anterior pole	14
Anterior, maximum	21
Equator	17
Posterior pole	4
Posterior, maximum	23

Table B7.8 Weight, volume, and density of the human lens in adult life [20]

Age interval (years)	Weight, mean (mg)	Volume, mean (mm ³)	Density (g/cm ³) ^a
20–30	172.0	162.9	1.034
30–40	190.3	177.3	1.048
40–50	202.4	188.1	1.061
50–60	222.3	205.4	1.072
60–70	230.1	213.0	1.082
70–80	237.1	218.3	1.091

^aCalculated at the beginning of a decade

Table B7.9 Refractive index of the human lens nucleus as a function of age (adapted from [21])

Age (years)	Refractive index
14	1.4325
82	1.4175

Table B7.10 Transmissivity of the human lens as a function of age [22]

Wavelength (nm)	Transmission of radiation (%)		
	Age (years)		
	25	54	82
350	1.2	1.2	1.2
400	4.8	4.8	4.8
450	38.0	30.6	21.7
500	70.0	42.7	30.0
700	75.0	51.7	37.0

Table B7.11 Variation with age of tensile modulus (Young's modulus of elasticity) of the decapsulated human lens [23]^a

Age (years)	Modulus (kPa)	
	Polar	Equatorial
At birth	0.85	0.75
20	1.0	0.75
40	1.5	1.1
63	3.0	3.0

^aDetermined by the spinning method**Table B7.12** Variation with age of the shear modulus of the human lens [4]

Age interval (years)	Shear modulus, G (Pa) ^a	
	Cortex	Nucleus
<30 ^b	98.3 ± 64.5	39.0 ± 13.8
>60 ^c	2040 ± 710	17,400 ± 4900

± Standard deviation

^aDetermined from penetration measurements^bSix samples^cTwelve samples**Table B7.13** Hardness of cataractous human lenses [24]^a

Age interval (years)	Mean force (N)	Number of lenses
<60	0.80	13
61–70	0.87	20
71–80	1.12	31
>80	1.38	27

^aMeasured by the force necessary to cut the lens in a guillotine

Table B7.14 Mechanical properties of the human anterior lens capsule [25]^a

Age (years)	Property	Value
20	Tensile modulus (MPa)	5.6
50		4.0
80		1.5
<20	Ultimate tensile stress (MPa)	2.3
>70		0.7
- ^b	Elongation (%)	29
- ^b	Poisson's ratio	0.47±0.5

± Standard deviation

^aDetermined from the volume–pressure relationship upon distension with isotonic saline

^bFound to be independent of age

Table B7.15 Variation with age of the mechanical properties of the human anterior lens capsule [26]

Age	Ultimate strain (MPa)	Ultimate stress (MPa)	Ultimate elastic modulus (MPa)
7 months	108	17.5	44.8
98 years	40	1.5	4.4

Table B7.16 Variation with age of the mechanical properties of the human posterior lens capsule [27]

Age	Ultimate strain (MPa)	Ultimate stress (MPa)	Ultimate elastic modulus (MPa)
1	101	16.9	55.7
94	34	1.1	5.4

Table B7.17 Force of contraction for maximum accommodation of the human lens [28]^a

Age (years)	Force (mN)
25	1.2
35	10.9
45	12.8
55	11.4

^aDetermined from the stress–dioptric power relationship

Table B7.18 Spring constants of human lens and zonules [29]^a

Spring constant at 10 % elongation (mN)	Age interval (years)	
	2–39	40–70
Lens, polar	13.5±0.80	25.4±0.24
Lens, equatorial	12.3±0.65	36.5±0.23
Zonules ^b	0.38±0.32	0.65±0.85

± Standard deviation

^aSpring constant is defined here as $S' = F/(\Delta l/l_0)$, where F is total force and $\Delta l/l_0$ is elongation^bDetermined on specimens zonule-lens-zonule, after the excision of the ciliary muscles**Table B7.19** Viscoelastic properties of the human lens [32]^a

Lens region	Storage modulus, G' (Pa)	Loss modulus, G'' (Pa)	Dynamic viscosity, η' (Pa s)	Loss tangent, δ (°)
Nucleus ^b	11.00±4.67	24.91±10.98	0.33	66.17
Cortex ^c	12.40±6.85	25.98±12.62	0.35	64.49

± Standard deviation

^aMeasured for postmortem lenses in a controlled strain rheometer at 75 Hz^bAverage results from 26 samples^cAverage results from eight samples**Table B7.20** Electrical properties of the isolated human lens

Property	Value	Source
Potential difference (mV) ^a	7	[33]
Short-circuit current density ($\mu\text{A}/\text{cm}^2$) ^b	5	[33]
Resistance ($\text{k}\Omega \text{ cm}^2$) ^c	1.5	[33]
Relative permittivity	39.1±0.12 (nucleus) ^{d,e}	[34]
	38.1±0.13 (nucleus) ^{e,f}	[34]
	55.6±0.17 (cortex) ^{d,e}	[34]
	52.1±0.16 (cortex) ^{e,f}	[34]
Conductivity (S/m)	0.31±0.005 (nucleus) ^{d,e}	[34]
	0.33±0.005 (nucleus) ^{e,f}	[34]
	0.73±0.07 (cortex) ^{d,e}	[34]
	0.72±0.005 (cortex) ^{e,f}	[34]

^aAnterior side positive^bReflects sodium transport from the posterior to the anterior lens side and is expressed as a current density^cCalculated as the ratio between potential difference and current density^dMeasured at 20 °C^eRange given for 95 % confidence interval^fMeasured at 37 °C

Large variations in the electrical properties of animal lenses have been reported, but it seems that the only measurements performed on human lenses are those shown in Table B7.20.

Additional Reading

Bellows, J.G. (ed.) (1975) *Cataract and Abnormalities of the Lens*, Grune & Stratton, New York.

A valuable collection of 42 contributions on the lens, its pathology, and surgery, written by known experts such as Barraquer, Bellows, Choyce, Girard, Hockwin, Kaufman, Rosen, and Yanoff. The first five introductory chapters present historical aspects, development, and characterization of the lens. However, most of the book is dedicated to cataract and its treatment.

Spector, A. (1982) Aging of the lens and cataract formation, in *Aging and Human Visual Function* (eds R. Sekuler, D. Kline and K. Dismukes), Alan R. Liss, Inc., New York, pp. 27–43.

A brief but comprehensive account of the changes which take place in the composition and metabolism of the lens during aging and cataractogenesis.

Duncan, G. and Jacob, T.J.C. (1984) The lens as a physicochemical system, in *The Eye*, vol. 1b, 3rd edn (ed H. Davson), Academic Press, Orlando, FL, pp. 159–206.

This text develops some topics usually neglected in other books, including the structural order in the lens, optical properties of the lens, role of lens membranes, and electrolyte transport and distribution in the lens.

Cotlier, E. (1987) The lens, in *Adler's Physiology of the Eye*, 8th edn (eds R.A. Moses and W.M. Hart), C.V. Mosby Co., St. Louis, pp. 268–290.

A systematic presentation of the anatomy, biochemistry, and physiology of the lens.

Moses, R.A. (1987) Accommodation, in *Adler's Physiology of the Eye*, 8th edn, (eds R.A. Moses and W.M. Hart), C.V. Mosby Co., St. Louis, pp. 291–310.

A thorough exposition of all aspects of the mechanism of accommodation and the role of the lens in vision. A text, by now classic, on a topic much more complex than it appears.

Jones, W.L. (1991) Traumatic injury to the lens. *Optom. Clin.*, **1**, 125–42.

This review article analyzes the effects of concussive trauma to the eye, emphasizing the types of injuries to the lens. The mechanical response of the anterior and posterior segments of the eye to external forces is also described.

Zampighi, G.A. (2006) The lens, in *The Biology of the Eye*, (ed J. Fischberg), Elsevier, Amsterdam, pp. 149–79.

A concise but informative chapter on relevant aspects of the human lens, including its cellular architecture and the mechanisms of the molecular processes and fluxes.

Beebe, D.C. (2011) The lens, in *Adler's Physiology of the Eye*, 11th edn (eds L.A. Levin et al.), Elsevier, Edinburgh, pp. 131–63.

Written by an expert, and beautifully illustrated, this text covers the current knowledge on the human lens and is supported by almost 500 references.

Recommended sources for ophthalmic terminology:

Cassin, B., Solomon, S.A.B. and Rubin, M.L. (1990) *Dictionary of Eye Terminology*, 2nd edn, Triad Publishing Co., Gainesville, FL, 286 pp.

Stein, H.A., Slatt, B.J. and Stein, R.M. (1992) *Ophthalmic Terminology. Speller and Vocabulary Builder*, 3rd edn, Mosby-Year Book Inc., St. Louis, MO, pp. 3–33, 243–257.

Myles, W.M. (1993) Ophthalmic etymology. *Surv. Ophthalmol.*, **37**, 306–9.

References

1. Grom E (1975) History of the crystalline lens. In: Bellows JG (ed) *Cataract and abnormalities of the lens*. Grune & Stratton, New York, pp 1–28
2. Smith P (1883) Diseases of crystalline lens and capsule. 1. On the growth of the crystalline lens. *Trans Ophthalmol Soc UK* 3:79–99
3. Burd HJ, Judge SJ, Flavell MJ (1999) Mechanics of accommodation of the human eye. *Vision Res* 39:1591–1595
4. Heys KR, Cram SL, Truscott JW (2004) Massive increase in stiffness of the human lens nucleus with age: the basis for presbyopia? *Mol Vis* 10:956–963
5. Wilde GS (2011) Measurement of human lens stiffness for modelling presbyopic treatments. Ph.D. Thesis, University of Oxford, 219 pp. <http://www.eng.ox.ac.uk/civil/publications/theses/wilde.pdf>. Accessed 12 Feb 2014
6. Kuck JFR (1970) Chemical constituents of the lens. In: Graymore CN (ed) *Biochemistry of the eye*. Academic, London, pp 183–260
7. Fisher RF, Pettet BE (1973) Presbyopia and the water content of the human crystalline lens. *J Physiol* 234:443–447
8. Bours J, Fodisch HJ, Hockwin O (1987) Age-related changes in water and crystalline content of the fetal and adult human lens, demonstrated by a microsectioning technique. *Ophthalmic Res* 19:235–239
9. Huizinga A, Bot ACC, de Mul FFM, Vrensen GFJM, Greve J (1989) Local variation in absolute water content of human and rabbit eye lenses measured by Raman microspectroscopy. *Exp Eye Res* 48:487–496
10. Deussen A, Pau H (1989) Regional water content of clear and cataractous human lenses. *Ophthalmic Res* 21:374–380
11. Siebinga I, Vrensen GFJM, de Mul FFM, Greve J (1991) Age-related changes in local water and protein content of human eye lenses measured by Raman microspectroscopy. *Exp Eye Res* 53:233–239
12. Salit PW (1943) Mineral constituents of sclerosed human lenses. *Arch Ophthalmol* 30:255–258
13. Tabandeh H, Thompson GM, Heyworth P, Dorey S, Woods AJ, Lynch D (1994) Water content, lens hardness and cataract appearance. *Eye* 8:125–129
14. Harding JJ, Crabbe MJC (1984) The lens: development, proteins, metabolism and cataract. In: Davson H (ed) *The eye*, vol 1b, 3rd edn. Academic, Orlando, FL, pp 207–492
15. Paterson CA (1985) Crystalline lens. In: Duane TD, Jaeger EA (eds) *Biomedical foundations of ophthalmology*, vol 2, 2nd edn. Harper & Row, Philadelphia, Chapter 10
16. Kuck JFR (1970) Metabolism of the lens. In: Graymore CN (ed) *Biochemistry of the eye*. Academic, London, pp 261–318
17. Davson H (1990) *Physiology of the eye*, 5th edn. Macmillan, London, Chapter 4
18. Dische Z, Zil H (1951) Studies on the oxidation of cysteine to cystine in lens proteins during cataract formation. *Am J Ophthalmol* 34:104–113

19. Strenk SA, Semmlow JL, Strenk LM, Munoz P, Gronlund-Jacob J, DeMarco JK (1999) Age-related changes in human ciliary muscle and lens: a magnetic resonance imaging study. *Invest Ophthalmol Vis Sci* 40:1162–1169
20. Scammon RE, Hesdorfer MB (1937) Growth in mass and volume of the human lens in postnatal life. *Arch Ophthalmol* 17:104–112
21. Moffat BA, Atchison DA, Pope JM (2002) Explanation of the lens paradox. *Optom Vis Sci* 79:148–150
22. Lerman S (1987) Chemical and physical properties of the normal and ageing lens: spectroscopic (UV, fluorescence, phosphorescence, and NMR) analyses. *Am J Optom Physiol Optics* 64:11–22
23. Fisher RF (1971) The elastic constants of the human lens. *J Physiol* 212:147–180
24. Heyworth P, Thompson GM, Tabandeh H, McGuigan S (1993) The relationship between clinical classification of cataract and lens hardness. *Eye* 7:726–730
25. Fisher RF (1969) Elastic constants of the human lens capsule. *J Physiol* 201:1–19
26. Krag S, Olsen T, Andreassen TT (1997) Biomechanical characteristics of the human anterior lens capsule in relation to age. *Invest Ophthalmol Vis Sci* 38:357–363
27. Krag S, Andreassen TT (2003) Mechanical properties of the human posterior lens capsule. *Invest Ophthalmol Vis Sci* 44:691–696
28. Fisher RF (1977) The force of contraction of the human ciliary muscle during accommodation. *J Physiol* 270:51–74
29. van Alphen GWHM, Graebel WP (1991) Elasticity of tissues involved in accommodation. *Vision Res* 31:1417–1438
30. Itoi M, Ito N, Kaneko H (1965) Visco-elastic properties of the lens. *Exp Eye Res* 4:168–173
31. Weeber HA, Eckert G, Pechhold W, van der Heijde RGL (2007) Stiffness gradient in the crystalline lens. *Graefe's Arch Clin Exp Ophthalmol* 245:1357–1366
32. Schachar RA, Chan RW, Fu M (2011) Viscoelastic properties of fresh human lenses under 40 years of age: implications for the aetiology of presbyopia. *Br J Ophthalmol* 95:1010–1013
33. Platsch KD, Wiederholt M (1981) Effect of ion substitution and ouabain on short circuit current in the isolated human and rabbit lens. *Exp Eye Res* 32:615–625
34. Gabriel C (1996) Compilation of the dielectric properties of body tissue at RF and microwave frequencies. Final Technical Report AL/OE-TR-1996-0004, Prepared for Brooks Air Force Base, Texas, 16 pp. www.dtic.mil/cgi-bin/GetTRDoc?AD=ADA303903. Accessed 27 Feb 2014

Chapter C1

Blood and Related Fluids

V. Turitto and S.M. Slack

C1.1—Introduction

This section provides data for several human biological fluids including blood, plasma or serum, cerebrospinal (CS) fluid, lymph, synovial fluid, and tear fluid. The material presented here was gleaned from a variety of sources, with emphasis placed on the most recently published work, and includes physicochemical properties (Table C1.1), cellular compositions (Table C1.2), concentrations of inorganics (Table C1.3), organics (Table C1.4), and major proteins (Table C1.5). In addition, various properties of the major proteins are presented in Table C1.7, while Tables C1.8 and C1.9 contain information regarding the components of the coagulation and complement cascades, respectively. Because of the variability in values for many properties of biological fluids, in many cases a normal singular range of such values is listed. In all cases, the data are those compiled for normal human adults and, where possible, differences with respect to gender are included. It must be stressed that fluid properties can readily change as a result of disease, aging, or drug ingestion.

The following equations can be used to estimate blood volume (BV, mL), erythrocyte volume (EV, mL), and plasma volume (PV, mL) from the known body mass (b, kg) with a coefficient of variation of approximately 10%:

V. Turitto (✉)

Department of Biomedical Engineering, University of Memphis, Memphis, TN 38152, USA

S.M. Slack

Department of Biomedical Engineering, University of Memphis,
Campus Box 526582, Memphis, TN 38152-6502, USA

Table C1.1 Physiochemical properties [1–3]

Property	Whole blood	Plasma (serum)
Dielectric constant	8.0–8.5	–
Freezing point Depression (°C)	0.557–0.577	0.512–0.568
Osmolality (mosmlkg)	–	276–295
pH	7.38–7.42	7.39–7.45
Refractive index	–	1.3485–1.3513
Relative viscosity	2.18–3.59	1.18–1.59
Specific gravity	1.052–1.061	1.022–1.026
Specific conductivity (S/cm)	–	0.0117–0.0123
Specific heat (cal/g/°C)	0.87	0.94
Surface tension (dyne/cm)	55.5–61.2	56.2

Property	Synovial fluid	CS fluid	Tear fluid
Dielectric constant	–	–	–
Freezing Point Depression (°C)	–	0.540–0.603	0.572–0.642
Osmolality (mosmlkg)	292–300	290–324	309–347
pH	7.29–7.45	7.35–7.70	7.3–7.7
Refractive index	–	1.3349–1.3351	1.3361–1.3379
Relative viscosity	> 300	1.020–1.027	1.26–1.32
Specific gravity	1.008–1.015	1.0032–1.0048	1.004–1.005
Specific conductivity (S/cm)	0.0119	–	–
Specific heat (cal/g/°C)	–	–	–
Surface tension (dyne/cm)	–	60.0–63.0	–

The refractive index, specific gravity, and surface tension were measured at 20°C, the specific conductivity at 25°C, and the relative viscosity at 37°C. The specific gravity is that relative to water. The viscosity of serum is slightly less than that of plasma due to the absence of fibrinogen. Blood viscosity depends strongly on shear rate and hematocrit and the value given in Table C1.1 is that at high shear rates (>200s⁻¹) and normal hematocrits (40–45%). Blood is a non-Newtonian fluid and exhibits increased viscosity with decreasing shear rate. Correlations relating blood viscosity to hematocrit, shear rate, and protein content have been described in the literature [4, 5]. The reader is referred to several excellent publications for further details regarding factors affecting blood viscosity [4, 6–11].

These equations, relating BY, PY, and EY to body weight, are taken from Lentner [12].

Males (M)	BY = 41.0 x b + 1530	Females (F)	BY = 47.16 x b + 864
	PY = 19.6 x b + 1050		PY = 28.89 x b + 455
	EY = 21.4 x b + 490		EY = 18.26 x b + 409

Additional correlations relating these volumes to body weight and surface area are available from the same source.

Table C1.2 Cellular composition of biological fluids [12]

A. Whole blood			
Whole blood: Cell type	Cells/ μL	Cell size (μm)	Half-life in circulation
Erythrocytes	4.6–6.2 x 10 ⁶ (M) 4.2–5.2 x 10 ⁶ (F)	7–8	25 \pm 2 days
Leukocytes			
Neutrophils	3000–6500	10–15	6–8 hours
Eosinophils	50–250	10–15	8–12 hours
Basophils	15–50	10–15	?
Monocytes	300–500	12–20	1–3 days
Lymphocytes	1000–3000	7–8	Variable
Platelets	1.5–3.5 x 10 ⁵	2–4	3.2–5.2 days
Reticulocytes	2.3–9.3 x 10 ⁴	7–10	–
<i>Synovial fluid:</i>			
<i>Cell type</i>	<i>Cells/μL</i>		
Leukocytes	4–5		
Monocytes	35–40		
Lymphocytes	15–16		
Synovial cells	2–3		

The variability in the half-life of circulating lymphocytes is a result of the many subsets of this cell type, e.g., B-cells, helper and suppressor T-cells, etc. Cerebrospinal fluid also contains ~ 1–5 cells/ μL , primarily lymphocytes.

Table C1.3 Inorganic content of various fluids [1]

Compound	Whole blood	Plasma (serum)	Synovial fluid
Bicarbonate	19.1–22.7	25–30	–
Bromide	0.033–0.074	0.043–0.093	–
Calcium	2.42	2.12–2.72	1.2–2.4
Chloride	77–86	100–108	87–138
Copper (μM)	11.3–19.5	13–22	–
Fluoride (μM)	5.3–23.7	–	–
Iodine (μM)	0.2–1.34	0.30–0.47	–
Iron	7.5–10.0	0.01–0.027	–
Magnesium	1.48–1.85	0.7–0.86	–
Phosphorous (total)	10.1–14.3	2.87–4.81	–
Potassium	40–60	3.5–4.7	3.5–4.5
Sodium	79–91	134–143	133–139
Zinc	0.076–0.196	0.011–0.023	–

(continued)

Table C1.3 (continued)

Compound	Cerebrospinal fluid	Tear fluid	Lymph
Bicarbonate	18.6–25.0	20–40	–
Bromide	0.018–0.048	–	–
Calcium	1.02–1.34	0.35–0.77	1.7–2.8
Chloride	119–131	110–135	87–103
Copper (μM)	0.13–0.37	–	–
Fluoride (μM)	55	–	–
Iodine (μM)	–	–	–
Iron	0.0003–0.0015	–	–
Magnesium	0.55–1.23	–	–
Phosphorous (total)	0.442–0.694	–	2.0–3.6
Potassium	2.62–3.30	6.6–25.8	3.9–5.6
Sodium	137–153	126–166	118–132
Zinc	–	–	–

Concentrations are in mM, unless otherwise specified.

Table C1.4 Organic content of various fluids [13–15]

Species	Whole blood	Plasma (serum)	CS fluid
Amino acids (mg/L)	48–74	20–51	10–15
Ammonia (mg/L)	0.26–0.69	0.22–0.47	0.14–0.26
Bilirubin (mg/L)	2–14	2–8	<0.1
Cholesterol	1.15–2.25	1.7–2.1	–
Creatine (mg/L)	3–5	1.3–7.7	4.6–19
Creatinine (mg/L)	10–20	5.6–10.5	6.5–10.5
Fat, neutral	0.85–2.35	0.25–2.6	trace
Fatty acids	2.5–3.9	3.5–4.0	trace
Glucose	630–870	650–966	430–640
Hyaluronic acid	–	–	–
Lipids, total	4.45–6.1	2.85–6.75	0.01–0.02
Total nitrogen	30–41	12–14.3	0.16–0.22
Nonprotein nitrogen	0.26–0.50	0.14–0.32	0.11–0.20
Phospholipid	2.25–2.85	2.0–2.5	0.002–0.01
Urea	0.166–0.39	0.18–0.43	0.14–0.36
Uric acid (mg/L)	6–50	30.5–70.7	1.1–6.3
Water	830–865	930–955	980–990

(continued)

Table C1.4 (continued)

Species	Synovial fluid	Tear fluid	Lymph
Amino acids (mg/L)	–	–	–
Ammonia (mg/L)	–	50	–
Bilirubin (mg/L)	–	–	8
Cholesterol	–	–	0.34–1.06
Creatine (mg/L)	–	–	–
Creatinine (mg/L)	–	–	8–89
Fat, neutral	–	–	–
Fatty acids	–	–	–
Glucose	–	0.025	1.36–1.40
Hyaluronic acid	3.32	–	–
Lipids, total	–	–	–
Total nitrogen	0.084–4.0	1.58	–
Nonprotein nitrogen	0.22–0.43	–	0.13–1.39
Phospholipid	–	–	–
Urea	0.15	0.33–1.4	–
Uric acid (mg/L)	39	–	17–108
Water	960–988	982	810–860

Concentrations are in mg/mL, unless otherwise specified.

Table C1.5 Major protein content of various fluids [12, 14]

Protein	Plasma (serum)	CS fluid ¹	Synovial fluid
Albumin	37.6–54.9	155±39	6–10
α ₁ -Acid glycoprotein (orosomucoid)	0.48–1.26	1.85±0.74	–
α ₁ -Antitrypsin	0.98–2.45	7.0±3.0	0.78±0.017
β ₂ -Microglobulin	0.58–2.24	0.1–1.9	–
Haptoglobin		2.24±1.5	0.1
Type 1.1	1.45±0.34		
Type 2.1	2.06±0.67		
Type 2.2	1.74±0.70		
Ceruloplasmin	0.09–0.51	0.88±0.21	0.043±0.016
Transferrin	1.52–3.36	8.42±3.5	–
C1 Inhibitor	0.15–0.35	–	–
α ₂ -Macroglobulin	1.45–4.43	4.64±1.84	0.31–0.21
IgA	0.7–3.12	2.26±0.95	0.62–1.15
IgG	6.4–13.5	13.9±6.6	1.47–4.62
IgM	0.56–3.52	–	0.09–0.22
Fibrinogen	2–4	0.65	–
Lysozyme	–	–	–
Fibronectin	0.09–0.25	–	–
Hemopexin	0.53–1.21	–	–

(continued)

Table C1.5 (continued)

Protein	Synovial fluid	Tear fluid
Albumin	3.94	15–26.7
α_1 -Acid glycoprotein (orosomucoid)	–	–
α_1 -Antitrypsin	0.015	–
β_2 -Microglobulin	–	–
Haptoglobin	–	–
Ceruloplasmin	0.04	–
Transferrin	–	–
C1 Inhibitor	–	–
α_2 -Macroglobulin	–	–
IgA	0.04–0.80	–
IgG	0.04–0.62	7.8
IgM	trace	–
Fibrinogen	–	–
Lysozyme	1–2.8	–
Fibronectin	–	–
Hemopexin	–	–

¹ Protein concentrations in CS fluid are given in mg/L. All others have units of mg/mL.

Table C1.6 Fluid volumes [16]

Fluid	Volume Male (mL)	Volume Female (mL)
Whole blood	4490	3600
Erythrocytes	2030	1470
Plasma	2460	2130
Cerebrospinal fluid	100–160	100–160
Tear fluid	4–13	4–13

Table C1.7 Properties of major plasma proteins [16, 17]

Protein	Plasma concentration (mg/mL)	Molecular weight (Da)	p ¹	S ¹	D ²
Prealbumin	0.12–0.39	54 980	4.7	4.2	–
Albumin	38–52	66 500	4.9	4.6	6.1
α ₁ - Acid Glycoprotein (Orosomuroid)	0.5–1.5	44000	2.7	3.1	5.3
α ₁ - Antitrypsin	2.0–4.0	54 000	4.0	3.5	5.2
α ₂ . Macroglobulin	1.5–4.5	725 000	5.4	19.6	2.4
α ₂ . Haptoglobin					
Type 1.1	1.0–2.2	100 000	4.1	4.4	4.7
Type 2.1	1.6–3.0	200 000	4.1	4.3–6.5	–
Type 2.2	1.2–2.6	400 000	–	7.5	–
α ₂ . Ceruloplasmin	0.15-.60	160 000	4.4	7.08	3.76
Transferrin	2.0–3.2	76 500	5.9	5.5	5.0
Hemopexin	0.56–0.89	57 000	5.8	4.8	–
Lipoproteins	5.5–6	140 000–20 000 000	–	–	5.4
IgA (Monomer)	1.4–4.2	162 000	–	7	3.4
IgG	6–17	150 000	6.3–7.3	6.5–7.0	4.0
IgM	0.5–1.9	950 000	–	18–20	2.6
C1q	0.05–0.1	459 000	–	11.1	–
C3	1.5–1.7	185 000	6.1–6.8	9.5	4.5
C4	0.3–0.6	200 000	–	10.0	–
Fibrinogen	2.0–4.0	340 000	5.5	7.6	1.97

Protein	Plasma concentration (mg/mL)	E ₂₈₀ ³	V ₂₀ ⁴	CH ₂ O ⁵	Half-life (days)
Prealbumin	0.12–0.39	14.1	0.74	–	1.9
Albumin	38–52	5.8	0.733	0	17–23
α ₁ . Acid glycoprotein (orosomuroid)	0.5–1.5	8.9	0.675	41.4	5.2
α ₁ . Antitrypsin	2.0–4.0	5.3	0.646	12.2	3.9
α ₂ . Macroglobulin	1.5–4.5	8.1	0.735	8.4	7.8
α ₂ . Haptoglobin					
Type 1.1	1.0–2.2	12.0	0.766	19.3	2–4
Type 2.1	1.6–3.0	12.2	–	–	
Type 2.2	1.2–2.6	–	–	–	
α ₂ . Ceruloplasmin	0.15-.60	14.9	0.713	8	4.3
Transferrin	2.0–3.2	11.2	0.758	5.9	7–10
Hemopexin	0.56–0.89	19.7	0.702	23.0	9.5

(continued)

Table C1.7 (continued)

Protein	Plasma concentration (mg/mL)	E_{280}^3	V_{20}^4	CH_2O^5	Half-life (days)
Lipoproteins	5.5–6	–	–	–	–
IgA (Monomer)	1.4–4.2	13.4	0.725	7.5	5–6.5
IgG	6–17	13.8	0.739	2.9	20–21
IgM	0.5–1.9	13.3	0.724	12	5.1
C1q	0.05–0.1	6.82	–	8	–
C3	1.5–1.7	–	0.736	–	–
C4	0.3–0.6	–	–	–	–
Fibrinogen	2.0–4.0	13.6	0.723	2.5	3.1–3.4

¹ Sedimentation constant in water at 20°C, expressed in Svedberg units.

² Diffusion coefficient in water at 20°C, expressed in 10^{-7} cm²/s.

³ Extinction coefficient for light of wavelength 280 nm traveling 1 cm through a 10 mg/ml protein solution.

⁴ Partial specific volume of the protein at 20°C, expressed as ml g⁻¹

⁵ Carbohydrate content of the protein, expressed as the percentage by mass.

Table C1.8 Proteins involved in blood coagulation [19]

Protein	Plasma concentration (µg/mL)	Relative molecular weight, M_r (Da)	Biological half-life $t_{1/2}$ (hr)
Fibrinogen	2000–4000	340 000	72–120
Prothrombin	70–140	71 600	48–72
Factor III (tissue factor)	–	45 000	–
Factor V	4–14	330 000	12–15
Factor VII	trace	50	2–5
Factor VIII	~0.2	330 000	8–12
Factor IX	~5.0	330 000	24
Factor X	~12	58 800	24–40
Factor XI	2.0–7.0	160 000	48–84
Factor XII	15–47	80 000	50–60
Factor XIII	~10	320 000	216–240
Protein C	~4.0	62 000	10
Protein S	~22	77 000	–
Protein Z	~2.9	62 000	60
Prekallikrein	35–50	85 000	–
High molecular weight kininogen	70–90	120 000	–
α_1 . Protease inhibitor	2500	55 000	–
Antithrombin III	230 ± 23	58 000	67

Table C1.9 Proteins in the compliment system

Protein	Serum concentration (mg/L)	Relative molecular weight, Mr (Da)	Sedimentation constant $S_{20W}(10^{-13}S)$
C1q	70 ± 14	459 000	11.1
C1r	39 ± 2	83 000	7.5
C1s	36 ± 3	83 000	4.5
C2	27 ± 5.6	108 000	4.5
C3	1612 ± 244	185 000	9.5
C4	498 ± 151	200 000	10.0
C5	153 ± 29	185 000	8.7
C6	50.9 ± 8	128 000	5.5
C7	4–60	121 000	6.0
C8	43.2 ± 6.5	151 000	8.0
C9	57.5 ± 12.7	71 000	4.5
Factor B	275 ± 55	92 000	5–6
Factor D	trace	24 000	3.0
Properdin	28.4 ± 5	220 000	5.4
C1 inhibitor	158 ± 14	100 000	–
Factor H	525 ± 58	150 000	6.0
Factor I	38.6 ± 5.5	88 000	5.5

Additional Reading

Ditmer, D.S. (ed.) (1961) *Blood and Other Body Fluids*, Federation of American Societies for Experimental Biology, Washington, D.C.

This text provides a thorough compilation of the physical properties and composition of numerous biological fluids. Unlike the *Geigy Scientific Tables*, this book also reports data for many non-human species. However, citations and some measurement techniques are somewhat outdated.

Kjeldsberg C.R. and Knight J.A. (eds) (1993) *Body Fluids: Laboratory Examination of Amniotic, Cerebrospinal, Seminal, Serous & Synovial Fluids*, 3rd ed., American Society of Clinical Pathologists, Chicago.

An excellent source of information, especially for a clinician or medical technologist. Includes numerous color photographs of fluids and cells. Discusses abnormal amounts or types of specific proteins and cells in fluids as potentially diagnostic of disease states.

Lentner, C. (ed.) (1984) *Geigy Scientific Tables*, Ciba-Geigy, Basle.

This is the most comprehensive source of information available on properties and composition of body fluids. Volumes 1 and 3 provide extensive data, generally in tabular form, on fluid content (as well as measurement technique), related to gender, age and disease state.

References

1. Dittmer, D.S. (ed.) (1961) *Blood and Other Body Fluids*, Federation of American Societies for Experimental Biology, Washington, D.C.
2. Fullard, R.J. (1988) *Current Eye Research*, **7**, 163–179.
3. Chmiel, H. and Walitza, E. (1980) *On the Rheology of Blood and Synovial Fluids*, Research Studies Press, New York.
4. Barbanel, J.C., Lowe, G.D.O. and Forbes, C.D. (1984), The viscosity of blood. in *Mathematics in Medicine and Biomechanics*, G.F. Roach (ed.), Shiva Publications, Nantwich, p. 19.
5. Begg, T.B. and Hearn, J.B. (1966) Components in blood viscosity: The relative contribution of hematocrit, plasma fibrinogen and other proteins. *Clinical Science*, **31**, 87–93.
6. Whitmore, R.L. (1968) *Rheology of The Circulation*, Pergamon Press, New York.
7. Merrill, E.W. (1969) Rheology of blood. *Physiology Reviews*, **49**, 863–867.
8. Harkness, J. (1971) The viscosity of human blood plasma: Its measurement in health and disease. *Biorheology*, **8**, 171–193.
9. Lowe, G.D.O., Barbanel, J.C. and Forbes, C.D. (eds) (1981) *Clinical Aspects of Blood Viscosity and Cell Deformability*, Springer-Verlag, New York.
10. Lowe, G.D.O and Barbanel, J.C. (1988) Plasma and blood viscosity, in *Clinical Blood Rheology*, G.D.O. Lowe (ed.), CRC Press, Boca Raton, pp. 11–44.
11. Schmidt-Schonbein, H. (1988) Fluid dynamics and hemorheology, in *Clinical Blood Rheology*, G.D.O. Lowe (ed.), CRC Press, Boca Raton, pp. 129–220.
12. Lentner, C. (ed.) (1984) *Geigy Scientific Tables*, Ciba-Geigy, Basle.
13. Bicks, R.L. (1993) *Hematology: Clinical and Laboratory Practice*, Mosby, St Louis.
14. Sokoloff, L. (ed.) (1978) *The Joints and Synovial Fluid*, Academic Press, New York.
15. Hermens, W.T., Willems, G.M. and Visser, M.P. (1982) *Quantification of Circulating Proteins: Theory and Applications Based on Analysis of Plasma Protein Levels*, Martinus Nijhoff, The Hague.
16. Colman, R.W., Hirsh, J., Marder, V.J., et al. (eds) (1993) *Hemostasis and Thrombosis*, Lippincott, Philadelphia.
17. Schultze, H.E. and Heremans, J.F. (1966) *Nature and Metabolism of Extracellular Proteins*, Elsevier, Amsterdam.
18. Bing, D.H. (ed.) (1978) *The Chemistry and Physiology of the Human Plasma Proteins*, Pergamon Press, Boston.
19. Stamatoyannopoulos, G., Nienhuis, A.W., Majerus, P.W., et al. (eds) (1994) *The Molecular Basis of Blood Diseases*, W.B. Saunders, Philadelphia.

Chapter C2

The Vitreous Humor

Traian V. Chirila and Ye Hong

C2.1 Introduction

The vitreous humor, also termed vitreous body, vitreus, or vitreous, is a clear and transparent mass (gel or liquid or a mixture of both) that fills the posterior cavity of the eye in vertebrates, between the lens and the retina.

The mammalian vitreous humor can be defined as an avascular, virtually acellular, highly hydrated gel located in the vitreous cavity of the eye and consisting of a dilute network of heterotypic collagen fibrils surrounded by a mixture of glycosaminoglycans where hyaluronan is the predominant component. In humans, the vitreous humor is perceived as a gel-like body that can provide an adequate support for the retina, allows the diffusion of metabolic solutes, and allows the light to reach the retina. Historically, there are two differing concepts on the nature of vitreous humor. A significant amount of evidence supports the view that the vitreous humor is basically an extracellular matrix. Another model has been developed in which the vitreous body is considered as a specialized, but simple, connective tissue. The two concepts are not yet reconciled; therefore the structure and role of the vitreous humor are usually regarded from both points of view. It is generally accepted that this gel-like material possesses a unique macromolecular organization in the form of a double-network system consisting of a scaffold of randomly spaced rodlike collagen fibrils surrounded by and entangled with a network of very large coiled-up macromolecules of hyaluronic acid (hyaluronan). The double-network model explains satisfactorily most of the properties of the vitreous body, as well as its remarkable mechanical stability, although it probably overestimates the importance of hyaluronan. The natural vitreous gel displays true viscoelastic properties which

T.V. Chirila (✉)

Queensland Eye Institute, 140 Melbourne Street, South Brisbane, QLD 4101, Australia

e-mail: traian.chirila@qei.org.au

Y. Hong

Cooper Vision, Inc., Pleasanton, CA 94588, USA

enable it to resist sudden compression shocks, offering much the best protection for the retina against contusion trauma. It is generally believed that the hyaluronan network imparts the latter feature, while the collagen network is responsible for the plasticity and tensile strength of the vitreous humor. The above considerations illustrate the understanding of the supramolecular organization of the vitreous humor as presented it in the first edition of this book [1]. Since that time, there was not much progress in this understanding [2]. However, our appreciation of the physiological role and functions of the vitreous humor in the eye has improved significantly [3, 4]. Further research revealed its central role in major diseases of the eye such as diabetic retinopathy, retinal vein occlusion, age-related macular degeneration, nuclear sclerotic cataract, and primary open-angle glaucoma [5].

Biochemically, the vitreous humor consists of collagen types I, V, IX, and XI, non-collagenous proteins (opticin, fibrillin-1, VIT1, fibronectin, proteoglycans, and others), and glycosaminoglycans [3, 6]. There has been considerable controversy regarding the existence of direct interactions between hyaluronan and the collagen fibrils, and the role of the former in maintaining the long-range spacing in the collagen network. There is no clear evidence for such interactions, but some experiments have suggested [7] that about 6 % of the total hyaluronan may be involved in maintaining the vitreous gel in a distended state. However, it is rather believed [3] that, due to indirect interfibrillar interactions, the collagen network has sufficient mechanical resilience to support itself in solution. It was suggested that the vitreous humor plays only a minor role in the regulation of intraocular pressure [8].

The role of the vitreous humor and its physiological functions in the human eye can be summarized as such: (a) contributes to the growth of the eye and to maintaining its volume, elasticity, and resilience, and provides protection during mechanical trauma; (b) contributes to the total transparency of the ocular pathways; (c) serves as a support for the intraocular lens and contributes to the accommodation; (d) acts as a repository and transport conduit for the substances involved in the metabolism of the surrounding ocular tissues; (e) acts as a barrier to biomolecules, biomacromolecules, and cells, and as an inhibitor of inflammation and neovascularization; (f) prevents the onset of certain types of cataract by protecting the intraocular lens against oxygen-induced damage; and (g) plays a significant role in the etiology of a number of major ocular diseases.

C2.1.1 Compendium of Physicochemical Characteristics of the Human Vitreous Humor

As is the case with many other structural elements of the eye, there are presently much more data on animal vitreous humor than on the human counterpart. The numerical data tabulated here cover almost everything reported so far on the analysis of the human vitreous. However, in many cases it is not possible to select a most reliable single value; dependable values representing a range are thus provided in several of the following tables, illustrating the large variability in the experimental methodology from one laboratory to another, in collecting and processing the

samples, and in the individual, inherent characteristics of samples as such. Also, considering that the vitreous samples processed and subjected to analysis were all postmortem, differences are expected in some characteristics as compared to the antemortem vitreous humor.

Being a very loose tissue, albeit well structured in a highly specialized way, the vitreous body becomes a homogeneous fluid during processing for measurements; therefore, the resulting data for its properties illustrate rather the behavior of a fluid consisting mainly of water and containing minute amounts of inorganic and organic components. The dimensional characteristics, bulk chemical composition, and optical properties are seemingly not affected by the homogenization process. However, some investigators considered the separate existence of gel and liquid fractions in the vitreous.

Over the past decades, the vitreous body was perceived as a typical viscoelastic material. Accounts of the earlier rheological studies of the mammalian vitreous humor have been summarized elsewhere [32, 33]. Since the first edition of this book, a number of rheological studies [34–39] have been reported on the animal vitreous, but almost none regarding the human vitreous. We can say that its characterization by rheometry (Table C2.9) is still in its infancy, perhaps due to the large sample variability. Indeed, in ten postmortem eyes, between the ages of 21 and 65 years, a range of 2–38 Pa was measured experimentally for the storage modulus G' [41], with no clear dependence upon age and with sample-to-sample variation observed even in two humors harvested from the same donor.

Table C2.1 Physical properties of the human vitreous humor

Property	Value	Source
Volume	3.9 mL	[9]
Weight	3.9 g	[9]
Water content	99.7 %	[10]
	99 %	[11]
pH	7.5	[12]
	7.4–7.52	[13]
	7–7.3	[14]
Osmolality	288–323 mOsm/kg	[15]
Osmotic pressure		
(freezing-point depression)	–0.554 to –0.518 °C	[12]
Density	1.0053–1.0089 g/cm ³	[16]
Intrinsic viscosity	3–5 × 10 ³ cm ³ /g	[17]
Dynamic viscosity	1.6 cP	[18]
Refractive index	1.3345	[19]
	1.3345–1.337	[9]

Table C2.2 Inorganic ion content of the human vitreous humor

Ion	Representative value	Source
Sodium	2.714–3.542 mg/cm ³	[23]
	135–151 mEq/L	[24]
	3.15 g/kg water	[11]
	2.603–5.805 mg/cm ³	[14]
Potassium	130–470 µg/cm ³	[23]
	0.15 g/kg H ₂ O	[11]
	4.2–7.2 mEq/L	[24]
Calcium	308–788 µg/cm ³	[14]
	56–106 µg/cm ³	[23]
	6.0–8.0 mg/100 mL	[24]
Phosphate	14–76 µg/cm ³	[14]
	0.1–3.3 mEq/dm ³	[23]
Chloride	3.155–5.140 mg/cm ³	[23]
	108–132 mEq/L	[24]
	4 g/kg water	[11]
	3.477–7.621 mg/cm ³	[14]
Bicarbonate	1.2–3.0 g/kg water	[11]

Table C2.3 Organic content of the human vitreous humor (low-molecular-weight components)

Component	Representative value	Source
Lipids	2 µg/mL	[25]
Glucose	17–105 mg/dL water	[23]
	37–180 mg/100 mL	[24]
	30–70 mg/dL water	[11]
Lactic acid	70 mg/dL water	[11]
Urea	24–172 mg/dL water	[23]
Creatinine	0.3–3.0 mg/dL water	[23]
Citrate	1.9 mg/dL water	[11]
Pyruvic acid	7.3 mg/dL water	[11]
Ascorbic acid	36 mg/100 g	[26]

Table C2.4 Organic content of the human vitreous humor (high-molecular-weight components)

Component	Representative value ($\mu\text{g}/\text{cm}^3$)	Source
Proteins ^a	280–1360	[25]
	450–1100	[27]
Hyaluronan	100–400	[27]
	42–399	[14]
	65–210	[28]
Versican ^b	60	[29]
Collagen	40–120	[27]
	30–532	[14]
Albumin	293 ± 18	[30]
Immunoglobulin (IgG)	33.5 ± 3	[30]
α_1 -Antitrypsin	141 ± 2.9	[30]
α_1 -Acid glycoprotein	4 ± 0.7	[30]

(\pm) represents standard deviation

^aTotal protein content

^bA high-molecular-weight proteoglycan based on chondroitin sulfate

Table C2.5 Variation with age of total protein content in the liquid fraction of human vitreous [27]

Age range (years)	Protein (mg/cm^3)
10–50	0.4–0.6
50–80	0.7–0.9
>80	0.9–1.0

Table C2.6 Axial length of the human vitreous body during maturation [20]^a

Age (years) and gender	Axial length (mm)
<13, male	10.48
<13, female	10.22
>13, male	16.09
>13, female	15.59

^aThe axial growth of the vitreous body is essentially completed by the age of 13 years

Table C2.7 Gel and liquid volume of the human vitreous as a function of age (adapted from [21])^a

Age (years)	Gel volume (cm ³)	Liquid volume (cm ³)
Birth	1.6	0
5	3.3	0
10	3.5	0.7
20	3.9	0.9
30	3.9	0.9
40	3.9	0.9
50	3.5	1.3
60	3.2	1.6
70	2.8	2.0
80	2.5	2.3
90	2.2	2.6

^aThe liquid vitreous appears first in childhood and by the seventh decade it occupies half of the vitreous [21, 22]

Table C2.8 Transmission of radiation through the human vitreous humor (adapted from [31])

Wavelength (nm)	Transmittance (total, %)
300	0
325	76
350	82
400	90
500	97
600	98
700	98

Table C2.9 Rheological characteristics of the human vitreous humor [40]

Parameter	Anterior	Region in the vitreous	
		Central	Posterior
Residual viscosity η_m (Pa s)	1.4	2.2	4.9
Internal viscosity η_k (Pa s)	0.3	0.35	0.5
Relaxation time τ_m (s)	0.38	0.30	1.61
Retardation time τ_k (s)	0.27	0.41	0.46
Elastic compliance, instantaneous, J_m (m ⁻² N ⁻¹)	0.1	0.3	0.3
Elastic modulus, internal, G_k (Pa)	2.5	1.3	1.2

Additional Reading

Balazs, E.A. (1968) The molecular biology of the vitreous, in *New and Controversial Aspects of Retinal Detachment* (ed A. McPherson), Harper & Row, New York, pp. 3–15.

This is a landmark paper on the nature of the vitreous body, describing the “mechanochemical” (or “double-network”) model. This model explains satisfactorily the correlations between some properties of the vitreous (composition, rheology, volume, cell population, transparency) and the physicochemical principles governing its stability (frictional interaction, expansion/contraction, the excluded-volume concept, and the molecular-sieve effect).

Berman, E.R. and Voaden, M. (1970) The vitreous body, in *Biochemistry of the Eye* (ed C.N. Graymore), Academic Press, London, pp. 373–471.

A comprehensive summary of knowledge at that time on animal and human vitreous humor, including development, chemical composition, metabolism, and aging effects.

Shields, J. A. (1976) Pathology of the vitreous, in *Current Concepts of the Vitreous Including Vitrectomy* (ed K.A. Gitter), C.V. Mosby Co., St. Louis, pp. 14–42.

This book chapter presents competently the pathologic vitreous, including developmental abnormalities, inflammation, hemorrhage, effects of trauma, systemic diseases, and degenerative processes.

Gloor, B.P. (1987) The vitreous, in *Adler’s Physiology of the Eye*, 8th edn (eds R.A. Moses and W.M. Hart), C.V. Mosby Co., St. Louis, pp. 246–267.

A concise description of all aspects of the vitreous humor, including properties, development, anatomy, structure, biochemistry, metabolism, and pathology.

Sebag, J. (1989) *The Vitreous. Structure, Function, and Pathology*, Springer-Verlag, New York.

This is probably only the second single-authored book in this century to be dedicated entirely to the topic of vitreous humor, written by the leading scholar in the field. It is a well-structured and updated compendium. The first half of the book is dedicated to structure, properties, and physiology of the vitreous. Pathology of the vitreous is analyzed in the other half from a biological angle. Although a clinician, the author manages to avoid typical clinical descriptions and to provide a text which integrates the basic scientific knowledge for both clinicians and scientists.

Williams, G.A. and Blumenkranz, M.S. (1992), Vitreous humor, in *Duane’s Foundations of Clinical Ophthalmology*, vol. 2 (eds W. Tasman and E.A. Jaeger), J.B. Lippincott Co., Philadelphia, chapter 11.

This chapter (27 pages) presents the modern concepts in the pathophysiologic mechanisms of vitreous diseases, and in the clinical conditions involving the vitreous (detachment, macular holes and membranes, diabetes, proliferative vitreoretinopathy, hyalosis, amyloidosis). Aspects such as separation of the vitreous from the retina and traction of the vitreous by hypocellular gel contraction are explained according to the most recent findings.

Lund-Andersen, H., Sebag, J., Sander, B. and la Cour, M. (2006) The vitreous, in *The Biology of the Eye* (ed J. Fischbarg), Elsevier, Amsterdam, pp. 181–94.

A concise but very informative text covering all aspects of the vitreous humor.

Lund-Andersen, H. and Sander, B. (2011) The vitreous, in *Adler's Physiology of the Eye*, 11th edn (eds L.A. Levin *et al.*), Elsevier, Edinburgh, pp. 164–81.

The most recent chapter on the vitreous humor to appear in the traditional textbook, covering the modern views on this part of the eye, and emphasizing biophysical and physiological aspects.

Sebag, J. and Green, W.R. (2013) Vitreous and vitreoretinal surface, in *Retina*, 5th edn (ed S.J. Ryan), vol. 1, part 2, Elsevier, Amsterdam, pp. 482–516.

A concise, update, and beautifully written account of the current knowledge of the vitreous humor, providing a balanced presentation of the structure, anatomy, physiology, and pathology of the vitreous and of its interface with the retina. This chapter in the classical monumental treatise displays also remarkable graphics.

Recommended sources for ophthalmic terminology:

Cassin, B., Solomon, S.A.B. and Rubin, M.L. (1990) *Dictionary of Eye Terminology*, 2nd edn, Triad Publishing Co., Gainesville, FL, 286 pp.

Stein, H.A., Slatt, B.J. and Stein, R.M. (1992) *Ophthalmic Terminology. Speller and Vocabulary Builder*, 3rd edn, Mosby-Year Book Inc., St. Louis, MO, pp. 3–33, 183–198, 275–278.

Myles, W.M. (1993) Ophthalmic etymology. *Surv. Ophthalmol.*, **37**, 306–9.

References

1. Chirila TV, Hong Y (1998) The vitreous humor. In: Black J, Hastings G (eds) *Handbook of biomaterial properties*. Chapman & Hall, London, pp 125–131
2. Sebag J (2009) Vitreous: the resplendent enigma. *Br J Ophthalmol* 93:989–991
3. Bishop PN (2000) Structural macromolecules and supramolecular organization of the vitreous gel. *Prog Retin Eye Res* 19:232–244
4. Kleinberg TT, Tzekov RT, Stein L, Ravi N, Kaushal S (2011) Vitreous substitutes: a comprehensive review. *Surv Ophthalmol* 56:300–323
5. Holekamp NM (2010) The vitreous gel: more than meets the eye. *Am J Ophthalmol* 149:32–36
6. Angi M, Kalirai H, Coupland SE, Damato BE, Semeraro F, Romano MR (2012) Proteomic analyses of the vitreous humour. *Mediat Inflamm* 2012; Article ID 148039 (7 pages). doi:10.1155/2012/148039
7. Bishop PN, McLeod D, Reardon A (1999) Effects of hyaluronan lyase, hyaluronidase, and chondroitin ABC lyase on mammalian vitreous gel. *Invest Ophthalmol Vis Sci* 40:2173–2178
8. Collins R, van der Werff TJ (1980) Mathematical models of the dynamics of the human eye. *Lect Notes Biomath* 34:5–6
9. Redslob E (1932) *Le corps vitré*. Masson & Cie, Paris, pp 299–305
10. Duke-Elder WS (1929) The physico-chemical properties of the vitreous body. *J Physiol* 68:155–165
11. Nordmann J (1968) Chimie. In: Brini A, Bronner A, Gerhard JP *et al* (eds) *Biologie et chirurgie du corps vitré*. Masson & Cie, Paris, pp 95–167

12. Mörner CT (1894) Untersuchung der Proteinsubstanzen in den licht-brechenden Medien des Auges. *Z Physiol Chem* 18:233–256
13. Gala A (1925) Observations on the hydrogen ion concentration in the vitreous body of the eye with reference to glaucoma. *Br J Ophthalmol* 9:516–519
14. Lee B (1994) Comparative rheological studies of the vitreous body of the eye. Ph.D. Thesis, University of Pennsylvania, 1992. U.M.I./Bell & Howell Co., Ann Arbor, MI, pp. 102, 138–152
15. Sturmer WQ, Dowdey ABC, Putnam RS, Dempsey JL (1972) Osmolality and other chemical determinations in postmortem human vitreous humor. *J Forensic Sci* 17:387–393
16. Visser-Heerema J (1936) Über das spezifische Gewicht der bei der Operation von Netzhautablösungen gewonnenen Flüssigkeit. *Arch Augenheilkd* 109:543–561
17. Berman ER, Michaelson IC (1964) The chemical composition of the human vitreous body as related to age and myopia. *Exp Eye Res* 3:9–15
18. Shafer DM (1965) Intraocular injections as adjuncts to other retinal detachment procedures. In: Schepens CL, Regan CDJ (eds) *Controversial aspects of the management of retinal detachment*. Little, Brown & Co., Boston, pp 186–204
19. Guggenheim I, Franceschetti A (1928) Refraktometrische Untersuchungen des Glaskörpers von Kaninchen und Mensch (unter physiologischen und pathologischen Bedingungen). *Arch Augenheilkd* 98:448–482
20. Larsen JS (1971) The sagittal growth of the eye. III. Ultrasonic measurement of the posterior segment (axial length of the vitreous) from birth to puberty. *Acta Ophthalmol* 49:441–453
21. Balazs EA (1992) Functional anatomy of the vitreous. In: Tasman W, Jaeger EA (eds) *Duane's foundations of clinical ophthalmology*, vol 1. J.B. Lippincott Co., Philadelphia, Chapter 17
22. Balazs EA, Denlinger JL (1982) Aging changes in the vitreous. In: Sekuler R, Kline D, Dismukes K (eds) *Aging and human visual function*. Alan R. Liss, Inc., New York, pp 45–57
23. Naumann HN (1959) Postmortem chemistry of the vitreous body in man. *Arch Ophthalmol* 62:356–363
24. Coe JI (1969) Postmortem chemistries of human vitreous humor. *Am J Clin Pathol* 51:741–750
25. Swann DA (1980) Chemistry and biology of the vitreous body. *Int Rev Exp Pathol* 22:1–64
26. Süllmann H (1951) *Chemie des Auges*. *Tabul Biol* 22:1–119
27. Balazs EA, Denlinger JL (1984) The vitreous. In: Davson H (ed) *The eye*, vol 1a, 3rd edn. Academic, Orlando, FL, pp 533–589
28. Grimshaw J, Kane A, Trocha-Grimshaw J, Douglas A, Chakravarthy U, Archer D (1994) Quantitative analysis of hyaluronan in vitreous humor using capillary electrophoresis. *Electrophoresis* 15:936–940
29. Theocharis DA, Skandalis SS, Noulas AV, Papageorgakopoulou N, Theocharis AD, Karamanos NK (2008) Hyaluronan and chondroitin sulfate proteoglycans in the supramolecular organization of the mammalian vitreous body. *Connect Tissue Res* 49:124–128
30. Clausen R, Weller M, Wiedemann P et al (1991) An immunochemical quantitative analysis of the protein pattern in physiologic and pathologic vitreous. *Graefe's Arch Clin Exp Ophthalmol* 229:186–190
31. Boettner EA, Wolter JR (1962) Transmission of the ocular media. *Invest Ophthalmol* 1:776–783
32. Chirila TV, Hong Y, Dalton PD, Constable IJ, Refojo MF (1998) The use of hydrophilic polymers as artificial vitreous. *Prog Polym Sci* 23:475–508
33. Swindle-Reilly KE, Ravi N (2010) Designing hydrogels as vitreous substitutes in ophthalmic surgery. In: Chirila T (ed) *Biomaterials and regenerative medicine in ophthalmology*. Woodhead Publishing Ltd/CRC, Oxford/Boca Raton, pp 339–373
34. Nickerson CS, Karageozian HL, Park J, Kornfield JA (2005) Internal tension: a novel hypothesis concerning the mechanical properties of the vitreous humor. *Macromol Symp* 227:183–189

35. Nickerson CS, Park J, Kornfield JA, Karageozian H (2008) Rheological properties of the vitreous and the role of hyaluronic acid. *J Biomech* 41:1840–1846
36. Zimmerlin JA, McManus JJ, Crosby AJ (2010) Cavitation rheology of the vitreous: mechanical properties of biological tissue. *Soft Matter* 6:3632–3635
37. Sharif-Kashani P, Nishida K, Kavehpour HP, Schwartz SD, Hubschman JP (2013) Effect of cut rates on fluidic behavior of chopped vitreous. *Retina* 33:166–169
38. Abdelkawi SA, Abdel-Salam AM, Ghoniem DF, Ghaly SK (2013) Vitreous humor rheology after Nd:YAG laser photo disruption. *Cell Biochem Biophys* 68:267–274
39. Watts F, Tan LE, Wilson CG, Girkin JM, Tassieri M, Wright AJ (2014) Investigating the micro-rheology of the vitreous humor using an optically trapped local probe. *J Opt* 16; Article ID #015301 (7 pp)
40. Lee B, Litt M, Buchsbaum G (1992) Rheology of the vitreous body. Part I: Viscoelasticity of human vitreous. *Biorheology* 29:521–533
41. Nickerson CS (2006) Engineering the mechanical properties of ocular tissues. Ph.D. Thesis, California Institute of Technology, 2005, pp. 57–59. <http://resolver.caltech.edu/CaltechETD:etd-03172005-145045>. Accessed 11 Dec 2013

Chapter C3

The Cornea

Traian V. Chirila and Shuko Suzuki

C3.1 Introduction

It would be perhaps unreasonable to rank various elements or segments of the human eye according to a criterion based on their level of importance. The eye works as an eminently complex system where each part plays a definite role in the process of maintaining normal vision. Yet, a tendency toward emphasizing the functional prominence of the cornea can be noticed in the ophthalmic literature. A possible reason may be the fact that the cornea is the first layer of the eye, in direct contact with the external environment, which results in functional tasks different from most of the other ocular elements. Indeed, the cornea acts as the essential barrier that protects the eye against physical and chemical injuries. Other functions of the cornea include the following: (a) it assures almost 100 % transmission of visible light and about 70 % of the total dioptric power of the human eye; (b) it protects the posterior ocular elements against damage from UV radiation by absorbing the rays between the wavelengths 200 and 300 nm; (c) it withstands the intraocular pressure (IOP) exerted from within the eye; (d) it functions as an impervious barrier against microbes and other pathogens. The intricate architecture of the cornea, comprising five discrete layers (epithelium, Bowman's layer, stroma, Descemet's membrane, and endothelium, as counted from outside toward inside), all within 500–600 μm of tissue, may be both a consequence and an indication of the diversity of the functional requirements the cornea must meet. As it is now in the vertebrate eye—a transparent, clear, smooth, elastic, tough, and relatively thick multilayered tissue—the cornea appears as an ideal result of evolution and the epitome of an expedient structure-to-function relationship.

T.V. Chirila (✉) • S. Suzuki

Queensland Eye Institute, 140 Melbourne Street, South Brisbane, QLD 4101, Australia

The corneal epithelium (about 10 % of the total corneal thickness) consists in 5 to 7 layers of specialized cells, which are interconnected. About 90 % of the corneal thickness is constituted by the stroma (*substantia propria*). This layer consists of water (about 78 % by weight [A6]), collagen fibrils, proteoglycans as ground substance, and a few specialized cells (keratocytes). The collagen fibrils are organized in lamellae in a highly specific fashion, imparting considerable mechanical strength to the stroma. The stroma manifests permanently a tendency to swell in water, due to the hydrophilicity of proteoglycan components. A cornea with a stroma that swells beyond the normal value becomes opaque and, if untreated, leads to reduced vision or blindness. The stroma rests upon Descemet's membrane, a strong and highly elastic membrane. The endothelium (or the posterior epithelium) is a single layer of hexagonal cells. The endothelium performs the crucial task of maintaining the normal hydration of the stroma, through its "leaky barrier-and-pump" function, with a complicated and not fully understood mechanism. This process puts extraordinary metabolic demands upon the endothelial cells.

The cornea is able to maintain indefinitely its integrity and transparency. Upon pathogenic attack or due to external insults, its defense capability may be overpowered and the ensuing disruption of any of the processes governing the cornea's performance will lead to reduced vision. The cornea can be afflicted by a large variety of disorders, of which many are able to cause loss of vision despite treatment [A5, 1–4]. It can be affected by pathologic disorders (inflammations, dystrophies, and degenerations), as well as by traumatic disorders (caused by mechanical, thermal, or chemical injuries). Modern ophthalmology provides a large range of treatment procedures, but in case of opaque or distorted corneas, only the transplantation of donor corneal grafts (known as penetrating keratoplasty) can restore vision. In fact, the first successful full-thickness allograft was performed in the cornea [5], and today the penetrating keratoplasty is still one of the most successful procedures for organ transplantation. However, this procedure has a poor outcome in cases of chemical burns, vascularized traumatic injuries, and a number of pathologic conditions. The alternative for such cases is either prosthokeratoplasty, a procedure where the damaged cornea is replaced with an artificial cornea, known also as a keratoprosthesis, or transplantation of tissue-engineered constructs [6–8].

C3.2 Compendium of Physicochemical Characteristics of the Cornea

It is rather surprising that, in spite of the prominence given to its study, the human cornea has been considerably less investigated than the animal corneas in some respects, perhaps less than any ocular element, which is rather peculiar considering that excised tissue rims from postmortem corneas are routinely discarded in the eye banks. Experimental data concerning certain properties of the human cornea, such as its composition or electrical properties, are actually available to a little extent,

and the investigators must rely upon information abundantly available for the cornea of a variety of other vertebrate species. Table C3.1 shows information available on the composition of the human cornea, as summarized by Ehlers and Hjortdal [A6] (likely as rounded-off values). The fact that our literature search did not result in more data confirms the above statement.

Another peculiarity of the study of the human cornea is the great attention and amount of research dedicated to its dimensional characteristics (diameter, thickness, geometry). However, this aspect has a justification. For instance, the corneal diameter is an important tool in identifying the congenital and developmental anomalies of the cornea, and for the design and fitting of contact lenses, intraocular lenses, and capsular tension rings. The early literature on the measurement of the corneal diameter has been reviewed by Martin and Holden [9]; more recent results, with an emphasis on the corneas of non-Caucasian subjects, have been summarized by Mashige [10]. As such, the concept of “corneal diameter” is poorly defined and still debated, and consequently the reported estimations differ to some extent between investigators. Table C3.2 presents a selection of data for the corneal diameter. Similarly, the measurement of the thickness of the human cornea triggered an inordinate amount of investigation. Since the corneal thickness is very sensitive to

Table C3.1 Composition of the human corneal stroma [A6]

Component	% (wt)
Water	78
Collagen	15
Other proteins	5
Keratan sulfates	0.7
Chondroitin sulfate	0.3
Salts	1

Table C3.2 Diameter of the cornea^a

Value (mm)	Remarks	Source
12.89±0.60 ^{b,c}	HCD ^d	[9]
11.64±0.49 ^{b,c}	HVID ^e	[9]
11.71±0.42 ^{b,f}	Horizontal WTW ^g diameter	[11]
11.46±0.48 ^{b,h}	Horizontal WTW diameter	[12]
10.63±0.63 ^{b,h}	Vertical WTW diameter	[12]
11.05±0.52 ^{b,h}	Average (horizontal, vertical)	[12]

^a early literature reviewed in [9] shows a variation for horizontal diameters between 10.25 and 13.5 mm; the recent literature reviewed in [10], with emphasis on non-Caucasian corneas, shows a variation between 10 and 14.6 mm for the HVID and between 10 and 11 mm for the VVID; ^b ± standard deviation; ^c measured in 50 persons aged between 20 and 29 years, using catoptric imaging and closed-circuit television; ^d horizontal corneal diameter; ^e HVID: horizontal visible iris diameter; VVID: vertical visible iris diameter; ^f measured in 370 right eyes and 373 left eyes (all Caucasians), using the Orbscan II topography system; ^g “white-to-white” diameter; ^h measured (in triplicate) in 78 postmortem eyes, using a Castroviejo caliper

an abnormal hydration of the stroma, and also related to the intraocular pressure in the eye, it became a diagnostic tool for certain pathological conditions, such as corneal degenerations. Exact measurement of the corneal thickness is also of great significance in the assessment of patients for corneal refractive surgery. The measurement of this quantity is associated with some difficulties; for instance, the thickness of postmortem corneas is much higher than in living persons due to uncontrolled hydration. Also, the thickness is not uniform throughout the cornea: it is the thinnest in the central region and becomes thicker toward the periphery. How important is this dimension is illustrated in the amount of research that has been reviewed in no less than four major papers [10, 13–15]. Table C3.3 contains representative values for the central corneal thickness (CCT).

An essential function of the cornea is to allow the formation of an image on the retina, and one of the prerequisites for this task is the existence of a curvature of the corneal surface(s) that can refract light sufficiently to focus on the retina. Corneal cur-

Table C3.3 Central corneal thickness in human subjects

Method	Value (μm) ^a	Source
Optical technique ^b	565 \pm 2.3 ^c	[16]
	559 \pm 4.5 ^d	[16]
	571 \pm 7.1 ^e	[16]
Optical technique ^b	507 \pm 4.2 ^f	[17]
Haag-Streit pachometer	520 \pm 18 (right eye) ^g	[18]
	524 \pm 20 (left eye) ^g	[18]
	534 (at wakening) ^h	[19]
	507 (at bedtime) ^h	[19]
Specular technique ^b	515 \pm 33 ⁱ	[20]
Ultrasound techniques	514.6 \pm 38.4 (right eye) ^j	[21]
	516.2 \pm 37.8 (left eye) ^j	[21]
	542 \pm 33 ^k	[22]
	545-556 ^l	[23]
Optical low-coherence reflectometry (OLCR)	519.6 \pm 1.2 (day 1) ^m	[24]
	519.9 \pm 0.9 (day 2) ^m	[24]
	523.8 \pm 0.6 (day 3) ^m	[24]
Orbscan pachometer (scanning slit principle)	596 \pm 40 ^k	[22]
Specular microscopy	566-578 ^l	[23]
	528.3 \pm 5.5 ⁿ	[25]
Ultrasound biomicroscopy	550-560 ^l	[23]

^a \pm standard error; ^b custom-made device; ^c measured in 224 corneas (from 125 persons) aged between <15 and >74 years; ^d measured in 55 corneas aged below 25 years; ^e measured in 28 corneas aged above 65 years; ^f measured in 44 persons aged between 18 and >35 years; ^g measured in 150 eyes (from 113 persons) aged between <15 and >74 years; ^h measured in 9 persons daily for 1 month; ⁱ measured in 115 persons aged between 10 and 90 years; ^j measured in 10 persons aged between 23 and 44 years; ^k measured in 20 persons, mean age 33.3 \pm 9 years; ^l measured in 31 persons (62 eyes), with the range given for 95 % confidence interval; ^m measured in one person for 3 consecutive days, 20 times each day; ⁿ measured in 40 persons (215 measurements)

vature, expressed commonly as the radius of curvature, has been of interest to vision scientists for centuries. A system of methodology and instrumentation, covered by the term “keratometry,” has been developed to measure the curvature of the central cornea. The refractive power of the cornea can be calculated from its radius of curvature, thickness, and refractive index. Representative values of the corneal radius of curvature and other derived parameters for the corneal optic system are summarized in Table C3.4.

Another parameter of significance for the light refraction through the cornea, intrinsic to the tissue as such, is the refractive index. Its measurement has a recorded history dating back to the nineteenth century, even before the introduction of refractometers. A refractive index of 1.376, which is commonly used in applications, has originated in the value of 1.3763 measured in human cornea by Matthiesen in 1891. However, as seen in Table C3.5, it has been seldom that refractive indices in the vicinity of 1.376 were reported. There is also substantial variability in the measured values, likely due to variation in tissues, subjects, and procedures. A similar level of

Table C3.4 Geometrical and optical properties of the human cornea^a

Property	Value	Source
Radius of curvature (mm) ^b	7.88 ± 0.045 ^{c,d}	[26] ^e
	7.796 (right eye)	[26] ^f
	7.746 (left eye)	[26] ^f
	7.7 (anterior surface) ^g	[27]
	6.8 (posterior surface) ^g	[27]
	7.249 to 8.993 (horizontal meridian) ^h	[28]
	6.637 to 8.001 (vertical meridian) ^h	[28]
	7.74 ± 0.26 ^{i,j}	[29]
	7.73 ± 0.29 ^{i,k}	[29]
	7.66 ± 0.26 ^{i,l}	[29]
	7.55 ± 0.28 ^{i,m}	[29]
	5.62 to 7.22 (posterior, vertical meridian) ⁿ	[30]
	7.84 (anterior, averaged) ^o	[31]
	6.42 (posterior, averaged) ^o	[31]
Refractive power (D)	8.03 ± 0.29 ^{c,p} (males)	[32]
	7.91 ± 0.28 ^{c,p} (females)	[32]
Refractive power (D)	43.05 ^r	[27]
First focal length (mm)	-23.227 ^r	[27]
Second focal length (mm)	31.031 ^r	[27]

^a for a review of the literature between 1975 and 2001 see [10], where the extreme values were reported in the ranges of 7.10 to 8.75 mm (in the horizontal meridian) and 7.06 to 8.66 mm (in the vertical meridian); ^b for a conversion table radius of curvature to refractive (dioptric) power see *Contact Lens Spectrum* (2012) at <http://www.clspectrum.com/printarticle.aspx?articleID=107267> (accessed 03/05/2014); ^c ± standard error; ^d measured in 12 eyes in living subjects; ^e [26]; ^f [26]; ^g measured in 2 persons; ^h measured in 26 persons, aged 19 to 36 years; ⁱ ± standard deviation; ^j measured in 27 emmetropic persons; ^k measured in 28 lowly myopic persons; ^l measured in 32 moderately myopic persons; ^m measured in 18 highly myopic persons; ⁿ measured in 120 children, aged 6 to 17 years; ^o measured in 25 persons, aged 60 to 80 years; ^p measured in 249 persons (498 eyes), aged between 18 and 29 years, all of Negroid race (African); ^r calculated from experimental values for radius of curvature and thickness, and assuming a refractive index of 1.376

Table C3.5 The refractive index of the human corneal tissue

Value	Remarks	Source
1.3569	Whole cornea	[33] ^a
1.377	Whole cornea, age 55 years	[27] ^b
1.3721	Whole cornea, age 2 days	[27] ^b
1.3763	Whole cornea	[27, 33] ^c
1.3751	Whole cornea, at 656.3 nm (red light)	[34] ^d
1.3818	Whole cornea, at 486.1 nm (blue light)	[34] ^d
1.401 ± 0.005 ^e	Corneal epithelium ^f	[35]
1.380 ± 0.005 ^e	Anterior corneal stroma ^g	[35]
1.373 ± 0.001 ^e	Posterior corneal stroma ^g	[35]
1.411 ± 0.001	Stromal collagen ^h	[36]
1.365 ± 0.003	Extracellular ground substance ^h	[36]
1.372 ^{g, i}	Stroma (from one enucleated eye)	[37]
1.404 ^{g, j}	Stroma (from one enucleated eye)	[37]
1.378 ^{h, i}	Stroma	[37]
1.399 ^{h, j}	Stroma	[37]
1.389 ± 0.004 ^{e, h, k}	At 1270 nm in 3 postmortem tissue specimens	[38]
1.3970 ± 0.001 ^{e, l}	Central epithelium	[39]
1.3946 ± 0.001 ^{e, l}	Nasal peripheral epithelium	[39]
1.3940 ± 0.001 ^{e, l}	Temporal peripheral epithelium	[39]
1.369 ± 0.008 ^{e, m}	Corneal stroma	[40]
1.373 ± 0.006 ^{e, n}	Corneal stroma	[41]

^a [33]; ^b [27]; ^c [27, 33]; ^d [34]; ^e ± standard deviation; ^f measured in 10 eyes, aged between 19 and 27 years; ^g measured in *ex vivo* tissue; ^h measured in postmortem eye(s); ⁱ measured immediately after removing the epithelium; ^j measured 35 min after removing the epithelium; ^k group refractive index (n_g) resulting from a low-coherence source; ^l measured in 10 persons, aged between 22 and 30 years; ^m measured during keratomileusis surgery (mechanical microkeratome) in 36 patients, aged between 18 and 56 years; ⁿ measured during keratomileusis surgery (femtosecond laser) in 115 patients, aged between 18 and 74 years

data spread can be noticed with respect to the measurement of radiation transmission through the cornea (Table C3.6).

Although the electrical properties of the ocular elements have been extensively investigated in the rabbit eye [47], there is little amount of such data on the human eye. Table C3.7 contains the available information regarding the human cornea.

Like any tissue in our body, the cornea undergoes changes with the passage of time. However, this tissue appears to be remarkably stable and to withstand elevated physical stress for long intervals, in most of the cases for our natural life duration. This dimensional stability, which is essential for normal vision, is a result of the inherent mechanical properties of the corneal tissues, and it is believed that the latter are ultimately determined by the properties and integrity of the stroma and the underlying Descemet's membrane. The biomechanics of the cornea is a rather well-established field. However, there are large discrepancies between the results of the mechanical characteristics measured for the human cornea. For instance, the variation in the reported experimental values for the elastic modulus covers three orders

Table C3.6 Transmission of ultraviolet and visible radiation through the human cornea

Wavelength (nm)	Transmittance (%)					
	Source:	[42] ^{a,b}	[43] ^{b,c}	[44] ^{b,d}	[45] ^{b,e}	[46] ^f
270		0	0	–	<0.01	–
290		0	0	–	0.1	–
300		0	~7	–	~2	–
310		58	~8	–	~8	27
325		63	33	–	~10	–
350		72	50	–	~12	–
400		81	58	–	~15	74
500		90	64	89.2	–	–
600		92	71	93.7	–	–
700		94	78	95.4	–	–

^a measured in 9 enucleated eyes, aged between 4 weeks and 75 years, on isolated cornea; ^b extrapolated from the transmission spectra; ^c measured on a 24-year-old cornea; ^d measured in 8 postmortem eyes, aged between 22 and 45 years, on the whole eyes; ^e measured in 20 corneal rims discarded from the eye bank; ^f measured in the central region of 4 postmortem corneas (aged 35 to 67 years) after removal of the epithelia; – not measured

Table C3.7 Electric properties of the human corneal tissue

Property	Value	Source
Relative permittivity	$62.6 \pm 0.13^{a,b}$	[48]
	$53.0 \pm 0.22^{a,c}$	[48, 49]
Conductivity ($S\ m^{-1}$)	$1.00 \pm 0.005^{a,b}$	[48]
	$1.05 \pm 0.01^{a,c}$	[48, 49]
	0.4 ^c	[50]
	0.26 ± 0.03^b	[51]
Transendothelial potential difference (μV)	200-500 ^{d,e}	[52-54]
Endothelial electrical resistance ($\Omega\ cm^2$)	$12.4 \pm 0.9^{d,f}$	[52]
	10.6 ^d	[54]
	10.26 ^d	[54]
Transendothelial short circuit current density ($\mu A\ cm^{-2}$)	$33.0 \pm 3.5^{d,f}$	[52]

^a range given for 95 % confidence interval; ^b measured at 20 °C; ^c measured at 37 °C; ^d postmortem corneas; ^e posterior side is negative; ^f \pm standard error

of magnitude! Diverse explanations have been advanced in order to explain such variation, including the following: (a) differences in methodology between laboratories; (b) nonuniform quality of the postmortem corneal specimens due to uncontrolled hydration; (c) nonlinearity of the stress-strain relationship in the corneal tissue; (d) occasionally, the measurements (e.g., elastic modulus) can be dramatically affected by the contribution of the adjacent sclera, a strong and highly elastic tissue, if the *in vitro* test specimens were not adequately isolated or when the measurements

Table C3.8 The mechanical properties of the human corneal tissue^a

Method	Remarks	Young's modulus (MPa)	Ultimate strength (MPa)	Elongation (%)	Source
Uniaxial tensile test	Cornea strips	57 ± 4.1 ^{b,c}	12.7 ± 0.6 ^{b,c}	35 ± 3 ^{b,c}	[55]
	Central cornea strips	0.34 ^d			[56]
	Central cornea strips	4.1 ^e			[56]
	Central cornea strip with Bowman's layer	0.282 ± 0.159 ^f			[57]
	Central cornea strip without Bowman's layer	0.245 ± 0.088 ^f			[57]
	Peripheral strips		3.81 ± 0.4 ^g		[58]
	Central strips	1.3 ^b			[59]
	Anterior hemisphere of globe	0.37 ⁱ			[60]
	Whole globe	1.11 ^j			[61]
	Descemet's membrane	5 ^k			[62]
Inflation	Whole globe	2.87 ± 0.38 ^{b,l,m}			[63]
	Whole globe	8.55 ± 0.83 ^{b,l,n}			[63]
	Whole globe	19.5 ± 0.98 ^{b,l,o}			[63]
	Excised cornea	0.79 ± 0.22 ^p			[64]
	Descemet's membrane	11.8 ± 1 ^{b,q}	1.72 ± 0.19 ^{b,q}	31.2 ± 1.4 ^{b,q}	[65]
	Cornea with scleral ring	0.624 ^{r,s}			[66]
	Cornea with scleral ring	0.777 ^{r,t}			[66]
	Cornea with scleral ring	0.961 ^{r,u}			[66]
	Whole globe	0.036 ^v			[67]
	Whole globe in saline	5.3 ± 1.1 ^w			[68]
Compression	Whole globe in 15 % dextran solution	20 ± 1.0 ^x			[68]

Rheometry	Central cornea strips (horizontal cut)	3 ^y		[69]
	Central cornea strips (Vertical cut)	1 ^z		[69]
	Central cornea strips (Diagonal cut)	0.3 ^{aa}		[69]
Optical methods	Living subjects	0.0245 ± 0.0057 ^{bb}		[70]
	Living subjects	9.03 ± 0.42 ^{cc}		[71]
	Living subjects	2.48 ± 091 ^{dd}		[72]
AFM indentation	Anterior basement membrane	0.0075 ± 0.0042 ^{ee}		[73]
	Descemet's membrane	0.050 ± 0.0178 ^{ff}		[73]
	Bowman's layer	0.1098 ± 0.0132 ^{gg}		[74]
	Anterior stroma	0.0331 ± 0.0061 ^{hh}		[74]
	Anterior stroma	1.14–2.63 ⁱⁱ		[75]
	Anterior stroma	0.25 ± 0.21 ^{jj}		[76]
	Posterior stroma	0.1 ± 0.06 ^{kk}		[76]

^a values are mean, or mean ± standard deviation, except in some cases as further specified; ^b mean ± standard error; ^c measured in 11 corneas, aged 14 to 76 years; ^d intraocular pressure (IOP)=30 mm Hg; ^e IOP=10 mm Hg; ^f measured in 5 pairs of eyes, aged 59 to 82 years, IOP=38 mm Hg; ^g measured in 10 corneal rings left from keratoplasty; ^h measured in 5 enucleated eyes, IOP=38 mm Hg; ⁱ at a strain of $\sim 3.3 \times 10^{-2}$ cm/cm for enucleated corneas; ^j measured in 5 pairs of eyes, aged 39 to 67 years, IOP=19 mm Hg; ^k aged 45 to 90 years, IOP=11 mm Hg; ^l measured in 8 eyes, aged 64 to 88 years; ^m IOP=2–10 mm Hg; ⁿ IOP=10–25 mm Hg; ^o IOP=25–100 mm Hg; ^p measured in 12 corneas, aged 20 to 69 years, IOP=15 mm Hg; ^q measured in 7 Descemet's membranes, aged 65 to 79 years; ^r measured in 13 corneas, aged 80 to 95 years; ^v measured in 2 enucleated eyes, IOP=35 or 40 mm Hg; ^w measured in 6 eyes, aged 75 to 82 years; ^x measured in 6 eyes, aged 78 to 84 years; ^y measured in 4 corneas; ^z measured in 3 corneas; ^{aa} measured in 7 corneas; ^{bb} measured in 28 persons in both eyes, aged 16 to 66 years using photokeratometry and topographic pachometry, IOP=10 mm Hg; ^{cc} measured in 29 persons, aged 17 to 66 years, using slit-lamp, photokeratometry, topographic pachometry, and Goldmann applanation tonometry, IOP=30 mm Hg; ^{dd} measured in 5 persons, aged 27 to 80 years, using Reichert ocular response analyzer (ORA); ^{ee} measured in 6 corneas, aged 58 to 67 years; ^{ff} measured in 5 corneas, aged 53 to 68 years; ^{gg} measured in 6 corneas, aged 19 to 73 years; ^{hh} measured in 5 corneas, aged 19 to 73 years; ⁱⁱ measured in 4 corneas; ^{jj} measured in 6 pairs of corneas, aged 39 to 89 years; ^{kk} measured in 6 pairs of corneas, aged 56 to 88 years

are carried out on living subjects. Table C3.8 presents a compilation, hopefully exhaustive, of the mechanical property measurements of the human cornea.

Additional Reading

[A1] Maurice, D.M. (1962) The cornea and sclera, in *The Eye. Vol. 1: Vegetative Physiology and Biochemistry* (ed H. Davson), Academic Press, New York, pp. 289-368.

This was the defining text to many generations of corneal researchers, written by one of the greatest scholars on the topic.

[A2] King, Jr., J.H. and McTigue, J.W. (eds) (1965) *The Cornea World Congress*, Butterworths, Washington, 754 pp.

A book containing the proceedings of the First World Congress on the Cornea, held in Washington, D.C. in 1964, attended by the most illustrious corneal surgeons and investigators of the period, such as Joachim Barraquer, José Barraquer, Bietti, Cardona, Castroviejo, DeVoe, Dohlman, Franceschetti, Maumenee, Refojo, Rycroft, and many others. The book covers the entire knowledge on the cornea up to that time. It is still a valuable reference book for all cornea scholars.

[A3] Sherrard, E.S. (1977) The cornea: structure and transparency, in *Scientific Foundations of Ophthalmology* (eds E.S. Perkins and D.W. Hill), Heinemann Medical Books, London, pp. 29-35.

A concise yet very informative text, explaining in accessible terms the structure and function of the cornea.

[A4] Fehér, J. (1996) *Pathophysiology of the Eye, Vol. 3: Transparency and Refraction of the Cornea*, Akadémiai Kiadó, Budapest, 230 pp.

This book presents in organized fashion many aspects of the cornea including its development, anatomy, structure, physiology, and new approaches to certain interrelations between the parts of the cornea.

[A5] Foster, C.S., Azar, D.T. and Dohlman, C.H. (eds) (2005) *Smolin and Thoft's The Cornea: Scientific Foundations and Clinical Practice*, 4th edn, Lippincott Williams & Wilkins, Philadelphia, 1323 pp. + 189 plates.

This monumental treatise does not need any recommendation, as its importance in the study of the cornea stood the test of time for generations of corneal investigators.

[A6] Ehlers, N. and Hjortdal, J. (2006) The cornea: epithelium and stroma, in *The Biology of the Eye* (ed J. Fischbarg), Elsevier, Amsterdam, pp. 83–111.

A well-balanced description of essential aspects of the corneal properties and function. Highly recommended as an introductory meaningful text for corneal investigators.

[A7] Fischbarg, J. (2006) The corneal endothelium, in *The Biology of the Eye* (ed J. Fischbarg), Elsevier, Amsterdam, pp. 113–25.

A significant contribution to the understanding of the corneal endothelium and the mechanism of its pump-barrier function, written by the proponent of the latest theory on the transendothelial fluid transport.

[A8] Dawson, D.G., Ubels, J.L. and Edelhauser, H.F. (2011) Cornea and sclera, in *Adler's Physiology of the Eye*, 11th edn (eds L.A. Levin *et al.*), Elsevier, Edinburgh, pp. 71–130.

The most recent chapter on the cornea in a traditional textbook, beautifully written and illustrated, and covering the latest views on the structure and function of this part of the eye.

[A9] Krachmer, J.H., Mannis, M.J. and Holland, E.J. (eds) (2011) *Cornea*, 3rd edn, vol. I & vol. II, Mosby Elsevier, St. Louis, MO, 1913 pp.

A comprehensive, state-of-the art coverage of the topic throughout 171 chapters organized in two volumes.

Recommended sources for ophthalmic terminology:

- Cassin, B., Solomon, S.A.B. and Rubin, M.L. (1990) *Dictionary of Eye Terminology*, 2nd edn, Triad Publishing Co., Gainesville, FL, 286 pp.
- Stein, H.A., Slatt, B.J. and Stein, R.M. (1992) *Ophthalmic Terminology. Speller and Vocabulary Builder*, 3rd edn, Mosby-Year Book Inc., St. Louis, MO, pp. 3–33, 135–55, 261–5.
- Myles, W.M. (1993) Ophthalmic etymology. *Surv. Ophthalmol.*, **37**, 306–9.

References

1. Grayson, M. (1979) *Diseases of the Cornea*, C.V. Mosby Co., St. Louis.
2. Donaldson, D.D. (1980) *Atlas of External Diseases of the Eye. Vol. III: Cornea and Sclera*, 2nd edn, C.V. Mosby Co., St. Louis.
3. Coster, D.J. (2002) *Cornea*, Fundamentals of Clinical Ophthalmology Series, BMJ Books, London.
4. Holland, E.J. and Mannis, M.J. (2002) *Ocular Surface Diseases. Medical and Surgical Management*, Springer-Verlag, New York.
5. Zirm, E. (1906) Eine erfolgreiche totale Keratoplastik. *Graefes Arch. Ophthalmol.*, **64**, 580–93.
6. Chirila, T.V., Hicks, C.R., Dalton, P.D., Vijayasekaran, S., Lou, X., Hong, Y., Clayton, A.B., Ziegelaar, B.W., Fitton, J.H., Platten, S., Crawford, G.J. and Constable, I.J. (1998) Artificial cornea. *Prog. Polym. Sci.*, **23**, 447–73.
7. Evans, M.D.M. and Sweeney, D.F. (2010) Synthetic corneal implants, in *Biomaterials and Regenerative Medicine in Ophthalmology* (ed T. Chirila), Woodhead Publishing Ltd, Oxford & CRC, Boca Raton, pp. 65–133.
8. Proulx, S., Guillemette, M., Carrier, P., Auger, F.A., Germain, L., Giasson, C.J., Gaudreault, M. and Guérin, S.L. (2010) Tissue engineering of human cornea, in *Biomaterials and Regenerative Medicine in Ophthalmology* (ed T. Chirila), Woodhead Publishing Ltd, Oxford & CRC, Boca Raton, pp. 150–192.
9. Martin, D.K. and Holden, B.A. (1982) A new method for measuring the diameter of the in vivo human cornea. *Am. J. Optom. Physiol. Opt.*, **59**, 436–41.
10. Mashige, K.P. (2013) A review of corneal diameter, curvature and thickness values and influencing factors. *S. Afr. Optom.*, **72**, 185–94.
11. Rüfer, F., Schröder, A. and Erb, C. (2005) White-to-white corneal diameter. Normal values in healthy humans obtained with the Orbscan II topography system. *Cornea*, **24**, 259–61.
12. Khng, C. and Osher, R.H. (2008) Evaluation of the relationship between corneal diameter and lens diameter. *J. Cataract Refract. Surg.*, **34**, 475–9.

13. Mishima, S. (1968) Corneal thickness. *Surv. Ophthalmol.*, 13, 57-96.
14. Doughty, M.J. and Zaman, M.L. (2000) Human corneal thickness and its impact on intraocular pressure measures: a review and meta-analysis approach. *Surv. Ophthalmol.*, 44, 367-408.
15. Ehlers, N. and Hjortdal, J. (2004) Corneal thickness: measurement and implications. *Exp. Eye Res.*, 78, 543-8.
16. von Bahr, G. (1948) Measurements of the thickness of the cornea. *Acta Ophthalmol.*, 26, 247-65.
17. Maurice, D.M. and Giardini, A.A. (1951) A simple optical apparatus for measuring the corneal thickness, and the average thickness of the human cornea. *Br. J. Ophthalmol.*, 35, 169-77.
18. Hansen, F.K. (1971) A clinical study of the normal human central corneal thickness. *Acta Ophthalmol.*, 49, 82-9.
19. Manchester, P.T. (1970) Hydration of the cornea. *Trans. Am. Ophthalmol. Soc.*, 68, 425-61.
20. Olsen, T. and Ehlers, N. (1984) The thickness of the human cornea as determined by a specular method. *Acta Ophthalmol.*, 62, 859-71.
21. Reinstein, D.Z., Silverman, R.H., Rondeau, M.J. and Coleman, D.J. (1994) Epithelial and corneal thickness measurements by high-frequency ultrasound digital signal processing. *Ophthalmology*, 101, 140-6.
22. Marsich, M.M. and Bullimore, M.A. (2000) The repeatability of corneal thickness measures. *Cornea*, 19, 792-5.
23. Tam, E.S. and Rootman, D.S. (2003) Comparison of central corneal thickness measurements by specular microscopy, ultrasound pachymetry, and ultrasound biomicroscopy. *J. Cataract Refract. Surg.*, 29, 1179-84.
24. Böhnke, M., Masters, B.R., Wälti, R., Ballif, J.J., Chavanne, P., Gianotti, R. and Salathé, R.P. (1999) Precision and reproducibility of measurements of human corneal thickness with rapid optical low-coherence reflectometry (OLCR). *J. Biomed. Opt.*, 4, 152-6.
25. Bovelle, R., Kaufman, S.C., Thompson, H.W. and Hamano, H. (1999) Corneal thickness measurements with the Topcon SP-2000P specular microscope and an ultrasound pachymeter. *Arch. Ophthalmol.*, 117, 868-70.
26. von Helmholtz, H. (1924) *Helmholtz's Treatise on Physiological Optics* (ed J.P.C. Southall), vol. 1 (trans. from the 3rd German edition), Optical Society of America, Rochester, NY, pp. 9-10.
27. Gullstrand, A. (1924) Procedure of the rays in the eye – Laws of first order, in *Helmholtz's Treatise on Physiological Optics* (ed J.P.C. Southall), vol. 1 (trans. from the 3rd German edition), Optical Society of America, Rochester, NY, pp. 301-58.
28. Chapman, H.C. and Brubaker, A.P. (1893) The radius of curvatures of the cornea. *Proc. Acad. Nat. Sci. Philadelphia*, 45, 349-60.
29. Carney, L.G., Mainstone, J.C. and Henderson, B.A. (1997) Corneal topography and myopia. A cross-sectional study. *Invest. Ophthalmol. Vis. Sci.*, 38, 311-20.
30. Garner, L.F., Owens, H., Yap, M.K.H., Frith, M.J. and Kinneer, R.F. (1997) Radius of curvature of the posterior surface of the cornea. *Optom. Vis. Sci.*, 74, 496-8.
31. Vojniković, B., Gabrić, N., Dekaris, I. and Jurić, B. (2013) Curvature analysis of the corneal front and back surface. *Coll. Antropol.*, 37 (Suppl. 1), 93-6.
32. Esenwah, E.C., Azuamah, Y.C. and Ekwe, C. (2013) An investigation into the radius of curvature of the cornea of young adults in relation to the conformity of an 8.6 mm base curve contact lens. *Int. J. Health Sci. Res.*, 3, 1-5.
33. Patel, S. (1987) Refractive index of the mammalian cornea and its influence during pachometry. *Ophthalm. Physiol. Opt.*, 7, 503-6.
34. Millodot, M. and Newton, I.A. (1976) A possible change of refractive index with age and its relevance to chromatic aberration. *Graefe's Arch. Clin. Exp. Ophthalmol.*, 201, 159-67.
35. Patel, S., Marshall, J. and Fitzke III, F.W. (1995) Refractive index of the human corneal epithelium and stroma. *J. Refr. Surg.*, 11, 100-5.
36. Meek, K.M., Leonard, D.W., Connon, C.J., Dennis, S. and Khan, S. (2003) Transparency, swelling and scarring in the corneal stroma. *Eye*, 17, 927-36.

37. Patel, S., Alió, J.L. and Pérez-Santonja, J. (2004) Refractive index change in bovine and human corneal stroma before and after LASIK: a study of untreated and re-treated corneas implicating stromal hydration. *Invest. Ophthalmol. Vis. Sci.*, 45, 3523-30.
38. Lin, R.C., Shure, M.A., Rollins, A.M., Izatt, J.A. and Huang, D. (2004) Group index of the human cornea at 1.3- μm wavelength obtained in vitro by optical coherence domain refractometry. *Opt. Lett.*, 29, 83-5.
39. Vasudevan, B., Simpson, T.L. and Sivak, J.G. (2008) Regional variation in the refractive-index of the bovine and human cornea. *Optom. Vis. Sci.*, 85, 977-81.
40. Patel, S., Alió, J.L., Amparo, F. and Rodriguez-Prats, J.L. (2011) The influence of age on the refractive index of the human corneal stroma resected using a mechanical microkeratome. *Cornea*, 30, 1353-7.
41. Amparo, F., Patel, S., Alió, J.L., Rodriguez-Prats, J.L. and Moreno, L.J. (2012) Relationship between patient age and refractive index of the corneal stroma during refractive surgery assisted by femtosecond laser flap creation. *Cornea*, 31, 751-5.
42. Boettner, E.A. and Wolter, J.R. (1962) Transmission of the ocular media. *Invest. Ophthalmol.*, 1, 776-83.
43. Lerman, S. (1984) Biophysical aspects of corneal and lenticular transparency. *Curr. Eye Res.*, 3, 3-14.
44. Beems, E.M. and van Best, J.A. (1990) Light transmission of the cornea in whole human eyes. *Exp. Eye Res.*, 50, 393-5.
45. Kolozsvári, L., Nógrádi, A., Hopp, B. and Bor, Z. (2002) UV absorbance of the human cornea in the 240- to 400-nm range. *Invest. Ophthalmol. Vis. Sci.*, 43, 2165-8.
46. Dutch, J.J., Quantock, A.J., Joyce, N.C. and Meek, K.M. (2012) Ultraviolet light transmission through the human corneal stroma is reduced in the periphery. *Biophys. J.*, 102, 1258-64.
47. Gabriel, C., Sheppard, R.J. and Grant, E.H. (1983) Dielectric properties of ocular tissue at 37 °C. *Phys. Med. Biol.*, 28, 43-9.
48. Gabriel, C. (1996) *Compilation of the dielectric properties of body tissues at RF and microwave frequencies*, Final Technical Report AL/OE-TR-1996-0004, Prepared for Brooks Air Force Base, Texas, www.dtic.mil/cgi-bin/GetTRDoc?AD=ADA303903 (accessed 02/27/2014), 16 pp.
49. Gabriel, S., Lau, R.W. and Gabriel, C. (1996) The dielectric properties of biological tissues: III. Parametric models for the dielectric spectrum of tissues. *Phys. Med. Biol.*, 41, 2271-93.
50. Gabriel, C. and Gabriel, S. (1996) *Compilation of the dielectric properties of body tissues at RF and microwave frequencies*, Final Report AL/OE-TR-1996-0037, Prepared for AFOSR/NL Bolling AFB DC 20332-0001, <http://niremf.ifac.cnr.it/docs/DIELECTRIC/Report.html> (accessed 03/03/2014), 10 pp.
51. Oksala, A. and Lehtinen, A. (1959) Comparative studies on the electrical conductivity of aqueous humour, vitreous body, cornea and sclera. *Acta Ophthalmol.*, 37, 388-94.
52. Wigham, C. and Hodson, S. (1981) Bicarbonate and the trans-endothelial short circuit current of human cornea. *Curr. Eye Res.*, 1, 285-90.
53. Hodson, S., Wigham, C., Williams, L., Mayes, K.R. and Graham, M.V. (1981) Observations on the human cornea in vitro. *Exp. Eye Res.*, 32, 353-60.
54. Hodson, S. and Wigham, C. (1983) The permeability of rabbit and human corneal endothelium. *J. Physiol.*, 342, 409-19.
55. Andreassen, T.T., Simonsen, A.H. and Oxlund, H. (1980) Biomechanical properties of keratoconus and normal corneas. *Exp. Eye Res.*, 31, 435-41.
56. Hoeltzel, D.A., Altman, P., Buzard, K. and Choe, K. (1992) Strip extensimetry for comparison of the mechanical response of bovine, rabbit, and human corneas. *J. Biomech. Eng.*, 114, 202-15.
57. Seiler, T., Matallana, M., Sendler, S. and Bende, T. (1992) Does Bowman's layer determine the biomechanical properties of the cornea? *Refr. Corneal Surg.*, 8, 139-42.
58. Zeng, Y., Yang, J., Huang, K., Lee, Z. and Lee, X. (2001) A comparison of biomechanical properties between human and porcine cornea. *J. Biomech.*, 34, 533-7.

59. Wollensak, G., Spoerl, E. and Seiler, T. (2003) Stress-strain measurements of human and porcine corneas after riboflavin-ultraviolet-A-induced cross-linking. *J. Cataract Refract. Surg.*, 29, 1780-5.
60. Woo, S.L.-Y., Kobayashi, A.S., Schlegel, W.A. and Lawrence, C. (1972) Nonlinear material properties of intact cornea and sclera. *Exp. Eye Res.*, 14, 29-39.
61. Kobayashi, A.S., Staberg, L.G. and Schlegel, W.A. (1973) Viscoelastic properties of human cornea. *Exp. Mech.*, 13, 497-503.
62. Jue, B. and Maurice, D.M. (1986) The mechanical properties of the rabbit and human cornea. *J. Biomech.*, 19, 847-53.
63. Hjortdal, J.Ø. (1996) Regional elastic performance of the human cornea. *J. Biomech.*, 29, 931-42.
64. Bryant, M.R. and McDonnell, P.J. (1996) Constitutive laws for biomechanical modeling of refractive surgery. *J. Biomech. Eng.*, 118, 473-81.
65. Danielsen, C.C. (2004) Tensile mechanical and creep properties of Descemet's membrane and lens capsule. *Exp. Eye Res.*, 79, 343-50.
66. Elsheikh, A., Wang, D., Brown, M., Rama, P., Campanelli, M. and Pye, D. (2007) Assessment of corneal biomechanical properties and their variation with age. *Curr. Eye Res.*, 32, 11-9.
67. Schwartz, N.J., Mackay, R.S. and Sackman, J.L. (1966) A theoretical and experimental study of the mechanical behavior of the cornea with application to the measurement of intraocular pressure. *Bull. Math. Biophys.*, 28, 585-643.
68. Wang, H., Prendiville, P.L., McDonnell, P.J. and Chang, W.V. (1996) An ultrasonic technique for the measurement of the elastic moduli of human cornea. *J. Biomech.*, 29, 1633-6.
69. Jayasuriya, A.C., Ghosh, S., Scheinbeim, J.I., Lubkin, V., Bennett, G. and Kramer, P. (2003). A study of piezoelectric and mechanical anisotropies of the human cornea. *Biosens. Bioelectron.*, 18, 381-7.
70. Sjøntoft, E. and Edmund, C. (1987) In vivo determination of Young's modulus for the human cornea. *Bull. Math. Biol.*, 49, 217-32.
71. Edmund, C. (1988) Corneal elasticity and ocular rigidity in normal and keratoconic eyes. *Acta Ophthalmol.*, 66, 134-40.
72. Glass, D.H. (2008) *Characterization of the biomechanical properties of the in vivo human cornea*, Ph.D. Thesis, Ohio State University, https://etd.ohiolink.edu/ap/1070::NO:10:P10_ACCESSION_NUM:osu1211920104 (accessed 02/27/2014), p. 60.
73. Last, J.A., Liliensiek, S.J., Nealey, P.F. and Murphy, C.J. (2009) Determining the mechanical properties of human corneal basement membranes with Atomic Force Microscopy. *J. Struct. Biol.*, 167, 19-24.
74. Last, J.A., Thomasy, S.M., Croasdale, C.R., Russell, P. and Murphy, C.J. (2012) Compliance profile of the human cornea as measured by atomic force microscopy. *Micron*, 43, 1293-8.
75. Lombardo, M., Lombardo, G., Carbone, G., De Santo, M.P., Barberi, R. and Serrao, S. (2012) Biomechanics of the anterior human corneal tissue investigated with atomic force microscopy. *Invest. Ophthalmol. Vis. Sci.*, 53, 1050-7.
76. Dias, J., Diakonis, V.F., Kankariya, V.P., Yoo, S.H. and Zierbath, N.M. (2013) Anterior and posterior corneal stroma elasticity after corneal collagen crosslinking treatment. *Exp. Eye Res.*, 116, 58-62.

Part II

Chapter 1a

Metallic Biomaterials: Introduction

H. Breme, V. Biehl, Nina Reger, and Ellen Gawalt

1a.1 Introduction

Metallic biomaterials are one of the most commonly used biomaterial groups along with ceramics, synthetic polymers, and naturally derived products. The utility of these metallic materials is based largely on the formation of a thin but protective oxide layer. The oxide layer forms upon exposure to oxygen and re-forms within milliseconds after damage [1]. This layer reduces corrosion in vivo, one of the major requirements of a robust biomaterial. The other requirements include biotolerability, bioadhesion, biofunctionality (bioactivity), and processability. In practice each metal or alloy, i.e., titanium alloys, stainless steel, and Co-Cr alloys, has their own advantages for different applications based on mechanical, chemical, and bio-functional properties. Generally, metallic biomaterials are used for structural applications such as implants, pins, and bone scaffolding due to their excellent mechanical properties such as Young's modulus, tensile strength, ductility, fatigue, and wear resistance. However, they can be used for unloaded, purely functional devices such as cages for pumps, valves, and heart pacemakers. The first generation of metallic biomaterials was designed for minimal toxicity. The second generation has been designed for functionality at both at the mechanical and molecular level to enhance integration of the material into the biological environment and increase longevity of the implant. The third generation has focused not only on functionality but also on regeneration of the surrounding tissue in conjunction with the bioactive material [2].

H. Breme • V. Biehl

Lehrstuhl für Metallische Werkstoffe, Universität des Saarlandes, Saarbrücken, Germany

N. Reger • E. Gawalt (✉)

Department of Chemistry and Biochemistry, Bayer School of Natural and Environmental Sciences, Mellon 337, 600 Forbes Avenue, Pittsburgh, PA 15282, USA

e-mail: gawalte@duq.edu

In the following chapters the metallic biomaterials are characterized in terms of their composition, physical and mechanical properties, and their corrosion and biological behavior.

1a.2 Alloys and Their Applications

Most metallic biomaterials in use today are alloys with Ti, Fe, Co, Cr, Ni, V, Al, and Ta as common components. Each alloy has different mechanical properties detailed herein making them preferred materials for different applications. Stainless steel 316 L (SS316L), Co-Cr, Ti6Al4V, and Nitinol are among the most common [3].

SS316L is a strong material that is used for small fixation devices such as pins, screws, and plates. It was originally used for prosthetics such as hip and knee replacements but the market size for SS316L prosthetics has been consistently shrinking due to the prevalent use of lighter alloys. The material is composed of 66 % Fe, 19 % Cr, 9 % Ni, 3 % Mo, and 2 % Mn with Si and C. The oxide surface of SS316L is predominately composed of Fe_2O_3 and Cr_2O_3 [4]. This surface is susceptible to pitting and corrosion, which is the largest cause of failure [5]. Subsequent to the corrosion, Ni ions may be released into the system. If the Ni ions collect in organs, toxicity becomes an issue [6]. Therefore, alloys where Ni is replaced with nitrogen are being introduced into the arena [7].

Cobalt-chromium (Co-Cr) alloyed with W, Mo, or other metals are used for both weight-bearing and non-weight-bearing applications. These lightweight materials are common in hip and knee prosthetics. Wear and fatigue are an issue with Co-Cr alloys. Therefore, metal-on-metal applications are limited and Co-Cr is used in metal-polymer applications or portions of an implant. This class of alloys is also common in arterial stent applications [8]. As a result of the wear issues, Cr ion toxicity questions have led to a reduction in usage.

Titanium and its alloys are the most common metallic biomaterials. Ti6Al4V is used in prosthetic devices including knees, hips, and vertebrae. The material is light with a favorable Young's modulus [9]. The oxide surface consists mainly of TiO_2 and Al_2O_3 in approximately the same percentage as the bulk. TiO_2 is an extremely stable and inert oxide under physiological and electrochemical conditions coupled with a high coefficient of friction making the material an ideal prosthetic and for use in metal-on-metal applications. Even though there are no detectable amounts of V present on the surface, concerns with V toxicity have been addressed and Ta or Nb has been used as replacements. Nitinol is a shape memory alloy that is used in stent and orthodontic applications. The surface of this 50–50 alloy is generally considered to be TiO_2 . In these applications, the inert oxide surface is important because integration into the surrounding tissue in its applications is not critical and in some cases undesirable. Due to these benefits, Ti alloys dominate the metallic biomaterials market [3].

1a.3 Mechanical Properties

The largest application for metallic biomaterials is in orthopedics. In these applications, stress shielding, tensile strength, elongation at fracture, fracture toughness, and fatigue strength are all important factors. For example, stress shielding is an issue because the Young's modulus of bone is 30 GPa while the modulus of the alloys is much higher, i.e., 100–110 GPa for Ti6Al4V. This mismatch can lead to fractures, failure, and eventual replacement of the prosthetic. Fatigue strength is extremely important in weight-bearing applications wherein repeated applied loads can cause structural damage. Another key property is fracture toughness. It is a measure of a material to resist fracture once a crack has formed and is therefore an essential measure in both weight- and non-weight-bearing applications. Specific strength data for each metal can be found in their respective chapters.

1a.4 Corrosion and Inertness

The primary corrosion products of metallic implants are mainly responsible for the biotolerability of the implanted alloy and their sustained interactions. The outer oxide layer of the metals and alloys provides protection from corrosion [5, 6]. However, the oxide layer does associate with hydroxyl groups and/or bound water that can facilitate corrosion either through electrochemical reactions or through reactions with biological fluids (in vivo or simulated). This can result in pitting or crevice corrosion and changes in surface composition, which can ultimately lead to metal ion release. This type of corrosion is particularly important in biological systems where the ions can be transported to various organs and due to an enrichment of the metal, toxicity may ensue.

The primary corrosion products of the most abundant elements in metallic implant materials vary due to their thermodynamic stability. While the oxides or hydroxides of Al, Cr, Nb, Ta, Ti, and V are stable due to a more negative heat of formation than that of water, the oxides and hydroxides of Co and Ni are unstable because of a less negative heat of formation than that of water [10]. The interaction between the oxide or hydroxide and body fluid is increased if the heat of formation for the oxide or hydroxide is increased. Therefore, the thermodynamically stable corrosion products have a low solution product and a low solubility in the body fluid. This is directly demonstrated by the pK_a values (negative logarithm) of the solution product of the primary corrosion products [11]. While Ti-, Ta-, Nb-, and Cr-oxides have pK_a values of >14 , i.e., hydrolysis cannot play a role, Co-, Fe-, and Ni-oxides possess negative pK_a values which cause considerable solubility. In spite of a high negative heat of formation for Fe_2O_3 and Fe- and Cr-hydroxide negative pK_a values and a high solubility are reported [11]. A remarkable solubility of Cr in serum was observed [12], while titanium is practically insoluble due to the formation of the thermodynamically stable oxide TiO_2 . It is this stability that favors Ti as a biomaterial over other materials.

Further, the oxide layers of Ti, Ta, and Nb are semi- or nonconductive oxides. These oxides are able to prevent to a great extent an exchange of electrons and therefore a flow of ions through the tissue [13] due to their isolating effect. This isolating effect may be demonstrated by the dielectric constants of the different metal oxides. While TiO_2 (rutile), Fe_2O_3 , and Nb_2O_5 have constants even higher than that of water, Al_2O_3 , Cr_2O_3 , and Ta_2O_5 have a lower isolating effect and a higher conductivity. For Ni- and V-oxides, dielectric constants are not available because of their high conductivity [14]. As a result of these electrochemical properties, it is clear why Ti alloys are much less susceptible to pitting and crevice corrosion than SS316L.

1a.5 Biofunctionality

The new generation of metallic biomaterials must be biofunctional not just biotolerable. A biofunctional material will integrate with the existing surrounding tissue or induce tissue growth *de novo*. This begins with cell adhesion, spreading, proliferation, and eventually tissue growth. However, the surface oxide layers are inert towards the surrounding tissue, protein- and environment-reducing integration, and potential functionality [15]. Therefore, the chemical bonding of a metallic implant with the tissue, which is observed between bioactive ceramics like hydroxyapatite and bone, seems to be limited and improbable, and the adhesion strength between the bone and the metal will have a primarily mechanical character. While metallic biomaterials, in general, do not induce *de novo* tissue formation they support adhesion and spreading of many cell types including fibroblast, endothelial, and osteoblast cells. Cell adhesion and growth have been studied in many systems with varying surface properties on the molecular, nano, micro, or macroscale.

Osseointegration of orthopedic alloys has been studied under many conditions, surface pretreatments, and modifications. For example, the slow formation of calcium phosphate mineral, the mineral component of bone, occurs on TiO_2 , Nitinol, and SS316L both *in vivo* and in Hanks' buffered saline solution without surface modification [1]. In another study, the bone ingrowth behavior of miniplates of cp-Ti and SS316L was investigated by the implantation of these plates on the legs of Hanford minipigs. The miniplates were fixed to the legs of the pigs by screws. After an 8-week exposure time, in the animals where Ti plates had been used, a new formation of bone could be observed in close contact to the surface of the plates. In contrast to this result, when SS316L was used, there was less new bone formation and undesired granulated tissue was found between the metallic surface and surrounding bone. This granulated tissue at the interface bone/implant has the disadvantage that it is not supplied with blood and unable to transfer or sustain forces, so that an eventual loosening of the implant will take place [16]. Successful growth of bone in close contact with metal and metal alloys has also been reported in similar investigations in which the contact area tissue/implant has been studied in detail [3, 5–7, 17–23].

Surface modifications are used to improve the functionality and integration of metallic materials. Many reported modifications include bioactive molecules, organic thin films, or metallic thin films. These modifications can improve soft tissue growth and osseointegration [1–3, 5, 7–9, 15, 17, 24–28]. Molecular and chemical coatings are increasingly important but outside the scope of this handbook. Physical modification of the oxide surface at the nano- and microscale increases cell adhesion. A Ti alloy femoral implant with nanomodifications, i.e., nanotrabeular and nanotuft-like structures, to the surface was implanted into a rat. The removed implant had a greater Ca phosphate content and a higher bone-to-implant contact percentage after 4 weeks compared to the rough surface control [29–31]. Additionally, TiO₂ nanotubes grown on the surface of Ti dental and tibial implants showed an increase in osseointegration compared to traditional smooth and unmodified Ti surfaces [29, 30, 32]. Therefore, adding nanostructures to microsmooth and microrough bone implants shows an improvement in early healing and long-term osseointegration [1, 29].

Two clinically relevant surface modifications, which improve biofunctionality, include surface roughness and surface porosity [28, 29, 33]. Surface roughness can affect cell adhesion and subsequent integration. Surface roughness is clinically used to improve cell adhesion and subsequent soft tissue integration and osseointegration in prosthetics. This influence was investigated using cylinders of Ti and Ti alloys which were implanted on the legs of rabbits. A measurable adhesion of the Ti alloys could be observed only on implants with a surface roughness of >22 μm [33]. With increasing roughness the adhesion strength is improved. Meanwhile, smooth, highly polished surfaces reduce soft tissue attachment. This is important in reducing scar tissue formation on some portions of implants or on parts of implants where sliding is necessary [28, 34, 35].

Porosity of the implant improves cell adhesion and eventual bone ingrowth into an implant. In addition to the improved fixation, the porous implant has two other advantages: its Young's modulus is decreased, which provides better transmission of the functional load and stimulation of new bone formation, and the damping capacity of the implant is increased. The shear stress generated by the functional loading is decreased because, similar to the thread of a screw, the load at this interface causes a normal stress perpendicular to the inclined area and a lower shear stress which is effective in the inclined area. An important example of this surface modification is the porous head of a metallic hip implant. In this application the decrease in load decreases potential fracturing along with the improved bone fixation [33].

In contrast to the Ti alloys, the adhesion of bioglass is not dependent on the surface roughness [33]. These results show that the growth of the bone and the tissue in close contact to Ti and its alloys with formation of a strong bond must have a more biomechanical than chemical-bioactive character. Consequently, it was shown that by an increase of the surface area, e.g., by drilling holes in the contact area of the implanted cylinders to the bone, the tear-off force necessary was increased. However, if the supplementary surface was taken into consideration, the adhesion

strength was not increased. A Ti5Al2.5Fe implant coated with hydroxyapatite had a maximum adhesion strength of 1.97 N/mm² [33].

The shape of non-weight-bearing biomaterials is also important. For example, those consisting of nanostructures of Al and Ti have shown to enhance cell adhesion and proliferation. The metals were formed into nanofibers and nanospheres. Both nanoshapes provided a platform for Ca deposition. This step is critical to long-term osseointegration of the implant material into the body. However, the nanofibers provided a superior platform for bone formation when compared to the nanospheres [9, 36, 37].

Traditionally, dental implants have outpaced the orthopedic implants in terms of longevity, biointegration, and functionality lasting up to 25 years. These materials include metals and ceramics. For example, implants made from different materials inserted into the jaws of dogs varied in their behavior. With Ti implants the bone grew in close contact to the metal surface. In contrast, when SS316L was used as the implant material, a fibrous encapsulation, which separated the implant from the surrounding tissue, was formed. In Ti implants instead of this fibrous encapsulation, an intercellular substance appeared. A similar unfavorable behavior was found in the case of dental implants of a Co-Cr alloy in dogs [38]. As in orthopedic research, recent dental studies have emphasized the surface properties of the materials. Due to the oxide nature of the implant surfaces, there are hydroxyl and μ -oxo groups on the surface. The presence of these hydrophilic groups increases mesenchymal stem cell adhesion and differentiation leading to enhanced integration. Combining micro-roughness with these hydrophilic groups provided the best environment for osseointegration in vivo [25].

1a.6 Future Directions

Metallic biomaterials are used in orthopedic, craniofacial, dental, and stabilizing implants each year affecting millions of patients. This multibillion dollar industry will continue to increase and diversify as the population ages and obesity-related health issues proliferate causing the need for more implants and innovation. Improving the lifetime of the biomaterial in the next generation is of paramount importance. In order to do this, the material's toxicity must be reduced. Toxicity may be changed by varying the alloy content, i.e., exchanging nitrogen for nickel in SS316L. Alternately, the surface corrosion could be reduced through surface passivation or modification such as plasma nitriding or enhancing the oxide layer. Continuing focused efforts on integration with the surrounding tissue and bone is important. For example, porous implants have been successful at increasing bone fixation while chemical modification of the surface will continue to be an important avenue for improving healing by delivering drugs, peptides, proteins, and growth factors to the wound site. This may lead to attraction and proliferation of cells and eventual growth of bone and tissue at the site or in some cases attraction of Ca and phosphate and the growth of hydroxyapatite. Biodegradable metals represent a

recent category of interest in biomaterials. Their use in applications from bone scaffolds to arterial stents is being evaluated. Issues with stability and degradation rates can hinder their performance and must be addressed in the future. Overall, metallic biomaterials are and will continue to be in high demand due to their strength parameters, which make them ideal for structural biomaterials as prosthetics, scaffolds, pins, screws, and plates.

References

1. Minagar S, Wang J, Berndt CC, Ivanova EP, Wen C (2013) Cell response of anodized nanotubes on titanium and titanium alloys. *J Biomed Mater Res A* 101A(9):2726–2739
2. Mantripragada VP, Lecka-Czernik B, Ebraheim NA, Jayasuriya AC (2013) An overview of recent advances in designing orthopedic and craniofacial implants. *J Biomed Mater Res A* 101A(11):3349–3364
3. Niinomi M, Nakai M, Hieda J (2012) Development of new metallic alloys for biomedical applications. *Acta Biomater* 8:3888–3903
4. Raman A, Dubey M, Gouzman I, Gawalt ES (2006) Formation of Self-assembled monolayers of alkylphosphonic acid on the native oxide surface of SS316L. *Langmuir* 22:6469–6472
5. Antunes RA, Lopes de Oliveria MC (2012) Corrosion fatigue of biomedical metallic alloys: mechanisms and mitigation. *Acta Biomater* 8:937–962
6. Singh R, Dahotre NB (2007) Corrosion degradation and prevention by surface modification of biometallic materials. *J Mater Sci Mater Med* 18:725–751
7. Talha M, Behera CK, Sinha OP (2013) A review on nickel-free nitrogen containing austenitic stainless steels for biomedical applications. *Mater Sci Eng C* 33:3563–3575
8. Zhang K, Liu T, Li J, Chen J, Wang J, Huang N (2014) Surface modification of implanted cardiovascular metal stents: from antithrombosis and antirestenosis to endothelialization. *J Biomed Mater Res A* 102A(2):588–609
9. Guduru D, Niepel M, Vogel J, Groth T (2011) Nanostructured material surfaces—preparation, effect on cellular behavior, and potential biomedical applications: a review. *J Artif Organs* 34(10):963–985
10. Kubashewski O, Evans EC, Alcock CB (1967) *Metallurgical thermochemistry*. Pergamon Press, London
11. Steinemann SG, Perren SM (1984) Titanium alloys as metallic biomaterials. In: Proc. of the 5th world conf. on titanium, vol 2, pp. 1327–1334
12. Zitter H (1976) Schädigung des Gewebes durch metallische Implantate. *Unfallheilkunde* 79:91
13. Zitter K, Plenck H, Strassl H (1980) Tissue and cell reactions *in vivo* and *in vitro* to different metals for dental implant. In: Heimke G (ed) *Dental implants*. C. Hanser, München, p 15
14. Ferguson AB, Akahashi Y, Laing PG, Hodge ES (1962) Characteristics of trace ions released from embedded metal implants in the rabbit. *J Bone Joint Surg* 44:323–336
15. Pound BG (2014) Passive films on metallic biomaterials under stimulated physiological conditions. *J Biomed Mater Res A* 102A:1595–1604
16. Breme J, Steinhäuser E, Paulus G (1988) Commercially pure titanium Steinhäuser plate–screw system for maxillo facial surgery. *Biomaterials* 9:310–313
17. Lyndon JA, Boyd BJ, Birbilis N (2014) Metallic implant drug/device combinations for controlled drug release in orthopaedic applications. *J Control Release* 179:63–75
18. Krekeler G, Schilli W (1984) Das ITI-Implantat Typ H: Technische Entwicklung, Tierexperiment und klinische Erfahrung. *Chirurgische Zahnheilkunde* 12:2253–2263
19. Kirsch A (1980) Titan-spritzbeschichtetes Zahnwurzel-implantat unter physiologischer Belastung beim Menschen. *Dt ZahnärztlZ* 35:112–114

20. Schröder A, van der Zypen E, Sutter F (1981) The reaction of bone, connective tissue and epithelium to endosteal implants with titanium- sprayed surface. *J Maxillofac Surg* 1981(9):15
21. Brånemark PI, Adell R, Albrektsson T, Lekholm U, Lundkvist S, Rockier B (1983) Osseointegrated titanium fixtures in the treatment of edentulousness. *Biomaterials* 4:25
22. Schröder A, Stich H, Strautmann F, Sutter F (1978) Über die Anlagerung von Osteozement an einem belasteten Implantatkörper. *Schweiz Monatsschr Zahnheilk* 4:1051–1058
23. Kydd WL, Daly CH (1976) Bone–titanium implant response to mechanical stress. *J Prosthet Dent* 35:567–571
24. Golish SR, Anderson PA (2012) Bearing surfaces for total disc arthroplasty: metal-on-metal versus metal-on-polyethylene and other biomaterials. *Spine J* 12:693–701
25. Bose S, Tarafder S (2012) Calcium phosphate ceramic systems in growth factor and drug delivery for bone tissues engineering: a review. *Acta Biomater* 8:1401–1421
26. Gittens RA, Scheideler L, Rupp F, Hyzy SL, Geis-Gerstorfer J, Schwartz Z, Boyan BD (2014) A review on the wettability of dental implant surfaces: II. Biological and clinical aspects. *Acta Biomater* 10:2907–2918
27. Purnama A, Hermawan H, Couet J, Mantovani D (2010) Assessing the biocompatibility of degradable metallic materials: state-of-the-art and focus on the potential of genetic regulation. *Acta Biomater* 6:1800–1807
28. Richards RG, Moriarty TF, Miclau T, McClellan RT, Grainger DW (2012) Advances in biomaterials and surface technologies. *J Orthop Trauma* 26(12):703–707
29. Gittens RA, Olivares-Navarrete R, Schwartz Z, Boyan BD (2014) Implant osseointegration and the role of microroughness and nanostructures: lessons for spine implants. *Acta Biomater* 10:3363–3371
30. Bjursten LM, Rasmusson L, Oh S, Smith GC, Brammer KS, Jin S (2010) Titanium dioxide nanotubes enhance bone bonding in vivo. *J Biomed Mater Res A* 92:1218–1224
31. Tsukimura N, Ueno T, Iwasa F, Minamikawa H, Sugita Y, Ishizaki K et al (2011) Bone integration capability of alkali- and heat-treated nanobimorphic Ti-15Mo-5Zr-3Al. *Acta Biomater* 7:4267–4277
32. Thakral GK, Thakral R, Sharma N, Seth J, Vashisht P (2014) Nanosurface—the future of implants. *J Clin Diagn Res* 8(5):7–10
33. Schmitz HJ, Gross V, Kinne R, Fuhrmann G, Strunz V (1988) Der Einfluß unterschiedlicher Oberflächenstrukturierung plastischer Implantate auf das histologische Zugfestigkeitsverhalten des Interface. *DVM-Vortragsreihe Implantate* 7
34. Hayes JS, Richards RG (2010) The use of titanium and stainless steel in fracture fixation. *Expert Rev Med Dev* 7:843–853
35. Hayes JS, Richards RG (2010) Surfaces to control tissue adhesion for osteosynthesis with metal implants: in vitro and in vivo studies to bring solutions to the patient. *Expert Rev Med Dev* 7:131–142
36. Webster TJ, Ergun C, Doremus RH, Siegel RW, Bizios R (2000) Enhanced functions of osteoblasts on nanophase ceramics. *Biomaterials* 21(17):1803–1810
37. Webster TJ, Gutwein LG, Tepper F (2008) Increased osteoblast function on nanofibered alumina. In: 26th annual conference on composites, advanced ceramics, materials, and structures B: ceramic engineering and science proceedings. John Wiley & Sons, Inc., pp. 817–824
38. Strassl H (1978) Experimentelle Studie über das Verhalten von titanbeschichteten Werkstoffen hinsichtlich der Gewebekompatibilität im Vergleich zu anderen Metallimplantaten. Teil 1. *Osterr Z Stomatol* 75(4):134–146

Chapter 1b

Metallic Biomaterials: Cobalt-Chromium Alloys

Gopinath Mani

1b.1 Introduction

Cobalt-chromium (CoCr) alloys have been extensively used for making various orthopedic, dental, and cardiovascular implants and devices. These alloys possess superior mechanical properties with high resistance to corrosion, wear, and fatigue. The biocompatibility and blood compatibility of these alloys have also been well demonstrated. In this chapter, the four types of CoCr alloys (ASTM F75 alloy, ASTM F799 alloy, ASTM F90 alloy, and ASTM F562 alloy) that are currently used for biomedical implants and devices are discussed. Also, the other types of CoCr alloy (ASTM F563, ASTM F1058, and Havar) that have been considered and investigated for biomedical implants and devices are discussed in this chapter. The chapter is divided into subsections based on these individual alloys.

1b.2 ASTM F75

ASTM F75 is a cast cobalt-chromium-molybdenum (Co-28Cr-6Mo) alloy. The unified numbering system (UNS) number for this alloy is R30075. The chemical composition of F75 alloy is provided in Table 1b.1. The different commercial names of F75 alloy are (a) Vitallium (Howmedica, Inc.); (b) Haynes Stellite 21 (Cabot Corp.); (c) Protasul-2 (Sulzer AG); and (d) Zimaloy (Zimmer). This alloy possesses excellent corrosion resistance even in highly corrosive chloride environments. This is mainly due to its bulk composition (Table 1b.1) and the surface chromium oxide (Cr_2O_3) layer.

G. Mani (✉)

Department of Biomedical Engineering, University of South Dakota,
4800 North Career Avenue, Sioux Falls, SD 57107, USA
e-mail: Gopinath.Mani@usd.edu

Table 1b.1 Chemical composition (wt.%) of F75 alloy^a

Co	Cr	Mo	W	Ni	Mn	Si	Fe	C	N	P	Al	S
58.9– 69.5	27.0– 30.0	5.0– 7.0	0.2	2.5	1.0	1.0	0.75	0.35	0.25	0.02	0.30	0.01

^aValues were taken from Refs. [1–6]

This alloy is made into the required shape of the final device by a process known as investment casting [1–4]. During this process, initially, a wax mold is made replicating the shape of the final device. Then, the mold is coated with a ceramic followed by melting the wax to leave a ceramic mold. After that, the alloy is melted at a temperature range of 1350–1450 °C, and poured into the ceramic mold. Once the metal is solidified, the ceramic mold is broken away, and the metal is further processed to obtain the final device.

The way how the casting conditions are carried out can produce different microstructural features and can adversely affect the mechanical properties of the alloy [1–4]. Firstly, as-cast F75 alloy typically consists of a Co-rich matrix (alpha-phase) with carbides (Co_{23}C_6 , Cr_{23}C_6 , and Mo_{23}C_6) in interdendritic spaces and grain boundaries. The relative amounts of alpha and carbide phases in the alloy are expected to be 85 % and 15 %, respectively. However, if there are any non-equilibrium conditions happened during cooling, the interdendritic regions become rich in solutes such as Cr, Mo, and C, along with carbides, and the dendrites will be rich in Co with lack of Cr. This situation is considered to be unfavorable since the regions with lack of Cr can act as an anode with respect to the rest of the alloy microstructure. However, this situation can be improved by solution annealing at 1225 °C for 1 h following casting. Secondly, the solidification step in the casting process not only creates dendrites but also large-size grains. This is not favorable since large-size grains can significantly decrease the yield strength of the alloy. Thirdly, defects may occur in the alloy during casting. For instance, if a ceramic mold piece is broken and entrapped in the alloy during its solidification, it could lead to stress concentrations and initiate cracks at the site where the ceramic piece is present. Such defects can cause fatigue fracture of the device under in vivo conditions. For the similar reasons, it is vital to avoid any porosity (macro- or micro-pores) in the alloy during casting conditions.

To circumvent the above-mentioned limitations and to improve the microstructural features and mechanical properties of the alloy, techniques such as hot isotactic pressing (HIP) have been developed [1–4]. In HIP, a fine powder of F75 alloy is compacted and sintered together under a pressure of 100 MPa at 1100 °C for 1 h, and then forged to obtain the final shape. The alloy prepared using HIP typically showed a much smaller grain size (approximately 8 μm), which not only provided higher yield strength but also improved fatigue properties when compared to those of as-cast alloy. The mechanical properties of as-cast and HIP F75 alloys are provided in Table 1b.2. F75 alloy is commonly used to make total hip arthroplasty components (femoral stems, modular head, and acetabular cup liner) and total knee arthroplasty components (metal femoral and tibial components). Also, this alloy is commonly used to make dental implants such as partial dentures and bridgeworks.

Table 1b.2 Mechanical properties of F75 alloy^a

F75 alloy types	Young's modulus (GPa)	Yield strength (MPa)	Tensile strength (MPa)	Fatigue strength (MPa)
As-cast/annealed	210	448–517	655–899	207–310
Powder metallurgy/hot isotactic pressing	253	841	1277	725–950

^aValues were taken from Refs. [1–5]

Table 1b.3 Chemical composition (wt.%) of F799 alloy^a

Co	Cr	Mo	Ni	Mn	Si	Fe	C	N
58–59	26.0–30.0	5.0–7.0	1.0	1.0	1.0	1.5	0.35	0.25

^aValues were taken from Refs. [1–6]

1b.3 ASTM F799

ASTM F799 is a thermomechanical cobalt-chromium-molybdenum (Co-28Cr-6Mo) alloy. The UNS number for this alloy is R31537. The chemical composition of F799 alloy is provided in Table 1b.3. The alloy is mechanically processed by hot forging at 800 °C after casting to obtain the final shape of the device [1–4]. The thermomechanical processing is the main difference between this alloy and F75 alloy. The processing is carried out in several steps to obtain the final desired shape, with different temperatures used at each step. Although a higher temperature can produce greater deformation, it can also lead to loss of strengthening. Hence, only during the initial stages of processing a higher temperature is applied to allow easier deformation followed by processing at lower temperature to induce cold working. By doing this, the final product of the alloy is obtained with very high strengths.

The microstructure of F799 alloy shows a more worked grain structure when compared to that of as-cast F75 alloy [1–4]. Also, a hexagonal close-packed (HCP) phase is formed through a shear-induced transformation of face-centered cubic (FCC) matrix to HCP platelets. The mechanical properties of F799 alloy are provided in Table 1b.4. As can be seen from this table, the yield and tensile strengths of this alloy are significantly greater than that of as-cast and HIP F75 alloys. Similar to F75 alloy, F799 alloy is also used for the different components of orthopedic and dental implants and devices.

1b.4 ASTM F90

ASTM F90 is a wrought cobalt-chromium-tungsten-nickel (Co-20Cr-15W-10Ni) alloy. The UNS number for this alloy is R30605. The chemical composition of F90 alloy is provided in Table 1b.5. The commercial name of F90 alloy is

Table 1b.4 Mechanical properties of F799 alloy^a

F799 alloy type	Young's modulus (GPa)	Yield strength (MPa)	Tensile strength (MPa)	Fatigue strength (MPa)
Hot forged	210	896–1200	1399–1586	600–896

^aValues were taken from Refs. [1–5]

Table 1b.5 Chemical composition (wt.%) of F90 alloy^a

Co	Cr	W	Ni	Mn	Si	Fe	C	P	S
45.5–56.2	19.0–21.0	14.0–16.0	9.0–11.0	2.0	0.4	3.0	0.15	0.04	0.03

^aValues were taken from Refs. [1–6]

Table 1b.6 Mechanical properties of F90 alloy^a

F90 alloy types	Young's modulus (GPa)	Yield strength (MPa)	Tensile strength (MPa)	Fatigue strength (MPa)
Annealed	210	448–648	951–1220	Not available
Cold worked to 44 %	210	1606	1896	586

^aValues were taken from Refs. [1–5]

Haynes 25 (L605). In this alloy, tungsten (W) and nickel (Ni) are added to improve the machinability and fabrication properties. The yield and tensile strengths of F90 alloy in annealed state are equivalent to those of F75 alloys. However, when the F90 alloy is cold worked to 44 %, the yield and tensile strengths significantly increased when compared to those of F75 alloys. The mechanical properties of F90 alloys in annealed and cold worked states are provided in Table 1b.6. F90 alloy is commonly used to make cardiovascular implants such as stents and mechanical heart valves. Also, this alloy is used in orthopedic applications such as cerclage cables and guide rods.

1b.5 ASTM F562

ASTM F562 is a wrought cobalt-nickel-chromium-molybdenum (Co-35Ni-20Cr-10Mo) alloy. The UNS number for this alloy is R30035. The chemical composition of F562 alloy is provided in Table 1b.7. This alloy is also known as MP35N. The “MP” in the name refers to multiple phases in its microstructure. This alloy can be heat treated and cold worked to produce a high-strength alloy with a controlled microstructure [1–4].

Under equilibrium conditions, the pure solid cobalt has a face-centered cubic (FCC) crystal structure above 419 °C and a hexagonal close-packed (HCP) crystal structure below 419 °C. When cobalt is alloyed with other elements for making the

Table 1b.7 Chemical composition (wt.%) of F562 alloy^a

Co	Cr	Mo	Ni	Mn	Si	Fe	C	P	Ti	S
29.0–38.8	19.0–21.0	9.0–10.5	33.0–37.0	0.15	0.15	1.0	0.025	0.015	1.0	0.010

^aValues were taken from Refs. [1–6]

Table 1b.8 Mechanical properties of F562 alloy^a

F562 alloy types	Young's modulus (GPa)	Yield strength (MPa)	Tensile strength (MPa)	Fatigue strength (MPa)
Hot forged	232	965–1000	1206	500
Cold worked and aged	232	1500	1795	689–793

^aValues were taken from Refs. [1–5]

F562 alloy, the processing involves cold working to 50 %, which greatly supports the transformation of FCC to HCC crystal structure. The HCP phase exists as platelets within the FCC grains to significantly strengthen the alloy. The alloy can also be further strengthened by a heat treatment of 430–650 °C. This heat treatment produces cobalt molybdenum (Co₃Mo) precipitates on the HCP platelets. Hence, this alloy is truly a multiphase material. The higher strength of the alloy is mainly due to the combination of a variety of processing methods such as cold working, solid solution strengthening, and precipitation hardening. The mechanical properties of F562 alloy in hot-forged, and cold-worked and aged forms are provided in Table 1b.8. As can be seen from this table, the tensile strength of cold-worked and aged F562 alloy is greater than that of all the other types (F75, F799, and F90) of CoCr alloy that are used for biomedical applications. F562 alloy is used for cardiovascular stents, lead wires for pacemakers, and heart valve components.

1b.6 Other Types of CoCr Alloy Investigated for Biomedical Applications

Although the above-discussed four types (F75, F799, F90, and F562) of CoCr alloy are currently used for making various biomedical implants and devices, the few other types of CoCr alloy such as ASTM F563, ASTM F1058, and UNS R30004 have also been investigated for biomedical applications. Each of these alloys (F563, F1058, and UNS R30004) has been shown to produce no harmful effects such as cytotoxicity, systemic toxicity, hemolysis, and pyrogenicity in intracutaneous irritation, intramuscular implantation, and skin sensitization tests [1].

1b.7 ASTM F563

ASTM F563 is a wrought cobalt-nickel-chromium-molybdenum-tungsten-iron (Co-20Ni-20Cr-3.5Mo-3.5W-5Fe) alloy. The UNS number for this alloy is R30563. The chemical composition of F563 alloy is provided in Table 1b.9.

F563 alloy can be significantly strengthened by cold working, and cold working and aging. The mechanical properties of the alloy are provided in Table 1b.10. F563 alloy was initially made in the form of bars, wires, and forgings for implant manufacture. However, this specification was withdrawn in 2005 since it was determined that this alloy is no longer being used for implants.

1b.8 ASTM F1058

ASTM F1058 is a wrought cobalt-chromium-iron-nickel-molybdenum (40Co-20Cr-16Fe-15Ni-7Mo) alloy. This alloy is available in two grades, grade 1 (UNS No. R30003) and grade 2 (UNS No. R30008). The chemical composition of grades 1 and 2 of F1058 alloy is provided in Tables 1b.11a and 1b.11b, respectively.

The grade 1 of F1058 alloy is commonly known as Elgiloy. This alloy has been used for making certain components (springs) of artificial heart. The grade 2 of F1058 alloy has been used for making carotid artery clamps for use in neurosurgery and vascular surgery. The tensile and yield strengths of cold-worked and aged F1058 wire for the different diameters of the wire are provided in Table 1b.12.

1b.9 UNS R30005

UNS R30005 is commonly known as Havar. The chemical composition of Havar is provided in Table 1b.13. The mechanical properties of Havar are provided in Table 1b.14. As can be seen from the table, the yield and tensile strengths of cold-rolled or cold-rolled and aged Havar are greater than those of most of the other CoCr alloy types that are used for biomedical applications.

Table 1b.9 Chemical composition (wt.%) of F563 alloy^a

Co	Cr	Mo	W	Ni	Mn	Si	Fe	C	Ti	S
Balance	18.0–22.0	3.0–4.0	3.0–4.0	15.0–25.0	1.0	0.50	4.0–6.0	0.05	0.5–3.50	0.010

^aValues were taken from Refs. [1, 2, 5]

Table 1b.10 Mechanical properties of F563 alloy^a

F563 alloy types	Young's modulus (GPa)	Yield strength (MPa)	Tensile strength (MPa)
Fully annealed	230	276	600
Cold worked or cold worked and aged (medium hard–hard)	230	827–1172	1000–1310
Cold worked and aged (extra hard)	230	1310	1586

^aValues were taken from Refs. [1, 5, 7]**Table 1b.11a** Chemical composition (wt.%) of F1058 alloy (grade 1)^a

Co	Cr	Mo	Ni	Mn	Si	Fe	C	P	Be	S
39.0–41.0	19.0–21.0	6.0–8.0	14.0–16.0	1.5–2.5	1.20	Balance	0.15	0.015	0.10	0.015

^aValues were taken from Refs. [1, 5, 8]**Table 1b.11b** Chemical composition (wt.%) of F1058 alloy (grade 2)^a

Co	Cr	Mo	Ni	Mn	Si	Fe	C	P	Be	S
39.0–42.0	18.5–21.5	6.5–7.5	15.0–18.0	1.0–2.0	1.20	Balance	0.15	0.015	0.001	0.015

^aValues were taken from Refs. [1, 5, 8]**Table 1b.12** Mechanical properties of F1058 alloy^a

F1058 alloy wire diameters (mm)	Yield strength (MPa)	Tensile strength (MPa)
0.02–0.12	–	2275
0.12–1.00	1450	2000
1.00–1.50	1380	1965
1.50–2.00	1380	1895
2.00–2.50	1345	1895
2.50–3.00	1275	1860
3.00–3.50	1240	1860

^aValues were taken from Refs. [1, 5, 7]**Table 1b.13** Chemical composition (wt.%) of Havar^a

Co	Cr	Mo	W	Ni	Mn	Fe	C
42.5	19.5	2.4	2.7	12.7	1.6	Balance	0.2

^aValues were taken from Refs. [1, 9, 10]

Table 1b.14 Mechanical properties of Havar^a

Havar types	Yield strength (MPa)	Tensile strength (MPa)	Hardness
Annealed	483	965	25
Cold rolled	1724	1862	50
Cold rolled and aged	2069	2275	60

^aValues were taken from Refs. [1, 9, 10]

References

1. Davis JR (2003) Handbook of materials for medical devices. ASM International, Materials Park
2. Park JB, Kim YK (2003) Metallic biomaterials. In: Park JB, Bronzino JD (eds) Biomaterials principles and applications. CRC Press, Boca Raton, pp 1–20
3. Brunski JB (2004) Metals. In: Ratner BD, Hoffman AS, Schoen FJ, Lemons JE (eds) Biomaterials science: an introduction to materials in medicine. Elsevier Academic Press, London, pp 137–153
4. Agrawal CM, Ong JL, Appleford MR, Mani G (2014) Introduction to biomaterials basic theory with engineering applications. Cambridge University Press, New York
5. Breme J, Biehl V (1998) Metallic biomaterials. In: Black J, Hastings G (eds) Handbook of biomaterial properties. Springer, New York, pp 135–213
6. Klarstrom D, Crook P (2001) Cobalt alloys: alloy designation system. In: Buschow KHJ, Cahn R, Flemings M, Ilshner B, Kramer E, Mahajan S, Veyssiere P (eds) Encyclopedia of materials: science and technology. Pergamon, Headington Hill Hall, pp 1279–1280
7. Chen Q, Thou G (2015) Biomaterials: a basic introduction. CRC Press, Boca Raton
8. Narushima T, Ueda K, Alfirano (2015) Co-Cr alloys as effective metallic biomaterials. In: Niinomi M, Narushima T, Nakai M (eds) Advances in metallic biomaterials tissues, materials and biological reactions. Springer, New York, pp 157–178
9. Robinson M (2005) Havar[®], a Co-Cr biocompatible alloy for medical implants, encyclopedia of materials: science and technology. Elsevier, pp 1–6
10. Robinson M (2004) Havar[®], a new, old Co-Cr biocompatible alloy for implants. In: Shrivastava S (ed) Medical device materials proceedings of the materials & processes for medical devices conferences. ASM International, Materials Park, pp 324–328

Chapter 1c

Metallic Biomaterials: Titanium and Titanium Alloys

H. Breme, V. Biehl, Nina Reger, and Ellen Gawalt

1c.1 Composition

Table 1c.1 Comparison of international standards for titanium and titanium alloys (Refs. 1, 2^a)

Alloy	Germany DIN	United Kingdom BS	France AIR	International Organization for Standardization ISO	United States ASTM	Japan JIS
Ti-1	17850	2TA1	9182 T-35	5832/II	F67/Grade 1	H4600
Ti-2	17850	2TA2	9182 T-35		F67/Grade 2	
Ti-3	17850	2TA6	9182 T-50		F67/Grade 3	
Ti-4	17850	2TA6, 2AT7 2AT8, 2AT9	9182 T-60		F67/Grade 4	
Ti6Al4V	17851	2TA10, 2TA11	9183T-A6V	5832/III	F136-13	H4607
		2TA13, 2TA28				
		TA56, TA59				
Ti5Al2.5Fe	17865	BS7252-10	–	5832/X	–	–
Ti6Al7Nb	17851		S94-081	5832/XI	FI295	–

^aTi-1–Ti-4 = commercially pure unalloyed titanium; others: direct chemical composition

H. Breme • V. Biehl

Lehrstuhl für Metallische Werkstoffe, Universität des Saarlandes, Saarbrücken, Germany

N. Reger • E. Gawalt (✉)

Department of Chemistry and Biochemistry, Bayer School of Natural and Environmental Sciences, Mellon 337, 600 Forbes Ave., Pittsburgh, PA 15282, USA

e-mail: gawalte@duq.edu

Table 1c.2 Chemical composition of commercially pure (cp)-titanium (wt%) (Refs. 1–3)

cp-Ti	Fe max.	O approx.	N max.	C max.	H max.	Ti
Grade 1	0.2	0.18	0.03	0.1	0.015	Balance
Grade 2	0.3	0.25	0.03	0.08	0.015	Balance
Grade 3	0.3	0.35	0.05	0.1	0.015	Balance
Grade 4	0.5	0.40	0.05	0.1	0.015	Balance

Table 1c.3 Chemical composition of ($\alpha+\beta$)-titanium alloys (wt%) (Ref. 1)

Alloy	Al	V	Fe	Nb	Ta	O	N	C	H	Others		Ti
										Single	Sum	
Ti6Al4V	5.5–6.5	3.5–4.5	0.25	–	–	0.13	0.05	0.08	0.012	0.1	0.4	Balance
Ti5Al2.5Fe	4.5–5.5	–	2.0–3.0	–	–	0.2	0.05	0.08	0.015	0.1	0.4	Balance
Ti6Al7Nb	5.5–6.5	–	0.25	6.5–7.5	0.5	0.2	0.05	0.08	0.009	–	–	Balance

Table 1c.4 Chemical composition (wt%) of β and near- β titanium alloys (Refs. 4–7)

Alloy	Al	Mo	Zr	Ta	Nb	Sn	Ti
Ti15Mo5Zr3Al	3.8	15	5				77
Ti12Mo5Zr5Sn		12	5			4.5	Balance
Ti30Nb					30		70
Ti30Ta				29.6			Balance

1c.2 Physical Properties

Table 1c.5 Physical properties of cp-Ti grade 1 (Refs. 8–11)

Young's modulus	102.7 GPa
Density	4.51 g/cm ³
Melting point	1670 °C
Boiling point	3260 °C
Transformation temperature α - β	890 °C
Crystal structure	>882 °C β bcc <882 °C α cph
Magnetic properties	Paramagnetic
Heat of transformation	67 kJ/kg
Thermal neutron-capture cross section	5.8×10^{-22} cm ²
Specific heat at 15 °C	0.52 kJ/kg K
Heat of fusion	419 kJ/kg
Thermal conductivity at room temperature	17 W/mK
Thermal expansion coefficient between 0 and 315 °C	9.6×10^{-6} °C ⁻¹
Specific heat resistivity at 20 °C	0.5 $\mu\Omega$ m

Table 1c.6 Physical properties of ($\alpha + \beta$)-titanium alloys (Refs. 4, 8–9, 12–14)

Property	Ti6Al4V	Ti5Al2.5Fe	Ti6Al7Nb
Young's modulus (GPa)	100–110	110	105
Density (g/cm ³)	4.43	4.45	4.52
Microstructure	A1–A9	A1–A9	A1–A9
Transformation temperature (°C)	990 ± 15	950 ± 15	1010 ± 15
Thermal conductivity at room temperature (W/mK)	6.6	–	7
Coefficient of thermal expansion between 30 and 200 °C ($\times 10^{-6} \text{ K}^{-1}$)	9.5	9.3	–
Specific heat at 20 °C (kJ/kg K)	0.56	–	0.54
Specific electrical resistivity at 20 °C (52 mm ² /m)	1.66	–	–

Table 1c.7 Influence of alloying elements and heat treatment on Young's modulus (Refs. 5, 15–18)

Alloy	Heat treatment	Young's modulus (GPa)
Ti30Ta	As rolled	69
	1 h/1000 °C/H ₂ O	63
Ti30Nb	As rolled	80
Ti15Mo5Zr3Al ELI ^a	Solution heat treated at 840 °C	75
	Solution heat treated at 740 °C	88
	Solution heat treated at 740 °C	113
	+ aged at 600 °C	

^aELI=extra-low interstitial

1c.3 Processing of cp-Ti and Ti Alloys

Provided that the following characteristics of titanium are taken into consideration, almost all processing procedures are possible:

1. High affinity to oxygen, nitrogen, and hydrogen gases
2. High reactivity to all metals to produce intermetallic compounds
3. Relatively low Young's modulus and therefore backspringing
4. Relatively low thermal conductivity
5. Tendency to stick to tools

1c.3.1 Hot Working and Heat Treatment

Titanium and titanium alloys are fabricated into semifinished products by conventional methods such as forging, rolling, pressing, and drawing. When Ti materials are heated, care must be taken to avoid an excessive adsorption of oxygen, nitrogen, and hydrogen. Therefore, heating and annealing should take place in a neutral or

slightly oxidizing atmosphere. During heating in a gas-fired furnace, direct contact with the flame must be avoided because of the risk of hydrogen pickup and local overheating. In a short heating period, oxygen pickup is restricted to the surface area. This surface zone must be removed by chemical or mechanical methods. Hydrogen is able to penetrate the matrix rapidly; therefore, a reducing atmosphere must be avoided. The hot working temperature depends on the alloy composition and should be selected to obtain the best mechanical properties and grain structure (A1–A9 according to ETTC2, Ref. 17). Table 1c.8 summarizes the deformation temperatures for the various Ti materials. Table 1c.9 lists the temperature ranges and recommended annealing times for stress relieving, soft annealing, and solution treating with age hardening. When the cross section is very small, annealing is favorably carried out in a high-vacuum furnace. Prior to this annealing treatment, the oxide film must be removed from the surface to avoid diffusion of oxygen into the material.

1c.3.2 Working of Sheet

At room temperature cp-Ti grades 1 and 2 can be worked very well, and grades 3 and 4 only moderately well. Titanium alloys, because of their high yield/tensile strength ratio, can be worked only under certain conditions.

Table 1c.8 Deformation temperatures for various titanium materials (Refs. 19, 20)

Alloy	Deformation temperature (°C)
cp-Ti Grade 1	650–870
cp-Ti Grade 2	650–870
cp-Ti Grade 3	700–900
cp-Ti Grade 4	700–930
Ti6Al4V	700–1100

Table 1c.9 Recommendation for the heat treatment of cp-Ti and Ti alloys (Refs. 2, 8)

Alloy	Stress relief	Soft annealing	Solution annealing + age hardening
Ti grade 1	15 min–4 h at 480–595 °C/air	6 min–2 h at 650–750 °C/air	–
Ti grade 2			
Ti grade 3			
Ti grade 4			
Ti6Al4V	3 min/mm 1–4 h at 480–650 °C/air	Min. 1 h max. 4 h at 700–850 °C air or furnace cool	15 min–1 h at 955–970 °C/H ₂ O +2 h at 480–595 °C/H ₂ O
Ti5Al2.5Fe	3 min/mm 15 min–4 h at 540–650 °C/air	Min. 10 min max. 4 h at 720–845 °C air or furnace cool	15–1 h at 800–920 °C/H ₂ O +2–4 h at 480–600 °C/air

For deep drawing, special coatings in the form of polymer foils have proved to be effective. At high temperatures colloidal graphite and common hot press greases with graphite or molybdenum disulfide additives have been successful. The Fe-, Ni-, and Cr-contents should be limited to 0.05, 0.1, and 0.33 wt%, respectively, to allow during a short annealing treatment (1–5 min at 750–850 °C) a grain growth producing an average grain size of 50–70 μm . Due to this grain growth a deformation by twinning, with a resulting increased deep drawability, occurs (Ref. 19).

Superplastic forming is a material-saving and cost-reducing process for manufacturing parts of a complicated shape because it can be carried out together with diffusion welding in a single operation. Fine-grained alloys like Ti6Al4V and Ti5Al2.5Fe can be used for superplastic deformation. Other special deformation processes such as stretch forming, spinning, or explosion forming are also possible.

1c.3.3 Descaling

The average thickness of the oxide layer on the surface of cp-Ti as a function of temperature can be found in Table 1c.10 and the composition of the oxide layer on cp-Ti and Ti alloys can be found in Table 1c.11. The oxide layer on the surface of thick-walled pieces generated during deformation and/or heat treatment is removed by sandblasting and/or pickling. The workpiece is treated in an aqueous solution of 20 wt% HNO_3 and 2 wt% HF.

Thin-walled pieces are merely pickled in an electrolytic solution or salt bath. It is important that not only the surface layer of oxide but also the underlying oxygen enriched diffusion zone is removed. Otherwise, the machinability and the service life of turning and milling tools would be negatively affected.

Table 1c.10 Thickness of oxide formed on the surface of cp-Ti as a function of temperature (Ref. 2)

Temperature (°C)	Measurable thickness (mm)
315	None
425	None
540	None
650	<0.005
705	0.005
760	0.008
815	<0.025
870	<0.025
925	<0.05
980	0.05
1040	0.10
1095	0.36

Table 1c.11 Nature of oxides formed on cp-Ti and titanium alloys (Ref. 22)

Alloy	Oxide				
	TiO ₂	Al ₂ O ₃	Nb ₂ O ₅	MoO ₃ /MoO ₂	ZrO ₂
cp-Ti	×				
Ti6Al4V	×	×			
Ti5Al2.5Fe	×	×			
Ti6Al7Nb	×	×	×		
Ti15Mo5Zr3Al	×	×		×	×

1c.3.4 Machining

The machining of titanium materials presents no difficulties provided that the following properties are taken into account:

1. Relatively low thermal conductivity which may cause high thermal stresses at the cutting edge of the tool
2. Low Young's modulus which applies pressure to the tool
3. Tendency to stick to the tool

Titanium materials must be machined at low cutting speeds, at a relatively high feed rate, and with an ample supply of coolant (sulfur-containing oil; mixture of tetrachloride carbon, molybdenum sulfide, and graphite; 5 % aqueous solution of sodium nitrite, 5–10 % aqueous solution of water-soluble oil or sulfurized chlorinated oil). The cutting tools should be sharp and mounted as rigidly as possible. Recommended parameters for turning and milling are given in Table 1c.12. Since titanium dust and chips can easily catch fire, safety precautions must be taken. Threads should be cut on a lathe, as thread-cutting discs are subject to seizure.

Sawing causes no difficulties if a high blade pressure is used and the coolant supply is sufficient. Coarse-toothed blades (4 teeth per inch) are recommended.

For grinding, aluminum oxide (5–10 m/s) and silicon carbide (20–30 m/s) can be used.

1c.3.5 Soldering and Brazing

Immediately before soldering and brazing, the oxide layer present on the surface of titanium material must be removed. For direct applications using a torch, aluminum–zinc and tin–zinc solders are suitable. The higher temperatures required for brazing present the difficulty of avoiding the formation of intermetallic phases. As with almost all metals, titanium forms brittle intermetallic phases in the fusion zone. The only exception is silver, so that this metal forms one of the main constituents of brazers. The sources of heat used for brazing and soldering are the acetylene torch, high-frequency induction coils, infrared radiation, an inert-gas-shielded arc with graphite or tungsten electrodes, furnaces with an argon atmosphere (min. 99.99 %

Table 1c.12 Recommendations for the cutting and milling of cp-Ti and Ti alloys (Ref. 8)

Alloy	Cutting speed (m/min)	Feed (mm/rev)	Depth of cut (mm)	Cutting angle	Relief angle
<i>Rough cutting</i>					
cp-Ti TC	30–75	0.2–0.4		0–6°	6–8°
HSS	7.5–4.0	0.1–1.25		6–15°	5–7°
			>2.5		
Ti alloys TC	15–25	0.2–0.4		0–6°	6–8°
HSS	3–15	0.1–0.4		6–15°	5–7°
<i>Forecutting</i>					
cp-Ti TC	60–100	0.1–0.4		6–6°	6–8°
HSS	18–50	0.075–0.2		6–15°	5–7°
			0.75–2.5		
Ti alloys TC	20–50	0.1–0.4		6–6°	6–8°
HSS	5–15	0.075–0.2		6–15°	5–7°
<i>Finish cutting</i>					
cp-Ti TC	60–100	0.075–0.3		0–15°	6–8°
HSS	20–50	0.05–0.1		5–6°	5–7°
			0.1–0.75		
Ti alloys TC	20–70	0.075–0.3		0–15°	6–8°
HSS	9–15	0.05–0.1		5–6°	5–7°
<i>Milling</i>					
cp-Ti TC	25–30	0.07–0.15			
HSS	50–60	0.1–0.2	>1.25 face cutter	–	–
Ti alloys TC	7.5–20	0.07–0.2	>2.5 gear cutter		
HSS	15–30	0.1–0.2			

TC hard metal (tungsten carbide)

HSS high-speed steel

and/or a dew point below -50 °C), and high-vacuum furnaces. If brazing is not performed under vacuum or in a controlled atmosphere, fluxes are necessary to dissolve the oxide layers and prevent a pickup of gases.

1c.3.6 Welding

The inert-gas-shielded arc processes (TIG and MIG) are mainly used for fusion welding. In special cases resistance, ultrasonic, electron beam, diffusion, and laser welding are applied. With the cp-Ti grades the weld attains mechanical properties approximating those of the base metal. A slight decrease in ductility may occur with high tensile grades. Under passivating conditions, titanium welds have the same corrosion resistance as the base metal. On the contrary, in reducing media the weld may be subjected to a more severe corrosive attack than the base metal. During the welding operation, the weld, the heat-affected zone, and the underside of the weld are shielded from the atmosphere. The filler rod used is an uncoated wire of the same grade or of a grade

with a lower hardness than the base metal. Careful preparation of the joint is necessary; that is, surface impurities must be removed by grinding or pickling in order to avoid porosity. Even fingermarks can produce a hardening of the weld. A single layer can weld sheets up to 2.5 mm thick. In order to avoid local oxygen concentrations oxidation products, such as those found at the tip of the electrode, must be cut off. The effectiveness of the inert gas is responsible for the welding rate. The optimum argon flow rate has proved to be about 6–8 l/mm. After welding, the appearance of a dark blue or gray oxide layer indicates an insufficient inert gas shielding and an embrittlement of the weld due to oxygen and/or nitrogen pickup. The hardness of a good weld may exceed that of the fully recrystallized base metal by a maximum of 50 VHN. If, after a slight grinding of the surface, a hardness test should give a higher value, the weld must be completely removed because of embrittlement.

Electron beam welding is particularly suitable for titanium materials. It offers many advantages such as very narrow seams and small heat-affected zones, weldability of thick diameters, high welding speed, and reproducibility of even complex welds.

Titanium materials can be spot welded without any particular preparation under similar conditions to those of stainless steel. Using flat-tipped electrodes, spot welding can be performed without inert gas. A hardening of the zone by up to 50 VHN compared with the base metal is regarded as normal and does not diminish the strength of the joint. Seam and flashbutt welding are also possible if an argon atmosphere is used.

Diffusion welding is of particular importance for titanium materials because these materials are more amenable to a homogeneous band in the solid state than other metals. After welding, the joint zone shows a higher temperature under high vacuum or, in an inert atmosphere, a microstructure very similar to that of the base metal.

1c.4 Mechanical Properties

Table 1c.13 Mechanical properties of commercially pure titanium (Ref. 3, 21)

Titanium ^a	Tensile yield strength (0.2 %) (MPa)	Ultimate tensile strength (MPa)	Ratio yield/tensile strength	Elongation at fracture ^b (%)	Reduction of area ^b (%)	Brinell hardness	Bend radius (105°) for sheet thickness (T)	
							<1.8 mm	>1.8–4.75 mm
Grade 1	170	240	0.71	24	30	110–170	3T	4T
Grade 2	275	345	0.80	20	30	140–200	4T	5T
Grade 3	380	450	0.84	18	30	140–200	4T	5T
Grade 4	483	550	0.88	15	25	200–275	5T	6T

^aCondition: Sheet, as rolled

^bMinimum values

Table 1c.14 Influence of a cold deformation on the mechanical properties of commercially pure titanium (Ref. 23)

cp-Titanium	Condition (%)	Tensile yield strength (0.2 %) (MPa)	Ultimate tensile strength (MPa)	Ratio yield/tensile strength	Elongation at fracture (%)
Ti grade 1	30	555	635	0.87	18
	40	560	645	0.87	16
	55	605	710	0.85	15
	60	620	725	0.86	14
	65	640	730	0.88	14.5
Ti grade 2	30	605	680	0.89	18
	40	645	740	0.87	17
	50	680	780	0.87	16
	60	685	795	0.86	16
	65	692	810	0.85	16.5

Table 1c.15 Mechanical properties of β and near- β -titanium alloys (experimental alloys) (Refs. 6, 15, 24–26)

Alloy	Tensile yield strength (0.2 %) (MPa)	Ultimate tensile strength (MPa)	Ratio yield/tensile strength	Elongation at fracture (%)	Reduction of area (%)
Ti5Mo5Zr3Al	838	852	0.98	25	48
Ti30Nb	500	700	0.71	20	60
Ti30Ta	590	740	0.80	28	58

Table 1c.16 Influence of heat treatment on the mechanical properties of β - and near- β -titanium alloys (Refs. 6, 15)

Alloy	Condition	Tensile yield strength (0.2 %) (MPa)	Ultimate tensile strength (MPa)	Ratio yield/tensile strength	Elongation at fracture (%)	Reduction of area (%)
Ti5Mo5Zr3Al	SHT at 840 °C	870	882	0.99	20	83.2
	SHT at 740 °C	968	975	0.99	16.9	64.5
	SHT at 740 °C	1087	1099	0.99	15.3	57.5
	+ aged at 600 °C					
	45 % cold worked	1284	1312	0.98	11.3	43.8
	+ aged at 600 °C					
Ti30Ta	Annealed at 1100 °C	650	800	0.81	8	42
	Annealed at 1200 °C	660	800	0.83	8	38
	Annealed at 1300 °C	665	800	0.83	8	30
	Annealed at 1400 °C	680	800	0.83	6	18

SHT solution heat treatment

Table 1c.18 Influence of a solution treating and ageing on the mechanical properties of Ti6Al4V

Condition	Tensile yield strength (0.2 %) (MPa)	Ultimate tensile strength (MPa)	Ratio yield/ tensile strength	Elongation at fracture (%)	Reduction of area (%)
Sheet ≤ 12.5 mm 15–60 min at 800–920 °C/H ₂ O + 2–4 h 480–600 °C/air	1070	1140	0.94	8	20

Table 1c.19 Influence of a plasma nitriding (PVD) on the mechanical properties of Ti6Al4V (Ref. 30)

Treatment	Tensile yield strength (0.2 %) (MPa)	Ultimate tensile strength (MPa)	Ratio yield/ tensile strength	Elongation at fracture (%)
Untreated	809	894	0.90	20
Vacuum annealed	815	924	0.88	21
20 h/850 °C				
Plasma nitrided ^a	805	914	0.88	20
20 h/850 °C/N ₂				
Plasma nitrided ^a	880	984	0.89	20
20 h/850 °C/NH ₃				

^aPlasma nitriding at 20–40 kW

Table 1c.20 Fracture toughness of Ti-alloys (Refs. 6, 31)

Alloy	Condition	Fracture toughness K_{IC} (N/mm ^{3/2})
Ti6Al4V	Annealed	1740
	Solution treated + annealed	2020
Ti5Al2.5Fe	Annealed (2 h/700 °C/air)	1225
	Solution treated + annealed	1785
	(1 h/900 °C/H ₂ O/2 h/700 °C/air)	
Ti5Mo5Zr3Al	Solution treated at 740 °C	4580
	Solution treated at 740 °C	2430
	+ annealed at 600 °C	
	40 % cold worked	980
	+ annealed at 600 °C	

1c.5 Fatigue

Table 1c.21 High cycle fatigue strength σ_B and rotating fatigue strength σ_R of pure titanium and titanium alloys (Wöhler curves) (Refs. 15, 32–37)

Alloy	R	σ_B (MPa)	R	σ_R (MPa)
cp-Ti	-1	230–280	-1	200
Ti6Al4V	-1	610–625	-1	500–660
Ti5Al12.5Fe	-1	580	-1	450–550
Ti6Al7Nb	-1	500–600	-1	450–600
cp-Nb	-1	270	-1	150
cp-Ta	-1	410	-1	200
Ti30Ta	-1	–	-1	400

Table 1c.22 Rotating bending fatigue tests of unnotched and notched titanium alloys (Ref. 31)

Alloy	R	Condition	Stress concentration factor	Fatigue strength for alternating tensile stresses ($>10^7$ cycles) (MPa)
Ti6Al4V	-1		1.0	725
Ti5Al12.5Fe	-1	Wrought + annealed	1.0	725
	-1	Wrought + solution	3.6	300
	-1	Treated + annealed		
	-1	Cast + HIP	3.6	300
	-1	Cast + HIP	1.0	450

Table 1c.23 High cycle fatigue strength of hip endoprostheses of titanium alloys, measured in 0.9 % NaCl solution at 37 °C. Testing conditions similar to DIN 58840 (simulated loosened shaft, 50 mm) (Refs. 34, 36, 38)

Alloy	Maximum load in 2×10^7 cycles (kN) 0.9 % NaCl ($f=2$ Hz)
Hot wrought Ti6Al4V	6.5–8.0
Wrought Ti5Al12.5Fe	8
Ti6Al7Nb	3.5–6.0

Table 1c.24 Influence of the mean stress S_m on the fatigue strength of Ti6Al4V (Ref. 39)

S_m (MPa)	R	Notch factor K_f	Fatigue strength (MPa) at 10^7 cycles
0	-1	1	400
		2.82	250
250	-0.1	1	300
	0.33	2.82	125
500	0.33	1	250
	0.66	2.82	100
750	0.7	1	125
	0.81	2.82	80

Table 1c.25 Influence of the notch factor on the fatigue strength of Ti6Al4V (Refs. 40–43)

Notch factor K_f	Stress ratio R	Fatigue strength (MPa)
1	-1	400
1.7	-1	300
3.7	-1	150
6.0	-1	100

Table 1c.26 Influence of interstitial elements on the rotating bending strength of Ti6Al4V (Ref. 44)

Chemical composition of the base alloy (wt%)							
Al	V	Fe	C	N	O	H	Ti
6.03	3.96	0.10	0.02	0.009	0.1	0.005	balance
Composition				Notch factor		Fatigue strength	
Heat treatment		K_f	R	(MPa)			
Base alloy		1 h 815 °C/furnace	1	-1	610		
		600 °C air	3	-1	210		
Base alloy		1 h 855 °C/furnace	1	-1	510		
+0.07 % N		600 °C air	3	-1	180		
Base alloy		1 h 870 °C/furnace	1	-1	550		
+0.2 % O		600 °C air	3	-1	210		
Base alloy		1 h 840 °C/furnace	1	-1	560		
+9.2 % C		600 °C air	3	-1	230		
Base alloy		1 h 930 °C/furnace	1	-1	580		
+0.07 % N		600 °C air	3	-1	240		
+0.2 % O							
+0.2 % C							

Table 1c.27 Influence of texture and test directions on the rotating bending fatigue strength of Ti6Al4V (fine equiaxed microstructure in rolled plates) (Ref. 45)

Type of texture and method of production	R	Text direction	Fatigue strength (MPa) test direction at 10^7 cycles
Basal (0002 tilted out of the rolling plane by about 30°) cross rolling in lower ($\alpha + \beta$)-field	-1	Rolling direction	625
Transverse (0002 aligned parallel to the rolling direction) unidirectional in the higher ($\alpha + \beta$)-field, 950 °C	-1	Rolling direction Transverse direction	630 590
Basal/transverse (both are present) Unidirectional roll at about 930 °C	-1	Rolling direction Transverse direction	720 690

Table 1c.28 Influence of heat treatment (annealing and precipitation hardening, respectively) on the fatigue strength of Ti6Al4V (Ref. 43, 46)

Condition	Yield strength (MPa)			Tensile strength (MPa)
As annealed	900			955
As hardened	1100			1195
				Fatigue strength (MPa)
Condition	s_m	K_f	R	at 10^7 cycles
As annealed	0	1	-1	510
	0	3.3	-1	300
As hardened	0	1	-1	600
	0	3.3	-1	280
As annealed	200	1	-0.3	425
	200	3.3	-0.01	200
As hardened	200	1	-0.5	600
	200	3.3	0	200
As annealed	300	1	0.14	400
	300	3.3	0.23	165
As hardened	300	1	-0.22	550
	300	3.3	-0.2	190

Table 1c.29 Influence of the beta field heat treatment on the fatigue strength of Ti6Al4V (Ref. 47)

Heat treatment	R	Fatigue strength (MPa) at 10^7 cycles
0.5 h 1010 °C/AC + 2 h 700 °C/AC	0	525
5 h 1000 °C/AC + 2 h 700 °C/AC	0	620
0.5 h 1010 °C/H ₂ O + 2 h 700 °C/AC	0	750
5 h 1010 °C/H ₂ O + 2 h 700 °C/AC ₂	0	650

Table 1c.30 Influence of the surface treatment on the rotating bending fatigue (fine lamellar microstructure, produced by annealing in 15 min/1050 °C/H₂O + 1 h/800 °C/H₂O) (Ref. 48)

Surface treatment	R	Fatigue strength (MPa) at 10^7 cycles
Electrically polished	-1	680
Mechanically polished (7 µm)	-1	750
Mechanically polished (80 µm)	-1	605
Mechanically polished (80 µm) + 1 h 500 °C	-1	550
Mechanically polished (180 µm)	-1	600
Mechanically polished (80 µm) + 1 h 800 °C	-1	450

Table 1c.31 Influence of the surface treatment on the rotating bending fatigue of Ti6Al4V (fine equiaxed microstructure produced by rolling at 800 °C/H₂O + 1 h/800 °C (HP)) (Ref. 48)

Surface treatment	<i>R</i>	Fatigue strength (MPa)
Electrically polished	-1	610
Shot peened	-1	710
Shot peened + 1 h 500 °C	-1	390
Shot peened + 1 h 500 °C 20 µm surface removed	-1	800
Shot peened + 20 µm surface removed	-1	820

Table 1c.32 Influence of surface working on the rotating bending of Ti6Al4V (Ref. 40, 49)

Surface working	Notch factor (<i>K_t</i>)	<i>R</i>	Fatigue strength (MPa)
Mechanically polished	1	-1	620
Mechanically polished + cold roll bent	1	-1	660
Ground	1	-1	540
Mechanically polished	2.02	-1	330

Table 1c.33 Influence of plasma nitriding (PVD) on the rotating bending fatigue of Ti6Al4V (Ref. 30)

Treatment	<i>R</i>	Maximum bending stress at 10 ⁷ cycles (MPa)
Untreated	-1	600
Vacuum annealed 20 h/850 °C	-1	370
Plasma nitrided ^a 20 h/850 °C/N ₂	-1	470
Plasma nitrided ^a 20 h/700 °C/NH ₃	-1	550
Solution treated 1 h/940 °C/vac. + Ar cooled	-1	530
Solution treated 1 h/940 °C/vac. + Ar cooled + plasma nitrided ^a at 20 h/770 °C/N ₂	-1	500

^aPlasma nitriding at 20–40 kW

1c.6 Corrosion and Wear

Table 1c.34 Electrochemical data for titanium and titanium alloys in 0.1 M NaCl under different conditions (Refs. 24, 50–54)

Alloy	Corrosion potential	Passive current density breakdown potential	
	E_{corr} (mV)	I_p ($\mu\text{A}/\text{cm}^2$)	E_b (mV)
cp-Ti			
pH 7	–628	2.5	
pH 2	–459	5–10	>1500
Ti5Al2.5Fe			
pH 7	–529	0.68	
pH 2	–567	0.71	>1500
Ti6Al4V			
pH 7	–510	0.92	
pH 2	–699	0.69	>1500
Ti6Al7Nb			
pH 7	–368	0.53	>1000
Ti30Ta			
pH 7	–419	0.3	>1500

Table 1c.35 Polarization current (i) and polarization resistance (R_c) of titanium and titanium alloys in pure saline at 37 °C (Ref. 50) and in 0.9 % NaCl with a stable redox system $[\text{Fe}(\text{CN})_6]^{4-}/\text{Fe}(\text{CN})_6^{3-}$ (Ref. 55)

Material	i ($\mu\text{A}/\text{cm}^2$)	R_c ($\text{k}\Omega \text{cm}^2$)	
		Pure saline	Saline + redox
cp-Ti	0.010	1000	714
Ti6Al4V	0.008	1250	455

Table 1c.36 Repassivation time in 0.9 % NaCl and breakdown potential in Hanks' solution of cp-Ti and Ti alloys (Refs. 24, 32, 56, 57)

Alloy	Breakdown potential (mV) vs. calomel electrode	Repassivation –500 mV	Time (ms) +500 mV
cp-Ti	2400	43	44.4
cp-Ta	2250	–	–
Ti30Ta	>1500	41.7	47.5
Ti40Nb	>1500	44.6	43.4
Ti6Al4V	>2000	37	41
Ti5Al2.5Fe		110–130	120–160

Table 1c.37 Electrochemical data for anodic titanium and Ti6Al4V at 37 °C in different solutions (de-aired) versus standard calomel electrode (SCE) (Ref. 58)

Alloy	Corrosion potential vs. SCE E_p (mV)	Passive current density I_b ($\mu\text{A}/\text{cm}^2$)	Breakdown potential E (mV)	Solution ^a
cp-Ti	-440 to 490	1.0–3.0	1300	1
	-94 to 140	0–1.0	1750	2
	-94	5.0–9.0	1950	3
Ti6Al4V	-200 to 250	0.9–1.0	1155–1240	1
	-240 to 300	0.8–1.5	1900	2
	-180 to 250	0.9–2.0	1550	3

^a1=Ringer's solution; 2=Hanks' solution; 3=0.17 M NaCl solution

Table 1c.38 Electrochemical data for cp-Ti and Ti alloys after 7 days in artificial saliva (Ref. 59)

Alloy	Corrosion potential (mV)	Current densities	
		I_{corr} (nA/cm ²)	I_{pass} ($\mu\text{A}/\text{cm}^2$)
cp-Ti	-260	21	9.5
Ti6Al4V	-230	31	10
Ti6Al7Nb	-220	32	9
Ti5Al2.5Fe	-180	30	6

Table 1c.39 Repassivation time of titanium and titanium alloys in contact with different metallic materials (Ref. 60)

NaCl pH=7.4 (shortcut alloy)	HCl pH=3 (activated alloy)	Repassivation time t_c (ms)
cp-Ti	cp-Ti	–
	Ti30Ta	37.7
	Ti6Al4V	41.8
	cp-Nb	480.0
	Co30Cr6.5Mo	38.7
	Co28Cr5Mo	38.4
	X3CrNiMo1812	1000.0
Ti30Ta	cp-Ti	43.0
	Ti30Ta	48.6
	Ti6Al4V	39.0
	cp-Nb	1080.0
	Co30Cr6.5Mo	44.1
	Co28Cr5Mo	(4200)
	X3CrNiMo1812	1000.0
Ti6Al4V	cp-Ti	44.0
	Ti30Ta	34.2

Table 1c.40 Influence of the surface treatment on the fretting corrosion behavior of Ti6Al4V (Ref. 61)

Material combination	Total weight loss (μg)	Ti (μg)	V (μg)
Untreated–untreated	2423	3925	78.5
Untreated–nitrogen ion implanted	1295	1260	31.2
Untreated–PVD coated with TiN	1002	902	15.0
Untreated–plasma ion nitrided	807	716	6.4
PVD–PVD	713	470	8.5
Plasma ion nitrided–plasma ion nitrided	273	87	0.5

Testing conditions: plate screw system (micromotion=100), 14 days in calf serum solution (1 Hz for 1,200,000 cycles)

Table 1c.41 Influence of the surface treatment on the wear behavior of Ti6Al7Nb as a result of a pin-on-disk test (Ref. 62)

Property	PVD coated with 3 μm TiN layer	Oxygen diffusion hardened (ODH) (30 μm hardened surface)
Wear factor ($10^{-7} \text{ mm}^3/\text{Nm}$)	2.111	1.353
Coefficient of friction	0.078	0.051
Surface roughness R_z (μm)	0.159	0.330
Wetting angle ($^\circ$)	47	49

Table 1c.42 Volumetric wear rate of Ti6Al4V and Ti6Al7Nb under different sliding speeds and normal load (Ref. 63)

Sliding speed	Load (N)	Volumetric wear ($\text{mm}^3 \text{ N/mm}$)	
		Ti6Al4V	Ti6Al7Nb
1 mm/s	3	4.45×10^{-3}	5.48×10^{-3}
	6	4.24×10^{-3}	9.64×10^{-3}
	10	11.08×10^{-3}	13.12×10^{-3}
15 mm/s	3	20.35×10^{-3}	22.06×10^{-3}
	6	37.98×10^{-3}	38.10×10^{-3}
	10	51.55×10^{-3}	57.35×10^{-3}
25 mm/s	3	27.32×10^{-3}	31.38×10^{-3}
	6	42.15×10^{-3}	45.28×10^{-3}
	10	54.21×10^{-3}	57.62×10^{-3}

Table 1c.43 Influence of ion implantation of nitrogen on the wear properties of commercial cp-Ti and Ti6Al4V (Ref. 64)

Material	Friction couple	Total wear (mg)	Friction coefficient
cp-Ti ^a	Untreated–untreated	632.3	0.48
	Nitrided–nitrided	54.3	0.10
	4 h/940 °C/N ₂ :H ₂ =2:1		
Ti6Al4V ^b	Untreated–untreated	600.0	0.46
	Nitrided–nitrided	40.1	0.10
	4 h/940 °C/N ₂ : H ₂ =2:1		
	Nitrided–nitrided	92.3	0.12
	6 h/800 °C/N ₂ :H ₂ =1:1		

^aFriction distance = 1257 m^bFriction distance = 1885 m**Table 1c.44** Rate of formation of corrosion products for cp-Ti in Hanks' solution during current-time-tests (Ref. 65)

Polishing method	Metal converted into compound (ng/cm ² h)
Mechanically polished	4.1
Chemically polished	3.5

1c.7 Biological Properties

Table 1c.45 Biocompatibility of cp-Ti and Ti alloys, survival rate of L132 cells incubated with powders (Ref. 66)

Alloy	Powder concentration (mg/L)	Survival rate of cells
cp-Ti	>400	
Ti6Al4V	>400	
Ti5Al2.5Fe	>400	>80 %
Ti30Ta	>400	
Ti30Nb	>400	

Table 1c.46 Influence of the implantation time (in vivo) on the surface roughness and peak-to-valley (P–V) height of Ti6Al4V femoral heads (Ref. 67)

Implantation time								
Position	Before implantation		85 months		110 months		124 months	
	R _a (nm)	P–V	R _a (nm)	P–V	R _a (nm)	P–V	R _a (nm)	P–V
Anterior	43±10	370±72	58±50	746±509	250±147	2044±1178	86±81	812±763
Posterior	41±6	591±333	150±125	2281±1842	114±96	1175±778	142±131	1045±890
Medial	51±14	411±159	44±29	649±259	118±69	1224±731	412±11	401±125
Lateral	52±9	364±68	71±55	722±474	117±106	1195±1009	40±16	527±156

1c.8 Nitinol: Shape Memory

Table 1c.47 Properties of Nitinol (shape memory, Ni₄₅Ti) alloy (Refs. 50, 68–71)

	Above (=austenitic)		Below (= martensitic)
	Transition temperature (–200 to 110 °C)		
Density (g/cm ³)		6.45	
Melting point (°C)		1310	
Young's modulus (GPa)	83		28–41
Tensile yield strength (0.2 %) (MPa)	195–690		70–140
Ultimate tensile strength (MPa)	640–1380		103–862
Ratio yield/tensile strength	0.75–0.68		0.33–0.16
Elongation at fracture (%)	1–15		up to 60
Thermal expansion coefficient (°C ⁻¹)	1.1 × 10 ⁻⁷		6.6 × 10 ⁻⁶
Specific heat (Cal/g °C)		0.20	
Electrical conductivity (S/m)		1–1.5	
Corrosion potential (mV)			
in 0.1 M NaCl pH 7		–431	
pH 2		–518	
Passive current density (A/cm ²)			
in 0.1 M NaCl pH 7		0.44	
pH 2		0.61	
Breakdown potential (mV)			
in 0.1 M NaCl pH 7		890	
pH 2		960	

Table 1c.48 Resulting oxide layer thickness on Nitinol stents using different preparation techniques (Ref. 72)

Surface treatment	Oxide layer thickness (Å)
Electropolished	34 ± 14
Passivated in 10 % HNO ₃	30 ± 1
Air aged at 450 °C	240 ± 70
Heat treated in a NO ₂ ⁻ /NO ₃ ⁻ solution 500 °C	911 ± 270

Table 1c.49 Ion release from Nitinol incubated with L132 cell culture (Ref. 73)

	Ni (ppm)		Ti (ppm)	
	3 days	6 days	3 days	6 days
hp-Ni	6.599 ± 0.037	11.364 ± 0.034	n.m.	n.m.
cp-Ti	n.m.	n.m.	0.001	0.002
NiTi	0.081 ± 0.006	0.176 ± 0.008	0.004	0.006

hp-Ni high-purity nickel, n.m. not measured

Table 1c.50 Survival rate of L132 cells incubated with Nitinol powder (Ref. 74)

Metal	Powder concentration ($\mu\text{g/mL}$)	Survival rate of cells
Nitinol	400	71.2 %

References

1. Cverna F, Horesh J, Whittle S, Yuko I (2001) Worldwide guide to equivalent nonferrous metals and alloys, 4th edn. ASM International, Materials Park, OH
2. Donachie MJ (2000) Titanium: a technical guide, 2nd edn. ASM International, Materials Park, OH
3. Standard specification for unalloyed titanium, for surgical implant applications (UNS R50250, UNS R50400, UNS R50550, UNS R50700) (2006) ASTM International, West Conshohocken, PA
4. Brunette DM, Tengvall P, Textor M, Thomsen P (2001) Titanium in medicine: material science, surface science, engineering, biological responses and medical applications, 1st edn. Springer, New York
5. Zhou YL, Niinomi M, Akahori T (2004) Effects of Ta content on Young's modulus and tensile properties of binary Ti-Ta alloys for biomedical applications. *Mater Sci Eng A* 371:283–290
6. Semlitsch M, Staub F, Weber H (1985) Development of a vital, high-strength titanium aluminium-niobium alloy for surgical implants. In: Proc. fifth European CONF. ON BIOMATERIALS, Paris, 4–6 Sept 1985
7. Mausli P-A, Steinemann SG, Simpson JP (1984) Properties of surface oxides on titanium and some titanium alloys. In: Proc. of the sixth world conference on titanium, vol 3, pp. 1759–1764
8. Material properties of titanium and titanium alloys (DIN 17869) (1990) Beuth Veriag, Germany
9. Microstructure standard for titanium alloy bars, Technical Committee of European Titanium Producers, Publication ETTC2 (1979)
10. Supra Alloys, Inc. (2013) Aerospace materials specifications for titanium and titanium alloys. <http://www.supraalloys.com/specs.php>
11. MatWeb Material Property Data. Titanium, Ti. <http://www.matweb.com/search/DataSheet.aspx?MatGUID=66a15d609a3f4c829cb6ad08f0dafc01>
12. Eliaz N (2012) Degradation of implants, 2012th edn. Springer, New York
13. Titanium alloys—Ti6Al7Nb properties and applications. AZO materials. <http://www.azom.com/properties.aspx?ArticleID=2064>
14. MatWeb Material Property Data. Titanium IMI 367 (Ti-6Al-7Nb). <http://www.matweb.com/search/datasheet.aspx?matguid=71fff43e6722453c8c9783d017d66977&ckck=1>
15. Breime J, Wadewitz V, Burger K (1988) Verbund Titanlegierungen/ Al_2O_3 -Keramik für dentale Implantate—Entwicklung geeigneter Legierungen. In: Ondracek G (ed) Verbundwerkstoffe—Stoffverbunde. DGM, pp. 123–130
16. Breime J, Biehl V, Schulte W, d'Hoedt B, Donath K (1993) Development and functionality of isoelectric dental implants of titanium alloys. *Biomaterials* 14(12):887–892
17. Akahori T, Niinomi M, Fukui H, Ogawa M, Toda H (2005) Improvement in fatigue characteristics of newly developed beta type titanium alloy for biomedical applications by thermo-mechanical treatments. *Mater Sci Eng C* 25:248–254
18. Kim SE, Jeong HW, Hyun YT, Lee YT, Jung CH, Kim SK, Song JS, Lee JH (2007) Elastic modulus and in vitro biocompatibility of Ti-xNb and Ti-xTa alloys. *Met Mater Int* 13(2):145–149
19. Zwicker U (1974) Titan und Titanlegierungen. Springer, New York
20. Lee W, Lin C (1998) High-temperature deformation behaviour of Ti6Al4V alloy evaluated at high strain-rate compression tests. *J Mater Process Technol* 75:127–136
21. Titanium and titanium wrought alloys forgings (hammer and drop forgings)—technical specification (DIN 17864) (1990) Beuth Veriag, Germany
22. Long M, Rack HJ (2008) Titanium alloys in total joint replacement—a materials science perspective. *Biomaterials* 19:1621–1639

23. Ramsdell JD, Hull ED (1960) Characteristics of cold-rolled and annealed Ti. Bureau of Mines Rep. of Inv. 5656
24. Breme J, Wadewitz V (1989) Comparison of Ti-Ta, Ti-Nb alloys. *J Oral Max Implants* 4(2): 113–118
25. Niinomi M (1998) Mechanical properties of biomedical titanium alloys. *Mater Sci Eng A243*: 231–236
26. Shuh A, Bigoney J, Höhle W, Zeiler G, Holzwarth U, Forst R (2007) Second generation (low modulus) titanium alloys in total hip arthroplasty. *Materwiss Werkstofftech* 38(12):1003–1007
27. Stemlitsch M, Staub F, Weber H (1985) Development of a vital, high-strength titanium aluminum-niobium alloy for surgical implants. In: Proc. fifth European conf. on biomaterials, Paris, 4–6 Sept 1985
28. Breme J, Zhou Y, Groh L (1995) Development of a titanium alloy suitable for an optimized coating with hydroxyapatite. *Biomaterials* 16:239–244
29. Titanium and titanium alloy strip, sheet and plate—technical conditions of delivery (DIN 17860) (1990) Beuth Verlag, Germany
30. Lanagan J (1988) Properties of plasma nitrided titanium alloys. In: Proc. of the sixth world conf. on titanium, vol 4, pp. 1957–1962
31. Borowy KH, Kramer KH (1984) On the properties of a new titanium alloy (TiAl₁₅Fe_{2.5}) as implant material. In: Proc. of the fifth world conf. on Ti, vol 2, pp. 1381–1386
32. Thull R (1979) Eigenschaften von Metallen, für orthopädische Implantate und deren Prüfung. *Orthopädie* 7:29
33. Breme J, Schmidt H-J (1990) Criteria for the bioinertness of metals for osseo-integrated implants. In: ed. Heimke G (ed) *Osseo-integrated implants*, CRC press, vol 1, pp. 31–80
34. Semlitsch M, Weber H (1992) Titanlegierungen für zementlose Hüftprothesen. In: Hipp E, Gradinger R, Asherl R (eds) *Die zementlose Hüftprothese*. Demeter Verlag, Grafelfingen, pp 18–26
35. Semlitsch M, Panic B (1994) 15 years of experience with test criteria for fracture-proof anchorage stems of artificial hip joints. In: Buchhorn GH, Willert H-G (eds) *Technical principles, design and safety of joint implants*. Hogrefe & Huber Publishers, Seattle, pp 23–36
36. Papakyriacou M, Mayer H, Pypen C, Plenck H Jr, Stanzl-Tschegg S (2000) Effects of surface treatments on high cycle corrosion fatigue of metallic implant materials. *Int J Fatigue* 22:873–886
37. Narayan R (2009) *Biomedical materials*, 2009th edn. Springer, New York
38. Kunze E (1988) Vergleichende Untersuchungen zum Langzeit-Ermüdungsverhalten von Hüftgelenkprothesen an Luft und in NaCl-Lösung. *Metall* 2:140–145
39. RMI-Titanium (1969) Reactive Metals Inc., Niles, OH
40. Weinberg IG, Hanna IE (1957) An evaluation of the fatigue properties of Ti and Ti-alloys. TML Rep. 77
41. Mote WM, Frost RB (1958) The engineering properties of commercial Ti-alloys. TML Rep. 92
42. Weltzin RB, Koves G (1968) Impact fatigue testing of Ti alloys. *J Mater* 3:469–480
43. Properties and selection of metals. In: ASM metals handbook, vol 1. ASM International (1961)
44. Dittmar CB, Bauer GW, Evers D (1957) The effect of microstructural variables and interstitial elements on the fatigue behavior of Ti and commercial Ti alloys, Mallory, Sharen Titanium Corp. AD-110726WADC-TR 56–304, 95
45. Liitjering G, Gysler A (1984) Fatigue. In: Proc. of the fifth conf. on Ti, pp. 2065–2083
46. Hempel M, Hillnhagen E (1966) Dauerschwingfestigkeit der technischen Titanlegierungen TiAl₁₅Sn_{2.5} und TiAl₁₆V₄. *Arch Eisenhüttenwesen* 37:263–277
47. Riidinger K, Fischer D (1984) Relationship between primary alpha content, tensile properties and high cycle fatigue behaviour of Ti₆Al₄V. In: Proc. of the fifth conf. on Ti, pp. 2123–2130
48. Wagner L, Gerdes C, Liitjering G (1984) Influence of surface treatment on fatigue strength of Ti₆Al₄V. In: Proc. of the fifth conf. on Ti, vol 4, pp. 2147–2154
49. Liu HW (1956) Effect of surface finish on the fatigue strength of TiAl₁₆V₄ alloy. Dept. of Theoretical and Applied Mechanics, University of Illinois, T.U.A.M. Rep. 533
50. Geis-Gerstorfer J, Weber H, Breme J (1988) Electrochemische Untersuchung auf die Korrosionsbeständigkeit von Implantatlegierungen. *Z Zahnarztl Implantol* 4(1):31–36

51. Titanium alloys; chemical composition (DIN 17851) (1990) Beuth Veriag, Germany
52. Luiz de Assis S, Wolynec S, Costa I (2006) Corrosion characterization of titanium alloys by electrochemical techniques. *Electrochim Acta* 51:1815–1819
53. Kesteven J, Kannan MB, Walter R, Khakbaz H, Choe H (2015) Low elastic modulus Ti–Ta alloys for load-bearing permanent implants: enhancing the biodegradation resistance by electrochemical surface engineering. *Mater Sci Eng C* 46:226–231
54. Cai Z, Nakajima H, Woldu M, Berglund A, Bergman M, Okabe T (1999) In vitro corrosion resistance of titanium made using different fabrication methods. *Biomaterials* 20:183–190
55. Breme J (1988) Titanium and titanium alloys, biomaterials of preference. In: Proc. of the sixth world conf. on Ti, vol 1, pp. 57–68
56. Fraker AC, Ruff AW et al (1983) Surface preparation and corrosion. Behaviour of titanium alloys for surgical implants. In: Luckey HA, Kubli F (eds) *Titanium alloys in surgical implants*. ASTM STP796, pp. 206–219
57. Breme J, Wadewitz V, Ecker D (1986) Untersuchungen zum Einfluf* des Geftigezustandes auf das Korrosionverhalten der Implantatlegierung TiAl5Fe2.5. *Z./Zahnarztl. Implantologie*, Bd. II 32–37
58. Gagg C (1988) Corrosion characteristics of Ti5V3Cr3Sn3Al (Ti5-3) alloy in a physiological environment
59. Mareci D, Ungureanu G, Aelenei DM, Mirza Rosca JC (2007) Electrochemical characteristics of titanium based biomaterials in artificial saliva. *Mater Corros* 58(11):848–856
60. Wadewitz V, Breme J (1989) Titan-Legierungen fur dentale Implantate. *Z Zahnarztl Implantol V*:116–120
61. Maurer A, Brown SA, Merrit K (1992) Effects of surface treatments on fretting corrosion of Ti6Al4V. In: Proc. of the fourth world biomaterials congress, p. 200
62. Streicher RM, Weber H, Schon R, Semlitsch M (1991) Wet behaviour of different ceramic surfaces in comparison to TiN and OHD treated Ti6Al4V alloy paired with polyethylene. In: Vincenzini P (ed) *Ceramics in substitutive and reconstructive surgery*. Elsevier, Amsterdam, pp 197–205
63. Fellah M, Assala O, Labaiz M, Dekhil L, Iost A (2013) Friction and wear behavior of Ti-6Al-4V and Ti-6Al-7Nb biomaterial alloy. *J Biomater Nanobiotechnol* 4:374–384
64. Hu Y-S, Dai D-H, Dong Y-L (1988) The ion nitriding of titanium materials and its applications. In: Proc. of the sixth world confer, on titanium, vol 4, pp. 1801–1804
65. Mears DC (1977) Metals in medicine and surgery. *Int Met Rev, Review* 218, 119–155
66. Hildebrand HF (1993) Biologische Aspekte beim Einsatz von Implantatwerkstoffen. DGM Hochschulseminar, Saarbrücken, Germany
67. Easter TL, Graham RM, Jacobs JJ, Black J, LaBerge M (1994) Clinical performance of Ti6Al4V femoral components: wear mechanisms vs. surface profile. In: Proc. of the 20th annual meeting of the society for biomaterials, p. 185
68. Ebel B (1990) Zur Biokompatibilitat von Implantatwerkstoffen. *KfK* 4476
69. Tautzenberger P, Stockel D (1987) Vergleich der Eigenschaften von Thermometallen und Memory-Elementen, 1, 26–32
70. Nitinol Technical Properties. Johnson Matthey Medical Components (2015) <http://jmmedical.com/resources/221/Nitinol-Technical-Properties.html>
71. Thompson SA (2000) An overview of nickel-titanium alloys used in dentistry. *Int Endod J* 33:297–310
72. Trépanier C, Tabrizian M, Yahia L, Bilodeau L, Piron DL (1997) Effect of modification of oxide layer on NiTi stent corrosion resistance; Nitinol: Freemont, CA. <http://www.nitinol.com/media/reference-library/033.pdf>
73. Rocher P, El Medawar L, Hornez JC, Traisnel M, Breme J, Hildebrand HF (2004) Biocorrosion and cytocompatibility assessment of NiTi shape memory alloys. *Scr Mater* 50:255–260
74. El Medawar L, Rocher P, Hornez JC, Traisnel M, Breme J, Hildenbrand HF (2002) Electrochemical and cytocompatibility assessment of NiTiNOL memory shape alloy for orthodontic use. *Biomol Eng* 19(2–6):153–160

Chapter 1d

Dental Restoration Materials

Jonathan Black and Garth Hastings

1D.1 Amalgams

1d.1.1 Composition of alloys

Table 1d.1 Chemical composition of dental amalgams (wt%) (Ref. 1, 2)

Alloy powder*	Ag	Sn	Cu	Zn	Hg
LCS	66–73	25–29	<6	<2	0–3
HCB	69	17	13	1	--
HCSS, HCSL	40–60	25–30	15–30	--	--

The mercury concentration after amalgamization is <50 %.

* LCS = low-copper spherical.

HCB = high-copper blended.

HCSS = high-copper single-composition spherical.

HCSL = high-copper single-composition lathe-cut.

1d.1.2 Physical properties

Table 1d.2 Physical and mechanical properties of amalgams (Ref. 2)

Thermal expansion coefficient	$25 \times 10^{-6}/\text{K}$
Thermal conductivity	23 W/mK
Ultimate tensile strength	≥ 60 MPa
Ultimate compression strength	≥ 300 MPa
Fracture toughness K_{IC}	< 1 MPa m ^{1/2}

J. Black (✉)

Principal: IMN Biomaterials, King of Prussia, PA, USA

G. Hastings

The Biomaterials Programme Institute of Materials Research and Engineering,
National University of Singapore, Singapore, Singapore

1d.1.3 General properties and processing

General properties of dental amalgams (Ref. 1, 2)

By definition amalgam is an alloy of mercury with one or more other metals. Dental amalgams are produced by mixing an alloy powder with mercury. Usually the alloy powder is called 'amalgam' and the composition of amalgam denotes the composition of the powder. The two basic physical shapes of the alloy powder are:

1. irregular shaped particles (length 20–120 μm , width 10–70 μm , thickness 10–35 μm) produced by lathe cutting.
2. spherical particles (diameter < 30 μm) produced by atomization.

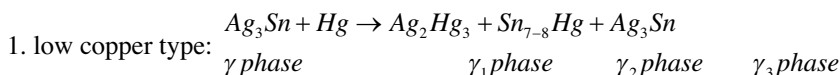
Amalgams for dental restorations are classified by their copper content in two basic types:

1. low-copper type, < 6 wt% Cu, used since the late 19th century.
2. high-copper type (non-gamma-2 amalgam), >6 wt% Cu, used since 1960.

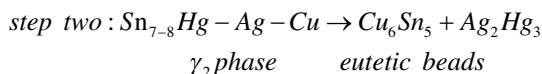
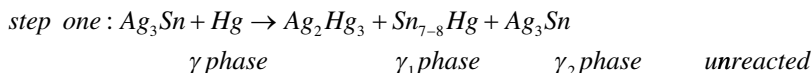
The high-copper type is available in two alloy groups, classified by the mixture of different powder shapes:

- 2.1 mixed alloys consisting of
 - 2.1.1 2/3 conventional lathe cutting + 1/3 spherical powder of Ag–Cu eutecticum (total composition see Table 1d.1 composition of eutecticum: Ag₃₀Cu)
 - 2.1.2 1/3 conventional lathe cutting powder + 2/3 spherical powder (Ag₂₅Sn₁₅Cu)
- 2.2 one-component amalgams consisting of
 - 2.2.1 ternary alloys, spherical shape
 - 2.2.2 ternary alloys, irregular shape
 - 2.2.3 quaternary alloys, non-spherical shape

During amalgamization the powder reacts with the mercury, producing different phases, depending on the amalgam powder:



2. high copper type, mixed alloy (a(i)), reacts in two steps:



The result of the amalgamization is a microstructure consisting of unreacted Ag₃Sn and Ag–Cu surrounded by a layer of Cu₆Sn₅ and the γ_1 matrix. The microstructure of the one-component non-gamma-2 amalgams is similar to that of the mixed alloy except that the Cu₆Sn₅ particles are decomposed in the γ_1 phase and form no layer.

Processing of dental amalgams

For dental restoration (fillings) the mercury is mixed with the (amalgam) alloy immediately before application. The alloy is delivered in powder or pellet form. The amount of mercury after amalgamization must be below 50 wt%. Trituration is accomplished manually in a mortar with a pestle or more often automatically using a capsule of mercury with a given weight and an alloy pellet. The amalgam is placed in the cavity of the tooth in small portions which are pressed with a force of 40–50 N. On the surface of the filling a mercury-rich phase should appear, allowing a good bonding to the following portion. When the cavity is completely filled, the mercury-rich phase must be removed, and the filling can be modelled to the desired shape. 24 hours after the amalgamization the filling must be polished in order to achieve a smooth surface, resulting in a low corrosion rate.

1d.1.4 Mechanical properties

Table 1d.3 Mechanical properties of dental amalgams (Ref. 2)

	Ultimate compression strength (MPa)		Creep (%) (7) days after amalgamization, pressure 38 MPa)
	After 1 h	After setting	
Amalgam*			
LCL	120–170	380–450	2.5–3.5
LCS	140–180	380–450	0.3–1.5
HCB	120–330	410–460	0.2–1.7
HCSS, HCSL ternary alloy	230–320	460–540	0.002–0.3
HCSS, HCSL quaternary alloy with indium	210–410	430–480	0.06–0.1

* LCL = low-copper lathe-cut. LCS = low-copper spherical. HCB = high-copper blended. HCSS = high-copper single-composition spherical. HCSL = high-copper single-composition lathe-cut.

1d.1.5 Corrosion and wear

Table 1d.4 Average passive current density, range of passivity, corrosion and breakdown potential of a non-gamma-2 amalgam in artificial saliva (Ref. 3)

Alloy	Passive Current Density ($\mu\text{A cm}^{-2}$)	Range of Passivity (mV vs. SCE)	Corrosion Potential (mV vs. SCE)	Breakdown Potential (mV vs. SCE)
Non-gamma-2 amalgam	1.5	-300 – +300	-400	300

Table 1d.5 Repassivation rates in artificial saliva versus standard calomel electrode (Ref. 3)

Material	Corrosion Potential (mV)	Potential (mV) after		
		1 h	2 h	36 h
Non-gamma-2 amalgam	-400	-408	-382	-290

Corrosion of amalgams

1. Corrosion of conventional amalgams

The heterogeneous structure of conventional amalgams is responsible for high corrosion. The γ_2 phase is the most active phase in electrochemical corrosion because it is less noble than γ and γ_1 . Therefore an anodic dissolution occurs. The corrosion products of the γ_2 phase are

1.1 Sn^{2+} ions, in the presence of saliva SnO_2 and $\text{Sn}(\text{OH})_6\text{Cl}$

2.2 the released Hg reacts with particles of the γ phase.

2. Corrosion of the high copper type amalgams

Because of the absence of the γ_2 phase, the Cu_6Sn_5 phase is the electrochemically based phase. However, the total corrosion current in the non-gamma-2 amalgams is much lower than in the conventional types. Therefore, the amount of corrosion products is much lower than in gamma-2 alloys. An additional advantage of these amalgams is the lack of mercury during corrosion.

Generally, to achieve a low corrosion in amalgams certain requirements must be fulfilled:

- a polished surface
- no contact with gold (this would lead to a high corrosion of the amalgams, setting mercury free and resulting in a reaction between gold and mercury).

Table 1d.6 Rate of release of mercury vapour per unit area of different types of amalgam dipped in an isotonic NaCl solution (pH = 6) (Ref. 4)

Alloy*		Rate of Hg Release (ng/min mm ²)
LCL	New	0.011
	Old	0.011
HCB	New	0.133
	Old	0.017
HCSS,	New	0.022
	HCSL	Old
In-containing one component	New	0.222
	Old	0.350

LCL = low-copper lathe-cut. HCB = high-copper blended. HCSS = high-copper single-composition spherical. HCSL = high-copper single-composition lathe-cut. New = tested within 2 months after amalgamization. Old = tested after 1.5 years after amalgamization.

Table 1d.7 Chemical composition of high gold-containing dental cast alloys (wt%) (Ref. 5, 6, 8)

Type*	Au + Pt Metals	Au	Pt	Pd	Ir	Rh	Ag	Cu	Zn	Ta	In	Re	Fe	Sn
HGC-1	88.6	87.5		1.0	0.1		11.5							
HGC-2	80.5-81.2	75.7-79.3	0.3-1.4	1.6-3.3			12.3-15.0	4.1-5.5	0.4-1.0	0-0.1				
HGC-3	78.0-78.5	74.0-74.4	0-2.4	2.0-3.5	0.1		9.6-13.5	7.0-11.5	0.9-1.0					
HGC-4	75.5-80.0	65.5-71.0	4.4-12.9	0.0-2.0	0.1	0-1.1	10.0-14.0	8.2-10.0	0.5-4.0					
HGC-1-C	95.0-97.0	80.0-85.0	5.0-11.0	3.3-4.4	0.2	1.6	3.0-5.0							
HGC-2-C	95.0	70.0	7.5	15.0	0.5	2.0	5.0							
HGC-3-C	98.0-99.0	82.6-86.0	9.7-10.4	0-2.2	0.1-0.3	0-1.6					1.0-2.0			
HGC-4-C	82.9-97.4	73.8-84.4	8.0-9.0	5.0-8.9	0.1		1.2-9.2	0.3-4.4	0-2.0	0-0.2	1.5-2.5	0-0.2	0-0.2	0.5-0.8

HGC = high gold-containing (Au + Pt metals > 75 wt%, Pt metals = Pt, Pd, Ir, Rh, Re, Os).

1 = soft, 2 = medium hard, 3 = hard, 4 = extra hard.

c = ceramic alloy (bonding with ceramic is possible).

Table 1d.8 Chemical composition of low gold-containing dental cast alloys (wt%) (Type 4: extra hard) (Ref. 5, 7, 8)

Type*	Au + Pt metals	Au	Pt	Pd	Ir	Ag	Cu	Sn	Zn	In	Ga	Re	Ta	Fe	Co
LGC-4	48.0–66.7	40.0–62.2	0–4.4	09.9	0.1	23.3–35.0	7.0–12.0	0–1.5	0.4–3.5	0–5.0					
LGC-4-C	74.8–89.8	43.0–55.1		29.0–38.5	0.1–0.2	0–19.5	0–0.3	0–0.5		0–9.0	0–1.5	0–2	0–0.1	0–0.2	0–2.8

* LGC-4 = low gold-containing, extra hard (60 wt% ≤ Au + Pt metals ≤ 75 wt%).

LGC-4-C = low gold-containing, extra hard, fusible (C = ceramic alloy (a bonding with ceramic is possible)).

Table 1d.9 Chemical composition of AgPd and Pd-alloys (wt%) (Ref. 5, 8)

Type	Au + Pt metals	Au	Pt	Pd	Ir	Ag	Cu	Sn	Zn	In	Ru	Ga	Ge
AgPd-1	29.5	2.0		27.5		70.0		0.2	0.3				
AgPd-4	29.5–40.0	≤2.0		27.4–39.9	0.1	52.0–58.5	0–10.5	≤2.0	1.5–4.0	≤2.0			
Pd-4-C	52–88	0–17	≤1.0	25–70		7.2–38.0	0–11.6	1.9–7.5	≤2.0	0–4.0	≤0.8	0–7.2	≤0.5

Key: see Table 1d.7

1D.2 Noble Metals

Table 1d.10 Physical Properties of precious dental alloys (Ref. 5, 8)

Alloy	Density (g/cm ³)	Melting Temperature (interval) (°C)	Mean Coefficient of Expansion (10 ⁶ /K) 25–600° C	Young's Modulus (GPa)
HGC-1	17.2	1030–1080		
HGC-2	16.1–16.4	900–1040		92–95
HGC-3	15.6–15.8	900–975		
HGC-4	15.6–16.8	900–1000		98–109
HGC-1-C	18.3–18.6	1090–1370	14.1–14.8	
HGC-2-C	17.3	1285–1370	13.6	
HGC-3-C	18.4–19.5	1045–1220	14.2–14.7	100–105
HGC-4-C	16.7–18.1	900–1260	14.0–16.8	102–113
LGC-4	12.1–14.1	770–1065		94–106
LGC-4-C	14.0–14.8	1150–1315	13.8–14.8	
AgPd-1	11.1			
AgPd-4	10.6–11.1	950–1150		
Pd-4-C	11.2–12.2	1100–1290	14.0–15.4	122–126

Key: see Table 1d.7.

1d.2.1 Composition of alloys

1d.2.2 Physical properties

1d.2.3 Processing of Precious Metal Alloys (Ref. 2, 5, 8)

Casting

Precious metal alloys are normally cast by means of the lost wax process. The well-known method of wax modelling is applied. For the commonly used casting procedure, centrifugal and vacuum pressure casting, the alloys can be heated by the following methods:

- resistance
- propane/oxygen torch (reducing flame zone)
- HF induction
- electrical arc

The alloys are melted in graphite or ceramic crucibles. After removal of the crucible the alloys can if required be hardened. After casting or brazing the alloys are descaled. Mechanical cleaning can be carried out with rotating tools, ceramic grinding wheels or rubber polishers.

Heat Treatment

Depending on the type of alloy and its application, the dental alloys are heat treated. After the casting the alloys are quenched. A homogenization at 700°C followed by rapid cooling should be carried out in order to decompose grain segregations, especially in alloys containing platinum. After a cold deformation the alloys should be stress-relieved. Precipitation hardening is performed by:

- slow cooling from 700°C to room temperature
- cooling from 450 to 250°C in 30 minutes, followed by quenching
- heating between 350 and 450°C for 15 minutes, followed by quenching

Table 1d.12 gives the recommended heat treatments for various noble metal alloys used in dental restoration.

Brazing

Brazing can be carried out with a torch or in a furnace. For larger surfaces furnace brazing is preferable. The best strength properties are obtained with a solder gap of 0.05 to 0.2 mm between the surfaces. Table 1d.11 shows the chemical composition and the brazing temperatures of various filler metals.

Bonding with Ceramics

Precious metal alloys are cast by the lost wax process. After removal of the crucible with carbide tools the castings are sand-blasted with alumina (100–150 μm, pressure 2 bar) to roughen the surfaces and to provide by increasing the surface an improvement in the adhesion strength. After cleaning with water and hot steam an additional cleaning of the alloys is performed by annealing for 10 minutes at 980°C. The bonding procedure takes place in the temperature range of 800–900°C. After bonding the surface must be carefully cleaned in order to provide good corrosion resistance. The final step of the process is a polishing operation with rotating cotton or wool buffers and a small amount of polishing paste.

Table 1d.11 Chemical composition (wt%) and brazing temperatures of various filler metals (Ref. 5, 8)

Filler Metals for Brazing	Brazing Temp. (°C)	Au	Pt	Pd	Ir	Ag	Cu	Zn	In	Re
HGC, LGC	700–840	50–73	≤19	≤1.0	≤0.1	8.0–28	0–9.0	6.0–14	≤2.0	≤0.1
AgPd	760–820	73	0.9	1.0	0.1	13.0		12.0		
HGC-C, LGC-C	700–1120	50–73	≤1.9	≤1.0	≤0.1	10.0–28.0	0–5.0	12.0–14.0	≤2.0	≤0.1
Pd-4-C	1030–1120	50–73	≤1.9	≤1.0		10.0–28.0	3.0–5.0	12.0–14.0	≤2.0	

Key: see Table 1d.7.

Table 1d.12 Recommended heat treatments for various noble metal alloys (Ref. 5, 8)

Alloy	Precipitation Hardening		Soft Annealing		Oxidizing without Vacuum	
	Time (min)	Temperature (°C)	Time (min)	Temperature (°C)	Time (min)	Temperature (°C)
HGC	15	400	15	700–800		
HGC-C	15	500–600	15	950	10	960–980
LGC	15	400–500	15	700–800		
LGC-C	15	600	15	950	10	980
AgPd	15	550				
Pd-4-C	15	600	15	950	10	980

Key: see Table 1d.7.

1d.2.4 Mechanical properties

Table 1d.13 Mechanical properties of high gold-containing dental cast alloys (Ref. 5, 8)

Type		Tensile Yield Strength (0.2 %) (MPa)	Ultimate Tensile Strength (MPa)	Ratio Yield/Tensile Strength	Elongation at Fracture (%)	Hardness HVHN
HGC-1		80	170	0.47	45	55
HGC-2		180–240	370–390	0.49–0.61	35–45	95–110
HGC-3	s	330–350	460	0.72–0.76	35–40	145
	h	350–390	550–590	0.64–0.66	20–23	170–190
HGC-4	s	300–420	500–580	0.60–0.72	15–37	155–195
	h	540–780	710–870	0.76–0.90	5–18	225–295
HGC-1-C	s	90–130	220–280	0.41–0.46	29–38	60–75
	h	105–140	230–300	0.46–0.47	27–38	70–90
HGC-2-C	s	230	400	0.58	20	105
	h	240	410	0.59	18	125
HGC-3-C	s	370–420	460–515	0.80–0.82	8–15	150–160
	h	470–490	530–590	0.83–0.89	6–9	185–200
HGC-4-C	s	380–480	530–580	0.72–0.83	7–14	150–200
	h	470–600	550–650	0.85–0.92	3–6	220–230

Key: see Table 1d.7.

s = soft, h = hardened.

Table 1d.14 Mechanical properties of low gold-containing dental cast alloys (Ref.: 5, 8)

Type		Tensile Yield Strength (0.2%) (MPa)	Ultimate Tensile Strength (MPa)	Ratio Yield/Tensile Strength	Elongation at Fracture (%)	Hardness VHN5
LGC-4	s	310–400	480–510	0.65–0.78	18–43	155–170
	h	555–830	640–890	0.87–0.93	3–13	220–275
LGC-4C	s	310–590	570–790	0.54–0.75	11–26	180–250
	h	550–700	710–900	0.77–0.78	6–18	235–285

Key: see Table 1d.7.
s = soft, h = hardened

Table 1d.15 Mechanical properties of AgPd and Pd-alloys (Ref.: 5, 8)

Type	Tensile Yield Strength (0.2%) (MPa)	Ultimate Tensile Strength (MPa)	Ratio Yield/Tensile Strength	Elongation at Fracture (%)	Hardness VHN5
AgPd-1	80	230	0.35	33	55
AgPd-4	285–595	510–950	0.56–0.63	3–31	140–310
Pd-4-C	340–630	630–900	0.54–0.70	8–30	180–285

Key: see Table 1d.7.

1d.2.5. Corrosion and wear

Table 1d.16 Polarization current (i) and polarization resistance (R_c) of gold in 0.9% NaCl and in 0.9% NaCl with a stable redox system $[\text{Fe}(\text{CN})_6]^{4-} / \text{Fe}(\text{CN})_6^{3-}$ at 37 °C corresponding to the potential of the body fluid of 400 mV (Ref. 7, 12)

Material	i ($\mu\text{A}/\text{cm}^2$)	R_c ($\text{k}\Omega\text{cm}^2$)	
		0.9% NaCl	saline + redox
Au	0.009	1100	0.28

Table 1d.17 Average passive current density, range of passivity, corrosion and breakdown potential of a high gold containing alloy (HGC) in artificial saliva (Ref. 3)

Alloy	Passive Current Density ($\mu\text{A cm}^{-2}$)	Range of Passivity (mV vs. SCE)	Corrosion Potential (mV vs. SCE)	Breakdown Potential (mV vs. SCE)
HGC	1.5	-100 – +400	-137	400

Table 1d.18 Repassivation rates in artificial saliva versus standard calomel electrode (Ref. 3)

Material	Corrosion Potential (mV)	Potential (mV) after		
		1 h	2 h	36h
HGC	-137	-48	-26	-26

1D.3 CoCr-Alloys

See Chapter 1b, CoCr-alloys.

1D.4 NiCr-Alloys (Ref. 9, 10, 11)

NiCr-alloys are difficult to classify because of the wide range of the chemical composition, as shown in Table 1d.19. The NiCr-alloys in dentistry are generally used for porcelain veneered and unveneered crowns, fixed and removable partial dentures and bridgework. As the processing is similar to that of the CoCr-alloys, it is not described here (see Chapter 1b.3). The requirements for these specific applications determine the chemical composition. The corrosion resistance of the NiCr-alloys is provided by the chromium content which produces a passive oxide layer on the surface. Beryllium is added as a solid solution strengthener and supports the self-fluxing at the porcelain veneering temperature. It is also responsible for the good chemical bonding to the porcelain. As it lowers the melting temperature, beryllium also improves the stability.

Aluminium also produces a passive oxide layer, aids in the bonding to the porcelain and strengthens the alloy due to the precipitation of $AlNi_3$. Silicon lowers the melting temperature and, like manganese, acts as a deoxidizer. Molybdenum and niobium are added to improve corrosion resistance and, like iron, are used to adapt the thermal expansion coefficient to the coefficient of the porcelain.

The wide composition range results in an equally wide range of physical (Table 1d.20) and mechanical properties (Table 1d.21). The high rigidity and strength of these alloys as compared to that of the precious metal alloys make them suitable for the production of small prosthetic devices.

Table 1d.19 Chemical composition (wt%) of the NiCr-alloys used in dentistry Ref. 11)

Ni	Co	Fe	Cr	Mo	Nb	Ti	W	Be	Ga	Si	C	Others
58	0	0	12	0.5	0	0	0	0	0	0	≤0.5	Al, Ce, B,
—	—	—	—	—	—	—	—	—	—	—		Mn, Sn, Y, V,
82	2	9	26	16	7	3	4	1.5	7.5	3		Ta, La, Cu

Table 1d.20 Physical and mechanical properties of NiCr-alloys used in dentistry (Ref. 11)

Melting interval	940–1430 °C
Young's modulus	170–220 GPa
Density	7.8–8.6 g/cm ³
Mean coefficient of linear thermal expansion between 25–600 °C	13.9–15.5 10 ⁻⁶ /K

Table 1d.21 Mechanical properties of NiCr-alloys used in dentistry (Ref. 12)

Tensile Yield Strength (0.2%) (MPa)	Elongation at Fracture (%)	Hardness (VHN5)
255–800	3–25	160–395

References

1. Cahn, R.W., Haasen, P. and Kramer, E.J. (eds) (1992) *Materials Science and Technology*, Vol. **14**, VCH.
2. Combe, E. (1984) *Zahnärztliche Werkstoffe*, Hanser.
3. Elagli, K., Traisnel, M. and Hildebrand, H.F. (1993) Electrochemical Behaviour of Titanium and Dental Alloys in Artificial Saliva. *Electrochimica Acta*, **38**(14), 1769–1774. 881.
4. Berglund, A. (1993) An *in vitro* and *in vivo* study of the release of mercury vapor for different types of amalgam alloys. *J. Dent. Res.* **72** (5), 939–945.
5. Product information, Degussa, Germany.
6. DIN 13906–1 (=EN 21562, ISO 1562) (1990). Beuth.
7. DIN 13906–2 (invalid, replaced by DIN 28891) (1990). Beuth.
8. Product information, Wieland Edelmetalle, Germany.
9. Fraker, A.C., Corrosion of Metallic Implants and Prosthetic Devices, in *Metals Handbook*, 9th Ed., Vol. **13**: Corrosion, p. 1351.
10. *Encyclopedia of Materials Science and Engineering*, Vol. **2**, (1986) Pergamon Press, pp. 1057–1058.
11. NiCo-alloy producing industries.
12. Zitter, H. and Plenk, H. (1987) The Electrochemical Behaviour of Metallic Implant Materials as an Indicator of their Biocompatibility. *J. of Biomedical Materials Research*, **21**, 881.

Chapter 2

Composite Materials

L. Ambrosio, G. Carotenuto, and L. Nicolais

2.1 Types of Composites and Component Materials

Composites are combined materials created by the synthetic assembly of two or more components – a selected reinforcing agent and a compatible matrix binder – in order to obtain specific and advanced characteristics and properties. The components of composite do not dissolve or otherwise merge completely into each other, but nevertheless do act in concert. The components as well as the interface between them can usually be physically identified, and it is the behavior and properties of the interface that generally control the properties of the composite. The properties of a composite cannot be achieved by any of the components acting alone.

The composites can be classified on the basis of the form of their structural components: fibrous (composed of fibers in a matrix), laminar (composed of layers of materials), and particulate (composed of particles in a matrix). The particulate class can be further subdivided into flake (flat flakes in a matrix) or skeletal (composed of a continuous skeletal matrix filled by a second material). In general, the reinforcing agent can be either fibrous, powdered, spherical, crystalline, or whiskered and either an organic, inorganic, metallic, or ceramic material.

2.2 Fibre Types and Properties

A summary of the most important reinforcing filaments and their properties is presented in Tables 2.1–2.7.

L. Ambrosio (✉) • G. Carotenuto • L. Nicolais
Department of Materials and Production Engineering, University of Naples Federico II
Institute of Composite Materials Technology CNR, Piazzale Technio, 80, 80125 Naples, Italy

Table 2.1 Compositions and properties of various glasses (4)

Compound	A	C	E	R	S
SiO ₂	72.0	64.6	52.4	60.0	64.4
Al ₂ O ₃ , Fe ₂ O ₃	1.5	4.1	14.4	25.0	25.0
CaO	10.0	13.4	17.2	9.0	–
MgO	2.5	3.3	4.6	6.0	10.3
Na ₂ O, K ₂ O	14.2	9.6	0.8	–	0.3
B ₂ O ₃	–	4.7	10.6	–	–
BaO	–	0.9	–	–	–

Table 2.2 Properties of fiberglass (2)

Property	Grade of class			
	A	B	E	S
Physical properties				
Specific gravity	2.50	2.49	2.54	2.48
Mohs gravity	–	6.5	6.5	6.5
Mechanical properties				
Tensile strength, psi×10 ⁶ (MPa)				
At 72°F (22 °C)	440 (3033)	440 (3033)	500 (3448)	665 (4585)
At 700°F (371 °C)	–	–	380 (2620)	545 (3758)
At 1000°F (538 °C)	–	–	250 (1724)	350 (2413)
Tensile modulus elasticity at 72°F (22 °C), psi×10 ⁶ (GPa)	–	10.0 (69.0)	10.5 (72.4)	12.4 (85.5)
Yield elongation, %	–	4.8	4.8	5.7
Elastic recovery, %	–	100	100	100
Thermal properties				
Coefficient of thermal linear expansion, in./in./°F×10 ⁻⁶ (m/m/°C)	4.8 (8.6)	4.0 (7.2)	2.8 (5.0)	3.1 (5.6)
Coefficient of thermal conductivity, Btu- in./hr/sq ft/°F (watt/motor K)	–	–	72	–
Specific heat at 72°F (22 °C)	–	0.212	0.197	0.176
Softening point, °F(°C)	1340	1380	1545	
Electrical properties				
Dielectric strength, V/mil	–	–	498	–
Dielectric constant at 72 °F (22 °C)				
At 60 Hz	–	–	5.9–6.4	5.0–6.4
At 10 ⁶ Hz	6.9	7.0	6.3	5.1
Dissipation (power) factor at 72 °F (22 °C)				
At 60 Hz	–	–	0.005	0.003

(continued)

Table 2.2 (continued)

Property	Grade of class			
	A	B	E	S
At 10 ⁶ Hz	–	–	0.002	0.003
Volume resistivity at 72 °F (22 °C) and 500 V	–	–	10 ¹⁵	10 ¹⁶
DC, ½-cm				
Optical properties				
Index of refraction	–	–	10 ¹³	10 ⁴
Acoustic Properties				
Velocity of sound, ft/sec (m/sec)	–	–	17,500 (5330)	19,200 (5850)

Table 2.3 Thermal Properties of Kevlar 49 (8)

Property	Value
Long-term use at elevated temperature in air, °C (°F)	160(320)
Decomposition temperature, °C (°F)	500 (932)
Tensile strength, MPa (Ksi)	
At room temperature for 16 months	No strength loss
At 50 °C (122°F) in air for 2 months	No strength loss
At 100 °C (212°F) in air	3170
At 200 °C (392°F) in air	2720
Tensile modulus, GPa (10 ³ Ksi)	
At room temperature for 16 months	No modulus loss
At 50 °C (122°F) in air for 2 months	No modulus loss
At 100 °C (212°F) in air	113.8 (16.5)
At 200 °C (392°F) in air	110.3 (16.0)
Shrinkage, %/°C (%°F)	4 x 10 ⁻⁴ (22 x 10 ⁻⁴)
Thermal coefficient of expansion, 10 ⁻⁶ cm/cm °C	
Longitudinal, 0–100 °C (32–212°F)	-2
Radial, 0–100 °C (32–212°F)	+59
Specific heat at room temperature, J/g°C (Btu/lb°F)	1.42 (0.34)
Thermal conductivity at room temperature, J cm/sec m ² °C (Btuin/hr ft ² °F)	
Heat flow perpendicular to fibers	4.110 (0.285)
Heat flow parallel to fibers	4.816 (0.334)
Heat of combustion, kJ/g (Btu/lb)	34.8 (15,000)

Table 2.4 Properties of Kevlar 29 (2)

Specific gravity	1.44
Tensile strength (GPa)	2.76
Tensile modulus (GPa)	58
Elongation (%)	4.0
Filament diameter (µm)	12.1

Table 2.5 Typical Properties of Boron fibers and of other Commercially Available Reinforcement Filaments (1)

Filament material	Diameter (μm)	Manufacturing technique	Average strength N/m^2 (Ksi)	Density (g/cm^3)	Modulus (GN/m^2)
Boron	100–150	CVD	34 (500)	2.6	400
SiC-coated boron	100–150	CVD	31 (450)	2.7	400
SiC	100	CVD	27 (400)	3.5	400
B_4C	70–100	CVD	24 (350)	2.7	400
Boron on carbon	100	CVD	24 (350)	2.2	—
Al_2O_3	250	Melt withdrawal	24 (350)	4.0	250
Beryllium	100–250	Wire drawing	13 (200)	1.8	250
Tungsten	150–250	Wire drawing	27 (400)	19.2	400
‘Rocket Wire’	50–100	Wire drawing	41(600)	7.9	180
AFC-77					

Table 2.6 Carbon fibre precursors (2)

Precursor material	Carbon content (%wt)	Carbonization yield (%wt)
Cellulose fibre	45	10–15
Polyacrylonitrile	68	40
Lignin	70	50
Hydrocarbon pitch	95	85–90

Table 2.7 Properties of some carbon fibers (2)

Fibre precursor	Fibre type	Trade name	Diameter (μm)	Specific gravity	Tensile strength (GPa)	Tensile modulus (GPa)	Elongation (%)	Carbon content (%wt)
Hydrocarbon pitch	Carbon	Kureha	10.5	1.6	1.03	—	2.5	99.5
Lignin	Carbon		10–15	1.5	0.6	—	1.5	90
Cellulose	Graphite	Thornel	6.6	1.67	2.0	390	0.6	99.9
Polyacrylonitrile	Carbon	Graphil	8	1.76	3.2	230	—	—
		HT						
Polyacrylonitrile	Graphite	Graphil	8	1.87	2.4	330	—	—
		HM						

2.2.1 Glass Fibers

Glass fibers are the most common of all reinforcing fibers for polymeric matrix composites. Their main advantages are low cost, high tensile strength, high chemical resistance and good insulating properties. On the other hand they display a low tensile modulus, a relatively high density compared to the other fibers, a high

sensitivity to wearing and a low fatigue resistance. Depending on the chemical composition of the glass they are commercially available in different grade: A, C, E, R, S. At one time 'A' or alkali glass was quite common as the basic material for glass fibre production. Today this has been virtually completely superseded by 'E' or electrical grade glass. E-glass is a very low alkali content borosilicate glass which provides good electrical and mechanical properties, coupled with good chemical resistance. Another glass produced in commercial quantities for fibers production is the C-glass, a special chemical resistant glass. This is used in the manufacture of surfacing tissues to provide additional chemical resistance over E-glass. For specific application 'R' and 'S' glasses are available as fibers. These are high strength glasses used mostly for aerospace applications.

2.2.2 Aramid Fibers

The most common aramid fiber available is the Kevlar 49. These fibers are composed of a highly oriented crystalline polymer and present the highest tensile strength/weight ratio. On the other hand the disadvantages that they present are the low compressive strength, difficulty of manufacturing and a sensitivity to ultraviolet light and water. However, Kevlar fibers find applications in sporting goods.

2.2.3 Boron Fibers

These fibers are characterized by an extremely high tensile modulus coupled with a large diameter, offering an excellent resistance to buckling that contributes to a high compressive strength of the composites. Their high cost is due to the processing operations. For this reason boron fibers find application only in aerospace and military contexts.

2.2.4 Graphite Fibers

Carbon fibers owe their success in high performance composites to their extremely high tensile modulus/weight and tensile strength/weight ratios, high fatigue strength and low coefficient of thermal expansion, coupled with a low ratio of cost to performance. Carbon fibers are commercially available with a variety of moduli ranging from 270 GPa to 600 GPa. They are produced following two different processes, depending on the type of precursors.

2.3 Matrix Materials

Polymer matrix resins bind the reinforcing fibers and fabrics together in composite structures. Resins also act as sizing, load distributors, and vibration dampeners in the composite structure. A wide variety of thermoset and thermoplastic resins are used in polymer composites. A summary of the most important materials used as composite matrix and their properties is presented.

2.4 Thermoplastic Matrix

Although many commercial applications for filled thermoplastics exist, use of thermoplastics in advanced composites is still in the developmental stage. In fact, the industry is still split on the use of thermoplastics for advanced composites. According to some, it is difficult to improve the rigidity, stability and thermal and chemical resistance of the thermoset resins currently available. Others believe that the majority of the thermoplastic resins available today not only possess the high-service temperature characteristics required, but also hold the potential of quicker and more economical processing once the existing problems are resolved. The various thermoplastics and their characteristics are described in the following paragraphs:

Polyamides commonly referred to as nylons, are produced by condensation between diamines and diacids or by self-condensation of an amino acid. Like many other resins, the exact chemistry of polyamides can vary and, therefore, so can the final properties. However, all polyamides have low-service temperatures and low melting points.

Polyamideimides are marketed by Amoco Chemicals under the trade name Torlon. A polyamideimide is also a good candidate for the production of thermoplastic prepregs.

Polycarbonates are noted for an extremely high-impact strength in an unreinforced state. However, compared to such other crystalline polymers as PEEK, a polycarbonate does not bond well to reinforcing fibers. It also has poor chemical resistance, which can be greatly improved by alloying it with thermoplastic polyesters. Although only a small quantity of polycarbonate with carbon fiber reinforcement is used today, primarily for interior aircraft structures, polycarbonate is potentially one of the more promising matrix resins for advanced composites, especially in alloyed versions such as General Electric's Xenoy and Bayer's Makroblend.

Polyetheretherketones (PEEK) have excellent properties for use in advanced polymer composites, including low flammability, low smoke and toxic gas emission, and broad chemical and solvent resistance. PEEK possesses a continuous service temperature of 200 °C to 240 °C (392 °F to 464 °F) and has a very high melting point of 334 °C (633 °F). PEEK also provides excellent abrasion resistance at its service temperature, radiation resistance, excellent fatigue and wear resistance and a relatively low specific gravity of 1.32. It is possible to process PEEK on conventional extrusion and molding equipment, and its highly crystalline nature responds well to fiber reinforcement.

Polyetherimides (PEI) have been commercially introduced by General Electric as ULTEM, and the company states that it could be a possible matrix for carbon fiber.

Polyether sulfones (PES) are also amorphous in structure. Although PES has poor resistance to solvents, it possesses several valuable properties. The resin is capable of providing thousands of hours of service at temperatures up to 180 °C (356 °F) and has very good load-bearing properties. It is dimensionally stable up to 200 °C (392 °F) and, like PEEK, possesses excellent flame resistance and favorable processing characteristics. In addition to thermoset polyimides, several thermoplastic polyimides are offered for high-temperature applications. Although difficult to process, these resins maintain favorable performance characteristics up to a higher temperature, 371 °C (700 °F), than their thermoset counterparts.

Polyphenylene sulfides (PPS), partially crystalline polymers, are produced by the reaction of p-dichlorobenzene and sodium sulfide. This polymer has metallic-like properties and responds well to reinforcement. PPS possesses good creep and good moisture resistance and a low coefficient of thermal expansion.

2.5 Thermosets Matrix

The basic difference between thermoset and thermoplastic resins is the reaction heat. A thermoset resin is cured by the application of heat and often by the addition chemicals called curing agents. Once cured, the material is infusible, insoluble and can softened or reworked with the addition of heat.

A thermoplastic, on the other hand, is capable of being repeatedly softened by addition of heat and hardened by decreasing temperature. The change occurring thermoplastic resin with the addition of heat is primarily physical, not chemical. This different provides one major advantage for thermoplastics: any scrap from fabrication can be reused.

Thermoset resins can vary greatly with respect to service temperature, solvent resist and other important characteristics. A description follows of the various thermoset resin their basic characteristics.

2.6 Vinyl Ester Resins

Vinyl ester resins are thermosetting resins that consist of a polymer backbone with acrylate or methacrylate termination. The backbone component of vinyl ester resins can derived from an epoxide resins, polyester resins, urethane resin, and so on, but those base epoxide resins are of particular commercial significance.

Vinyl ester resins are produced by the addition of ethylenically unsaturated carbo acids (methacrylic or acrylic acid) to an epoxide resin (usually of the bisphenol epichlorohydrin type). The reaction of acid addition to the epoxide ring (esterification exothermic and produces a hydroxyl group without the formation of

by-products. Appropriate diluents and polymerization inhibitors are added during or after esterification. Epoxide resins that have been used to produce vinyl ester resins include:

- bisphenol A types (general-purpose and heat-resistant vinyl esters)
- phenolic-novolac types (heat-resistant vinyl esters)
- tetrabromo bisphenol A types (fire-retardant vinyl esters)

Vinyl ester resins contain double bonds that react and crosslink in the presence of free radicals produced by chemical, thermal or radiation sources.

2.7 Epoxide Resins

Epoxide are materials which contain two or more glycidyl groups per molecule. The uncured resins range from free flowing liquids to high melting solids, which can be cross-linked by reaction with an appropriate curing agent.

Typical curing agents include primary and secondary amines, polyamides and organic anhydrides. Other curing agents used are the catalytic curing agents, such as the boron trifluoride complexes. No by-products are evolved during cure. The resultant cured resins are generally hard thermoset materials with excellent mechanical, chemical and electrical properties.

These materials can be conveniently divided into six classes of resins:

- bisphenol A based (e.g. diglycidyl ether of bisphenol-A (DGEBA))
- glycidyl esters
- glycidyl amines (e.g. tetraglycidyl amine of 4,4-diamino-diphenyl-methane)
- novolacs brominated resins (e.g. diglycidyl ether of tetrabromo-bisphenol A)
- cycloaliphatic resins (e.g. Tetraglycidyl ether of tetraphenylene ethane)

2.8 Diluents

Diluents are added to epoxide resins primarily to lower viscosity and thus to improve handling characteristics. They also modify the cured properties of the resin. Diluents can be divided into two classes: (a) the reactive diluents and (b) the non-reactive diluents.

2.8.1 Reactive Diluents

- Butane-1, 4-diol diglycidyl ether
- n-Butyl glycidyl ether (nBGE)
- Glycidyl methacrylate

- Phenyl glycidyl ether (PGE)
- 2-Ethylhexyl glycidyl ether (2EHGE)
- Iso-octyl glycidyl ether (IOGE)
- Diethylene glycol monobutyl glycidyl ether
- Cresyl glycidyl ether (CGE)
- p-t-Butylphenil glycidyl ether
- Epoxide 7 (C8–C10 glycidyl ether)
- Epoxide 8 (C12–C14 glycidyl ether)
- Dibromocresyl glycidyl ether (BROC)
- Dibromophenyl glycidyl ether (DER 599)

2.8.2 Non Reactive Diluents

- Benzyl alcohol
- Furfuryl alcohol
- Dibutyl phthalate (DBP)

2.9 Curing Agents for Epoxide Resins

These are known variously as curing agents, hardeners, activators or catalysts. They are required to convert liquid and solid epoxide resins into tough infusible thermoset polymers. The curing agents promote this curing reaction by opening the epoxide ring and become chemically bound into the resin in the process. Each of the curing agents for epoxide resins will now be discussed in turn.

2.9.1 Amine Curing Agents

Amine curing agents may be primary or secondary amines, aliphatic, alicyclic or aromatic. The reaction with an epoxide resin is an addition reaction where the amine links directly with an epoxide group to form a combined polymer, with hydroxyl groups formed during the reaction. The amines commonly used are the following

- Ethylenediamine (EDA)
- Trimethylhexamethylenediamine (TMD)
- Diethylenetriamine (DTA)
- 2-Hydroxyethyldiethylenetriamine (T)
- Dipropylenetriamine (DPTA)
- Triethylenetetramine (TETA)
- Tetraethylenepentamine (TEPA)
- Diethylaminopropylamine (DEAPA)

- Dimethylaminopropylamine (DMAPA)
- m-Xylylenediamine (mXDA)
- N-Aminoethylpiperazine (AEP)

2.9.2 Anhydride Curing Agent

These consist of organic anhydrides and are used in roughly stoichiometric proportions with epoxide resins. The anhydride commonly used are the following:

- Phthalic anhydride (EPA)
- Tetrahydrophthalic anhydride (THPA)
- Methyltetrahydrophthalic anhydride (MTHPA)
- Endomethylenetetrahydrophthalic anhydride (NA)
- Hexahydrophthalic anhydride (HHPA)
- Methylhexahydrophthalic anhydride (MHPA)
- Trimellitic anhydride (TMA)
- Pyromellitic dianhydride (PDMA)
- Dodecenylsuccinic anhydride (DDSA)

2.9.3 Accelerators for Anhydride Cured Systems

Various accelerators can be used with epoxy/anhydride systems to promote cure. Some accelerators in use are:

- Benzyl dimethylamine (BDMA)
- Tris(dimethylaminomethyl)phenol
- 1-Methylimidazole (DY 070 from Ciba-Geigy)
- N-Butylimidazole
- 2-Ethyl-4-methylimidazole
- Triamylammonium phenate (DY 063 from Ciba-Geigy)

2.9.4 Polyamide Curing Agents

The polyamides used to cure epoxide resins are all reactive compounds with free amine groups. They may be amidopolyamines, aminopolyamides or imidazolines. They are mostly used in coating systems and in adhesive formulations. Some suppliers of polyamide curing agents are listed below:

- Ancamide (Anchor Chemical Co, Ltd)
- Araldite (Ciba-Geigy Plastics & Additives Co.)

- Versamid, Genamid, Synolide (Cray Valley Products Ltd)
- Plastamid (Croda Resin Ltd)
- Grilonit (Grilon (UK) Ltd)
- Beckopox (Hoechst AG(Reichhold Albert Chemie AG))
- Euredur (Schering Chemicals Ltd)
- Epikure (Shell Chemicals UK Ltd)
- Casamid (Thomas Swan & Co. Ltd)
- Uracure (Synthetic Resins Ltd)
- Thiokol (Thiokol Chemicals Ltd)
- Wolfamid (Victor Wolf Ltd)

2.9.5 Other Curing Agents

Several other types of curing agent are used with epoxide resins for laminating applications or in moulding compounds. Examples of these curing agents are:

- Dicyandiamide (Dicy)
- Boron trifluoride complexes
- Boron trifluoride monoethylamine
- 2-Ethyl-4-methylimidazole
- N-n-Butylimidazole

2.10 Polyester Resins

The basic materials used to make a polyester resin are a dibasic organic acid or anhydride and a dihydric alcohol.

2.10.1 Catalysts or Initiators

Catalyst or initiators for unsaturated polyester resin system consist of organic peroxides. Some commercially available catalysts are:

- Diacyl peroxides (benzoyl peroxide, 2,4-dichlorobenzoyl peroxide, dilauroyl peroxide, diacetyl peroxide).
- Ketone peroxides (methyl ethyl ketone peroxide, cyclohexanone peroxide, acetylacetone peroxide, methyl isobutyl ketone peroxide).
- Hydroperoxides (t-butyl hydroperoxide, cumene hydroperoxide).
- Dialkyl and diaralkyl peroxides (dicumyl peroxide, di-t-butyl peroxide, t-butyl cumyl peroxide, 2,5-dimethyl-2,5-bis(t-butylperoxy)hexane).

- Peroxyesters (t-butyl peroxybenzoate, t-butyl peroxydiethylacetate, t-butyl peroxyester, t-butyl peroxyisononanoate, t-butyl peroctoate, dit-butyl diperoxyphthalate, t-butyl peroxyvalate).
- Perketals (2,2-bis(t-butylperoxy)butane, 1,1-bis(t-butylperoxy)cyclohexane, 1,1-bis(t-butylperoxy)-3,3,5-trimethylcyclohexane).

2.10.2 Accelerators or Promoters

These are materials which when used in conjunction with an organic peroxide catalyst increase the rate at which that peroxide breaks down into free radicals. Some of the commercially available accelerators are:

- Cobalt accelerators: cobalt siccatoate, naphthenate or octoate
- Manganese accelerators: manganese salts
- Vanadium accelerators
- Tertiary amine accelerators: dimethylaniline (used to accelerate diacyl peroxide catalysed system); diethylaniline (used to accelerate benzoyl peroxide catalysed system); dimethyl-p-toluidine (used to accelerate benzoyl peroxide catalysed system).

2.11 Laminate Properties

Current attitudes regarding composite materials emphasize the relationship of structural performance to the properties of a ply. A 'ply' is a thin sheet of material consisting of an oriented array of fibers, embedded in a continuous matrix material. These plies are stacked one upon other, in a definite sequence and orientation, and bonded together yielding a laminate with tailored properties. The properties of the laminate are related to the properties of the ply by the specification of the ply thickness, stacking sequence, and the orientation of each ply. The properties of the ply are, in turn, specified by the properties of the fibers and the matrix, their volumetric concentration, and geometric packing in the ply. Generally, the material is preformed and can be purchased in a continuous compilant tape or sheet form which is in a chemically semicured condition. Fabrication of structural items involves using this 'prepreg' material, either winding it on to a mandrel or cutting and stacking it on to a mold, after which heat and pressure or tension is applied to complete the chemical hardening process.

The basis for engineering design of a such material is then the properties of a cured ply or lamina as it exists in a laminate. This ply is treated as a thin two-dimensional item and is mechanically characterized by its stress-strain response to: (i) loading in the direction of the filaments, which exhibits a nearly linear response up to a large fracture stress; (ii) loading in the direction transverse to the filament

orientation, which exhibits a significantly decreased moduli and strength, and (iii) the response of the material to an in-plane shear load.

By the contrast with isotropic metallic materials, an oriented ply, in the form of a thin sheet, is anisotropic and requires four elastic (plane stress) constants to specify its stiffness properties in its natural orientation

$$\begin{aligned}\sigma_1 &= Q_{11}\epsilon_1 + Q_{12}\epsilon_2 \\ \sigma_2 &= Q_{12}\epsilon_1 + Q_{22}\epsilon_2 \\ \sigma_6 &= Q_{66}\epsilon_6\end{aligned}\quad (2.1)$$

where $\sigma_6=\tau_{12}$ and $\epsilon_6=\gamma_{12}$ or in matrix form

$$\begin{bmatrix} \sigma_1 \\ \sigma_2 \\ \sigma_3 \end{bmatrix} = \begin{bmatrix} Q_{11} & Q_{12} & 0 \\ Q_{12} & Q_{22} & 0 \\ 0 & 0 & Q_{66} \end{bmatrix} \cdot \begin{bmatrix} \epsilon_1 \\ \epsilon_2 \\ \epsilon_3 \end{bmatrix}\quad (2.2)$$

where the plane stress stiffness moduli are

$$\begin{aligned}Q_{11} &= E_{11} / (1 - \nu_{12} \nu_{21}) \\ Q_{22} &= E_{22} / (1 - \nu_{12} \nu_{21}) \\ Q_{12} &= \nu_{21} E_{11} / (1 - \nu_{12} \nu_{21}) \\ Q_6 &= G_{12}\end{aligned}\quad (2.3)$$

where ν_{ij} is the Poisson ratio, defined as $-\epsilon/\epsilon_j$.

If, however, the ply is rotated with respect to the applied stress or strain direction additional moduli appear, which results in the direction-indicated shear coupling rotation simple extension

$$\begin{bmatrix} \sigma_1 \\ \sigma_2 \\ \sigma_3 \end{bmatrix} = \begin{bmatrix} Q_{11}^* & Q_{12}^* & Q_{16}^* \\ Q_{12}^* & Q_{22}^* & Q_{26}^* \\ Q_{16}^* & Q_{26}^* & Q_{66}^* \end{bmatrix} \cdot \begin{bmatrix} \epsilon_1 \\ \epsilon_2 \\ \epsilon_3 \end{bmatrix}\quad (2.4)$$

where

$$\begin{aligned}Q_{11}^* &= U_{11} + U_2 \cos(2\theta) + U_3 \cos(4\theta) \\ Q_{22}^* &= U_{11} + U_2 \cos(2\theta) + U_3 \cos(4\theta) \\ Q_{12}^* &= U_4 + U_3 \cos(4\theta) \\ Q_{66}^* &= U_5 + U_3 \cos(4\theta) \\ Q_{16}^* &= -1/2 U_2 \sin(2\theta) - U_3 \sin(4\theta) \\ Q_{26}^* &= -1/2 U_2 \sin(2\theta) - U_3 \sin(4\theta)\end{aligned}\quad (2.5)$$

The invariants U_i to the rotation are

$$\begin{aligned}
 U_1 &= \frac{1}{8}(3Q_{11} + 3Q_{22} + 2Q_{12} + 4Q_{66}) \\
 U_2 &= \frac{1}{2}(Q_{11} - Q_{22}) \\
 U_3 &= \frac{1}{8}(Q_{11} + Q_{22} - 2Q_{12} - 4Q_{66}) \\
 U_4 &= \frac{1}{8}(Q_{11} + Q_{22} + 6Q_{12} - 4Q_{66}) \\
 U_5 &= \frac{1}{8}(Q_{11} + Q_{22} - 2Q_{12} - 4Q_{66})
 \end{aligned} \tag{2.6}$$

In addition, lamination can result in up to 18 elastic coefficients and increased deformational complexities, but the additional coefficients can all be derived from the four primary coefficients using the concept of rotation and ply-stacking sequence. These complications are the result of geometric variables. If the laminate is properly constructed, the in-plane stretching or stiffness properties can still be specified by four elastic coefficients. We shall consider laminates of this nature.

Note that both short and continuous fibers are handled in the same manner. These calculations, while tedious, are analytically simple. The ‘plane stress’, the Q_{ij} terms, are employed because lamination neglects the mechanical properties through the ply thickness. These stiffnesses are sometimes regrouped into new constants called ‘invariants’, the U_i terms, for analytical simplicity. To compute the properties of the laminate one then sums the ply (h_k) properties through the thickness of the laminate, weighted by the thickness (h_k) of each oriented ply

$$A_{ij} = \sum_{k=1}^N (Q_{ij})_k h_k$$

For a balanced (same number of $\pm\theta$) and symmetrical system ($+\theta$ or $-\theta$ at same distance above and below the midplane) the laminate solution is

$$\begin{aligned}
 A_{11} &= U_1 + U_2 \cos(2\theta) + U_3 \cos(4\theta) \\
 A_{22} &= U_1 + U_2 \cos(2\theta) + U_3 \cos(4\theta) \\
 A_{12} &= U_4 - U_3 \cos(4\theta) \\
 A_{66} &= U_5 - U_3 \cos(4\theta)
 \end{aligned} \tag{2.7}$$

Note the inverted terms A_{ij} yield the required elastic properties of the laminate in terms of the individual ply properties E_{11} , E_{12} and G_{12} .

$$\begin{aligned}
 E_{11} &= (A_{11}A_{22} - A_{12}^2) / A_{22} \\
 E_{22} &= (A_{11}A_{22} - A_{12}^2) / A_{11} \\
 \nu_{12} / E_{11} &= A_{12} / (A_{11}A_{22} - A_{12}^2) G_{12} = A_{66}
 \end{aligned} \tag{2.8}$$

These calculations have been thoroughly tested and agree closely with experiment. The circles and squares are the experimental points and the lines are the theoretical predictions for a nylon fiber reinforced rubber. The angle ply laminate is predicted from the ply properties. The ply properties are in turn correlated with the transformation equations and the micromechanics. The micromechanics employed in this demonstration are based upon the 'self-consistent method' developed by Hill (8). Hill rigorously modeled the composite as a single fiber, encased in a cylinder of matrix, with both embedded in an unbounded homogeneous medium which is macroscopically indistinguishable from the composite. Hermann (9) employed this model to obtain solution in terms of Hill's 'reduced moduli'. Halpin and Tsai (10) reduced Hermann's solution to simpler analytical form and extended its use for a variety of filament geometries

$$\begin{aligned} E_{11} &= E_f V_f + E_m V_m \\ \nu_{12} &= \nu_f V_f + \nu_m V_m \\ p/p_m &= (1 + \eta \xi V_f) / (1 - \eta V_f) \end{aligned} \quad (2.9)$$

where

$$\begin{aligned} \eta &= (t_f / t_m - 1) / (p_f / p_m + \zeta) \\ \xi &= (e / d); \zeta_{G12} = 1 \zeta_{G23} = 1 / (3 - 4\nu_m) \\ p &= E_{22}, G_{12}, G_{23}; p_f = E_f, G_f; p_m = E_m, G_m \end{aligned} \quad (2.10)$$

These equations are suitable for single calculation and were employed previously for the single ply and angle ply properties. The short fiber composite properties are also given by the Halpin-Tsai equations where the moduli in the fiber orientation direction is a sensitive function of aspect ratio ($1/d$) at small aspect ratios and has the same properties of a continuous fiber composite at large but finite aspect ratios.

If the ply is used in the construction of a balanced and symmetrical 0/90 laminate and is mechanically tested, bilinear stress/strain curve is obtained, and the stiffness is the sum, through the thickness of the plane stress stiffness of each layer. As the laminate is deformed each ply possesses the same in-plane strain, and when the strain on the 90 layers in the laminate prevents the 90° layer from carrying its share of the load, $Q_{ij}(90^\circ) = 0$. This load is transferred to the unbroken layers, the 0° layers for our illustration, and results in a loss of laminate stiffness or modulus. Continual loading will ultimately produce a catastrophic failure of the laminate when the strain capability of the unbroken, 0°, layers is exceeded. For a 0/90 construction, employing glass/epoxy material, the ratio of the ultimate failure stress to the crazing stress is 6.1. Note a change in stiffness as the 90° and then the 45° layers fail, and the correspondence of the theoretical ultimate strength of 356 MPa with the experimental results of 346 MPa. While the strain for transverse ply failure is constant from laminate to laminate, the stress required to craze the system as well as cause final failure is a function of laminate geometry, because the construction of the

laminate specifies the stiffness properties (crazing stress = stiffness \times allowable transverse ply strain). It must be noticed that the area under the stress/strain curve is proportional to the impact energy. Therefore, lamination permits the engineer to tailor a fixed prepreg system to meet the conflicting stress/strain demands at different points in a structure. A further point, the crazing stress threshold is generally at or below the creep fracture or fatigue limit for all classes of composites (for glass/epoxy the fatigue limit lies between 0.25 and 0.30 of static ultimate strength). Boron and graphite are fatigue insensitive filaments, thus no fatigue damage is realized below first ply failure.

Thus, the material properties of a laminate are specified in terms of the ply engineering moduli, E_{11} , E_{22} , ν_{12} and G_{12} ; the engineering strains to failure, ϵ_1 , ϵ_2 and ϵ_6 ; and the thermal expansion coefficients, ϵ_1 and ϵ_2 .

2.12 Composite Fabrication

Various fabrications used in the reinforced plastics industry are discussed below:

2.12.1 *Hand Lay-Up and Spray-Up Procedures*

In one of the simplest and labor intensive procedures, pigmented, catalysed resin is applied to the surface of the mold. This gel coat in room temperature lay-up techniques will end up on the surface of the finished composite (FRP). Catalysed resin-impregnated mat is then applied over the gel coat and this and subsequent layers are brushed or rolled to assure good contact between layers and to remove any entrapped air. This procedure is continued until the desired thickness of the composite is attained.

The assembled composite may be cured at room temperature or at elevated temperatures for faster cycles. This procedure, which was originally called contact molding, may be upgraded by the application of a vacuum or pressure bag placed over a Cellophane film on the final layer to reduce void formation in the composite. The laminate may also be built up by a spray-up process in which a mixture of chopped glass strands and catalysed resin is sprayed on the gel coat instead of resin-impregnated mat. In any case, the inner surface will be less smooth than the first layer formed by the gel coat. Tanks, boats and pipe may be fabricated by this technique.

2.12.2 *Centrifugal Casting*

Fiber-reinforced plastic pipe (FRP) can be produced by rotating a mixture of chopped strand and catalysed resin inside a hollow mandrel. Because of differences in specific gravity, there is a tendency for these composites to be less homogeneous than those produced by other techniques.

In addition to being available as continuous filaments and staple fibers in mats, fiberglass textiles are also available as biaxial, triaxial, knitted and three dimensional braided patterns. Many different resin matrices are in use but the emphasis in this chapter will be on unsaturated polyester and epoxy resins. While the strength and stiffness are controlled primarily by the reinforcements, the resinous matrix contributes to thermal conductivity and flexibility. The ultimate properties of these composites are based on a harmonious contribution of both the continuous and discontinuous phases.

2.12.3 *Matched Die Molding*

Matched die molding of a premix of chopped glass, roving, and catalyzed resin is used for relatively large scale production of reinforced articles. Uncured dough-like compositions are called bulk molding compounds (BMC). Uncured resin-impregnated sheets are called sheet molding compound (SMC). These compounds are supplemented by thick molding compounds (TMC) and XMC. TMC is produced continuously on a machine that resembles a 2 roll mill. XMC, in which the continuous impregnated fiber are arranged in an X-pattern, is produced on a filament winding machine.

Autoclave Molding Autoclave molding, the process of curing thermoset resins at elevated temperature and pressure in an inert environment, has an important role in the fabrication of continuous fiber reinforced thermoplastics. While most companies view thermoplastics as an alternative to traditional autoclave long-cycle processing, they have come to accept the following reasons for the autoclave processing of thermoplastic matrices:

- Availability
- High temperature and pressure capability
- Reduced tooling requirements
- Uniform pressure distribution.

The dominant reason for the autoclaves' role in thermoplastics production is its availability. Aerospace first- and second-tier contractors, who conducted much of the developmental work in parts fabrication, all have autoclaves on hand.

While it may seem defeatist to use the autoclave for thermoplastic resins which undergo no chemical reaction and lend themselves to rapid fabrication, autoclave use offers other advantages.

In the industry, many fabricators own autoclaves capable of processing high temperature thermosets (e.g. polyimides) at operating temperatures up to 800 °F and pressures of 150 to 200 psi; which can also accommodate high temperature thermoplastics such as PEEK, which is normally processed in the 700 to 750 °F range. One disadvantage, particularly for production-sized autoclaves, is the inability to finely control cool-down rate – a critical process step for the semicrystalline thermoplastics. This situation can be improved by implementing integrally cooled tooling.

Where high consolidation pressures are required, the autoclave can reduce tooling costs by eliminating the need for matched metal tooling, when compared to a molding process (e.g. compression molding or thermoforming). Less expensive tooling aids can be used for consolidation via the autoclave's pressurized environment. The autoclave also provides uniform pressure over the part's area and eliminates pressure distribution concerns associated with a matched tool in a press.

Thermoforming Thermoforming offers vast potential for high volume thermoplastic composite parts fabrication. There are many thermoforming variations; but by basic definition, thermoforming is the heating of a reinforced thermoplastic matrix sheet or kit above the softening temperature, followed by forcing the material against a contour by mechanical (e.g. matched tooling, plug) or pneumatic (e.g. differential air or hydraulic) means. The material is then held and cooled sufficiently for shape retention, and removed from the mold. Thermoforming implies only those processes applicable to thermoplastic resins, and is often used in the same context as the term 'compression molding' which also applies to thermosets. In this section, the process is defined as the preheating of the lay-up or reconsolidated sheet, followed forming via a matched mold.

Phillips Petroleum has applied this technology to fabric reinforced Ryton (PPS) materials. A conveyORIZED infrared oven is used to rapidly preheat the lay-up to 600 °F in two to three minutes. The charge is quickly transferred to a preheated mold in a fast closing press for part forming. Total cycle times of one to three minutes are feasible with this automated approach.

High production rates can be achieved using thermoforming technology. However, it is difficult to form high quality continuous fiber reinforced thermoplastic parts with demanding geometries, due to the restricted movement of the fiber.

Du Pont's long discontinuous fiber sheet products with PEEK and J-2 resins provide easier fabrication of complex shapes. This product form is particularly attractive to helicopter manufacturers for the press forming of highly contoured secondary structure parts.

Transfer molding Transfer molding is used for the manufacture of small components and is particularly useful with multi-cavity tools and where small inserts are to be moulded in. Materials used are polyester and epoxide dough moulding compounds, although a new liquid resin injection technique is reported.

Heated steel molds, preferably hard chrome plated, are used, which may be of multicavity design. Tooling costs are higher than for compression moulding since appropriate gates and runners must be included in the mould.

A pre-weighed quantity of DMC is placed in a heated transfer pot by hand. A punch or ram compresses the material and causes it to flow into the heated tool cavity where it cures. The tool is mounted between the platens of a press.

Factors to be considered with transfer molding are transfer and tool clamping pressures and transfer time. To reduce transfer time and increase overall efficiency the molding compound may be pre-heated in an oven or high frequency pre-heater such as a micro-wave oven.

Mold temperatures range from 155 to 170 °C both for polyester and epoxide resin compounds, with molding pressures ranging from 5 to 100 MPa depending on the type of compound to be processed, mold design and temperature. Cure time in the mold (excluding pre-heat time) is usually of the order of 10–30 s per millimetre of wall thickness for both types of compound.

Injection molding Injection molding, a technique used extensively for the processing of thermoplastic materials, has also been developed to process thermosetting resin systems. Due to high mould costs it is generally only suitable for the large scale production of small-to-medium sized components. Materials processed in this way are polyester and epoxy DMC and also phenolics, ureas, melamines and diallyl phthalate moulding compounds. These latter materials are generally more difficult to process than either polyester or epoxy DMC.

Thermoset moldings produced by injection moulding are used widely in the electrical and automotive fields, thus large production runs are common.

Injection molding has advantages over both compression and transfer molding in that the process is more automated and far higher production rates can be achieved. Although mould costs are higher than for compression molding, overall finished component costs are generally lower. With small weight components, scrap from runners can be high compared with compression molding but for large moldings this becomes relatively insignificant. Injection molding is also better for thick parts since, with the pre-heating of the DMC before injection into the mold, shorter molding cycles are possible.

While injection molding machines designed specifically for processing thermoset materials are available, a number of manufacturers offer replacement screw and barrel assemblies and stuffer hoppers to convert conventional thermoplastic injection moulding machines to process thermosets.

Molding compound is transferred in the cold state by pressure from the material hopper into the main injection chamber. Here it can be preheated before injection into the heated mould tool. Injection, through a special nozzle, can be either by ram or screw pressure. If screw feed is used, the screw must be of the type designed to process thermosets as opposed to thermoplastics.

Early machines were designed with vertical clamping pressure on the mold but today horizontal machines are mostly used. Since thermosetting materials are liquid until gelation occurs, clamping pressure has to be maintained on the mould until the resin has cured. Unless this is done, excessive flash will form. Heated matched metal molds are used, which may be of multi-cavity design. These molds must be designed for use with thermosetting resins, taking into account the fact that thermoset moldings are harder, more rigid and less easily deformed than thermoplastics.

A typical temperature sequence for injection molding DMC would be: feed hopper and feed zone – ambient temperature; metering section 50–60 °C; nozzle 80–90 °C; mould temperature 135–185 °C for polyester DMC or 160–22 °C for epoxy DMC; injection pressure 80–160 MPa. Cure time is generally of the order of 10–20 s per millimetre of wall thickness. Very little finishing of moldings is necessary.

Where fully automatic molding machines are used, hydraulic ejection with perhaps a 'joggle' facility is necessary, since thermosets have a tendency to stick in the mold.

2.12.4 Filament winding

Filament winding is a technique used for the manufacture of pipes, tubes, cylinders and spheres and is frequently used for the construction of large tanks and pipework for the chemical industry. By suitable design, filament wound structures can be fabricated to withstand very high pressures in service. In general, products fabricated by filament winding have the highest strength to weight ratios and can have glass contents of up to 80 % by weight.

The process is suitable for use both with polyester and epoxide resin systems and a variety of fibres including glass, carbon, aramid and metals, providing that these materials are available in continuous filament lengths. Glass fibre is by far the most common reinforcement used and will be used as the example in the description of the process.

Filament winding is basically a simple process, although numerous modifications have been developed to improve product quality. Moldings can be produced by either a wet lay-up process or from prepreg.

In recent years filament winding has been extended to the continuous production of pipe using a continuous steel band mandrel. In this way continuous lengths of pipe can be produced, with diameters ranging from about 0.3 to 3.5 m.

2.12.5 Wet lay-up

With the wet lay-up process glass rovings are drawn through a resin bath to impregnate them with resin. The impregnated rovings are then wound under tension round a rotating mandrel. Generally the feed head supplying the rovings to the mandrel traverses backwards and forwards along the mandrel.

The mandrel, which may be segmented for large diameter pipes, is generally wrapped with a release film, such as Cellophane, prior to wrapping with glass and resin. The mandrel may incorporate some means of heating the resin system, such as embedded electric heaters, or provision for steam heating. Alternatively, the fully wrapped mandrel and laminate may be transferred to a curing oven to effect cure.

In order to provide a resin-rich, corrosion resistant inner lining to the pipe, the mandrel may be wrapped with a surfacing tissue followed by one or two layers of chopped strand mat or woven tape prior to filament winding. This first layer is usually allowed to cure partially before winding commences to prevent the resin from being squeezed out into the main laminate.

The winding angle used during construction of pipes or tanks depends on the strength/performance requirements and may vary from longitudinal through helical to circumferential. Often a combination of different winding patterns is used to give optimum performance. Accurate fibre alignment is possible.

For pipe construction, steel mandrels are generally used. However, where cylinders or spheres are to be made, an alternative material has to be used so that it can be removed once the resin system has cured. In these cases the mandrel can be made from wax, a low melting metal alloy, or an inert plaster held together with a water soluble binder. Clearly, in these cases the mandrel can only be used once. Material choice for the mandrel will depend on the cure cycle needed for the resin system.

In addition to winding with continuous filament rovings, machines have been developed which permit winding with tapes or slit-width chopped strand mat and woven rovings. These reinforcements may be used alone or combined with continuous filament rovings. Thus considerable design flexibility exists for the production of large simple shapes.

Improved chemical resistance can be achieved by the use of a thermoplastic or synthetic rubber liner. If the liner is sufficiently rigid it can be supported on a light frame and used as the mandrel, if not then it can be wrapped round the mandrel first. A grade of polypropylene is available which has a woven glass cloth partially rolled into one side to improve adhesion of the resin system (Celmar).

Dunlop has recently developed a new process for pipe production to produce pipes in the range 200–2000 mm diameter. Essentially the process is similar to conventional filament winding. A mandrel, suitably coated with release agent, is wrapped with an epoxide resin impregnated glass tape over this is wound a 150 mm high-strength steel strip angled to give 50 % overlap. Epoxide resin system is applied to the steel strip to ensure that each layer is fully encapsulated. From three to 13 layers of steel may be applied to satisfy different pressure ratings. The pipe is finished by wrapping with further resin impregnated glass tape and the resin system cured. Pipe produced in this way has excellent corrosion resistance coupled with a high strength/weight ratio. It is said to provide up to 50 % weight saving over conventional steel pipe.

Various processes are available for the 'on-site' construction of large filament wound storage tanks. By manufacturing these on site, transport problems are overcome and integral structures can be produced. With the various processes either horizontal or vertical mandrels are first constructed from preformed GRP sheets. These are then wrapped with resin impregnated glass rovings.

Filament wound vessels can be produced from prepreg tapes and rovings. This technique is often used with carbon fibre to reduce fibre damage during the winding operation and to permit the use of resin systems which cannot be handled by wet lay-up techniques. Here, it is essential to use a heated mandrel to melt the resin and hence displace air and consolidate and cure the laminate. Resin content of the laminate can be controlled more accurately with prepreg since the prepreg can be made with exactly the right resin content. The use of prepreps also makes for cleaner operation.

Filament winding has been used to provide a protective laminate on the outside of steel pressure pipes where external corrosion can take place. An example of this use is in the protection of the splash zone of steel riser pipes used on sea based oil and gas production platforms. Here, care has to be taken in the design of such a composite structure since the coefficient of expansion of the filament wound glass wrap can be lower than that of the steel core. If such a composite structure is produced using a heat cured resin system (say 120 °C cure) and then subjected to sub-zero temperatures in use, the steel pipe can shrink away from the laminate and permit entry of water by capillary action. Thus the object of wrapping the pipe to prevent corrosion can be defeated, since corrosion can then still take place under the laminate. once the bond has broken it can never be remade.

2.12.6 Centrifugal Moulding

Centrifugal moulding or casting is a method used for making cylindrical objects with uniform wall thickness. It is mainly used for the production of large diameter pipes, up to 5 m in diameter, from either polyester or vinyl ester resin systems, although epoxide resin systems may also be used. Pipes produced in this way are void-free and smooth on both the inner and outer surfaces. Threaded sections can be molded into the external wall if required. More recently, a system has been developed for producing tapered and curved poles by centrifugal casting.

Molds need to be bored and polished to a mirror finish and of sufficient strength to withstand, without distortion, the high G-force exerted during spinning. A steam jacket or other means of heating may be built into the mould to cure the resin system, or alternatively hot air may be blown through the mold.

Release agents used include silicones, bake-on PTFE types or PVA, although silicones are generally preferred. If the exterior of the finished pipe is to be painted then a silicone release agent should not be used. Choice of resin system must depend on application and a heat cured resin may be used, particularly where chemical resistance is required. In addition, the process lends itself to the use of several different resin systems incorporated in the one pipe, such as an abrasion resistant outer skin, a general purpose centre and a chemically resistant inner skin. The resin system used should have some degree of flexibility to give good impact resistance to the pipe, coupled with good chemical resistance. To achieve both of these requirements in the one resin system may require a compromise in properties.

Various methods of fabrication can be used. With large diameter moulds, glass and resin can be applied by the hand lay-up technique using a slow gel resin system so that the whole mold can be coated and the mould spun before gelation of the resin takes place. Here, it is necessary to tailor the reinforcement to shape to avoid overlaps.

Alternatively, the reinforcement may be wrapped round a mandrel, inserted into the mould and then unwound onto the mould surface. The mandrel is removed before resin is injected into the mold. With this technique a faster gelling resin system may be used. Woven fabrics and chopped strand mat are suitable reinforcements.

A third method, capable of being fully automated, is generally preferred. Here, resin and glass are applied to the mold surface utilizing a travelling feeder arm fitted with a chopper and spray gun, which passes slowly backwards and forwards through the mold while the mold is rotated. The laminate can be built up in layers of 0.5–1 mm thickness per pass once the reinforcement and resin system have been placed in the mold it is rotated at up to 2500 revolutions per minute (rpm) depending on mold diameter, the larger the mould diameter the slower the speed. For example, with a 2 m diameter mould a rotation speed of about 180 rpm is used. At this speed the mould surface is rotating at about 68 km/h (42.4 mph).

After the main resin system has gelled, a chemically resistant topcoat may be applied while the mold is still rotating. Mold rotation is continued until all the resin has cured.

In all of the above techniques, a relatively flexible glass reinforced resin pipe is produced, with properties similar to some of those made by filament winding. To produce stiffer pipes a modification to the spray technique has been developed and is in use commercially. Stiffer pipes, particularly in the larger diameter range, offer considerable advantages in handling and installation and maintain their shape during installation.

With this modified process, which is fully automatic, the mold is coated with release agent and rotated at a suitable speed. The feeder arm is designed in such a way that it can deliver programmed amounts of resin, chopped glass and a filler such as sand, to the mold surface as it moves in and out of the mold. In this way a layer of abrasion resistant sand filled resin system can be applied to the mold surface over this is applied a layer of glass reinforced resin. By suitable design of the chopper unit, fibre orientation can be controlled. Next a layer of sand filled resin is applied followed by a further layer of glass reinforced resin. Depending on the type and size of pipe to be produced, several more layers of GRP alternated with filled resin may be added. Finally, the inner surface is coated with a suitable chemically resistant layer of resin, which may be lightly filled or reinforced, to give a smooth corrosion resistant lining.

The equipment used can be programmed to feed materials to the mould to build up the pipe wall thickness at a rate of between 0.5 and 1 mm per pass and to compact the materials by centrifugal force throughout the whole production cycle once the final layer of resin has been applied, hot air is passed through the mold to assist curing of the resin system. The mould is cooled to ambient temperature to assist removal of the finished pipe, which is pushed out using a hydraulically operated ram. Using this technique, rigid hard wearing pipes can be produced, tailored to meet end user requirements. This is a simplified version of the pipes produced commercially, to illustrate pipe construction. In practice several more layers of glass and sand filled system may be incorporated in the pipe wall. A range of bends and joints is also available to meet most needs.

In the Usui process for producing tapered pipes, the glass fibre reinforcement is wound round a tapered mandrel to make a preform. This is inserted into the mould in the centrifugal machine and the mandrel removed. Resin is poured in and the mold tilted to a pre-determined angle and then rotated until the resin has cured.

To produce a curved tapered pipe, a flexible mold is used. This is bent to the required shape once the preform has been placed in position. It is also claimed that base plates can be simultaneously molded on by this method. These base plates are first preformed and then inserted into the mold where they become firmly bonded into the pole. Typical applications include poles for street lighting, flag poles and aerials.

2.12.7 Continuous Sheet Manufacture

For the purposes of this book, only those processes for which polyester resins and, to a limited extent, epoxide resins are used will be described. It should be noted, however, that the decorative laminates used in building and transport applications are in the main manufactured from melamine faced phenolic resin/paper laminates.

Several patented processes exist for continuous sheet production, all of which are similar in broad principle.

Resin and glass reinforcement are sandwiched between two sheets of release film, such as Melinex, Mylar or Cellophane and passed through rollers to consolidate the laminate before curing in an oven. Resin is applied to the release film either by spray or trickle process, care being taken to ensure that application is uniform. Glass reinforcement is laid in the resin and a second layer of release film applied. This sandwich is passed through a series of rollers to expel all air bubbles and consolidate the laminate to the correct thickness. During the next stage the laminate sandwich is either passed directly through an oven to produce flat sheet or through rollers or dies and then an oven to produce corrugated sheet. Once cured the sheet is trimmed to the required width and cut into suitable lengths. Depending on the process, corrugations may run longitudinally or transversely. Production speeds of up to 12 m/min are possible.

To produce clear sheeting the refractive index of the resin system must match that of the glass reinforcement. For this reason special resins have been developed which match the refractive index of E-glass. For translucent sheeting A-glass may be used but, due to its low refractive index, it is unsuitable for use in transparent sheeting. In any case today A-glass is rarely found.

Generally the glass reinforcement used consists of chopped strand mat with a soluble polyester powder binder or chopped rovings deposited directly into the resin film. However, for certain applications woven fabrics may be used. With the latter and to a much lesser extent with chopped strand mat, the glass cloth may be drawn through a resin bath and excess resin removed between doctor blades or rollers, before placing between two layers of release film and processing as before.

With high quality sheeting a surfacing tissue may be used to ensure a resin-rich finish. Such sheeting must be installed with the resin-rich surface exposed to the weather.

Resin systems are generally specifically formulated for each machine, since gel time and viscosity must suit the particular operating conditions of the machine. Resin systems used include those suitable for producing clear fire retardant sheeting.

By the correct choice of resin system, sheeting can be manufactured which will not yellow to any extent after exposure to tropical weather conditions for several years. However, to ensure that this is the case the resin system must be chosen with care and must be fully cured. Also the release film must be removed before installation and the laminate should contain not less than 75 % by weight of resin. In other cases the resin content of the laminate may fall between 65 and 75 % by weight.

2.12.8 Pultrusion

Pultrusion is a technique used for producing continuous fibre reinforced sections in which the orientation of the fibres is kept constant during cure. The process is suitable for use with both polyester and epoxide resin systems, reinforced with glass, carbon or synthetic fibres. An infinite number of profiles can be produced using appropriate dies and includes rods, tubes and flat and angled sections. All profiles have high strength and stiffness in the lengthwise direction, with fibre content generally around 60–65 % by volume.

The reinforcements used consist of continuous fibres such as glass rovings or continuous carbon fibre tows, woven rovings or chopped strand mat or a combination of the two, depending on the strength and rigidity required in the molded profile.

Two processes are available which use liquid resin systems. In the first the reinforcement is drawn through an impregnating bath containing catalysed resin. For this process, a resin system with a long pot-life at room temperature is necessary. The reinforcement is then drawn through a heated die which removes excess resin, determines the cross-sectional shape and cures the resin system.

In the second process the reinforcement, accurately positioned and under tension, is drawn through a heated metal die where impregnation of the fibres and cure of the resin system takes place. Here, by the use of appropriate resin injection equipment, a short pot-life system can be used. Typical resin injection pressures are between 0.1 and 0.5 MPa. To speed up cure, the reinforcement may be pre-heated to about 100°C before passing through the die. Production rates of 1 m/min can be achieved. By careful design of the pulling mechanism, consistent profiles can be produced with no bending or twisting of the fibres. With some resin systems a tunnel oven may be required after the die to give a suitable post cure.

Apart from the wet processes it is also possible to make pultruded sections from prepregs. The forming procedure is the same as that used with wet resin systems. The prepreg is drawn through a heated die which melts the resin, compresses the prepreg into the required shape and cures the resin. This is a somewhat cleaner process than that using a resin bath.

It is reported that sandwich panels are being produced in the USA by pultrusion. In this process a plywood core is completely encased in a 3 mm thick glass polyester skin, resin penetrating the plywood during production to give increased bond strength and moisture resistance.

2.13 Mechanical Properties

A summary of the mechanical properties of the most important matrix materials and their composites with different reinforcing fibers are presented in Tables 2.8–2.39.

Table 2.8 Properties of a Typical Filled and Unfilled Polypropylene (1)

Properties	PP	PP 40% Talc	PP 40% CaCO ₃	PP 40% Glass	PP 30% Graphite
T _g °C	170	168	168		
Heat deflection temperature, 1.82 MPa °C	55	100	80	160	120
Maximum resistance to continuous heat °C	100	120	110	135	125
Coefficient of linear expansion cm/cm $\times 10^{-5}$ °C	9	6	4	3	3
Tensile strength, MPa	35	32	26	82	47
% Elongation	150	5	15	2	0.5
Flexural strength MPa	48	60	45	100	62
Compressive strength, MPa	45	52	35	64	55
Notched Izod impact J/m	42	27	42	90	56
Hardness Rockwell	R90	R100	R88	R105	R100
Specific gravity	0.90	1.25	1.23	1.22	1.04

Table 2.9 Properties of a Typical PEEK Resin (1)

Properties	PEEK	PEEK 30% Glass	PEEK 30% Graphite
T _g °C	334	334	334
Heat deflection temperature, 1.82 MPa °C	165	282	282
Maximum resistance to continuous heat °C	150	270	270
Coefficient of linear expansion cm/cm $\times 10^{-5}$ °C	5.5	2.1	1.5
Tensile strength, MPa	100	162	173
% Elongation	40	2	2
Flexural strength MPa	110	255	313
Notched Izod impact J/m	150	110	70
Hardness Rockwell	R123	R123	R123
Specific gravity	1.32	1.44	1.32

Table 2.10 Properties of a Typical Polyetherimide Resins (1)

Properties	PEI	PEI 10% Glass	PEI 20% Glass	PEI 30% Glass	PEI 30% Graphite
T _g °C	216	216	216	216	216
Heat deflection temperature, 1.82 MPa °C	195	200	205	210	210
Maximum resistance to continuous heat °C	165	170	175	180	180
Coefficient of linear expansion cm/cm×10 ⁻⁵ °C	5	4	3	2	2
Tensile strength MPa	105	114	138	169	216
% Elongation	7	5	4	3	2
Flexural strength MPa	144	193	205	225	283
Compressive strength MPa	140	155	162	175	220
Notched Izod impact J/m	55	60	85	110	75
Hardness Rockwell	M110	M116	M120	M125	M127
Specific gravity	1.3	1.35	1.45	1.5	1.4

Table 2.11 Properties of Typical Polycarbonate Sheets (1)

Properties	PC	PC 10% Glass	PC 30% Glass	PC 40% Glass	PC 40% Graphite	Polyester Carbonate
T °C g	150	150	150	150	150	160
Heat deflection temperature, 1.82 MPa °C	139	142	144	144	146	150
Maximum resistance to continuous heat °C	125	130	130	130	130	135
Coefficient of linear expansion cm/cm×10 ⁻⁵ °C	7	2	1	1	1	8
Tensile strength MPa	65	65	135	165	165	73
% Elongation	110	6	3	3	2	90
Flexural strength MPa	93	105	155	93	240	240
Notched Izod impact J/m	130	110	90	100	90	300
Hardness Rockwell	M70	M75	M92	R118	R119	M85
Specific gravity	1.2	1.28	1.4	1.35	1.35	1.2

Table 2.12 Properties of Polyphenylene Sulfide Resins (1)

Properties	PPS	PPS 40% Glass	PPS 40% Graphite
T _g °C	290	290	280
Heat deflection temperature, 1.82 MPa °C	133	260	260
Maximum resistance to continuous heat °C	120	240	240
Coefficient of linear expansion cm/cm×10 ⁻⁵ °C	5	2	1
Tensile strength MPa	65	135	160
% Elongation	2	2	1.5
Flexural strength MPa	95	185	210
Compressive strength MPa	95	160	180
Notched Izod impact J/m	25	80	55
Hardness Rockwell	R123	R123	R123
Specific gravity	1.3	1.65	1.45

Table 2.13 Properties of a Typical Polyarylate (1)

Heat deflection temperature, 1.82 MPa °C	174
Maximum resistance to continuous heat °C	150
Coefficient of linear expansion cm/cm×10 ⁻⁵ °C	6.5
Tensile strength MPa	68
% Elongation	50
Flexural strength MPa	74
Compressive strength MPa	93
Notched Izod impact J/m	210
Hardness Rockwell	R125
Specific gravity	1.2

Table 2.14 Properties of Typical Polyamide-Imide Plastics (1)

Properties	PA	PAI 30 % Glass	PAI 30 % Graphite
T _g °C	275	275	275
Heat deflection temperature, 1.82 MPa °C	275	275	275
Maximum resistance to continuous heat °C	260	260	260
Coefficient of linear expansion cm/cm×10 ⁻⁵ °C	3.6	1.8	2.0
Tensile strength MPa	150	195	205
% Elongation	13	6	6
Flexural strength MPa	200	315	315
Compressive strength MPa	258	300	300
Notched Izod impact J/m	135	105	45
Hardness Rockwell	E78	E94	E94
Specific gravity	1.39	1.57	1.41

Table 2.15 Properties of Typical Polysulfones (1)

Properties	Polysulfone (Udel) Gloss	Polysulfone 30 % Graphite	Polysulfone 30 %	Polyether Sulfone (Victrex)	PES 20 % Glass	PES 20 % Graphite	Modified Polysulfone	Modified Polysulfone 30 % Glass
Heat deflection temperature, 1.82 MPa °C	190	198	190	200	210	210	150	150
Maximum resistance to continuous heat °C	170	175	175	185	200	200	150	150
Coefficient of linear expansion $\text{cm/cm} \cdot 10^{-5}$ °C	6	2.5	2.5	5.5	2	1	4	5
Tensile strength MPa	70	100	100	138	127	190	43	115
% Elongation	5	115	115	85	2	115	50	2
Flexural strength MPa	106	200	215	120	175	250	85	175
Compressive strength MPa	176	95	175	95	150	150	125	150
Notched Izod impact J/m	64	58	64	110	75	75	150	75
Hardness Rockwell	M69	M95	M80	M88	M98	R123	R117	M80
Specific gravity	1.25	1.5	1.36	1.4	1.5	1.5	1.35	1.5

Table 2.16 Properties of typical Nylons (1)

Properties	Nylon 6	Nylon-6 30 % glass	Nylon-6 30 % graphite	Nylon 66	Nylon 66 30 % glass	Nylon 66 30 % graphite	Nylon 66 40 % clay	Nylon 66 50 % mica
T _g °C	226	215	215	265	265	265	265	215
Heat deflection temperature, 1.82 MPa °C	78	210	215	75	250	260	190	230
Maximum resistance to continuous heat °C	65	190	205	100	225	240	150	170
Coefficient of linear expansion cm/cm x 10 ⁻⁵ °C	8	4	5	8	2	2	3	3
Tensile strength MPa	62	138	205	82	180	227	75	90
% Elongation	30	5	3	60	4	3	9	9
Flexural strength MPa	96	150	135	103	180	170	160	150
Compressive strength MPa	55	130	155	55	110	88	50	85
Notched Izod impact J/m	R119	M85	M80	M85	M85	R120	M80	M80
Hardness Rockwell	1.13	1.38	1.28	1.14	1.37	1.35	1.4	1.4
Specific gravity	96	275	315	103	275	330	205	400

Table 2.17 Properties of typical Nylons (1)

Properties	Nylon 69	Nylon 6-10	Nylon 6-12	Nylon 6-12 35 % Glass	Nylon 11	Nylon 12	Aramid
T _g °C	205	220	210	210	192	177	275
Heat deflection temperature, 1.82 MPa °C	55	60	69	216	150	146	260
Maximum resistance to continuous heat °C	60	70	75	200	140	135	150
Coefficient of linear expansion cm/cm x 10 ⁻⁵ °C	8	8	8	6	10	8	3
Tensile strength MPa	58	60	50	145	55	55	120
% Elongation	80	125	200	4	200	225	5
Flexural strength MPa	40	40	44	80	40	42	172
Compressive strength MPa	100	90	90	150	80	80	207
Notched Izod impact J/m	60	60	60	96	96	110	75
Hardness Rockwell	R111	R105	M78	M93	R108	R105	E90
Specific gravity	1.09	1.08	1.08	1.35	1.04	1.01	1.2

Table 2.18 Typical properties of Discontinuous Graphite-Fiber-Reinforced Thermoplastic Composites (8)

Property	Nylon 66 30 %	Polysulfone 30 %	Polyester 30%	Polyphenilene sulfide 30%C	ETFE 30 % C
Specific gravity	1.28	1.32	1.47	1.45	1.73
Water absorption (24 hr), %	0.5	0.15	0.04	0.004	0.015
Equilibrium, %	2.4	0.38	0.23	0.1	0.24
Mold shrinkage, %	1.5–2.5	2–3	1–2	1	1.5–2.5
Tensile strength, ksi (MPa)	35 (241)	19 (131)	20 (138)	27 (186)	15 (103)
Tensile elongation, %	3–4	2–3	2–3	2–3	2–3
Flexural strength, ksi (MPa)	51 (351)	25.5 (176)	29 (200)	34 (234)	20 (138)
Flexural modulus of elasticity, Msi (GPa)	2.9 (20)	2.05 (14.1)	2.0 (13.8)	2.45 (16.9)	1.65 (11.4)
Shear strength ft-lb/in (<i>J/m</i>)	13 (89.6)	7 (48.1)	–	–	7 (48.2)
Izod impact strength ft-lb/in (<i>J/m</i>)	1.5 (80.1)	1.1 (58.7)	1.2 (64.1)	1.1 (58.7)	4–5 213–267)
Thermal deflection temperature at 264 psi (1.82 MPa), °F	495 (257)	365 (185)	430 (221)	500 (260)	465 (241)
Coefficient of linear thermal expansion, in./in., °F×10 ⁻⁵ (m/m/°C×10 ⁻⁵)	1.05 (1.89)	0.7 (1.26)	0.5 (0.9)	0.6 (1.08)	0.8 (1.44)
Thermal conductivity, BTU-in/hr ft ² °F (<i>W/m°C</i>)	7.0 (12.1)	5.5 (9.5)	6.5 (11.2)	5.2 (9.0)	5.6 (9.7)
Surface resistivity, Ω/m ²	3–5	1–3	2–4	1–3	3–5

Table 2.19 Typical properties of Discontinuous Graphite-Fiber-Reinforced Thermoplastic Composites (8)

Property	Polypropilene 30% C	Polycarbonate 30% C	VF2-TFE 20% C
Specific gravity	1.06	1.36	1.77
Water absorption (24 hr), %	—	—	0.03
Equilibrium, %	—	—	—
Mold shrinkage, %	5	2	2.5–3.5
Tensile strength, ksi (MPa)	5.4 (37.2)	11.5 (79.2)	12.3 (84.7)
Tensile elongation, %	2.2	2.1	3–4
Flexural strength, ksi (MPa)	6.7 (46.2)	17.1 (118)	17.2 (119)
Flexural modulus of elasticity, Msi (GPa)	0.60 (4.1)	1.08 (7.44)	1.10 (7.58)
Shear strength ft-lb/in (<i>J/m</i>)	—	—	7.5 (51.7)
Izod impact strength ft-lb/in (<i>J/m</i>)	0.7 (37.4)	3.0 (160.2)	2.6 (138.8)
Thermal deflection temperature at 264 psi 1.82 MPa), °F	295 (146)	293 (145)	248 (120)
Coefficient of linear thermal expansion, in./in., °F×10 ⁻⁵ (m/m/°C×10 ⁻⁵)	3.0 (5.4)	1.6 (2.8)	1.6 (2.8)
Thermal conductivity, BTU-in/hr ft ² °F (<i>W/m°C</i>)	3.0 (5.7)	—	—
Surface resistivity, Ω/m ²	3–5	—	—

Table 2.20 Properties of a Typical Styrene Polymer (1)

Properties	PS	PS 30% Glass
Heat deflection temperature, 1.82 MPa °C	90	105
Maximum resistance to continuous heat °C	75	95
Coefficient of linear expansion cm/cm×10 ⁻⁵ °C	7.5	4.0
Tensile strength MPa	41	82
% Elongation	1.5	1.0
Flexural strength MPa	83	117
Compressive strength MPa	90	103
Notched Izod impact J/m	21	20
Hardness Rockwell	M65	M70
Specific gravity	1.04	1.2

Table 2.21 Properties of Typical Polyester Resins (1)

Properties	PET	PET 30% Glass	PET 45% Glass	PET 30% Glass	PBT	PBT 30% Glass	PBT 45% Glass	PBT 30% Glass
T _g °C	255		255	255	245	245	245	245
Heat deflection temperature, 1.82 MPa °C	220		225	225	85	210	210	215
Maximum resistance to continuous heat °C	200		210	210	80	200	200	205
Coefficient of linear expansion cm/cm×10 ⁻⁵ °C	6.5		2	3	6	2.5	2	3
Tensile strength MPa	58		165	175	50	220	90	155
% Elongation	100		3	115	100	3	3	2
Flexural strength MPa	110		175	260	100	175	140	215
Compressive strength MPa	90		155	105	98	145	105	100
Notched Izod impact J/m	35		75	75	40	50	50	70
Hardness Rockwell	M97		R118	R125	M72	M90	M80	R120
Specific gravity	1.35		1.6	1.4	1.34	1.5	1.7	1.41

Table 2.22 Properties of Typical Polyimides (1)

Properties	PI	PI 40 % graphite
T_g °C	330	365
Heat deflection temperature, 1.82 MPa °C	315	360
Maximum resistance to continuous heat °C	290	810
Coefficient of linear expansion cm/cm $\times 10^{-5}$ °C	5	4
Tensile strength MPa	96	44
% Elongation	9	3
Flexural strength MPa	165	145
Compressive strength MPa	240	125
Notched Izod impact J/m	83	38
Hardness Rockwell	E70	E27
Specific gravity	1.4	1.65

Table 2.23 Properties of DAP (1)

Properties	DAP	Fiber glass filled	Mineral filled
Heat deflection temperature, 1.82 MPa °C	155	225	200
Maximum resistance to continuous heat °C	100	210	200
Coefficient of linear expansion cm/cm $\times 10^{-5}$ °C	—	3	3.5
Tensile strength MPa	27.6	50	45
% Elongation	4.6	4	4
Flexural strength MPa	62.0	90	65
Compressive strength MPa	150	205	170
Notched Izod impact J/m	14	50	16
Hardness Rockwell	E115	E84	E61
Specific gravity	11.3	1.80	1.75

Table 2.24 Properties Of Typical Amino Plastics (1)

Properties	Cellulose-filled UF	Fberglass-filled MF
Heat deflection temperature, 1.82 MPa °C	175	200
Maximum resistance to continuous heat °C	100	175
Coefficient of linear expansion cm/cm $\times 10^{-5}$ °C	4.0	1.6
Tensile strength MPa	65	50
% Elongation	0.7	0.7
Flexural strength MPa	90	130
Compressive strength MPa	275	310
Notched Izod impact J/m	16	100
Hardness Rockwell	M120	M120
Specific gravity	1.50	1.9

Table 2.25 Properties of fiberglass Composites with Different Thermosets (1)

Properties	Diallyl phthalate	Epoxy	Phenolic	Polyester	Polyamide
Heat deflection temperature 1.8 MPa °C	225	150	200	200	350
Maximum continuous use temperature °C	210	140	175	160	310
Coefficient of linear expansion cm/cm $\times 10^{-5}$ °C	3	2	2	2.5	1.3
Tensile strength, MPa	50	83	41	70	44
% Elongation	4	4	1.5	1	1
Flexural strength, MPa	90	103	172	172	145
Compressive strength, MPa	205	100	200	200	300
Notched Izod impact J/m	50	25	175	200	300
Hardness Rockwell	E84	M105	M110	M50	M118
Specific gravity	1.8	1.9	1.5	2	1.6

Table 2.26 Properties of the Most Common Resin for High Performance Composites

Materials	Tensile strength (MPa)	Flexural modulus (MPa)	Density (gcm ⁻³)	Max service temperature (°C)	Coefficient of thermal expansion (10 ⁻⁵⁰ °C ⁻¹)	Water absorption (24 h%)
Epoxy	35–85	15–35	1.38	25–85	8–12	0.1
Polyimide	120	35	1.46	380	9	0.3
PEEK	92	40	1.30	140	6–9	0.1
Polyamide/imide	95	50	1.38	200	6.3	0.3
Polyether/imide	105	35	1.27	200	5.6	0.25
Polyphenylene/sulfide	70	40	1.32	75	9.9	0.2
Phenolics	50–55	10–24	1.30	50–175	4.5–11	0.1–0.2

Table 2.27 Properties of Polyester Composites Reinforced by Continuous and Chopped Fiberglass

Continuous Filament (%)	Chopped Glass (%)	Tensile Strength MPa	Flexural Strength MPa	Transverse Tensile Strength MPa	Transverse Flexural Strength MPa
75	0	690	1200	24	35
65	10	660	1135	27	90
45	20	570	980	60	155
25	20	500	810	95	200
15	60	410	680	125	260

Table 2.28 Typical properties of cured polyester resins

Resin	Cast resin properties				Laminate properties					
	Flexural strength (MPa)	Tensile strength (GPa)	Tensile Modulus (GPa)	% Elongation	HDT(°C)	% glass	Flexural Strength(MPa)	Tensile Strength(MPa)	Tensile modulus(GPa)	
Orthophthalic	100	65-75	3.2	2.0-4.0	55-110	30	150	90	7	
Isophthalic	140	70-75	3.5	3.5	75-130	30	230	120	8	
Neo-pentylglycol	130	70	3.4	2.4	110	30	170	90	7	
Isophthalic/ neopentylglycol	130	60	3.4	2.5	90-115	30	160	90	7	
HET acid	80	40-50	3.2	1.3-4.0	55-80	30	150	85	7	
Isophthalic/HET acid	85	55	3.2	2.9	70	30	150	90	7	
Bisphenol A	130	60-75	3.2	2.5-4.0	120-136	30	170	90	7	
Chlorinated paraffin	110	50-60	3.4	1.2-4.8	55-80	30	140	90	7	
Isophthalic/ chlorinated paraffin	90	60	2.0	4.8	50	30	140	100	7	

Table 2.29 Characteristics of Epoxy resins (8)

Resin	Description	Characteristics and end uses
Epocryl® Resin 12	A neat dimethacrylate ester of a low-molecular weight bisphenol A epoxy resin	Nominal 1 000 000 cp (1 kPa sec) viscosity designed for molding, adhesives, and electrical prepreg
Epocryl® Resin 370	A neat diacrylate ester of a low-molecular-weight bisphenol A epoxy resin	Base resin for formulation of UV-cure inks and coating
CoRezyn VE-8100 Derakane® 411-C-50 Epocryl® Resin 321	A dimethacrylate ester of an intermediate-molecular-weight bisphenol A epoxy resin containing 50 wt% styrene	Nominal 100 cP (5 dPa sec) viscosity designed for chemical-resistant FRP applications: hand lay-up and filament winding
Corrolite 31–345 CoRezyn VE-8300 Derakane® 411–45 Epocryl® Resin	A dimethacrylate ester of a high-molecular-weight bisphenol A epoxy resin containing 45 wt% styrene	Nominal 500 cP (5 dPa sec) viscosity designed for Chemical-resistant FRP applications: hand lay-up and filament winding
Derakane® 470–36	A methacrylate ester of a phenolicnovolac epoxy resin containing 36 wt% styrene	Nominal 200 cP (2 dPa sec) viscosity designed for solvent resistance and high-service-temperature FRP applications
Epocryl® Resin	A methacrylate ester of a low-molecular-weight bisphenol A epoxy resin containing 40 wt % styrene	Nominal 500 cP (5 dPa sec) viscosity designed for solvent resistance and high-service-temperature FRP applications. Exhibits high tensile strengths and elongation with high modulus. Designed for filament winding and hand lay-up applications
Derakane® 510A40	A dimethacrylate ester of a brominated bisphenol A epoxy resin containing 40 wt% styrene	Nominal 350 cP (3.5 dPa sec) viscosity designed to impart fire retardancy for chemical-resistant FRP applications

Table 2.30 Shear Properties of Composites of Kevlar 49 Fiber in Epoxy Resins (8)

Epoxy System (weight ratio)	Cure Cycle hours/°C (hours/°F)	Shear Failure Stress MPa (CV)	Shear Strain at Failure Stress % (CV)	Secant Shear Modulus at 0.5% Shear Strain MPa (CV)
XD 7818/ERL	2.5/80 + 2/160	21.4 (2.6)	1.35 (2.2)	1884 (3.9)
4206/Tonox 60–40	(2.5/176 + 2/320)			
DER 332/ Jeffamine	24/60	29.4 (2.0)	173 (2.3)	1923 (4.7)
T-403 (100/39)	(24/140)			
ERL 2256/Tonox	16/50 + 2/120	23.0 (8.6)	1.49 (2.2)	1775 (0.9)
60–40 (100/25/28.3)	(16/122 + 2/248)			
Epon 826/RD2/	3/60 + 2/120	23.4 (6.3)	1.91 (6.5)	1520 (3.9)
Tonox 60–40	(3/140 + 2/248)			
(100/25/28.3)				
XB 2793/Tonox	2/90 + 2/160	21.9 (0.3)	1.69 (2.9)	1600
60–40 (100/25.6)	(2/194 + 2.320)			

(continued)

Table 2.30 (continued)

Epoxy System (weight ratio)	Cure Cycle hours/°C (hours/°F)	Shear Failure Stress MPa (CV)	Shear Strain at Failure Stress % (CV)	Secant Shear Modulus at 0.5% Shear Strain MPa (CV)
XD 7818/XD	5/80 + 3/120	39.7 (0.9)	2.43 (2.5)	1852 (1.7)
7575.02/XD	(5/176 + 3/248)			
7114/Tonox 60/DAP (50/50/45/14.1/14.1)				
XD 7818/XD	5/60 + 3/120	31.9 (3.4)	1.91 (4.5)	1850 (1.5)
7114/Tonox LC (100/45/50.3)				

Table 2.31 Properties of a typical PMMA Sheet* (1)

Heat deflection temperature at 1.8 MPa (°C)	96
Maximum resistance to continuous heat (°C)	90
Coefficient of linear expansion cm/cm/°C x 10 ⁻⁵	7.6
Tensile strength (MPa)	72
Percent elongation	5
Flexural strength (MPa)	110
Compressive strength (MPa)	124
Notched Izod impact(J/m)	74
Hardness Rockwell	M93
Specific gravity	1.19

*Polymethyl methacrylate (PMMA) is largely used for bio-medical applications, optical fibers and cultured marble.

Table 2.32 Properties of Typical Polyfluorocarbons (1)

Properties	PFTE	PCTFE	PVDF	PVF
Heat deflection temperature 1.8 MPa (°C)	100	100	80	90
Maximum resistance to continuous heat (°C)	250	200	150	125
Coefficient of linear expansion cm/cm °C x 10 ⁻⁵	10	14	8.5	10
Tensile strength, MPa	24	34	55	65
Flexural strength MPa	50	60	75	90
Notched Izod impact J/m	160	100	150	100
% Elongation	200	100	200	200
Hardness, Rockwell	D52	R80	R110	R83
Specific gravity	2.16	2.1	1.76	1.4

Table 2.33 Properties of typical Filled PTFE (1)

Properties	Unfilled PTFE	15% Glass	25% Glass	15% Graphite	60% Bronze
Thermal conductivity mW/MK	0.244	0.37	0.45	0.45	0.46
Tensile strength MPa	28	25	17.5	21	14
% Elongation	350	300	250	250	150
Notched Izod impact J/m	152	146	119	100	75
Coefficient of friction, 3.4 MPa load	0.08	0.13	0.13	0.10	0.10
Wear factor 1/pPa	5013	280	26	102	12
Shore durometer hardness	51D	54D	57D	61D	70D
Specific gravity	2.18	2.21	2.24	2.16	3.74

Table 2.34 Properties of Typical LDPE Plastics (1)

Glass transition temperature (°C)	-25
Coefficient of linear expansion cm/cm°Cx10 ⁻⁵	15
Tensile strength MPa	20
%Elongation	350
Shore hardness	47D
Specific gravity	0.925

Table 2.35 Properties of a typical Filled and Unfilled HDPE (1)

Properties	HDPE	30% Glass-Filled HDPE
Melting point (°C)	130	140
Heat deflection temp. at 1.82 MPa (°C)	40	120
Maximum resistance to continuous heat (°C)	40	110
Coefficient of linear expansion cm/cm°Cx10 ⁻⁵	10	5
Tensile strength MPa	27	62
% Elongation	100	1.5
Flexural strength MPa	—	76
Compressive strength MPa	21	43
Notched Izod impact J/m	133	64
Hardness Rockwell	D40	R75
Specific gravity	0.95	1.3

Table 2.36 Thermal and Electrical Properties of Kevlar 49 Fabric/Epoxy Composites (8)

Property	Value
Thermal conductivity (46 volume % fiber)	
Across fabric layers, W/m °K	0.22
Parallel to warp, W/m °K	0.91
Thermal coefficient of expansion (20–100°C)	0
Dielectric constant (58 volume % fiber)	
Perpendicular at 9.3x10 ⁹ Hz (room temperature)	3.3
Parallel at 9.3x10 ⁹ Hz (room temperature)	3.7
Perpendicular (48 volume % fiber) at 10 ⁶ Hz	4.1
Dielectric strength (48 volume % fiber), V/mm (V/mil)	24.4
Volume resistivity (48 volume % fiber), 1/2 -cm	5x10 ¹⁵
Surface resistivity (48 volume % fiber), 1/2 cm	5x10 ¹⁵
Arc resistance (48 volume % fiber), seconds	125

Table 2.37 Property of Unidirectional Thornel 300-Kevlar 49/Epoxy Hybrid Composites (8)

Ratio Thornel to Kevlar	Specific gravity	Tension		Compression				Flexure			Short- beam shear stress	Short- beam shear stress			
		Modulus GPa	Modulus (Msi)	Ultimate stress MPa	Ultimate stress (ksi)	Stress at 0.02% offset (ksi)	Stress at 0.02% offset MPa	Ultimate stress (ksi)	Ultimate stress sMPa	Stress at 0.02% offset (ksi)					
100/0	1.60	145	(21.1)	1565	(227)	678	(98.4)	1007	(146)	1605	(223)	1606	(233)	91	(13.2)*
75/25	1.56	120	(17.4)	1281	(186)	469	(68.8)	938	(136)	1248	(181)	1358	(197)	76	(11.0)
50/50	1.51	108	(15.7)	1213	(176)	413	(59.9)	688	(99.8)	827	(120)	1103	(160)	56	(8.1)
0/100	1.35	77	(11.2)	1262	(183)	182	(26.4)	286	(41.5)	339	(49.2)	634	(91.9)	49	(7.1)

Table 2.38 Properties of Epoxy Resin Composites with Different Reinforcing Fibers

Properties	E-Glass	S-Glass	Aramid Kevlar 49	Graphit	Boron
Thermal conductivity W/mK	0.9	1.1	0.9	5	1
Linear expansion cm/cm°C×10 ⁻⁵	1.2	1.1	1	2	1
Tensile strength MPa	450	700	800	700	1600
Elastic modulus MPa	24 000	30 000	33 000	60 000	207 000
Fracture toughness MPa m ^{1/2}	22	25	34	18	35
Specific gravity	2.1	2.0	1.4	1.6	2.1

Table 2.39 Properties of Fiberglass-reinforced Polyester Composites with Different Fabrication Techniques (1)

Properties	SMC	BMC	Preform mat	Cold-molding	Spray-press up	Filament wound (epoxy)	Pultruded
Glass content %	22	25	30	25	40	55	60
Heat deflection temp.	225	225	205	190	190	190	175
Maximum resistance to continuous heat °C	180	175	185	180	185	150	200
Coefficient of linear expansion °C×10 ⁻⁵	1.0	1.0	1.4	1.4	1.6	4	5
Tensile strength KPa	90	48	110	110	95	120	80
% Elongation	1	0.5	1.5	1.5	1.0	2.0	2.0
Flexural strength KPa	165	100	220	190	150	1250	1000
Compressive strength MPa	80	30	150	125	135	400	340
Notched Izod impact J/m	640	240	800	560	425	2660	2750
Hardness Rockwell	H75	H95	H70	H70	H70	M110	H96
Specific gravity	1.9	1.9	1.9	1.6	1.5	1.9	1.8

2.14 Antioxidants and Effect of Environmental Exposure

Many of the polymeric matrices will require some type of antioxidants to improve aging properties. The most common primary antioxidants are hindered phenols such as butylated hydroxytoluene (BHT). Typical low toxic antioxidants are reported in Tables 2.40–2.42.

The toxicity of commonly used polymer stabilizers and additives are classified in the following table.

Table 2.40 Typical antioxidants of low toxicity (3)

Primary antioxidants (usually hindered phenols)	Butylated hydroxy toluene (BHT)
Thioester antioxidants (usually derivatives of thiodipropionic acid)	Dilaryl thiodipropionate (DLTDP) Distearyl thiodipropionate (DSTDP)
Phosphite antioxidants (usually derivatives of aromatic phosphites)	Distearyl pentaerythritol diphosphite Tris (nonylphenyl) phosphite

Table 2.41 Toxicity of commonly used polymer stabilizers and additives (3)

Stabilizer	Toxicity
Fatty acid derivatives of calcium, zinc and magnesium	Low toxicity. Used in non-toxic medical applications
Barium fatty acid compounds	Moderately toxic
Lead & cadmium derivatives	Highly toxic. Not recommended in the US for use in medical applications (cadmium pigments considered of low toxicity in England)
Amines (antioxidants)	Generally toxic, with aromatic amines showing carcinogenic tendencies. Newer types less toxic
Butylated hydroxy toluene (BHT) (antioxidant)	Considered non-toxic as also used in foods. Recently investigated and found non-carcinogenic
Octyl tin compounds	Only class of tin compound classified as of low toxicity and used in medical applications e.g. di-(n-octyl)tin maleate polymer

Table 2.42 Toxicity data on some common plasticizers used in plastic manufacture (3)

Plasticizer	Toxicity
Adipates	To date animal experiments indicate possible carcinogenicity
Glycolates	Generally of low toxicity levels. However studies underway as commercial form are phthalyl derivatives
Phosphates	Generally cause irritation to skin and mucous membranes
Phthalates	Although commercially used in medical devices, environmental effects and toxicological properties continually under investigation
Epoxidized soya bean oil	Chelating type of plasticizer with low toxicity

2.15 The Radiation Stability of Commercial Materials

The radiation resistance of common polymeric materials used as matrix for composite are shown in Tables 2.43–2.52. Generally, polystyrene and urethane rubber have the most resistance.

Table 2.43 The radiation resistance of common materials used as matrix of polymeric composites (3)

Material	Stability effect
ABS	Stable for single dose of 2.5 Mrad
Polyamides	Suitable for single doses of 2.5 Mrad level
Polyethylene	Stable under ordinary conditions at 2.5 Mrad
Polypropylene	Embrittles – newer variations more resistant
Poly(vinyl chloride)	Withstands single dose radiation cycle – but discolors – some HCl liberated
Polystyrene	Most radiation – stable of common polymers
Poly(tetrafluoroethylene)	Poor resistance to radiation – copolymers less affected
Polysulfone	Stable under ordinary conditions at 2.5 Mrad
Polyacetals	Embrittles – discolors
Polyurethane	Stable under ordinary conditions at 2.5 Mrad
Polymethylmethacrylate	Embrittles – discolors
Rubber natural	Stable under ordinary conditions when properly compounded
Rubber butyl	Poor stability at low radiation levels
Rubber silicones	Stable under ordinary conditions at 2.5 Mrad
Urethanes	Excellent radiation resistance

Table 2.44 The radiation resistance of common materials used as matrix of polymeric composites (3)

Material Thermoplastics	Stability	
Acrylonitrile/Butadiene/Styrene(ABS)	Good	
Cellulosics esters more stable	Fair	Undergoes chain scission,
Fluoinated ethylene propylene (FEP)	Fair	Copolymers more resistant than Homopolymer
Polyacetal	Poor	Embrittles
Polyamides aromatic	Excellent	
Polyamides aliphatic	Fair	Hardens as levels increased
Polycarbonates	Good	Yellow – mechanical properties unchanged
Polyesters (aromatic)	Good	
Polyethylene	Good	lowers melt flow
Polymethylmethacrylate	Poor	Degrades-turns brown
Polyphenylene sulfide	Good	
Polypropylene	Fair	Improved stability if properly stabilized
Polysulfone	Excellent	Yellow natural color
Polystyrene	Excellent	
Polytetrafluoroethylene	Poor	Acid evolved
Polyvinylchloride homopolymer	Good	If properly stabilized
Polyvinylchloride Copolymer	Fair	HCl evolved – turns brown
Styrene/ Acrylonitrile (SAN)	Good	More resistant than ABS

Table 2.45 The radiation resistance of common materials used as matrix of polymeric composites (3)

Material	Thermosetting resin	Stability
Epoxies		Excellent
Phenol or urea formaldehyde		Good
Polyimides		Excellent
Polyesters		Good
Polyurethanes		Excellent

Table 2.46 The radiation resistance of common materials used as matrix of polymeric composites (3)

Material elastomers	Stability
Polyisobutylene (butyl)	Poor
Natural	Good
Urethanes	Excellent
Nitrile	Good
Polyacrylic	Poor
Styrene-butadiene	Good
EPDM	Good
Silicones	Good

Table 2.47 The radiation resistance of polymers (3)

Textiles	Stability
Polyesters	Excellent
Cellulosics	Poor
Nylon	Fair

Table 2.48 Synergism between a UV absorber and a thermal antioxidant (6)

Additive (0.4 pph) UV stabilizer	Antioxidant	Time to embrittlement of low-density polyethylene (in hours)
None	None	400
Octylphenyl salicylate	None	1600
None	Tri (nonylphenyl) phosphite	1800
Octylphenyl salicylate	Tri (nonylphenyl) phosphite	7000
2-Hydroxy-4-n-octoxybenzophenone	None	2000
None	Tri (nonylphenyl) phosphite	1000
2-Hydroxy-4-n-octoxybenzophenone	Tri(nonylphenyl) phosphite	8500

Table 2.49 Stability of hydrocarbon polymers with bound phenolic antioxidants (6)

Material	Hours to react with 10 cc of O ₂ at 140°C
Low-density polyethylene:	
Uninhibited	3
Reacted with diazooxide	14
High-density Polyethylene:	
Commercially stabilized	175
Reacted with diazooxide	411
Polypropylene	
Uninhibited	<1
Reacted with diazooxide	31

Table 2.50 Additives incorporated into natural rubber and as bound antioxidants (6)

Additive	Hours to absorb 1 % by wt. of O ₂	
	Before extraction	After extraction
N,N'-Diethyl-p-nitrosoaniline	39	30
p-Nitrosodiphenylaniline	60	53
p-Nitrosophenol	31	30
2,6-Diter-butyl-p-cresol	47	4

Table 2.51 Summary of effects of moisture and ambient aging on epoxy composites (7)

Flexural strength, MN/m ² (ksi)										
Orient	Temperature K(°F)	Control	24-h H ₂ O boil	Retention %	6-week humidity	Retention	20-week ambient	Retention %	52-week ambient	Retention %
B/5505 boron/epoxy										
[0]	297 (75)	2070 (300)	1950 (283)	94	2120 (308)	103	2180 (316)	105	2280 (330)	110
[0]	450 (350)	1730 (251)	393 (57)	23	683 (99)	39	1030 (149)	59	910 (132)	53
[0±45]	450 (350)	862 (125)	545 (79)	63	641 (93)	74	882 (128)	102	807 (117)	94
A-S/3501 graphite/epoxy										
[0]	297 (75)	1680 (244)	1680 (244)	100	1680 (244)	100	1850 (268)	110	1620 (235)	96
[0]	450 (350)	1300 (188)	434 (244)	34	386 (56)	30	703 (102)	54	593 (86)	46
[0±45]	450 (350)	676 (98)	365 (53)	54	276 (40)	41	545 (79)	81	386 (56)	57

Table 2.52 Summary of thermal aging of epoxy and polyimide system (7)

Material system	Orientation	Aging temperature K(°F)	Test temperature K(°F)	Aging time, h	Retention of tensile strength, %
B/E	[O]	394 (250)	450 (350)	1000	99
	[CP]				94
	[O]	450 (350)	450 (350)	1000	100
	[CP]				100
G/E	[O]	394 (250)	450 (350)	1000	94
	[CP]				100
	[O]	450 (350)	450 (350)	1000	100
	[CP]				100
G/PI	[O]	505 (450)	505 (450)	1000	98
	[CP]				92
	[O]	561 (550)	561 (550)	1000	87
	[CP]				100

2.16 Polymers Aging

2.17 Composite Materials in Medicine

In recent years, carbon fiber has been recognized as a material with many exciting applications in medicine. Several commercial products utilize carbon fiber as a reinforcing material which serves to enhance the mechanical properties of the polymeric resin systems in which it is included. The attractive feature of carbon reinforced polymer for this application is that the orientation and fiber content can be varied in the implant to provide the mechanical property orientation necessary for good function. The carbon fiber can be distributed in matrix material to provide strength in only those locations and directions where it is needed. The implant must be designed in a way that fatigue failure does not occur and the matrix material is not attacked by the physiological environment. The matrix materials used are listed in Table 2.53.

These polymers were combined with unsized carbon fiber, into $\pm 15^\circ$ laminated, test specimens approximately 2.5 cm \times 7.5 cm \times 0.3 cm. Testing was performed in three point bending giving the results in Table 2.55.

Because a composite hip will be subjected to the physiological environment in use, an accelerated test was performed to evaluate changes in properties. In this test, the samples were immersed in 0.9 % saline solution maintained at 90°C for one week; the results are shown in Table 2.56.

Blood compatible materials are essential to circulatory support devices. Numerous materials have been considered for use in prosthetic devices.

Table 2.53 Polymeric materials used as matrix for carbon fibers composites (3)

Polymer	Polymer type	Commercial name and manufacturer
Polysulfone	Thermoplastic	UDEL MG-11, Union Carbide, Dallas, TX
Poly-methyl methacrylate	Thermoplastic	PMMA I.V. 0.4, Rohm & Haas, Philadelphia, P A
Epoxy (low viscosity)	Thermoset	Stycast 1267
Epoxy (high viscosity)	Thermoset	C-8W795 & H.R. 795, Hysol Corp., Los Angeles, CA

Table 2.54 Mechanical properties of carbon fibers used in carbon prosthesis

Fibre-type	Density (g/cm ³)	Diameter (µm)	Tensile strength (MPa)	Elastic modulus (GPa)	Strain to failure (%)	$\alpha/(10^{-6} K)$
T300	1.75	7	3430	230	1.5	-1.5
HM 35	1.79	6.7	2350	358	0.6	-0.5

Table 2.55 Typical Mechanical Properties of Polymer-Carbon Composites (3)

Polymer	Ultimate strength (MPa)	Modulus (GPa)
PMMA	772	55
Polysulfone	938	76
Epoxy Stycast	535	30
Epoxy Hysol	207	24

Table 2.56 Accelerated Test Data (3)

Matrix	Strength (MPa)		Modulus (GPa)	
	Before	After	Before	After
Polysulfone	807	723	77	67
PMMA	687	594	76	73
Epoxy (Stycast)	535	323	30	21

2.17.1 Carbons In Heart Valve Prostheses

Carbons are widely used in prosthetic heart valves, as a result of their favorable mechanical and biological properties. Pyrolytic carbons, deposited in a fluidized bed, have high strength, and high fatigue and wear resistance. Compatibility with blood and soft tissue is good.

Table 2.57 Representative Mechanical Properties of LTI, Glassy, and Vapor-Deposited Carbons (3)

Property	Glassy carbon	Vapor deposited carbon	LTI carbon	LTI carbon with silicon (5–12%)
Density, g/cm ³	1.5	1.9	1.9	2.1
Crystallite size, Å	30	10	35	35
Flexural strength 1000 psi	20	80	70	85
Young's modulus, 10 ⁶ psi	4.0	2.5	3.0	4.0
Strain to fracture, %	1.0	5.0	2.0	2.0
Fatigue limit/fracture strength	1.0	1.0	1.0	1.0
Strain energy to fracture, 100 psi	1	12	7	9

Table 2.58 Mechanical Properties of Suture Materials (3)

Suture	Yield stress (GPD)	Breaking stress (GPD)	Yield strain (%)	Breaking strain (%)	Modulus of elasticity	Specific work of rupture (N/Tex)×10 ⁻²
Dexon	0.80	6.30	1.9	22.6	55	6.63
Vicryl	0.97	6.55	1.8	18.4	67.5	5.46
Mersilene	1.20	4.20	2.7	8	53	1.32
Silk	1.33	3.43	1.9	11.5	79.0	2.36
Nurolon	0.34	3.80	1.6	18.2	21.0	2.80
Ethilon	0.41	6.25	2.2	33	20.0	8.96
Prolene	0.52	5.14	1.2	42	58.5	14.69

2.17.2 Wound Closure Biomaterials

Virtually every operation requires the use of materials to close the wound for subsequent successful healing. The material must retain adequate strength during the critical period of healing; it should also induce minimal tissue reaction that might interfere with the healing process. The complexity involved in wound healing calls for different types of wound closure materials.

2.18 Metal Matrix Composites

The metal matrix composites can be described as materials whose microstructure comprises a continuous metallic phase into which a second phase (ceramic materials) has been artificially introduced during processing, as reinforcement.

2.18.1 Matrix Materials

The most common matrices are the low-density metals, such as aluminum and aluminum alloys, and magnesium and its alloys. Some work has been carried out on lead alloys, mainly for bearing applications, and there is interest in the reinforcement, for example, of titanium-, nickel- and iron- base alloys for higher-temperature performance. However, the problems encountered in achieving the thermodynamic stability of fibers in intimate contact with metals become more severe as the potential service temperature is raised, and the bulk of development work at present rests with the light alloys.

2.18.2 Reinforcements

The principal reinforcements for metal matrices include continuous fibers of carbon, boron, aluminum oxide, silica, aluminosilicate compositions and silicon carbide. Some ceramic fibers are also available in short staple form, and whiskers of carbon, silicon carbide and silicon nitride can be obtained commercially in limited quantities. There is also interest in the use of refractory particles to modify alloy properties such as wear and abrasion resistance. In this case, particle sizes and volume fractions are greater than those developed metallurgically in conventional alloys, and incorporation of the particles into the metal is achieved mechanically rather than by precipitation as a consequence of heat treatment. Most metal-matrix composites consist of a dispersed reinforcing phase of fibers, whiskers or particles, with each reinforcing element ideally separated from the next by a region of metal. A summary of properties of the most important metal matrix composites is presented in Tables 2.59–2.69.

Table 2.59 Summary of Mechanical Properties of A13 Aluminum-28 v/o Thornel- 50 Composite (5)

Property	Value
Ultimate tensile strength	730 MN/m ² (106 000 psi) at 20 °C
	660 MN/m ² (95 000 psi) at 500 °C
Rule-of-mixtures strength	700 MN/m ² (101 000 psi) at 20 °C
	550 MN/m ² (80 000 psi) at 500 °C
Transverse tensile strength	~83 MN/m ² (~12000 psi)
Tensile elastic modulus, E	145 GN/m ² (21.0x10 ⁶ psi)
Shear modulus, G (calculated)	55 GN/m ² (7.9x10 ⁶ psi)
Density	2.4 g/cm ³ (0.0805 lb/in. ³)
Strength-to-density ratio	2.4x10 ⁶ cm (1.25x10 ⁶ in.)
Modulus-to-density ratio	620x10 ⁶ cm (248x10 ⁶ in.)
Poisson's ratio, m (calculated)	0.306

Table 2.60 Summary of Transverse Tensile Strengths of Various Aluminum- Graphite Composite Systems (5)

Composite		Average				Number of tests
Fiber	Matrix	(MN/m ²)	(psi)	High (psi)	Low (psi)	
Thornel-50	Al-12Si	26	3777	6500	433	9
Courtaulds	220 Al	42	6117	8690	3760	20
Courtaulds	356 Al	70	10,008	14,600	5500	26
Courtaulds HM	Al -10Mg	29.5	4280	4500	3600	5
Whittaker-Morgan	356 Al	50	7300	11,300	4100	5
Whittaker-Morgan	7075 Al	21	3040	5100	400	5

Table 2.61 Uniaxial Tensile Data for Aluminum-Silicon Alloy-Thornel-50 Composite Thermally Cycled 20 Times from -193 to +500°C (5)

Sample number	Ultimate tensile strength (psi)	Rule-of-mixture strength (%)
C7	103 000	103
C8	100 000	99
C9	100 000	00
C10	99 000	99
Average	101 000	100

Table 2.62 Transverse Tensile Strengths for 356 Aluminum-Courtaulds HM Graphite Composite (5)

Sample number	Transverse strength	
	(MN/m ²)	(psi)
808A	91	13 100
808A	88	12 700
808A	74	10 700
808A	68	9900
808B	79	11 500
837A	67	9700
837A	67.5	9800
837A	76	11 100
837B	67	9700
837B	72	10 400

Table 2.63 Corrosion Behavior of Aluminum–Graphite Composite for 1000hr (5)

	356 aluminum (23°C)	(50°C)	356 aluminum–25 v/o (23°C)	Thornel-50 (50°C)
Environment	Nil	Nil	1.2	1.2
Distilled water	1.1	4.9	4.7	9.8
3.5% NaCl solution				

Table 2.64 Tensile Properties of Al₂O₃-Whisker-Nickel Composites at 25 and 1000 °C(5)

Type of composite	Test temperature (°C)	Whisker volume fraction (v/o)	Composite strength (MN/m ²)	Strength-to-density ratio (10 ⁶ cm)
Continuous	25	22	1230	1.63
	25	51	1050	1.68
	25	39	1350	2.0
	1000	16	282	0.114
	1000	21	495	0.665
	1000	21	495	0.67
	1000	29	759	1.08
	Discontinuous	25	28	621
25		19	1180	1.52
25		11	938	1.14
1000		17	451	0.542
1000		28	106	0.144
1000		10	269	0.33
1000		20	618	0.80

Table 2.65 Off-Axis Tensile Properties of Ti-6Al-4V-28 v/o SiC (5)

Average Strength (ksi)				
Filament orientation (degrees)	Ultimate tensile strength	Proportional limit	Elastic modulus (10 ⁶ psi)	Poisson 's ratio
0	142	117	36	0.275
15	135	117	35	0.277
30	113	104	32	0.346
45	107	75	31	0.346
90	95	53	28	0.250

Table 2.66 Properties of Ti-6Al-4V-50 v/o Borsic Composites (5)

Temperature (°F)	Orientation (degrees)	Tensile strength (ksi)	Failure strain (min./in.)	Elastic modulus (10 ⁶ psi)	Elastic modulus (10 ⁶ psi)	Coefficient of expansion (10 ⁻⁶ /°F)
				Tensile	Flexure	
70	0	140	3340	41.5	34.4	2.50
70	15	100	3220	36.8	33.3	—
70	45	66	4220	31.2	31.8	—
70	90	42	3130	29.8	31.2	3.17
500	0	119	—	—	33.2	2.80
700	0	107	—	—	32.4	—
850	0	109	—	—	31.5	3.17
850	15	86	—	—	29.9	—
850	45	53	—	—	27.6	—
850	90	35	—	—	24.4	3.64

Table 2.67 Summary of Mechanical Properties of Magnesium-Graphite Composites (5)

Composite	Strength (psi)	Strength (MN/m ²)	E (10 ⁻⁶ psi)	E (GN/m ²)	Density (gm/cm ³)	Strength/density (10 ⁻⁶ cm)	Modulus/density (10 ⁻⁶ cm)
Mg-42v/o	65 000	450	26.6	184	1.77	2.5	1000
Thornel-75							
Mg-ZK60A	50 000	345	6.5	45	1.80	1.9	250

Table 2.68 Room-Temperature Properties of Lead-Graphite Composites (5)

Composite	Strength lb/in. ²	Modulus of elasticity 10 ⁻⁶ lb/in. ²	Density lb/in. ³	Strength/density 10 ⁻⁶ in.	Modulus/density 10 ⁻⁶ in.
Pure lead	2 000	2.0	0.41	0.005	4.9
Lead-base bearing (75Pb-15Sb-10Sn)	10 500	4.2	0.35	0.03	12.0
Lead-graphite 41 vol% Thornel-75 Fibers	104 000	29.0	0.270	0.385	107.0
Lead-graphite 35 vol% Courtaulds HM	72 000	17.4	0.28	0.26	62.3

Table 2.69 Summary of Mechanical Properties of Zinc and Zinc-Graphite Composite (5)

System	Strength (psi)	Modulus of elasticity (10 ⁻⁶ psi)	Density lb/in. ³	Strength density 10 ⁻⁶ in.	Modulus/density (10 ⁻⁶ in.)
Z-35 v/o Thornel/75	110 900	16.9	0.191	0.58	88.5
Alloy AG40A	41 000	10.0	0.240	0.17	41.7

2.19 Ceramic Matrix Composites

Composite structures in ceramics have been developed for two major reasons. First, they provide a means to enhance dramatically the performance of the so-called functional ceramics; these are systems where electrical, dielectrical, piezoelectric or sensitizing properties are greatly amplified by appropriate composite design. Secondly, they are used to avoid or diminish the brittle behaviour of structural ceramic systems.

A summary of properties of the most important ceramic matrix composites is presented in Tables 2.70–2.74.

Table 2.70 Glass and Glass ceramics suitable as matrices (4)

Matrix type	Major constituent	Minor constituent	Maximum use temperature
Glass			
7740 Boro-silicate	B ₂ O ₃ , SiO ₂	Na ₂ O, Al ₂ O ₃	600 ⁰
1723 Alumino-silicate	Al ₂ O ₃ , MgO, CaO, SiO ₂	B ₂ O ₃ , Bao	700 ⁰ C
7930 High silica	SiO ₂	B ₂ O ₃	1150 ⁰ C
Glass ceramics			
LAS I	Li ₂ O, Al ₂ O ₃ , MgO, SiO ₂	ZnO, ZrO, BaO	1000 ⁰ C
LAS II	Li ₂ O, Al ₂ O ₃ , MgO, SiO ₂ , Nb ₂ O ₅	ZnO, ZrO ₂ , BaO	1100 ⁰ C
LAS III	Li ₂ O, Al ₂ O ₃ , MgO, SiO ₂ , Nb ₂ O ₅	ZrO ₂	1200 ⁰ C
MAS	MgO, Al ₂ O ₃ , SiO ₂	BaO	1200 ⁰ C
BMAS	BaO, MgO, Al ₂ O ₃ , SiO ₂	—	1250 ⁰ C

Table 2.71 Properties of silicon nitride and carbon/silicon nitride (4)

Property	Si ₃ N ₄	C/Si ₃ N ₄
Bulk density (g/cm ³)	3.44	2.7
Fibre content (vol.%)	—	30
Bending strength (MPa)	473±30	454±42
Young's modulus (GPa)	247±16	188±18
Fracture toughness (MPa m ^{1/2})	3.7±0.7	15.6±1.2
Work of fracture (J/m ²)	19.3±	4770±770

Table 2.72 Room temperature strengths of RBSN* and SiC/RBSN (4)

Test	Axial strength (MPa)		
	0 % Fiber	23 % Fiber	40 % Fiber
Four point bend	107 ± 26	539 ± 48	616 ± 36
Three point bend	—	717 ± 80	958 ± 45
Tensile	—	352 ± 73	536 ± 20

* RBSN - Reaction bonded silicon nitride.

Table 2.73 Properties of brittle fibre/SiC matrix composites (4)

Reinforcement	Matrix	Vol %	Comp.density % Th.	Fracture toughness (MPa m ^{1/2})	4 Point bending strength, MPa
SiC Fibers	SiC	45 39.5	70–77 68–75	–	213–230 224–410
SiC Cloth	SiC	41.6 37.9	75–90 73–89	–	419–437 187–217
SiC chopped fibers	SiC	25.4 21.9	51–81 71–77	– –	90–177 50–94
SiC cloth plain weave satin	SiC	35.5 46.3	62–83 65–85	1.8–3.6 –	72–107 71–196
weave		50.2	68–84	–	44–97
SiC chopped fibers	SiC	16.8 24.3 25.4	69–82 68–76 51–81	– – –	61–106 74–98 90–177
SiC cloth	SiC	41–45	64–90	–	107–476
SiC fibers	SiC	39–57	68–77	–	38–410
SiC fibers	SiC	–	>90	>25	320
C fibers	SiC	–	>90	>25	530

Table 2.74 Room temperature of some unreinforced ceramics and ceramic matrix composite (4)

Material	Flexural strength MPa	Fracture toughness MPa m ^{1/2}
Ai ₂ O ₃	550	4–5.0
SiC whiskers/Al ₂ O ₃	800	8.7
SiC	500	4.0
SiC fibers/SiC	750	25.0
ZrO ₂	200	5.0
SiC/ZrO ₂	450	22.0
Borosilicate glass	60	0.6
SiC fibers/borosilicate glass	830	18.9
Glass ceramic	200	2.0
SiC fibers/glass ceramics	830	17.0
Reaction bonded Si ₃ N ₄	260	2–3.0
SiC whiskers/reaction bonded Si ₃ N ₄	900	20
Hot pressed Si ₃ N ₄	470	3.7–4.5
SiC whiskers/hot pressed Si ₃ N ₄	800	56

References

1. Seymour, R.B. (1990) *Polymer Composites*, VSP, Utrecht, The Netherlands.
2. Weatherhead, R.G. (1980) *FRP Technology*, Applied Science Publishers, London.
3. *Biocompatible Polymers, Metals, and Composites*, edited by M. Szycher, Technomic Publishing Co. Inc.

4. Islam, M.U., Wallace, W. and Kandeil, A.Y. (1985) *Artificial Composites for High Temperature Applications*, Noyes Data Corporation, Park Ridge, New Jersey, USA.
5. Kreider, Kenneth G. (1974) *Metallic Matrix Composites*, Vol. 4, Academic Press, New York and London.
6. Hawkins, W.L. (1984) *Polymer Degradation and Stabilization*, Springer-Verlag.
7. Environmental Effects on Advanced Composite Materials, symposium presented at the seventy-eighth Annual Meeting ASTM, Philadelphia, 1975.
8. Hill, R. (1964) *J. Mech. Phys. Solids*, **12**, 199.
9. Hermann, J.J. (1970) *Proc. Konigl. Nederl. Akad. Wetenschappen Amsterdam*, **B70**, 1.
10. Halpin, J.C. and Pagano, N.J. (1964) *J. Compos. Mater.*, **3**, 720.

Chapter 3

Thermoplastic Polymers In Biomedical Applications: Structures, Properties and Processing

S.H. Teoh, Z.G. Tang, and Garth W. Hastings

3.1 Introduction

In general thermoplastic polymers are made up of long linear chain molecules which exhibit large scale chain mobility and deformation under shear forces above their softening temperature. This change is reversible. Above this temperature the thermal motions of the chain segments are sufficient to overcome inter- and intramolecular forces. At room temperature the material is a viscoelastic solid. Their behaviour is dependent on chain morphology, structure, crystallinity and the types of additives added (often to aid processing). The materials can easily be processed into different type of products and are considered to be the most important class of plastic materials commercially available. The processability of this class of plastics is a key characteristic for developing biomedical applications.

Nine potential biomedical applications areas have been identified (Jones and Denning, 1988):

1. Membranes in extracorporeal applications such as oxygenators;
2. Bioactive membranes e.g., controlled release delivery systems and artificial cells;
3. Disposable equipment e.g., blood bags and disposable syringes;
4. Sutures and adhesives including biodegradable and non-biodegradable materials;
5. Cardiovascular devices such as vascular grafts;
6. Reconstructive and orthopaedic implants;
7. Ophthalmic devices such as corneas and contact lens;

S.H. Teoh (✉) • G.W. Hastings

Institute of Materials Research & Engineering – IMRE Block S7, Level 3, Room 17B,
National University of Singapore, Singapore, 10 Kent Ridge Crescent, 119260, Singapore

Z.G. Tang

BIOMAT Centre, National University of Singapore, Singapore 119260, Singapore

8. Dental restorative materials including dentures;
9. Degradable plastic commodity products.

This section focuses on 12 thermoplastic polymers which have found wide application in the above. Each part deals with one polymer or one group of polymers of structural similarity. The content includes the chemical structure, structure-property relationships, tables of physical, mechanical and thermal properties, and processing conditions of each candidate thermoplastic. Some properties can be predicted from the structural characteristics of the polymers.

In general, for a given polymer, higher molecular weight tends to improve mechanical properties, but the increase in the resistance to flow in the fluid state makes processing more difficult and costly. A wide range of molecular weight is generally more appropriate for processing of each polymer. The effect of branching in otherwise linear molecules is significant. Short but numerous branches irregularly spaced may reduce considerably the ability of portions of linear chains to form crystal-like domains, and the corresponding polymer will display a lower stiffness, a good example being the highly branched low-density polyethylene of lower degree of crystallinity than the less branched high density product. Tacticity of polymer molecules greatly affects crystallinity and stiffness. For example, commercial polypropylene is usually about 90–95% isotactic, and is stiff, highly crystalline and with a high melting point, whereas the atactic polypropylene is an amorphous somewhat rubbery material of little value. Within the range of commercial polymers, the greater the amount of isotactic material the greater the crystallinity and hence the greater the softening point, stiffness, tensile strength, modulus and hardness. The inter-molecular and intra-molecular forces also influence the properties of polymers. The hydrogen bonds or van der Waal's and other dispersion forces between adjacent molecules produce a large increase in melting temperature. A high energy barrier to molecular rotations hinders the ability of molecules to take up the required conformations to form crystals. Polymethylmethacrylate (PMMA), and polycarbonate exist in an amorphous state and are completely transparent. The crystallinity is controlled by both structural factors and processing conditions. From the processing standpoint, the higher the crystallinity, the bigger the shrinkage observed after product processing. Thermoplastic polymers exist in semi-crystalline and amorphous states. The ratio of these two states affects material properties strongly and can be characterized using X-ray analysis and by observing the thermal behaviour of the polymers. Amorphous thermoplastics are normally transparent and do not have a fixed melting temperature like that of the semi-crystalline thermoplastics. They are also less resistant to solvent attack. Semi-crystalline thermoplastics, because of the presence of crystallites, are more fatigue and wear resistant. A typical case is polyacetal which has more than 20 years of *in vivo* experience as an occluder in the Björk–Shiley tilting disc mechanical heart valves.

A main requirement for a polymeric candidate is its biocompatibility with biological tissues and fluids. Biocompatibility will depend on the polymer intrinsic chemical nature and the additives present. It is a complex issue not dealt with here. It is not always possible to distinguish the medical-grade polymers from the

conventional polymers. They may come from a batch intended for general purposes, but are selected on the basis of clean condition or trace element analysis or mechanical properties. Subsequent processing requires clean room conditions and care to avoid any contamination. There is still some inherent uncertainty about constituents unless there has been complete disclosure and/or only a 'pure' polymer is used. With new developments in polymeric biomaterials, the situation should improve.

It is hoped that the following sections will be of value to researchers in science and engineering and to clinical practitioners who are engaged in the development and material selection of new thermoplastic polymers for biomedical applications.

3.2 Polyethylene

Commercially, polyethylene is produced from ethylene in various densities (from linear low to ultra high). There are four quite distinct processes to the preparation of commercial polymers of ethylene: (a) high pressure processes, (b) Ziegler processes, (c) the Phillips process, (d) the Standard Oil (Indiana) process. High pressure polymers (British patent 471590, 1930) are of the lower density range for polyethylene ($0.915\text{--}0.94\text{ g/cm}^3$) and usually also of the lower range of molecular weights. Until the mid- 1950s, all commercial polyethylenes were produced by high pressure processes. These materials were branched materials and of moderate number average molecular weight, generally less than 50 000. Ziegler polymers (Ziegler, 1955) are intermediate in density (ca. 0.945 g/cm^3) between the high pressure polyethylenes and those produced by the Phillips and Standard Oil processes. Phillips polymers have the highest density of any commercial polyethylenes (ca. 0.96 g/cm^3) Ziegler and Phillips processes produce polymers at lower temperature and pressures with a modified structure giving a higher density, greater hardness higher softening points. The Standard Oil process gives a density of about 0.96 g/cm^3 similar to the Phillips materials. Processes, such as a gas phase process developed by Union Carbide for making linear low density polyethylene (LLDPE), were aimed to produce polyethylenes with short chain branch but no long chain branch. High pressure polymers have more branching and even with side chains as long as the main chain. In contrast, the high density polyethylene (HDPE) produced by the Ziegler or Phillips methods has only 3 to 5 branches per 1000 C-atoms and the linear low density PE has very few branches. The weak point in the chain which is sensitive to degradative environmental effects is located at the branching site. The amount of branches in polyethylene also influences the crystallinity of polyethylene. A higher degree of crystallinity and associated denser packing leads to higher density and larger crystals (LDPE < $1\text{ }\mu\text{m}$; LLDPE, $2\text{--}4\text{ }\mu\text{m}$; HDPE, $2\text{--}8\text{ }\mu\text{m}$). The crystallinity is increased with slower cooling rate. Only the HDPE and the ultra high molecular weight polyethylene (UHMWPE) find extensive medical applications.

Chemically, polyethylene is inert and there are no effective solvents at room temperature. However, polyethylene is subject to oxidation and halogenation. Chemicals like nitric acid produce oxidative deterioration and affect mechanical properties of polyethylene. The environmental oxidation of polyethylene happens at high temperature, under ultra-violet light and/or high energy irradiation, e.g., gamma irradiation. Polyethylene should be kept from contact with halogenating agents and environments. The lower molecular weight polyethylene may be dissolved at high temperature and swollen by chemicals such as benzene and xylene. The resistance to environmental stress cracking (ESC) increases with molecular weight, (copolymers being more resistant than homopolymers).

3.3 Polypropylene

Polypropylene is an addition polymer of propylene. The chemical structure of polypropylene is often described as the repeating unit of 2-methyl ethylene. During polymerization, the CH_3 groups characteristic of this olefin can be incorporated spatially into the macromolecule in different ways. The resulting products have different properties and are classified as a. isotactic polypropylene, where the CH_3 groups are on the same side of the main chain; b. syndiotactic polypropylene, where the CH_3 groups are symmetrically arranged on the two sides of the main chain; c. atactic polypropylene, where the CH_3 groups are randomly distributed in the spatial relationship to the main chain.

The atactic polymer is an amorphous somewhat rubbery material of little value, whereas the isotactic polymer is stiff, highly crystalline and with high melting point. Commercial polymers are usually about 90–95% isotactic. Within the range of commercial polymers, the greater the amount of isotactic material, the greater the crystallinity, and hence the greater the softening point, stiffness, tensile strength, modulus, and hardness. The properties of the polymer will depend on the size and type of crystal structure formed in its construction.

Molecular weights of polypropylenes are in the range $M_n = 38\,000\text{--}60\,000$ and $M_w = 220\,000\text{--}700\,000$ with the values of $M_w/M_n = 5.6\text{--}11.9$, higher than those encountered normally in polyethylene. The high molecular weight polymer from propylene was introduced in 1954 by G. Natta using a modified Ziegler process, and commercialized in 1957 by Montecatini under a trade name Moplen. This was followed in 1983 by the Spheripol process; in 1988, the Valtec process; and in 1990, Himont process. The greatest influence of molecular weight and molecular weight distribution is on the rheological properties. Rheological investigations show that polypropylene deviates more strongly from Newtonian behaviour than does polyethylene. The effect of shear rate on the apparent melt viscosity is greater for polypropylene.

Although polypropylene and polyethylene are similar structurally, polypropylene has a lower density around 0.90 g/cm^3 and a higher T_g and T_m . The higher melting point of polypropylene gives the option for autoclave sterilization. The chemical

resistance of polypropylene is similar to high density polyethylene, but it is more susceptible to oxidation, chemical degradation and crosslinking (irradiation, violet light and other physical means) than polyethylene. Polypropylene is better in creep resistance and in resisting environmental stress cracking than polyethylene.

3.4 Polyurethane

Polyurethanes are block copolymers containing blocks of low molecular weight polyethers or polyesters linked together by a urethane group. The variety of linkages in polymers results from the further reaction of urethane groups with isocyanates and of isocyanates with amines, water, or carboxylic acids.

Attention in this section will be focussed on the thermoplastic polyurethane elastomers. These polymers are based on three monomers: (1) an isocyanate source, (2) a macroglycol or carbonate, and (3) a chain extender, or curing agent. The isocyanates can be either aromatic or aliphatic. Although the aliphatic based polyurethanes are more expensive, and inferior in physical properties they do not show the embrittlement, weakening, and progressive darkening of the aromatic equivalents.

The final physical and biological properties of the polyurethanes depend principally on the type of macroglycol used in the synthesis. The polyether-based polyurethanes are less sensitive to hydrolysis, and are thus more stable *in vivo*. The polycaprolactone-based polyurethanes, due to their quick crystallization, can be used as solvent-activated, pressure-sensitive adhesives. For medical applications, the polyether-based polyurethanes, particularly those based on polytetramethylene ether glycol (PTMEG) have been used. Among chain extenders, there are two choices: either difunctional or multifunctional monomers. For the production of linear elastomers, only difunctional chain extenders are used, of these, diols and diamines are by far the most important. The chain extenders for the thermoplastic polyurethanes must be linear diols, among which, 1,4-butane diol has been chosen for medical applications. This chain extender produces thermoplastic polyurethanes with high physical properties, excellent processing conditions and clear polymers.

Polyurethane elastomers are a mixture of crystalline (hard segment) and amorphous domains (soft segment), and the hard segments are considered to result from contributions of the diisocyanate and chain extender components. They significantly affect mechanical properties, particularly modulus, hardness and tear strength. Soft segments therefore affect the tensile strength and elongation at yield and break.

Polyurethanes are sensitive to strong acids, strong alkalis, aromatics, alcohols, hot water, hot moist air and saturated steam. The hydrolytic stability of polyurethanes in applications must be considered carefully. However, polyurethanes are resistant to weak acids, weak alkalis, ozone, oxygen, mineral grease, oils and petroleum. There are doubts for the oxidation stability of polytetramethylene ether glycol

based polyurethanes. Polycarbonate urethane is a promising substitute with good oxidation stability.

The thermoplastic polyurethanes are characterized by the following properties: a. high elongation at break and high flexibility (also at low temperature), b. low permanent deformation on static and dynamic loading, c. favourable friction and abrasion performance, d. high damping power, e. high resistance to high energy and UV radiation, and f. plasticizer free,

3.5 Polytetrafluoroethylene

Polytetrafluoroethylene, PTFE, is the polymerization product of tetrafluoroethylene discovered in 1938 by R.J. Plunkett of Du Pont. The polymer is linear and free from any significant amount of branching. The highly compact structure leads to a molecule of great stiffness and results in a high crystalline melting point and thermal stability of the polymer.

The weight average molecular weights of commercial PTFE are in the range 400 000 to 9 000 000. The degree of crystallinity of the polymer reaches 94%. The properties of PTFE moldings are considerably influenced by the processing conditions and polymer grades. After processing, cooling conditions determine the crystallinity of the molding. Slow cooling leads to higher crystallinity which affects the physical properties as well as mechanical and thermal properties.

PTFE is a tough, flexible material of moderate tensile strength with excellent resistance to heat, chemicals and to the passage of an electric current. The polymer is not wetted by water and absorption is not detectable. The permeability to gases is low, the water vapour transmission rate being approximately half that of low density polyethylene and polyethylene terephthalate. It has the lowest coefficient of friction of all solids and the dynamic and static coefficients of friction are equal, i.e. stick-slip does not occur. Abrasion resistance is low. The thermal stability of PTFE is excellent up to 300 °C but it is degraded by high energy radiation.

Phase transition behaviour precludes the use of the conventional molding methods, and PTFE can be processed by employing a process similar to that of metallurgical sintering. In 1963, Shinsaburo Oslinge of Sumitomo Industries in Japan discovered a process for expanding PTFE during extrusion. The e-PTFE has been considered for fabrication of vascular grafts.

Apart from its good slip and wear characteristics the advantages of PTFE are: a. almost universal chemical resistance, b. insolubility in all known solvents below 300 °C, c. high thermal stability, d. continuous service temperature range -270 to 260 °C, e. low adhesion, f. low coefficient of friction, g. outstanding electrical and dielectric properties, h. resistant to stress cracking and weathering, but limited use in structural components because of the low modulus of elasticity.

3.6 Polyvinylchloride

Commercial PVC polymers are largely amorphous, slightly branched molecules with the monomer residues arranged in a head-to-tail sequence. The molecular weights for most commercial polymers are in the range of $M_w = 100\,000\text{--}200\,000$, $M_n = 45\,000\text{--}64\,000$ although values may be as low as 40 000 and as high as 480 000 for the weight average molecular weight. The ratio of M_n/M_w is usually about 2 for the commercial material although it may increase with the higher molecular weight grades.

The polarity and strong inter-chain attraction gives a higher hardness and stiffness than polyethylene. Thus PVC has a higher dielectric constant and power factor than polyethylene, although at temperatures below the glass transition temperature the power factor is still comparatively low (0.01–0.05 at 60 Hz) because of the immobility of the dipole. PVC is mainly used in a plasticized form. There are many materials that are suitable plasticisers for PVC. They have similar solubility parameters to PVC, i.e., about $19.4\text{ MPa}^{1/2}$ and are also weak proton acceptors and may be incorporated by mixing at elevated temperatures to give mixtures stable at room temperature.

The release of low molecular weight plasticizer has resulted in polymeric plasticisers being developed, but esters are still widely used and are effective in plasticisation. (Black, 1992; Brydson, 1982, and Park and Lakes, 1992).

Characteristic properties are:

3.6.1 Unplasticized PVC

a. high mechanical strength, rigidity and hardness, b. low impact strength in unmodified form, c. translucent to transparent (depending on method of manufacture), d. good electrical properties in the low voltage and low frequency range, and e. high chemical resistance.

3.6.2 Plasticized PVC

a. flexibility adjustable over a wide range, b. depending on type of plasticiser, toughness very temperature dependent, c. translucent to transparent, d. good electrical properties in the low voltage and low frequency range, e. chemical resistance is dependent on the formulation and very dependent on temperature, and f. the polymers contain less than 1 ppm vinyl chloride monomer.

3.7 Polyamides

Chemically, the polyamides may be divided into two types: a. those based on diamines and dibasic acids, and b. those based on amino acids or lactams (Chapman and Chruma, 1985). Commercial use of nylons is dominated by two products, one from each type, nylon 66 and nylon 6 from ϵ -caprolactam.

Aliphatic polyamide is linear and easy to crystallize but crystallinity varies widely with conditions. Crystalline content may be 50–60% by slow cooling and 10% by fast cooling. High interchain attraction in the crystalline zones and flexibility in the amorphous zones leads to polymers which are tough above their apparent glass transition temperatures (Brydson, 1982).

Polyamides have excellent fibre-forming capability due to interchain H-bonding and a high degree of crystallinity which increases strength in the fibre direction (Park and Lakes, 1992). Polyamides are hygroscopic and lose strength *in vivo*. The amorphous region of polyamide chains is sensitive to the attack of water. The greater the degree of crystallinity, the less the water absorption and hence the less the effect of humidity on the properties of the polymer. The reversible absorption of water is associated with a change in volume and thus of dimensions.

The mechanical properties of moulded polyamide materials depend on molecular weight, crystallinity and moisture content. In the dry, freshly molded state, all polyamide grades are hard and brittle. When conditioned they are tough and wear resistant. High melting points result in good mechanical properties up to temperatures in the region of 120–150 °C.

They are only soluble in a few solvents (formic acid, glacial acetic acid, phenols and cresols), of similar high solubility parameter. Nylons are of exceptionally good resistance to hydrocarbons. Esters, alkyl halides, and glycols have little effect on them. Alcohols can swell the polymers and sometime dissolve some copolymers. Mineral acids attack the nylons but the rate of attack depends on the type of nylon and the nature and concentration of the acid. Nitric acid is generally active at all concentrations. The nylons have very good resistance to alkalis at room temperature. Resistance to all chemicals is more limited at elevated temperature (Brydson, 1989).

Generally, polyamides are characterized by: a. high strength, stiffness and hardness, b. high heat distortion temperature, c. high wear resistance, good slip and dry-running properties, d. good damping capacity, e. good resistance to solvents, fuels and lubricants, f. non-toxicity, g. good processability, h. aliphatic polyamides are partially crystalline and thus opaque, and i. moisture content impairs mechanical properties and affects dimensions of moldings.

3.8 Polyacrylates

Polyacrylates are based on acrylic acid, methacrylic acid, and their esters. Among them, polymethylmethacrylate (PMMA) and polyhydroxy ethylmethacrylate (PHEMA) have found wide applications as biomedical materials. The clinical

history of polyacrylates began when it was unexpectedly discovered that the fragments of PMMA plastic aircraft canopies stayed in the body of the wounded without any adverse chronic reactions (Jones and Denning, 1988; Park and Lakes, 1992).

In normal conditions, PMMA is a hard transparent material. Molecular weight is the main property determinant. High molecular weight PMMA can be manufactured by free radical polymerization (bulk, emulsion, and suspension polymerisation). Bulk polymerization is used for cast semi-finish products (sheet, profiles and even tubes), and the cast polymer is distinguished by superior mechanical properties and high surface finish (Brydson, 1982 and Dominghaus, 1993). Cast material has a number average molecular weight of about 10^6 whilst the T_g is about 106°C . The extensive molecular entanglement prevents melting below its decomposition temperature (approx. 170°C).

An amorphous polymer, PMMA has a solubility parameter of about $18.8 \text{ MPa}^{1/2}$ and is soluble in a number of solvents with similar solubility parameters. Solvents include ethyl acetate (δ : $18.6 \text{ MPa}^{1/2}$), ethylene dichloride (δ : $20.0 \text{ MPa}^{1/2}$), trichloroethylene (δ : $19 \text{ MPa}^{1/2}$), chloroform (δ : $19 \text{ MPa}^{1/2}$), and toluene (δ : $20 \text{ MPa}^{1/2}$). The polymer is attacked by mineral acids but is resistant to alkalis, water and most aqueous inorganic salt solutions. A number of organic materials although not solvents may cause crazing and cracking (e.g. aliphatic alcohols).

The characteristic properties of PMMA are, a. high hardness, stiffness and strength, b. homopolymers are brittle, copolymers are tough, c. scratch-resistant, high gloss surface capable of being polished, d. water-white transparency, copolymers exhibit inherent yellowish color, e. high heat distortion temperature, f. good electrical and dielectric properties, g. resistant to weak acids and alkaline solution as well as to non-polar solvents, grease, oils and water, h. susceptible to stress cracking, i. flammable, j. good processability and machinability, k. rather low resistance to creep at temperature only slightly above room temperature, and l. high melt viscosity due to the high chain stiffness caused by restricted rotations about the C-bonds in the backbone chains

3.9 Polyacetal

Polyacetal can be divided into two basic types, acetal homopolymer and acetal copolymer. Both homopolymer and copolymer are available in a range of molecular weights ($M_n = 20\,000\text{--}100\,000$). The homopolymer is a polymer of formaldehyde with a molecular structure of repeated oxymethylene units (Staudinger, 1932). Large-scale production of polyformaldehyde, i.e. polyacetal, commenced in 1958 in the USA (US Patent 2 768 994, 1956) (British patent 770 717, 1957). Delrin (1959) was the first trade mark for this polymer by Du Pont Company. The copolymers were introduced by the Celanese Corporation of America, and the first commercial product named Celcon (1960). One of the major advantages of copolymerization is to stabilize polyacetal because the homopolymer tends to depolymerize and eliminate formaldehyde. The most important stabilization method is structural modification of the polymer by, for example, copolymerization with cyclic ether.

As can be seen polyacetal has a very simple structure of a polyether. Unlike polyethylene, polyacetal has no branching, and its molecules can pack more closely together than those of polyethylene. The resultant polymer is thus harder and has a higher melting point than polyethylene (175°C for homopolymer), exhibiting a high crystallinity (77–85%).

No effective solvents have been found for temperatures below 70°C. Swelling occurs with solvents of similar solubility parameter (δ : 22.4 MPa^{1/2}). However, polyacetal should be kept away from strong acids, strong alkalis, and oxidizing agents. Water can not degrade it but may swell it or permeate through it and affect the dimensions of its products. Prolonged exposure to ultra-violet light will induce surface chalking and reduce the molecular weight of the polymers. Polyacetals, both homopolymer and copolymer are also radiation sensitive. The radiation damage threshold is estimated at 0.5 Mrad with 25% damage at 1.1 Mrad (Szycher, 1991).

Generally, the polyacetals have the following characteristics, a. high tensile strength, shear strength, stiffness, and toughness, b. predictable stress/ strain relationships, c. predictable dimensional behavior, d. chemical and corrosion resistance, e. abrasion resistance, f. light weight and good appearance, g. acceptability for food contact application (most grades), h. ease of processing, and i. competitive costs.

The enormous commercial success of the polyacetals is owed to their very high resistance to creep and fatigue. The acetal resins show superior creep resistance to the nylons.

3.10 Polycarbonate

Polycarbonate, PC, is a linear thermoplastic based on the bis-phenol A dihydroxy compound. In 1898 Einhorn reacted dihydroxybenzenes with phosgene in solution in pyridine (Brydson, 1982), and production began in both Germany and USA in 1958. General purpose polycarbonate is a linear polyester of carbonic acid in which dihydric phenols are linked through carbonate groups, while standard grades are made from bisphenol A and phosgene (Carhart, 1985).

The rigid molecular back bone of bis-phenol A PC leads to high melting temperature ($T_m = 225\text{--}250^\circ\text{C}$) and high glass transition temperature ($T_g = 145^\circ\text{C}$). The polymer does not show any crystallinity. After annealing polymer between 80 and 130°C there is a small increase in density and hence there must be a decrease in free volume, and a large drop in impact strength; impact strength may be reduced by annealing crystallization and aging (Brydson, 1982).

The limited crystallinity contributes to the toughness of PC. Highly crystalline samples prepared by heating for prolonged periods above their T_g or by precipitation from solution are quite brittle. Although of good impact strength and creep resistance tensile strain of 0.75% or more produces cracking or crazing. The refractive index of PC lies in the range of 1.56 to 1.65 (higher than PMMA and silicone rubber) and the transparency of 85 to 90% is reached in the region of visible light (Domininghaus, 1993).

The chemical resistance of PC is poor and hydrolysis of aliphatic PC s is more prominent than that of bis-phenol A PC s. There is resistance to dilute (25%) min-

eral acids and dilute alkaline solutions other than caustic soda and caustic potash. Where the resin comes into contact with organophilic hydrolysing agents such as ammonia and the amines, the benzene rings give little protection and reaction is quite rapid. The absence of both secondary and tertiary C-H bonds leads to a high measure of oxidative stability. Oxidation takes place only when thin films are heated in air to temperatures above 300°C.

Typical properties include: a. low density, b. high strength, stiffness, hardness and toughness over the range from -150 to +135°C unreinforced and from -150 to +145°C when reinforced, c. crystal clear transparency, high refractive index, high surface gloss, d. can be colored in all important shades, transparent, translucent or opaque with great depth of color, e. good electrical insulation properties which are not impaired by moisture, f. high resistance to weathering for wall thicknesses greater than 0.75 mm, g. high resistance to high energy radiation, and h. self-extinguishing after removal of the ignition source.

The main disadvantages are: a. processing requires care, b. limited chemical resistance, c. notch sensitivity and susceptibility to stress cracking.

3.11 Polyethylene Terephthalate

Polyethylene terephthalate, PET, is a thermoplastic polyester made by condensation reaction of ethylene glycol with either terephthalic acid or dimethyl terephthalate (Margolis, 1985). By the end of the 1920s J.R. Whinfield and J.T. Dickson discovered PET (BP 578079). It was first commercialized by Du Pont in 1930 (Brydson, 1982) as Dacron[®], followed by ICI with Terylene[®] Films and blow-molded articles have become very important commercially.

The average molecular weights are distributed from 15 000 to 20 000. The physical properties of PET are largely determined by the degree of crystallinity, which varies between 30 and 40% depending on the processing conditions. The rate of crystallization of PET is considerably less than that of polyacetal (POM) and HDPE. The growth rate of the spherulites is only 10 µm/mm for PET compared with 400 µm/mm for POM and 5000 (µm/mm for HDPE (Domininghaus, 1993). To achieve better crystallinity, the mould temperature should be equivalent to that for maximum growth. This point is about 175°C, higher than for POM and HDPE. Rapid-crystallization agents, nucleating agents, reduce the process cycle time and permit lower mould temperatures below 100°C, leading to very fine spherulites and hard stiff mouldings. Extrusion and rapid quenching below the temperature at which most crystallization occurs (between 120 and 200°C), produces amorphous materials and this may be followed with uniaxial orientation for fibres and biaxial orientation for films. The orientation is carried out at 100–120°C, the glass transition temperature, T_g being 86°C.

The permeability of water vapor through PET is higher than that of polyolefins but lower than that of polycarbonate, polyamide, and polyacetal. Antioxidants are necessary to prevent to the oxidation of polyether segments in thermoplastic

polyester elastomer. Chemical resistance of PET is generally good to acids, alkalis, and organic solvents.

Typical properties for partially crystalline PET include, a. high strength and stiffness, b. favorable creep characteristics in comparison with POM, c. hard surface capable of being polished, d. high dimensional stability, e. good electrical, mediocre dielectric properties, and f. high chemical resistance except to strong acid and alkaline solution.

3.12 Polyetheretherketone

Polyetheretherketone, PEEK, is a polymer combining stiff conjugated aromatic groups and flexible ether segments. It was first prepared in the laboratory in 1977 and then marketed in 1978 by ICI, under the trade name of Victrex (Brydson, 1982).

The distribution of aromatic rings and polar flexible groups in the chain affects the glass transition temperature, such that PEEK has a T_g around 145°C and T_m ca. 335°C, PEK (polyether ketone) T_g ca. 165°C and T_m ca. 342°C. Normally the chain stiffness and bulkiness of aromatic rings make it difficult for these polymers to crystallize and although they invariably remain mainly amorphous (Mascia, 1989), PEEK is a partially crystalline thermoplastic. The maximum crystallinity of 48% is achieved from the melt at 256°C and by subsequent conditioning of moldings at 185°C (Domininghaus, 1993). PEEK polymers are capable of melt processing (Brydson, 1982). Other specific features are excellent gamma radiation resistance, and good resistance to environmental stress cracking. PEEK shows excellent chemical resistance and can be used in aggressive environments.

Generally, the main characteristics of this material include, a. high tensile and flexural strength, b. high impact strength, c. high fatigue limit, d. high heat distortion temperature (315°C for 30 glass reinforced), e. good electrical properties over a wide range of temperature, f. favourable slip and wear properties, g. high chemical resistance, h. high resistance to hydrolysis, j. high resistance to radiation, k. low flammability, very low gas and smoke emission, and l. easy processing, no thermal after-treatment of injection moldings.

3.13 Polysulfone

Polysulfone is a polymer which has properties matching those of light metals (Park and Lakes, 1992). The first commercial polysulfone was introduced in 1965 by Union Carbide as Bakelite Polysulfone, now called Udel®. In 1967 3M offered Astrel 360 referred to as a polyarylsulfone. In 1972 ICI introduced a polyethersulfone Victrex®. A high toughness polysulfone was released in the late 1970s by

Union Carbide. Although the commercial polymers are linear and most have regular structures they are all principally amorphous. The backbone aromatic structure leads to high values of the glass transition temperature between 190 and 230°C. The Union Carbide materials have a secondary transition at -100°C and the ICI polymer at -70°C. Typical M_n values are ca. 23 000. Commercial materials are described variously as polysulfones (Udel), polyarylsulfones (Astrel), polyether sulfones or polyarylethersulfones (Vitrex) (Brydson, 1982).

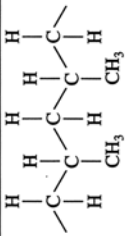
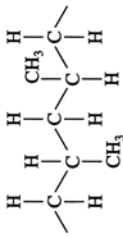
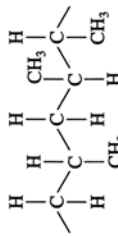
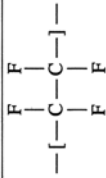
The polymer is manufactured from bisphenol A and 4, 4-dichlorosulphonyl sulfone by multi-step condensation. The most distinctive feature of the backbone chain of those polymers is the diphenylene sulfone group. The sulphur atom in each group is in its highest state of oxidation and tends to draw electrons from the adjacent benzene rings, hence resisting any tendency to lose electrons to an oxidizing agent. Polysulfones thus show outstanding oxidation resistance. The aromatic nature of the diphenylene sulphone can absorb considerable energy applied as heat or radiation and so resists thermal degradation. The diphenylene sulfone group thus confers on the entire polymer molecule the inherent characteristics of thermal stability, oxidation resistance, and rigidity at elevated temperatures.

The potential for energy dissipation confers good impact strength and ductility down to -100°C with high elongation to break and tensile strength. Under most conditions, impact properties rival those of bisphenol A polycarbonate. Unlike polycarbonate, however, polysulfone can exhibit excellent resistance to hydrolysis or reduction of molecular weight even at elevated temperatures. Tests on the hydrolysis stability of polysulfones have been carried out up to 10 000 hours without observed loss of molecular weight.

The polymers are stable in aqueous inorganic acids, alkalis, salt solutions, aliphatic hydrocarbons, and paraffin oils, are transparent, capable of steam sterilization, and free from taste and smell. They should not come in contact with ketones, aromatic solvents, chlorinated hydrocarbons, and polar organic solvents. They may show stress crazing on exposure to steam or water. A polyethersulfone, however, exhibited no crazing even after 300 hours and retained 90% of initial tensile impact strength. For a thermoplastic material, creep is low at moderate temperatures but is significant at temperatures approaching the glass transition. However, the wear properties of this material are not as good as PE and POM (Teoh *et al.*, 1994).

Generally polysulfone has the following characteristic properties, a. high strength, stiffness and hardness between -100 and +150°C short-term to 180°C, b. high thermal stability and heat distortion temperature, c. crystal clear (slightly yellowish) transparency, d. high processing temperature, e. high melt viscosity, f. high chemical resistance, g. susceptibility to stress cracking with certain solvents, h. high resistance to β -, γ -, X- and IR-radiation, i. high transmittance for microwaves, and j. high flame resistance and low smoke development.

Table 3.1 Chemical structures of thermoplastic polymers in biomedical applications

1. Polyethylene (PE)	$\text{---} [\text{---} (\text{CH}_2\text{---CHR})_m \text{---} (\text{CH}_2\text{---CH}_2)_n \text{---}] \text{---}$ <p> $\text{R} = \text{H, Me, Et, ...}$ $m = 1, 2, \dots$ $n = 1, 2, \dots$ if $\text{R} = \text{H}$, linear and high density if $\text{R} \neq \text{H}$, branched and lower density </p>
2. Polypropylene (PP)	$\text{---} [\text{CH}_2\text{---CH}(\text{CH}_3) \text{---}] \text{---}$ <p>isotactic</p>  <p>syndiotactic atactic</p>  
3. Polyurethane (PU)	$\text{---} [\text{O} \text{---} (\text{CH}_2)_x \text{O} \text{---}]_n \text{---} \text{CONH---R---NHCO---O}(\text{CH}_2)_y \text{---} \text{OCONH---R---NHCO} \text{---}] \text{---}$ <p> $\text{R} = \text{aliphatic or aromatic groups}$ x and n for soft segment, y for extender in rigid segment </p>
4. Polytetrafluoroethylene (PTFE)	$\text{---} [\text{---} \text{C} \text{---} \text{C} \text{---}] \text{---}$ 

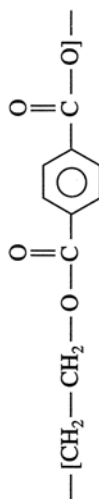
(continued)

Table 3.1 (continued)

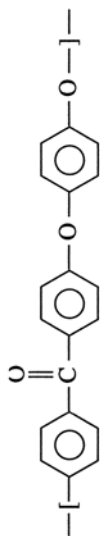
5. Polyvinylchloride (PVC)	$\begin{array}{c} \text{H} & \text{H} \\ & \\ -[\text{C}-\text{C}-] - \\ & \\ \text{H} & \text{Cl} \end{array}$
6. Polyamide (PA)	$-\text{NH}-(\text{CH}_2)_x-\text{NHCO}-\text{nylon}_{x+1,y+1}-(\text{CH}_2)_y-\text{CO}-$ and $-\text{NH}-(\text{CH}_2)_x-\text{CO}-\text{nylon}_{x+1}$
7. Polyacrylate (PMMA)	$\begin{array}{c} \text{R} \\ \\ -(\text{CH}_2-\text{C}-) - \\ \\ \text{COOR}' \end{array}$
8. Polyacetal (POM)	$-[(\text{CH}_2-\text{O})_n-[\text{CH}_2-\text{CH}_2-(\text{R})_x-\text{O}]_m]-$ $\text{R} = \text{CH}_2$ $x = 0, 1, 2$ $m = 0, 1, 2$ $n = 1, 2, 3$ if $x = m = 0$, homopolymer if $x \neq m \neq 0$ copolymer
9. Polycarbonate (PC)	$\begin{array}{c} \text{CH}_3 \\ \\ -[\text{O}-\text{C}_6\text{H}_4-\text{C}-\text{C}_6\text{H}_4-\text{O}-\text{C}(=\text{O})-] - \\ \\ \text{CH}_3 \end{array}$

Table 3.1 (continued)

10. Polyethylene terephthalate (PET)



11. Polyetheretherketone (PEEK)



12. Polysulfone (PS)

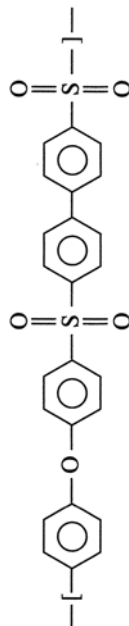
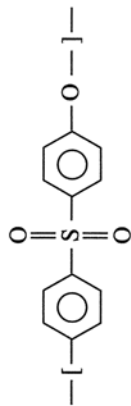
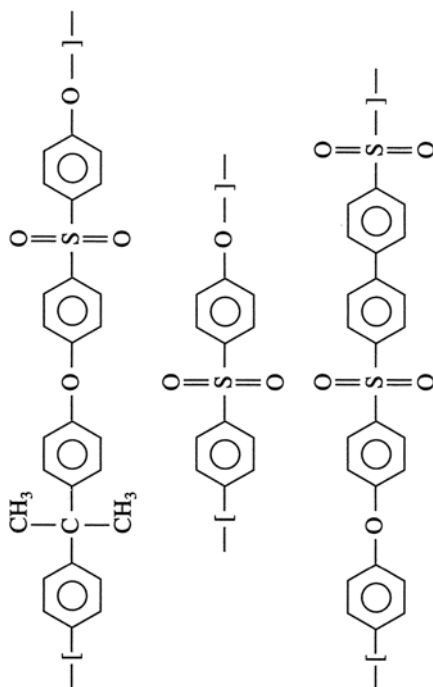


Table 3.2 Properties of thermoplastic polymers in biomedical applications

a. Physical properties									
Physical properties	Unit	PE	PP	PU	PTFE	PVC	PA		
Density	g/cm ³	0.954-0.965	0.90-0.915	1.02-1.28	2.10-2.20	1.16-1.70	1.02-1.15		
Water absorption	%	0.001-0.02	0.01-0.035	0.1-0.9	0.01-0.05	0.04-0.75	0.25-3.5		
Solubility parameter	MPa ^{1/2}	16.4-16.6	16.3	16.4-19.5	12.6	19.4-21.5	23.02		
Refractive index, n _p ²⁰		1.52-1.54	1.47-1.51	1.5-1.65	1.35-1.38	1.52-1.57	1.52-1.57		
b. Mechanical properties									
Physical properties	Unit	PMMA	POM	PC	PET	PEEK	PS		
Density	g/cm ³	1.12-1.2	1.40-1.42	1.2-1.26	1.31-1.38	1.29-1.49	1.13-1.60		
Water absorption	%	0.1-0.4	0.2-0.4	0.15-0.7	0.06-0.3	0.15-0.51	0.14-0.43		
Solubility parameter	MPa ^{1/2}	18.58	22.4	19.4-19.8	21.54	20.2	20.26-22.47		
Refractive index, n _p ²⁰		1.49-1.51	1.48	1.56-1.60	1.51	1.56-1.67	1.56-1.67		
b. Mechanical properties									
Mechanical property	Unit	PE	PP	PU	PTFE	PVC	PA		
Bulk modulus	GPa	0.8-2.2	1.6-2.5	1.5-2	1-2	3-4	2.4-3.3		
Tensile strength	MPa	30-40	21-40	28-40	15-40	10-75	44-90		
Elongation at break	%	130-500	100-300	600-720	250-550	10-400	40-250		
Young's modulus	GPa	0.45-1.3	1-1.6	0.0018-0.009	0.3-0.7	1.0-3.8	1.4-2.8		
Elastic limit	MPa	20-30	20-33	28-40	15-30	23-52	40-58		
Endurance limit	MPa	13-19.6	11-18.2	21-30	9-18	13.8-31.2	22-31.9		
Fracture toughness	MPa m ^{1/2}	2.2-4	1.7-2.1	0.1-0.4	2.5-3	1-4	1.8-2.6		
Hardness	MPa	60-90	60-100	50-120	27-90	70-155	100-160		
Compressive strength	MPa	30-40	30-45	33-50	30-60	32-80	60-100		
Poisson's ratio		0.4-0.42	0.4-0.45	0.47-0.49	0.44-0.47	0.37-0.43	0.38-0.42		
Shear modulus	GPa	0.18-0.46	0.4-0.6	0.0008 ^{1/4} -0.003	0.11-0.24	0.7-1.1	0.52-0.9		

(continued)

Table 3.2 (continued)

b. Mechanical properties										
Mechanical property	Unit	PMMA	POM	PC	PET	PEEK	PS			
Bulk modulus	GPa	3–4.8	4–5.6	2.8–4.6	3–4.9	4–4.5	3.8–4.6			
Tensile strength	MPa	38–80	70–75	56–75	42–80	70–208	50–100			
Elongation at break	%	2.5–6	15–80	80–130	50–300	1.3–50	25–80			
Young's modulus	GPa	1.8–3.3	2.55–3.5	2–2.9	2.2–3.5	3.6–13	2.4–2.9			
Elastic limit	MPa	35–70	65–72	53–75	50–72	12–60	58–70			
Endurance limit	MPa	19.3–38.5	28–42	29.2–41.3	30–43.2	33–36	34.8–42			
Fracture toughness	MPa m ^{1/2}	0.8–1.3	1–1.5	2.5–3.2	1.2–2	2.3–2.5	1.3–2			
Hardness	MPa	100–220	110–220	110–180	97–210	100–120	180–240			
Compressive strength	MPa	45–107	70–80	100–120	65–90	80–120	72–100			
Poisson's ratio		0.4–0.43	0.38–0.43	0.39–0.44	0.38–0.43	0.38–0.43	0.38–0.43			
Shear modulus	GPa	0.6–1.2	0.79–1	0.95–1.05	0.83–1.1	1.2–1.4	0.8–1			
c. Thermal properties										
Thermal property	Unit	PE	PP	PU	PTFE	PVC	PA			
Service temperature in air without mechanical loading (short-term)	°C	90–130	140	80–130	300	55–100	130–200			
Service temperature in air without mechanical loading (long-term)	°C	70–100	100	60–80	250	50–85	70–120			
Minimum service temperature	°C	–63 to –53	–123 to –23	–123 to –23	–263 to –253	–43 to –28	–60 to –50			
Melting(T _m)/decomposing (T _d) ranges	°C	125–135	160–180	180–250*	322–327	150*	220–267			
Glass transition temperature T	°C	–113 to –103	–30 to –3	–73 to –23	20 to 22	–23 to 90	20 to 92			

c. Thermal properties										
Thermal property	Unit	PE	PP	PU	PTFE	PVC	PA			
Softening temperature	°C	40-50	70-100	100		40-110	80-200			
Specific heat	J/g.K	1.95-2.20	1.70-2.35	0.4-1.76	1.00-1.01	0.85-1.80	1.26-1.8			
Thermal expansion	106/K	100-200	80-200	150-210	100-150	60-210	80-150			
Thermal conductivity	W/m K	0.42-0.52	0.12-0.24	0.29-1.80	0.19-0.25	0.13-0.26	0.23-0.29			
Thermal property	Unit	PMMA	POM	PC	PET	PEEK	PS			
Service temperature in air without mechanical loading (short-term)	°C	76-108	110-140	160	180-200	300	160-260			
Service temperature in air without mechanical loading (long-term)	°C	65-98	90-110	135	100	250	150-200			
Minimum service temperature	°C	-123 to -73	-123 to -73	-133 to -123	-133 to -38	-123 to -103	-123 to -73			
Melting (T _m)/decomposing (T _d [*]) ranges	°C	~170*	164-175	225-250	245-255	335	>500*			
Glass transition temperature T _g	°C	106-115	-13-75	145	67-127	144	167-230			
Softening temperature	°C	70-115	110-163	138-148	70-185	140-315	150-216			
Specific heat	J/gK	1.28-1.5	1.40-1.46	1.17-1.30	1.05-1.60	1.5-1.6	1.1-1.30			
Thermal expansion	106/K	62-105	90-125	40-75	50-120	15-47	53-58			
Thermal conductivity	W/mK	0.10-0.19	0.22-1.1	0.14-0.22	0.15-0.34	0.25-0.92	0.13-0.28			

Table 3.3 Processing conditions for thermoplastic polymers in biomedical applications

a. Physical properties			
<i>Thermoplastics</i>			
<i>Process</i>	<i>Special process</i>	<i>Pre-treatment</i>	<i>Remarks</i>
<p>1. Polyethylene</p> <p>Injection moulding Extrusion Blow film extrusion Flat film extrusion Blow moulding Thermoforming Compression moulding</p>	<p>Film processing for PE-LD Rotational moulding for PE-powders Block, sheet, tube, profile, and film processings for PE-HD and PE-HD-UHMW Powder sintering technology for PE-UHMW</p>	<p>No pre-drying treatment except hygroscopic additives are added. Stabilizers and antioxidants are needed for specific processing.</p>	<p>PE-UHMW in solid or porous form has been used in biomedical study and application. Its most outstanding properties are wear or abrasion resistance, excellent impact resistance, and fatigue resistance.</p>
<p>2. Polypropylene</p> <p>Injection moulding Extrusion Blow moulding Compression moulding Thermoforming</p>	<p>Extrusion: blown film, flat film, sheet, tube, monofilaments Injection: Long-lasting integral hinges Biaxially oriented packaging film Tapes</p>	<p>No pre-drying treatment except hygroscopic additives' are added. Stabilizers and antioxidants are needed for specific processing.</p>	<p>Polypropylene has exceptionally high flex life, excellent environmental stress cracking resistance, excellent wear resistance, higher temperature resistance (withstanding steam sterilization), and low cost. Fiber applications such as suture, sewing ring, braided ligament, skin and abdominal patches. Promising applications in thin-wall packaging competing with polystyrene. Polypropylene has lower specific heat and the flow properties are more sensitive to temperature and shear rate. The mold shrinkage is lower than polyethylene but higher than with polystyrene. It has higher melt strength is important for extrusion blow molding of hollow objects. Lower molecular weight grades are suited for extrusion of monofilaments and injection molding of thin-walled articles. Cold forming may be done at room temperature (rolling), and forging, pressure forming, rolling and stamping at temperatures below the crystallite melting region (150 to 160°C). Film processing especially in oriented form competing with polyethylene.</p>

3. Polyurethane	Injection moulding Extrusion	Sheet extrusion Shape extrusion Cast or blow film extrusion Fiber processing	Polyurethane, especially aliphatic type is hygroscopic; the pellets must be dried before extrusion.	Characteristics high flexibility and high impact resistance, and excellent biocompatibility. Film forms of polyurethane have been used in fabrication of vascular graft and patches, heart valve leaflets, blood pumps, diaphragms for implantable artificial heart, and carriers for drug delivery. Elastomeric fibers (Spandex) made from polyurethane copolymer have been used in surgical hoses. Unfavorable processing conditions will induce residual stresses in the products which impair the biostability of polyurethane-based prostheses. To avoid residual stresses in polyurethane tubes, an upper limit of drawn down ratio of 1.5:1.0 are recommended for the appropriate stretching during extrusion. If water bath for tube processing is too cold, residual stresses are also induced. A recommended temperature for the water bath is between 21–27°C.
4. Polytetrafluoroethylene	Sintering Ram extrusion Paste extrusion Coating followed by sintering Impregnation	High temperature sintering process for parts, sheets, plates Ram extrusion for rods, tubes, profiles, wire coatings, and fibers Insulating films, crucibles Expanded tubular form	PTFE is a hydrophobic polymer and pre-drying is not necessary.	Exceptional chemical resistance, temperature resistance, and radiation and weathering resistance. Outstanding electrical properties as insulator or dielectric material. Low adhesion and low coefficient of friction. Exceptional flame resistance. Expanded PTFE (Gortex) has been used in fabrication of blood vessel prostheses.

(continued)

Table 3.3 (continued)

<p>5. Polyvinylchloride</p>	<p>Extrusion Calendering Injection molding Extrusion blow molding Stretch blow molding Compression molding Sintering</p>	<p>Blown film Flat film Sheets Tubes and profiles Cable sheathing Bristles and mono filaments</p>	<p>Proper stored polyvinylchloride can be used without pre-drying. Premixing of ingredients will be considered for plasticized PVC.</p>	<p>Plasticized PVC favours calendering, while unplasticized PVC prefers extrusion. Injection moulding is difficult for both plasticized and unplasticized PVCs except careful control of processing conditions or special design of machine. Characteristic flame resistance. Decomposition happens at high temperature. Overheat in processing should be avoided. Tubular, sheet, plate, and film forms of PVC have been used in medical devices such as blood bags and catheters. Implants of PVC are not encouraged.</p>
<p>6. Polyamides</p>	<p>Injection molding Extrusion Extrusion blow molding</p>	<p>Injection: thin-wall articles, engineering components Extrusion: bristles, packaging, tapes, fiber, wire, film, sheet, tubes, profiles, sheathing</p>	<p>Polyamides, especially aliphatic types are hygroscopic. Pre-drying is needed before processing, and also precaution will be considered during and after process.</p>	<p>Excellent friction properties and good wear and abrasion resistance. Excellent hydrocarbon resistance. Films are used for packaging. Fiber form is employed as suture materials.</p>
			<p>Polyacrylates can easily pick up moisture from environment. Pre-drying is necessary.</p>	<p>Excellent transparency, good scratch resistance. Good processability and machinability. Monomer and polymer powder casting to produce bone cement. Hydrogel has been used to fabricate contact lens. Monomer-polymer doughs is used for processing dentures.</p>

7. Polyacrylates	Injection molding Extrusion Compression molding Thermoforming	Primary forms: sheet, rod, and tube Casting from monomer for optical properties Extrusion from thermoplastic resins to produce sheet. Injection moulding for small complex parts	Polyacrylates can easily pick up moisture from environment. Pre-drying is necessary.	Excellent transparency, good scratch resistance. Good processability and machinability. Monomer and polymer powder casting to produce bone cement. Hydrogel has been used to fabricate contact lens. Monomer-polymer doughs is used for processing dentures.
8. Polyacetal	Injection molding Extrusion Blow molding Compression molding	Injection moulding Extrusion	Polyacetal is less hygroscopic than nylon. However, acetal polymer must be stored in dry place.	Outstanding creep and fatigue resistance. Good toughness and impact resistance. Excellent strength for engineering application. Processing temperature must be carefully controlled. Fiber and film forms of polyacetal are not available. Polyacetal, Delrin, has been used in disc of mechanical heart valves.
9. Polycarbonate	Injection molding Extrusion Blow moldings Thermoforming Hot bending	Injection and extrusion Films: extruded and solvent cast, uniaxially oriented amorphous and partially, crystalline Tube, rod, profile, sheet: extrusion	Polycarbonate can pick up enough moisture to deteriorate quality of products. Pre-drying is necessary.	Applications have been found in consideration of toughness, rigidity, transparency, self-extinguishing characteristics, good electrical insulation and heat resistance. Polycarbonate has been used in the manufacture of contact lenses.

(continued)

Table 3.3 (continued)

<p>10. Polyethyleneterephthalate</p>	<p>Injection moulding Extrusion Blow moulding</p>	<p>Fiber process Uniaxially oriented tapes Films, packaging film, sheet, articles Biaxially oriented film and sheet</p>	<p>Polyethyleneterephthalate is hygroscopic. Pre-drying is necessary.</p>	<p>Characteristic crystallization. Both amorphous and crystallized products can be made through control of crystallization. The benefits from PET products are their stiffness, warp resistance, and dimension stability. Fiber form of PET has been used to fabricate blood vessels and by-pass prostheses. Suture made from PET. Dacron® sewing ring and medical fabrics.</p>
<p>11. Polyetheretherketone</p>	<p>Injection moulding Compression molding Extrusion Composite</p>	<p>Injection moulding for articles Extrusion: film/cast and oriented monofilament wire covering Composite: carbon fiber/PEEK composite</p>	<p>PEEK is hydrophobic polymer but pre-drying is necessary for quality control.</p>	<p>Characteristic high strength at high temperature. Excellent resistance to hydrolysis and environmental stress cracking. Carbon fiber/PEEK composite investigated in bone fracture fixation.</p>
<p>12. Polysulphone</p>	<p>Injection moulding Extrusion Blow moulding Thermoforming</p>	<p>Injection moulding for articles Extrusion: film and sheet which can be thermoformed</p>	<p>Polysulphone is hygroscopic and predrying is required to avoid vapor formation during processing.</p>	<p>Good rigidity, creep resistance, and toughness. Hydrolysis resistance and can undergo repeated steam sterilization. Transparent products can be made and used in medical field. Hollow fiber and membrane devices have been used in hemodialysis. Carbon fiber/polysulphone composite has been used for bone fracture fixation.</p>

Table 3.4 Trade names of thermoplastic polymers in biomedical applications

I. Polyethylene (PE)		
<i>PE-LD and PE-HD</i>		
Eltex(Solvay, BE)	Fertene Maplen (Hirmnont, IT)	Ladene (SABIC, Saudi Arabia)
Finathene (Fina, BE)	Rurmiten (Rumianca, IT)	Escorene (Exxon Chem, US)
Alathon, Sclair (Du Pont Canada Inc., CA)	NeoZex (Mitsui, JP)	Fortiflex (Soltex Polymer, US)
Boalen (Petrinex, CS)	Nipolon (Toyo Soda, JP)	Norechem (USI, US)
Hostalen (Hoechst, DE)	Novatec (Mitsubishi, JP)	Paxon (Allied Signal Corp., US)
Lupolen (BASF, DE)	Hi Zex (Mitsol, JP)	Microthene, Petrothene (US I Chem., US)
Vestolen (Huls, DE)	Mirason (Mitsui Polychem., JP)	HiFax (Himont, US)
Ertileno (Union ERT, ES)	Sholex (Showa Denko, JP)	Marlex (Phillips Petrol., US)
Natene (Rhône-Poulenc, FR)	Sumikathene (Sumitomo Chem., JP)	Super Dylan (Arco Chem., US)
Lacqtene (Atochem, FR)	Suntec (Asahi Chem., JP)	Tenite (Easrman Chem., US)
Carlona (Shell, GB)	Staflene (Nisseki Plastic Chem., JP)	Hipten (Hernijska Ind., YU)
Rigidex, Novex (BP Chemicals, GB)	Yukalon (Mitsubishi Petroleum, JP)	Okiten (INAOKI, YU)
Tipolen (Tiszai Vegyi Kombinát, HU)	Stamylan (DSM, NL)	
Eraclene (EniChem Base, IT)	Ropol (Chem. Komb. Borcesti; RO)	
	<i>PE-HD-UHMW</i>	
Hostalen GUR (Hoechst AG, DE)	Lupolen UHM (BASF AG, DE)	
<i>PE-LLD</i>		
Eltex (Solvay, BE)	Rurmiten (Rumianca, IT)	Escorene (Exxon Chem., US)
Alathon, Sclair (Du pont Canada, CA)	Mirason (Mitsui Polychem., JP)	Marlex TR 130 (Phillips Petroleum, US)
Novapol LL (Novacor Chem., CA)	Novatex (Mitsubishi Chem., JP)	Microthene, Petrothene (USI Chem., US)
Lupolen (BASF, DE)	Sumikathene (Sumitomo Chem., JP)	Norechem (USIExxon Chem., US)
Lotrex (Orkono Norsolor SA, FR)	Ultzex (Mitsui Petrochemical, JP)	Rexene (EI Paso Chem., US)
News (Neste Oy Chem., FI)	Stamylex (DSM, NL)	Tenite (Eastman Chem., US)
Visqueen (ICI, GB)	Ladene (SABIC, Saudi Arabia)	
Eraclene (EniChem., IT)	Dowlex (Dow Chemical, US)	

(continued)

Table 3.4 (continued)

2. Polypropylene (PP)		
Asota, Ecofelt (Chemic Linz, AT)	Eltex (Solvay, FR)	Stamylan (DSM, NL)
Marlex (Phillips Petroleum Co., BE)	Carlona (Shell, GB)	Bicor (Mobil Chem., US)
Istrono (Chern., Werke J. Dimitrow, CS)	Propathene (ICI, GB)	Extrel, Twistlock, Vistalon (Exxon Chem, US)
Tatren (Petrimex, CS)	Biofol (Chem. Kombinat. Tisza, HU)	Fortilene (Soltex Polymer Corp. US)
Hostalen PP (Hoechst, DE)	Afax, Moplen, Valtec (Himont, IT)	Liteplate S (Hercules, US)
Platlion (Deutsche A TOchem., DE)	Bifax (Showa denko. JP)	Profax (Himont, US)
Trovidur (HulsTroisdorf, DE)	Eperon (Kanegafuchi Chem., JP)	Rexene (EI Paso Chem., US)
Ultralen (Lonza Werke, DE)	Noblen (Mitsubishi Petrochemical, JP)	Tenite (Eastman Chemical, US)
Vestolen P (Huls, DE)	Novatec (Mitsubishi Chem., JP)	
Apryl, Lacqtene P (Atochem., FR)	PolyPro, Sunlet (Mitsui Petrochem., JP)	
3. Polyurethane (PU)		
<i>General</i>		
Ucefex, Ucellex (UCB, BE)	Europolymers (Avalon Chemical Co., GB)	Urafil (Akzo-Wilson-Fiberfil, US)
Fabeltan (Tubize Plastics, BE)	Jectothane (Dunlop Holdings, GB)	Hi-Tuff (J.P. Stevens & Co., US)
Caprolan, Elastolen, Elastolan (Elastogran Polyurethane, DE)	Pemullex (Pemu ChemolimpeX, HU)	Esteloc, Estane, Roylar (B.F. Goodrich Chemical Co., US)
Desmopan (Bayer, DE)	Uthane (Urethanes India, IN)	Irogran, Plastothane (Morton Thiokol, US)
Lurolex (Lehmann u. Voss Co., DE)	Pelprene (Toyobo Co., Resins Div., JP)	Proplastic (Pro Lam, US)
Oldopren (Busing u. Fasch & Co., DE)	Durane (Swanson, US)	Q-Thane (Quinn & Co., US)
Durelast (B & T polymers, GB)		
	<i>Medical special</i>	
Angiollex (Abiomed Danvers, MA)	Mitrathane (PolyMedica Burlington, MA, US)	Corplex (Corvita Miami, FL, US)
Biomer (Ethicon Somerville, NJ, US)	Pellethane (Dow Chemical La Porte, TX, US)	Unithane 80F (NICBPB Beijing, China)

3. Polyurethane (PU)				
Cardiothane (Kontron Everett, MA, US)	Surethane (Cardiac Control Palm Coast, FL, US)			Corethane (Corvita Miami, FL, US)
Chronollex (PolyMedica Burlington, MA, US)	Tecollex (Thermedics Inc Woburn, MA, US)			PU 10 (Univ. NSW, Australia)
Hemothane (Sams, Div 3M Ann Arbor, MI, US)	Toyobo TMS5 (Toyobo Co. Osaka, Japan)			
4. Polytetrafluoroethylene (PTFE)				
Hostallon TF (Hoechst, DE)	Neollon (Daikin Ind., JP)			RT duroid (Rogers Corp., US)
Pamllon (Norton Pampus, DE)	Pollyllon (Daikin Kogyo Co., JP)			Rulon (Dixon Ind. Corp., US)
Forallon (A TOCHEM, FR)	Ferrottron, Fluorosint (Polymer Corp., US)			Salox (Allegheny Plastics, US)
Sorellon (Pechiney U.K., FR)	Fluoroloy (Fluorocarbon, US)			Tellon (Du Pont de Numours, US)
Gallon (Plastic Omnium, FR)	FluoroMet (Raymark, US)			Turcite (W.S. Shamban & Co., US)
Fuon (ICI, GB)	Goretex (W.L. Gore Assoc., US)			Tygalor (American Cyanamid Aerospace, US)
Algollon (Montedison, IT)	Halon (Ansimont, US)			Xylon (Whitford Corp., US)
5. Polyvinylchloride (PVC)				
Benvic (Solvay, BE)	Corvic, Vynide, Welvic (ICI, GB)			Rosevil (Chern. Kombinat Borzesti, RO)
Plastilit, Selchim, Solvic (Solvay & Cie., BE)	Ongrovil (Barsodi Veggi Komb., HU)			Ensolite (Uniroyal Chem., US)
Vipopham (Lonza, CH)	Ravinil, Siron, Vipla, Viplast (EniChem, IT)			Ethyl (Ethyl Corp., Polymer Div., US)
Astralon, Trocal, Trospilast, Trovidur, Vestolit (Huls-Troisdorf, DE)	Vixir (S.I.R. (Montedison), IT)			Fiberloc, Geon (B.F. Goodrich, US)
Decelith (VEB Ellenburger Chemiewerk, DE)	Hishiplate (Mitsubishi Plastics Ind., JP)			Pliovic, Vinacel, Vycell (Goodyear, US)
Vinnol (Wacker Chemie, DE)	Kureha, Vicolon (Kureha Chem. Ind., JP)			Vygen (General Tire & Rubber Co., US)
Genopak, Genotherm, Hostalit (Hoechst, DE)	Vinychlon (Mitsui Toatsu Chem., JP)			Vynaloy (B.F. Goodrich Chem. Co., US)
Armodur (Rhone-Poulenc, FR)	Vinylfoil (Mitsubishi Gas Ind., JP)			Hipnil (Hemijiska Industria, YU)
Bipeau, Orgavyl, Polycal (ATOCHEM., FR)	Varian (DSM, NL)			Jugotherm, Juvinil (Jugovinil, YU)
Ekavyl (PCUK, FR)	Norvinyl, Pevikon (Norsk Hydro, NO)			Zadrovil (Polikem, YU)
Carina, Duraflex (Shell Intern. Chern Co., GB)	Olitivil (Chern. Komb. Pitesti, RO)			

(continued)

Table 3.4 (continued)

6. Polyamide (PA)	
	PA 6
Faberyl (Tubize Plastics,	Maranyl (ICI, GB)
	Akulon (Engineering Plastics of AKZO Plastics, NL)
Grilon (Ems Chemie, CH)	Latamid (L.A.T.I., IT)
Durethan B (Bayer, DE)	Nivionplast (EniChem, IT)
Ultramid B (BASF, DE)	Renyl (Snia Technopolimeri, IT)
Orgamide (ATOCHEM, FR)	Amilan, Amilon (Toray Ind., JP)
Technyl C (Rhone-Poulenc Specialites Chimiques, FR)	Torayca (Toray Ind., JP)
	PA 66
Durethan A (Bayer, DE)	Leona (Asahi Chemical Ind., JP)
Technyl A (Rhone-Poulenc Specialites Chimiques, FR)	Torayca (Toray Ind., JP)
Maranyl A (ICI, GB)	Akulon (Engineering Plastics of AKZO Plastics, NL)
7. Polyacrylates	
Umaplex (Synthesia, CS)	Asterite (ICI, GB)
Acifix (Rohm, DE)	Diakon (ICI, GB)
Lucryl (BASF, DE)	Perspex (ICI, GB)
Degaplast (Degussa, DE)	Unilok (British Vita Co., GB)
Deglas, Dewglas (Degussa, DE)	Vetredil (Vetril, IT)
Dewoglas (Degussa, DE)	Vedril (Montedison, IT)
Paraglas (Degussa, DE)	Acrypanel (Mitsubishi Rayon Co., JP)
Plexidur, Plexiglas (Rohm, DE)	Delmer, Depet (Asahi Chem. Ind., JP)
Resarit (Resart, DE)	Eska (Mitsubishi Rayon, JP)
Vestiform (Huls, DE)	Palapet (Kyowa Gas Chem., JP)
Altuglas (Altulor, Orekem, FR)	Shinkolite (Mitsubishi Rayon Co.,JP)
	Sumipex (Sumitomo Chern. Co., JP)
	Casoglas (Casolith, NL)
	Acrylite (Cy/Ro Industries, US)
	Lucite (Du Pont de Nemours, US)
	Corian (Du Pont de Nemours, US)
	Crofon (Du Pont de Nemours, US)
	Electroglas (Glasfex Corp., US)
	Exolite (Cyro Industries, US)
	Gardlite (Southern Plastics Co., US)
	Oroglas (Rohm & Haas Co., US)
	Swedcast (Swedlow, US)

Table 3.4 (continued)

8. Polyacetal (POM)			
	<i>Homopolymers</i>		
Delrin (Du Pont, US)		Tenal (Asahi Chemical Ind., JP)	
	<i>Copolymers</i>		
Celcon, Hostaform (Hoechst, DE)		Duracon, Alkon, and Kematal (Daicel Polyplastic Co., JP)	Ultraform (BASF, DE)
9. Polycarbonate (PC)			
Sparlux (Solvay & Cie., BE)		Sinvet (EniChem, IT)	Lexan (General Electric Plastics, US)
Durolon (Polycarbonates do Brazil, BR)		Novarex (Mitsubishi Chem. Ind., JP)	Merlon (Mobay Chemical Corp., US)
Makrolon (Bayer, DE)		Panlite (Teijin Chemicals, JP)	Polycarbafil (Akzo-WilsonFiberfil, US)
Orgalan (A TOCHEM, FR)		Xantar (DSM, NL)	Polygard (Poly tech, US)
Star-C (Ferro Eurostar, FR)		Calibre (Dow Chemical Corp., US)	Stat-Kon (LNP Corp., US)
Royalite (British Vita Co., GB)		Ekonol (Carborundum Co., US)	
10. Polyethyleneterephthalate			
		(PET)	
Craslin (Ciba Geigy, CH)		Melinar, Melinite (ICI, GB)	Pelton (Mobay Chem. Corp., US)
Grilpet (Ems Chemie, CH)		Amite (Akzo Engng. Plastics, NL)	Petra (Allied Signal, US)
Impet (Hoechst, DE)		Etar (Eastman Chem. Intern., US)	Ropet (Rohm & Hass Co., US)
Ultradrur (BASF, DE)		Mindel (Amoco Performance Products, US)	Rynite (Du Pont de Nemours, US)
11. Polyetheretherketone			
		(PEEK)	
		Victrex PEEK (ICI, UK)	
12. Polysulphone			
U. Polysulphone		Stabar (ICI, UK)	Udel (Amoco Performance Products, US)
Sumilik FST (Sumitomo, Chem. Co., JP)			

References

- Black, J. (ed.) (1992), in *Biological Performance of Materials: Fundamentals of Biocompatibility*, Second edition, Marcel Dekker, Inc, New York.
- Brydson, J.A. (ed.), *Plastics Materials*, Butterworths Scientific, fourth edition, 1982; fifth edition, 1989.
- Carhart, R.O. (1985) Polycarbonate, in *Engineering Thermoplastics, Properties and Applications*, Margolis, J.M. (ed.), Chapter 3, pp. 29–82..
- Chapman, R.D. and Chroma, J.L. (1985) Nylon plastics, in *Engineering Thermoplastics, Properties and Applications*, Margolis J.M. (ed.), pp. 83–122.
- Charrier, J.M. (ed.) (1990) *Polymeric Materials and Processing: Plastics, Elastomers and Composites*, Hanser.
- Dominghaus, H. (ed.) (1993) *Plastics for Engineers, Materials Properties, Applications*, Car-Hanser Verlag.
- Goodman, S.B. and Fomasier, V.L. (1992) Clinical and experimental studies in the biology of aseptic loosening of joint arthroplasties and the role of polymer particles, in *Particulate Debris from Medical Implants: Mechanisms of Formation and Biological Consequences*, ASTM ATP 1144, K.R St John, (ed), American Society for Testing and Materials, Philadelphia, pp. 27–37.
- Harper, C.A (eds) (1992) *Handbook of Plastics, Elastomers, and Composites*, McGraw-Hill.
- How, T.V. (1992) Mechanical properties of arteries and arterial grafts, in *Cardiovascular Biomaterials*, Hastings, G.W. (ed.), Springer-Verlag, London, pp.1–35.
- Jones, A.J. and Denning, N.T. (1988) in *Polymeric Biomaterials: Bio- and Eco-compatible Polymers, A Perspective for Australia*, Department of Industry, Technology and Commerce.
- Lilley, P.A, Blunn, G.W., and Walker, P.S. (1993) Wear performance of PEEK as a potential prosthetic knee joint material, in *7th International Conference on Polymers in Medicine and Surgery*, 1–3 September 1993, Leeuwenhorst Congress Center, Noordwijkerhout, The Netherlands, pp. 320–326.
- Margolis, J.M. (1985) *Engineering Thermoplastics: Properties and Applications*, Dekker, New York.
- Mascia, L. (1989), in *Thermoplastics: Materials Engineering*, Second Edition, Elsevier Applied Science, London and New York.
- McMillin, C.R (1994) Elastomers for biomedical applications, *Rubber Chem. and Tech.* **67**, 417–446.
- Park, J.B. and Lakes, R.S. (1992) *Biomaterials, an Introduction*, Second Edition, Plenum Press, New York and London.
- Rubin, I.I. (ed.) (1990), *Handbook of Plastic Materials and Technology*, John Wiley & Son.
- Staudinger, H. (1932) *Die Hochmolekularen Organischer Verbindungen*, Julius Springer.
- Stokes, K., McVenes, R., and Anderson, J.M. (1995) Polyurethane elastomer biostability, *J. Biomaterials Applications*, **9**, 321–355.
- Szycher, M. (1991) in *Blood Compatible Materials and Devices: Perspectives Towards the 21st Century*, Sharma, C.P. and Szycher, M. (eds), Technomic Publishing CO., Inc., Lancaster, Basel, pp. 33–85.
- Teoh, S.H., Lim, S.c., Yoon, E.T., and Goh, K.S. (1994a) A new method for *in vitro* wear assessment of materials used in mechanical heart valves, in *Biomaterials Mechanical Properties*, ASTM STP 1173, H.E. Kambic and AT. Yokobori, Jr. (eds), American Society for Testing and Materials, Philadelphia, pp.43–52.
- Teoh, S.H., Martin, R.L., Lim, S.c., et al. (1990) Delrin as an occluder material, *ASAIO Transactions*, **36**, M417–421.
- Watson, M., Cebon, D., Ashby, M., Charlton, C., and Chong, W.T. (eds) (1994) *Cambridge Materials Selector V2.02*, National University of Singapore, Granta Design Ltd.
- Wenz, L.M., Merritt, K., Brown, S.A, and Moet, A (1990) In-vitro biocompatibility of polyetheretherketone and polysulphone composites, *J. Biomed. Mater Res.*, **24**, 207–215.
- Ziegler, K.E. (1955) *Angew. Chem.* **67**(426),541.

Chapter 4

Biomedical elastomers

J.W. Boretos and S.J. Boretos

4.1 Introduction

Elastomers are described as materials that possess pronounced elasticity and rebound. They can be tough, relatively impermeable to air and water and exhibit resistance to cutting, tearing and abrasion. Often they are modified by compounding to increase their hardness and strength. Or, conversely, they can be soft, compliant and absorbent to water if the need exists. In some instances their properties can closely simulate that of the tissues which they must contact. As biomedical materials they may have originated from commercial formulations or been custom designed from basic chemistry. Those that have been judged as biocompatible have made significant contributions towards the development of successful medical devices. Literally, every basic elastomer has been evaluated at some time for its possible suitability in contact with the body. This would include such materials as natural rubber, styrene rubber, polybutyl rubber, silicone rubber, acrylate rubber, Hypalon[®], polyurethanes, fluorinated hydrocarbon rubbers, polyvinyl chloride, thermoplastic vulcanizates and others. Of these, only special medical grade formulations of silicone, polyurethane, polyvinyl chloride and thermoplastic elastomer have continued to be commercially successful.

There are important differences between materials and differences among similar materials within a given generic class. These differences are due to the chemical composition of the polymer, the molecular configuration of the polymer and the presence of functional groups. For instance, polyurethanes of a polyester base were initially tried and found unstable for implantation whereas polyether based polyurethanes were decidedly more stable. Elastomers with aromatic structures behave differently than the polymer having aliphatic structure. Not every material is suitable

J.W. Boretos (✉) • S.J. Boretos
Consultants for Biomaterials, 6 Drake Court, Rockville, Maryland 20853, USA

for every application. Some have been found to perform successfully under static conditions but fail or perform undesirably under dynamic situations. Often, the design of a device and the demands upon it will determine if the elastomer chosen is the proper selection. Therefore the material and its use are inseparable. They must be evaluated together. Merely passing an array of physical and biological tests do not confer success. Biocompatibility is an essential element of medical grade elastomers. A set of compatibility tests determine the general physiological acceptability of an elastomer. These consist of passing USP Class VI tests. Additional testing may be required depending upon the device, its area of application and the time it is in contact with tissues. A Master File is often registered by the manufacturer of the basic elastomer with the FDA to attest to its properties, composition and response to biological testing. Demands on medical device manufacturers have never been more stringent. Regulatory pressures, more indepth testing, the threat of litigation plus the constraints of health care cost containment are affecting all aspects of the design and development process and the availability of some biomedical elastomers. A variety of elastomeric materials are available to meet the design challenges presented by medical devices. However, there is still a need for even better materials.

The elastomers that are listed here should be considered in light of their suitability for a specific application. The properties tables should serve as a guide to design options for those in the early stages of the development process. Keep in mind that these properties listed in the tables and the compatibility standings are only indicative of the performance characteristics that an elastomer may exhibit.

4.2 Types of Elastomer

Biomedical elastomers can be classified as to whether they are thermoplastic or thermosetting in nature. Thermoplastic biomedical elastomers are gaining in commercial importance and in some cases replacing traditionally used vulcanized versions. Thermosetting elastomers are irreversibly crosslinked and have had the longest history of medical use. Both groups will be described citing representative medical elastomers that are either commercially available or that may replace elastomers that have been recently withdrawn from the market.

4.2.1 Thermoplastic elastomers

Thermoplastic elastomers (TPEs) are a special class of materials that process similarly to other thermoplastic polymers, yet possess many of the desirable properties of thermoset elastomers. Some TPEs are elastomeric alloys consisting of cross-linked particles of rubber surrounded by a thermoplastic matrix. Others consist of block copolymers and are typified by polyurethanes and styrene polymers.

Depending upon which thermoplastic elastomer is chosen, physical properties can vary over a wide range. They can be either hard, or soft, flexible or stiff, elastic or rigid. For the most part, they are smooth to the touch, yet will form tight seals to surfaces they contact. They can be processed using conventional techniques and equipment and in automated modes. Medical applications consist of such examples as pacemaker lead wire coatings, artificial hearts, and catheters. A wide variety of sundry uses have contributed to patient care and consists of bulbs and bladders, serum caps and tubes, cushions, diaphragms, electrical connectors, flexible medical wire coatings, gaskets, needle shields, pharmaceutical closures, seals, stoppers, tubing, and valves. Most of the TPEs can be sterilized using gas, steam and radiation with very little change in their molecular structures or properties (Table 4.13).

Thermoplastic vulcanizates

Thermoplastic vulcanizates are a separate class of thermoplastic elastomers (TPEs) with Santoprene® as the representative biomedical elastomer.

Santoprene®

This thermoplastic vulcanizate is an olefin based elastomer; an elastomeric alloy. It is totally synthetic and does not contain any natural rubber thereby avoiding many of the allergic reaction problems associated with natural rubber latex. It exhibits outstanding flex-fatigue resistance, low temperature flexibility (-40 °C) and resistance to tearing and abrasion. Its resistance to plastic deformation under tensile and compression stress is another of its features. Santoprene® is reported to be superior to natural rubber in some situations and replaces silicone elastomers in others. It has found use in peristaltic pump tubing, syringe plungers, seals, and caps, tracheal and enteral tubing, vial closures and pump seals, disposable anesthetic hoses, intravenous delivery systems, and other hospital devices. Santoprene® has met USP Class IV requirements for *in vivo* biological reactivity and conforms to the Tripartite Biocompatibility Guidance standards. However, the manufacturer does not recommend Santoprene® for use as part of human implants. The material may be injection molded, extruded, blow molded and thermoformed. For details on physical properties, processing and biocompatibility see Tables 4.1, 4.2, 4.13 and 4.14.

Copolyester ether elastomer

Ecdel™

This copolyester ether TPE is essentially polycyclohexanedimethylcyclohexanedicarboxylate (PCCE). It is reported to possess the chemical resistance, toughness and inertness yet exhibits elastic flexibility over a broad temperature range. Ecdel™ is an unusual elastomer since it has a crystalline structure. Quenching during molding can reduce its crystallinity and impart increased clarity. The material is being used for uniquely designed intravenous bags with built-in bottle necks and fasteners. The material can be injection or blow molded and extruded into film or sheet; but only Ecdel™ 9967 may be processed into tubing. This TPE is also manufactured under the name CR3 by Abbott Labs (Tables 4.2, 4.12, 4.13, and 4.14).

Polyurethane-based elastomers

Polyurethanes are another class of TPEs. They are a large family of chemical compounds that can consist of ether-based, ester-based, polycarbonate-based or polypropylene-based varieties. A number of copolymers are also included; polyurethanes are combinations of macroglycols and diisocyanates that have been polymerized into tough and elastic materials. TPE polyurethanes have been used for peristaltic pump tubing, parenteral solution tubing and catheters. The tables list the majority of those that are commercially available. Among others are those either of limited supply, available for proprietary use only or that have been successful, but recently discontinued such as:

- Hemothane Sarns Div. of 3M. Restricted to proprietary use.
- Biomer Ethicon, Inc. No longer available through this source.
- Surethane Cardiac Control Systems, Inc. Redissolved Lycra® thread. Some formulations may have a few percent PDMS blended with it. Limited availability.
- Pellethane™ 2360 Dow Chemical, USA. This material is no longer available for medical implant use (see also Pellethane™).
- Angioflex ABIOMED, Danvers, Mass. Restricted to proprietary use.
- Cardiothane Kontrol, Inc. A silicone-urethane interpenetrating polymer network. Limited availability.

Internationally, polyurethanes for medical use have been developed by Italy, China and Japan.

Biospan®

This TPE is a segmented polyurethane and is reported to be not significantly different from biomer in chemistry and molecular weight. It is a polytetra-methyleneoxide-based aromatic polyurethane urea with mixed aliphatic and cycloaliphatic diamine chain extenders. A copolymer of diisopropylamino-ethyl methacrylate and decyl methacrylate are added as a stabilizer. The material is supplied as 25% solids in dimethyl acetamide solvent (Tables 4.3, 4.12, 4.13, and 4.14).

Biospan®-S

This is a silicone modified analog of Biospan® with a different stabilizer. It possesses a silicone-rich surface to enhance thromboresistance while maintaining the bulk properties of Biospan® (Tables 4.3, 4.12, 4.13, and 4.14).

Biospan®-D

This is another version of Biospan® with surface modification by an oligomeric hydrocarbon covalently bonded to the base polymer during synthesis. The additive has a pronounced effect on the polymer surface chemistry but little effect on the bulk properties of the base polymer according to the manufacturer (Tables 4.3, 4.12, 4.13, and 4.14).

Table 4.1 Typical Properties of Thermoplastic Vulcanizates

Product and Manufacturer	Product no.	Property							
		Specific gravity	Durometer hardness shore	Tensile strength, psi	Elongation, percent	Modulus ASTM D-412	Tear strength pli.,die C	Compression set, percent	
Santoprene® Rubber,	281-45	0.97	45A	435	300	psi	ASTM D-624	ASTM D-395	
	281-55	0.97	55A	640	330	175	80	11	
	281-64	0.97	64A	1,030	400	250	108	23	
Advanced Elastomer Systems	281-73	0.98	73A	1230	460	340	140	23	
	281-87	0.96	87A	2,300	520	520	159	26	
	283-40	0.95	40 D	2,750	560	1,010	278	29	
						1,250	369	32	

Table 4.2 Typical Properties of Copolyester Elastomers, PCCE

Product and Manufacturer	Product no.	Property						
		Specific gravity	Durometer hardness shore	Tensile strength, psi	Elongation, percent	Modulus ASTM D-412	Tear strength pli, die B	Compression set, percent
Ecdel™	9965	ASTM D-792	ASTM D-2240	ASTM D-412	ASTM D-412	psi	ASTM D-624	ASTM D-395
Elastomer,	9966	1.13	95 A	3,500	380	16,000	100	40
Eastman Chemical Co.	9967						135	

Table 4.3 Typical Properties of Polyurethane-based Elastomers

Product and Manufacturer	Product no.	Specific gravity	Durometer hardness shore	Tensile strength, psi	Elongation, percent	Modulus		Tear strength pli, die C	Compression set, percent
						ASTM D-412	psi		
Biospan segmented polyurethane, The Polymer Technology Group, Inc.	Biospan®	ASTM D-792	75A	ASTM D-412	ASTM D-412	psi	%	ASTM D-624	ASTM D-395
	Biospan® D		70 D	6000	850	575	100		
	Biospan® S		70 D	6000	1000	550	100		
				5500	1050	450	100		
Hydrothane™, Poly Medica Biomaterials, Inc.	Dry		93 A	7800	580				
	Very dry		95 A	5800	475				
	Wet		85 A	5600	500				
	MF-5000	1.15	50 A	3000	500	300	100		
	MF-5001	1.15	55 A	3000		300	100		
	MF-5040	1.15	60 A	5000	700	300	100		
	MF-5041					300	100		
	MF-5056	1.15	65 A	5000	750	500	100		
	MF-5057					550	100		
	MF-5062	1.14	60 A	5000	800	500	100		
	2363-55D	1.15	55 D	6900	390	2500	100	650	25
	2363-55DE	1.15	53 D	6500	450	2300	100	600	30
	2363-65D	1.17	62 D	6460		2900	100	1100	30
	2363-75D	1.21	76 D	5810	380		1470		
	2363-80A	1.13	81 A	5200	550	880	100	470	25

(continued)

Table 4.3 (continued)

		Property							Modulus ASTM D-412	Tear strength pli, die C	Compression set, percent
		Specific gravity	Durometer hardness shore	Tensile strength, psi	Elongation, percent						
Dow Chemical Co.	2363-80AE	1.12	85 A	4200	650	890	100	420	30		
	2363-80A	1.30	81 A	6860	670	970	100				
	R0120										
	2363-90A	1.14	90 A	5850	500	1700	100	570	25		
	2363-90AE	1.14	90 A	6000	550	1475	100	540			
PolyBlend™	PB1000-650		65 D to 75	D6500	350	5300	100	-	-		
1000 and	PB1100-55	1.02	55 A	2150	800	135	100	140	55-66		
PolyBlend™	PB1100-60	1.02	60 A	2400		210	100	150	50-60		
1100,											
Poly Medica	PB1100-75	1.02	75 A	3250	575	420	100	240	45-50		
Biomaterials, Inc.	PB1100-80	1.02	80 A	4600	590	555	100	330	25-30		
	EG60D	1.09	51 D	7829	363	2000	100				
Tecoflex®	EG60D-B20	1.32	55 D	7484	370						
	EG65D	1.10	60 D	8074	335	2500	100				
	EG65D-B20	-	63 D	6986	321						
Thermedics, Inc.	EG68D	1.10		8686	332						
	EG72D	1.11	67 D	7739	307	3400	100				
	EG80A	1.04	72 A	5640	709	400	100				
Thermedics, Inc.	EG80A-B20	1.24	73 A	5571	715						
	EG85A	1.05	77 A	6935	565	700	100				
	EG85A-B20	1.25	83 A	5282	632						
	EG85A-B40	1.51	84 A	5093	559						
	EG93A	1.08	87 A	7127	423	1100	100				

	EG100A	1.09	94 A	8282	370	1800	100		
	EG100A-B20	1.29	93 A	7104	369				
	EG100A-B40	1.54	96 A	5607	360				
	1055D	1.16	54 D	9600	350	2500	100		
	1065D	1.18	64 D	10 000	300	3200	100		
	1074A	1.10	75 A	6000	530	530	100		
	1075D	1.19	75 D	8300	240	3600	100		
	1085A	1.12	85 A	7000	450	800	100		
	1095A	1.15	94 A	9400	400	1600	100		
	2055D	1.36	55 D	9000	360	2700	100		
	2065D	1.38	67 D	8500	300	3100	100		
	2074A	1.30	77 A	5500	580	510	100		
	2075D	1.40	77 D	7600	230	3000	100		
	2085A	1.32	87 A	6600	550	800	100		
	2095A	1.35	97 A	8200	450	1600	100		
	5187	1.20	87 A	6000	500	750	100	500	12
	5265	1.17	65 D	6000	460	3300	100	1200	20
	5286	1.12	86 A	6000	550	700	100	500	16
	5370	1.21	70 D	6000	180	4500	100	900	
	DP7-3002		88 A	2208	579	815	100	399	—
	DP7-3003	—	50 D	3714	458	1049	100	564	
	DP7-3004		55 D	4783	392	1766	100	819	

Table 4.4 Typical Properties of Polycarbonate-based Polyurethane

	Product no.	Specific gravity	Durometer hardness shore	Tensile strength, psi	Property			Tear strength pli, die C
					Elongation, percent	Modulus ASTM D-412	%	
Product and Manufacturer		ASTM D-792	ASTM D-2240	ASTM D-412	ASTM D-412		ASTM D-624	
	PC-3555D	1.15	60 D	7000	350	1500	100	
Carbothane™	PC-3555D-B20	1.36	57 D	8300	380	1600	100	
	PC-3572D	1.15	71 D	8500	300	4100	100	
Thermedics, Inc.	PC-3572D-B20	1.35	71 D	8400	310	3400	100	
	PC-3575A	1.15	73 A	4400	500	380	100	
	PC-3575A-B20		73 A	3500	600	410	100	
	PC-3585A	1.15	84 A	6500	390	640	100	
	PC-3585A-B40	1.68	89 A	3800	521	700	100	
	PC-3595A	1.15	95 A	6500	520	900	100	
	PC-3595A-B20	1.36	96 A	8300	390	1100	100	
Chronoflex™	Chronoflex™		70 A	7500	500	700	100	
AR, Poly Medica Bio-materials, Inc.	AR							
Corethane®	TPE 55D	1.211	55 D	7000-8500	365-440	1850-2200	100	
and	TPE 75D	1.216	75 D	7000-9100	255-320	5300-5700	100	
	TPE 80A	1.179	80 A		400-490	770-1250		
Corthesive™, Corvita Corp.	Corthesive™ (cured)	1.179	80 A	6500-7500	400-900	770-1250	100	
Texin™ 5370, 5370 Miles, Inc.		1.21	70 D	6000	180	4500	900	

Table 4.5 Typical Properties of Polypropylene-based Elastomers

		Property					
Product and Manufacturer	Product no.	Specific gravity	Durometer hardness shore	Tensile strength, psi	Elongation, percent	Tear strength pli, die B	Compression set, percent
		ASTM D-792	ASTM D-2240	ASTM D-412	ASTM D-412	ASTM D-624	ASTMD-395
Sarlink®	3260	0.95	60 A	870	619	183	42
medical grade							
DSM Thermoplastic							
Elastomers, Inc.							

Hydrothane™

Hydrothane™ is a TPE hydrogel belonging to the polyurethane family of polymers. Hydrothane™ is an aliphatic material with water absorption capabilities ranging from 5 to 25% by weight while still maintaining high tensile strength and elongation. Because of its water absorption capacity, Hydrothane™ is reported to be bacteria-resistant and lubricious. The polymer can be processed by conventional extrusion and injection molding techniques. It can also be dissolved in dimethyl acetamide solvent to produce a 25% solids solution suitable for dip-coating and other solution processing techniques (Tables 4.3, 4.12, and 4.13).

Medicaflex™

The Lambda series of Medicaflex is a polyurethane-based TPE polymer that exhibits low modulus characteristics with high tear strength and abrasion resistance. Those listed in the tables have passed USP Class VI compatibility tests and have been used as replacements in some natural rubber latex and silicone rubber applications. The polymer has been applied to uses such as catheters, tubing and films where softness, low durometer hardness, low modulus or high elongation are needed (Tables 4.3, 4.12, and 4.13).

Pellethane™ polyurethane elastomers

The 2363 series Pellethane™ TPE elastomers have a wide range of durometer hardness and are noted for their high tensile and tear strength and abrasion resistance. Chemically they are classed as polytetramethylene glycol ether polyurethanes. The ether series is the most widely used for medical applications although polyester versions of Pellethane™ are useful for some applications. None of these polymers have the disadvantage of containing plasticizers which can migrate out of the polymer over time resulting in reduction in physical properties. Medical tubing made from Pellethane™ polymer is widely used. These TPEs are unaffected by ethylene oxide gas, gamma radiation and electron beam sterilization procedures. Pellethane™ can be processed by injection molding and extrusion. For details on physical properties, processing and biocompatibility (Tables 4.3, 4.12, and 4.13).

Table 4.6 Typical Properties of Plasticized Polyvinyl Chloride

		Property					
Product and Manufacturer	Product no.	Specific gravity	Durometer shore	Tensile strength, psi	Elongation, percent	Modulus	
		ASTM D-792	ASTM D-2240	ASTM D-412	ASTM D-412	ASTM D-412	psi
	3511TX-02	1.12	35 A	1110	525	235	100
Elastichem™	4011TX-02	1.16	40 A	1300	500	266	100
PVC,	5011TX-02	1.16	50 A	1650	465	426	100
Colorite	5511TX-02	1.18	55 A	1790	465	455	100
Plastics Co.	6011TX-02	1.18	60 A	1936	465	488	100
	7011TX-02	1.21	70 A	2667	400	952	100
	7511TX-02	1.22	75 A	3000	360	1400	100
	8011TX-02	1.23	80 A	3646	330	2025	100
	0-1234	1.21	58 A	1400	400	600	100
Ellay™ PVC,	0-1290	1.26	83 A	2750	275	1500	100
	0-1541	1.23	81 A	2400	300	1400	100
	0-1554	1.21	70 A	2000	400	950	100
Ellay, Inc.	0-2112	1.24	82 A	2650	320	1200	100
	0-2129	1.24	83 A	2670	310	1500	100
	0-2202	1.54	75 A	2360	270	1190	100
	0-2609	1.20	68 A	1950	410	800	100
	0-2610	1.24	83 A	2460	295	1450	100
	0-2623	1.24	82 A	2550	325	1350	100
	0-2631	1.19	65 A	1800	390	650	100
	0-3110	1.22	74 A	2100	355	1000	100
	0-3115R	1.20	68 A	1900	400	800	100
	0-3119	1.22	75 A	2150	350	1100	100
	0-3138R	1.22	75 A	2200	350	1075	100
	0-3140R	1.25	87 A	2850	330	1600	100
	0-3147	1.28	95 A	3100	250	2350	100
	0-3149R	1.23	78 A	2400	340	1150	100
	0-3154	1.19	65 A	1750	410	725	100
	0-3155R	1.20	68 A	1850	390	780	100
	0-3166R	1.25	85 A	2700	320	1650	100
	0-3195	1.27	90 A	2950	280	2210	100
	0-3200	1.18	60 A	1600	450	525	100
Ellay™ PVC,	0-3201	1.21	70 A	2000	340	800	100
	0-3224R	1.21	77 A	2300	345	1100	100
	0-3231R	1.26	88 A	3000	280	1800	100
Ellay, Inc.	0-4106R	1.25	85 A	2650	300	1600	100
	0-4108	1.25	85 A	2750	300	1600	100
	0-4109R	1.25	85 A	2800	310	1700	100
	0-4113	1.31	100 A	3960	184	3200	100

(continued)

Table 4.6 (continued)

		Property					
Product and Manufacturer	Product no.	Specific gravity	Durometer shore	Tensile strength, psi	Elongation, percent	Modulus	
		ASTM D-792	ASTM D-2240	ASTM D-412	ASTM D-412	ASTM D-412	psi
	0-4114	1.20	67 A	1900	400	780	100
	0-4115	1.26	87 A	2800	295	1650	100
	0-4116R	1.27	90 A	2950	265	2100	100
Ellay, Inc.	0-4120	1.21	68 A	2180	400	830	100
	0-4121	1.23	81 A	2550	325	1400	100
	0-4122	1.33	110 A	4500	135	4180	100
	0-4124R	1.28	95 A	3050	250	2200	100
	0-4125	1.24	80 A	3150	355	1310	100
	0-4129	1.18	63 A	1670	430	620	100
	0-4132	1.21	70 A	2000	395	900	100
	0-4135	1.23	80 A	2550	320	1260	100
	0-4140	1.23	80 A	2500	330	1250	100
	0-4150	1.26	88 A	2900	290	2200	100
	0-5210C	1.26	82 A	2300	225	1250	100
	BB-69	1.23	78 A	2200	340	1150	100
	EH-222C	1.21	70 A	2050	365	1100	100
	ES-2967ZPH	1.22	75 A	2300	360	1200	100
Geon® PVC,	121AR	1.4		2800	380		
	213	1.4		2205	379	1010	100
B. F. Goodrich Co.	250x100						
				1700-1850	430-460	400-500	100
Multichem™ PVC,	6014	1.15	60 A	1640	540	400	100
	7014	1.19	70 A	2040	600	625	100
Colorite	8014	1.22	80 A	2100	500	1000	100
Plastics Co.	8514	1.24	85 A	2250	530	880	100
	3300-45 NT	1.13	45 A	1100	480	325	100
Teknor™ PVC,	3300-50 NT	1.14	50 A	1220	460	370	100
	3300-55 NT	1.16	55 A	1500		520	100
	3300-60 NT	1.17	60 A	1550	450	560	100
Teknor Apex Co.	3300-68 NT	1.18	68 A	1850	430	690	100
	3300-75 NT	1.20	75 A	2150	420	900	100
	3300-80 NT	1.21	80 A	2400		1,320	100
	3300-85 NT	1.23	85 A	2800	380	1,560	100
	3300-90 NT	1.25	90 A	3100	340	2,100	100
	3310-50 NT	1.35	50 A	1000	430	330	100
	3310-55 NT	1.35	55 A	1100	410	400	100
	3310-60 NT	1.35	60 A	1300	400	480	100

(continued)

Table 4.6 (continued)

		Property					
Product and Manufacturer	Product no.	Specific gravity	Durometer shore	Tensile strength, psi	Elongation, percent	Modulus	
		ASTM D-792	ASTM D-2240	ASTM D-412	ASTM D-412	ASTM D-412	psi
	3310-65 NT	1.35	65 A	1500	390	590	100
	3310-70 NT	1.35	70 A	1770	380	700	100
	3310-75 NT	1.35	75 A	1900	370	800	100
	3310-80 NT	1.35	80 A	2200	360	1,050	100
	3310-85 NT	1.35	85 A	2500	340	1,470	100
	3310-90 NT	1.35	90 A	2900	330	1,900	100
Teknor Apex Co.	90A471R-60NT	1.16	60 A	1500	450		
	90A471R-65NT	1.17	65 A	1750	440		
	90A471R-70NT	1.18	70 A	1900	430		
	90A471R-75NT	1.20	75 A	2150	420		
	90A471R-80NT	1.23	80 A	2690	380		
	90A471R-85NT	1.23	85 A	2800			
	90A471R-90NT	1.27	90 A	3350	360		

Notice Regarding Long-Term Medical Implant Applications

The Dow Chemical Company does not recommend Pellethane™ elastomers for long-term medical implant applications in humans (more than 30 days). Nor do they recommend the use of Pellethane™ elastomers for cardiac prosthetic devices regardless of the time period that the device will be wholly or partially implanted in the body. Such applications include, but are not limited to, pacemaker leads and devices, cardiac prosthetic devices such as artificial hearts, heart valves, intra-aortic balloon and control systems, and ventricular bypass assist devices. The company does not recommend any non-medical resin (or film) product for use in any human implant applications.

PolyBlend™ polyurethane

This TPE has been described as an aromatic elastoplastic polyurethane alloy. It possesses a low coefficient of friction, low extractables, and dimensional stability. Hardness ranges from 65 to 75 Shore D. The material is classified for short-term (29 days or less) implantation. Clear and radiopaque formulations are available. Tubing should be annealed at 80°C for four hours to reduce crystallinity (Tables 4.3, 4.4, 4.12, and 4.14).

Tecoflex® polyurethane

Tecoflex is an aliphatic polyether-based polyurethane that is available in clear and radiopaque grades. They are reaction products of methylene bis (cyclohexyl) diisocyanate (HMDI), poly (tetramethylene ether glycol) (PTMEG), and 1,4 butane diol chain extender. The manufacturer claims that the aliphatic composition of Tecoflex®

eliminates the danger of forming methylene dianiline (MDA) which is potentially carcinogenic. MDA can be generated from aromatic polyurethanes if they are improperly processed or overheated. Tecoflex has been reported to crack under stress when implanted, long-term, in animals. An advantage of Tecoflex is that it softens considerably within minutes of insertion in the body. This feature can offer patient comfort for short-term applications such as catheters and enteral tubes; it is also reported to reduce the risk of vascular trauma (Tables 4.3, 4.12, and 4.13).

Tecothane[®]

Tecothane[®] is an aromatic polyether-based TPE polyurethane polymer. It has processibility and biocompatibility characteristics similar to Tecoflex[®] except that it is an aromatic rather than an aliphatic polyurethane. Tecothane[®] is synthesized from methylene diisocyanate (MDI), polytetramethylene ether glycol and 1,4 butanediol chain extender. By varying the ratios of the reactants, polymers have been prepared ranging from soft elastomers to rigid plastics. The manufacturer of Tecoflex[®] and Tecothane[®] point out that there is not much difference between medical-grade, aliphatic and aromatic polyether-based polyurethanes with regard to chemical, mechanical and biological properties. However, they caution that with improper processing of Tecothane[®] (e.g., high moisture content or steam sterilization) it is possible to form measurable amounts of methylene dianiline (MDA), a listed carcinogen. The use of ethylene oxide or gamma radiation are suitable sterilizing agents that do not affect the chemical or physical properties (Tables 4.3, 4.12, and 4.13).

Texin[™]

There are four basic polymer formulations of Texin polyurethane TPE that may be suitable for medical applications. They range in hardness and flexural modulus. Texin elastomers are produced by the reaction of diisocyanate with a high molecular weight polyester or polyether polymer and a low molecular weight diol. The polyethers (products 5286 and 5265) offer greater hydrolytic stability and stress crack resistance. The polyesterbased polyurethane (product 5187) and the polyester polyurethane/ polycarbonate blend (product 5370) possess high impact strength and high stiffness along with useful low-temperature properties. Texin is not recommended for implants of greater than 30 days duration. Texin should not be sterilized by autoclave or use of boiling water. Other advantages offered by Texin TPUs are that plasticizers are not necessary to achieve flexibility, the amount of extractables are low, and they possess high tensile strength, high tear strength, and high abrasion resistance. Texin polyurethanes are hydroscopic and will absorb ambient moisture. They can be processed by extrusion and injection molding if thoroughly dried beforehand. As with all chemical systems, the proper use and handling of these materials can not be over-emphasized (Tables 4.3, 4.12, and 4.13).

Texin[™] 5370 is a blend of polyester-based polyurethane and polycarbonate. It offers high impact strength and high stiffness. Steam sterilization or boiling should be avoided (Tables 4.3, 4.12, and 4.13).

Table 4.7 Typical Properties of Styrene-based Thermoplastic Elastomers

Product and Manufacturer	Product no.	Property							
		Specific gravity	Durometer hardness shore	Tensile strength, psi	Elongation percent	Modulus ASTM D-412	Tear strength pli, die B	Compression set, percent	
C-Flex [®] ,	R70-001	ASTM D-792	ASTM D-2240	ASTM D-412	ASTM D-412	psi	%	ASTM D-624	ASTM D-395
	R70-003	0.90	50	1200	900	150	100		16
	R70-005	0.90	70	1280	760	340	100		25
	R70-026	0.90	30	1400	950	100	100		11
	R70-028	0.90	90	1830	650	1,010	100		
Consolidated Polymer	R70-046	0.90	35	990	800	120	100		13
	R70-050	0.90	34	1320	940	110	100	135	12
Technologies, Inc.	R70-051	0.90	48	1250	880	170	100	100	18
	R70-051	0.90	74	1140	680	370	100	150	28
	R70-058	0.94	70	2080	660	300	100	120	55
	R70-057	0.92	40	1220	890	100	100	90	33
	R70-068	0.93	50	1630	850	140	100	110	38
	R70-072	0.90	60	1270	780	240	100		20
	R70-081	0.90	45	1440	920	120	100		17
	R70-082	0.90	61	1270	860	230	100	130	19
	R70-085	0.90	50	1380	750	200	100		17
	R70-089	0.90	45	1640	700				
	R70-091	0.90	50	1280	780	130	100		
	R70-116	0.90	30	1105	810	100	100	84	24
	R70-190	0.90	5	270	1010	20	100		
R70-214	0.90	18	450	780					
D-2103	0.94	70	4300	880	400	300	205		

Kraton®,	D-2104	0.93	27	A	1700	1350	200	300	180	
	D-2109	0.94	44	A	950	800	300	300	160	
Shell	G-2701	0.90	67	A	1600	800	480	300	260	
Chemical	G-2703	0.90	63	A	1200	670	470	300	230	
Co.	G-2705	0.90	55	A	850	700	400	300	140	38
	G-2706	0.90	28	A	850	950	130	300	140	
	G-2712	0.88	42	A	840	820	250	300	140	

Polycarbonate-based polyurethanes

Carbothane™

This medical grade TPE polyurethane is the reaction product of an aliphatic diisocyanate, a polycarbonate-based macrodiol, and a chain terminating low molecular weight diol (Tables 4.4, 4.12, and 4.13).

ChronoFlex™ AR.

Available as a dimethyl acetamide solution, this segmented, aromatic, polycarbonate-based TPE polyurethane was designed to mimic Ethicon Corporation's Biomer. The polymer is made from the addition of diphenylmethane 4,4'-diisocyanate to a polycarbonate diol followed by addition of a mixture of chain extenders and a molecular weight regulator. The polymer is believed to be resistant to environmental stress cracking such as that experienced by other polyurethanes coated onto pacemaker leads (Tables 4.4, 4.12, and 4.13).

Coremer™

Specifically designed as an 80 Shore A durometer TPE, this is a diamine chain extended version of Corethane®. Coremer™ solution cast films have a low initial modulus and high flex fatigue life. Information as to long-term biostability is not available at this time (Tables 4.4 and 4.13).

Corethane®

A polycarbonate TPE polyurethane that claims biostability is achieved through its replacement of virtually all ether or ester linkages with carbonate groups. The soft segment is composed of a polycarbonate diol formed by the condensation reaction of 1,6-hexanediol with ethylene carbonate. The polycarbonate diol is converted to a high molecular weight polyurethane by the reaction with 1,4-methylene bisphenyl diisocyanate (MDI) and 1,4-butanediol. It is reported to be resistant to environmental stress cracking as experienced with insulation on pacemaker lead wires. The polymer can be extruded, injection molded or compression-molded, and can be bonded with conventional urethane adhesives and solvents (Tables 4.4, 4.12, 4.13, and 4.14).

Corhesive™

Corhesive™ is a solvent-free, two-component reaction adhesive system for use with polyurethanes, plasma treated silicones and certain metals (Tables 4.4, 4.12, 4.13, and 4.14).

Polypropylene-based elastomers Sarlink®

This is a polypropylene-based TPE that has been used as a replacement for medical stoppers previously made from butyl rubber. Sarlink® has the characteristics typical of rubber vulcanizates such as elasticity, flexibility, high coefficients of friction and softness. Sarlink® combines gas impermeability without concern for contamination of biological medium. Applications for medical grade Sarlink® are inserts on syringe plungers, reusable injection caps, vacuum assisted blood sampling tubes, plus

flexible grade tubing. The number of stoppers produced from Sarlink annually number in the billions. The material can be injection molded, blow molded, extruded, calendered, and thermoformed on standard processing equipment. It can be thermal bonded or adhesive bonded (Tables 4.5, 4.12, and 4.13).

Polyvinyl chloride elastomers

Polyvinyl chloride polymer is polymerized from vinyl chloride monomers. It is a hard material which can be made soft and flexible through the addition of a plasticizer or a copolymer. As such, it resembles an elastomer and can be included with other TPEs. Also optionally added to PVC are fillers, stabilizers, antioxidants and others. A typical PVC plasticizer for medical products is di(2-ethylhexyl) phthalate (also known as dioctyl phthalate, DOP). Some producers of PVC also offer non-phthalate formulations. PVC has been used extensively for blood bags, blood tubing, endotracheal tubes, catheters and fittings, urology tubes, intravenous tubing, respiratory devices and dialysis sets. Leaching of the plasticizer can offer difficulties if the application is not short-term. Medical grade PVC is available from B.F. Goodrich under the name Geon[®] RX, Elastichem[™] PVC, Ellay[™] PVC, Multichem[™] PVC, Teknor[™] PVC, AlphaGary and others. PVC polymers have also been incorporated as additives to polyurethane to alter the properties of the latter.

Elastichem[™] PVC.

This polyvinyl chloride compound family is highly elastomeric and exhibits a dry non-tacky surface even at hardnesses as low as 40 Shore A durometer. Their rubber-like resilience, high elongation and low permanent set and fatigue resistance offer advantages over conventional formulations (Tables 4.6, 4.12, and 4.13).

Ellay[™] PVC.

Compounds from Ellay Corp. are available with Shore hardness ranges from 55 A to 100 A. The polymers have been applied to medication delivery systems, blood collection, processing and storage, gastro-urological devices and collection systems. Product numbers ending in 'R' are special radiation resistant grades (Tables 4.6, 4.12 and 4.13).

Geon[®] PVC.

Geon[®] PVC is associated with vinyl examination gloves. For this use, Geon[®] recommends a combination of Geon[®] 121 AR and 213. For a more 'latex type' feeling, Goodtouch 250x100 is recommended. Typical film samples have passed patch insult tests when worn against the skin for extended periods (Tables 4.6, 4.12 and 4.13).

Multichem[™] PVC

This line of PVC polymers consist of alloys of PVC in combination with other polymers. They display notable dynamic properties and resistance to migration and extraction. These non-toxic PVC compounds (includes Multichem[™] and Elastichem[™]) have over 25 years of experience in the medical field (Tables 4.6, 4.12 and 4.13).

Teknor™ Apex PVC

This extrudable PVC has found use as tubing for blood transport and delivery systems, dialysis and enteral feeding systems, oxygen delivery systems, catheters, and drainage systems. Product numbers containing an R are special radiation resistant grades (Tables 4.6, 4.12 and 4.13).

Styrene-based elastomers

C-Flex®TPE.

C-Flex® thermoplastic elastomers are based on styrene/ethylene-butylene/styrene block copolymers. C-Flex® polymers designated as 'medical grade' are clear and can be processed using conventional extrusion and injection molding equipment. They have been tested using Good Laboratory Practices and have successfully passed USP Class VI, biocompatibility tests. Translucent versions have high rebound values at ultimate elongation. Medical tubing, ureteral stents, blood pumps, feeding tubes and nephrostomy catheters are successful uses of this material (Tables 4.7, 4.12 and 4.13).

Kraton®

Kraton® elastomer consists of block segments of styrene and rubber monomers and are available as Kraton® D and G series. The D series is based on unsaturated mid-block styrene-butadiene-styrene copolymers whereas the G series is based on styrene-ethylene/butylene-styrene copolymers with a stable saturated midblock. Listed among the attributes of both series are such features as low extractables, dimensional stability, vapor and gas transmission properties, ease of sterilization, softness and clarity. They exhibit elastomeric flexibility coupled with thermoplastic processibility (Tables 4.7, 4.12, 4.13).

4.2.2 crosslinked elastomers

Natural rubber

Natural rubber (cis-polyisoprene) is strong and one of the most flexible of the elastomers. The material has been used for surgeon's gloves, catheters, urinary drains and vial stoppers. However, because it has the potential to cause allergic reactions thought to be due to the elution of entrapped natural protein, this elastomer is being used less now than in the past. Safer substitutes are being selected.

Silicone elastomers

Silicone elastomers have a long history of use in the medical field. They have been applied to cannulas, catheters, drainage tubes, balloon catheters, finger and toe joints, pacemaker lead wire insulation, components of artificial heart valves, breast implants, intraocular lenses, contraceptive devices, burn dressings and a variety of

associated medical devices. A silicone reference material has been made available by the National Institutes of Health to equate the blood compatibility of different surfaces for vascular applications. This material is available as a silica-free sheet. Contact the Artificial Heart Program, NHBLI, NIH, Bethesda, Md. for further information.

The silicone elastomers most commonly used for medical applications are the high consistency (HC) and liquid injection molding (LIM) types. The former is most often peroxide cured and the latter platinum cured although there are variations. Both materials are similar in properties. LIM offers greater advantages to the medical device molder and is gaining in popularity. This form of silicone may become the molder's material of choice within the next few years.

High consistency (HC) silicone elastomer

High consistency silicone elastomer consists of methyl and vinyl substituted silicones with aromatic and fluorinated functional groups in some formulations. For the most part, they are peroxide crosslinked. Items are usually compression or transfer molded (Tables 4.8).

Liquid injection molding (LIM) silicone elastomer

Liquid injection molding (LIM) with liquid silicone rubber (LSR) is fast becoming the technique of choice for processing silicone elastomers. Modifications of conventional injection molding equipment are required. For example, pumps to handle two components being injected simultaneously are required. The heaters on the injection barrel and nozzle are replaced by water cooled jackets. The mold is heated in the range of 300 to 400°F. Because the (LSR) flows easily, injection pressures are low (800 to 3000 psi). Elastomeric items cure rapidly in the mold (e.g., a 7 gram part will crosslink in about 15 seconds at 350 °F). Many formulations rely on platinum as a crosslinker. Perhaps in the future, the majority of silicone rubber molded parts will be made in this fashion. Appropriate equipment is commercially available.

Tables 4.8, 4.9, 4.10 and 4.11 list the silicones made by Applied Silicone Corp., Dow Corning Corp., and NuSil Technologies. Table 4.12 lists their biocompatibility status and Table 4.13 recommended sterilization methods. Dow Corning no longer offers the following materials for general sale:

- Silastic MDX 4-4515
- Silastic MDX 4-4515
- Silastic Q7-2245
- Dow Corning Q7-2213

Further, they have discontinued the sale of all implant grade materials.

Other silicones

Silicones and polyurethanes have been used to produce denture liner materials and maxillofacial prostheses. Most of these materials are silicone based, e.g., Flexibase,

Table 4.8 Typical Properties of High Consistency (HC) Silicone Elastomers

		Property				
Product and Manufacturer	Product no.	Specific gravity ASTM D-792	Durometer hardness, shore ASTM D-2240	Tensile strength, psi ASTM D-412	Elongation, percent ASTM D-412	Tear strength pli, die B ASTM D-624
	40039	1.12	35 A	1600	1200	200
Applied Silicone	40040	1.15	50 A	1500	900	220
Medical Implant	40041	1.20	66 A	1200	900	260
Grade,	40042	1.20	78 A	1200	600	280
Applied Silicone	40043	1.12	23 A	1100	1500	160
Corp.	40044	1.12	33 A	1600	1015	150
	40045	1.15	51 A	1400	600	190
	40046	1.20	66 A	1200	500	250
	40063	1.20	70 A	1400	850	280
	MED-2174	1.15	52 A	1200	715	200
NuSil Silicone,	MED-2245	1.13	41 A	1300	700	140
	MED-4515	1.15	52 A	1350	450	90
NuSil Technology	MED 4516	1.21	72 A	1175	370	80
	MED-4735	1.10	35 A	1310	1250	200
	MED 4750	1.15	50 A	1350	810	230
	MED 4755	1.14	57 A	1375	800	300
	MED 4765	1.20	65 A	1100	900	240
	MED-4770	1.17	70 A	1375	700	300
	MDX4-4210	1.10	25 A	550	350	50
Silastic [®]	Q7-4535	1.10	33 A	1200	1015	160
Medical Materials,	Q7-4550	1.14	51 A	1375	600	170
	Q7-4565	1.20	66 A	1000	550	210
Dow Corning	Q7-4720	1.10	23 A	1200	1100	150
Corp.	Q7-4735	1.10	35 A	1050	1200	200
	Q7-4750	1.14	50 A	1300	900	230
	Q7-4765	1.14	50 A	1300	900	230
	Q7-4780	1.22	78 A	850	600	190

Table 4.9 Typical Properties of Liquid Injection Molding (LIM) Silicone Elastomers

Product and Manufacturer	Product no.	Property				
		Specific gravity ASTM D-792	Durometer hardness, shore ASTM D-2240	Tensile strength, psi ASTM D-412	Elongation, percent ASTM D-412	Tear strength pli, die B ASTM D-624
	40023	1.11	10 A	500	750	80
Applied Silicone	40024	1.11	20 A	800	600	140
Medical Implant	40025	1.12	30 A	950	600	150
Grade,	40026	1.12	40 A	980	450	170
Applied Silicone	40027	1.13	50 A	1000	400	190
Corp.	40028	1.13	60 A	1100	350	220
	40029	1.10	30 A	900	300	80
	40071	1.14	70 A	1200	350	220
	40072	1.10	25 A	650	400	60
	40082	1.10	40 A	900	250	110
NuSil Silicone,	MED-6210	1.04	50 A	1000	100	35
	MED-6233	1.03	50 A	1200	300	75
NuSil Technology	MED-6382	1.13	45 A	400	200	
	MED-6820	1.05	40 A	750	125	25
Silastic®	Q7-4840	1.12	40 A	950	425	150
Medical Materials,	Q7-4850	1.14	50 A	1350	550	225
Dow Corning Corp.	Q7-6860	1.16	60 A	1300	450	250

Molloplast-B, Prolastic, RS 330 T-RTV, Coe-Soft, Coe-Super Soft, Vertex Soft, PERform Soft, and Petal Soft. Other custom made elastomers have been applied to maxillofacial prostheses, e.g., Cosmesil, Silastic® 4-4210, Silastic® 4-4515, Silicone A-102, Silicone A-2186, Silskin II, Isophorone polyurethane, and Epithane-3. Denture liners with acrylic and silicone include Coe-Soft, Coe Super-Soft, Vertex Soft, Molloplast-B and Flexibase.

Dispersions

Solvent solutions of polyurethane elastomers and silicone elastomers are given in Table 4.10. These materials are helpful in casting thin films and odd or complex shapes.

Table 4.10 Typical Properties of Elastomeric Dispersions

Product and Manufacturer	Product no.	Specific gravity	Durometer hardness	Property				Tear strength pli, die B
				Tensile strength, psi	Elongation percent	Modulus ASTM D-412	Modulus ASTM	
	40000	1.10	ASTM D-2240 35 A	ASTM D-412 1800	ASTM D-412 800	psi	% 185	ASTM D-624
Applied Silicone	40001	1.18	32 A	1200			200	
Medical Implant	40002	1.08	24 A	800	700		60	
Grade,	40016	1.10	35 A	1800	800		185	
Applied Silicone	40021	1.08	24 A	1000			100	
Corp.	40032	1.19	40 A		500		120	
	MED-2213	1.13	Shore 00,82	1300	700	190	200	140
NuSil Silicone,	MED-6400	1.08	32 A	1250		325	300	150
	MED2-6400	1.08	32 A	1250	800			
NuSil Technology	MED-6600	1.10	20 A	1000		275	300	90
	MED2-6600	1.10	25 A	1000	750	325	300	
	MED-6605	1.08	25 A	900	1000	75	175	100
	MED3-6605	1.08	25 A	900	1000	100	200	125
	MED-6607	1.10	40 A	900	650	-		130
	MED-6640	1.12	30 A	1650	1100	150	100	280
	MED2-6640	1.12	30 A	1750		100	100	275
	MED2-6650	1.15	35 A	1100	750	200	300	
Silastic® Medical Materials, Dow Corning Corp.	Q7-2630	-	Shore 00, 70	800	900	50	200	-

Product no.	Form	viscosity cp.	Solvent System Used	Cure System	Chemical Type
40000	35% solids, 1 part	2000	Xylene	Platinum addition	Methyl vinyl siloxane
40001				Phenyl vinyl	
40002	32% solids, 1 part	500		Acetoxy	siloxane Dimethyl siloxane
40016	27% solids, 1 part	2000	1,1,1 trichloroethane	Platinum addition	Methyl vinyl siloxane
40021	32% solids, 1 part	500	Xylene	Acetoxy	Dimethyl siloxane
40032	21 % solids, 1 part	800	1,1,1 trichloroethane	Platinum addition	Fluorovinyl methyl siloxane
MED-2213	15% solids, 1 part	7000	1,1,1 trichloroethane		Dimethyl-methyl vinyl siloxane
MED-6400	35% solids, 2 part, 1:1	600	Xylene	Platinum addition	
MED2-6400	25% solids, 2 part, 1:1	800	1,1,1 trichloro-ethane		Vinyl methyl siloxane
MED-6600	35% solids, 2 part	300	Xylene		
MED2-6600		1600	1,1,1 trichloroethane		
MED-6605	30% solids, 1 part	800	Xylene	Acetoxy	
MED3-6605	22% solids, 1 part	1250	1,1,1 trichloroethane		Dimethyl siloxane
MED-6607	33% solids, 1 part	5500	trichloroethane	Oxime	
MED-6640	25% solids, 2 part	7000	VM&P naphtha		
MED2-6640	15% solids, 2 part	5000	Xylene		Methyl vinyl siloxane
			1,1,1 trichloroethane	Platinum addition	
MED2-6650	20% solids, 2 part	3000			Fluorovinyl methyl siloxane
Q7-2630 10% solids		-	Q7-2650	Acetoxy	Dimethyl siloxane

Table 4.11 Typical Properties of Silicone Elastomeric Adhesives

Property							
Product and Manufacturer	Product no.	Specific gravity	Durometer hardness Shore	Tensile strength, Psi	Elongation, Percent	Tear strength, die B, pli	Adhesive strength (to silicone) pli
Applied Silicone	40064	ASTM D-792	ASTM D-2240	ASTM D-412	ASTM D-412	ASTM D-624	pli
Medical Implant Grade,	Medical Grade RTV Silicone Adhesive	1.08	24 A	850	750	70	18
Applied Silicone Corp.	Medical Grade High Strength RTV Silicone Adhesive			950	770		18
NuSil Silicone, NuSil Technology	MED-1137	1.07	29 A	550	450		
Silastic® Medical Materials	Medical Adhesive A	1.06	29 A	450	400	30	20+
Dow Corning Corp.	355 Medical Grade Pressure Sensitive			1.40			
Product no.	Cure Conditions			Comments			
40064	Produces acetic acid. Cures @ RT with atmospheric moisture, 20 to 60% RH.			Bonds silicones to each other and some synthetics, metals.			
Medical Grade RTV Silicone Adhesive Medical Grade High Strength RTV Silicone Adhesive	24 hours @ 25°C, aged 24 hours @ RT.			Bonding silicone to polyester, etc. High strength bonds to polyester, nylon, polyurethane and metals.			
MED-1137	Produces acetic acid. Cure 3 days @ RT with atmospheric moisture, 20 to 60% RH.			Bonding silicones to each other & some synthetics/metals. When fully cured resembles some conventional silicone elastomers.			

(continued)

Table 4.11 (continued)

Property							
Product and Manufacturer	Product no.	Specific gravity ASTM D-792	Durometer hardness Shore ASTM D-2240	Tensile strength, Psi ASTM D-412	Elongation, Percent ASTM D-412	Tear strength, die B, pli ASTM D-624	Adhesive strength (to silicone) Pli
Medical Adhesive A 355 Medical Grade Pressure Sensitive	Produces acetic acid, requires 50% RH & 7 days to cure. Non-curing dispersion - becomes adhesive as solvent evaporates.			Bonding silicone rubber to itself. Useful for cast films or parts from dispersions. Adheres to skin for use with ileostomy and colostomy appliances.			

4.3 Establishing Equivalence

Specific polymeric materials traditionally used for medical applications have been recently withdrawn from the medical market. Silicone elastomers are among those withdrawn. To maintain continued supply of vital implants, methods of determining equivalence for withdrawn elastomers with new or existing ones has been adopted by the FDA in the form of an FDA Guidance Document.

4.3.1 *FDA Guidance document for substitution of equivalent elastomers*

The FDA will allow manufacturers to change sources of silicone elastomers (and others) if they can show that the replacement material is ‘not substantially different’ from materials described in existing approved applications. The device manufacturer is still required to certify that the processes of fabrication, cure and sterilization it uses in the manufacture of its device are appropriate for the new material and that the device will perform as intended. Premarket notification submission under section 510(k) of the Federal Food, Drug, and Cosmetic Act (21 USC 360(k) and 21 CFR 807.81(a)(3)(i), or a supplemental premarket approval application under 21 USC 360(k) section 515 and 21 CFR 814.39 is necessary when change could significantly affect the safety or effectiveness of the device. These submissions are required to be submitted and approved before the device may be marketed with the change.

There are a number of tests necessary for comparison of silicone elastomers as indicated by ‘Guidance for Manufacturers of Silicone Devices Affected by Withdrawal of Dow Corning Silastic® Materials’ (Federal Register, Vol. 58, No. 127, Tuesday, July 6, 1993/ Notices, 36207). They compare the physical, chemical and biological properties of the bulk polymers as they are received from the supplier and also compare the molded elastomer as it exists in the final medical device.

Table 4.12 Biocompatibility of Various Elastomers

Classification	Product and Manufacturer	Product no.	Biocompatibility Status*					Skin Sensitization
			Hemolysis	Intracutaneous Pyrogenicity	Systemic Injection	Injection		
Thermoplastic elastomer	Santoprene®	281-45	passed	passed	passed	passed	passed	passed
	Rubber,	281-55	passed	passed	passed	passed	passed	passed
		281-64	passed	passed	passed	passed	passed	passed
	Advanced Elastomer	281-73	passed	passed	passed	passed	passed	passed
		281-87	passed	passed	passed	passed	passed	passed
		283-40	passed	passed	passed	passed	passed	passed
PCCE copolyester	Ecdel™ Elastomer,	9965	passed					
	Eastman Chemical Co.	9966						
elastomer Polyurethane-based elastomers	Biospan® Segmented, Polyurethane, The Polymer Technology Group, Inc.	Biospan®	passed	passed	passed	passed	passed	passed
	Hydrothane™, Poly Medica Biomaterials, Inc.	Hydrothane™						
Medicaflex™,		MP-5000						
		MF-5001		passed	passed	passed	passed	
		MF-5040						
		MF-5041						
		MF-5056						
	Technology	MF-5057						

		MF-5062							
	Pellethane™	Pellethane™							
	2363 series,	2363 series		passed			passed		passed
	Dow Chemical Co.								
	PolyBlend™ 1000 ,	PolyBlend™							
	and PolyBlend™	1000 and							
	1100	PolyBlend™							
	Poly Medica	1100							
	Biomaterials, Inc.								
<i>Biocompatibility Status*</i>									
<i>Intramuscular</i>									
<i>Product no.</i>	<i>10 days</i>	<i>30 days</i>	<i>90 days</i>	<i>Culture</i>	<i>Comments</i>				
281-45									
281-55		passed	passed	passed	Passed USP Class VI testing, Tripartite testing, mouse embryo toxicity testing and Ames				
281-64					Mutagenicity testing.				
281-73									
281-87									
283-40									
9965				passed					
9966									
Biospan®				passed					

(continued)

Table 4.12 (continued)

Hydrothane™						See text for status.	
MF-5000	passed				passed		
MF-5001	passed				passed	Passed USP Class VI testing.	
MF-5040					passed		
MF-5041					passed		
MF-5056	passed				passed		
MF-5057					passed		
MF-5062					passed		
Peliethane™						Passed USP Class VI testing.	
2363 series					passed	See text for status.	
PolyBlend™						See text for status.	
1000 and							
PolyBlend™							
<i>Biocompatibility Status*</i>							
<i>Classification</i>	<i>Product and Manufacturer</i>	<i>Product no.</i>	<i>Hemolysis</i>	<i>Intracutaneous Systemic</i>			<i>Skin Sensitization</i>
				<i>Pyrogenicity</i>	<i>Injection</i>	<i>Injection</i>	
Polyurethane based elastomers	Tecoflex® and Tecothane®	EG60A EG80D 1055D 1065D	passed		passed	passed	passed

		1074A	passed		passed	passed
	Thermedics, Inc.	1075D				
		1085A				
		1095A				
	Texin™,					
		Texin™		passed	passed	passed
	Miles, Inc.					
Polycarbonate based polyurethanes	Carbothane™, Thermedics, Inc.	PC-3555D	passed		passed	passed
		PC-3572D				
		PC-3575A				
		PC-3585A				
		PC-3595A				
	ChronoFlex™ AR,					
	Poly Medica	ChronoFlex™	passed	passed	passed	passed
	Biomaterials, Inc.	AR				
	Coremer™,	Coremer™				
	Corethane®,	TPE 55D			passed	passed
	and	TPE 75D		passed		
		TPE 80A	passed		passed	passed
	Corhesive™,	Corhesive™,	passed	passed	passed	passed
	Corvita Corp.					
Polypropylene based elastomers	Sarlink® medical grade, DSM Thermoplastic Elastomers, Inc.	Sarlink® medical grade				

(continued)

Table 4.12 (continued)

Product no.	Intramuscular			Tissue Cell Culture	Comments
	10 days	30 days	90 days		
EG60A					
EG80D					
1055D					
1065D					
1074A					
1075D					
1085A					
1095A					
Texin™		passed		passed	Passed USP Class VI testing. See text for status.
PC-3555D					
PC-3572D					
PC-3575A					
PC-3585A					
PC-3595A					
ChronoFlex™ AR		passed		passed	Passed USP Class VI testing. See text for status.
Coremer™					
TPE 55D	passed	passed	passed	passed	
TPE 75D				passed	
TPE 80A	passed	passed	passed	passed	

Corhesive™	passed	passed	passed	passed	passed	See text for status.		
Sarlink® medical grade								
<i>Biocompatibility Status*</i>								
<i>Classification</i>	<i>Product and Manufacturer</i>	<i>Product no.</i>	<i>Hemolysis</i>	<i>Intracutaneous Systemic Pyrogenicity</i>	<i>Injection</i>	<i>Injection</i>	<i>Skin Sensitization</i>	
Polyvinyl chloride elastomers	Elastichem™ PVC, Geon® PVC, B. F. Goodrich Co. Plastics Co.	Elastichem™ PVC, PVC						
Ellay™ PVC	Ellay™ PVC Ellay, Inc. Geon® PVC, B. F. Goodrich Co. Multichem™ PVC, Colorite Plastics Co.	Geon® PVC Multichem™ PVC	passed	passed	passed			
		3300-45 NT						
		3300-50 NT						
		3300-55 NT						
		3300-60 NT						
		3300-68 NT						
		3300-75 NT						
		3300-80 NT						
		3300-85 NT						
		3300-90 NT						

(continued)

3300-45 NT				passed			
3300-50 NT				passed			
3300-55 NT				passed			
3300-60 NT				passed			
3300-68 NT				passed			
3300-75 NT				passed			
3300-80 NT		passed		passed		Passed USP Class VI testing.	
3300-85 NT				passed		Passed USP Class VI testing.	
3300-90 NT				passed			
3310-50 NT				passed			
3310-55 NT				passed			
3310-60 NT				passed			
3310-65 NT				passed			
3310-70 NT				passed			
3310-75 NT				passed			
3310-80 NT				passed			
3310-85 NT				passed			
3310-90 NT				passed			
90A471R-60NT		passed				Passed USP Class VI testing.	
90A471R-65NT		passed				Passed USP Class VI testing.	

(continued)

Table 4.12 (continued)

90A471R-70NT	passed					Passed USP Class VI testing.	
90A471R-75NT	passed					Passed USP Class VI testing.	
90A471R-80NT	passed					Passed USP Class VI testing.	
90A471R-85NT	passed					Passed USP Class VI testing.	
90A471R-90NT	passed					Passed USP Class VI testing.	
<i>Biocompatibility Status*</i>							
<i>Classification</i>	<i>Product and Manufacturer</i>	<i>Product no.</i>	<i>Hemolysis</i>	<i>Intracutaneous Pyrogenicity</i>	<i>Systemic Injection</i>	<i>Injection</i>	<i>Skin Sensitization</i>
Styrene-based elastomers	C-Flex [®] ,	R70-001	passed	passed	passed	passed	
		R70-003	passed	passed	passed	passed	
		R70-005	passed	passed	passed	passed	
	Consolidated Polymer Technologies, Inc.	R70-026	passed	passed	passed	passed	
		R70-028	passed	passed	passed	passed	
		R70-046	passed	passed	passed	passed	
		R70-050	passed	passed	passed	passed	
		R70-051	passed	passed	passed	passed	
		R70-058	passed	passed	passed	passed	

		R70-067	passed	passed	passed	passed	passed
		R70-068	passed	passed	passed	passed	passed
		R70-072	passed	passed	passed	passed	passed
		R70-081	passed	passed	passed	passed	passed
		R70-082	passed	passed	passed	passed	passed
		R70-085	passed	passed	passed	passed	passed
		R70-089	passed	passed	passed	passed	passed
		R70-091	passed	passed	passed	passed	passed
		R70-116	passed	passed	passed	passed	passed
		R70-190	passed	passed	passed	passed	passed
		R70-214	passed	passed	passed	passed	passed
		D-2103	passed	passed	passed	passed	passed
		D-2104	passed	passed	passed	passed	passed
		D-2109	passed	passed	passed	passed	passed
		G-2701	passed	passed	passed	passed	passed
		G-2703	passed	passed	passed	passed	passed
		G-2705	passed	passed	passed	passed	passed
		G-2706	passed	passed	passed	passed	passed
		G-2712	passed	passed	passed	passed	passed

Biocompatibility Status*

<i>Product no.</i>	<i>Intramuscular</i>		<i>Tissue Cell</i>		<i>Comments</i>
	<i>10 days</i>	<i>30 days</i>	<i>90 days</i>	<i>Culture</i>	
R70-001	passed	passed	passed	passed	
R70-003	passed	passed	passed	passed	C-Flex testing data is available from manufacturer.
R70-005					
R70-026	passed	passed	passed	passed	

(continued)

Table 4.12 (continued)

R70-028	passed	passed	passed	passed	passed	passed	passed	passed
R70-046	passed	passed	passed	passed	passed	passed	passed	passed
R70-050	passed	passed	passed	passed	passed	passed	passed	passed
R70-051	passed	passed	passed	passed	passed	passed	passed	passed
R70-058	passed	passed	passed	passed	passed	passed	passed	passed
R70-067	passed	passed	passed	passed	passed	passed	passed	passed
R70-068	passed	passed	passed	passed	passed	passed	passed	passed
R70-072	passed	passed	passed	passed	passed	passed	passed	passed
R70-081	passed	passed	passed	passed	passed	passed	passed	passed
R70-082	passed	passed	passed	passed	passed	passed	passed	passed
R70-085	passed	passed	passed	passed	passed	passed	passed	passed
R70-089	passed	passed	passed	passed	passed	passed	passed	passed
R70-091	passed	passed	passed	passed	passed	passed	passed	passed
R70-116	passed	passed	passed	passed	passed	passed	passed	passed
R70-190	passed	passed	passed	passed	passed	passed	passed	passed
R70-214	passed	passed	passed	passed	passed	passed	passed	passed
D-2103	passed	passed	passed	passed	passed	passed	passed	passed
D-2104	-	passed	-	-	-	-	passed	Passed USP Class VI testing.
D-2109		passed					passed	Passed USP Class VI testing.
G-2701		passed					passed	Passed USP Class VI testing.

G-2703		passed			passed	Passed USP Class VI testing.	
G-2705		passed			passed	Passed USP Class VI testing.	
G-2706		passed			passed	Passed USP Class VI testing.	
G-2712		passed			passed	Passed USP Class VI testing.	
Biocompatibility Status*							
Classification	Product and Manufacturer	Product no.	Hemolysis	Intracutaneous Systemic		Skin Sensitization	
				Pyrogenicity	Injection		
Polydimethylsiloxane	Applied Silicone Medical Implant Grade, Applied Silicone Corp.	Applied Silicone Medical Implant Grade					
	NuSii Silicone, NuSil Technology	NuSii Silicone					
	Silastic®	MDX4-4210		passed	passed	passed	
	Medical Materials,	Q7-4535	passed	passed	passed	passed	passed
		Q7-4550	passed	passed	passed	passed	passed
		Q7-4565	passed	passed	passed	passed	passed
	Dow Corning Corp.	Q7-4720	passed	passed	passed	passed	passed
Q7-4735		passed	passed	passed	passed	passed	
Polydimethyl	Silastic®	Q7-4750	passed	passed	passed	passed	

(continued)

Table 4.12 (continued)

siloxane	Medical Materials,	Q7-4765	passed	passed	passed	passed	passed	passed
		Q7-4780	passed	passed	passed	passed	passed	passed
	Dow Corning Corp.	Q7-4840	passed	passed	passed	passed	passed	passed
		Q7-4850	passed	passed	passed	passed	passed	passed
		Q7-6860	passed	passed	passed	passed	passed	passed
	Medical							
	Adhesive A			passed	passed	passed	passed	passed
	355 Medical			passed	passed	passed	passed	passed
	Grade Pressure							
	Sensitive							
<i>Biocompatibility Status*</i>								
<i>Intramuscular</i>								
<i>Product no.</i>	<i>10 days</i>	<i>30 days</i>	<i>90 days</i>	<i>Culture</i>	<i>Comments</i>			
Applied Silicone					Applied Silicone testing data is available from manufacturer.			
Medical								
Implant								
Grade								
NuSii Silicone					See text for status.			
MDX4-4210	passed	passed		passed	See text for status.			
Q7-4535	passed	passed			See text for status.			

Q7-4550	passed	passed				See text for status.
Q7-4565	passed	passed				See text for status.
Q7-4720				passed		See text for status.
Q7-4735	passed			passed		See text for status.
Q7-4750	passed					See text for status.
Q7-4765	passed					See text for status.
Q7-4780	passed					See text for status.
Q7-4840	passed					See text for status.
Q7-4850		passed			passed	See text for status.
Q7-6860	passed					See text for status.
Medical Adhesive A						See text for status.
355 Medical	passed	passed		passed		See text for status.
Grade Pressure Sensitive	passed	passed		passed	passed	See text for status.

*Biocompatibility based on comparison with USP negative controls

Note: It is the user's responsibility to adequately test or determine that these materials are suitable or safe for any application.

Table 4.13 Sterilization Methods for Elastomers

Product	Steam/autoclave	Cobalt 60	Ethylene oxide	Cold solution
Biospan	OK	—	OK	—
Biospan D	—	—	—	—
Biospan S	—	—	—	—
C-Flex R70-001	OK	OK	OK	—
R70-003	OK	OK	OK	—
R70-005	no	OK	OK	—
R70-026	OK	no	OK	—
R70-028	no	OK	OK	—
R70-046	no	OK	OK	—
R70-050	OK	OK	OK	—
R70-051	OK	OK	OK	—
R70-072	OK	OK	OK	OK
R70-081	OK	OK	OK	—
R70-082	OK	OK	OK	—
R70-085	OK	OK	OK	—
R70-089	NR	OK	OK	—
R70-091	NR	OK	OK	—
R70-116	no	OK	OK	—
R70-190	no	OK	OK	—
R70-214	no	OK	OK	—
Carbothane	with caution	—	OK	—
ChronoFlex	—	—	—	—
Coremer	—	OK	OK	OK
Corethane 80A	—	OK	OK	OK
55D	—	OK	OK	OK
75D	—	OK	OK	OK
Corhesive	—	—	—	—
Ecdel elastomers	OK	no	OK	—
Hydrothane	—	—	—	—
—	—	—	—	—
Kraton G-series	—	OK	—	—
D-series	—	—	OK	—
Medicaflex	no	OK	OK	—
Natural rubber, gum	OK	OK	OK	—
Natural rubber, latex	with caution	OK	OK	—
Pellethane	no	OK	OK	—
Poly blend	—	—	—	—
Poly blend 1100	—	—	—	—
PVC Elasticchem	OK	OK	OK	—
Ellay	OK	OK	OK	—
Geon	—	—	—	—
Multi-Chem	OK	OK	OK	—
Teknor	OK	OK	OK	—

(continued)

Table 4.13 (continued)

Product	Steam/autoclave	Cobalt 60	Ethylene oxide	Cold solution
in general	Flexible	with caution	OK	—
	PVC, OK			
	rigid PVC, no			
Santoprene	OK	OK	OK	OK
Sarlink 3260	—			—
Silicone High consistency	OK	OK	OK	—
LIM	OK	OK	OK	—
Adhesives	OK	OK	OK	—
Dispersions	OK	OK	OK	—
Tecoflex	with caution	OK	OK	with caution
Tecothane	—	OK	OK	with caution
Texin	no	OK	OK	—

Caution: with some aromatic polyurethanes methylene dianiline (MDA) can be generated with steam sterilization.

Table 4.14 Water Absorption of Various Elastomers

Classification	Product and manufacturer	Product no.	Water absorption, percent (after 24 hours) ASTM-D 570	
Thermoplastic vulcanizate	Santoprene® Rubber,	281-55 281-64	6.0	
	Advanced Elastomer Systems	281-87 283-40	0.0	
PCCE copolyester elastomer	Ecdel™ Elastomer,	9965		
		9966	0.4	
Polycarbonate-based polyurethanes	Eastman Chemical Co. Corethane®,	TPE 80A	1.2	
		TPE 55D	0.9	
		TPE 75D	0.8	
Polyurethane-based elastomers	Corvita Corp. Corhesive™,		1.2	
		Biospan® segmented	Biospan®	1.5
		polyurethane, The Polymer Technology Group, Inc.	Biospan®D Biospan®S	1.3 1.5
	PolyBlend™ 1000, and PolyBlend™ 1100	PB1000-650	<	
		PB1100-55		
		PB1100-60	<0.4	
		PB1100-75		
Silicone rubber	Poly Medica Biomaterials, Inc.	PB1100-80		
			0.1-0.5	
Silicone type A adhesive			<0.2	

4.3.2 Equivalent silicone elastomers

Two manufacturers, NuSil Technology and Applied Silicone Corp., are providing equivalent silicone materials for the Dow Corning products that have been withdrawn. Tables 4.15 and 4.16 gives reported comparisons.

Table 4.15 Equivalent Silicone Elastomers for Existing Dow Corning Silicones

Dow Corning Silicone*	NuSil [‡] Silicone Equivalent	Applied Δ Silicone Equivalent	Medical Grade Silicone Description
Medical Adhesive A	MED-1137	40064	Medical RTV Adhesive, Acetoxy System (see also Rehau, Table 4.16)
Q7-4535	MED-4535	40044	High Consistency, 35 Durometer, Peroxide Cure
Q7-4550	MED-4550	40045	High Consistency, 50 Durometer, Peroxide Cure
Q7-4565	MED-4565	40046	High Consistency, 65 Durometer, Peroxide Cure
Q7-4720	MED-4720	40043	High Consistency, 20 Durometer, Platinum Cure
Q7-4735	MED-4735	40039	High Consistency, 35 Durometer, Platinum Cure
Q7-4750	MED-4750	40040	High Consistency, 50 Durometer, Platinum Cure
Q7-4780	MED-4780	40042	High Consistency, 80 Durometer, Platinum Cure
MDX4-4210	MED-42111	40072	Liquid Silicone, 25 Durometer, Platinum Cure
		40029	Liquid Silicone, 30 Durometer, Platinum Cure
Q7-4840	MED-4840	40026	Liquid Silicone, 40 Durometer Platinum Cure
Q7-4850	MED-4850	40027	Liquid Silicone, 50 Durometer, Platinum Cure
Q7-4865	MED-4865		Liquid Silicone, 65 Durometer, Platinum Cure
DC-360	MED-360	40047	Medical Grade Silicone Fluid, 1000 cps.
	Specify	40073	Medical Grade Silicone Fluid, 350 cps.
	viscosity	40074	Medical Grade Silicone Fluid, 20 cps.

* Dow Corning Corp., Midland, MI. [‡] NuSil Silicone Technology, Carpinteria, CA

Δ Applied Silicone Corp., Ventura, CA Note: It is the user's responsibility to adequately test or determine that these materials are suitable or safe for any application.

Table 4.16 Equivalent Silicone Elastomers for Withdrawn Dow Corning silicones

Dow Corning Silicone*	NuSilt‡ Silicone Equivalent	Applied Δ Silicone Equivalent	Medical Grade Silicone Description
MDX4-4515	MED-4515	40045	50 Durometer, peroxide cure
MDX4-4516	MED-4516	40046	60 Durometer, peroxide cure
Q7-2245	MED-2245	40009	40 Durometer, platinum cure
Q7-2213	MED-2213	40076	Dispersion in 1, 1, 1 trichloroethane
Rehau 1511¥		40076	Medical RTV adhesive, acetoxy system

*Dow Corning Corp., Midland, MI. ‡ NuSil Silicone Technology, Carpinteria, CA.

Δ Applied Silicone Corp., Ventura, CA. ¥ Rehau AG and Co., Rehau, Germany.

Note: It is the user's responsibility to adequately test or determine that these materials are suitable or safe for any application.

4.4 Sterilization of Elastomers

4.4.1 Sterilization methods

Not all materials respond alike when subjected to various means of sterilization. Some are heat sensitive, some will absorb sterilization fluids, some will be affected by molecular changes when subjected to radiation sterilization and others will absorb and hold irritating gases for extended periods of time. Table 4.13 gives sterilization methods that have been judged most appropriate for each elastomer. The consequences of using an inappropriate method can be loss in physical properties and an adverse biological response.

4.5 Relevant ASTM Standards

Standard methods of testing elastomers used for medical applications are given by specific ASTM test methods. Physical and biological tests are provided here to serve as references for the data cited in the tables and listed in Table 4.17. They are also designated in the FDA Guidance Document.

4.6 Biocompatibility

Table 4.12 on biocompatibility of various elastomers is intended to show the status of *in vitro* and *in vivo* testing. The successful outcome of these tests can serve as guides to potentially acceptable performance of an elastomeric product in a medical device under development. However, the use of elastomeric products in medical devices is the responsibility of the device manufacturer who must establish their safety and efficacy with the FDA.

Table 4.17 Relevant ASTM Standards

D 395	Test Method for Rubber Property - Compression Set
D 412	Test Method for Vulcanized Rubber, Thermoplastic Rubbers and Thermoplastic Elastomer - Tension
D 471	Test Method for Rubber Property - Effect of Liquids
D 570	Test Method for Water Absorption of Plastics
D 624	Test Method for Tear Strength of Conventional Vulcanized Rubber and Thermoplastic Elastomer
D 638	Test method for Tensile Properties of Plastics
D 792	Test Method for Specific Gravity (Relative Density) and Density of Plastics by Displacement
D 797	Test Methods for Rubber Property - Young's Modulus at Normal and Subnormal Temperatures
D 1630	Test Method for Rubber Property - Abrasion Resistance (NBS Abrader)
D 1708	Test method for Tensile Properties of Plastics by Use of Microtensile Specimens
D 1790	Test method for Brittleness Temperature of Plastic Film by Impact
D 1938	Test method for Tear Propagation Resistance of Plastic Film and Thin Sheetting by a Single-Tear Method
D 2240	Test Method for Rubber Property - Durometer Hardness
D 2702	Standard Practice for Rubber Chemicals - Determination of Infrared Absorption Characteristics
D 3418	Test Method for Transition Temperatures of Polymers by Thermal Analysis
D 3593	Test Method for Molecular Weight Averages and Molecular Weight Distribution of Certain Polymers by Liquid Size-Exclusion Chromatography (Gel Permeation Chromatography, GPC) Using Universal Calibration
D 5023	Test Method for Measuring the Dynamic Mechanical Properties of Plastics Using Three Point Bending
D 5026	Test Method for Measuring the Dynamic Mechanical Properties of Plastics in Tension
E 355	Standard Practice for Gas Chromatography, Terms and Relationships
E 1356	Test Method for Glass Transition Temperatures by Differential Scanning Calorimetry or Differential Thermal Analysis
F 604	Classification for Silicone Elastomers Used in Medical Applications
F 619	Standard Practice for Extraction of Medical Plastics
F 720	Standard Practice for Testing Guinea Pigs for Contact Allergens: Guinea Pig Maximization Test
F 748	Standard Practice for Selecting Generic Biological Test Methods for Materials and Devices
F 749	Standard Practice for Evaluating Material Extracts by Intracutaneous Injection in the Rabbit
F 750	Standard Practice for Evaluating Material Extracts by Systemic Injection in the Mouse
F 813	Standard Practice for Direct Contact Cell Culture Evaluation of Materials for Medical Devices
F 895	Standard Practice for Agar Diffusion Cell Culture Screening for Cytotoxicity
F 981	Standard Practice for Assessment of Compatibility of Biomaterials (Non-porous) for Surgical Implants with Respect to Effect of Materials in Muscle and Bone

4.7 Sources

- AlphaGaryAlphaGary, Leominster, MA
- Applied SiliconeApplied Silicone Corp., Ventura, CA
- Biospan[®]Polymer Technology Group, Inc., Emeryville, CA
- C-Flex[®]Consolidated Polymer Technologies, Inc., Largo, FL
- Carbothane[™]Thermedics, Inc., Woburn, MA
- ChronoFlex[™]PolyMedica Industries, Inc., Woburn, MA
- Coremer[™]Corvita Corp., Miami, FL
- Corethane[®]Corvita Corp., Miami, FL
- Corhesive[™]Corvita Corp., Miami, FL
- Ecdel[™]Eastman Chemical Co., Kingsport, TN
- Elasticchem[™]Colorite Plastics Co., Ridgefield, NJ
- Ellay[™]Ellay, Inc., City of Commerce, CA
- Geon[®]B.F. Goodrich Co., Chemical Group, Cleveland, OH
- Hydrothane[™]PolyMedica Industries, Inc., Woburn, MA
- Kraton[®]Shell Chemical Co., Oak Brook, IL
- Medicaflex[™]Advanced Resin Technology, Manchester, NH
- Multichem[™]Colorite Plastics Co., Ridgefield, NJ
- Natural rubberExxon Chem. Co., Buffalo Grove, IL Goodyear Tire and Rubber Co., Akron, OH
- NuSil SiliconeNuSil Technology, Carpinteria, CA
- Pellethane[™]Dow Chemical Co., Midland, MI
- PolyBlend[™]PolyMedica Industries, Inc., Woburn, MA
- Santoprene[®]Advanced Elastomer Systems, St Louis MO
- Sarlink[®]DSM Thermoplastic Elastomers, Inc., Leominster, MA
- SilasticDow Corning Corp., Midland, MI
- Tecoflex[®]Thermedics, Inc., Woburn, MA
- Tecothane[®]Thermedics, Inc., Woburn, MA
- Teknor[™]Teknor Apex Co., Pawtucket, RI
- Texin[™]Miles, Inc., Pittsburgh, PA

Chapter 5

Oxide Bioceramics: Inert Ceramic Materials in Medicine and Dentistry

J. Li and G.W. Hastings

5.1 Introduction

Single oxide ceramics, e.g. aluminium oxide (Al_2O_3 , alumina) and zirconium dioxide (ZrO_2 , zirconia), are bioceramics of an inert nature. An inert ceramic does not form a bonding to bone similar to those bioceramics of bioactive nature. Alumina bioceramics are in the pure aluminium oxide form, whereas zirconia bioceramics are partially stabilized by additional oxides, e.g. yttrium oxide, calcium oxide or magnesium oxide.

Oxide ceramics exhibit superior mechanical properties, corrosion and wear resistance. Since the oxides are the highest oxidation state of the metal, they are stable even in the most invasive industrial and biomedical environments. Alumina and zirconia are utilized as load-bearing hard tissue replacements and fixation implants in dentistry and surgery.

5.2 Short History

Although the use of alumina as implants can be traced back to the 1930s as described by Hulbert *et al.* (1) (Table 5.1), the extensive use of alumina since the 1980s has depended on new powder processing technology enabling grain size reduction of the sintered ceramics from 10 micrometers down to 2 micrometers (Figure 5.1, microstructure of alumina). This significantly improves the performance of the

J. Li (✉)

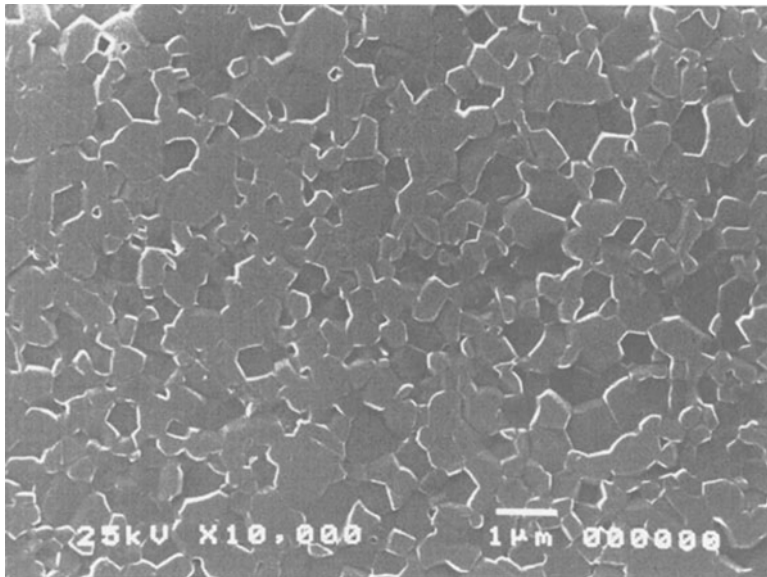
Centre for Oral Biology, Karolinska Institute, Huddinge S 141–4, Sweden

G.W. Hastings

Institute of Materials Research and Engineering, Singapore, Singapore

Table 5.1 Evaluation of oxide ceramic implants: alumina and zirconia

1932	First suggestion of application of alumina ceramics in medicine	Rock (2)
1963	First orthopaedic bone substitute application	Smith (3)
1964	First dental implant of alumina	Sandhaus (4)
1970	French hip prosthesis: Alumina ceramic ball and cup	Boutin (5)
1974	German hip prosthesis	Mittelmeier (6)
1977	28 mm alumina ball	Shikita (7)
1981	Alumina total knee prosthesis	Oonishi <i>et al.</i> (8)
1982	FDA approval for non-cemented alumina ceramic cup and ball and CoCrMo-stem of Mittelmeier type	
1986	First zirconia ball of 32 mm	Lord <i>et al.</i> (9)
1993	First dental implant of zirconia	Akagawa <i>et al.</i> (10)
1995	First zirconia dental post	Meyenberg <i>et al.</i> (11)
1996	First zirconia inlay	Johansson (12)

**Figure 5.1** SEM micrograph of dense alumina, etched in boiling H_3PO_4 for 6 minutes to show the microstructure.

alumina ceramic hip balls. Alumina and partially stabilized zirconia are currently in extensive use as implants in consequence of their high strength, excellent corrosion and wear resistance and stability, non-toxicity and biocompatibility *in vivo*. A summary of alumina- and zirconia-based implants is presented in Table 5.2. The most established example is in the total hip endoprosthesis with a combination of metallic stem, ceramic ball and ultra high molecule weight polyethylene (UHMWPE)

Table 5.2 Biomedical applications of oxide ceramics

Materials	Applications	References
Alumina	Hip ball & cup	Clarke and Willmann (13)
	Knee joint	Oonishi <i>et al.</i> (8)
	Bone screws	
	Dental implant	Kawahara (14)
	Dental crowns & brackets	Sinha <i>et al.</i> (15)
Zirconia	Hip ball	Christel (16)
	Dental implants	Akagawa <i>et al.</i> (10)
	Dental post, brackets and inlay	(10, 11), Keith <i>et al.</i> (17)

acetabular cup. A ten year clinical success rate better than 90% is reported for the cemented total hip endoprosthesis.

Dental implants of polycrystalline alumina were suggested by Sandhaus in Germany (4). Type Tübingen was produced by Frialit in the 1970s. These devices have not been generally accepted, due to the fracture failure of the implants, particularly for those of polycrystalline type produced in the early 1970s. The single crystal sapphire type, introduced in Japan by Kawahara in the 1970s (18) is, however, still being used and a recent 10-year clinical follow-up report from Sweden showed a 92% success rate (19) for the single crystal dental implants.

Alumina and zirconia ceramics are also being used for alveolar ridge reconstruction (20), maxillofacial reconstruction, as ossicular bone substitutes (21), and in ophthalmology (22), knee prosthesis (8), bone screws as well as other applications as dental biomaterials, such as dental crown core, post, bracket and inlay (23, 24).

5.3 Material Properties and Processing

5.3.1 Materials properties

Although alumina is chemically more stable it is mechanically weaker than zirconia, and the phase changes or transformation mechanisms in zirconia produce a unique ceramic material having much higher strength and higher fracture toughness compared with alumina and other ceramics. The excellent mechanical properties of zirconia allow the design of hip balls of smaller diameter in order to reduce the wear of the UHMWPE cup with expected increased long-term clinical performance as a result.

The chemical stability of alumina is related to its phase stability, whereas the phase changes of zirconia result in degradation in strength and wear resistance. Release of substances from zirconia and alumina implants to the surrounding tissue is very low and neither local nor systemic effects have been reported.

Aluminium oxide: alumina

Aluminium oxide is produced by heating its hydrates. At least seven forms of alumina have been reported, but six of these forms have traditionally been designated ‘gamma alumina’. When heated above 1200°C, all other structures are irreversibly transformed to the hexagonal alpha-alumina, corundum, a close-packed arrangement of oxygen ions. Thus alphaalumina is the only stable form above 1200°C and by far the most commonly used of structural ceramics. Alpha-alumina is thermodynamically stable and is crystallographically identical with the single crystal ruby and sapphire ceramics. Each aluminium ion is surrounded by six oxygen ions, three of which form a regular triangle on one side, the other three form a similar triangle on the other side, with the two planes of the triangles being parallel and the triangles being twisted 180° (25).

Physical and mechanical properties

Table 5.3 and 5.4. Resulting from a strong chemical bond between the Al and O ions, as expected from the value of heat of formation (-400K cal/mol), Al₂O₃ has a high melting point, the highest hardness among known oxides, and high mechanical strength (26).

Table 5.3 Engineering Properties of Alumina and Zirconia (At 25 °C)*

Property	Al ₂ O ₃	ZrO ₂ **
<i>Physical</i>		
Crystallography	Hexagonal	Tetragonal***
a(Å)	4.76	3.64
c(Å)	13.0	5.27
Space group	D ⁶ _{Ba}	P4 ₂ /nmc
Melting point (°C)	2040	2680
Density (g/cm ³)	3.98	6.08
Grain size (µm)	1–6	0.54
Hardness (GPa)	22	12.2
Modulus of elasticity, (GPa)	366	201
Poisson's ratio	0.26	0.30
Thermal coefficient of expansion 25–200 °C	6.5	10.1
<i>Mechanical</i>		
Flexural strength (MPa)	551	1074
Compressive Strength (MPa)	3790	7500
Tensile strength (MPa)	310	420
Fracture toughness (MPa m ^{1/2})	4.0	6–15

* Sources: refs 26, 44 and 45

** Zirconia presented is the yttria-partially stabilized material

*** Most of the medical-grade zirconia is partially stabilized tetragonal zirconia

Table 5.4 Properties of medical-grade ceramic materials according to the standards to the standards and the manufacturer's technical date – alumina and zirconia

Property	Alumina according to ISO-6474 ASTM F 603–83 DIN 58 8353	Frialit bioceramic alumina	Zirconia according to ISO/DIS 13356	Prozyr® zirconia
Purity (%)	>99.5	>99.5	>99.5*	>95
Density (g/cm ³)	>3.9	>3.98	>6.0	6
Porosity (%)	0	**	0	0
Grain size (µm)	<4.5	>2.5	<0.6	<1
Microhardness (GPa)	23	23	—	13
Young's modulus (GPa)	380	380	—	220
Flexural strength (MPa)	>400	>450	>900	>920
Biaxial flexural strength (MPa)	250	—	>550	—
Impact strength (cm MPa)	>40	>40		124
Fracture toughness (MPa m ^{1/2})				10
Wear resistance (mm ³ /h)	0.01	0.001		—
Corrosion resistance (mg/m ² d)	<0.1	<0.1	—	—

* ZrO₂+HfO₂+Y₂O₃

** Not available.

Chemical properties

Alumina is chemically stable and corrosion resistant. It is insoluble in water and very slightly soluble in strong acids and alkalis. Therefore, practically no release of ions from alumina occurs at a physiological pH level, 7.4.

Wear resistance

Arising from the chemical stability and high surface finish and accurate dimensions, there is a very low friction torque between the alumina femoral heads and the acetabular cup, leading to a low wear rate. Combinations of ceramic head/UHMWPE cup and ceramic head/ceramic cup were tested and compared to the metal head/UHMWPE cup. The wear resistance of the ceramic head/UHMWPE cup combination over metal/UHMWPE has improved from 1.3 to 34 times in the laboratory and from three to four times clinically (27, 28). No alumina wear particles from retrieved ceramic/UHMWPE were found, whereas UHMWPE wear particles from microns to millimetres in size were found in the retrieved surrounding tissues. However, from the ceramic/ceramic combination, ceramic particles resembling 'fine grains and great fragments in the ranges from 0.5 to 10 micrometers diameter, with the predominant size of about 1 micrometer' were found in the surrounding tissue (29). The advantage of ceramic/ceramic combination over ceramic/UHMWPE is, therefore, doubtful. For wear tests, we refer to ISO-6474 ASTM F-603.

Clinical performance

The fracture of ceramic balls in ceramic: UHMWPE combination has been virtually zero. Fritsch and Gleitz (30) published a failure analysis on 4341 alumina ceramic heads articulating with 2693 alumina ceramic and 1464 polymer sockets implanted over 20 years (1974 to 1994), and concluded that the use of ball type neckless heads brought the fracture rate close to zero. The success rate of 10 years follow-up is normally above 90% for the 'elderly' patient population. Stem and cup loosening are the causes of failure, where the consistent wear debris from UHMWPE and bone cement remain the problems.

Zirconium dioxide: zirconia

Zirconia ceramics are termed polymorphic because they undergo several transformations on cooling from a molten state to room temperature. It exhibits three well-defined polymorphs, the monoclinic, tetragonal and cubic phases and a high pressure orthorhombic form also exists. The monoclinic phase is stable up to about 1170°C where it transforms to the tetragonal phase, stable up to 2370°C, while the cubic phase exists up to the melting point 2680°C. A large volume change of 3 to 5% occurs when zirconia is cooled down and transforms from the tetragonal to the monoclinic phase.

Partially stabilized zirconia (PSZ) and tetragonal zirconia polycrystals (TZP)

The volume change due to phase transformation is sufficient to exceed elastic and fracture limits and causes cracking of the zirconia ceramics. Therefore, additives such as calcia (CaO), magnesia (MgO) and/or yttria (Y_2O_3) must be mixed with zirconia to stabilize the material in either the tetragonal or the cubic phase. PSZ is a mixture of cubic and tetragonal and/or monoclinic phases, whereas TZP is 100% tetragonal (phase diagram Figure 5.2). Both PSZ and TZP are suggested for medical implant applications. Yttria-TZP ceramics have a strength and fracture toughness approximately twice that of alumina ceramics used in the biomedical field. This makes zirconia heads less sensitive to stress concentrations at the points of contact with metal cones.

Physical and mechanical properties

Zirconia ceramics have a high density because of heavy zirconium ions, and a low microhardness and elastic modulus, together with high strength and fracture toughness compared to other ceramics including alumina. The superior mechanical strength provides the possibilities for producing ceramic ball heads of size below 32 mm.

Figure 5.2(a) Part of the equilibrium phase diagram for the system ZrO₂-CaO. C_{ss} refers to the cubic solid-solution phase, T_{ss} to the tetragonal solid-solution phase, and M_{ss} to the monoclinic solid-solution phase (ref. 21).

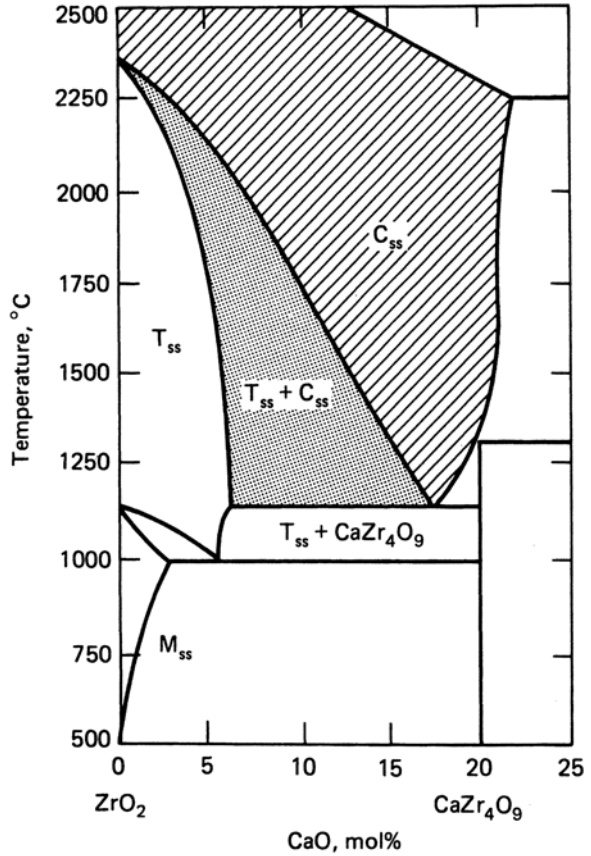
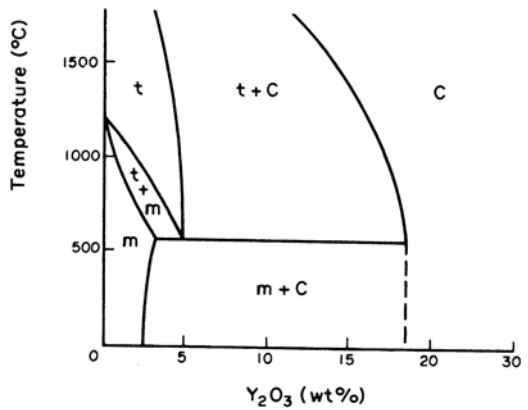


Figure 5.2(b) Y₂O₃-ZrO₂ phase diagram: the addition of less than 5% of Y₂O₃ to ZrO₂ allows the sintering of a fully tetragonal material (t=tetragonal phase; m=monoclinic phase; c=cubic phase) (ref. 16).



Fracture toughness mechanisms:

Garvie *et al.* were the first to realize the transformation toughening mechanism for zirconia ceramics. Increase of both strength and fracture toughness can be obtained by utilizing the tetragonal-monoclinic phase transformation of metastable tetragonal grains induced by the presence of the stress field ahead of a crack (31). The volume change and the shear strain developed in the martensitic reaction were recognized as opposing the opening of the crack and therefore acting to increase the resistance to crack propagation.

Wear resistance and chemical stability:

The published results of *in vitro* wear tests demonstrated that zirconia has a superior wear resistance. Saikko (32) showed no wear of zirconia femoral heads on his hip simulator wear test against 10.9 mm UHMWPE cup, and Praveen Kumar *et al.* (33) demonstrated the high wear resistance of zirconia against UHMWPE and the superiority of zirconia ceramics even over alumina ceramics in terms of low wear and low friction. A significant reduction in the wear rate of zirconia ball heads compared to the metal ball heads was reported on a pin-on-disc wear test and on a hip simulator (34). However, there are two potential limitations for the use of zirconia as bioceramics: degradation and radiation. It is known that the phase transformation is accelerated in aqueous environment, but little is known about how this phase transformation will occur in biological environment, particularly under dynamic loadings. A warning against steam reesterilization has been issued in the UK. Radioactive U-235 impurity was detected in some 'pure zirconia', both alpha- and gamma-irradiation were measured from zirconia femoral balls. Although the radioactivity was low, more work is required to verify this matter (13).

Clinical performance

The surface degradation of the zirconia balls due to the phase transformation under loading seems to be a problem, although no significant change in mechanical strength was reported in some long-term *in vivo* and *in vitro* studies (35, 36). Seriously, catastrophic failure of modular zirconia ceramics femoral head components after total hip arthroplasty was reported (37). Since zirconia femoral heads have a short clinical history and few clinical results are available, more investigation is required to eliminate the factors which impair the clinical stability of zirconia ceramics under loading.

5.3.2 *Materials processing*

An advanced ceramic is processed in such a way that the structure of the materials on different levels, including atomic, electronic, grain boundary, microstructural and macrostructural, is under strict control. In the manufacturing processes, emphasis is placed on producing dense ceramics with a fine microstructure. However, other factors such as chemical composition, the nature and distribution of the impurities, crystal structure, grain size, and defects are also of importance to the performance of the ceramic materials. Three basic processes are involved in the production of fine ceramic components, namely: 1. powder technology, 2. densification or sintering and 3. machining. Both alumina and zirconia hip balls are produced by compacting fined-grained powder (green bodies), and sintering at 1500–1700 °C and finally grinding or lapping to obtain a high surface finish and sphericity ($R_a < 0.02 \mu\text{m}$).

5.4 Biocompatibility of Oxide Bioceramics

No materials placed within a living tissue can be considered to be completely inert. However, oxide bioceramics, by their very nature, do not suffer from corrosion or degradation in biological environments, as metals or plastics do. Ceramics, having molecular structures completely different from those of living tissues, are generally stable inside the living body and provide a high degree of acceptance by the apposition to the surrounding tissue as shown by *in vitro* and *in vivo* studies Ichikawa *et al.* observed no adverse soft tissue responses to zirconia and alumina implants after 12 months of implantation (38). Takamura *et al.* reported that alumina and zirconia did not possess chronic toxicity to mice (39), whereas Stefflik *et al.* found a biological seal at the alumina dental implant and epithelium interface (40). However, oxide bioceramics do not form a chemical bond to bone tissue and are therefore defined as inert biomaterials. Oxide bioceramics are defined as inert biomaterials.

The ASTM standards (F 748/82, 763/82) and ISO standards No 10993 have set the guidance for biological testing of biomaterials for orthopaedic application. The materials should be tested in soft tissue as well as in hard tissue environments, for both short-term and long-term experiments. A summary of recommended biological testing is presented in Table 5.5. Both alumina and zirconia have shown non-toxicity and good biocompatibility according to the tests. Testing results for zirconia made by a French Company are shown in Table 5.6. Although some serious problems occurred with zirconia balls, the basic biocompatibility of the zirconia remains. Soft tissue and bone responses to zirconia and alumina were studied in our lab: no adverse tissue reaction to these ceramics were found. The patterns of tissue-materials interface after 1 month implantation in muscle and femur of rat are shown in Figure 5.3.

Table 5.5 Guidance for Biologic Evaluation Tests of the Implant Device in Contact to bone Tissue (According to ISO 10993–1:1992 (E))

	Contact duration		
	A-limited (>24 h)	B-prolonged (<24 h to 30 days)	C-permanent (<30 days)
Biological tests			
Cytotoxicity	x	x	x
Sensitisation	x	x	x
Irritation/Intracutaneous Reactivity	x	x	x
Irritation/Intracutaneous	x		
Genotoxicity		x	x
Implantation		x	x
Chronic toxicity			x
Carcinogenicity			x

The related tests see ISO standards from No. 10993–1 to 10993–6

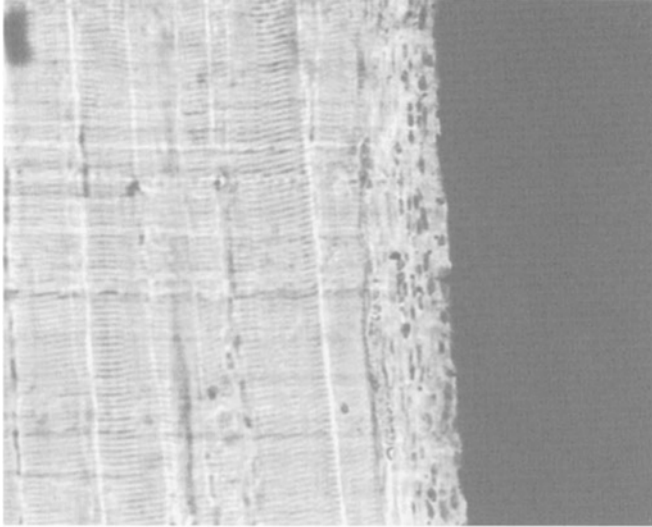
Table 5.6 Biological evaluations of zirconia ceramics (Prozyr®, Ceramiques Desmarquest, France)

Biocompatibility	Standard used	Results
Short-term <i>in vivo</i> biocompatibility	ASTM F 763/82	Very good
<i>In vitro</i> biocompatibility	ASTM F 748/82	
Cell culture cytotoxicity	PRIS 90.702	Good cytocompatibility
Mutagenicity	Ames test Micronucleus test	No mutagenic activity
Systemic injection acute toxicity	ASTM F 750/82	According to standard
Intracutaneous injection	ASTM F 749/82 ASTM F720/81	No irritation
Sensitization	Magnusson	No sensitization

5.5 Applications

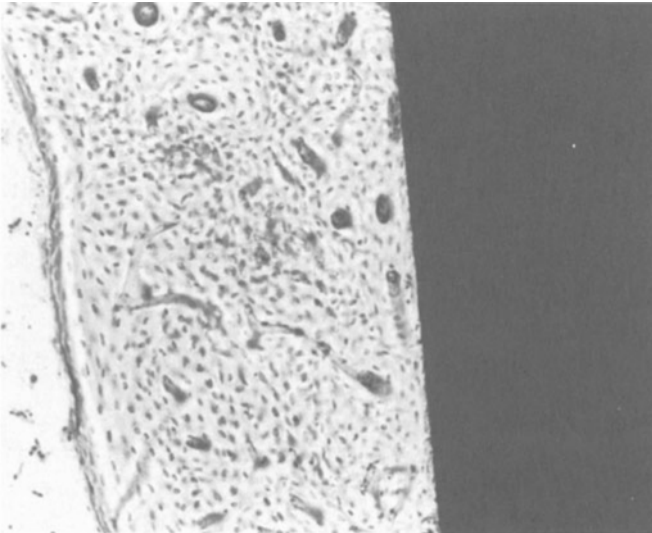
5.5.1 Orthopaedic applications

The dominating application of alumina and zirconia is as hip balls as well as cups of total femoral prosthesis. The neckless hip balls are the most popular design. In 1981, Oonishi *et al.* (8) reported on the use of an alumina ceramic total knee prosthesis. High alumina ceramic middle ear implants (Frialit) are used clinically in Europe since 1979 (21). An ophthalmological implant device consisting of a combination of a single crystal alumina optional cylinder and a polycrystalline alumina holding ring was introduced clinically in 1977 (22). Kawahara (12) has reported extensively on single crystal alumina bone screws.



(a)

Figure 5.3(a) Optical micrograph of alumina and soft tissue interface.



(b)

Figure 5.3(b) Zirconia and bone interface 1 month after implantation. Arrows are pointing to the interfaces.

Table 5.7 Ceramic manufacturers known for their bioceramic productions

Manufacturer	Country	Primary Materials	Secondary Materials	Trade Names Al ₂ O ₃ (ZrO ₂)
Astroment	USA	ZrO ₂	Al ₂ O ₃	
Ceraver	France	Al ₂ O ₃	ZrO ₂	
Cerasiv	Germany	Al ₂ O ₃	ZrO ₂	Biolox
Desmarquest	France	ZrO ₂		(ProyZR)
HiTech	France	ZrO ₂	Al ₂ O ₃	
Kyocera	Japan	Al ₂ O ₃	ZrO ₂	Bioceram
Metoxit	Switzerland	ZrO ₂		
Morgan Matroc	England	ZrO ₂	Al ₂ O ₃	
NGK	Japan	ZrO ₂		
Biocare	Sweden	Al ₂ O ₃		Procera
Unitek	USA	Al ₂ O ₃		Transcend 2000
Maillefer	Switzerland	ZrO ₂		

5.5.2 Dental applications

Alumina and zirconia ceramics have been utilized for root analogue, endosteal screws, blades and pin-type dental implants. The root and blade form dental implants used during the 1970s tended to fracture after a few years in function (41, 42) (Brose *et al.*, 1987, Driskell, 1987). Although initial testing of these polycrystalline alumina materials showed adequate mechanical strength, the long-term clinical results demonstrated functional limitations related to material properties and implant design. However, single crystalline alumina showed mechanical strength superior to that of polycrystalline alumina. It allows a much higher load. One-stage dental implants of single crystalline alumina are used clinically with a high success rate. McKinnery (43) had also reported on single crystal alumina blade and screw dental implants. Dental implants of zirconia have not been widely used clinically although zirconia has a similar mechanical strength and a much higher fracture toughness in addition to lower cost of production compared to single crystalline alumina. The term dental implant is used only for materials in contact with bone and soft tissue (14). Alumina and zirconia are also used in other dental applications, alumina ceramic crowns, Procera® (23), zirconia dental post, (10) and recently a dental inlay of zirconia was introduced (11). Orthodontic brackets made of oxide ceramics were also produced, tested and used clinically. Unfortunately, tooth surface damage was observed when the brackets were taken away (15). Modification of the debonding technique is under developing.

5.6 Manufacturers and Their Implant Products

Clarke and Willmann (13) make a comprehensive summary about the bioceramic manufacturers (Table 5.6). Some dental companies are included.

5.7 Problems and Future Prospects

Hip balls of polycrystalline alumina have a minimum size limitation to ca. 28 mm due to strength limitations. A reduced ball size might have two positive effects on the applications: reduced wear and better suitability (smaller) for Asian patients. Although single crystalline alumina might overcome the strength limitation, the cost of manufacturing is unreasonably high and in addition, some processing problems remain. Zirconia, on the other hand, has a high strength and high fracture toughness, but it suffers from potential biodegradation. Therefore, the future research and development will focus on the understanding of degradation mechanisms of zirconia in the body and the improvement of stability of this material. Of course, combinations, such as alumina/zirconia composite and even non-oxide ceramic, such as nitrides and carbides, ought also to be investigated.

References

1. Hulbert, S.F., Bokros, J.C., Hench, L.L., Wilson, J. and Heimke, G. In *Ceramics in Clinical Applications*, ed. by Vincenzini, P. Elsevier, Amsterdam, 1987, pp. 3–27.
2. Rock, M. German Patent 583 589, 1933.
3. Smith, L. *Arch. Surg.* 1963; **87**: 653–661.
4. Sandhaus, S. British Patent 1083769, 1967.
5. Boutin, P. *Presse Med.* 1971; **79**: 639.
6. Mittelmeier, H. *Z. Orthop. Ihre Grenzgeb* 1974; **112** : 27.
7. Shikita, T. Paper presented at the XIV World Congress of SICOT, Kyoto, Japan, October 15–20, 1978.
8. Oonishi, H., Okabe, N., Hamaguchi, T. and Nabeshima, T. *Orthopaedic Ceramic Implants I*, 1981; 11–18.
9. Lord, G. *et al.* Paper presented at the Harrington Arthritis Research Centre Symposium, November 18–21, 1990.
10. Akagawa, Y. *et al. J. Prosthet. Dent.* 1993; **69**: 599–604.
11. Meyenberg, K.H., Luthy, H. and Scharer, P. *J. Esthet. Dent.*, 1995; **7**(2): 73–80.
12. Johansson, B. *Tandläkartidningen* 1996; 14746–749.
13. Clarke, I.C and Willmann, G. In *Bone implant Interface* ed. H.V. Cameron, Hugh U., Mosby, 1994, pp. 222.
14. Kawahara, H. In *Encyclopedic handbook of biomaterials and bioengineering* ed. by Wise, Donald L. *et al.* Marcel Dekker, Inc., New York, 1995, pp. 1469–1524.
15. Sinha, P.K., Rohrer, M.D., Nanda, R.S. and Brickman, C.D. *American J. Orthodont & Dentofacial Orthop*, 1995; **108**: 455–63.
16. Christel, P.S. In *Condse Encyclopedia of Medical & Dental Materials*, ed. by Williams, D.F., Pergamon Press, Oxford, 1990, pp. 375–379.
17. Keith, O., Kusy, R.P. and Whitley, J.Q. *American J. Orthodont. & Dentofacial Orthop.*, 1994; **106**(6): 605–614.
18. Kawahara, H. *Orthopaedic Ceramic Implants I*, 1981; 1–10.
19. Fartash, B. Single Crystal Sapphire Dental Implants: Experimental and Clinical Studies. PhD thesis, Karolinska Institute, Sweden, 1996.
20. Hammer, N.B., Topazian, R.G., McKinney, P.V. and Hulbert, S.F. *J. Dent. Res.* 1973; **52**: 356–361.

21. Jahnke, K. *Biomaterials in Otolaryngology*, Martinus Nijhoff, The Hague, 1984:205–209.
22. Polack, F.M. and Heimke, G. *Ophthalmology*, 1980; **87**(7): 693–698.
23. Andersson, M. and Odén, A. *Acta Odont. Scand.*, 1993; **51**: 59–64.
24. Kittipibul, P. and Godfrey, K. *American J. Orthodont & Dentofacial Orthopedics*, 1995; **108**(3): 308–315.
25. Heimke, G. In *Metal and Ceramic Biomaterials Vol I Structure*, ed. by Ducheyne, P. and Hastings, G.W. CRC Press Inc., Boca Raton. Florida, 1984, pp. 41–42.
26. Miyayama, M. *et al.* In *Ceramics and Glass, Engineered Materials Handbook Volume 4*, ASM International, 1991, pp. 748–757.
27. Griss, P. In *Functional Behavior of Orthopaedic Biomaterials 11*, Ch 2, 1984.
28. Jager M. and Plitz, W. *Triobology of aluminium ceramics, Symposium of Biomaterials*, pp. 114–122, 1981.
29. Willert, H.G. *et al.* In *Implant Retrieval: Material and Biological Analysis*, ed. by Weinstein, A., Gibbons, D., Brown, S. and Ruff, W. 1981.
30. Fritsch, E.W. and Gleitz, M. *Clin. Orthop. & Related Res.*, 1996; **328**: 129–136.
31. Garvie, R.C, Hannink, R.H. and Pascoe, R.T. *Nature*, 1975; **258**: 703.
32. Saikka, V.O. *Acta Orthop. Scand.*, 1995; **66**(6): 501–506.
33. Kumar, P. *et al.* *J. Biomed. Mater. Res.*, 1991; **25**: 813–828.
34. Derbyshire, B. *et al.* *Medical Eng. & Phys.*, 1994; **16**(39): 229–36.
35. Shimizu, K. *et al.* *J. Biomed. Mater. Res.*, 1993; **27**: 729–734.
36. Cales, B., Stefani, Y. and Lilley, E. *J. Biomed. Mater. Res.*, 1994; **28**: 619–624.
37. Hummer, C.D., Rothman, R.H. and Hozack, W.J. *J. Arthroplasty*, 1995; **10**(6): 848–850.
38. Ichikawa, Y. *et al.* *J. Prosthet. Dent.* 1992; **68**: 322–6.
39. Takamura, K. *et al.* *J. Biomed. Mater. Res.*, 1994; **28** : 583–589.
40. Stefflik, D., McKinney Jr R.V. and Koth, D. In *Bioceramics: Materials characteristics versus in vivo behavior*, ed. by Ducheyne, P. and Lemons, J.E. *Ann. N. Y. Acad. Sci.* **523**, pp. 4–18.
41. Brose, M. *et al.* *J. Dent. Res.*, 1987; **66**: 113.
42. Driskel, T.D. *J. Calif Dent. Assoc.*, 1987; 16–25.
43. Mckinney, R.V. and Koth, D.L. *J. Prosthet. Dent.*, 1982; **47** : 69–84.
44. Park, J.B. and Lakes, R.S. *Biomaterials: an Introduction*, 2nd edition, Plenum Press, New York, 1992.
45. Bajpai, P.K. and Billotte, W.G. In *The Biomedical Engineering Handbook*, ed. by Bronzino, J.D. CRC Press, 1995, pp. 552–580.

Chapter 6

Ceramic Materials Testing and Fracture Mechanics

Garth Hastings, Ishbel Gair, and D. Daily

6.1 Introduction

6.1.1 Ductile and Brittle Behaviour

In general, metals deform by dislocation movement which is essentially a shearing process as the planes of atoms slip over each other. The process is referred to as “slip”. To be completely ductile there should be five systems in a crystal capable of independent slip movement (this is known as the von Mises criterion). Most FCC metals with a face-centred cubic lattice structure deform quite easily by slip, while other systems less so. If the criterion cannot be met, the behaviour is that of semi-brittle or brittle solids.

Ductile behaviour is quite well known in inorganic solids. Single crystals of most alkali metal halides can be deformed at room temperature, and it is also possible to strain a pure single crystal of magnesium oxide by 10%. To obtain NaCl as a polycrystalline ceramic the powder is simply pressed to 100% density at room temperature in a die. This is impossible by sintering. Many ceramics become ductile at high temperatures when slip planes which are inactive at room temperature become activated eventually to meet the von Mises criterion. Ceramics also become deformable by grain boundary sliding at high temperature, and in creep both types of

The original version of this chapter was revised. An erratum to this chapter can be found at DOI [10.1007/978-1-4939-3305-1_36](https://doi.org/10.1007/978-1-4939-3305-1_36)

G. Hastings

Staffordshire University (Emeritus), Lyme, Staffordshire, UK

e-mail: garth.hastings@btinternet.com

I. Gair

Technical Consultant, Lucideon Ltd, Staffordshire, UK

e-mail: ishbel-@hotmail.co.uk

D. Daily

(deceased)

deformation behaviour are possible. At room temperature both ceramics and glasses fall into the brittle category and any significant deformation is accompanied by cracking. This may be intergranular, i.e. within the grain boundaries in materials like alumina, or within the grains as in zirconia.

It is very difficult to identify obvious properties which relate to strength of a ceramic, but there are a number of factors to which one can point.

6.1.2 Microstructure

6.1.2.1 Effect of Grain Size

$$\sigma_g = \sigma_\infty + \sigma_1 G^{-1/2}$$

σ_g =strength of the ceramic, G =mean grain size. σ_1 and σ_∞ are material constants. This is the Orowan–Petch relation first observed in steels in 1953 and holds for all crystalline materials. It implies that the finer the grain size, the stronger the material, although it fails for small grain sizes.

Carniglia [33] has identified a two-stage relationship in which the strength dependence changed at a critical grain-size G_0 . Davidge and Evans enlarged on this [34] and related the grain-size/strength dependence to the fracture mechanism. In the larger grain size region, to which the above relations refer, fracture occurs as a consequence of the extension of inherent flaws while for the lower grain sizes, plastic flow is the dominant cause. The changeover in behaviour is a property of the material considered, related to its purity, and environmental factors such as temperature. In ceramics where there are large and small grains, an initial flaw in a large grain region propagates until it reaches a finer region where the apparent fracture surface energy is higher. Here it is held up until the stress becomes critical for the new region.

Producers of structural bio ceramic components devote much effort towards the choice and quality of raw materials used in the manufacture of these devices. This is of particular importance to load-bearing orthopaedic implant applications where strength and fracture toughness properties are critical to the long-term performance of the device. The need therefore is to produce high purity, dense ceramic with fine grain crystalline microstructures, free from inclusions and/or impurities often introduced through raw materials and production processes. The introduction inhomogeneity within the microstructure of the ceramic does have a detrimental effect on the strength and fracture toughness properties of the device. Inclusion or defects as small as $\sim 10 \mu\text{m}$ in a sintered ceramic microstructure have contributed in vivo failure. It must also be mentioned that other factors such as device design (see Chap. 7—Ceramic hip joint endoprosthesis) and processing surface treatment, for example grinding, honing and polishing, do influence the strength of the ceramic component and ultimately the long-term success of a device.

The majority of ceramics currently used in the manufacture of orthopaedic devices are high-purity zirconia toughened alumina (ZTA), alumina (>99.9%), zirconia, and all contain grain size substantially sub-micrometre. In recent years various ISO, BSI, ASTM and CEN Standards have been developed and published,

specifying the material performance requirements and testing methodologies for implantable grade ceramics. Microstructural specifications including grain size are stated in the ISO 6474: part 1 for alumina, ISO 6474: part 2 for ZTA and the ISO 13356 for zirconia. The ISO 6474 part 1 grain size specification for load bearing orthopaedic implantable alumina is $\leq 2.5 \mu\text{m}$ although the grain size in commercial grades has significant proportion of sub-micrometre microstructure. Zirconia (ISO 13356) specifies a grain size $\leq 0.4 \mu\text{m}$; commercial grades are typically $0.3\text{--}0.4 \mu\text{m}$. ZTA forms a matrix of alumina and zirconia have two size specifications $\leq 1.5 \mu\text{m}$ for the crystalline alumina phase and $\leq 0.6 \mu\text{m}$ for the zirconia, the typical grain size $0.5\text{--}0.8 \mu\text{m}$ for alumina phase and $0.1\text{--}0.2 \mu\text{m}$ for zirconia.

6.1.2.2 Strength of Individual Grains

Sapphire single crystals are stronger than polycrystalline alumina, so a crack would be expected to follow the grain boundaries, so that the smaller the grains, the greater the surface free energy of sapphire, — about $6\text{--}7 \text{ J/m}$, while for polycrystalline alumina, this is about 30 J/m . It should therefore be harder to create new surfaces in ceramic alumina than in sapphire. The only explanation for this is that in the ceramic, the cracks are there already, as surface and volume flaws, while in sapphire they need to be nucleated.

Pure cubic zirconia is a relatively weak material and normal sintering invariably generates very large grains. One concludes that it is easier for a crack to go across a grain rather than travel through the grain boundaries.

6.1.2.3 Multiphase and Multicomponent Structures

New considerations have to be introduced for these materials such as (1) the coherency of the boundaries between different crystalline components; (2) the stress imparted at the interfaces between components (and this can be severe enough to crack the material) as a consequence of cooling components or phases of different thermal expansion; (3) different elastic moduli of non-equilibrium of solutes within phases once these can create internal stresses which oppose crack propagation.

6.1.3 Porosity

Porosity reduces the strength of ceramics. Approximately a 50% decrease in strength results from a 10% increase porosity. Duckworth [35] proposed the following relationship:

$$\sigma = \sigma_0 \exp^{-bP}$$

where σ = strength of the porous material, σ_0 = strength of the fully dense material, P = porosity, b is a constant.

Coble and Kingery measured the flexural strength of polycrystalline aluminas for porosities between 5% and 50% porosity, and using the symbols above, proposed the following empirical equation:

$$0.6P = \exp \frac{-\sigma}{8000(1-p)}$$

Knudsen [36] and Passmore et al. [37] derived formulae to describe the coincident effects of grain size and porosity on alumina at both 25 and 1200 °C. These were of the form:

$$\sigma = k \cdot \exp(-bP) \cdot G^{(-1+cP)},$$

where c , k and b are constants, and G is the grain size. This relationship becomes increasingly in error as the porosity approaches zero.

It is usually considered that the reduction of strength by porosity is caused by stress concentrations around individual pores. In some instances pores can interact with a moving crack front to produce a reduction of localised stress [37]. Other porosity concepts include the assumption by Eudier [38] that the strength is lowered by the simple reduction of load-bearing cross-sectional area, for which he proposed the equation:

$$\frac{\sigma}{\sigma_0} = 1 - kP^{2/3}$$

k is a constant approximately equal to 1.21.

Porosity will be reconsidered after the Griffith concept has been discussed.

6.1.4 Valency Type

In general covalent substances are stronger than ionic. Diamond, silicon carbide, silicon nitride, cubic boron nitride (borazon), boron carbide are typical; they contain very few flaws and usually have a rigid framework structure.

Alumina and silica are substances with both ionic and covalent character. At very high stresses (e.g. at the tips of cracks) deformation by slip is possible causing a dissipation strain energy.

The relationship between failure stress, surface energy and concentration of flaws is a complicated one, but a number of approaches to this problem have been made, giving rise to the science of fracture mechanics.

6.2 Strength Testing of Ceramics

6.2.1 Tensile Testing

In contrast with metals, stress does not cause deformation by slip in ceramics, and eventual failure along the planes of maximum shear stress. Ceramics fail by the propagation of cracks, and in particular when one of them reaches a critical length. Ceramics also are 8–10 times stronger in compression than in tension, and so the

ceramic member is designed for use in compression, while is specified its strength as a result of tensile test.

Metals are usually tested in tension on a tensile machine where a machined specimen is trained and the strain is measured as the increase in separation of a pair of marks divided by the original distance separating them (called the “gauge length”), and the stress is determined from a load cell reading. This method of testing is not convenient for ceramics for the following reasons.

6.2.2 Ceramic Machining

Machining ceramics to precise dimensions requires diamond grinding. This is a costly operation, and a specially prepared piece may have to be made in a separate operation. Consequently this may not be representative of the batch of material about which information is required. The grinding operation itself can introduce surface flaws which may impair the strength of the test piece.

6.2.3 Test Pieces

The test piece will probably be dumbbell shaped and carefully have avoided sharp corners which would create a stress concentration. It would be supported by a ring, and another ring would be used to supply the extension force.

The alignment of such a test piece would be critical, requiring a universal joint between the extending crosshead of the machine and the test piece. Failure to do this would cause a stress intensification where the ring makes contact.

6.2.4 Flexion and Flexure Testing

Direct tensile measurement is therefore not a practical proposition and testing is performed by flexion of bars, rods, discs or other shapes, which easily allow representative samples to be made. It will be shown that it is possible to normalise the results of flexure tests to a tension equivalent. The theory behind flexure testing will now be examined in some detail.

6.2.5 Beam Theory [12]

In the process of bending a material, cross section mm and pp (Fig 2.1) rotate with respect to each other about axes perpendicular to the plane of bending, so that longitudinal fibres on the convex side are extended and longitudinal fibres on the concave side are compressed.

Fig. 2.1 Beam Theory

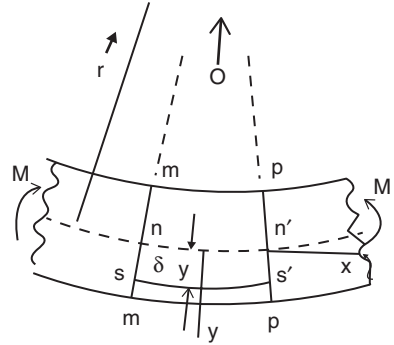
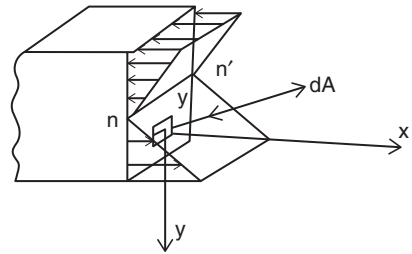


Fig. 2.2 Neutral Surface



There is also some intermediates surface which is neither extended nor compressed, called the “neutral surface” represented by nn' . The radius of curvature r is measured from the neutral surface nn' . Let ss' be any surface at a distance y from the neutral axis, then, from similar triangles,

$$\frac{nn'}{r} = \frac{ss'}{r + \delta_y} = \frac{nn' + \delta_x}{r + \delta_y} = \frac{\delta_x}{\delta_y} \tag{6.1}$$

$$\text{strain} = \epsilon_x = \frac{\delta_x}{nn'} = \frac{\delta_y}{r}$$

$$\text{From Hooke's Law, } \frac{\sigma_x}{\epsilon_x} = E \tag{6.2}$$

$$\text{Therefore } \sigma_x = E \frac{\delta_y}{r}$$

This diagram represents the distribution of stresses. They increase numerically with distance from nn' .

Let dA represent an elemental area of cross section at distance y from nn'

$$\text{Force acting on } dA = \sigma_x dA = \frac{E y}{r} dA \tag{6.3}$$

Sum of all such forces over the cross section represent a couple resultant in the x direction, therefore $= \phi$

$$\int \frac{E y}{r} dA = \frac{E}{r} \int y dA = \phi \tag{6.4}$$

Moment of force acting on dA , with respect to nn' is $\frac{E y}{r} dA \cdot y$.

Adding all the moments over the cross section, and equating to the moment of the external forces M ,

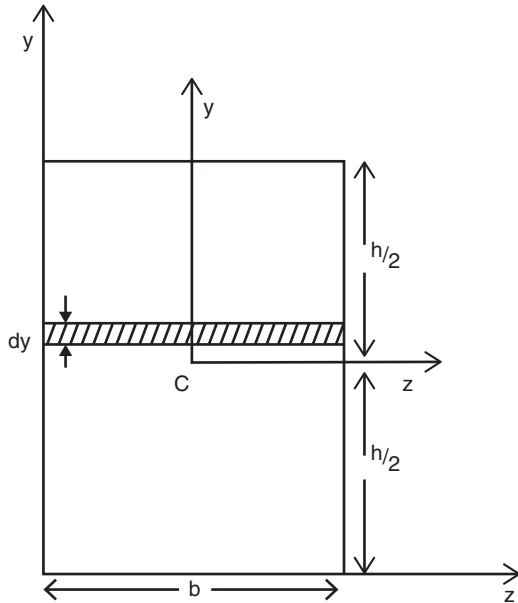
$$\frac{E y^2}{r} dA = \frac{E I_z}{r} = M \tag{6.5}$$

6.2.5.1 Rectangular Section Test Piece

This defines the relation $\frac{1}{r} = \frac{M}{E I}$, where $I = \int y^2 dA$ (6.6)

I_z is the “moment of inertia of bending” (analogous to the expression used in describing a rotating body).

Fig. 2.3 Rectangular Section Test Piece



For a rectangle,

$$I_z = 2 \int_0^{h/2} y^2 b dy = \frac{bh^3}{12}. \quad (6.7)$$

For a circular section (diameter d)

$$I_z = \frac{\pi d^4}{64}. \quad (6.8)$$

Eliminating r , we have,

$$\sigma_z = \frac{My}{I_z}$$

For a rectangle,

$$I_z = 2 \int_0^{h/2} y^2 b dy = \frac{bh^3}{12} \quad (6.9)$$

For a circular section (diameter d)

$$I_z = \frac{\pi d^4}{64} \quad (6.10)$$

Eliminating r , we have,

$$\sigma_z = \frac{My}{I_z}$$

Maximum tensile or compressive stress is in the outermost fibre. If nm' is the middle of the section, and the thickness = h

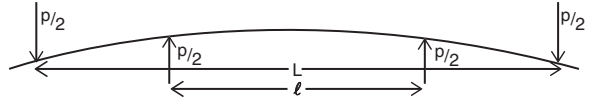
$$(\sigma_x)_{\max} = \frac{Mh}{2I_z} \quad (6.11)$$

6.2.6 3 and 4 Point Bending

For a rectangular, four-point bending system,

$$M = \frac{P(L-2)}{2} \frac{P(L-2)}{2}$$

Fig. 2.4 4 Point Bending



$$\begin{aligned} \text{Stress in outermost fibre} &= \frac{p}{2} \cdot \frac{(L-l)}{2} \cdot \frac{h}{2} \cdot \frac{12}{bh^3} \\ &= \frac{3 p(L-l)}{2 bh^2} \end{aligned}$$

Frequently 1/4 point loading is used, i.e. where $L = 4a$ and $l = 2a$ so that maximum stress $= \frac{3Pa}{bh^2}$. This is the failure stress (sometimes called modulus of rupture)

$$\begin{aligned} \sigma_F &= \frac{3Pa}{bh^2} \left\{ = \frac{3 PL}{4 bh^2} \right\} \\ \left(\text{For a cylinder } \sigma_F &= \frac{16Pa}{\pi d^3} \right) \end{aligned}$$

For a three-point bend, let $l = \phi$

$$\sigma_F = \frac{6Pa}{bh^2} = \frac{3PL}{2bh^2} \tag{6.12}$$

$$\left(\text{For a cylinder } \sigma_F = \frac{32Pa}{\pi d^3} \right) \tag{6.13}$$

6.2.6.1 Calculation of Deflections

6.2.6.2 Simple Cantilever

$$P(L-x) = M = \frac{EI}{R} = EI \frac{d^2L}{dx^2} *$$

Integrate,

$$\frac{dy}{dx} = \frac{P}{EI} \left(Lx - \frac{x^2}{2} \right) + A$$

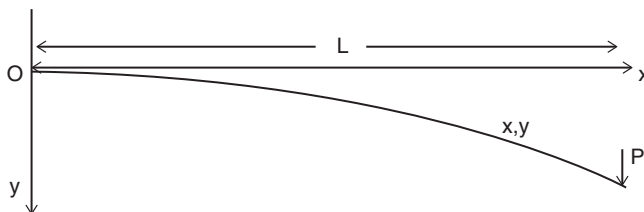


Fig. 2.5 Simple Cantilever

Now $A = 0$, because $\frac{dy}{dx} = 0$ at the origin

$$y = \frac{P}{EI} \left\{ \frac{Lx^2}{2} - \frac{x^3}{6} \right\} + B$$

Now $B = 0$ because $y = 0$ when $x = 0$ at origin.

Depression at the free end is therefore

$$\Delta_{\max} = \frac{PL^3}{3EI} \quad (6.14)$$

For a curve $y = f(x)$ at a specific point,

$$R = \frac{\left[1 + (dy/dx)^2 \right]^{3/2}}{d^2y/dx^2} = \frac{1}{d^2y/dx^2}$$

(In this instance)

6.2.6.3 Three-Point Bend

This is equivalent to two cantilevers symmetrically opposed. Point of application of P equivalent to simple cantilever fixation point.

Let L be the length of the test specimen

$$\Delta_{\max} = \frac{(P/2)(L/2)^3}{3EI} = \frac{PL^3}{48EI} \quad (6.15)$$

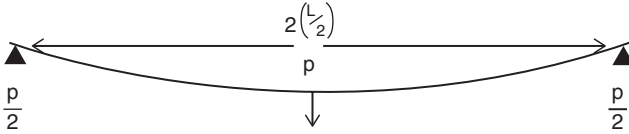


Fig. 2.6 3 Point Bending

6.2.6.4 Four-Point Bend

We require to determine:

- (a) radius of curvature.
- (b) maximum elevation of the centre of the beam above the support points.
- (c) depression of ends below support points.

Let h be elevation above supports, then from the similar triangles OPC and CPQ

$$\frac{R-h}{(\ell/2)} = \frac{(\ell/2)}{(2h)}$$

Neglecting h cf. R ,

$$\frac{\ell^2}{4} = 2Rh, \quad h = \frac{\ell^2}{8R}$$

The important aspect of the four-point bend test is that there is a circular arc with a constant bending moment between the loading points (B and C in Fig. 7). Effectively the specimen selects its own weakest point for failure within this region.

$$\begin{aligned} \text{Over BC, } M &= \frac{P}{2} \cdot \frac{(L-\ell)}{2} = \frac{EI}{R} \\ R &= \frac{2EI}{(P/2)(L-\ell)} \\ h &= \frac{(P/2)(L-\ell)\ell^2}{16EI} \end{aligned}$$

(6.16)

Let C represent the origin. Inclination to horizontal at $c = \frac{(\ell/2)}{R}$

$$= \arcsin \theta \quad \theta = \frac{(P/2)(L-\ell)\ell}{4EI}$$

Let right hand part of the beam contain the points (x, y) .

Taking moments,

$$M = \frac{P}{2} \left\{ \frac{(L-\ell)}{2} - x \right\} = \frac{d^2y}{dx^2} EI$$

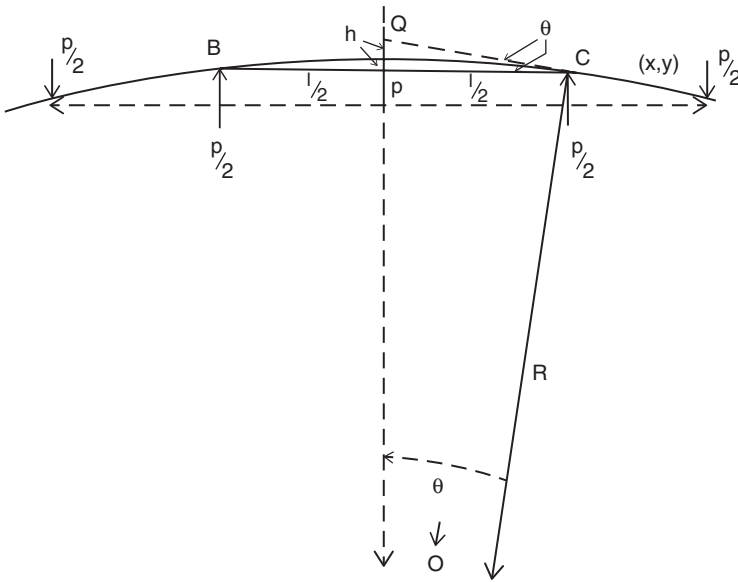


Fig. 2.7 4 Point Bend Test

$$\frac{dy}{dx} = \frac{(P/2)}{EI} \left\{ \frac{(L-\ell)x - x^2}{2} \right\} + A$$

At C, the origin, $x = 0$, $A = \left(\frac{dy}{dx} \right) = \theta$

$$\frac{dy}{dx} = \frac{(P/2)}{2EI} \left\{ (L-\ell)x - x^2 + \frac{(L-\ell)}{2} \cdot \ell \right\}$$

By integration,

$$y = \frac{(P/2)}{2EI} \left\{ \frac{(L-\ell)}{2} x - \frac{x^3}{3} + \frac{(L-\ell) \cdot \ell x}{2} \right\} + B$$

At C, $x = 0$, $y = 0$, therefore $B = 0$.

To find the depression at the ends, let $x = \frac{L-\ell}{2}$.

Depression of the ends below the origin,

$$= \frac{(P/2)}{8EI} \left\{ \frac{(L-\ell)^3}{2} - \frac{(L-\ell)^3}{6} + (L-\ell)^2 \cdot \ell \right\}$$

For $\frac{1}{4}$ point, symmetrical loading, let $L = 4a$, $\ell = 2a$

$$\begin{aligned}
 &= \frac{(P/2)}{8EI} \left(\frac{8a^3}{2} - \frac{8a^3}{6} + 8a^3 \right) \\
 &= \frac{2Pa}{3EI}
 \end{aligned}
 \tag{6.17}$$

These deflection formulae may be used to determine the elastic modulus. At high stresses the machine deflection becomes significant, and a blank run has to be performed to determine this.

6.2.7 Test Configurations

6.2.7.1 Biaxial Flexure of Discs

R_L is the loaded radius; R_O is the outer radius; R_S is the supported radius; t is the plate thickness; P is the loading force; V is Poisson’s ratio.

Principal stresses in the plate are $\sigma_r = \sigma_\theta$

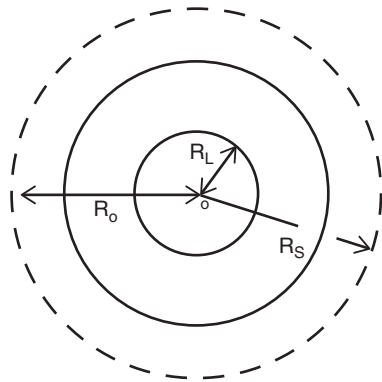
$$\sigma_r = \sigma_\theta = \frac{3P}{2\pi t^2} \left\{ (1+\nu) \ln \frac{R_S}{R_L} + (1+\nu) \frac{(R_S^2 - R_L^2)}{2R_O^2} \right\}
 \tag{6.18}$$

These are effectively the failure stresses for the ceramic.

This test is especially valuable for ceramics in that:

- (a) it tests simultaneously in two dimensions at right angles.
- (b) there are no sharp edges in the stress field to initiate cracks.
- (c) discs are easy to press, fire and polish.
- (d) they take up little room in a furnace, and a batch of ten can expect to have identical firings.

Fig. 2.8 Biaxial Flexure Disc Test



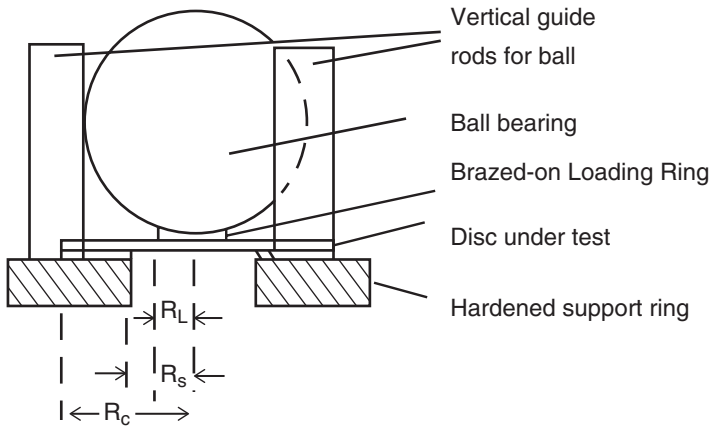
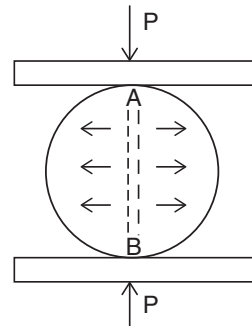


Fig. 2.9 Test configuration

Fig. 2.10 Forces Applied During test



Alternatively the hardened support ring may be replaced by three balls at the apexes of an equilateral triangle. This overcomes the problem of flatness in discs.

R_s becomes the radius of the circumcircle of the latter.

(Ref. Ph.D. Thesis, A.D. Sivill, University of Nottingham, 1974) [32].

6.2.7.2 Diametrical Compression Test [19, 29]

A disc specimen is compressed between two flat plates. Tensile splitting occurs along the loaded diameter AB. It was developed originally in Brazil and Japan for testing concrete about 1943. A biaxial stress distribution is set up in the disc, provided the thickness is small compared with the diameter.

$$\sigma_{\max} = \frac{2P}{DtT} \tag{6.19}$$

6.2.7.3 Brittle Ring Test [19, 31]

$$= \frac{6W \cdot (OD + ID)}{\pi \cdot t (OD - ID)^2} \quad (6.20)$$

(Tensile stresses are indicated at W, X, Y, Z .)

This configuration is especially useful for high temperature testing in that it avoids the use of testing jigs (at 1600–1700 °C it would be deforming as fast as the test piece). The specimen undergoes fracture in four places, often showing separate maxima on the testing machine. In some respects it resembles two three-point bend tests superimposed above and below the horizontal diameter. The mathematical derivation is tedious, but the test is capable of high reproducibility.

6.2.7.4 Theta Specimen [13, 14, 19]

This is also used for high temperature strength determinations. Photoelastic studies indicate that central bar is in pure uniform tension. This pattern was selected out of 60 shapes, but the difficulty of precision shaping has restricted its application. This

Fig. 2.11 Brittle Ring Test

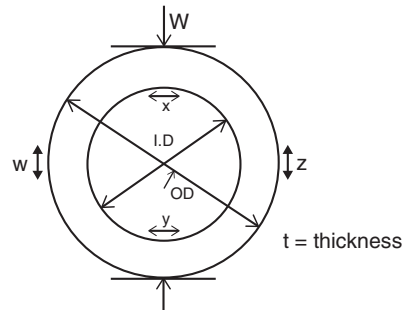
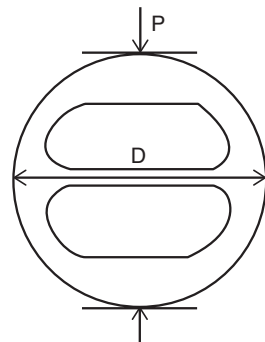


Fig. 2.12 Force applied during Brittle Ring testing



should no longer be a problem exploiting the high reproducibility of the computer-machining technique of P. Barnes and D.F. Dailly, at the North Staffordshire Polytechnic. The relation to evaluate the stress in the central bar is

$$\sigma = kP / Dt \quad (6.21)$$

σ =stress in bar, P =applied load, D =outer diameter, t =thickness: k is a constant = 13.8 (Daniels) or 16.4 (Durelli).

K can be easily determined using a strain gauge and a knowledge of the elastic modulus.

6.2.8 *Significance of Test Results*

To appreciate the problems associated with ceramic design it would be useful to compare the elastic behaviour with those of metals. For a non-ferrous metal such as copper (Fig. 14), the stress developed as a consequence of the strain can be represented in two stages. The initial region is Hookean, where the slope of the curve is the elastic modulus, but beyond this it departs from linearity and the resultant stress is proportionately less because of slip caused by dislocation movement on the favourably oriented slip planes in the crystal lattice. In an FCC metal like copper, with four slip planes per unit cell this process is easy. With hexagonal or body-centred cubic systems slip is less easy.

It is therefore usual to specify such metals in terms of the ultimate tensile strength (UTS) and a 1% or 0.1% proof stress, the percentages referring to the amount of permanent deformation resulting from the strain (Fig. 2.14).

For ferrous metals the situation is slightly different, in that a “yield point” is displayed. Once again the dislocations are responsible in that a threshold stress has to be supplied to overcome the stabilising effect of the interstitial carbon and nitrogen atoms which have anchored themselves in the strained region of the lattice immediately adjacent to the dislocation core. We have therefore to specify the UTS and the yield point (Fig. 2.15).

For a ceramic (Fig. 2.15) the stress–strain graph displays an entirely Hookean behaviour, and this continues until the test-specimen breaks. However, the fracture stress can vary over a wide range, and no ultimate tensile stress is able to be specified. For a design specification this introduces an entirely new concept. It must be recognised that there is no realistic lower limit below which the test specimen cannot fail, and the best that can be given is finite probability of failure under a given tensile stress. It will further be shown that many factors are likely to influence the value of the strength of a ceramic. These may emerge from the conditions under which the test is performed, the size of test piece chosen, the smoothness of its surface which is under tension and the particular configuration of the test. So that all test results are comparable, there should be a normalisation of the results to unit volume under pure tension.

Fig. 2.13 Stress/Strain Graph of Non-Ferrous Metal

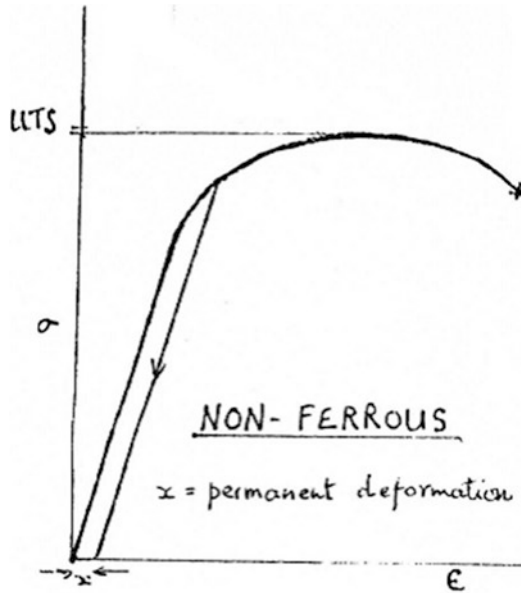
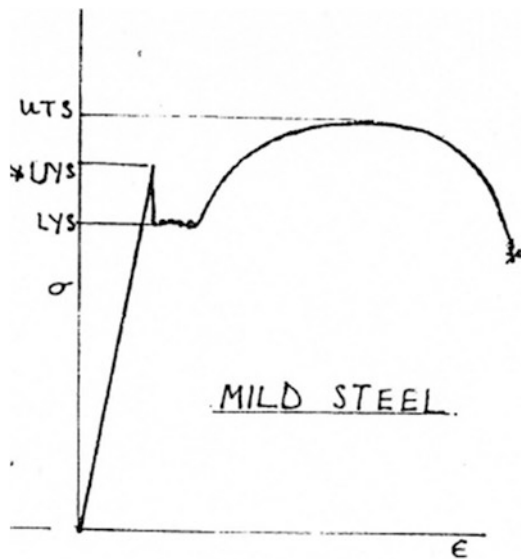


Fig. 2.14 Ultimate Tensile Strength of Mild Steel

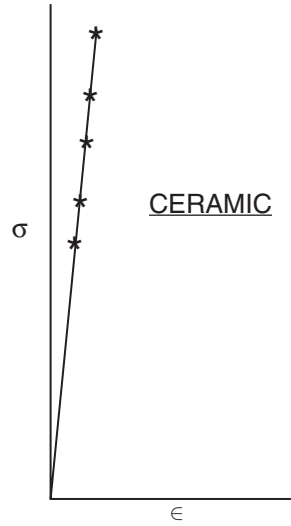


6.2.9 Processing of Failure Data [7]

The following expression was given by Weibull for the probability of failure, and it is especially applicable to brittle materials.

$$P_f = 1 - \exp \left\{ \left(\frac{-\sigma - \sigma_u}{\sigma_0} \right)^m \right\} \tag{6.22}$$

Fig. 2.15 Stress/Strain graph of Ceramic (Hookean behaviour)



σ_u is a “threshold stress” below which the probability of failure is zero. The threshold stress when compared to the mean stress is relatively small and typically set as zero rather than given a finite number which may result in over estimation of the probability of failure. It does have significance for glasses.

σ_0 is a normalising factor.

σ is the stress in the material.

m is the “Weibull modulus” and it is a measure of the variability of σ . The higher the value of m , the more consistent the material.

The function is valid for all stresses in the range $\sigma_u \leq \sigma \leq \infty$.

Failure probabilities are in the range $0 \leq P_f < 1$.

For ceramic materials it is usual to find m in the range $5 < m < 20$.

The curve can be fitted to the experimental points by the manipulation of the values m , σ_u and σ_0 .

Stress/mean stress of batch.

(Ph.D. University of Nottingham 1973)

While this may be the best method of obtaining m , it is time-consuming and laborious, but with the help of a few assumptions a very rapid procedure is possible, particularly if a computer is employed.

Assume $\sigma_u = 0$. Let F be the probability of failure corresponding to an applied stress σ .

$$\begin{aligned} \text{Then } F &= 1 - \exp\left\{-\left(\frac{\sigma}{\sigma_0}\right)^m\right\} \\ \text{Then } \frac{1}{1-F} &= \exp\left(\frac{\sigma}{\sigma_0}\right)^{m--} \quad \text{---Takelogs} \\ \ln \frac{1}{1-F} &= \left(\frac{\sigma}{\sigma_0}\right)^{m--} \quad \text{---Takelogs again} \end{aligned}$$

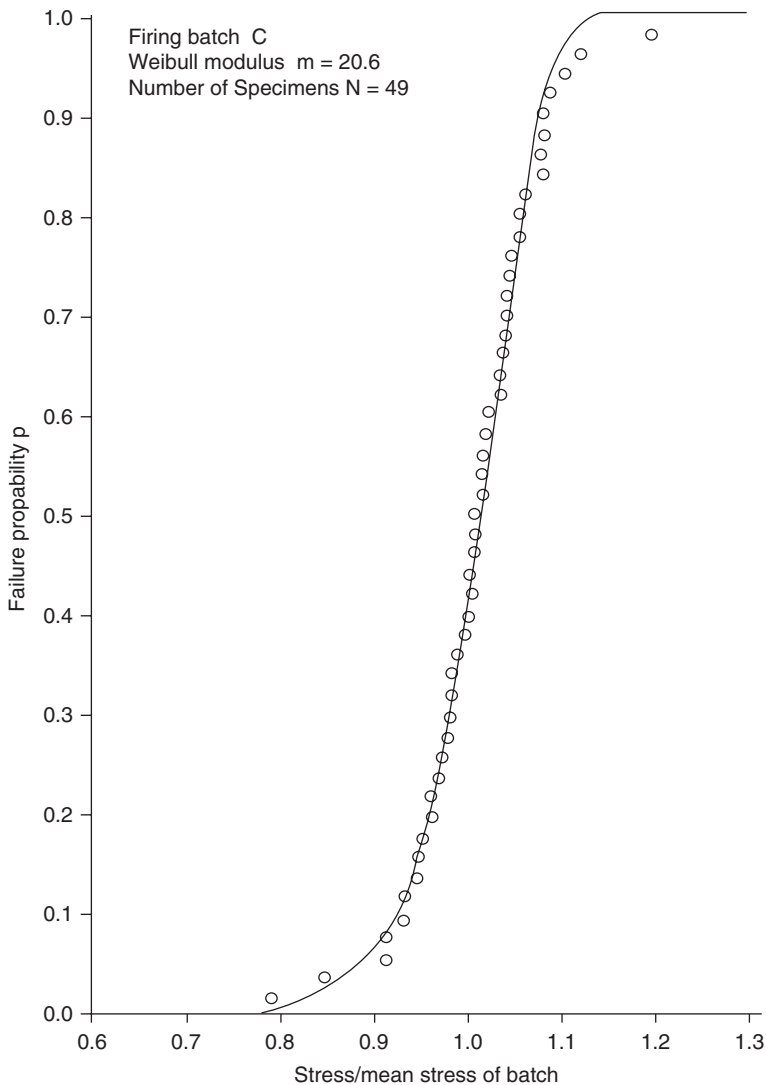


Fig. 2.16 Weibull distribution of the fracture data of a sintered batch of Reaction bonded silicon nitride

$$\ln . \ln . \frac{1}{1-F} = m \ln \sigma - m \ln \sigma^0 . \tag{6.23}$$

Weibull graph paper is ruled with $\ln . \ln . \left(\frac{1}{1-F} \right)$ as the ordinate units and one simply plots F against σ to obtain straight line graph of which m is the slope.

Note : when $\sigma = \sigma_0 \ln . \ln . \frac{1}{1-F} = 0 \ln \frac{1}{1-F} = 1$

$$\exp^{-1} = (1 - F) \quad F = 1 - \exp^{-1} = 0.632$$

This makes σ_0 the value of σ when 63.2% of failures have occurred.

If one fails to obtain a straight line, or there is a sharp gradient change, it is a sign that more than one process is occurring during the failure, e.g. if there is an unexpected decrease in strength at the lower end of failure stresses it suggests a processing fault, or a bimodal distribution (Fig. 2.22) suggests a wide disparity of particle sizes (e.g. in abnormal grain-growth).

6.2.10 Ranking (or How We Arrive at the Value of F)

One must remember that the purpose of the Weibull statistics is to be able to take a limited number of data from the breakage of test-specimens and obtain a reasonable value for m . This will act as a control for our processing schedule. Twenty is a convenient number, but if the quantity of raw material is limited, even ten results can be useful.

Consider a very large population of N data. If one value has to be chosen at random, then each has a $1/N$ chance of being picked.

If the data is placed in ascending order, the chance of picking a value less than, or equal to the i th number in the list is i/N .

Each value in the data list is therefore associated with a cumulative probability of $P = i/N$.

Let the large circle contain N data (in a bag if the analogy is helpful). Let us withdraw i' data at random and arrange it in ascending order. (Think of $i' = 20$ for a convenient number.)

Assemble the data in order on the ladder diagram (Fig. 2.18) and represent it with the full lines. Return the data to the bag, shake it and withdraw another 20 (i'').

Set these up in ascending order, and indicate them with the short dashed lines. Return, shake and withdraw another 20 (i''').

Fig. 2.17 "N" data ring

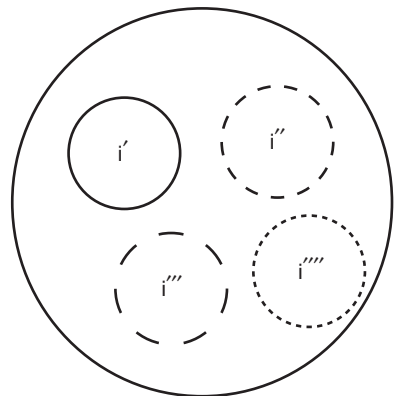
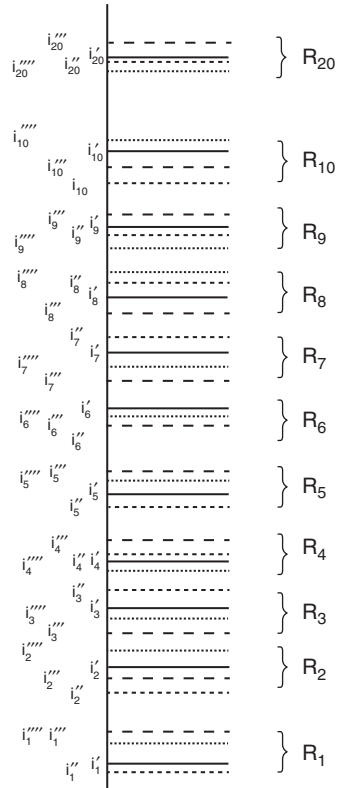


Fig. 2.18 Ladder Diagram



Set these up in ascending order, and indicate with the long dashed lines. Return, shake and withdraw another $2(i''')$ (dotted lines).

Repeat until i' is obtained.

Each sequence of first values $i', i'', i''', \dots \dots i'$

second values $i', i'', i''', \dots \dots i'$

third values $i', i'', i''', \dots \dots i'$

twentieth values $i', i'', i''', \dots \dots i'$

is called a “rank”.

Each value is a binomial distribution of 20 values (or other number if chosen) which will have a most probable value represented by the mean or median of the distribution. There are formulae for calculating these or there are tabulated values for convenient numbers. Procedure:

When an appropriate number of tests have been made,

1. the results are arranged in sequence.
2. the table of “ F ” values for the number of tests is obtained (Table 6.1).
3. using Weibull paper, we plot F is ordinate and σ as abscissa the lowest value of F is made to correspond with the lowest failure stress and so on.
4. using the least squares method, the best line is obtained through the points.
5. gradient of the line is m , the Weibull modulus.

Table 6.1 Median ranks (F_{50}) [7]

Rank	Sample size		
	<u>5</u>	<u>10</u>	<u>20</u>
1	12.95	6.70	3.41
2	31.38	16.23	8.25
3	50.00	25.86	13.15
4	68.62	35.51	18.06
5	87.06	45.17	22.97
6		54.83	27.88
7		64.49	32.80
8		74.14	37.71
9		83.77	42.63
10		93.30	47.54
11			52.46
12			57.37
13			62.29
14			67.21
15			72.12
16			77.03
17			81.95
18			86.85
19			91.75
20			96.59

By producing the line backwards it is possible to predict the failure probability at any stress loading. This is probably the most satisfactory way to specify the strength of a brittle material such as a ceramic.

6.2.11 Nature of the Test [7]

To compare three point bend specimens with those tested in pure tension, the following expression relates

$$\frac{\sigma_{B3}}{\sigma_T} = \left[(m+1)^2 \cdot \frac{v_T}{v_{B3}} \right]^{1/m} \tag{6.24}$$

For a Weibull modulus of 10 and specimens of equal volume,

$$\frac{\sigma_{B3}}{\sigma_T} = 1.614 \tag{6.25}$$

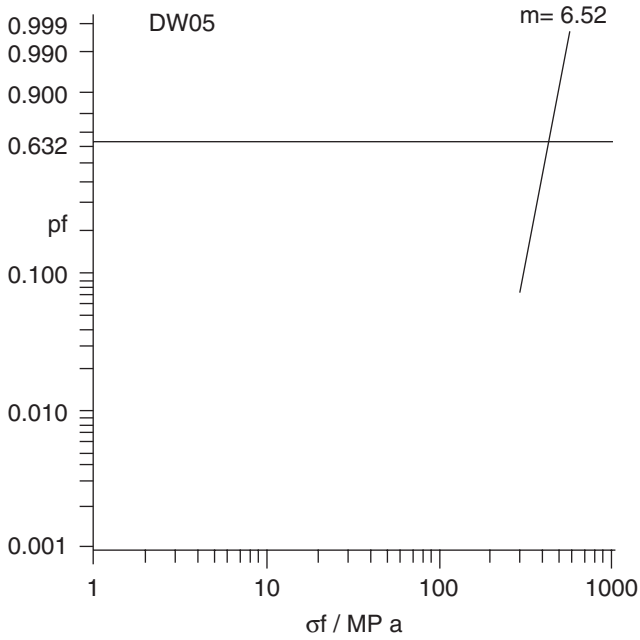


Fig. 2.19 95 % alumina 1600 °C 120 min. 50 mm × 3 mm bars, ¼ point loading

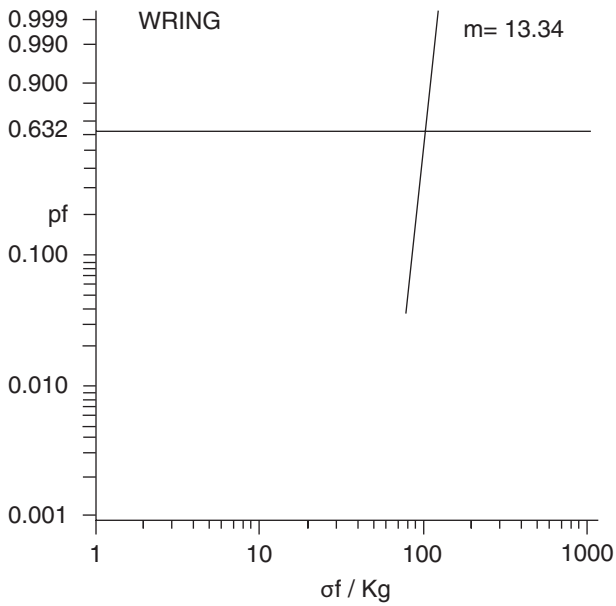


Fig. 2.20 Ground and refined alumina ring specimens

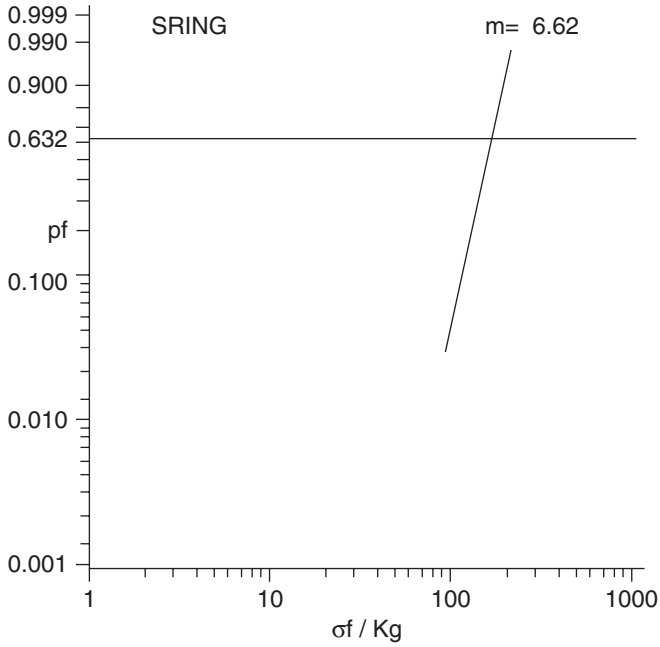


Fig. 2.21 Grand alumina ring specimens

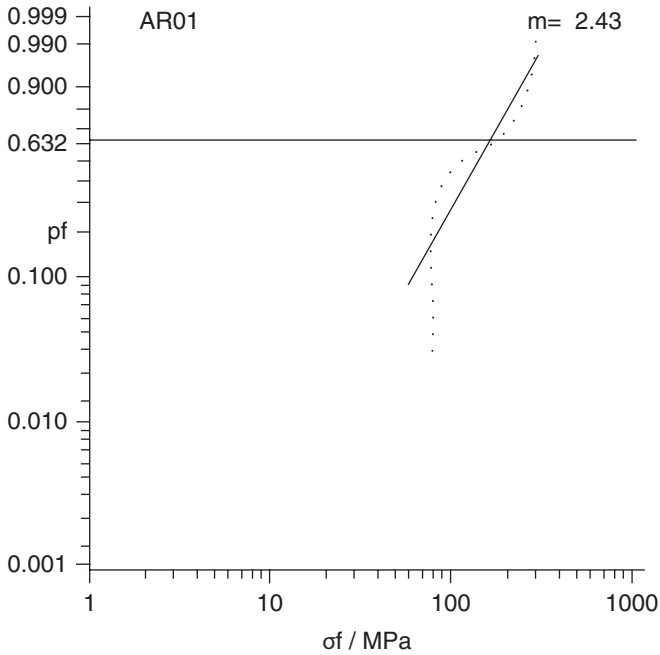


Fig. 2.22 AIS alumina, showing bimodal distribution

Comparison of four point with tension uses the following expression

$$\frac{\sigma_{B4}}{\sigma_T} = \left[(m+1) \cdot \frac{V_T}{V_{B4}} \right]^{1/m} \quad (6.26)$$

and for a Weibull modulus of 10 and equal volumes of test pieces

$$\frac{\sigma_{B4}}{\sigma_T} = 1.27 \quad (6.27)$$

Relating four point to three point under the same conditions gives

$$\frac{\sigma_{B4}}{\sigma_{B3}} = 0.785 \quad (6.28)$$

6.2.12 Volume of Test Piece [7]

Because brittle fracture depends on the largest crack in the stress field growing until it reaches a critical length, the larger the volume of the test specimen the higher will be the probability of a crack being present which is large enough to cause failure. It is for this reason that one uses large test pieces, and chooses four-point loading instead of three-point. The relationship is simple, i.e.

$$\frac{\sigma_{V_1}}{\sigma_{V_2}} \left(\frac{V_2}{V_1} \right)^{\frac{1}{m}} \quad (6.29)$$

In a rearranged form, $\sigma_{V_1}^m V_1 = \sigma_{V_2}^m V_2$. This expression will be used in the following chapter.

6.3 Strength of Solids [11]

6.3.1 Theoretical Strength of Crystals

The shear stress at which deformation should begin in an ideally perfect crystal was calculated by Frenkel in 1926. Referring to Fig. 2.1 representing two adjacent planes of atoms in a simple crystal structure, we see that if the upper plane were displaced relative to the lower in the slip direction b , causing atoms A' , B' , C' , etc. to lie over B , C , D , etc. respectively, slip would have taken place. The crystal would remain perfect as the atoms had moved to equivalent lattice sites. The shear stress

necessary to produce this permanent plastic deformation is the critical shear stress τ_c of the ideally perfect crystal.

To obtain its value we first consider the form of the stress displacement curve (Fig. 2.2) measuring displacements indicated in Fig. 2.1.

Now $\tau=0$, when $x=0$ and $x=b$;

The crystal is in equilibrium in both cases.

When $x = \frac{1}{2}b$, the atoms in the upper layer can be seen to be in a position of unstable equilibrium; the force in the slip direction is zero, for each atom is equally attracted to the right and to the left.

Consequently $\tau=0$, also at $x = \frac{1}{2}b$.

Further, we know from the elastic behaviour of crystals that the shear stress increases linearly with strain within the elastic range. The slope of the displacement curve at $x=0$ and $x=b$ must therefore comply with Hook's law.

$$\frac{\tau}{\gamma} = G \quad (6.30)$$

where

$$\gamma = x/a, \tau = \frac{Gx}{a} \quad (6.31)$$

Thus

$$\frac{dx}{dx} = G/a (x \ll a)$$

Now $\tau(x)$ must be a periodic function with wavelength b , and we therefore taken the relation as typical,

$$\tau = K \sin\left(\frac{2\pi x}{b}\right) \quad (6.32)$$

Other harmonic functions satisfying the boundary conditions at $x=0$, $\frac{1}{2}b$ and b could have been chosen, without affecting the result. As Eq. (6.32) must reduce to Eq. (6.30) for small strains, one finds that

$$\tau = G \frac{x}{a} = K \frac{(2\pi x)}{b}$$

Re-presenting a very small angle, so that

$$K = \frac{Gb}{2\pi a} \quad (6.33)$$

The highest stress occurs when

$$2\pi \frac{x}{b} = \frac{1}{2}\pi$$

i.e. at $x = \frac{1}{4} \cdot b$, and is numerically equal to K . In practice a and b will not differ from one another appreciably and one therefore obtains the result that the critical shear stress of the ideally perfect crystal is

$$\tau_c \approx G/10 \quad (6.34)$$

The maximum elastic shear strain occurs when $x = \frac{1}{4}b$ and is therefore equal to $\frac{1}{4} \cdot \frac{b}{a}$ which, with $a \approx b$, yields

$$\gamma_c \approx 25 \% \quad (6.35)$$

Perfect crystals necessary to check this theory can only be obtained in the form of microscopically thin whiskers. They have, nevertheless, established the correctness of the foregoing results. However, the critical shear stress of pure copper is only about 20 kg/cm², while $G/10$, Eq. (6.34) yields about 40,000 kg/cm². The strength of the ideal crystal is therefore about 2000 greater than the real one. In metals this discrepancy is accounted for by the presence of dislocations, while in non-metals, and in particular in ceramic substances, the discrepancy is caused by cracking, although both processes can be present to some degree in either class of material.

6.3.2 Elastic Constants and Interatomic Forces [11]

If we recollect the Born equation, which is $u = \frac{Ae^2}{r} + \frac{B}{r^n}$ and plot U , the potential energy against r , the interionic distance, the curve displays a minimum of energy, resulting from a balance of attractive and repulsive forces. This minimum is at the distance r_0 , which is the equilibrium interionic spacing in the lattice. (The first term in the Born equation represents the Coulombic energy, and the latter represents the repulsion caused by quantum exchange energy as the electron shells of adjacent ions approach.) Similar curves exist for covalent and van der Waals bonds. The elastic constants can be estimated from the function U . A crude calculation illustrates the principle involved. The force between the atoms is $\frac{du}{dr}$ and stress is

$$\sigma \approx \left(\frac{du}{dr} \right) \cdot \frac{1}{r_0^2} \quad (6.36)$$

dr = force

r_0 = area of one atom plane

i.e. the force divided over the approximate area over which it operates. Now

$$d\sigma = cd \in = c \frac{dr}{r_0} \quad (6.37)$$

and thus

$$c = r_0 \frac{d\sigma}{dr} \sim \frac{1}{r_0} \left(\frac{\partial^2 u}{\partial r^2} \right) \quad (6.38)$$

For a shear deformation, the Born repulsive term may be neglected, and thus for ionic crystals $u \propto \frac{1}{r_0}$. Substitution in Eq. (6.32) predicts a proportionality between C_{44} and r_0^{-4} .

When we try to shear the lattice we have to overcome the peak of maximum resistance. Over small displacements the stress-distance curve is approximately a sine wave so we may write

$$\sigma = \sigma_{th} \sin \frac{\Pi}{2\alpha} (r - r_0) \quad (6.39)$$

where a is the atomic displacement corresponding to the theoretical strength, and the material is assumed isotropic.

If E is the elastic modulus, then, $E = \frac{d\sigma}{d\epsilon}$, and

$$\frac{d\sigma}{d\epsilon} = r_0 \frac{d\sigma}{dr} = \frac{r_0 \sigma_{th} \Pi}{2\alpha} \cos \frac{\Pi}{2\alpha} (r - r_0)$$

For very small strains, $r - r_0 \rightarrow 0$, the cosine term $\rightarrow 1$, so that

$$\sigma_{th} = \frac{2E\alpha}{\Pi r_0} \quad (6.40)$$

To estimate the constant a , Orowan's argument is that the work done in stressing the material to σ_{th} , must be at least equal to the energy required to create two new fracture faces. If γ_0 is the surface energy per unit area,

$$\int_{r_0}^{r_0+2\alpha} \sigma dr = \frac{2E\alpha}{\Pi r_0} \int \sin \frac{\Pi}{2\alpha} (r - r_0) dr = 2\gamma_0 \quad (6.41)$$

and this reduces to

$$\frac{4E\alpha^2}{\Pi^2 r_0} = \gamma_0 \quad (6.42)$$

Eliminating α using Eq. (6.35) gives

$$\sigma_{th} = \left(\frac{E\gamma_0}{r_0} \right)^{\frac{1}{2}} \quad (6.43)$$

High surface energy and stiffness, together with a small lattice spacing, contribute to high strength, although a high fabricated density is also required. It has been shown that $\alpha \approx 0.14 r_0$ for ionic crystals. Note in the previous hypothetical approach $\alpha = r_0/4$ substituting in Eq. (6.37), gives

$$\gamma_0 \approx \frac{Er_0}{125} \quad (6.44)$$

Substituting values for alumina where $E = 4 \times 10^{11} \text{ N/m}^2$, $r_0 = 4 \times 10^{-10} \text{ m}$ gives $\gamma_0 \approx 1.2 \text{ Jm}^{-2}$ (This is for a sapphire and not a polycrystal) and agrees with experimental data.

In general, two lines of approach to the study of fracture have been made. These are:

1. The Griffith's approach, where the reduction of strain energy in the test sample is equated to the increase of surface energy of the crack.

Formulae for fracture energy have been derived and practical evaluation methods described.

2. The elastic continuum approach, where the intensified stresses at the edge of the crack-tip are considered. From this the 'Stress Intensity Factor' can be defined, the critical value of which is a materials property can be used in engineering design. Equations from the two approaches can be related to provide a number of useful testing methods to evaluate the fracture toughness of a material.

6.3.3 Griffith's Theory [2]

6.3.3.1 Basic Derivation of Expression

Let a plate contain a thin elliptical crack of length $2c$, represented by AOB in Fig. 3.1, under a uniform stress σ . To find an expression for the relaxation of the strain energy as the crack is formed, assume that the plate consists of a number of independently operating linear elements. Behind the crack front there will be a stress free zone, caused by the shrinkage of the elements. Let it be assumed that the length of this zone, measured along each element from the line AOB representing the centre of the crack is y_0 . This figure will obviously vary from zero at the crack edges to y_0 in the centre.

Fig. 3.1 Elliptical Crack Diagram

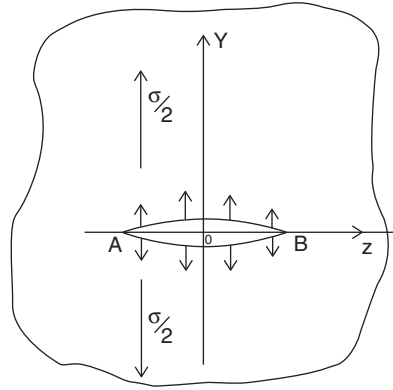
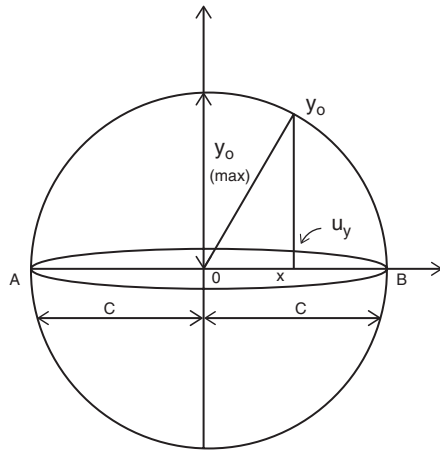


Fig. 3.2 Stress Free Zone AOB



The original strain can now be calculated:
Strain imparted to each element is

$$\frac{\mu_y}{y_0} = \frac{E}{\sigma / 2} \tag{6.45}$$

Therefore $\mu_y = \frac{E}{\sigma / 2} y_0$

μ_y represent the y coordinates of the ellipse and y are lengths of the stress-free zone.
For the ellipse,

$$\frac{x^2}{c^2} + \frac{\mu_y^2}{b^2} = 1, \mu_y^2 = \frac{b^2}{c^2} (c^2 - x^2) \tag{6.46}$$

$$y_0^2 \cdot \left(\frac{E}{\sigma / 2} \right) = \frac{b^2}{c^2} (c^2 - x^2) \tag{6.47}$$

Consider an element at $x = \emptyset$

$$y_{0(\max)}^2 \left(\frac{E}{\sigma/2} \right)^2 = b^2$$

$$\frac{y_0^2 c^2}{y_{0(\max)}^2} = (c^2 - x^2)$$

The locus of the lengths of y_0 is a circle if

$$\frac{c^2}{y_{0(\max)}^2} = 1$$

We may confirm this if we let $x = c/2$

$$\frac{y^2}{y_{0(\max)}^2} = 3/4 \quad (\text{Fig. 3.2})$$

$$\frac{y}{y_{0(\max)}} = \frac{\sqrt{3}}{2}$$

Since $0_x = c/2$, $xy = \frac{\sqrt{3}}{2}$, then $0_y = c$. Which is a radius of the same circle.

Therefore y_0 lies on a circle, and $y_0 = \sqrt{(c^2 - x^2)}$

In order to compute these relaxing stresses, we require to know the displacement of the upper surface of the ellipse, given by the following expression:

$$\mu_y = \sqrt{(c^2 - x^2)} \cdot \left(\frac{E}{\sigma/2} \right) \quad (6.48)$$

Work done by the relaxation of the elements (μ_ϵ) is also the strain energy released, and is given by,

$$U_\epsilon = \frac{1}{2} \sigma \mu_y dx \quad (\text{per element})$$

$$U_\epsilon = \frac{1}{2} \int_0^c \sigma \mu_y dx \quad (\text{per quadrant})$$

$$U_\epsilon = 2 \int_0^c \sigma \mu_y dx \quad (\text{for circle}) \quad (6.49)$$

That is

$$U_{\epsilon} = \frac{\sigma^2}{E} \int_0^c \sqrt{(c^2 - x^2)} dx \tag{6.50}$$

$$\int_0^c \sqrt{(c^2 - x^2)} dx = 1/2x\sqrt{(c^2 - x^2)} + 1/2c^2 \arcsin(x/c)$$

When $x=0$, $\arcsin = 0$; when $x=c$, $\arcsin = \pi/2$.

Leaving the notion of independent elements and returning to the continuous sheet, the elastic constraints must now be put in, so that the expression becomes modified to

$$U_{\epsilon} = \frac{\sigma^2}{E} (1+r)(k+1) \int_0^c \sqrt{(c^2 - x^2)} dx \tag{6.51}$$

where $k=3-4r$ for plane strain,

and $k = \frac{(3-r)}{(1+r)}$ for plane stress

(r is Poisson's ratio).

On integration, Eq. (6.51) gives

$$U = \frac{\sigma^2 \Pi c^2}{4E} (1+r)(k+1) \tag{6.52}$$

This expression represents the total crack surface and it should be noted that the expression is independent of the semi-minor axis of the ellipse b

6.3.4 Griffith's Criterion [2]

According to the Griffith criterion, the surface energy, U_s , needed to create new surfaces, is supplied by the energy released, U_{ϵ} . The total free energy, U , for the cracked body is expressed as,

$$\mu = \mu_s - \mu_{\epsilon} + \bar{\mu} \tag{6.53}$$

where $\bar{\mu}$ is the component of the strain energy independent of the crack in the body (i.e. $\frac{d\bar{\mu}}{dc} = 0$) and is equal to $\frac{\sigma^2}{2E}$ per unit volume for this system. In Griffith's terminology, U is the total potential energy for the system. In terms of the total energy of the system

$$\frac{du}{dc} < 0 \quad \text{when the crack is unstable}$$

$$\frac{du}{dc} = 0 \quad \text{when the crack is in equilibrium}$$

$$\frac{du}{dc} > 0 \quad \text{when the crack is stable}$$

The surface energy per unit thickness, U_s , equals $4c\gamma_0$. Substituting for U_s and U_e in Eq. (6.53) we have,

$$u = 4c\gamma_0 - \frac{\sigma^2 \Pi c^2}{4E} (1+r)(k+1) + \bar{\mu} \quad (6.54)$$

For the equilibrium situation $\frac{du}{dc} = 0$, and if the applied stress be equal to σ_f .

$$\frac{du}{dc} = \frac{du_s}{dc} - \frac{du_e}{dc} = 4\gamma_0 - \frac{\sigma_f^2 \Pi c}{2E} (1+r)(k+1) = 0$$

Therefore

$$\sigma_f = \sqrt{\frac{8\gamma_0}{\Pi c(1+r)(k+1)}} \quad (6.55)$$

For plane stress and plane strain the expression takes the form,

$$\sigma_f = \sqrt{\frac{2E\gamma_0}{(1+r^2)\Pi c}} \quad \text{Plane strain} \quad (6.56)$$

$$\sigma_f = \sqrt{\frac{2E\gamma_0}{\Pi c}} \quad \text{plane stress} \quad (6.57)$$

The results of tests carried out by Griffith indicated that the theoretical predictions were justified provided that there was little or no plastic flow in the region of the crack tip. Because there is always some dissipation of energy due to plastic flow, the Griffith expression tends to give a higher value than the true thermodynamic one.

The theory does bring out a very important point, namely that the strength of a solid is dependent on the flaw size in a direction normal to the applied stress, and the probability of failure will, in turn, depend on the probability of there being a flaw in excess of the critical size.

6.3.5 Energy Release Rate

We define G as the energy release rate. This is either the strain energy release or the potential energy release rate, and it is the energy released per unit extension of the crack front per unit thickness of the body (rate in this instance relates to distance rather than time).

In the opening mode (or mode 1, in Fig. 4.3), if the crack moves at both ends a distance $2dc$, relative to a crack size $2c$,

From equation, at equilibrium,

$$\frac{du}{dc} = \frac{du_s}{dc} - \frac{du_\epsilon}{dc} = 0. \tag{6.58}$$

$$G = \frac{du_\epsilon}{dc} \left(= \frac{du_s}{dc} \right) \quad du_s = 4\gamma_0 dC \tag{6.59}$$

For the case where the crack operates from one end only,

$$G = \frac{du_\epsilon}{dc} \left(= \frac{du_s}{dc} \right) \quad du_s = 2r_o dC \tag{6.60}$$

where the crack size is critical (Fig. 3.2) $c=c$ and G is equal to twice the thermodynamic surface energy.

I.e. $G = 4\gamma_0$ (for the double-ended crack) [1–5] and $2\gamma_0$ (for the single ended crack).

This defines the strain-energy-release rate per unit width of crack front.

The conclusion of this analysis is that we can relate the failure stress σ_f with the size of the crack c , provided we have some knowledge of γ_0 the fracture energy, or G , the strain energy release rate.

What follows is a discussion of the significance of G , followed by practical evaluation methods for γ_0

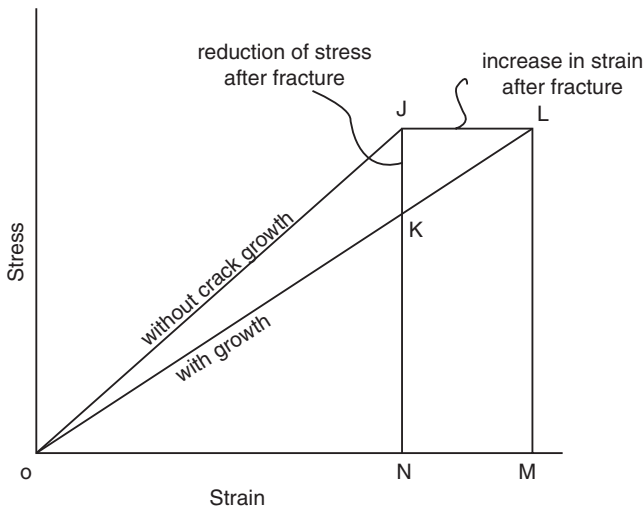
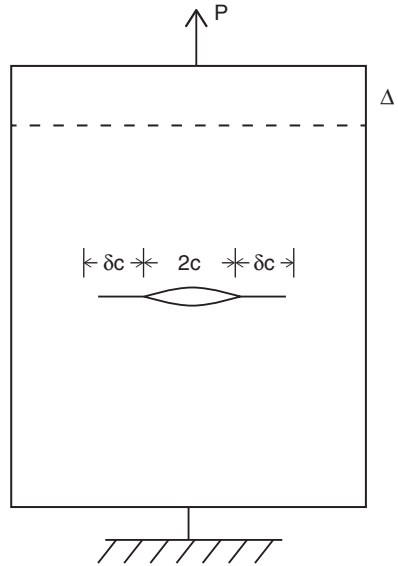


Fig. 3.3 Strain Energy Release Rate

Fig. 3.4 Failure stress associated with Size of crack



6.3.6 Geometric Illustration of Compliance

An energy balance criterion has been developed by Davidge [3] using a simple geometrical argument (Fig. 3.3). Suppose the stress/strain curve of the sheet containing the crack is represented by OJ . Let the crack now grow in length from $2C$ to $2(C+dC)$, i.e. equal amounts at both ends. The sheet will then be less stiff. The stress/strain curve is now represented by OKL . When deformation is by dead loading (i.e. constant stress), the strain increases by JL . When a rigid machine is used the strain is constant and therefore the reduction of stress is given by JK . Let the fracture energy per unit area be given by γ_0 . As the crack grows, the energy required to form new fracture faces is $4\gamma_0 dC$.

The elastic strain energy is du .

The external work done on the sheet is dW .

The condition for fracture is therefore,

$$d(w - u) \geq 4\gamma_0 dC \tag{6.61}$$

We need to estimate W and U .

Note that the energy is proportional to the area under the graph, so that when fracture occurs at constant strain, $dW = \emptyset$ and an amount of elastic strain energy, proportional to OKJ is released (dU is negative).

When fracture occurs at constant stress, dW is proportional to $JLMN$ and the elastic strain energy increases proportional to $OLM - OJN = OJL$. Because JKL becomes negligible in the limit, $d(W - U)$ is again proportional to OJK .

Note that $dW=2dU$; half the external work is absorbed as elastic energy, and half is available to assist crack propagation.

For either type of loading, we can continue the discussion solely in terms of U . The condition for fracture reduces to

$$\frac{du}{dC} \geq 4\gamma_o \quad (6.62)$$

6.3.7 Analytical illustration of Compliance

Following Lawn and Wilshaw [1], another approach to the understanding of G is as follows (Fig. 3.4):

A crack is made in sheet of brittle solid of unit thickness and one end is loaded with a tensile force P . The test piece behaves according to Hooke's law as follows:

$$\delta = P\lambda \quad (6.63)$$

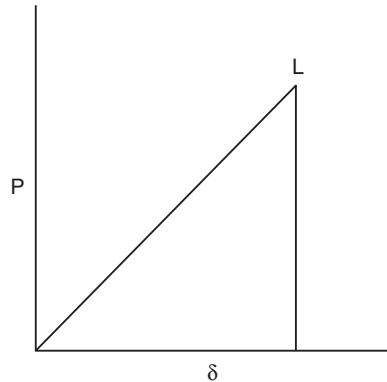
where δ is the elongation of the test piece and λ is the elastic compliance. The strain energy is therefore,

$$u_\epsilon = \int_0^\delta Pd\delta = \frac{1}{2}P\delta$$

(P is a function of δ and is area under curve)

$$= \frac{1}{2}P^2\lambda = \frac{1}{2}\frac{\delta^2}{\lambda} \quad (6.64)$$

Fig. 3.5 Hooke's Law



Let us now consider two extreme loading configurations,

1. Constant force (i.e. dead-weight loading)

Let U be the strain energy in the test piece, and W be the work done by the load, then, as the consequence of crack-growth,

$$\delta w \approx P\delta(\delta) = P^2\delta\lambda \quad (6.65)$$

$$\delta u = \frac{1}{2}P^2\delta\lambda \quad (6.66)$$

and the total change in mechanical energy is

$$\delta(-w+u) \approx \frac{-1}{2}P^2\delta\lambda \quad (6.67)$$

2. Constant displacement

$$\begin{aligned} \delta W &= 0 \\ \delta u &= -\frac{1}{2}P^2d\lambda \end{aligned} \quad (6.68)$$

giving

$$\delta(-w+u) = -\frac{1}{2}P^2\delta\lambda \quad (6.69)$$

It will be seen that the two results are identical, i.e. the mechanical energy released during incremental crack extension is independent of the loading configuration. We can therefore define a crack extension force, which is the strain energy release rate with respect to the crack length in a test piece of unit thickness.

The strain energy release rate is a measure of available potential energy, and the given the symbol G and is equal to

$$\frac{-d(-w+u)}{dC}$$

and is equivalent to

$$G = -\left(\frac{\partial u}{\partial c}\right)_\delta$$

Because $W = \emptyset$, for the constant strain situation (i.e. where the fixation is rigid).

6.3.7.1 Practical Methods [1]

From equations $G = \frac{1}{2}P^2 d\lambda/dc$ and $\frac{1}{2}(\delta^2/\lambda^2)d\lambda/dc$, G can be deduced in two ways. At constant stress, all that is needed is the load, and a calibration for the compliance. At constant strain, one needs to know the compliance, and then its rate of change with the crack-length. Because of the negative sign the strain energy actually decreases under constant strain, but under constant stress it increases. For this reason constant stress methods are preferable, because the crack configuration is stable.

Davidge and Tappin [10] describe a practical method for compliance analysis with a notched bar specimen. The “stiffness” k is determined from the load/deflection curve, and it is given by:

$$P = k\delta \quad (6.70)$$

Stored energy at the instant of fracture is given by

$$U = \frac{P_F \delta_F}{2}$$

Now $\gamma_c = -\left(\frac{\partial u}{\partial A}\right)_\delta$, fracture occurring at a fixed deflection, or

$$\gamma_c = -\left(\frac{\partial u}{\partial k}\right)_\delta \cdot \left(\frac{\partial K}{\partial A}\right)_\delta$$

But,

$$\left(\frac{\partial u}{\partial k}\right) = \delta^2$$

and thus

$$\gamma_c = -\delta^2 \left(\frac{\partial K}{\partial A}\right) / 2 \quad (6.71)$$

Experimentally, one has to measure the specimen stiffness k as a function of the initial crack area $A = 2bc$. For each notch depth used, $\partial K/\partial A$ is obtained from the slope of the curve at the appropriate value of A , as in Fig. 3.4. If we substitute these values of $\partial K/\partial A$ in Eq. (6.70) with the experimental values of δ_F , a series of values of γ_c is given for each notch depth.

The equivalence of the two equations is shown as follows:

Remembering that $k(\text{stiffness}) = 1/\lambda$ ($\lambda = \text{compliance}$) and stating Hooke's law $P = k\delta$ (P is the applied force, δ is the deflection)

$$\begin{aligned}
 G &= \frac{1}{2} P^2 \frac{d\lambda}{dc} \\
 &= \frac{1}{2} P^2 \frac{d\left(\frac{1}{k}\right)}{dc} = -\frac{1}{2} P^2 \frac{1}{k^2} \frac{dk}{dc} \\
 &= -\frac{\delta^2}{2} \left(\frac{dk}{dc}\right)_\delta = \frac{b\delta^2}{2} \left(\frac{\partial k}{\partial A/2}\right)_\delta \\
 &= -\frac{\delta^2}{2} \left(\frac{\partial k}{\partial \frac{A}{2}}\right)_\delta
 \end{aligned}$$

(both sides of a single-ended crack)

Since

$$G = 2\gamma_c \text{ (at equilibrium)}$$

$$\gamma_c = \frac{G}{2} = \frac{-\delta^2}{2} \left(\frac{\partial k}{\partial A}\right)_\delta \quad (6.72)$$

6.3.8 *Experimental Technique for Compliance: Calculating of γ [10]*

Five test bars of $\varnothing.5$ cm square section and 4 cm length are prepared as accurately as possible (allowing for sintering shrinkage) with progressively increasing notch-depths, cut accurately with a diamond saw, so that the crack area increases conveniently in units of $\varnothing.1$ cm of cross-sectional area. The bar is then subject to a three-point bend test, and the stiffness is obtained from dividing the applied load by the deflection obtained. It is advisable to find the average value of a number of tests, particularly at low crack areas. This deflection may be measured directly by a transducer or in terms of movement of the chart, making corrections for the deformation of the load cell of the testing-machine at comparable loads. Note that the first objective is not to extend the crack or break the specimen, but merely to obtain plots from which k and $\left(\frac{\partial k}{\partial A}\right)_\delta$ can be broken and δ_F obtained (at the point of fracture).

The tabulation is completed for each specimen, the stiffness against crack area curve drawn, and $\left(\frac{\partial k}{\partial A}\right)_\delta$ obtained for each specimen area, by measuring the gradients of the curve.

Fig. 3.6 Stiffness versus Crack Area

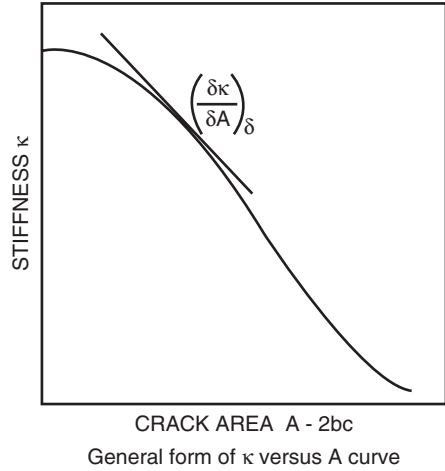
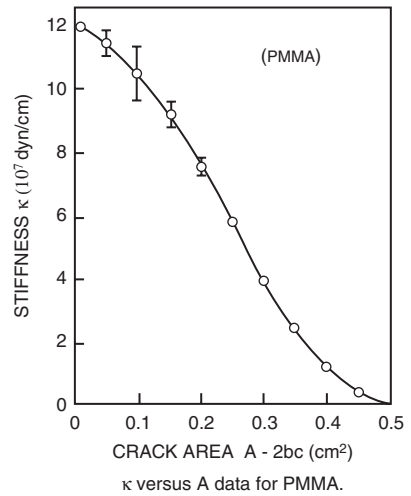


Fig. 3.7 Stiffness Gradient Curve



6.3.8.1 Compliance Results

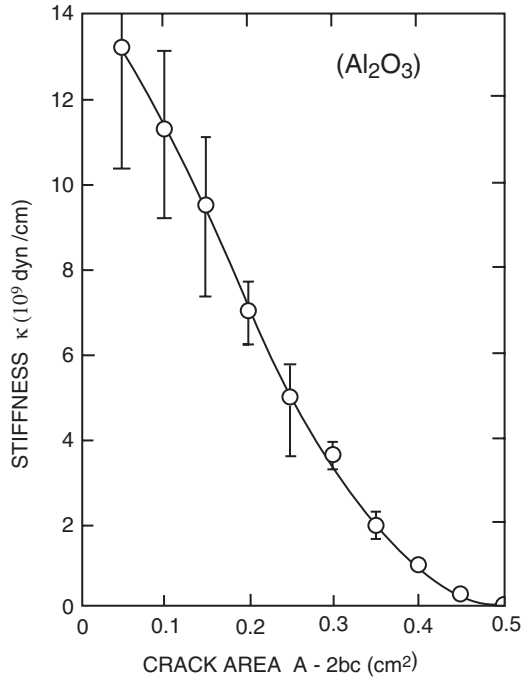
From the knowledge of δ_f for each specimen, γ_c can be calculated [10].

6.3.9 Work of Fracture

This requires a crack to propagate in a specimen while its growth is under control. The stronger the specimen the more difficult this becomes. It is essential to have:

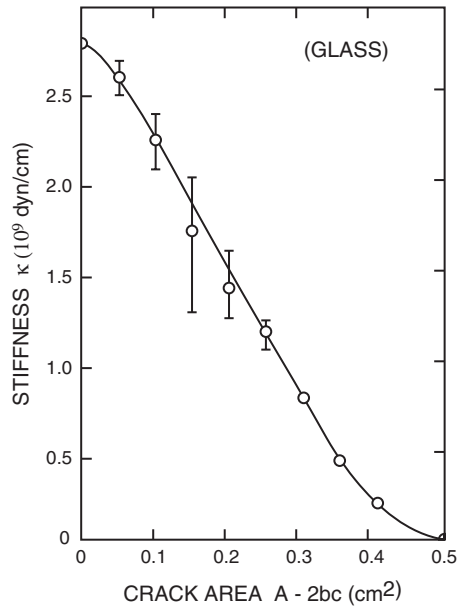
- (a) a very hard machine.
- (b) the facility for very slow rates of strain.

Fig. 3.8 Alumina Ceramic gradient Curve



κ versus A data for alumina

Fig. 3.9 Glass Gradient Curve



κ versus A data for glass

Table 6.2 Experimental Tabulation Data for Material Testing

P	δ	k	Ave k	b	c	$A = zbc$	$-\left(\frac{\partial k}{\partial A}\right)$	δ_F
Testing Speed Crosshead gears								
Testing Speed Chart gears								

Fig. 3.10 Specimen geometry. l =span; b =breadth; d =crack depth

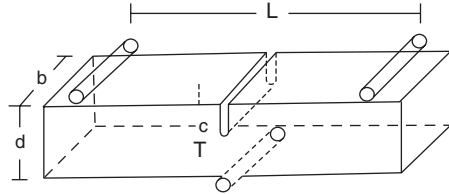
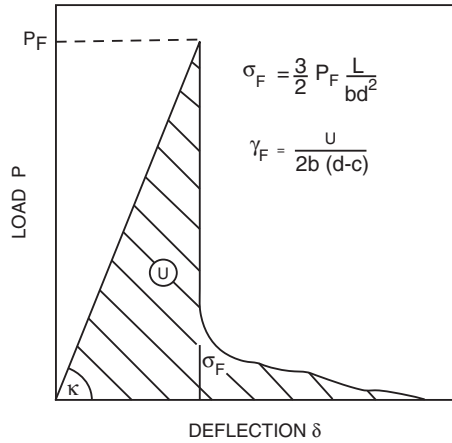


Fig. 3.11 Load/deflection curve. P_f =fracture load; δ_f =fracture deflection; k =specimen stiffness; σ_f =fracture stress



Controlled cracking can only occur in brittle material when the notch depth is so large that the test specimen is substantially weakened. One then arrives at a situation where the residual strain energy in a specimen is less than that of the increase in surface energy required when fracture occurs. Increasing the external strain then goes directly into providing the energy for overcoming the surface and propagating the crack.

Measure the area under the curve to obtain U Record P Calculate γ_F and δ_F

Fig. 3.12 Controlled load/deflection curve for graphite

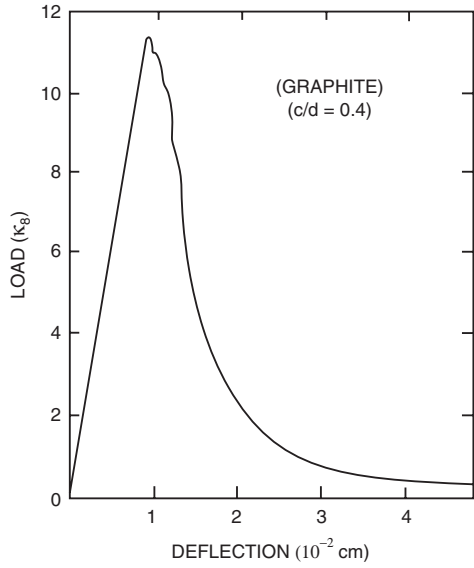


Fig. 3.13 Load/deflection curves for PMMA. Numbers on graph refer to notch depth ratio c/d . X indicates catastrophic failure

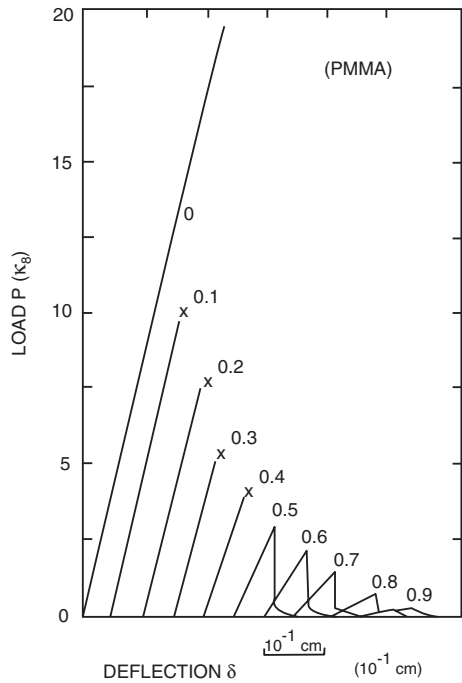


Table 6.3 Experimental Tabulation for Fracture Mechanics

Work of fracture						
L	b	d	c	P_δ	σ_F	u

Materials: Alumina test-bars $L=8$ cm, $b=0.5$ cm, $d=1.0$ cm
 These are cut with diamond saw to give $c=0.7, 0.8, 0.85, 0.9, 0.95$ cm
 Breaking is carried out at 0.005 cm/min. and the graph is automatically plotted by the recorder
 Repeat with Perspex (i.e. polymethylmethacrylate)
 $L, b,$ and d similar, $c=0.4, 0.5, 0.6, 0.7, 0.8, 0.9$ cm

6.3.10 Significance of γ_o , the Fracture Energy

Davidge [3] also draws attention to the fact that the γ_o in the Griffith equation is an ideal value, requiring perfectly sharp cracks to propagate through a material and creating planer fracture surfaces. Fracture in ceramics is not far from ideal, but there are energy-dissipating processes in what is a relatively complex process. For example fracture may be due to:

- (a) a combination of transcrystalline and intercrystalline microstructure, manifesting as steps in the fracture surface.
- (b) Because of the high stresses near the crack-tip (approaching...) there is a possibility that plastic flow may occur.
- (c) Cracking branching in the microstructure causing subsidiary cracking.

All of these are energy-consuming processes which make the apparent fracture energy γ_1 , somewhat higher than the thermodynamic surface energy γ_o . The effective surface energy γ_1 , is only a valid concept when plastic flow is localised near the crack tip and would not apply to metals where plastic flow is the normal deformation mode.

6.3.11 Double Cantilever Beam [15]

Attach the test piece show above, to the Instron in the tensile mode, i.e. P (up) to the load-cell and P (down) to the cross-head via a universal coupling. Follow the progress of the crack front (L) and measure $2d$ with a transducer system.

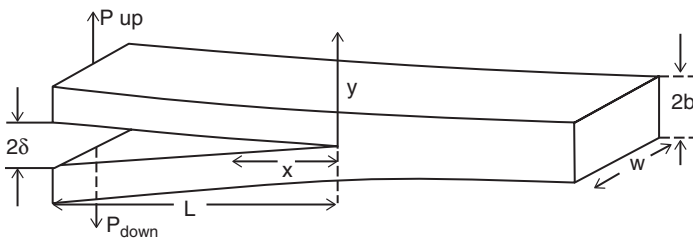


Fig. 3.14 Double Cantilever Beam

Bending moment is distributed along the beam, and is caused by the applied force P , so that

$$M(x) = P(L - x) \quad \text{where } 0 < x < L$$

Beam theory predicts that the strain energy U will be,

$$U = \frac{1}{2EI} \int_0^L M^2(x) dx = \frac{P^2 L^2}{6E \cdot I} \left(\text{where } I = \frac{wb^3}{12} \right) \quad (6.73)$$

(E is the elastic modulus and I the moment of inertia of bending)

Deflection of beam at point of application of force is obtained using Castigliano's theorem.

$$\delta = \left(\frac{\partial U}{\partial P} \right)_{x=L} = \frac{PL^3}{3EI} \quad (6.74)$$

Strain energy is therefore

$$U = \frac{3EI\delta^2}{2L^3} \quad (6.75)$$

By the conservation of energy

$$\underbrace{Pd\delta}_{\text{Workdone by external force}} + \underbrace{\gamma WdL}_{\text{Energy expended in new surface}} + \underbrace{dU}_{\text{Change in stored energy}} = 0 \quad (6.76)$$

From above

$$dU = \left(\frac{\partial U}{\partial L} \right)_{\delta} dL + \left(\frac{\partial U}{\partial \delta} \right)_{L} d\delta = -\frac{9EI\delta^2 dL}{2L^4} + Pd\delta$$

$$\text{Therefore } \gamma^w = \frac{9EI\delta^2}{2L^3} \text{ or } \gamma_{\delta} = \frac{3Eb^3\delta^2}{8L^4} \text{ (measuring } \delta) \quad (6.77)$$

$$(3.24) \text{ and } (3.27) \text{ give } \gamma_p = \frac{6P^2 L^2}{Ew^2 b^3} \text{ (measuring } P) \quad (6.78)$$

Both of these formulas can be used. A problem is to make the crack grow straight, and to clearly see the tip of it. This will be a problem with opaque bodies, where one cannot use total internal reflection to see the crack tip. The crack may be guided by the use a rectangular grooved. Specimen

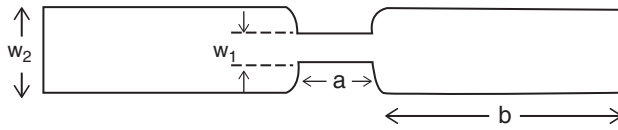


Fig. 3.15 Test Specimen

$$dS = \gamma w_1 dL$$

$$\left(\frac{\partial U}{\partial L} \right) = \frac{-9EI\delta^2}{2L^4} \left(\text{where } I = \frac{w_2 b^3}{12} \text{ and where } a \ll b \right) \quad (6.79)$$

$$\text{Thus } \gamma_\delta = \frac{3Ew_2 b^3 \delta^2}{8w_1 L^4} \text{ and } \gamma_P = \frac{6P^2 L^2}{w_2 w_1 b^3 E}$$

6.4 Stress Concentrators

6.4.1 Elliptical Cracks [1, 2]

An important historical precursor to the Griffith study was the street analysis of Inglis (1913) of an elliptical hole in a uniformly stressed plate. This showed that the local stresses about a sharp notch or corner could rise to several times that of the applied stress. It thus became apparent that even submicroscopic flaws might be potential sources of weakness in solids. In the limiting case a crack could be regarded as an infinitesimally narrow ellipse.

Let us therefore examine the modifying effect of the hole on the distribution of stresses in the solid plate. Let it be assumed that Hooke's law applies everywhere in the plate, and the dimensions b, c (Fig. 4.1) are small in comparison with those of the plate. The problem then reduces to one of linear elasticity.

Beginning with the equation of an ellipse

$$\frac{x^2}{c^2} + \frac{y^2}{b^2} = 1 \quad (6.80)$$

One can show that at C the radius of curvature is:

$$P = \frac{b^2}{c} \quad (6.81)$$

It is at the point C where the greatest concentration of stress occurs. The apparently simple equation (6.81) is obtained as a result of a complex analysis [1-3, 5]

$$\sigma_{yy}(C, \theta) = \sigma_A \left(1 + \frac{2C}{b} \right) = \sigma_A \left[1 + \left(\frac{C}{P} \right)^{1/2} \right]. \quad (6.82)$$

Fig. 4.1 Effect of Hole on the Distribution of Stress in a Solid

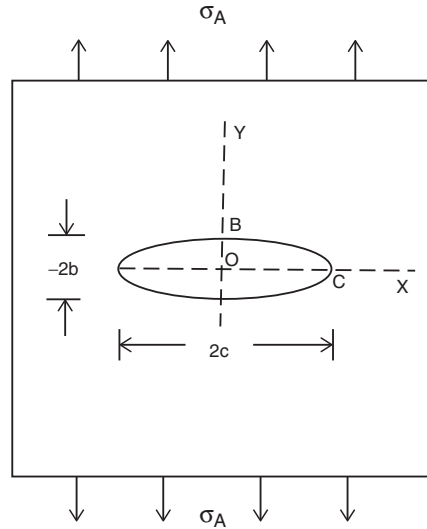
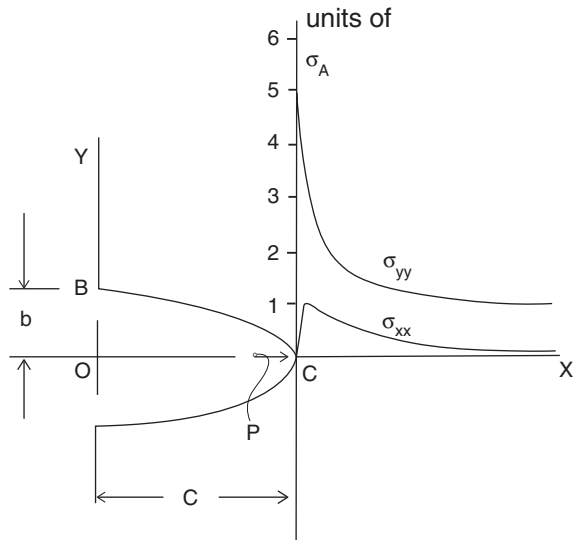


Fig. 4.2 Stress Concentration



It appears that stress concentration depends on the shape of the hole rather than its size. The variation of local stress along OX is also of interest. Figure 4.2 illustrates the case where $C = 3b$. σ_{yy} drops from its maximum at C approach the value of σ_A asymptotically for large values of x , while σ_{xx} rises to a sharp peak within a small distance from the stress-free surface and subsequently drops to zero at high x . (It can be appreciated that when $C/b = 5$, $\sigma_{yy} = \sigma_{max} = 11$.)

For the case where $b \ll C$, this equation reduces to

$$\frac{\sigma_{\max}}{\sigma_A} = \frac{2C}{b} = 2 \left(\frac{C}{P} \right)^{1/2}. \quad (6.83)$$

(C/P) is “the Stress concentration factor”.

Rearranging this equation, and multiplying by the factor $\sqrt{\pi}$, yields the following equation.

$$\sigma_A \sqrt{\pi_c} = \frac{1}{2} \sigma_{\max} \sqrt{\pi_P}. \quad (6.84)$$

in which we can call the *L.H.S.* $K_1 = \sigma \sqrt{\pi_c}$, and is known as the “stress intensity factor”.

It is important to realise that K_1 contains only the macroscopic quantities (the external tensile stress) and the half crack-length, C , both of which are measurable. It should be appreciated that the Eq. (6.95) implies a physical limit restricted by the properties P and σ_{\max} without breaking at the tip of the crack, for P is given by the microstructure of the material, and σ_{\max} cannot be larger than the internal molecular strength, σ_M . There should exist therefore a specific material limit given by

$$K_{1C} = \frac{1}{2} \sigma_M \sqrt{\pi_P} \quad (6.85)$$

the so-called “critical stress intensity factor”, for “fracture toughness”.

In Davidge’s treatment [3] the expression (6.85) is related to the Orowan value for the theoretical strengths of solids, i.e. the latter value for σ_{th} is made equivalent to the stress at the edge of the crack tip. For the failure this gives

$$\sigma_f = \frac{E}{4_c} \cdot \frac{P}{r_o}. \quad (6.86)$$

Now if the tip of the crack were infinitesimally small the stresses would be infinitely large. It is reasonable to assign the value half an atomic spacing to P if the crack passes between adjacent planes of atoms. Substitution in (6.38) gives a second value for i.e.

$$\sigma_f = \left(\frac{E\gamma_o}{S_C} \right)^{1/2} \quad (6.87)$$

The stress is somewhat lower than the Griffith stress at which therefore, fracture should certainly occur and Orowan’s value for could only be accurate to within a factor of two. Hence we conclude the Griffith criterion is adequate and sufficient.

A criticism of this solution is that the elastic stresses in the direction of the applied force rapidly reach infinity as the crack becomes sharper, and so become insensitive to the differences in the mode of cracking and the stress configurations.

6.4.2 K_I Values for Specific Crack Systems [2]

1. Internal crack in infinite body length of crack = $2a$ app. stress = σ .

$$K_I = \sigma\sqrt{\pi a}. \quad (6.88)$$

2. Internal crack in a plate of finite width.

As above, only width = $2w$.

$$K_I = \sigma \left[2w \tan \left(\frac{\pi a}{2W} \right)^{1/2} \right] \quad (6.89)$$

Expanding the above expression we have,

$$K_I = \sigma\sqrt{\pi a} \left[1 + \frac{\pi a^2}{24W} \right] \pm \quad (6.90)$$

as $a/w \rightarrow \theta$, becomes

3. Surface crack in a semi infinite body.

$$K_I = 1.12\sigma\sqrt{\pi a} \quad (6.91)$$

Fig. 4.9a Internal Crack in plate with infinite body length

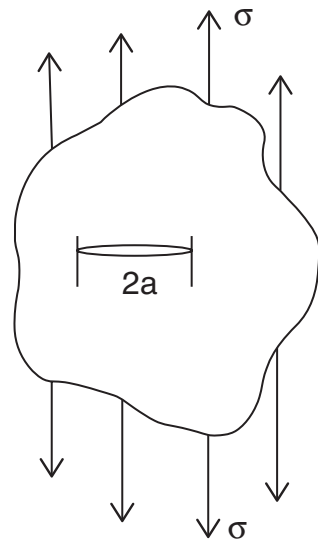


Fig. 4.10a Internal crack in plate of finite width

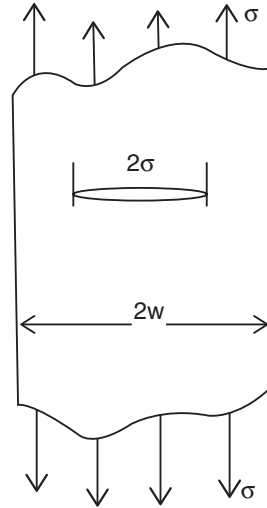
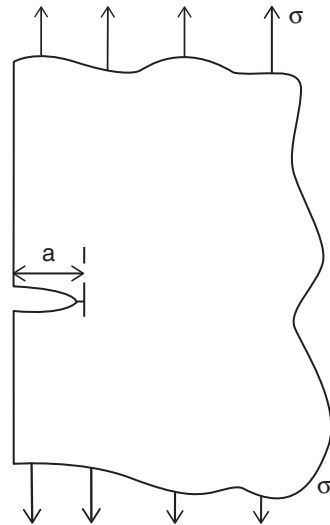


Fig. 4.12a Surface Crack



4. Two symmetrical edge cracks in a plate of finite width.

$$K_1 = \sigma \left[2w \tan\left(\frac{\pi a}{2w}\right) + \theta \cdot 2w \sin\left(\frac{\pi a}{w}\right) \right]^{1/2}. \tag{6.92}$$

5. Central penny-shaped crack in an infinite body.

$$K_1 = 2\sigma \sqrt{a/\pi} \tag{6.93}$$

Fig. 4.13a Two Symmetrical edge cracks in plate of finite width

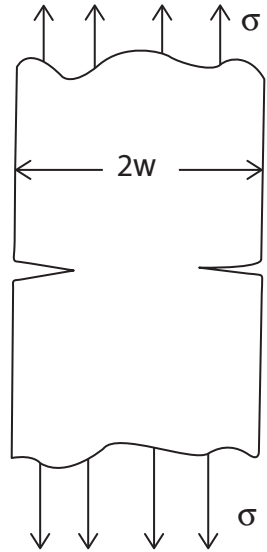


Fig. 4.14a Central penny shaped crack in an infinite body

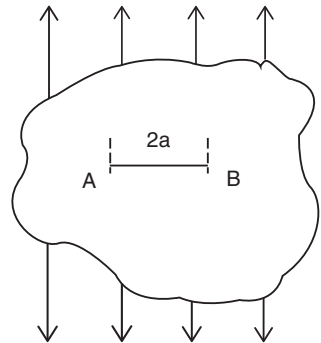
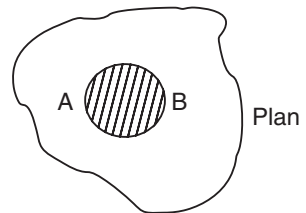


Fig. 4.14b Plan view of Penny Crack



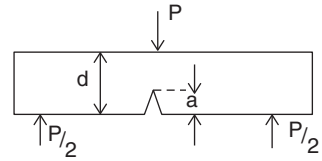
6. Surface crack in a three-point bend system.

Flexural strength in a system without a surface crack is given by

$$a = \frac{3}{2} \cdot \frac{Pl}{bd^2} \tag{6.94}$$

b = breadth, d = thickness, l = span.

Fig. 4.15a Surface crack in 3pt bend System



When a surface crack is introduced, and $l = 4d$.

$$K_1 = \frac{3Pl}{2bd} \sqrt{\frac{3}{2}} \left[1.93 \left(\frac{a}{d} \right)^{1/2} - 3.07 \left(\frac{a}{d} \right)^{3/2} + 14.53 \left(\frac{a}{d} \right)^{5/2} + \dots \right] \quad (6.95)$$

for $0.2 < a/d < 0.6$.

In terms of the flexural strength, the expression (6.95) becomes

$$K_1 \sigma \sqrt{a} \left[1.93 - 3.07 \left(\frac{a}{d} \right) + \dots \right]$$

This application is continued in the testing methods latter on.

Functions have been developed which satisfy the requirements of linear elasticity theory for the stresses in the vicinity of a sharp slit. Their derivations are mathematically complex, and only the solutions are reported here. Reference can be made to the following text-books and papers [1–5].

6.4.3 Crack Propagation [1, 2, 4, 5, 20]

A crack may propagate in three different modes as represented in Fig. 4.3. While the opening mode is likely to predominate, the other modes do exist, and combinations of mode 1 with others are possible. The other modes will only operate if the crack or the test piece is not free to move into a favourable orientation for mode 1. The modes are referred to as

1. the opening mode
2. the shearing or sliding mode
3. the tearing mode

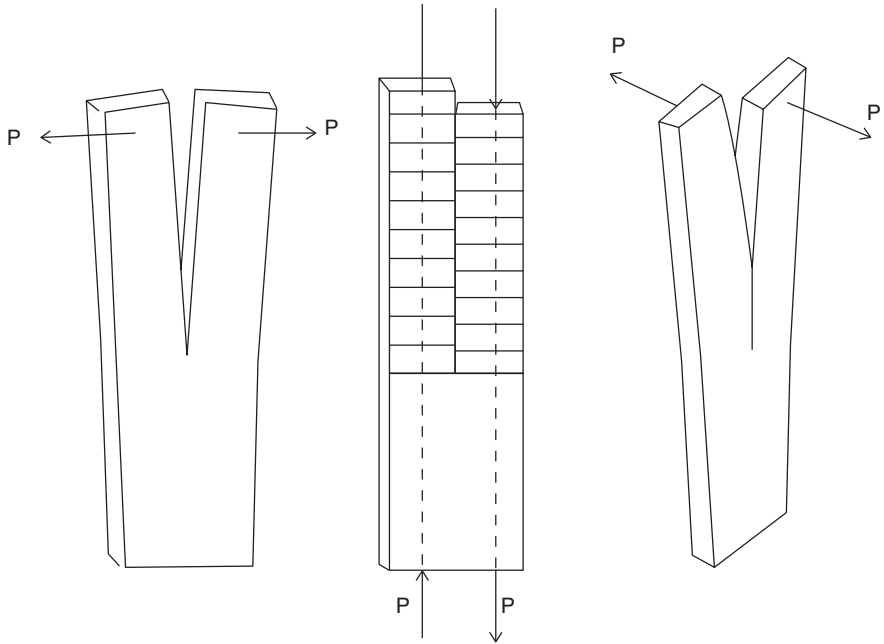


Fig. 4.3 Open Mode, shearing or Sliding Mode, Tearing Mode fracture of a Brittle Material

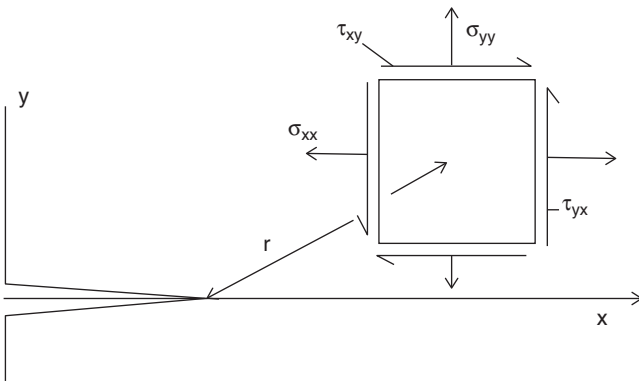


Fig. 4.4 Stress Analysis at Crack Tip

6.4.4 K4 Application: Stress Analysis at Crack Tip

The stress distributions near to the end of a Griffith's crack has been analysed as follows:

6.4.4.1 Mode 1 Stresses

$$\left. \begin{array}{l} \sigma_{xx} \\ \sigma_{yy} \\ \tau_{xy} \end{array} \right\} = \frac{K}{\sqrt{2\pi r}} \left\{ \begin{array}{l} \cos(\theta/2) \left[1 - \sin(\theta/2) \sin(3\theta/2) \right] \quad (\text{tensile}) \\ \cos(\theta/2) \left[1 + \sin(\theta/2) \sin(3\theta/2) \right] \quad (\text{tensile}) \\ \sin(\theta/2) \cos(\theta/2) \cos(3\theta/2) \quad (\text{shear}) \end{array} \right. \quad (6.96)$$

$$\begin{aligned} \sigma_{zz} &= \nu(\sigma_{xx} + \sigma_{yy}) \quad (\text{P. strain}) \quad (\text{tensile}) \\ &= \theta \quad (\text{P. stress}) \\ \tau_{zz} &= \tau_{yz} = \theta \quad (\text{shear}) \end{aligned}$$

6.4.4.2 Mode 1 Displacements

$$\begin{aligned} \mu &= \frac{K}{2E} \left(\frac{r}{2\pi} \right)^{1/2} (1+\nu) \left[(2K-1) \cos(\theta/2) - \cos(3\theta/2) \right] \\ \nu &= \frac{K}{2E} \left(\frac{r}{2\pi} \right)^{1/2} (1+\nu) \left[-(2K+1) \sin(\theta/2) + \sin(3\theta/2) \right] \\ W &= (\nu z / E) (\sigma_{xx} + \sigma_{yy}) \quad (\text{Plane strain}) \\ &= \theta \quad (\text{Plane strain}) \end{aligned} \quad (6.97)$$

These equations follow from those derived in Ref. [5] an example of which is

$$\sigma_x = \sigma \sqrt{\frac{c}{2r}} \cdot \cos(\theta/2) (1 - \sin(\theta/2) \sin(3\theta/2)) \quad (6.98)$$

σ represents the general stress in the material, and the trigonometrical terms are the resolved components of it.

6.4.4.3 For Mode 2

Similar expressions also exist e.g.

$$\left. \begin{array}{l} \sigma_{xx} \\ \sigma_{yy} \\ \tau_{xy} \end{array} \right\} = \frac{K_{\pi}}{\sqrt{2\pi r}} \left\{ \begin{array}{l} -\sin(\theta/2) \left[(2 + \cos(\theta/2) \cos(3\theta/2)) \right] \\ \sin(\theta/2) \cos(\theta/2) \cos(3\theta/2) \\ \cos(\theta/2) \left[(1 - \sin(\theta/2) \sin(3\theta/2)) \right] \end{array} \right.$$

$$\begin{aligned} \sigma_{zz} &= \tau_{xz} = \tau_{yz} = \theta \quad \text{for plane stress,} \\ &= \nu(\sigma_{xx} + \sigma_{yy}) \quad \text{and } \tau_{xz} = \tau_{yz} = \theta \quad \text{for plane strain} \end{aligned} \quad (6.99)$$

6.4.4.4 For Mode 2 Displacements

$$\begin{aligned}\mu &= \frac{K_{II}}{2E} \left(\frac{r}{2\pi} \right)^{1/2} (1+\nu) \left[(2K+3) \sin\left(\frac{\theta}{2}\right) + \sin\left(3\frac{\theta}{2}\right) \right] \\ \nu &= \frac{K_{II}}{2E} \left(\frac{r}{2\pi} \right)^{1/2} -(1+\nu) \left[(2K-3) \cos\left(\frac{\theta}{2}\right) + \cos\left(3\frac{\theta}{2}\right) \right] \\ W &= (\nu z / E) (\sigma_{xx} + \sigma_{yy}) (\text{Plane stress}) = \theta (\text{Plane stress})\end{aligned}$$

6.4.4.5 For Mode 3

$$\begin{aligned}\tau_{xz} &= \frac{K_{III}}{\sqrt{2\pi r}} - \sin\left(\frac{\theta}{2}\right), \text{ and } \tau_{yz} = \frac{K_{III}}{\sqrt{2\pi r}} \cos\left(\frac{\theta}{2}\right) \\ \sigma_{xx} &= \sigma_{yy} = \sigma_{zz} = \tau_{xy} = \theta\end{aligned} \quad (6.100)$$

The K values depend on the applied loading and crack geometry, and determine the intensity of the local field.

It is also possible to express the above equations in polar coordinates.

The value of r has certain limitations, i.e. the equations are not valid if $r \rightarrow \theta$ or becomes large in relation to the length of the crack.

Where two crack modes operate simultaneously, the resolved components of each in a specific direction are additive.

6.4.5 The Application of K_I in terms of is a Materials Property [2]

There is a direct relation between K_I and E_γ .

Because E and γ are materials properties then, by inference, K_I should also be.

The actual determination of has shown it to be structure sensitive and depends on the energy losses incurred in its measurement. This problem will also be encountered with K_I .

The equivalence of K and G parameters.

Extension of the crack involves:

- (a) Linear opening in the y direction Strain energy = $\frac{1}{2} \sigma_{yy} \cdot u_y$.
- (b) Shear in x direction Strain energy = $\frac{1}{2} \tau_{xy} \cdot u_z$.
- (c) Shear in z direction Strain energy = $\frac{1}{2} \tau_{zy} \cdot u_x$.

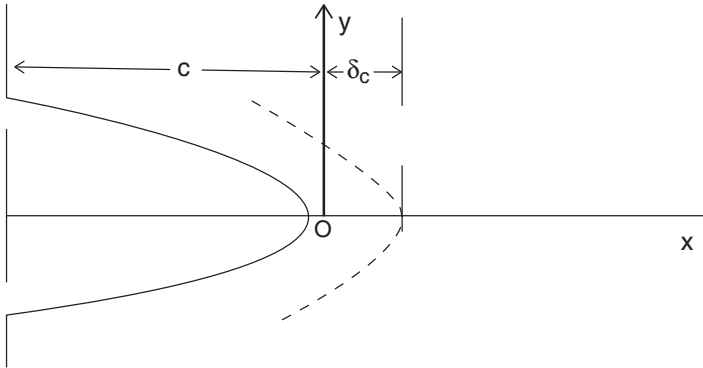


Fig. 4.5 The K1 a material property

Energy is additive, therefore total strain energy =

$$\frac{1}{2}(\sigma_{yy}\mu_y + \tau_{xy}\mu_z + \tau_{xy}\mu_z) \tag{6.101}$$

If crack extends from \emptyset to δc , strain energy increase =

$$\begin{aligned} (\delta U_E) &= 2 \int_0^{\delta c} U_E dx \\ &= \int_0^{\delta c} (\sigma_{yy}\mu_x + \tau_{zy}\mu L_z) dx \end{aligned} \tag{6.102}$$

In the limit $\left(\frac{\delta\mu_E}{\delta_c}\right) = \frac{d\mu_E}{dc}$

Let X be measured from the \emptyset (closed position) where $\phi < X < \delta c$ and let failure be in mode 1.

Work done by BOTH crack surfaces

$$\delta U = 2 \int_0^{\delta c} \frac{1}{2} \tag{6.103}$$

Now σ is the stress normal to the crack surface before it opens or extends (i.e. crack is in the closed position).

U is the normal displacement of the crack surfaces after the crack has opened.

$$G = \frac{\delta U_E}{\delta c} = (\text{in the limit}) \frac{1}{\delta c} \int_0^{\delta c} \sigma u dx. \tag{6.104}$$

Derived from the K_I equation (see p. 49)

$$\sigma_{yy} = \frac{K_I}{\sqrt{2\pi r}} \cos(\theta/2) \cdot [1 + \sin(\theta/2) \cdot \sin(3\theta/2)] \quad (6.105)$$

$$\mu = \frac{K_I}{2E} \sqrt{\frac{r}{2\pi}} (1+\nu) [(2k+1)\sin(\theta/2) - \sin(3\theta/2)] \quad (6.106)$$

so that for σ_{yy} (σ directed towards the surface) $\theta = \phi$ and $r = x$.

And for μ (μ displaced away from the surface) $\theta = \pi$ and $r = \delta c - x$.

Substituting,

$$\sigma_{yy} = \frac{K_I}{\sqrt{2\pi x}} \mu = \frac{K_I}{2E} \sqrt{\frac{(\delta c - x)}{2}} (1+\nu)(2k+2) \quad (6.107)$$

$$G = \frac{\delta U_c}{\delta c} (\text{mode 1}) = \frac{1}{\delta c} \frac{K_I^2}{2\pi E} (1+\nu)(k+1) \int_0^{\delta c} \frac{(\delta c - x)^{\frac{1}{2}} dx}{x} \quad (6.108)$$

The value of the integral (Hahn, p. 149) is $\frac{\delta c \cdot \pi}{2}$ [5].

Giving

$$G = \frac{K_I^2}{4E} (1+\nu)(k+1) \quad (6.109)$$

At fracture, for plane strain and stress

$$G = \frac{K_{Ic}^2}{E} (\text{plane stress}) \quad G = \frac{K_{Ic}^2}{E} (1-\nu^2) (\text{plane stress}) \quad (6.110)$$

By these simple expressions therefore, it is possible to relate fracture energy and fracture toughness.

6.4.6 Crack Stability

In most sources of information, fracture mechanics tends to concern itself with mode I, and information on other cracking modes is not readily available. There are two ways of regarding this problem:

- By subjecting a crack inclined at an angle to a uniform stress, and
- By subjecting a crack to a complex stress pattern.

A relatively clear analysis for (a) is given in Ref. [1], which is summarised below, while the mathematically more complex (b) is given in Ref. [5].

It is equally possible to express the resolved stresses in terms.

Of K_I , K_{II} and K_{III} and polar coordinates, shown below (Fig. 4.6).

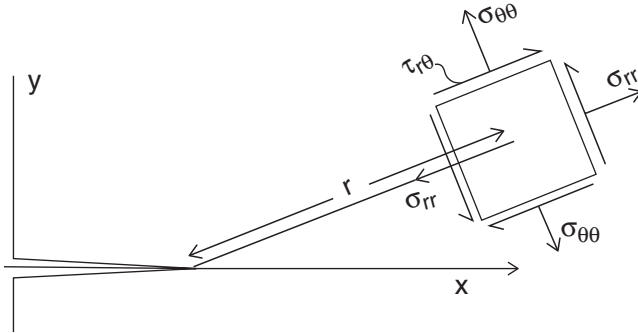


Fig. 4.6 KI, KII and KIII and Polar coordinates

For mode 1

$$\begin{aligned} \sigma_{\theta\theta} &= \frac{K_I}{2\pi r} \cos^3(\theta/2) = K_I f_{\theta\theta}(\theta) \\ \sigma_{rr} &= \frac{K_I}{\sqrt{2\pi r}} \cos(\theta/2) [1 + \sin^2(\theta/2)] = K_I f_{rr}(\theta) \\ \tau_{r\theta} &= \frac{K_I}{\sqrt{2\pi r}} \sin(\theta/2) \cos^2(\theta/2) = K_I f_{r\theta}(\theta) \end{aligned} \tag{6.111}$$

For mode 2

$$\begin{aligned} \sigma_{rr} &= \frac{K_{II}}{\sqrt{2\pi r}} \sin(\theta/2) [1 - 3\sin^2(\theta/2)] = K_{II} f_{rr}(e) \\ \sigma_{\theta\theta} &= \frac{K_{II}}{\sqrt{2\pi r}} - 3\sin(\theta/2) \cos^2(\theta/2) = K_{II} f_{\theta\theta}(e) \\ \tau_{rc} &= \frac{K_{II}}{2\pi r} \cos(\theta/2) [1 - 3\sin^2(\theta/2)] = K_{II} f_{r\theta}(\theta) \end{aligned} \tag{6.112}$$

Fig. 4.7, is from Lawn and Wilshaw’s “Fracture of Brittle solids and is a graphical illustration of Figs. 4.32 and 4.33, with θ extended over the range $-\pi$ to $+\pi$ [1].

Fig. 4.8, from the same source, demonstrates the effect of adding these curves. Assuming $K_I = K_{II}$, it is possible to see how an asymmetric function develops for K when the $f(\theta\theta)$ are added.

An inclined crack in a loaded plate will be subject to two stresses and the stress intensity factors are transformed accordingly as

Total normal component

$$K'_1(\theta) = K_I f_{\theta\theta}^I + K_{II} f_{\theta\theta}^{II}$$

Fig. 4.7 Fracture of Brittle Solids: Mode I Curves

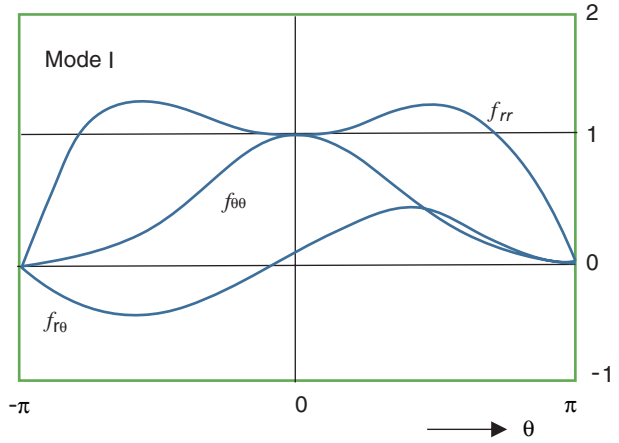


Fig. 4.8 Mode 2 Curves

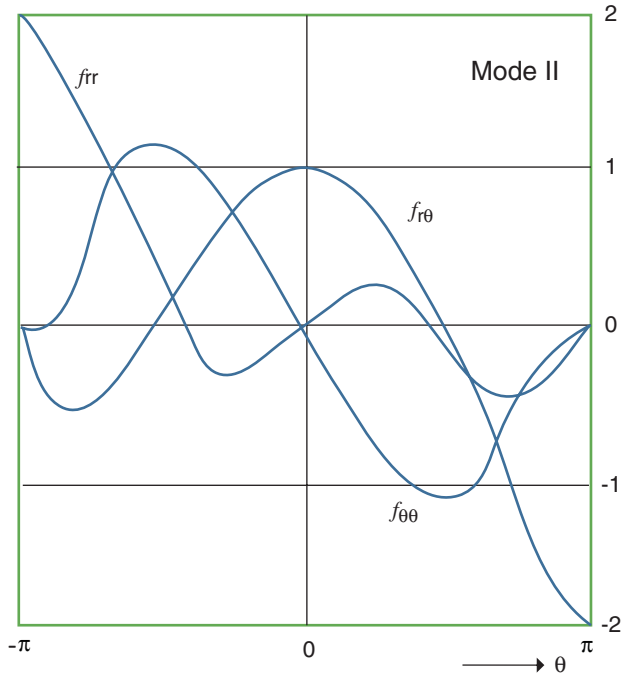


Fig. 4.8 Mode 1 and 2

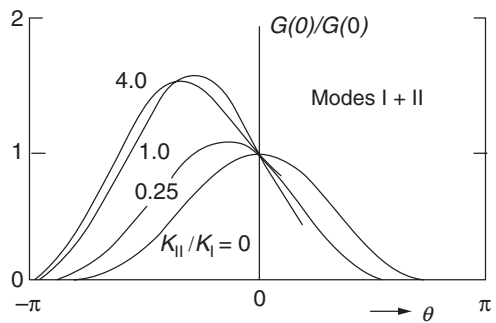
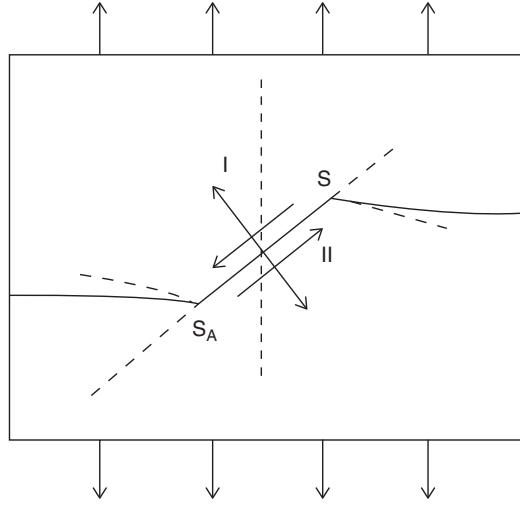


Fig. 4.9 Principle Stress in Applied Field



Total shear component

$$\begin{aligned}
 K'_{II}(\theta) &= K_I f_{r\theta}^I + K_{II} f_{r\theta}^{II} \\
 K'_{III}(\theta) &= \phi
 \end{aligned}
 \tag{6.113}$$

Initially, when the new crack is still $\ll c$, the original crack length, it will move in a direction determined by the ratio K_I/K_{II} , but as it moves clear of the crack it turns to move normal to the applied stress and is subsequently influenced only by K_I .

Deviant paths therefore are not permanent features but the system restores itself and the path becomes orthogonal to the greatest principal stress in the applied field.

6.5 Testing Methods for Determination of K_I [6]

6.5.1 Notched Bar (S.E.N.B.)

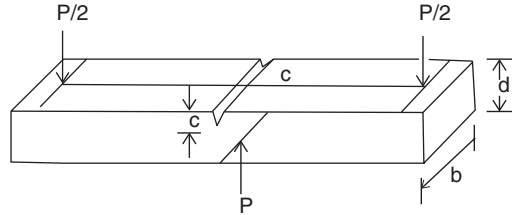
From the Griffith equation,

$$\sigma_f = \sqrt{\frac{2E_\gamma}{\pi c}} = \sqrt{\frac{K_I}{\pi c}}
 \tag{6.114}$$

where c = crack length

$$K_I = \sigma_f \sqrt{\pi c}
 \tag{6.115}$$

Fig. 5.1 Notched Bar Specimen



$\sqrt{\pi}$ can be incorporated into a factor Y along with geometric constants

$$\sigma_f = \frac{K_{Ic}}{Y \cdot c^{\frac{1}{2}}} = \frac{3P1}{2bd^2} \tag{6.116}$$

$$K = \frac{3PYc^{\frac{1}{2}}}{2bd} \text{ where}$$

$$Y = A_0 + A_1(c/d) + A_2(c/d)^2 + A_3(c/d)^3 + A_4(4/d)^4 \tag{6.117}$$

The curves (Fig. 5.2) relate Y with c/d . It clearly shows that a c/d value between 0.1 and 0.2 is most favourable and contrasts with the work of fracture experiment.

Values of A coefficients

Loading	A_0	A_1	A_2	A_3	A_4
Type					
$1/w=8$	+1.96	-2.75	+13.66	-23.98	+25.22
$1/w=4$	+1.93	-3.07	+14.53	-25.11	+25.80
Four point	+1.99	-2.47	+12.97	-23.17	+24.80

This method of K_I determination depends on a knowledge of the crack depth, which has been made by a saw-cut.

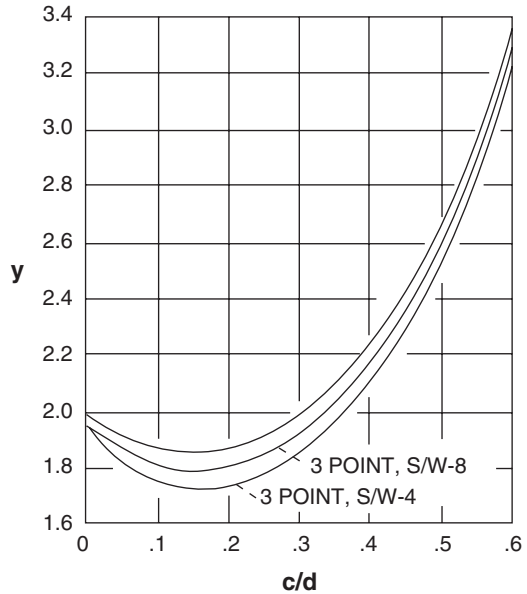
It presupposes that:

1. The rate of loading will be sufficiently fast, so that growth is not significant as the machine is loaded.
2. The end of the saw-cut will generate a network of micro cracks, one of which will grow and eventually fracture the specimen.

(Another way of looking at this formula is $K = \frac{6Mc^{\frac{1}{2}}}{bd^2}$ where M is the applied bending moment. This is useful for four-point bends)

The curves show the variation of Y with the ratio c/d .

Fig. 5.2 The Variation of Y with the Ratio c/d



6.5.2 The Double Torsion Method [3, 16, 21, 24, 30]

6.5.2.1 Double Torsion Test Piece

Where a greater degree of control over the crack progress is required, then the double torsion or double cantilever methods are preferred. They also lend themselves to the study of stress corrosion effects.

If y is the displacement of the loading points, P is the applied load and a is the crack length, from the compliance relationship,

$$y = P(Ba + c) \tag{6.118}$$

Differentiating w.r.t. time,

$$\frac{dy}{dt} = \frac{dP}{dt}(Ba + c) + \frac{PBda}{dt} \tag{6.119}$$

Note that $\frac{da}{dt}$ is the crack velocity, which at constant displacement

$$\frac{dy = \phi}{dt} \text{ is given by, } \frac{da}{dt} = \frac{(Ba + c) \frac{dP}{dt}}{BP} \tag{6.120}$$

The values for P and a are interrelated, when the specimen is subject to constant displacement. When the crack has finished growing, we have P_f and a_f , hence

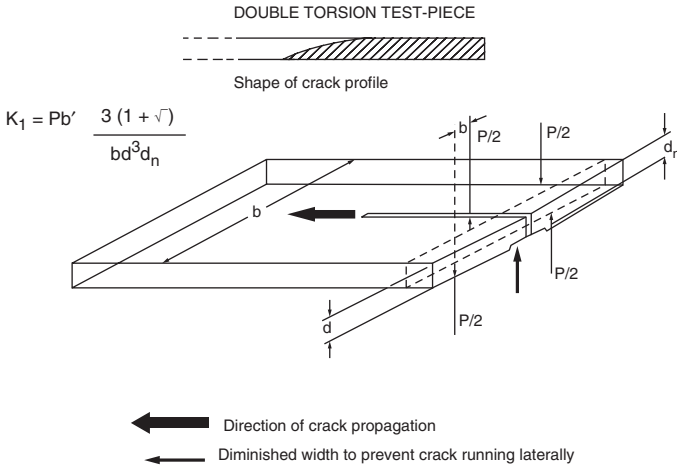


Fig. 5.3 Double Torsion Test Piece

$$P(Ba + c) = P_f(Ba_f + c) \tag{6.121}$$

Substituting for $(Ba + c)$ in eq. (6.120), we obtain,

$$\frac{da}{dt} = \frac{P_f}{p^2 B} (Ba_f + c) \frac{dp}{dt} \tag{6.122}$$

For a relatively large crack length, where $c \ll B$, the equation simplifies to

$$\frac{da}{dt} = -\frac{P_f}{p^2} a_f \frac{dp}{dt} \tag{6.123}$$

The crack velocity can be found if the initial and final loads, the rate of load relaxation with time, and the final crack length can be measured. The specimen is loaded to a suitable level (below K_I) and for a fixed displacement, the load decay with time is followed on the pen recorder coupled to the load-cell of the testing machine. The final crack length is measured, probably with the aid of a dye penetrant in the crack.

Also we note that

$$K_I \text{ (or } K_{Ic}) = P_1 \text{ (or } P_{1c}) w_m \left[\frac{3(1+\nu)}{wt^3 t_n} \right]^{\frac{1}{2}} \tag{6.124}$$

$$K_I = PW_m \left[\frac{3(1+\nu)}{wt^3 t_n} \right]^{\frac{1}{2}}$$

Fig. 5.4 Crack Velocity Test

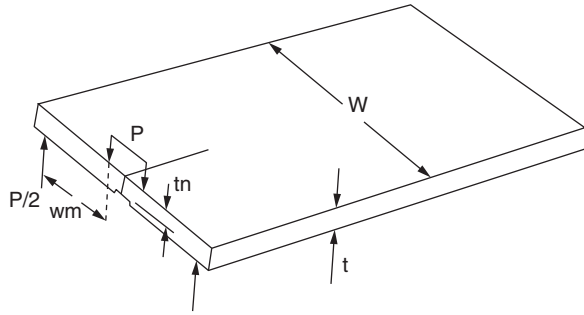
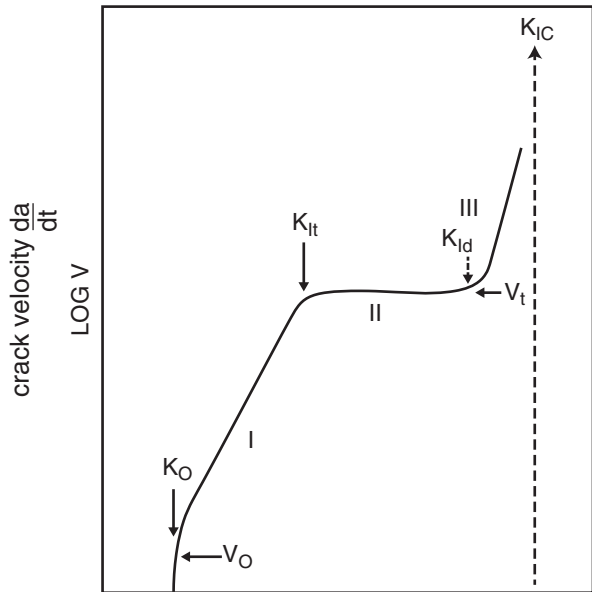


Fig. 5.5 Crack Velocity Curve



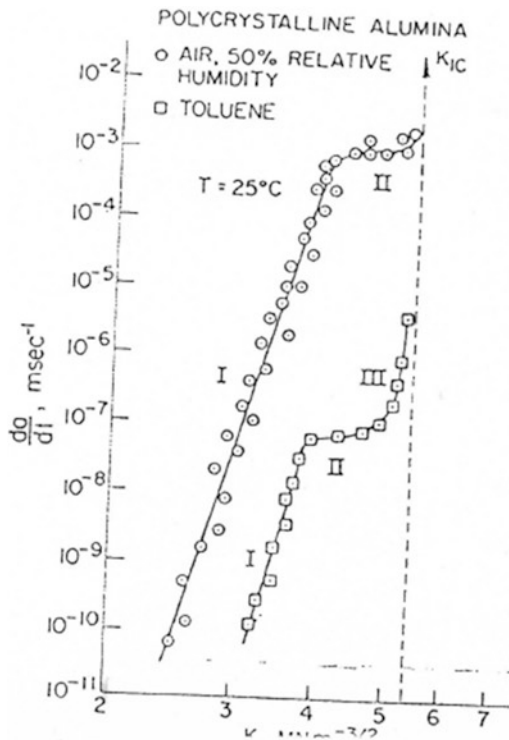
Figures 5.5 and 5.6 show the characteristic shapes of the curve when $\frac{da}{dt}$ is plotted against K_I . In the results for polycrystalline alumina, K_{Ic} is equal to $5.2 \text{ MN m}^{-3/2}$.

The slope in region 1 is often referred to by the symbol “ n ” and called the “crack susceptibility.” One can contrast the behaviour of alumina in moist air with that in toluene (where air is excluded). In air the onset of stress corrosion is at a lower stress level than in toluene and in vacuum it is depressed still further.

Region 2 is depressed in high corrosion situations [24] and the effect of Ca and Mg ions in the alumina depresses the value of n . Increasing the purity of the alumina increases n to the extent that measurement becomes very difficult because the initial reading approaches K_{Ic} , although the early detection of the movement of the crack by acoustic emission should simplify this measurement [25].

An important consideration in the double torsion technique is that the crack front has a curved profile [16]. Allowance can be made for this in the calculation, but a method which almost eliminates this to use very thin specimens.

Fig. 5.6 A Comparison of the Crack Velocity of Alumina Ceramics in Dry and Humid Conditions



Alumina of various categories has been used for the manufacture of microcircuits and these can be obtained in 50 mm squares which are very suitable for the double torsion test. Some difficulty has been encountered in making an initial crack in the edge to begin the process. The following technique has been successful. A small cut (<1 mm) is made in the edge, and this is dipped symmetrically into a bath of Silicone oil at 180–200 °C. When the edge with the crack has attained the temperature, it is then plunged into cold water. With practice the thermal shock can be used to make a short crack in the side of the specimen which can then be placed in the equipment and tested.

Results of Double Torsion Experiments (Davidge [3])

6.5.3 Double Cantilever Beam

This technique was the original method for the investigation of fracture energy and K_1 . The formula for K_1 is

$$K_1 = \frac{3.45Pa}{bt^{3/2}} \left[1 + 0.7 \left(\frac{t}{a} \right) \right] \tag{6.125}$$

The technique suffers in that it is dependent on a , the crack length. Glass and epoxy resins etc. create no problems, because the crack can be seen due to total reflection on the air surface within the crack. K_I for sapphire was also measured in this way. But for opaque ceramics it is not very successful because the exact end of the crack cannot be seen, unless the specimen is dismantled and a dye penetrant used to reveal the end of the crack. This will alter the surface conditions and destroy the value of the experiment.

Another difficulty is caused by the asymmetric loading of the specimen on a conventional hard testing machine. The weight of the test piece will influence the result. It can be used successfully in certain purpose built machines which put the test piece in tension horizontally [15]. This technique also allows stress-corrosion measurements to be made.

It has been said [28] that this technique measures the pure K_I fracture mode. While this is probably true, the results do not differ significantly from those obtained by the double torsion technique.

Because the DCB method depends on a knowledge of the crack length, an alternative method has been proposed which eliminates this, carefully removed and the specimen dried before use. The moment arms were attached with high strength epoxy resin which was cured at 70 °C. Small lugs were also incorporated in the moment arms to meet with a transducer for measuring the separation of the crack surfaces. Alumina proved to be a very difficult material to measure in this way. When one attempted to work at constant strain, the crack did not extend even though one approached within 90 % of K_{Ic} . Any further increase simply shattered the specimen which was clearly too stiff.

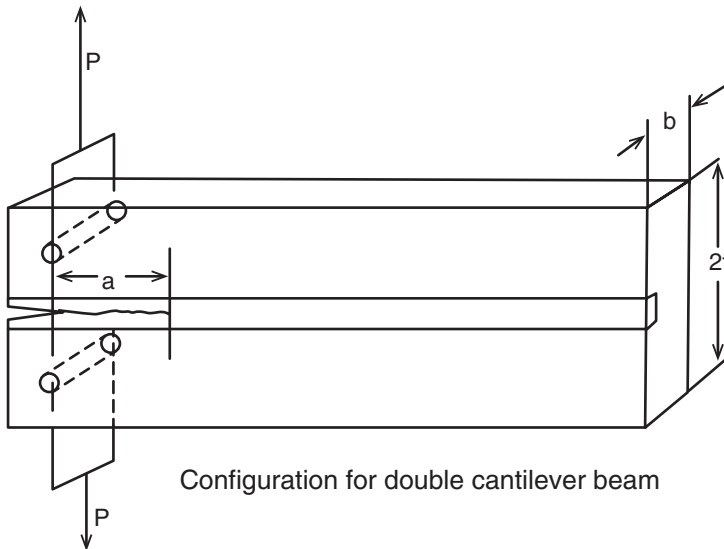


Fig. 5.7 Configuration for Double Cantilever Beam

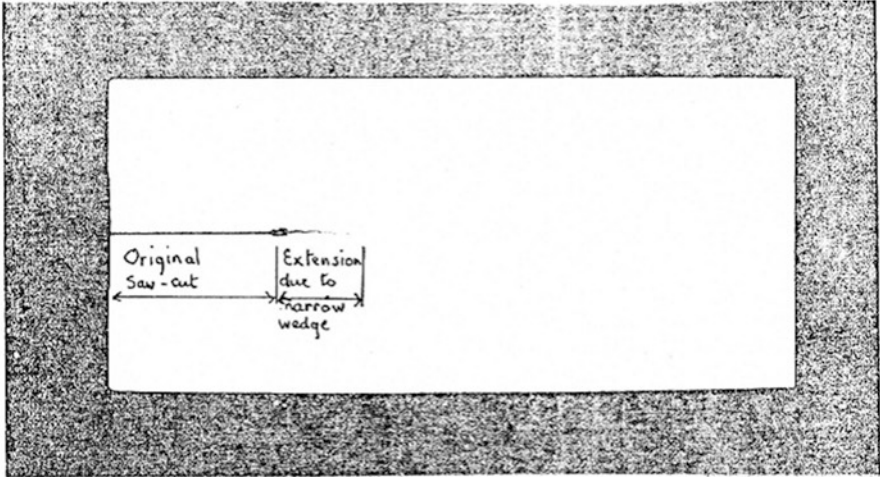
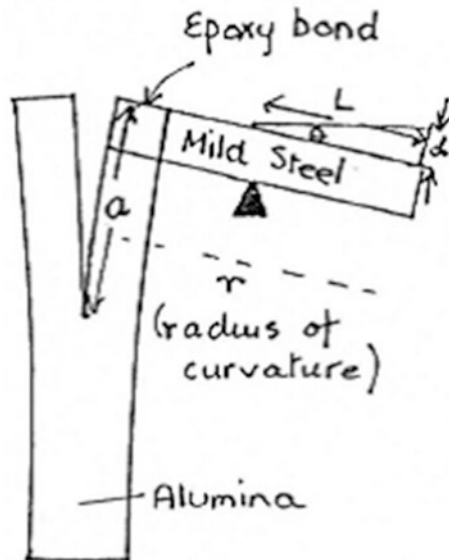


Fig. 5.8 Crack Opening Measurement

Fig. 5.9 Specimen Fracturing across Width due to Surface Imperfections



The crack velocity can be obtained from the measurement of the crack opening, or from the depression of the loading points by a simple relation.

If the beam deflects through an angle θ , then $\tan \theta = d/L = a/r = aM/EI$. Hence $a = (EI/ML) \cdot d$.

Like the DT, or DCB this method is easy to operate if there is significant stress corrosion, but with increased purity of materials the stress intensity factor K_I approaches K_{Ic} as the regions I and II of the curve of Fig. 7.4 diminish and if one

attempts to allow the stress to relax from an initial constant strain it is more than likely the specimen will fracture prematurely.

An alternative to this is to perform the experiment under constant stress. This can be generated by means of a long lever arm on the end of which is a container of zircon sand (chosen for its high density). This system, which admittedly appears crude, is capable of very fine adjustment, and the stress actually on the moment arms is read off from the testing machine chart as before. It proved quite possible to control the growth of the crack by this method, but the values of K_1 in those specimens which fractured were twice as high as expected. This was because in the constant loading method an equal quantity of energy is used to strain the specimen as that used in extending the crack (p. 51). Before it is possible to accept these results as reliable, a check for the influence of crack kinetic energy should be made [1]. Attempts to use the constant moment method in this manner for pure alumina gave results which were no better than the double torsion. A large number of plots were made with K_1 ranging from 2.2 to 2.5 MN m^{-3/2} over a velocity range from 10⁻⁸ to 10⁻⁵. The constant velocity region (II) was assumed to be about 10 m/s and this had a particularly wide scatter of results. K_{1c} was in the range 4.5–5 MN m^{-3/2}.

A possible advantage of this configuration is that by adjustment of the position of the test-specimen one can perform fracture experiments in the K_3 mode. Precautions have to be taken to prevent

- (a) the specimen rotating back into the normal K_1 mode, and
- (b) the specimen fracturing across its width from a surface imperfection near the point of attachment of the moment arms. Cladding with a thin piece of metal attached with epoxy resin accomplishes this, and it does not significantly alter the moment of inertia of bending of the specimen.

6.5.4 The “C” Specimen

An elegant method for the measurement of fracture toughness in the tensile mode has been reported by Kapp et al. [26]. It is intended for use with hollow cylinder geometries, and one can appreciate that it can be used in reverse, i.e. from a knowledge of K it is capable of detecting critical sizes of flaw in a hollow cylinder geometry. Much of the mathematical theory is available in Refs. [17, 18, 26], but the paper of Kapp et al., presents the formula for K in a readily applicable form.

$$K = \left(\frac{P}{BW \frac{1}{2}} \right) \left[3X/W + 1.9 + 1.1a/w \right]$$

$$X \left[1 + 0.25 \left(1 - a/w \right)^2 \left(1 - r_1/r_2 \right) \right] F(a/w) \quad (6.126)$$

$$\text{where } F(a/w) = \left[\left(a/w \right)^{1/2} / \left(1 - a/w \right)^{3/2} \right] \left[3.74 - 6.30a/w + 6.32 \left(a/w \right)^2 - 2.45 \left(a/w \right)^3 \right]$$

Limits:

For $0.45 \leq a/w \leq 0.55$

For all r_1/r_2 values, Accuracy within $\pm 1\%$

For X/W either 0.5 or 0

For $0.2 \leq a/w \leq 1.0$

For all r_1/r_2 values, Accuracy within $\pm 1.5\%$

For X/W either 0.5 or 0

For $0.2 \leq a/w \leq 1.0$

For all r_1/r_2 values, Accuracy within $\pm 3\%$

For $0 \leq X/W \leq 1$

An application of this method is found in Tan and Davidge's paper [18]. This paper also describes an alternative mode of gripping the specimen, and making it more applicable for evaluating the quality of tube materials.

6.5.5 Short Rod, Short Bar or "Stub" Test Piece

The basis of this test is a short cylindrical or block specimen which has a notch machined into it of such a shape that it leaves a "V" configuration behind in the remaining ceramic. A basic requirement for this must be a very precise fabrication

Fig. 5.10 Short Cylindrical or Block Specimen

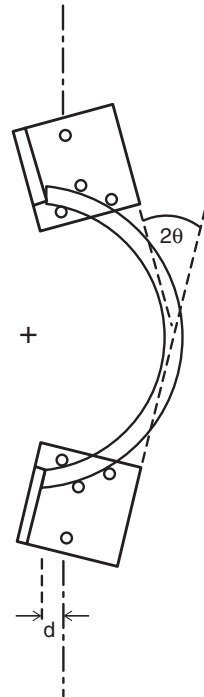
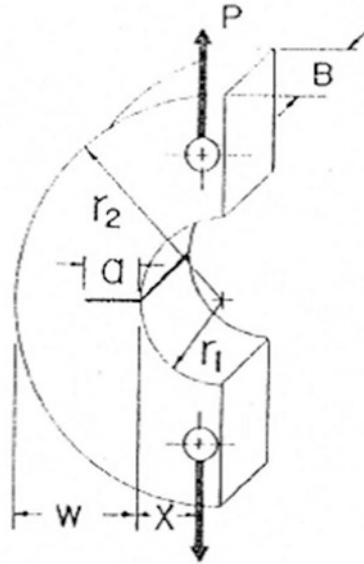


Fig. 5.11 The “C” shaped Specimen indicating geometric parameters



— The C-shaped specimen indicating geometric parameters.

method for the initial cylinder or block, and a means of sawing in the notch to very precise specifications after firing. Testing is carried out by opening up the notch and this may be achieved in two ways.

1. By pulling the specimen apart using a specially shaped tensile jig.
2. Inserting a thin inflatable bag into the notch and pressuring it until the test-piece breaks.

The latter method is clearly quite attractive if expensive test machines are not available.

The crack growth from the point of the V-shaped slot in the specimen is initially stable, even for the most brittle materials. Thus a real crack is obtained during the initial loading of the specimen and an ever increasing load is required for continued crack growth until the crack reaches a critical length a_c . Thereafter, the load to produce further crack growth decreases. a_c depends upon the specimen geometry, but is independent of the specimen material, provided only that it behaves in accordance with linear elastic fracture mechanics. The equation for K_{Ic} is as follows:

$$K_{Ic} = A_F P_c \sqrt{B} \quad (6.127)$$

P_c is the peak pressure on the notch face during the test.

B is the specimen diameter.

A_F is a dimensionless constant dependent on the specimen geometry and loading configuration.

For the rod specimens these are the ratios (related to B)

$$W / B = 1.5000 + 0.006$$

$$C / B = 0.03 + 0.002$$

$$a_0 / B = 0.531 + 0.006$$

$$a_p / B = 0.482 + 0.002$$

$$\delta = 55.2 + 0.5^\circ$$

For block specimens $L/B=0.870$.

Figures 5.13 and 5.14 are the alternative configurations. Figure 5.15 is a section through the notch.

For the ration given above, $A=7.51$.

Typical dimensions are going to be determined by the width of the notch. For a 1 mm notch, one requires a 33.3 mm diameter.

Main reference is L.M. Barker in ASTM/STP 678 (p. 73 [6]). (The author discusses the use of a curved profile on the “V”. This might be achievable with computer machining.)

6.5.6 Indentation Methods

One of the difficulties of obtaining fracture toughness data is that for the most part specially prepared specimens with characteristic shapes have to be produced. It would be very desirable to have a technique which would eliminate these difficulties even at the expense of accuracy if it could be used to sort bodies into categories, so that when a promising material was forthcoming, fewer refined test specimens would have to be prepared. It is possible to do this with a hardness indenter which is a standard piece of equipment in metallurgical and engineering laboratories. Figure 5.17 represents the impression left by a Vicker’s diamond pyramid indenter and showing cracks emanating from each corner.

Figure 5.16 is a longitudinal section through the diagonal of the pyramid base. The advancing crack front is the semicircle of diameter $2D'$ (surface extremities of the crack) and of sub-surface depth D .

$2a$ is the length of the diagonal indentation, and to be Effective, $D/a \geq 2$.

An expression K_{1c} , given by Lawn and Swain [3] is

$$K_{1c} = \frac{(1-2\gamma)(\alpha\rho_o)^{1/2}}{2^{1/2}\pi^2\beta} \left(\frac{P}{D}\right)^{1/2} \quad (6.128)$$

where

P = indenter load.

D = crack depth.

Fig. 5.13 Short Bar Specimen

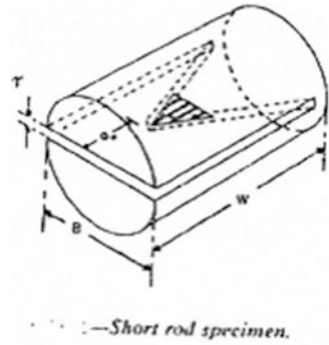


Fig. 5.14 Short Bar Specimen

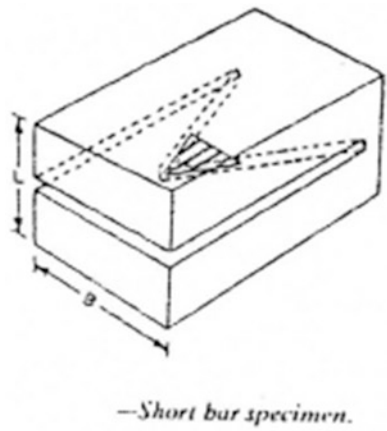
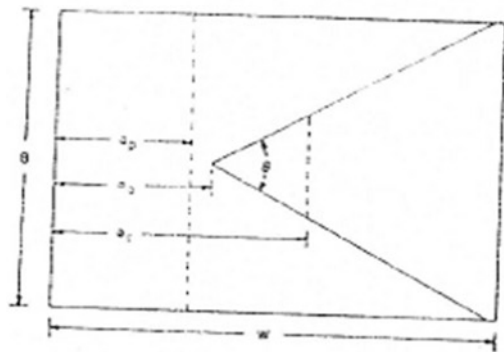


Fig. 5.15 Plan view of Short Bar specimen



γ = Poisson's ratio.

ρ_0 = mean contact pressure.

α = dimensionless constant determined by indenter geometry (for Vicker's $\alpha = 2 / \pi$).

β = dimensionless constant determined by the deformation zone geometry (for Vicker's or Knoop indenter $\beta \sim 2$).

For a pointed indenter which leaves geometrically similar impressions in a homogeneous specimens at all loads, the mean indentation pressure remains invariant. And is equal to the hardness of the material. Equation (6.128) predicts that a plot of P against D will be a Straight line for a given material. By measuring the hardness (ρ_o) and the slope of P/D , the fracture toughness can be calculated.

There is a second, simpler treatment, predicting a different relationship between the parameters [27]

$$K_{Ic} = \frac{1}{\pi^{3/2} \tan \psi} \left(\frac{P}{D^{1/2}} \right) \quad (6.129)$$

where ψ is the indenter cone half angle (Strictly it is only valid for conical indenters) but it gives a good fit to crack growth obtained with a Vicker's indenter. In this case ψ is assumed to be 68° , the half angle between the faces. Analysis predicts that $P/D^{3/2}$ will be a straight line and the hardness is not needed.

Other points about the methods:

1. Crack length should be ten times the max-grain size.
2. Crack depth should be less than 1/3 specimen thickness.
3. For ceramics loading rate was 5.0 mm/min with as Vickers's indenter.
4. Measurement of crack length was by travelling microscope with dye-penetrant to render crack.
5. Data collected at four indenter loads with a min. Of three indents at each load.

For materials with high stress corrosion rates, the indenter may be covered with paraffin oil otherwise tests are carried out in air. For transparent materials photography is probably a better method to measure crack lengths.

Fig. 5.16 Illustration of parameters defining the medium crack which forms during indentation

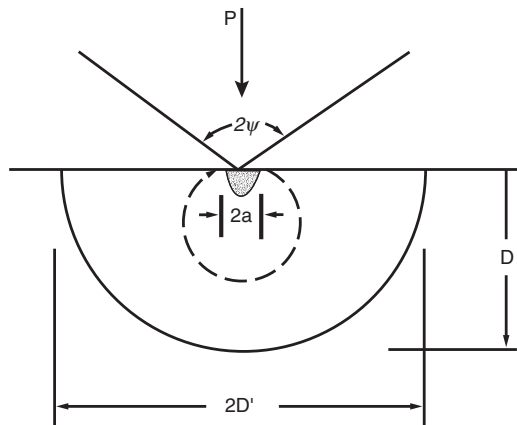


Fig. 5.17 Indentation cracks introduced by a Vickers indenter. (a) Schematic showing the parameters used in the test. (b) A typical crack pattern obtained in Si_3N_4 (polarised light reflected micrograph)

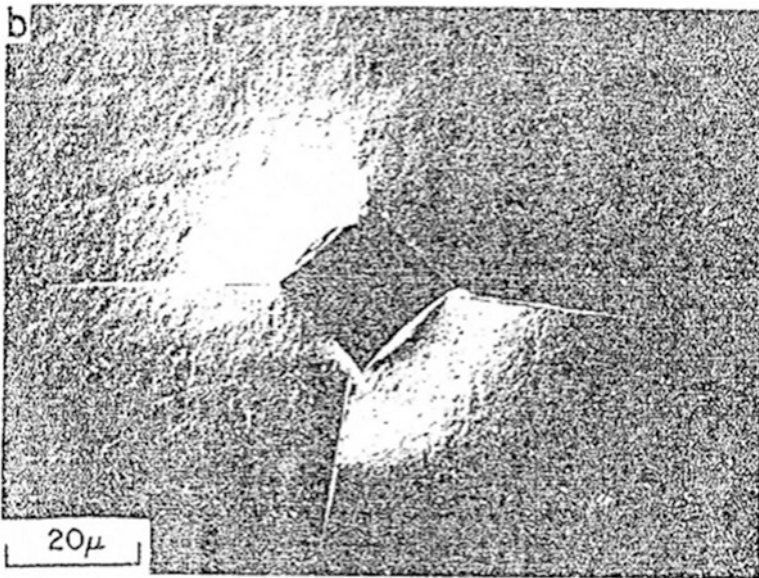
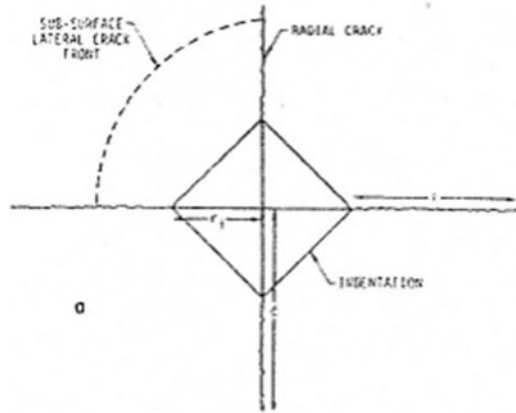


Fig. 5.18 Indentation cracks introduced by a Vickers indenter (a) schematic showing the parameters used in the test

6.6 Time Dependence of Strength [3]

6.6.1 Stress Corrosion

When a crack in a ceramic is exposed to the air, or other environment, the freshly exposed, very reactive surfaces will undergo a chemical reaction with whatever is nearest to it. If you consider that the bonds which hold the crystal together have been disrupted, and there are the free unbounded electrons of the valency forces available to react, then this effect is inevitable. If it were possible to compress a

crack before the atmosphere was able to attack it, the crack would heal up again, and this can be demonstrated in glass. The net effect of the atmosphere is to stabilise the crack in the open position. The most deadly corrosion agent is simply water vapour, and the amount present in normal moist air is quite enough to cause damage. Obviously more active agents, e.g. saline solution, present in animal tissues will be even more dangerous. In effect the $(OH)^-$ groups from the water (or Cl^- ions) satisfy the released valency forces. The combined effect of stress in the material and the activation energy of the chemical attack causes a crack to steadily grow until it eventually reaches the critical Griffith flaw size, and if the stress is sustained, the material will break.

Referring to the double torsion graph (Fig. 5.5), the linear region (I) is that for sub-critical crack growth (or stress corrosion) and for a particular stress (on the abscissa) the appropriate crack velocity can be read off on the ordinate. As the crack grows the stress intensity factor increases, the velocity increases, and a catastrophic situation ensues (i.e. when the stress intensity factor becomes critical).

Under constant stress σ time to failure is given by:

$$t = \int_{C_i}^{C_c} \frac{dc}{v} \tag{6.130}$$

C_i is the initial crack size and C_c is the critical size, and $K_{1c} = \gamma \sigma C_c^{\frac{1}{2}}$.

Because generally $K_1 = \gamma \sigma C^{\frac{1}{2}}$, differentiation given

$$dC = \frac{2K_1}{\sigma^2 \gamma^2} dK_1 \tag{6.131}$$

Substituting for dc in Eq. (6.130).

$$t = \frac{2}{\sigma^2 \gamma^2} \int_{K_{1i}}^{K_{1c}} \frac{K_1}{v} dK_1 \tag{6.132}$$

Referring to the double torsion graph (Fig. 5.5), we have,

Region I, $\log v = \text{const.} \times \log K_1$ i.e. $v = \alpha_1 K_1$.

Region II, Constant velocity region $v = \alpha_2$.

Region III, A third term is possible, but is usually not considered, because crack is reaching sonic velocities, and the specimen is in effect broken at the end of region II.

Let K_1^* be the limiting value of K_1 separating regions I and II

$$\text{then } t_{(\text{minimum})} = \frac{2}{\sigma^2 \gamma^2} \left(\frac{1}{\alpha_1} \int_{K_1}^{K_1^*} K_1^{(1-n)} dK_1 + \frac{1}{\alpha_2} \int_{K_1^*}^{K_{1c}} K_1 dK \right) \tag{6.133}$$

For a real situation, the limit of tolerable stress corrosion should be the end of region I, so if we simply integrate this part of the equation we get,

$$t_{(\min)} = \frac{2}{\sigma^2 \gamma^2 \alpha_1 (n-2)} (K_{li}^{2-n} - K_{1*}^{2-n}) \quad (6.134)$$

Furthermore if n is large (typically) 10, $K_{li}^{2-n} \gg K_{1*}^{2-n}$ so that

$$t_{(\min)} = \frac{2K_{li}^{2-n}}{\sigma^2 \gamma^2 \alpha_1 (n-2)} \quad (6.135)$$

Let a particular specimen have an initial crack length c_1 , then $K_{li} = \sigma \gamma c_i^{\frac{1}{2}}$; combining with Eq. (6.135), (6.136) we see that $t\sigma^n$ is constant (for this particular specimen). Thus the ration of the lifetimes $t\sigma_i, t\sigma_j$, at two subcritical stresses σ_i and σ_j , is given by

$$\left(\frac{\sigma_i}{\sigma_j} \right)^n = \frac{t\sigma_j}{t\sigma_i} \quad (6.136)$$

This relation allows the strength/probability/time diagram to be made, combining the statistical and time-dependent properties of ceramics.

6.6.2 The SPT Diagram

The failure times under constant stress conditions are likely to be inconveniently short compared with those measured a constant rate of strain. These times are related by the expression

$$t_\varepsilon = (n-1)t_\sigma \quad (6.137)$$

(where n is the slope of the K_I/v curve in region I).

Suppose a specimen fails under stress $\sigma_{\varepsilon i}$, in testing time $t_{\varepsilon i}$ then $\sigma_{\varepsilon i} = E_{\varepsilon i} t_{\varepsilon i}$.

For another specimen failing under stress $\sigma_{\varepsilon j}$, in time $t_{\varepsilon j}$, then $\sigma_{\varepsilon j} = E_{\varepsilon j} t_{\varepsilon j}$.

for which

$$\left(\frac{\sigma_{\varepsilon i}}{\sigma_{\varepsilon j}} \right) = \frac{\varepsilon_i t_{\varepsilon i}}{\varepsilon_j t_{\varepsilon j}} \quad (6.138)$$

Eliminating the time using Eqs. (6.137) and (6.138), we have,

$$\left(\frac{\sigma_{\varepsilon i}}{\sigma_{\varepsilon j}} \right)^{n+1} = \frac{\varepsilon_i}{\varepsilon_j} \quad (6.139)$$

Fig. 6.1 A typical crack Pattern obtained in Si3N4 (polarized light reflected micrograph)

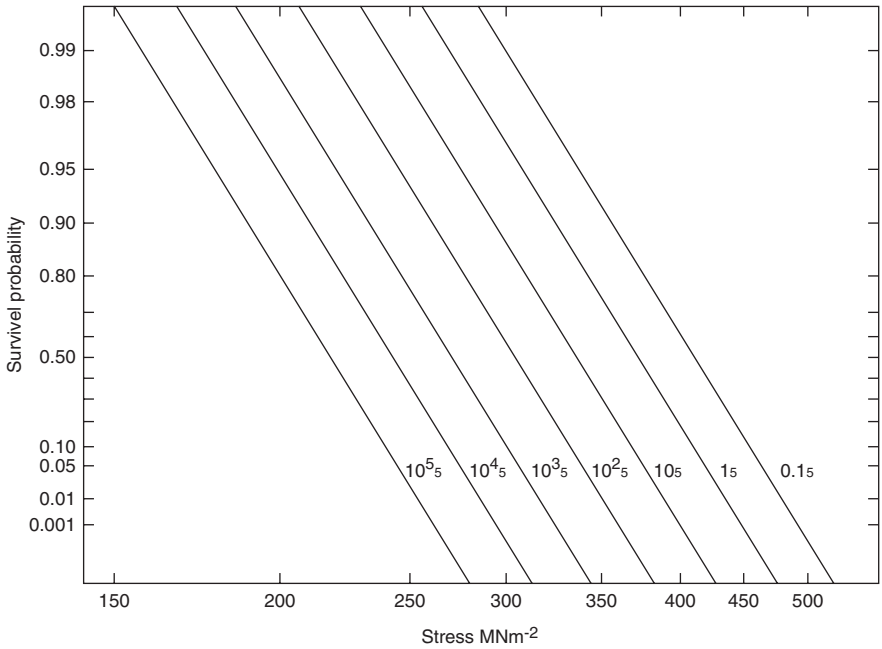
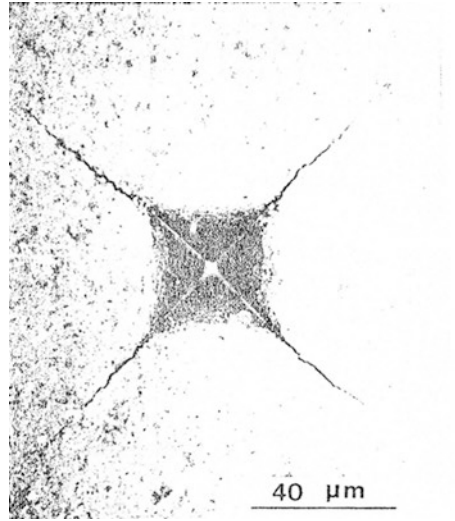


Fig. 6.2 S.P.T diagram for 95 % alumina

S.P.T. diagram for 95 % alumina [1, 3].

S.P.T. diagram for Co-WC alloy at different temperatures (Braiden et al. [23]).

This enables n to be estimated independently of the K_I/v diagram.

6.6.2.1 Procedure

- (1) About 100 test specimens (bars or discs) are prepared and the side which becomes under tension is polished.
- (2) Tests on five batches of 20 are conducted over a wide range of strain rates (each batch having a constant rate). The Weibull modulus for each is obtained.
- (3) A representative stress is chosen for each batch (usually the median) and n is calculated between pairs of batches from the median stress and the straining rate.
- (4) Select a standard failure time (usually 1 s) and normalise the most convenient Weibull spread to this time (using Eq. 6.137)?.
- (5) On the basis of this, draw parallel Weibull slopes in decades of seconds until the desired life of the component is reached. For convenience remember that 3×10^7 s is equivalent to 1 year.

For $n = 10$ each decade represents a reduction of strength of 21 %.

6.6.2.2 Application

This procedure is necessary when ceramic components are designed for use in corrosive environments. Typical applications are hip-joints and grinding wheels. For the hip prosthesis the corrosive environment is the body fluid which is approximately normal saline (e.g. tears). A projected life is 50 years, which makes a revision of the operation unlikely!, and the stress chosen as a basis for calculation is 10 times body weight (i.e. if one jumped down four stairs and landed on one leg.) The calculation is pessimistic because this is an exceptional stress condition and not a constantly applied one.

Apart from the knee these strictures do not apply to any other ceramic joint replacement because they are not under stress.

In the case of grinding wheels, the normal moist air we live in is corrosive agent, and the centrifugal force of its rotation creates the stress. Failure of the wheel catastrophic and fatal accident. Manufacturers of wheel should therefore specify the maximum number of hours for safe usage.

One should be able to apply this reasoning to any kind of ceramic component which will be under stress during its useful life. How do you regard ceramic engines in cars, in lorries, or in aircraft!? Perhaps they may be regarded as disposable items since they should become cheaper than conventional materials and thereby create and environmental disaster with all the indestructible ceramic litter.

6.6.3 Proof Testing [3, 22]

The inherently brittle nature of ceramics makes their use in high stress situations attended with some risk, and before use can be contemplated one has to make a very careful assessment of this risk.

Typically the questions which might be asked are:

“Given the characteristics of its design, is it possible for a hit joint ball to last 40 years, subject to a maximum loading of $10\times$ body weight (chosen to account for impacts during stumbles or other unusual situations. Will it survive the corrosive body environments)”.

“Will a ceramic-bladed jet-engine survive 1 flight, 5 flights, 20 flights etc. in service across the Atlantic” What is quite certain is that only whole numbers are acceptable, and that a fair number of flights are required before the engine can be taken out of service to be operated economically.

“How many hours will a grinding wheel survive at its normal speed of rotation, working in normal humid air before it must, for safety’s sake be taken out of service”.

Putting these questions in another way would be to say “What is the chance of a catastrophically large flaw being present in a highly stressed region of the ceramic”.

A rough method of improving their survival probability would be to simply place all the specimens under a testing load and deliberately allow a few of them break to remove those which had manufacturing defects. This is better than nothing, but it is possible to be much more precise. Initially one must decide what is a realistic load for the ceramic component. It is then overloaded for a finite length of time during which the cracks will grow. Some, of course, will exceed the critical length and the ceramic will fail, but it is possible to calculate a critical crack length under a proof-test load, at which the ceramic will be just short of the point of failure. This represents a “worst case” situation because most of the survivors will be far better than this.

If we now go back to the realistic load, the critical cracks will now be longer than they were before testing, and the service life will be the time required for the cracks to grow by stress corrosion from the proof-test worst crack length to the working load critical crack length. If it assumed that the specimens are being proof tested at the top end the K_I region we can state that,

$$K_{I_p} = Y\sigma_p\sqrt{cp} < K_{I_c} \quad (6.140)$$

In subsequent service

$$K_{I_a} = Y\sigma_a\sqrt{c_p} \quad (6.141)$$

Thus

$$K_{I_a} = \frac{\sigma_a}{\sigma_p} K_{I_c} \quad (6.142)$$

$$K_{(\min)} = \frac{2K_{I_c}^{2-n} (\sigma_a / \sigma_p)^{2-n}}{\sigma_a^2 Y_{\alpha 1}^2 (n-2)} \quad (6.143)$$

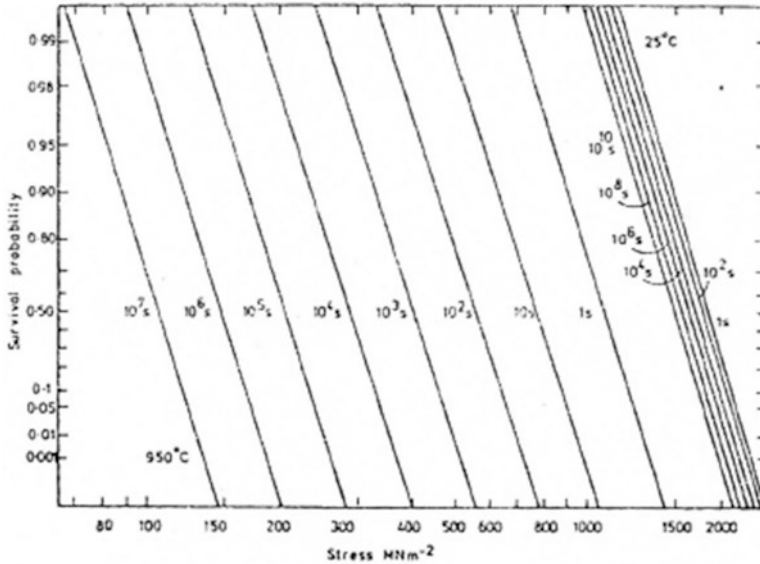


Fig. 6.3 S.P.T diagram for Co-WC alloy at different temperatures (Braiden et al. [23])

Choosing different ratios of σ_d/σ_p the stress, σ_a may be plotted against the time for which it is applied (Eq. 6.143), on a log-log plot this must have a slope of -2 . We can superimpose on this diagram curves which relate the time in seconds to the stress for a specific probability of failure. These can be obtained from the S.P.D. diagram. It is possible to predict therefore, for a specific ratio of failures to survivors, what the service time would be under a given stress, and also the proof testing ratio σ_p/σ_a which would guarantee this performance.

Figure 6.3 shows that if we allow a one per thousand (10^{-3}) proof-testing failure ratio, a service life of 5×10^7 s is guaranteed for a service stress of 30 MPa, if the proof testing ratio had been 2.6/1.

(Check that if we allow one per hundred failures during proof-testing at a ratio of 3.6/1, the service life under the same stress is 10^{16} s. Since this is about 10^8 years they would have to have been made before mankind appeared.)

For hip joint balls designed to operate with a conical fixation, σ_a is 9000 N applied over the effective conical surface, and σ_p is 25,000 N. This should last about 50 years. Because there is some slight degree of failure when the load is removed, the specimens are reloaded to the working stress level to ascertain they are still sound.

6.7 Ceramic Hip Joints Endoprosthesis

The design of the ceramic head for the hip joint prosthesis requires the solution of a number of problems, important among which are as follows:

1. Using a conical fixation to the metal stem creates a hoop stress which will be severe if the cone is forced or impacted too violently into ball.
2. It is unlikely that the conical surfaces will be machined so precisely that stress will not be concentrated at some point on the cone.¹
3. A working stress limit on the ball is considered to be about ten times weight, taking account of sudden impacts on one limb.
4. The effect of stress corrosion after 30–40 years may weaken the ceramic.

6.7.1 Finite Element Analysis (FEA)

The testing of every combination of a hip device design with multiple modular heads and neck arrangements and sizes are not practical in terms of time or cost for the pre-market approval process of a device. To overcome this issue often “the worst case” prosthesis design/combination is identified and used as the bases for the approval of the range of similar devices. The identification of the “worse case” design may not always be obvious; however, it is generally accepted that femoral heads with the largest off set of +12 mm [29] on the smallest stem in terms of diameter produce the most extreme stress conditions in the neck of the femoral stem. In particular with new device designs where there is no historical data to draw from then Finite Element Analysis (FEA) can be a valuable tool to determine the worst case design combination to test. When this chapter was written in the 1990s FEA was a relatively recent computational technique; however, it is now widely used in medical devices to verify a design is “fit for purpose”. FEA is used to simulate the loading conditions within a human body and therefore assisted in the development of more realistic testing protocols.

In the original investigation, the aim was to answer questions raised (Sect. 6.7) questions 1, 2 and 3. In the original computational process the optimum mesh of 152 elements was drawn and eight nodes per element were defined at which the stresses were measured. In modern computational studies it is common to use 4000 [30] mesh units to represent the possible contact areas using a new range of analytical models; however, the original work describes the basic theory behind the analysis therefore it was decided to retain much of the original texts.

Three load cases and three restraints were defined, as follows (Fig. 7.2).

¹ Accurately machined cone and socket sections from epoxy resin were analysed photoelastically. However, careful the machining, a “high spot” which concentrated the stress was always revealed. Much depends on the confidence one has in the machining operation.

6.7.1.1 Load Cases

Case (A) was chosen to represent the very small area of contact of the prosthesis ball with a ceramic acetabular cup.

Case (B) was chosen to represent the wider distribution of the load when a less rigid UHMWPE (ultra high molecular weight polyethylene) acetabular cup was used.

Case (C) was chosen to represent the situation in the body, where the load was not applied axially but spread over an arc between 20° and 55° to the cone axis. This case is somewhat exaggerated and chosen to accommodate the computational system. It serves to indicate that in a realistic situation where the load is applied at 25° to the axis there will be more distortion than is represented by cases A and B.

6.7.1.2 Restraints

1. The load was transmitted to the shaft via the ball across the lower third of the conical interface, i.e. at the end of the cone remote from the centre of the ball.
2. Load transmitted via the middle third, and
3. Load transmitted via the upper third, i.e. at the end of the cone nearest the centre.

6.7.1.3 Results and Conclusions from FEA

The finite element system requires information about the physical properties of the material e.g. modulus of elasticity, Poisson's ratio etc. and the load applied, which was 9000 N (i.e. about ten times body weight. The body in this instance is rather large, but not untypical of the type of elderly patient needing a hip replacement) [8].

Because the ceramic heads were symmetrical, the problem was considerably simplified, and the analysis was able to provide plane strain diagrams of the following:

1. The highly magnified "displaced shape" of the ball under load (Figs. 7.3, 4, 5). The diagrams were chosen to represent ("worst cases"). The diagrams appear to display very large distortions, but the scale of these is very large, i.e. 1 cm on the diagrams represents the order of micrometres.
2. Diagrams representing the magnitude and direction of the two principle stresses at the nodal points in the xy plane.
3. Diagrams showing equal stress contour lines through the nodal points for the maximum and minimum principle stresses and for the hoop stress which is in the z direction.

A stress printout for all the nodes which surround each element was also provided, from which it was possible to derive the average stress at the centre of each element.

The finite element analysis was able to point to several factors about the design of the prosthesis shape, the manner of application of the load and to enable specifications for the alumina to be drawn.

6.7.1.4 Shape Factors

Examination of the diagrams for the principle stress (2) above and the equal stress contour lines (3) show large tensile stresses at the base of the cone and at the cone opening. This can be remedied by undercutting the base of the cone to turn it into a dome, and by relieving the corner at the cone opening.

6.7.1.5 Application of Load

The displaced shape diagrams (1) and the stress contours (3) clearly show that the application of the load over a larger area from the polyethylene cup produces a higher concentration of large tensile stresses than is the case with the alumina acetabular cup.

6.7.2 Weibull Equation

This involved the application of the four function Weibull equation [9, 32] as follows:

The probability of failure of a test specimen can be represented by the standard Weibull equation.

$$P_f = 1 - \exp \left\{ - \left[\frac{(\sigma_u - \sigma)}{\sigma_0} \right]^m \right\} \quad (6.144)$$

Another form of this equation is given by

$$P_f = 1 - \exp \left\{ - \left(\frac{1}{m} \right)! \left(\frac{\sigma}{\bar{\sigma}_f} \right)^m \right\} \quad (6.145)$$

which employs the relation $\bar{\sigma}_f = \sigma_0 (1/m)!$, where $(1/m)!$ are the ‘‘gamma function’’ and is available in tables, and $\bar{\sigma}_f$ is the mean stress of the batch.

The failure stress of a specimen is also related to its volume, given by the expression (based on 6.144)

$$\bar{\sigma}_f^m V = \bar{\sigma}_{f_v}^m v \tag{6.146}$$

$\bar{\sigma}_{f_v}$ is the tensile breaking stress of a test piece of reference volume v . The purpose of the exercise is to evaluate this.

Combining the two we arrive at the four function Weibull equation

$$P_f = 1 - \exp \left\{ - \left(\frac{1}{m} \right)!^m \cdot \left(\frac{1}{\bar{\sigma}_{f_v}} \right)^m \cdot \frac{V}{v} \cdot \sigma^m \right\} \tag{6.147}$$

The stress in each volume element dV is made up from the three principal stresses so $\sigma^m dV$ has to be applied three times over in each element, i.e. $(\sigma_1^m + \sigma_2^m + \sigma_3^m) dV$. Account has also to be taken of whether the stress is tensile or compressive. Use is made of the Heaviside function $H(\sigma)$. Its value is unity for positive tensile stresses, and $-\alpha$ for negative compressive stresses, α is the modulus of the ratio of the mean failure stresses per unit volume in uniaxial tension and compression. In this exercise α was conveniently given the value of -10 for the alumina under compression.

The final expression for the failure probability of the specimen is given by

$$P_{\text{total}} = 1 - \exp \left\{ - \left(\frac{1}{m} \right)!^m \cdot \left(\frac{1}{\bar{\sigma}_{fr}} \right)^m \cdot \frac{1}{v} \int_r \left[\left(\frac{\sigma_1}{H(\sigma_1)} \right)^m + \left(\frac{\sigma_2}{H(\sigma_2)} \right)^m + \left(\frac{\sigma_3}{H(\sigma_3)} \right)^k \right] dv \text{ (Ref. 10)} \right\} \tag{6.148}$$

where the ‘‘stress-volume integral’’ is taken over all the elements in the body.

From the finite element diagrams, the area of each element was calculated in square millimetres by approximating each to a trapezoid. The volume of revolution of each element about the centre line of the section was then calculated.

To construct Tables 6.4 and 6.5 the 152 elements were divided into eight separate computer programmes to estimate the stress-volume-integral, the sum of which is shown in the first column. For convenience of calculation the stress unit chosen was 10 MPa.

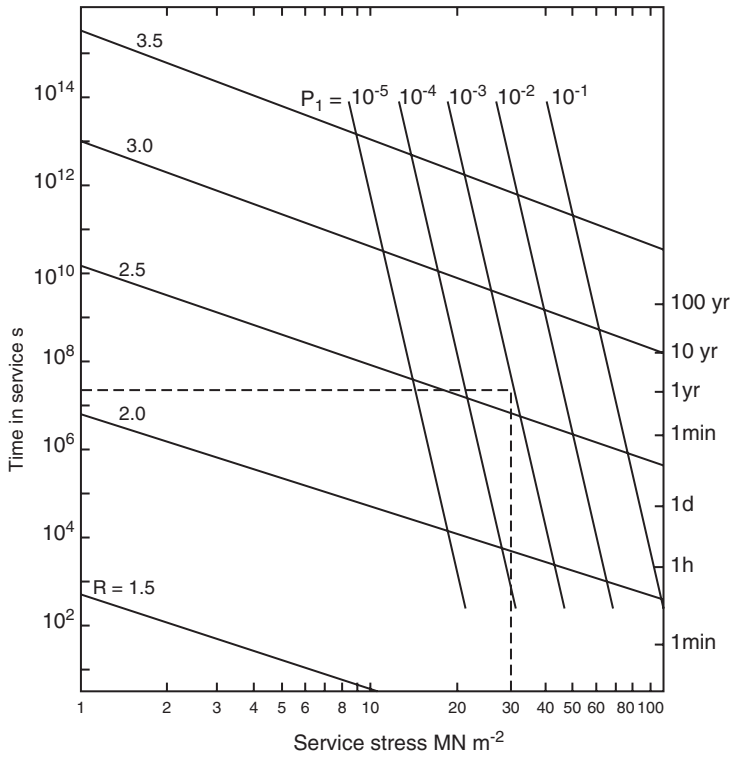


Fig. 7.1 Finite element mesh—elements numbered (1–152)

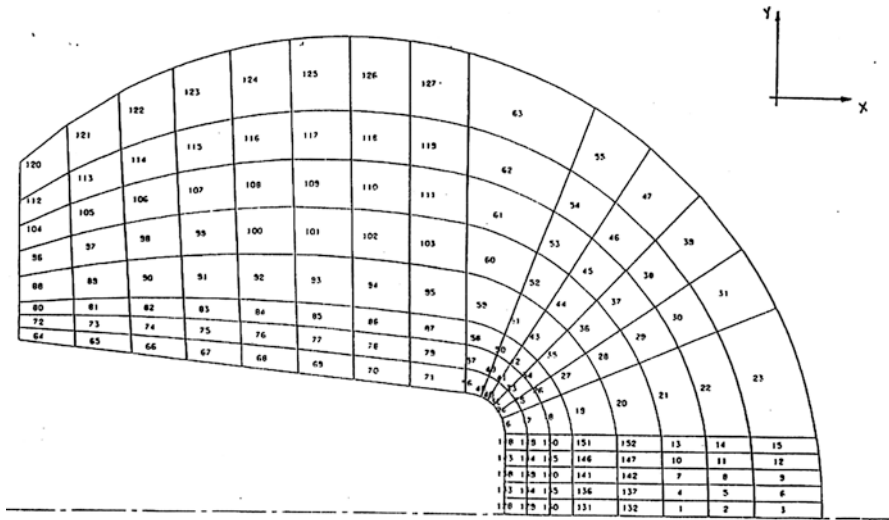


Fig. 7.2 Loadcases (A, B and C) and restraints (1, 2 and 3)

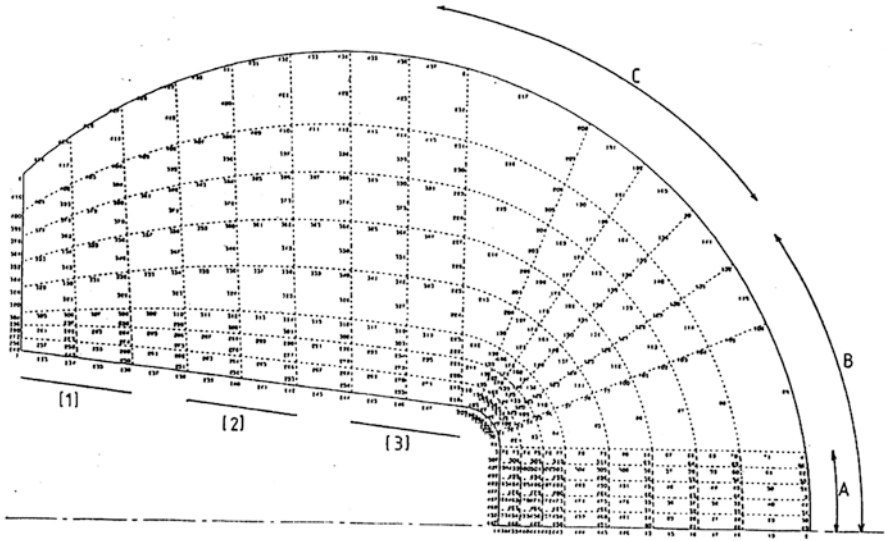


Fig. 7.3 Displaced shapes of prosthesis head. Load case A. Constraints 1 and 3

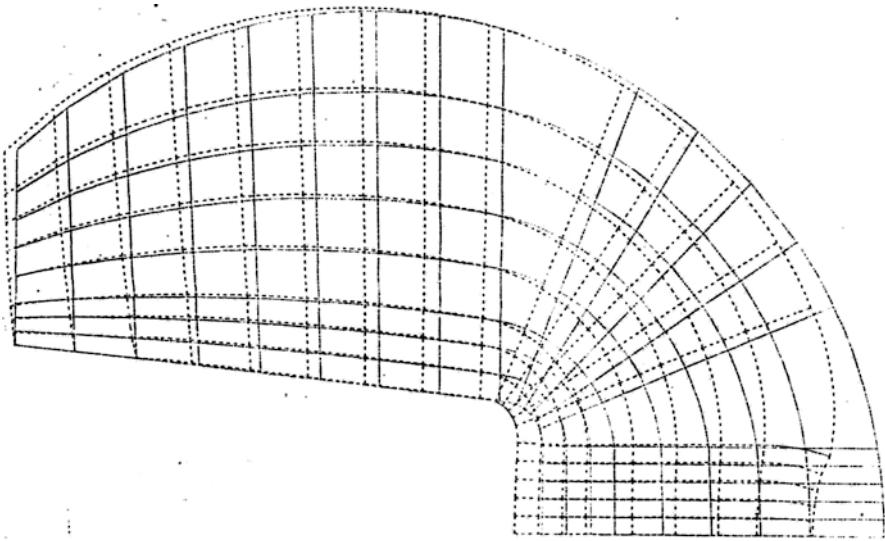


Fig. 7.4 Displaced shape of prosthesis head. Load case B. Constraint 1

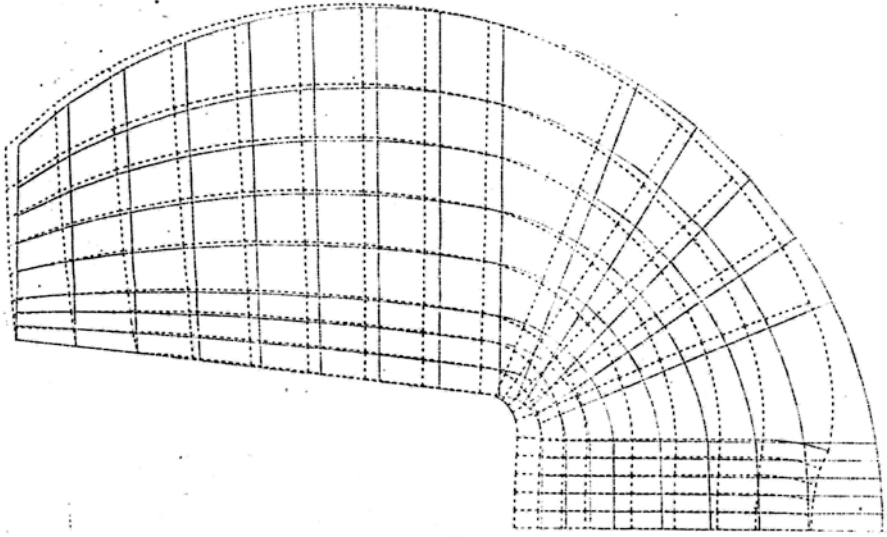


Fig. 7.4 (continued)

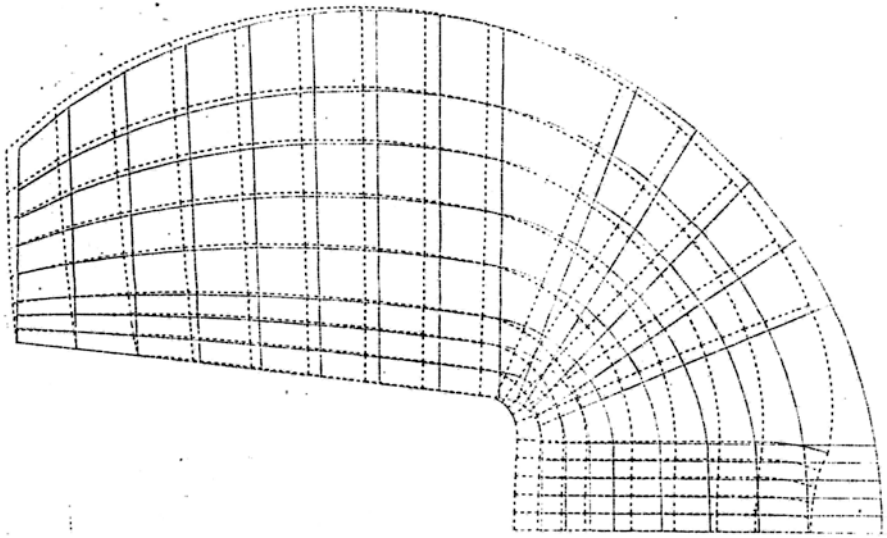


Fig. 7.5 Asymmetric load. Constraint 3

Table 6.4 Experimental Data for Notched Bar Test

Str/vol. Int $S_{i(-\dots)}dv$	Ref., vol. (v)	Weibull mod. (m)	Gamma for "m" value $(1/m)!$	Failure prob. reqd. (P_r)
1.050E14				
8.890E10	mm ³	10.000	0.610	0.100
6.890E13	1000.000			ln(1 - Pr)
9.280E15				-0.105
1.030E12			-Gamma	
1.140E10			-0.610	
5.330E14				
5.800E14				
Total	Total/Ref. V	S/V Int x Gamma	"A"/E-14	Req. str/10
1.057E16	1.057E13	-6.446E12	1.634	23.91 MPa
Str/vol. Int $S_{i}(dv)$	Ref. vol. (v)	Weibull mod. (m)	Gamma for "m" value $(1/m)!$	Failure prob. reqd. (P_r)
1.05E14				
9.890E10	mm ³	10.000	0.610	0.100
6.890E13	1000.000			ln (1 - Pr)
9.280E15				-0.105
1.030E12			-Gamma	
1.140E10			-0.610	
5.330E14				
5.800E14				
Total	Total/Ref. V	S/V Int x -Gamma	"A"/E-14	Req. str/10
1.057E16	1.057E13	-6.446E12	0.016	38.099 MP a

"A" = (S/V Int x Gamma)/log(1 - Pr)
 With a Weibull modulus of 10 the required tensile strength of a 1 cc test specimen is 381 MPa for a 0.1 % failure probability
 The required tensile strength is 239 MPa for a 10 % failure probability

Table 6.5 Survival Probability Vs. Stress

Str/vol. Int $S_i(-\dots)dv$	Ref., vol. (v)	Weibull mod. (m)	Gamma for "m" value (1/m)!	Failure Prob. reqd. (P)
3.500E20				
3.210E15	mm ³	15.000	0.590	0.100
3.520E19	1000.000			ln(1 - Pr)
9.940E18				-0.105
1.460E17			-Gamma	
1.140E10			-0.590	
2.400E21				
8.820E20				
Total	Total/Ref. V	S/V Int x -Gamma	"A"/E-14	Req. str/10
3.677E21	3.677E18	-2.170E18	4.856E-6	19.39 MPa
Str/vol. Int	Ref. Vol.	Weibull mod.		Failure prob. reqd.
3.500E20				
3.210E15	mm ³	15.000	0.590	0.001
3.520E19	1000.000			ln(1 - Pr)
9.940E18				-0.001
1.460E17			-Gamma	
1.140E10			-0.590	
2.400E21				
8.820E20				
Total	Total/Ref. V	S/V Int x -Gamma	"A"/E-14	Req. str./10
1.057E16	3.677E18	-2.170E18	4.61E-8	26.449 MPa

"A" = (S/V. Int x -Gamma)/log(1 - Pr)
 With a Weibull modulus of 15, the required tensile strength of a 1 cm test specimen is 264.5 MPa for a 0.1 % failure probability
 The required tensile strength is 194 MPa for a 10 % failure probability

6.7.3 *A Design solution to the Stem Fixation Problem*

An obvious solution to the problems created by the conical fixation is to avoid this if possible. A cylindrical fixation would have the following advantages:

Dangerous hoop stresses would not be created by impacting the ball in service or during fixation.

It is easier and less expensive for the manufacturer to press solid spheres and afterwards machine out the cylindrical fixation hole, rather than having to machine out a precise conical hole or include it in the original pressing.

To obtain the degree of bonding required needs a very precise frictional fit between the stem and the ball. This has been achieved by

- (a) Covering the stem with a plastic sleeve and forcing it into the cavity.
- (b) Diffusion bonding a biocompatible metallised layer of precise thickness into the surface of the cylindrical cavity in the ceramic so that it becomes integral with the ceramic. A titanium shaft is subsequently fitted into the cavity. This is still under active development.

6.7.4 *Summary and Conclusions*

Testing methods for alumina have to be chosen so that

- (a) a representative proportion of the material is actually tested
- (b) they can all receive identical processing
- (c) they can be easily polished
- (d) they are as large as the facilities permit

The required parameters are the strength and Weibull modulus. These can be used, along with the “stress-volume-integral” obtained from the results of finite element analysis, to provide the factors in the four function Weibull equation. From this the minimum strengths of the representative test pieces may be defined.

The clearly emerging results from this analysis are as follows:

- (a) The required strength of the material is increased as the specified risk of failure is reduced.
- (b) The required strength is reduced if the Weibull modulus is increased.

A combination of high strength, high “*n*” value (making allowance for stress corrosion projected over the length of time in service), and high Weibull modulus should ensure a satisfactory materials performance.

Considering therefore the results in Tables 6.4 and 6.5, to ensure to safety of a hip prosthesis, a value of 400 MPa for the flexural strength should be expected, having made an appropriate deduction for stress corrosion, and expecting to attain a Weibull modulus of at least 15 (which should be attainable after polishing). These figures would demand a very fine grained alumina and is in line with current thinking. To convert the tensile strengths into experimental flexural strengths or modulae of rupture requires them to be multiplied by factors given in (1.3) and (1.4) which in turn depend on the Weibull modulus.

Comparing Fig. 7.3 with Figs. 7.4 and 7.5, it seem evident that load cases B and C contribute to shear stress, which when resolved cause higher tensile stresses than in load case A. This would indicate that the ceramic acetabular cup is safer to use than the polyethylene.

It should be emphasised that this degree of rigour is required only for highly stressed components. Many of the other applications of alumina (e.g. in the dental field) do not require such high specifications.

6.7.5 *Alternatives Approach to Design*

With increased pressure from regulatory bodies demanding stringent testing throughout the design, validation and manufacturing phases of health care product development, alternative aids are emerging to assist in the pre-market product performance evaluation studies. Digital Imaging Correlation [31] is one such aid using digital cameras to quantitatively analysis the surface deformation of device under load. This system is based on the ability of the high resolution cameras to track a speckle pattern on the surface of an object as it deforms and provides a visual and quantitative analysis of surface strains of materials and products undergoing stress testing. Digital Imaging Correlation has been used in the analysis of prosthetic stress shielding. Stress shielding occurs as the result of a discrepancy between the elastic properties of the bone and the implant. The strain characteristics of differing materials on the femur have been demonstrated in laboratories using strain gauges and photoelastic techniques.

FEA can still present problems when modelling stress and strain complex geometries, often associated with uncertainty surrounding boundary conditions and material properties of the modelling. Digital Imaging Correlation can aid in the validation of FEA theoretical computer models with a view to reducing the risks associated with development of new increasing more complex device designs.

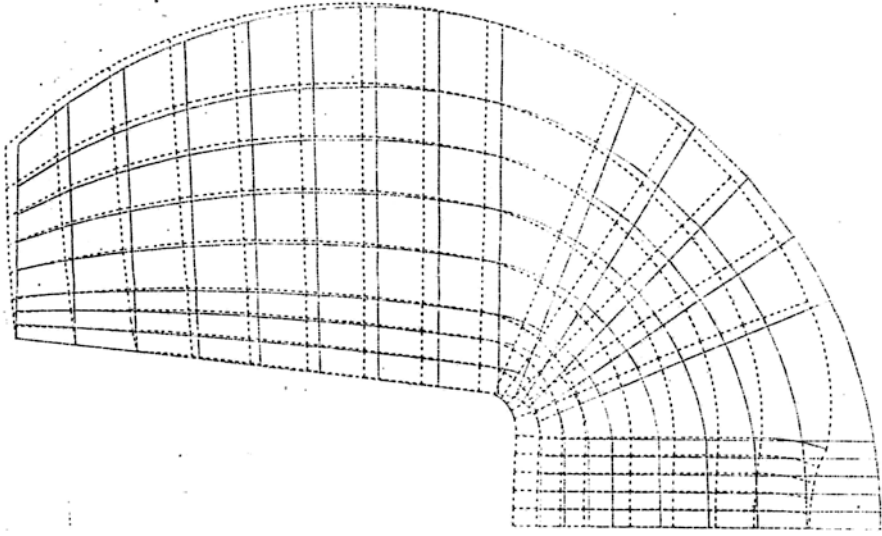


Fig. 7.6 Femoral head under axial loading, Image supplied by Lucideon

References

1. Lawn BR, Wilshaw TR (1975) *Fracture of brittle solids*. Cambridge University Press, London
2. Jayatilaka A de S (1979) *Fracture of engineering brittle materials*. Applied Science Publishers, London
3. Davidge RW (1979) *Mechanical behaviour of ceramics*. Cambridge University Press, Cambridge
4. Kerkhof F (1983) *Handbook of ceramics*. Schmidt, Freiburg im Breisgau
5. Hahn HG (1976) *Bruchmechanik*. Teubner, Stuttgart
6. Freiman SW (ed) (1979) *Fracture mechanics applied to brittle materials*. A.S.T.M., S.T.P. 678
7. Braiden P (1975) An introduction to Weibull statistics. A.E.R.E.R 7165
8. Maier HR, Staerk N, Krauth A (1983) In: Hastings GW, Williams DF (eds) *Mechanical properties of biomaterials*. Wiley, New York
9. Stanley P, Fessler H, Sivill AD (1973) An engineer's approach to the prediction of failure probability of brittle components. *Proc Br Ceram Soc* 22:453–487
10. Davidge RW, Tappin G (1968) The effective surface energy of brittle materials. *J Mater Sci* 3:165–173
11. Feltham P (1966) *Deformation and strength of materials*. Butterworths, London
12. Timoshenko S (1976) *Strength of materials, vol 1*. Van Nostrand-Reinhold, New York, p 92
13. Durelli AJ, Morse S, Parks V (1962) The theta specimen for determining tensile strength of brittle materials. *Mater Res Stand* 2(2):114–117
14. Daniel IM, Weil NA (1962) Effect of non-uniform stress fields. *Studies of the brittle behaviour of ceramic materials*. Report AD 277659
15. Griffiths R, Holloway DG (1970) The fracture energy of some epoxy resin materials. *J Mater Sci* 5:302–307
16. Evans AG (1972) A method for evaluating the time-dependent failure characteristics of brittle materials and its application to polycrystalline alumina. *J Mater Sci* 7:1137–1146

17. Evans JRG, Stevens R (1984) The “C”-ring test for the strength of brittle materials. *Trans Br Ceram Soc* 83:14–18
18. Tan SR, Davidge RW et al (1980) Strength-controlling flaws in beta-alumina. *Trans Br Ceram Soc* 79:120–127
19. Mordfib L, Kerper MJ (1969) Strength testing of ceramics. Office of Aerospace Research, Arlington, VA
20. Paris PC, Sih GC (1965) Stress analysis of cracks. *ASTM Spec Tech Publ* 381
21. Williams P, Evans AG (1973) A simple method for studying slow crack growth. *J Test Eval* 1(4):264–270
22. Evans AG, Wiederhorn SM (1973) Proof testing of ceramic materials—an analytical basis for failure prediction. *Int J Fract* 10(3):379–373
23. Braiden PM, Davidge RW, Airey R (1977) Time dependent strength parameters for tungsten carbides containing 6 or 16% cobalt at room and elevated temperatures. *J Mech Phys Solids* 25:257–268
24. Lach S, Dailly DF, Hastings GW (1982) Stress corrosion of debase alumina. *Proc Br Ceram Soc* 31:191–200
25. Dalgleish BJ, Pratt PL, Rawlings RD, Fakhr A (1980) The fracture toughness testing of ceramics and acoustic emission. *Mater Sci Eng* 45:9–20
26. Lawn BR, Swain MV (1975) Microfracture beneath point indentations in brittle solids. *J Mater Sci* 10:113–122
27. Champonier RP (1979) A.S.T.M./S.T.P. No. 678, p 60
28. Shaw MC, Braiden PM, de Salvo GJ (1975) The disc test for brittle materials. *J Eng Ind* 97(1):77–87
29. Khan I, Naylor M, Gupta G (2013) Characterization of Orthopaedic Devices. In: Bandyopadhyay A, Bose S (eds) *Characterization of biomaterials*. Elsevier, Amsterdam, pp 323–351
30. Cilingir A (2010) Finite element analysis of the contact mechanics of ceramic-on-ceramic hip resurfacing prostheses. *J Bionic Eng* 7(3):244–253
31. Smith R (2015) The application of digital image correlation technology in healthcare. Lucideon White Paper
32. Lach S (1981) Ph.D. Thesis, C.N.A.A.
33. Carniglia SC (1972) Working model for porosity effects on the uniaxial strength of ceramics. *J Am Ceram Soc* 55(12):610–618
34. Davidge RW, Evans AG (1970) The strength of ceramics. *Mater Sci Eng* 6(5):281–298
35. Duckworth W (1953) Discussion of Ryshkewitch paper compression strength of porous sintered alumina and zirconia. *J Am Ceram Soc* 36(2):68
36. Knudsen FP (1959) Dependence of mechanical strength of brittle polycrystalline specimens on porosity and grain size. *J Am Ceram Soc* 42(8):376–387
37. Passmore EM, Spriggs RM, Vasilos T (1965) Strength-grain size-porosity relations in alumina. *J Am Ceram Soc* 48(1):1–7
38. Eudier M (1962) The mechanical properties of sintered low-alloy steels. *Powder Metall* 5(9):278–290

Chapter 7

Properties of Bioactive Glasses and Glass-ceramics

L.L. Hench and T. Kokubo

7.1 Definition of bioactivity:

A bioactive material is one that elicits a specific biological response at the interface of the material which results in the formation of a bond between the tissues and the material. A common characteristic of bioactive glasses, bioactive glass-ceramics, and bioactive ceramics is that their surface develops a biologically active hydroxy carbonate apatite (HCA) layer which bonds with collagen fibrils. The HCA phase that forms on bioactive implants is equivalent chemically and structurally to the mineral phase of bone. It is that equivalence which is responsible for interfacial bonding¹⁻³.

7.2 Bioactive Bonding

Bioactive materials develop an adherent interface with tissues that resist substantial mechanical forces. In many cases the interfacial strength of adhesion is equivalent to or greater than the cohesive strength of bone. The interfacial strength of a bioactive implant bonded to bone is 15–40 times greater than the interfacial adherence of non-bioactive materials (such as Al_2O_3) (Table 7.1 and Figure 7.1), tested in the same animal model (rabbit tibia) (Figure 7.2)⁴.

L.L. Hench (✉) • T. Kokubo

Division of Material Chemistry Faculty of Engineering, Imperial College Department of Materials, Kyoto University, Sakyo-ku Kyoto, 606-01, Japan, Prince Consort Road, London SW7 2BP, UK

Table 7.1 Failure Loads of Bioceramics by Detaching (Pull-Off) Test

Materials	Failure Load (kg)		Location of Fracture
	8 Weeks	24 Weeks	
Dense sintered alumina ^{1,2}	0.13 ± 0.02		Interface
Bioglass [®] 45S5-type glass ^{1,2}	2.75 ± 1.80		within material
Ceravital [®] KGS-type glass-ceramic ³	3.52 ± 1.48	4.35 ± 1.45	within material
Cerabone [®] A-W glass-ceramic ^{1,2}	7.44 ± 1.91	8.19 ± 3.6	within bone
Dense sintered hydroxyapatite ^{1,2}	6.28 ± 1.58	7.77 ± 1.91	within material
Dense sintered β -3CaO • P ₂ O ₅ ⁴	7.58 ± 1.97		not specified
Natural polycrystalline calcite ⁵	4.11 ± 0.98		within material

¹. T. Nakamura, T. Yamamuro, S. Higashi, T. Kokubo and S. Ito (1985) A New Glass- Ceramic for Bone Replacement: Evaluation of its Bonding to Bone Tissue, *J. Biomed. Mater. Res.* **19**, 685–698.

². T. Nakamura, T. Yamamuro, S. Higashi, Y. Kakutani, T. Kitsugi, T. Kokubo and S. Ito, 1985, A New Bioactive Glass-Ceramic for Artificial Bone, in *Treatise on Biomedical Materials, 1*, T. Yamamuro, ed., Research Center for Medical Polymers and Biomaterials at Kyoto University, Kyoto, Japan, pp. 109–17.

³. S. Kotani, T. Yamamuro, T. Nakamura, T. Kitsugi, Y. Fujimuta, K. Kawanabe, T. Kokubo and C. Ohtsuki (1990) The Bone-Bonding Behavior of Two Glass-Ceramics (KGS and A-W GC), in *Bioceramics*, Vol. 2, G. Heimke, ed., German Ceramic Society, Cologne, pp. 105–112.

⁴. S. Kotani, Y. Fujita, T. Kitsugi, T. Nakamura, T. Yamamuro, C. Ohtsuki and T. Kokubo (1991) Bone Bonding Mechanisms of β -tricalcium Phosphate, *J. Biomed. Mater. Res.* **25**, 1303–15.

⁵. Y. Fujita, T. Yamamuro, T. Nakamura, S. Kotani, C. Ohtsuki and T. Kokubo (1991) The Bonding Behavior of Calcite to Bone, *J. Biomed. Mater. Res.* **25**, 1991–2003.

⁷. T. Yamamuro (1993) A/W Glass-Ceramic: Clinical Applications, in *Introduction to Bioceramics*, eds L.L. Hench and J. Wilson, World Scientific Publishing Co., London, 1993, pp. 89–104.

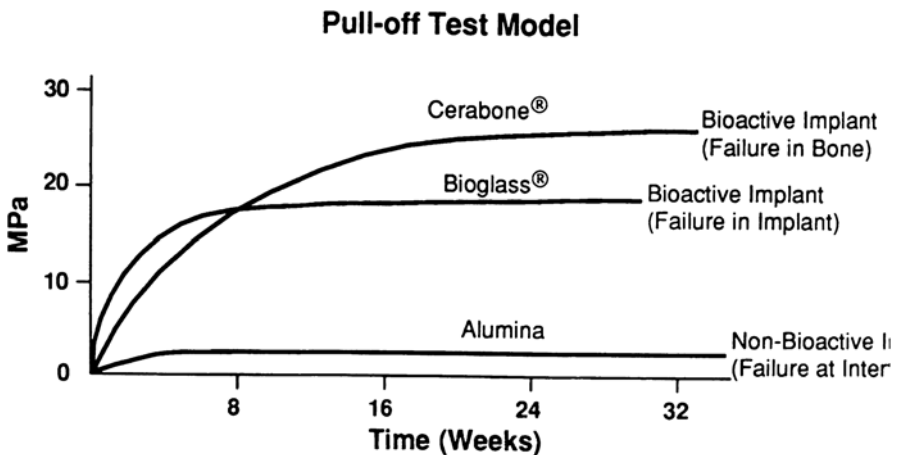


Fig. 7.1 Comparison of interfacial bond strengths of bioactive implants with non-bonding implants (alumina) using ‘pull off’ detaching test [4, 5]

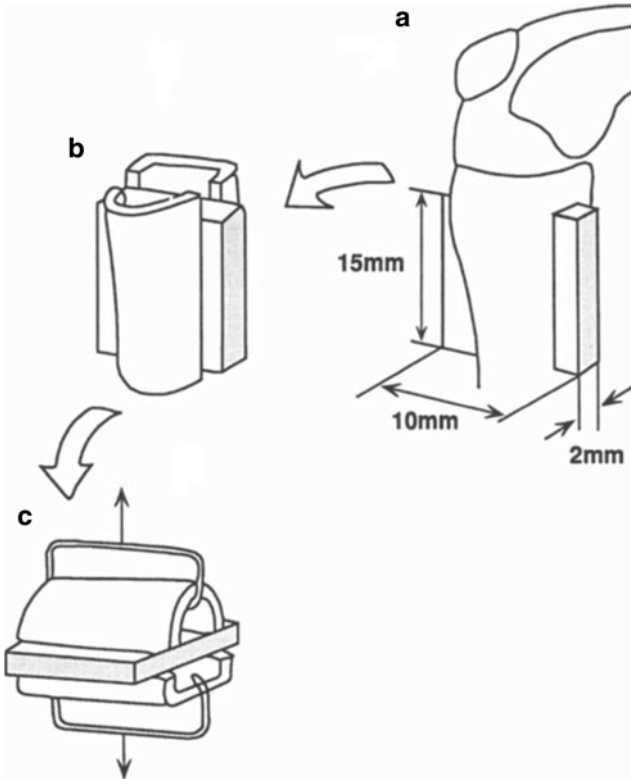


Fig. 7.2 Schematic of 'pull off' detaching test for determining bone-implant bonding (based upon T. Yamamuro, ref. 4)

7.3 Bioactive Compositions

Bioactive materials are composed of very specific compositional ranges of Na_2O , CaO , P_2O_5 and SiO_2 due to the importance of these compounds in the *in vivo* formation of hydroxy carbonate apatite (HCA) bone mineral (Table 7.2) [1, 2]. All compositions either form a HCA layer on their surface or partially dissolve (resorb) as HCA crystals are formed during the mineralization of osteoid. The rate of formation of HCA and bone depends upon the composition of the material (Figure 7.3) with bioactive glasses and glass-ceramics containing $<52\%$ SiO_2 being the most rapid. The time difference in time dependence of interfacial bond strength (Figure 7.1) is due to the different rates of growth of the interfacial HCA layer. The bioactivity index of a materials (I_B) is defined as:

$$I_B = 100/t_{0.5bb}$$

I_B is obtained from Figure 7.3, and is proportional to the reciprocal of the time required for one half (0.5) of the interface to be bonded to bone. I_B values are shown in Table 7.2 for the various bioactive implants.

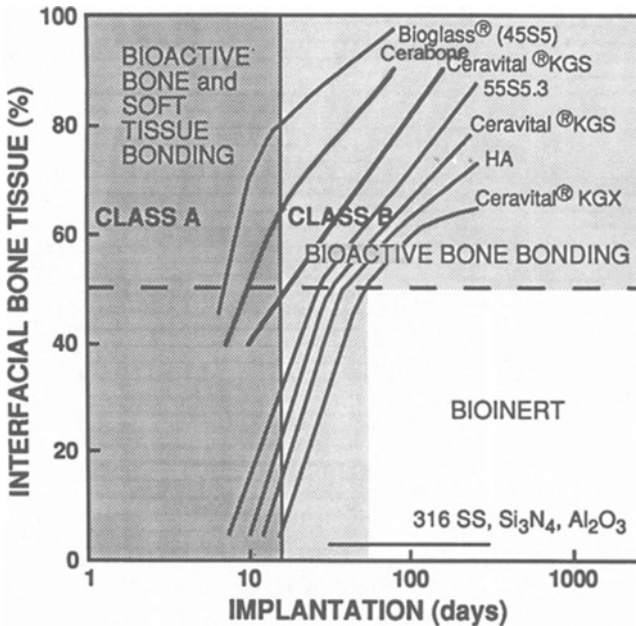


Fig. 7.3 Time dependence of interfacial bone formation for various types of bioceramic implants

The compositional dependence of bonding of bone to various bioactive glasses is illustrated in Figure 7.4 for the $\text{Na}_2\text{O}-\text{CaO}-\text{SiO}_2$ system, with a constant 6 weight percent P_2O_5 and in Figure 7.5 for the $\text{CaO}-\text{P}_2\text{O}_5-\text{SiO}_2$ system. Figure 7.4 also shows iso I_B values for the $\text{Na}_2\text{O}-\text{CaO}-\text{P}_2\text{O}_5-\text{SiO}_2$ system. When $I_B = 0$ there is no interfacial bond with bone; i.e., the material develops a non-adherent fibrous capsule and is nearly bioinert.

7.4 Physical Properties

Table 7.2 summarizes the physical properties of the bioactive glasses, glassceramics, and ceramics in clinical use, with references. The bioactive glasses are single phase amorphous materials which have high I_B values (rapidly form a bone bond) but have low mechanical strength and toughness. These materials should be used in particulate form (as powders), as coatings, or in low load bearing applications, as listed in Table 7.3. Bioactive glass-ceramics are multi-phase materials with a fine, homogeneous grain size and good mechanical strength and toughness⁵ and intermediate I_B values. They can be used in moderate load bearing

¹ L.L. Hench and E.C. Ethridge, *Biomaterials, An Interfacial Approach*, p. 137, Academic Press, New York, 1982.

² ö.H. Andersson, K.H. Karlsson, K. Kangasniemi, and A. Yli-Urpo, *Models for Physical Properties and Bioactivity of Phosphate Opal Glasses*, *Glastech. Ber.*, **61**, 300–305 (1988).

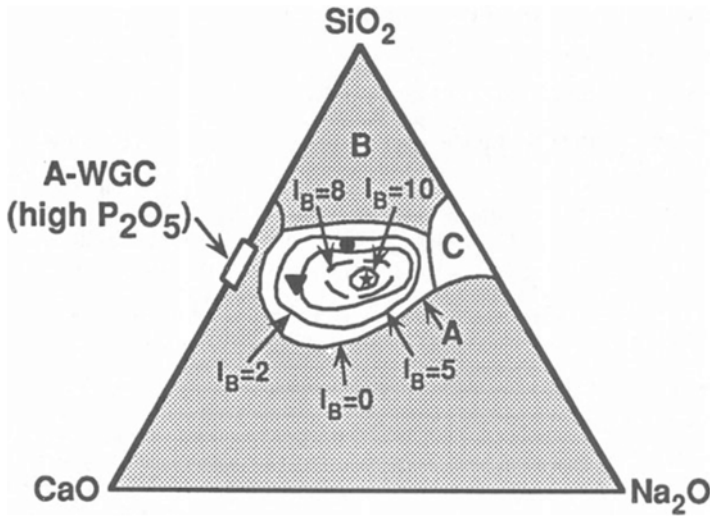


Fig. 7.4 The compositional dependence of bone bonding to bioactive glasses (region A) containing 6 weight % P_2O_5 . Soft tissue bonding occurs for compositions with I_B values >8 (see text). Region B: non-bioactive compositions. Glasses in Region C are resorbable. (Based upon chapters 1 and 3 in ref. 1.)

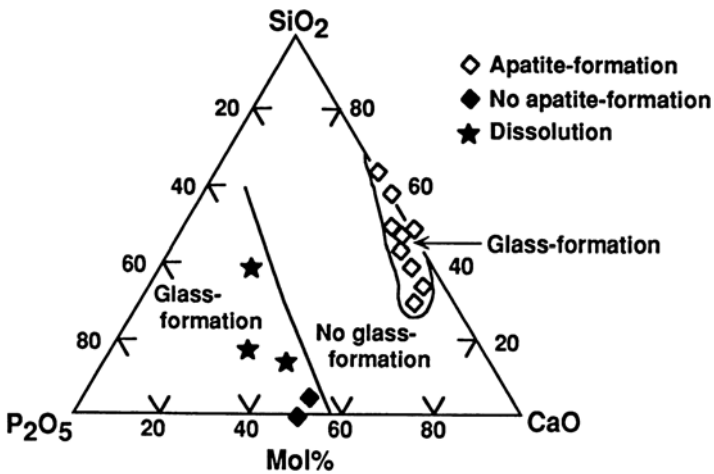


Fig. 7.5 Compositional dependence of bioactivity for glasses in the $CaO-P_2O_5-SiO_2$. (Based upon T. Kokubo, ref. 5.)

Table 7.3 Clinical Uses of Bioactive Glasses and Glass-Ceramics

Material	Form	Application	Function
45S5 Bioglass®	Bulk	Endosseous alveolar ridge maintenance	Space filling and tissue bonding
	Bulk	Middle ear prostheses	Restore conductive hearing by replacing part of ossicular chain
	Powder	Repair of periodontal defects	Restore bone lost by periodontal disease and prevent epithelial down growth
	Powder	Fixation of revision arthroplasty	Restore bone loss due to loosening of hip prostheses
Cerabone® (A/W glass-ceramic)	Bulk	Vertebral prostheses	Replace vertebrae removed in tumor surgery
		Iliac crest prostheses	Replace bone removed for autogenous graft
	Coating	Fixation of hip prostheses	Provide bioactive bonding of implant
S53P4	Bulk	Orbital floor prostheses	Repair damaged bone supporting eye
	Powder	Cranial repair	Repair bone lost due to trauma

³. H. Bromer, K. Deutscher, B. Blenke, E. Pfeil and V. Strunz, Properties of the Bioactive Implant Material Ceravital®, in *Science of Ceramics*, Vol. 9, 1977, pp. 219–223.

⁴. T. Kokubo, Mechanical Properties of a New Type of Glass-Ceramic for Prosthetic Applications, in *Multiphase Biomedical Materials*, T. Tsuruta and A. Nakajima, eds, VSP, Utrecht, Netherlands, 1989.

⁵. G. Berger, F. Sauer, G. Steinborn, F.G. Wishmann, V. Thieme, St Kohler and H. Dressel, Clinical Application of Surface Reactive ApatitelWollastonite Containing Glass-Ceramics, in Proceedings of XV International Congress on Glass, Vol. 3a, O.V. Mazurin, eds, Nauka, Leningrad, 1989, pp. 120–126.

⁶. W. Vogel and W. Holland, The Development of Bioglass® Ceramics for Medical Applications, *Angew Chem. Int. Ed. Engl.* **26**,527–544 (1987).

⁷. M. Jarcho, C.H. Bolen, M.B. Thomas, J. Bobick, J.F. Kay and R.H. Doremus, Hydroxyapatite Synthesis and Characterization in Dense Polycrystalline Form, *J. Mater. Sci.* **11**, 2027–2035 (1976).

⁸. M. Akao, H. Aoki, and K. Kato, Mechanical Properties of Sintered Hydroxyapatite for Prosthetic Applications, *J. Mater. Sci.* **16**,809–812 (1981).

⁹. G. Dewith, H.J.A. Van Dijk, N. Hattu and K. Prijs, Preparation, Microstructure and Mechanical Properties of Dense Polycrystalline Hydroxyapatite, *J. Mater. Sci.* **16**, 1592–1598 (1981).

¹⁰. M. Jarcho, R.L. Salsbury, M.B. Thomas and R.H. Doremus, Synthesis and Fabrication of β -tricalcium Phosphate (Whitlockite) Ceramics for Potential Prosthetic Applications, *J. Mater. Sci.* **14**, 142–150 (1979).

¹¹. M. Akao, M. Aoki, K. Kato and A. Sato, Dense Polycrystalline β -tricalcium Phosphate for Prosthetic Applications, *J. Mater. Sci.* **17**, 343–346 (1982).

¹². L.L. Hench, Bioactive Ceramics, in *Bioceramics: Materials Characteristics Versus In Vivo Behavior*, P. Ducheyne, J.E. Lemons, eds, *Annals of the NY Academy of Sciences*, **523**, 1988, pp. 54–71

applications as bulk materials (Table 7.3). Polycrystalline bioactive ceramics, such as synthetic hydroxyapatite (HA), have moderate strengths and relatively low I_B values and should be used as particulate or in nonload bearing applications. Compo-

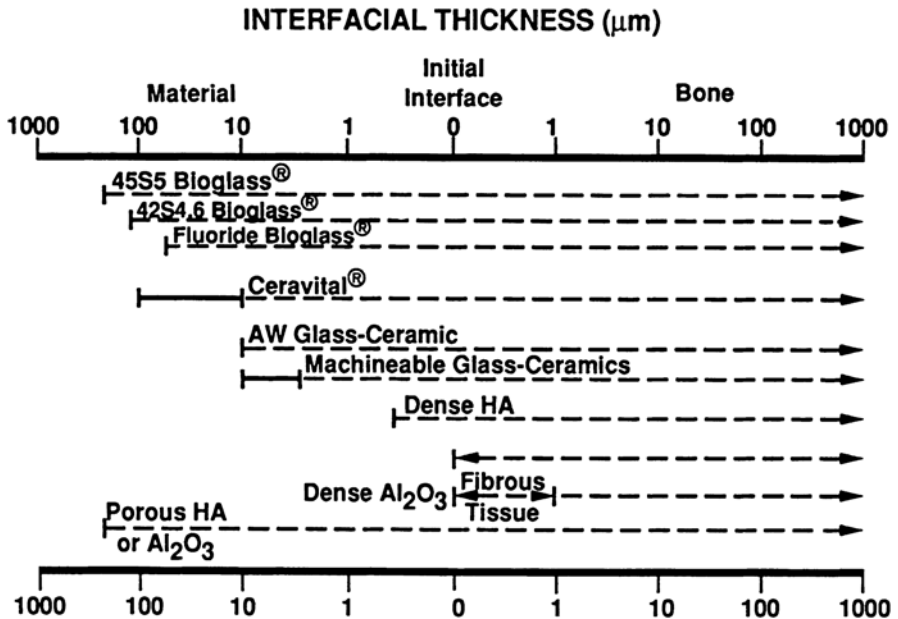


Fig. 7.6 Thickness of interfacial bonding layers for various bioceramics

sitions with the highest I_B values develop interfacial bonding layers (Figure 7.6) composed of both hydrated silica gel layers and Ca, P-rich layers. Compositions with low to moderate I_B values form thinner bonding zones composed primarily of Ca-P-rich compounds. Non-bonding implants have a non adherent fibrous tissue layer at the implant interface.

References

1. Hench, L.L. and Wilson, J. (eds) (1993) *Introduction to Bioceramics*, World Scientific Publishers, London and Singapore, pp. 1–24.
2. Gross, U., Kinne, R., Schmitz, H.J. and Strunz, V. (1988) The response of bone to surface active glass/glass-ceramics. *CRC Critical Reviews in Biocompatibility*, **4**, 2.
3. Yamamuro, T., Hench, L.L. and Wilson, J. (eds) (1990) *Handbook of Bioactive Ceramics, Vol 1: Bioactive Glasses and Glass-Ceramics*, CRC Press, Boca Raton, FL.
4. Yamamuro, T. (1993) A/W glass-ceramic: clinical applications, in *Introduction to Bioceramics* (eds L.L. Hench and J. Wilson), World Scientific Publishers, London and Singapore, pp. 89–104.
5. Kokubo, T. (1993) A/W glass-ceramic: processing and properties, in *Introduction to Bioceramics* (eds L.L. Hench and J. Wilson), World Scientific Publishers, London and Singapore, pp. 75–88.

Chapter 8

Wear

M. LaBerge and J.D. Desjardins

8.1 Introduction

Biomaterials used in the fabrication of implants are subjected to wear. Wear of biomaterials and devices has been shown to be detrimental to their long term success resulting in implant retrieval and revision. One of the most dramatic impacts of the wear of biomaterials and its consequences is observed with artificial joints. As stated by [1] wear has emerged as a central problem limiting the long-term longevity of total joint replacements. Ultra-high-molecular-weight polyethylene (UHMWPE) wear debris has been shown by many authors to trigger an osteolytic reaction which leads to implant loosening [2]. Wear is a process resulting in the progressive loss of material involving many diverse mechanisms and phenomena which are often unpredictable (Table 8.1). The wear process of materials is predominantly governed by their mechanical and/or chemical behavior. More often than not, the wear processes listed in Table 8.1 do not act independently. However, even though several wear mechanisms are involved, it is often the case that one particular mechanism dominates (Dowson, 1981).

Unfortunately surface wear of an implant results from its use, and therefore, cannot be avoided or eliminated. Because wear is a limiting factor in the successful outcome and lifetime of an implant, it is of the utmost importance to characterize the wear resistance of materials used in implant design, and the effect of the design on wear. The volume of material removed from surfaces in specific tribosystems as a result of wear processes has been described phenomenologically and estimated by different models (Table 8.2). Several experimental wear studies have been conducted to (1) predict the amount of material removed in specific conditions,(2)

M. LaBerge (✉) J.D. Desjardins
Department of Bioengineering, 301 Rhodes Clemson University,
Clemson, SC 29634-0905, USA

Table 8.1 Wear mechanisms

<i>Wear mechanisms</i>	<i>Definition</i>
Adhesive wear	Characterized by the transfer of material from one surface to another surface during relative motion. This type of wear is a consequence of adhesive forces acting at the junction of surface asperities. The transferred fragments may either be permanently or only temporarily attached to the other surface. Adhesive wear has been denoted as being the most commonly detected mechanism of wear, unfortunately it is also the least preventable (Dowson, 1981).
Abrasive wear	Results from a hard asperity damaging or ploughing the surface of a softer material. The presence of hard particles may be due to the original material properties of one of the surfaces or loose debris particles which have become entrapped between the two sliding surfaces and/or embedded into one of the surfaces expediting abrasive wear. Generally, the resistance to abrasion can be related to the hardness of the material, however, this relationship is not directly proportional (Suh, 1986).
Delamination wear	Involves material removal subsequently to plastic deformation, crack nucleation, and propagation in the subsurface (Jahanmir and Suh, 1977; Suh, 1986)
Fatigue wear	Associated with cyclic stress variations and therefore, the lifetime of the material is dependent on the number of cycles. Cyclic deformation of the contacting surfaces leads to the initiation and propagation of microcracks (Rowe, 1980). Subsurface crack initiation generally occurs in the region of maximum shear stress which will depend upon the geometry of the materials
Fretting wear	Generated by a relative oscillatory tangential movement of small amplitudes (damage can be caused by movement with amplitudes as small as 0.125 μm) which may occur between two surfaces in contact subjected to vibration [7]
Corrosive wear	Observed when the environment interacts chemically or electrochemically with one or both of the surfaces. Therefore, the wear rate is dependent on the environmental conditions affecting the chemical reactivity of the surfaces. This type of wear mechanism is important for biomaterials since they function in an extremely harsh environment, the human body [8].
Cavitation wear	Occurs from the collapse of cavitation bubbles where the surrounding liquid rushes to refill the void and collides with the material surface. Craters form on the surface of a softer material while a harder surface will experience cracks and spalls which come from subsurface damage. Subsurface damage induced by cavitation is observed in the softer or weaker phases of the material [9, 10]

compare the effect of different fabrication and sterilization processes on materials, (3) produce wear debris to be used in biocompatibility studies, and (4) characterize the behavior of a new material destined for biomedical applications. Overall wear tests are primarily conducted to ascertain the basic mechanisms of wear for a particular combination of materials, or the more restrictive yet equally elusive determination of the rate of wear to facilitate the estimation of their 'clinical' life. Experimental results are highly dependent on the geometry of the contact, the lubricant, the tribological conditions including velocity and load, and material properties [4]. Therefore, experimental protocols aimed at investigating the wear properties of

Table 8.2 Selected wear models

Wear process	Model	Specifications
Adhesive wear ^a [12]	Archard equation: $W_{ad} = \frac{V}{L} = K \frac{F_N}{H}$	<ul style="list-style-type: none"> Use hardness as the only material property, even though K depends on various properties of both materials
	W_{ad} = wear rate (worn volume per unit sliding distance) K = wear coefficient V = volume of wear L = sliding distance F_N = normal load H = hardness of the softer material	<ul style="list-style-type: none"> Implies that wear rate is proportional to real contact area in plastic contacts and may not be applicable for cases involving elastic contacts
[13]	Hornbogen equation: $W_{ad} = N^2 \frac{P_y E' F_N^{1.5}}{K_{IC}^2 H^{1.5}}$ W_{ad} = wear rate K_{IC} = fracture toughness P_y = yield strength N = work hardening factor E' = equivalent elastic modulus $E' = 1/[(1 - \nu_1^2)/E_1 + (1 - \nu_2^2)/E_2]$	<ul style="list-style-type: none"> Based on a comparison of the strain occurring during asperity interactions with the critical strain at which crack growth is initiated. If the applied strain is smaller than the critical strain, the wear rate is independent of toughness, and follows Archard's
Abrasive wear [1]	Rabinowicz model: $W_{ab} = \frac{V}{L} = \frac{K F_N}{\pi H} \tan \theta$ W_{ab} = wear rate (worn volume per unit sliding distance) K = wear coefficient V = volume of wear L = sliding distance F_N = normal load H = hardness of the softer material $\tan \theta$ = weighted average of the $\tan \theta$ values of all the individual cones θ = average slope of the asperities	<ul style="list-style-type: none"> Assumes that asperities of the harder surface are conical
[14]	Zum Gahr model: $W_{ab} = \frac{f_{ab}}{K_1 K_2 \tau_c} \frac{\cos \rho \sin \theta}{[\cos(\theta/2)]^{0.5} \cos(\theta - \rho)} F_N$	<ul style="list-style-type: none"> Considers the processes of microcutting, microploughing, and microcracking in the abrasive wear of ductile metals
	W_{ab} = wear rate f_{ab} = model factor (1 for microcutting) K_1 = relaxation of normal and shear stress K_2 = texture factor (1 for fcc metals) τ_c = shear stress for dislocation movement ρ = friction angle at abrasive-material interface	<ul style="list-style-type: none"> This model includes the effects of work hardening ductility homogeneity of strain crystal anisotropy

(continued)

Table 8.2 (continued)

Wear process	Model	Specifications
Fatigue wear [15]	Halling model: $W_{fa} = K \frac{\eta\gamma}{e_1^2 H} F_N$ $W_{fa} = \text{wear rate}$ $\eta = \text{line distribution of asperities}$ $\gamma = \text{constant defining particle size}$ $e_1 = \text{strain to failure in one loading cycle}$ $H = \text{hardness of the softer material}$ $K = \text{wear coefficient}$	<ul style="list-style-type: none"> Incorporates the concept of fatigue failure as well as simple plastic deformation failure
Corrosive wear [16, 17]	Quinn model: $W_{corr} = \frac{dA_c \exp[-Q/R_c T_c]}{3e^2 \rho^2 vH} F_N$ $W_{corr} = \text{wear rate}$ $\rho = \text{density of material}$ $A_c = \text{Arrhenius constant}$ $Q = \text{activation energy}$ $R_c = \text{gas constant}$ $T_c = \text{contact temperature}$ $d = \text{asperity contact diameter}$ $v = \text{sliding velocity}$ $e = \text{critical thickness of reaction layer}$	<ul style="list-style-type: none"> Explains wear in steel and assumes that surface asperity layers formed tribochemically are detached at a certain critical thickness
Ultrahigh-molecular-weight polyethylene (UHMWPE) wear [18]	Wang model: $k = k' \frac{d(\mu - \mu_0)}{2\gamma_c} \left(\frac{1}{X_c} - \frac{1}{X_0} \right) \times \left(1 - \frac{\sin 2\alpha}{2\alpha} \right)$ $k' = \text{constant}$ $d = \text{diameter of fibrils (mm)}$ $\mu = \text{coefficient of friction}$ $\mu_0 = \text{coefficient of friction for initiating surface failure}$ $X_c = \text{cross-link density (mole/g)}$ $X_0 = \text{critical cross-link density (mole/g)}$ $\gamma_c = \text{C-C bond energy (Joule)}$ $\alpha = \text{maximum cross-shear angle (radian)}$	<ul style="list-style-type: none"> For ultrahigh-molecular-weight polyethylene in lubricated multi-directional sliding Assumes the occurrence of preferential molecular alignment in the principal direction of sliding and rupture or splitting of the oriented molecules in the perpendicular direction associated with secondary sliding

^aNote

- The wear factor (k) is a measure of the rate at which a given combination of materials wears in the environment of the test. k is widely used for comparative purposes (mm^3/Nm)
- According to Dowson [19], if the mean contact stresses are not too high the wear of polymer against a hard surface (metal or ceramic) is obtained with fair accuracy with the relationship $V = kFL$
- K is directly influenced by the roughness average (Ra) of the metallic counterface for the contact UHMWPE–stainless steel in water under reciprocating pin-on-plate conditions given by the relationship $k = 4.0 \times 10^{-5} \text{ Ra}^{1.2}$ [20]

biomaterials should be designed to assess or predict their behavior in simulated clinical conditions [21].

In Vitro Wear Testing

Although wear is a very complex process, apparatuses are available which allow for the accumulation of data resulting in an estimate of the wear resistance of a combination of materials or a device. Preliminary material studies will commonly be performed on laboratory wear benches while devices will be evaluated with simulators. The classic arrangement of articulating surfaces in material wear testing involves an upper bearing part that is attached to a pin, and a lower bearing material that is attached to a specimen holding plate, or disk. The primary advantage of this configuration is that any combination of candidate bearing materials can be incorporated into the testing setup. Typically, this involves either a spherical or a flat material geometry on the pin, and a flat material geometry at the disk counterface. The sacrificial material (which experiences the greatest amount of wear) can be fabricated into either the pin or the disk; the decision regarding location of the sacrificial material depends on the particular type of analysis desired. Although it has an important effect on the resulting wear, primarily because the material on the surface of the pin is under constant load while the disk is loaded only periodically in discrete regions, the importance of this decision is often overlooked. Historical configurations of this pin-on-flat wear testing arrangement are most often referred to as a “pin-on-disk” (POD) wear test. Many variations of this arrangement reported in the literature include rotary pin-on-disk, reciprocating pin-on-disk, circularly translating pin-on-disk, and multi-axis pin-on-disk configurations [22]. For clarity, the translations and rotations of both the pin and disk have been described using consistent terminology as follows: (1) translations are given with respect to a fixed point of observation not on either the pin or the disk; circular translation does not imply rotation about an internal axis; and (2) rotations are given with respect to the central axis of either the pin or the disk being described, wherein the axis is normal to the bearing surface.

One of the most basic wear testing configurations is the rotary pin-on-disk method. In this method the pin is neither translated nor rotated, and the disk is rotated without translation, producing a circular wear track on the flat specimen. This configuration is often used to produce constant-velocity, unidirectional shearing forces at the pin and disk surfaces. The pin surface is under continuous load and unidirectional shear conditions, while only discrete locations of the flat specimen are periodically loaded in unidirectional shear during each cycle. In this manner, the pin specimen experiences the majority of the wear potential. Depending upon material fabrication and geometric constraints, the candidate material under wear investigation can be fabricated into either pins or sheets; typically the softer material (the polymer in a metal/polymer combination) is used as the upper bearing surface.

A similar type of wear testing configuration is the reciprocating pin-on-disk method. In a reciprocating pin-on-disk wear test, the pin is linearly translated back and forth along a single line trajectory without rotation, while the disk neither translates nor rotates [22]. This produces a linear wear track, with a stop/start condition at either end of the wear track, and a variable (usually sinusoidal) velocity profile along the trajectory. In this configuration, the pin surface is under continuous load and reciprocating shear conditions, while the discrete locations of the flat specimen of the wear track are periodically loaded in reciprocating shear. Similar to the rotary pin-on-disk method, the pin specimen experiences the majority of the wear potential. Historically, this reciprocating pin-on-disk configuration has been extensively used in all types of material-pair wear evaluations.

Many polymers have been shown to wear more severely under conditions that produce multi-directional shear forces [23] than under unidirectional and reciprocating wear testing conditions. This has been theorized to be a result of a process whereby the long molecular chains of the polymer reorient themselves along the directions of the shear vector [24], and has been assessed using soft X-ray absorption spectroscopy to measure molecular orientation at UHMWPE surfaces [25]. Such findings have resulted in the introduction of a new class of pin-on-disk wear testing systems that attempt to subject the material surfaces to multi-directional shearing forces similar to those seen in total joint replacements [26–28]. The circularly translating pin-on-disk (CTPOD) system was introduced as a method by which the pin material could be subjected to continuous multi-directional shearing conditions [29]. Multi-axis pin-on-disk wear testing incorporates one or two additional degrees of motion into a standard reciprocating wear testing profile to produce specific cross-shear conditions [26, 28, 30]. The multi-axis wear testing devices utilize a simplified rectangular path as a wear pattern [18, 26, 31–33], more representative multi-directional shearing conditions [29] with shear vector orientations changing gradually over a complete range of angles during constant sliding [32], or more multi-axis cross-shear system incorporating the kinematics of bearing surfaces in total joint replacements [22]. Overall, the latter systems have provided valuable insight into the implications of multi-directional motion on wear rates.

In general, most pin-on-disk wear testing configurations produce the highest wear potential for the material that is placed at the pin. For this reason, the polymeric material is most often located there, with the metallic material acting as the disk. Intrinsic to this configuration, however, is the fact that the polymer experiences constant load across the entire contacting surface area of the pin, and wear is measured by gravimetric analysis of material removal. This is contrary to the *in vivo* condition of total knee joint bearing surfaces whereby the polymer is cyclically loaded in discrete locations. The greater physiological relevance of the opposite situation (metal pin on polymer flat) has been noted [34, 35] (Tables 8.3 and 8.4).

The standard procedure under the American Society for Testing and Materials (ASTM F-732-00, 2011—Standard Test Method for Wear Testing of Polymeric Materials Used in Total Joint Prostheses) describes the testing protocol for characterizing the wear resistance of material combinations to be used in the design of orthopaedic total joint replacements. Several investigators have used modified or

Table 8.3 Example of biomaterial combinations tribologically characterized with POD and simulators

Material combinations	Test apparatus
Stainless steel-UHMWPE	Pin-on-disc; joint simulator [36–38]
Co-Cr-alloys-UHMWPE	Pin-on-disc; joint simulator [38–43]
Titanium alloys-UHMWPE	Pin-on-disc; joint simulator [40, 44, 45]
Alumina-UHMWPE	Pin-on-disc; joint simulator [38, 42, 43, 46]
Zirconia-UHMWPE	Pin-on-disc; joint simulator [37, 42, 47]
CoCrMo-CoCrMo	Pin-on-disc; joint simulator [46, 48–52]
CoCrMo-Delrin	Disc-on-flat [53]
PEEK-CoCrMo	Pin-on-plate [54, 55]
CoCrMo-alumina	Joint simulator [42]
Ti6Al4V-alumina	Joint simulator [42]
Alumina-alumina	Wear and friction benches; joint simulator [46, 51, 56–59]
Elastomers-metal	Reciprocating friction benches; joint simulator [22, 60–68]
Dental resins-enamel	Pin-on-flat [69]
Modified UHMWPE-metal	Pin-on-disc [70–72] Joint Simulator [73–75]

Table 8.4 In vitro measurement of wear machines

Wear apparatus type	Comments
Pin-on-disc or pin-on-plate	Useful in studying basic wear mechanisms. Steady and well-controlled operating conditions. Fails to replicate the reciprocating motion observed in joints
Reciprocating pin-on-disc (POD)	Simulates the reciprocating motion observed in vivo and fatigue loading (loading and unloading)
Multi-directional/multi-axis pin-on-disc	Incorporates one or two additional degrees of motion into a standard reciprocating wear testing profile to produce specific cross-shear conditions
Joint simulators (knee, hip, spine/disc simulators)	Improved understanding of the wear processes encountered in prostheses by simulating mechanical conditions observed in patients

adapted versions of this standard to assess the wear resistance of bearing surfaces for orthopaedic applications [48, 60, 76–82]. Other ASTM methods and protocols from the International Organization for Standardization (ISO) pertinent to the evaluation of wear performance of engineering materials and devices are listed in Table 8.5.

Wear resistance is usually reported in terms of wear rate, either linear or volumetric, with different units such as volume lost per 10^6 cycles (MC), mass loss per 10^6 cycles, or linear displacement per 10^6 cycles. A complete walking cycle is represented by two steps. One cycle on a reciprocating pin-on-flat system is obtained

Table 8.5 In vitro friction and wear measurement standards

^a ASTM G40-13	Standard Terminology Relating to Wear and Erosion
ASTM G77-05(2010)	Standard Test Method for Ranking Resistance of Materials to Sliding Wear Using Block-on-Ring Wear Test
ASTM G118-02(2015)	Standard Guide for Recommended Format of Wear Test Data Suitable for Databases
ASTM G119-09	Standard Guide for Determining Synergism Between Wear and Corrosion
ASTM G133-05(2010)	Standard Test Method for Linearly Reciprocating Ball-on-Flat Sliding Wear
ASTM G176-03(2009)	Standard Test Method for Ranking Resistance of Plastics to Sliding Wear Using Block-on-Ring Wear Test—Cumulative Wear Method
ASTM G190-15	Standard Guide for Developing and Selecting Wear Tests
ASTM G206-11	Standard Guide for Measuring the Wear Volumes of Piston Ring Segments Run against Flat Coupons in Reciprocating Wear Tests
ASTM F732-00(2011)	Standard Test Method for Wear Testing of Polymeric Materials Used in Total Joint Prostheses
ASTM F1714-96(2013)	Standard Guide for Gravimetric Wear Assessment of Prosthetic Hip Designs in Simulator Devices
ASTM F1875-98(2014)	Standard Practice for Fretting Corrosion Testing of Modular Implant Interfaces: Hip Femoral Head-Bore and Cone Taper Interface
ASTM F1877-05(2010)	Standard Practice for Characterization of Particles
ASTM F2025-06(2012)	Standard Practice for Gravimetric Measurement of Polymeric Components for Wear Assessment
ASTM F2385-04(2010)	Standard Test Method for Determining Femoral Head Penetration into Acetabular Components of Total Hip Replacement Using Clinical Radiographs
ASTM F2423-11	Standard Guide for Functional, Kinematic, and Wear Assessment of Total Disc Prostheses ASTM F2694-07(2013) Standard Practice for Functional and Wear Evaluation of Motion-Preserving Lumbar Total Facet Prostheses
ASTM F2624-12	Standard Test Method for Static, Dynamic, and Wear Assessment of Extra-Discal Single Level Spinal Constructs
ASTM F2694-07(2013)	Standard Practice for Functional and Wear Evaluation of Motion-Preserving Lumbar Total Facet Prostheses
ASTM F2979-14	Standard Guide for Characterization of Wear from the Articulating Surfaces in Retrieved Metal-on-Metal and other Hard-on-Hard Hip Prostheses
ASTM F3047M-15	Standard Guide for High Demand Hip Simulator Wear Testing of Hard-on-hard Articulations
ASTM D7596-14	Standard Test Method for Automatic Particle Counting and Particle Shape Classification of Oils Using a Direct Imaging Integrated Tester
^b ISO 14242-1:2014	Implants for surgery—Wear of total hip-joint prostheses—Part 1: Loading and displacement parameters for wear-testing machines and corresponding environmental conditions for test
ISO 14242-2:2000	Implants for surgery—Wear of total hip-joint prostheses—Part 2: Methods of measurement

(continued)

Table 8.5 (continued)

ISO 14243-1:2009	Implants for surgery—Wear of total knee-joint prostheses—Part 1: Loading and displacement parameters for wear-testing machines with load control and corresponding environmental conditions for test
ISO 14243-2:2009	Implants for surgery—Wear of total knee-joint prostheses—Part 2: Methods of measurement
ISO 14243-3:2014	Implants for surgery—Wear of total knee-joint prostheses—Part 3: Loading and displacement parameters for wear-testing machines with displacement control and corresponding environmental conditions for test
ISO/TS 14569-2:2001	Dental materials—Guidance on testing of wear—Part 2: Wear by two and/or three body contact
ISO 16428:2005	Implants for surgery—Test solutions and environmental conditions for static and dynamic corrosion tests on implantable materials and medical devices
ISO 17853:2011	Wear of implant materials—Polymer and metal wear particles—Isolation and characterization
ISO 18192-1:2011	Implants for surgery—Wear of total intervertebral spinal disc prostheses—Part 1: Loading and displacement parameters for wear testing and corresponding environmental conditions for test
ISO 18192-2:2010	Implants for surgery—Wear of total intervertebral spinal disc prostheses—Part 2: Nucleus replacements

^aAmerican Society for Testing and Materials, Philadelphia, PA (www.astm.org)

^bInternational organization for Standardization, Geneva, Switzerland (www.iso.org)

by two passes (return to starting point), while the other cycle on a rotating pin-on-disc system corresponds to one revolution. It is assumed that a normal individual will make two million steps per year while an active subject may make more than 10 million steps [21] at a maximum frequency of 1 Hz. Investigators have also reported wear rates as cubic millimeters (volume) per millimeter (sliding distance) (mm^3/mm). The volume is calculated by measuring the mass loss and using the density of the polymer as a conversion factor. Tables 8.6 and 8.7 present a critical selection of wear data available for biomaterial tribosystems useful to the orthopaedic design community. Both friction coefficient and wear rate are used as design parameters. Unless independently monitored, friction coefficients are usually acquired during wear tests. The static coefficient of friction is calculated using the force required to initiate motion. The kinetic coefficient of friction may vary during a test for a constant velocity and should be calculated from averaged force readings during the duration of the test. The ASTM method G115–10 (2013) proposes a guide for “*Measuring and Reporting Friction Coefficients*” which is designed to assist investigators in the selection of an appropriate method for measuring the frictional properties of materials.

Table 8.6 Friction coefficients of various implant materials from representative in vitro studies

Material contact	Average (or range) friction coefficient	Testing apparatus	Tribological conditions	References
Stainless steel (316LVM) + UHMWPE	0.07–0.13	Pin-on-disk	<ul style="list-style-type: none"> • Load=3.45 M Pa • Velocity=50 × 106 mm/year • Lub#: serum • Duration: 2 years test • 28–32 °C 	[40]
Stainless steel (316L) + UHMWPE	0.078	Pin-on-disk	<ul style="list-style-type: none"> • Load=3 MPa • Velocity=60 mm/s • Lub: bovine serum, 40–50 ml • 24–26 °C 	[37]
Stainless steel (100CR6-German) + UHMWPE (Chirulene-German)	0.17 (a); 0.10 (b); 0.16 (c); 0.14 (d)	Ball-on-disk vibrottribometer (Optimol SRV-German)	<ul style="list-style-type: none"> • 10 mm diameter ball • Oscillation=10 Hz; 1.65 mm amplitude • Load=50 and 300 N • Lub: (a) none; (b) human synovial fluid; (c) yellow bone marrow; (d) red bone marrow • 37 °C 	[83]
Stainless steel + UHMWPE	0.03–0.09	Reciprocating flat-on-flat	<ul style="list-style-type: none"> • Load=445 N • Velocity=100 cycles/min • Lub: bovine serum • Duration: 3.7 × 106 cycles 	[38]
Stainless steel + UHMWPE (Charnley)	0.05	Dual hip simulator	<ul style="list-style-type: none"> • Velocity=30 cycles/min • Load=250 kg • Duration: 1000 h • Lub: serum • Room temperature 	[84]
Stainless steel (Ortron 90) + UHMWPE (ASTM F 648)	0.034	Single-channel hip joint simulator	<ul style="list-style-type: none"> • Range of motion =30° • Lub: Deionized water at 37 °C • Load=1–4 kN • Angular Velocity=0.6–2.4 rad/s 	[85]

Stainless steel (316L) + UHMWPE	0.040	Single-channel hip joint simulator	<ul style="list-style-type: none"> • Range of motion = 30° • Lub: Detonized water at 37 °C • Load = 1–4 kN • Angular velocity = 0.6–2.4 rad/s 	[85]
Stainless steel (316L) + UHMWPE (ASTM F 648)	0.03–0.09	Twelve-channel friction and wear machine FW-12	<ul style="list-style-type: none"> • Conforming, flat-on-flat configuration • Velocity = 100 cyc./min • Pressure = 6.90 MPa • Duration: 3.7 × 106 cycles • Lub: bovine calf serum w/55 sodium azide 	[86]
CoCrMo (Protasul-2) + UHMWPE	Dry 0.13 Lub: 0.21	Rolling-sliding apparatus	<ul style="list-style-type: none"> • Velocity = 25 m/min • Pressure = 30 N/cm² • Duration: 20 h • Lub: none or distilled water • Room temperature 	[46]
Co-Cr + UHMWPE	0.05–0.11	Pin-on-disk	<ul style="list-style-type: none"> • Load = 3.45 M Pa • Velocity = 50 × 106 mm/year • Lub: serum • Duration: 2 years test • 28–32 °C 	[40]
Co-Cr + UHMWPE	00.07–0.25	Pin-on-flat	<ul style="list-style-type: none"> • Axial load = 223 N • Duration 250,000 cycles • Lub: bovine serum 	[87]
Co-Cr–Mo (Vitalium) + UHMWPE	0.08–0.15	Pin-on-flat	<ul style="list-style-type: none"> • Contact pressure = 4.8 MPa • Frequency = 1 Hz • Sliding dist. = 50 mm • Lub: distilled, detonized H₂O • 37.1 °C 	[42]

(continued)

Table 8.6 (continued)

Material contact	Average (or range) friction coefficient	Testing apparatus	Tribological conditions	References
Co-Cr-Mo (ASTM F799) + UHMWPE (GUR 415)	0.060–0.093	Reciprocating motion friction bench (line/flat)	<ul style="list-style-type: none"> • Maximum stress = 6 MPa • Lub: 86 % Glycerine • Frequency = 1 Hz • Duration: 500,000 cycles • Sliding Dist. = 100 mm/cycle 	[88]
Co-Cr-Mo (Muller) + UHMWPE	0.018–0.045	Durham hip function simulator	<ul style="list-style-type: none"> • Range of motion = 20° • Lub: Carboxymethyl cellulose • Dynamic load = 2000 N • Frequency = 1 Hz 	[89]
Co-Cr-Mo (Vitalium) + UHMWPE (ASTM F 648)	0.057	Single-channel hip joint simulator	<ul style="list-style-type: none"> • Range of motion = 30° • Load = 1–4 kN • Angular velocity = 0.6–2.4 rad/s • Lub: deionized water at 37 °C 	[85]
Co-Cr-Mo (Zimalloy) + UHMWPE (ASTM F 648)	0.038–0.063	Single-channel hip joint simulator	<ul style="list-style-type: none"> • Range of motion = 30° • Load = 1.4 kN • Angular velocity = 0.6–2.4 rad/s • Lub: deionized water at 37 °C 	[85]
Co-Cr-Mo (ASTM F75) + UHMWPE	0.044	Hip simulator machine	<ul style="list-style-type: none"> • Lub: synovial fluid • Peak load = 150 kg 	[90]
Co-Cr-Mo (ASTM F 799) + UHMWPE (ASTM F 648)	0.052–0.070	Single-channel hip joint simulator	<ul style="list-style-type: none"> • Range of motion = 30° • Load = 1.4 kN • Angular velocity = 0.6–2.4 rad/s • Lub: deionized water at 37 °C 	[85]
CoCrMo + UHMWPE (Charnley-Muller)	0.06	Dual hip simulator	<ul style="list-style-type: none"> • Velocity = 30 cycles/min • Load = 250 kg • Duration: 100 h • Lub: serum • Room temperature 	[84]

Co-Cr-Mo+UHMWPE	0.05-01.1	Twelve-channel friction and wear machine FW-12	<ul style="list-style-type: none"> • Conforming, flat-on-flat configuration • Velocity = 100 cyc./min • Pressure = 6.90 MPa • Duration: 3.7×10^6 cycles • Lub: bovine calf serum w/55 sodium azide 	[86]
Co-Cr-Mo+UHMWPE	0.06-0.07 (a,c) 0.10-0.12 (b,d)	Hip joint simulator	<ul style="list-style-type: none"> • Load 2.5 kN static load • Lub: (a) serum, (b) serum albumin, (c) synovial fluid, (d) veronate buffer 	[91]
Co-Cr-Mo+UHMWPE	0.04-0.06	Hip joint simulator	<ul style="list-style-type: none"> • Load 2.5 kN static load • Velocity: 30 cycles/min • Duration: 1.8 million cycles • Lub: serum 	[92]
Co-Cr-Mo+UHMWPE	0.03-0.05	Pin-on-disk	<ul style="list-style-type: none"> • Load = 100 N • Lub: Ringer's solution • Velocity = 0.05 m/s • Duration: 48 h 	[93]
Ti-6Al-4V+UHMWPE	0.04-0.26	Pin-on-flat	<ul style="list-style-type: none"> • Axial load = 223 N • Duration: 250,000 cycles • Lub: bovine serum 	[87]
Ti-6Al-4V+UHMWPE	0.05-0.121	Reciprocating flat on-flat	<ul style="list-style-type: none"> • Load = 445 N • Velocity = 100 cycles/min • Lub: bovine serum • Duration: 4.1×10^6 cycles 	[38]
Ti-6Al-4V (1on implanted)+UHMWPE (ASTM F 648)	0.058	Single-channel hip joint simulator	<ul style="list-style-type: none"> • Range of motion = 30° • Lub: deionized water at 37°C • Load = 1-4 kN • Angular velocity = 0.6-2.4 rad/s 	[85]

(continued)

Table 8.6 (continued)

Material contact	Average (or range) friction coefficient	Testing apparatus	Tribological conditions	References
Ti-6Al-4VELI (ASTM F 136) + UHMWPE (ASTM F 648)	0.123–0.133	Single-channel hip joint simulator	<ul style="list-style-type: none"> • Range of motion = 30° • Lub: deionized water at 37 °C • Load = 1–4 kN • Angular velocity = 0.6–2.4 rad/s 	[85]
Alumina + UHMWPE	0.06–0.10	Reciprocating flat-on-flat	<ul style="list-style-type: none"> • Load = 223 N • Velocity = 60 cycles/min • Lub: bovine serum 	[38]
Alumina + UHMWPE	0.056	Pin-on-disk	<ul style="list-style-type: none"> • Load = 3 MPa • Velocity = 60 mm/s • Lub: bovine serum, 40–50 ml • 24–26 °C 	[37]
Alumina (Vitox) + UHMWPE	0.06–0.18	Pin-on-flat	<ul style="list-style-type: none"> • Contact pressure = 4.8 MPa • Frequency = 1 Hz • Sliding dist. = 50 mm • Lub: distilled, deionized H₂O • 37.1 °C 	[42]
Alumina + UHMWPE	0.06–0.25	Pin-on-flat	<ul style="list-style-type: none"> • Axial load = 223 N • Duration: 250,000 cycles • Lub: bovine serum 	[87]
Alumina + UHMWPE	Dry: 0.16 Lub: 0.05	Rolling-sliding apparatus	<ul style="list-style-type: none"> • Velocity = 25 m/min • Pressure = 30 N/cm² • Duration: 20 h • Lub: none or distilled water • Room temperature 	[46]
Alumina (BIOLOX) + UHMWPE (ASTM F 648)	0.022–0.062	Single-channel hip joint simulator	<ul style="list-style-type: none"> • Range of motion = 30° • Lub: deionized water at 37 °C • Load = 1–4 kN • Angular velocity = 0.6–2.4 rad/s 	[85]

Alumina (ASTM F 603) + UHMWPE (ASTM F 648)	0.050	Single-channel hip joint simulator	<ul style="list-style-type: none"> • Range of motion = 30° • Lub: deionized water at 37 °C • Load = 1–4 kN • Angular velocity = 0.6–2.4 rad/s 	[85]
Zirconia (Y-PSZ) + UHMWPE	0.049	Pin-on-disk	<ul style="list-style-type: none"> • Load = 3 MPa • Velocity = 60 mm/s • Lub: bovine serum, 40–50 ml • 24–26 °C 	[37]
Zirconia (Zyranox) + UHMWPE	0.05–0.16	Pin-on-flat	<ul style="list-style-type: none"> • Contact pressure = 4.8 MPa • Frequency = 1 Hz • Sliding dist. = 50 mm • Lub: distilled, deionized H₂O • 37.1 °C 	[42]
Zirconia + UHMWPE (ASTM F 648)	0.059	Single-channel hip joint simulator	<ul style="list-style-type: none"> • Range of Motion = 30° • Lub: deionized water at 37 °C • Load = 1–4 kN • Angular velocity = 0.6–2.4 rad/s 	[85]
Stainless steel (100CR6-German) + Stainless steel (100CR6-German)	0.6 (a); 0.26 (b); 0.106 (c); 0.1 (d)	Ball-on-disk vibrottribometer (Optimol SRV-German)	<ul style="list-style-type: none"> • 10 mm diameter ball • Oscillation = 10 Hz; 1.65 mm amplitude • Load = 50 and 300 N • Lub: (a) none; (b) human synovial fluid; (c) yellow bone marrow; (d) red bone marrow • 37 °C 	[83]
Co-Cr-Mo + Co-Cr-Mo	0.03–0.04	Pin-on-disk	<ul style="list-style-type: none"> • Load = 100 N • Lub: Ringer's solution • Velocity = 0.05 m/s • Duration: 48 h 	[93]

(continued)

Table 8.6 (continued)

Material contact	Average (or range) friction coefficient	Testing apparatus	Tribological conditions	References
CoCrMo (Protasul-2) + CoCrMo (Protasul-2)	Dry: 0.4 Lub: 0.35	Rolling-sliding apparatus	<ul style="list-style-type: none"> • Velocity = 25 m/min • Pressure = 30 N/cm² • Duration: 20 h • Lub: none or distilled water • Room temperature 	[46]
Co-Cr-Mo + Co-Cr-Mo	0.12-0.13 (a,b,c) 0.22 (d)	Hip joint simulator	<ul style="list-style-type: none"> • Load 2.5 kN static load • Lub: (a) serum, (b) serum albumin, (c) synovial fluid, (d) veronate buffer 	[91]
Co-Cr-Mo + Co-Cr-Mo	0.13-0.14	Hip joint simulator	<ul style="list-style-type: none"> • Load 2.5 kN static load • Velocity: 30 cycles/min • Duration: 1.8 million cycles • Lub: serum 	[92]
Co-Cr-Mo (ASTM F75)	0.16	Hip simulator machine	<ul style="list-style-type: none"> • Lub: synovial fluid • Peak load = 150 kg 	[90]
CoCrMo + CoCrMo (McKee-Farrar)	Serum and synovial fluid: 0.12 Saline: 0.22	Dual-hip simulator	<ul style="list-style-type: none"> • Velocity = 30 cycles/min • Load = 250 kg • Duration: 1000 h • Lub: serum and synovial fluid or saline • Room temperature 	[84]

CoCrMo + CoCrMo (McKee-Farrar)	0.13	Dual-hip simulator	<ul style="list-style-type: none"> • Velocity = 30 cycles/min • Load = 250 kg • Duration: 1000 h • Lub: serum • Room temperature 	[84]
Alumina + alumina	0.26-0.35	Pin-on-disk	<ul style="list-style-type: none"> • Load = 100 N • Lub: Ringer's solution • Velocity = 0.05 m/s • Duration: 48 h 	[93]
Alumina + alumina	Dry: 0.71 Lub: 0.09	Rolling-sliding apparatus	<ul style="list-style-type: none"> • Velocity = 25 m/min • Pressure = 30 N/cm² • Duration: 20 h • Lub: none or distilled water • Room temperature 	[46]

Table 8.7 Wear rates of various material combination from in vitro studies

Material contact	Wear rate	Wear coefficient	Tribological conditions	Wear mechanisms	References
Stainless steel (316LVM) + UHMWPE	0.4 mm/year	NA	<ul style="list-style-type: none"> Pin-on-disk Luba: bovine serum Duration: 2 years test Load = 3.45 MPa Velocity = 50 × 106 mm/year 28–32 °C 	Smooth polymer, metal—scratches	[40]
Stainless steel (316L) + UHMWPE	0.17–0.23 mm ³ /106	NA	<ul style="list-style-type: none"> Reciprocating flat-on-flat Load = 445 N Velocity = 100 cycles/min Lub: bovine serum Duration = 3.7 × 106 cycles 	Surface scratching	[38]
Stainless steel (316L) + UHMWPE	NA	27.7 × 10 ⁻⁷ mm ³ /Nm	<ul style="list-style-type: none"> Pin-on-disk Lub: bovine serum, 40–50 ml Load = 3 MPa Velocity = 60 mm/s 24–26 °C 	Original machine marks gone, new wear marks	[37]
Stainless steel (316L) + Machined UHMWPE (HiFax 1900)	Machined UHMWPE: 3.23 in./in. × 10–9 UHMWPE: 1.70 in./ in. × 10–9	NA	<ul style="list-style-type: none"> Annular disk on flat pin Range of motion = 110° Sliding velocity = 43.3 in./ min Stress = 500 psi Lub: Ringer's solution 	UHMWPE transfer film	[45]
Stainless steel + UHMWPE (Charnley)	Max. depth of wear: 0.15 mm	NA	<ul style="list-style-type: none"> Dual-hip simulator Velocity = 30 cycles/min Load = 250 kg Duration: 1000 g Lub: serum Room temperature 	Evidence of brittle fracture	[84]

Stainless steel (316L)	UHMWPE: 0.20 mm ³ /106 cycles UHMWPE 0.65 µm ³ /year	NA	<ul style="list-style-type: none"> • Twelve-channel friction and wear machine FW-12 • Conforming, flat-on-flat configuration • Velocity = 100 cyc./min • Pressure = 6.90 MPa • Duration: 3.7 × 106 cycles • Lub: bovine calf serum w/55 sodium azide 	Quantification of wear separately from creep deformation. Adhesive/abrasive wear emphasizes over fatigue wear	[86]
Stainless steel + UHMWPE	UHMWPE: 40 mg/106 cycles	NA	<ul style="list-style-type: none"> • Ten station hip simulator • Range of motion = 46° • Lub: Bovine blood serum at 37 ° C • Load = Oscillating 0–2030 N • Frequency = 1 Hz • Duration: 1 × 106 cycles 	Highly loaded region of UHMWPE smooth and shiny, peeling, pitting	[94]
Stainless steel + UHMWPE	1.62 × 10 ⁻⁷ mm ³ /Nm	NA	<ul style="list-style-type: none"> • Ball-and-socket simulator • Ra < 0.016 • Sterilized with 2.5 Mrad g rad • Lub: bovine serum with sodium azide • Load = 2000 N • Speed = 100 mm/s 	Uniform superficial scratches, occasional deeper marks. Metal particles, acrylic cement particles	[44]

(continued)

Table 8.7 (continued)

Material contact	Wear rate	Wear coefficient	Tribological conditions	Wear mechanisms	References
Cast Co-Cr-Mo pins (ASTM F-75)+ UHMWPE (GUR 415 plate)	PE thickness change: 64±13 µm	NA	<ul style="list-style-type: none"> Reciprocating pin-on-flat Sterilized with 2.5 Mrad Lub: deionized water 36 MPa Line contact stress Frequency = 2.1 Hz Stroke length = 15 mm Duration = 2 × 106 cycles Final friction = 0.079 ± 0.001 	Abrasive wear of PE. Transfer of PE on Co-Cr pins. Oxidative wear of Co-Cr pins	[95]
Wrought Co-Cr pins (ASTM F-90)+ UHMWPE GUR 415 plate	PE thickness change: 71±25 µm	NA	<ul style="list-style-type: none"> Reciprocating pin-on-flat Sterilized with 2.5 Mrad Lub: deionized water 36 MPa Line contact stress Frequency = 2.1 Hz Stroke length = 15 mm Duration = 2 × 106 cycles Final friction = 0.101 ± 0.019 	Abrasive wear of PE. Transfer of PE on Co-Cr pins. Oxidative wear of Co-Cr pins	[95]
Co-Cr-Mo (Protasul-2)+ UHMWPE	CoCrMo: 0.1 mg/20 h UHMWPE: 1 mg/20 h	NA	<ul style="list-style-type: none"> Rolling-sliding wear and Friction apparatus Velocity • 25 m/min Pressure = 30 N/cm² Duration: 20 h Dry condition Room temperature 	NA	[40]
Co-Cr-Mo (hot pressed)+ UHMWPE	0.5 mm/year	NA	<ul style="list-style-type: none"> Pin-on-disk Lub: bovine serum Duration: 2 years test Load = 3.45 MPa Velocity = 50 × 106 mm/year 28–32 °C 	Smooth polymer, metal — scratches	[87]

Co-Cr+ UHMWPE	1.05 mg/106 cycles	NA	<ul style="list-style-type: none"> • Pin-on-flat • Lub: distilled, deionized water • Contact pressure: 4.8 MPa • Frequency = 1 Hz • Sliding dist. = 50 mm • 37.1 °C 	Transfer of PE to Co-Cr Surface Adhesive wear	[42]
Co-Cr-Mo (passivated)+ UHMWPE (HiFax 1900)	Machined UHMWPE: 3.23 in./in. x 10–9 UHMWPE: 1.50 in./in. x 10–9	NA	<ul style="list-style-type: none"> • Annular disk on flat pin • Range of motion = 110° • Sliding velocity = 43.3 in./min • Stress = 500 psi • Lub: Ringer's solution • Twelve-channel friction and wear machine FW-12 	UHMWPE transfer film Quantification of wear separately from creep deformation	[45]
Co-Cr-Mo+ UHMWPE	UHMWPE: 0.17 mm ³ /106 cycles 0.55 μm/year	NA	<ul style="list-style-type: none"> • Conforming, flat-on-flat configuration • Velocity = 100 cyc./min • Pressure = 6.90 MPa • Duration: 3.7 x 106 cycles • Lub: bovine calf serum w/55 sodium azide 	Adhesive/abrasive wear emphasizes over fatigue wear	[86]
Co-Cr–Mo+ UHMWPE	UHMWPE: 68 mg/106 cycles	NA	<ul style="list-style-type: none"> • Ten-station hip simulator • Range of motion = 46° • Lub: bovine blood serum at 37 °C • Load = Oscillating 0–2030 N • Frequency = 1 Hz • Duration: 1 x 106 cycles 	Highly loaded region of UHMWPE smooth and shiny Peeling Pitting	[94]

(continued)

Table 8.7 (continued)

Material contact	Wear rate	Wear coefficient	Tribological conditions	Wear mechanisms	References
Co-Cr-Mo + UHMWPE (Charnley-Muller)	Max. depth of wear: 0.08 mm	NA	<ul style="list-style-type: none"> • Dual hip simulator • Velocity = 30 cycles/min • Load = 250 kg • Duration: 1000 h • Lub: serum • Room temperature 	Evidence of brittle fracture	[84]
Co-Cr-Mo + UHMWPE (Charnley)	0.15 mm/1.8 × 10 ⁶ cycles	NA	<ul style="list-style-type: none"> • Hip joint simulator • 2.5 kN static load • Lub: bovine serum • Duration: 1.8 × 10⁶ cycles • Velocity = 30 cycles/min 	Creep, abrasion, adhesion. Max cup wear depth	[91]
Co-Cr-Mo + UHMWPE (Charnley-Muller)	0.075 mm/1.8 × 10 ⁶ cycles	NA	<ul style="list-style-type: none"> • Hip joint simulator • 2.5 kN static load • Lub: bovine serum • Duration: 1.8 × 10⁶ cycles • Velocity = 30 cycles/min 	Creep, abrasion, adhesion. Max cup wear depth	[91]
Co-Cr-Mo + UHMWPE (Duo-Patella)	1.8 mg/105 cycles	NA	<ul style="list-style-type: none"> • Knee joint simulator • 700 lb peak load • Velocity = 33 cycles/min • Duration: 105 cycles • Lub: double-spun bovine serum 	Creep and fatigue cracks evident	[41]
Co-Cr-Mo + UHMWPE (Ewald)	1.1 mg/105 cycles	NA	<ul style="list-style-type: none"> • Knee joint simulator • 700 lb peak load • Velocity = 33 cycles/min • Duration: 105 cycles • Lub: double-spun bovine serum 	Creep and fatigue cracks evident	[41]

Co-Cr-Mo + UHMWPE (Spherocentric)	0.3 mg/105	NA	<ul style="list-style-type: none"> • Knee joint simulator • 700 lb peak load • Velocity = 33 cycles/min • Duration: 105 cycles • Lub: double-spun bovine serum 	Creep and fatigue cracks evident	[41]
Co-Cr-Mo + UHMWPE (Geometric)	0.4 mg/105 cycles	NA	<ul style="list-style-type: none"> • Knee joint simulator • 700 lb peak load • Velocity = 33 cycles/min • Duration: 105 cycles • Lub: double-spun bovine serum 	Creep and fatigue cracks evident	[41]
Co-Cr-Mo + UHMWPE (Geometric)	0.3 mg/105 cycles	NA	<ul style="list-style-type: none"> • Knee joint simulator • 700 lb peak load • Velocity = 33 cycles/min • Duration = 105 cycles • Lub: double-spun bovine serum 	Creep and fatigue cracks evident	[41]
Ti-6Al-4V + UHMWPE	0.47 mg/106 cycles	NA	<ul style="list-style-type: none"> • Pin-on-flat • Axial load = 223 N • Duration: 250,000 cycles • Lub: bovine serum 	Surface scratching	[87]
Ti-6Al-4V + UHMWPE	0.3 mm/year	NA	<ul style="list-style-type: none"> • Pin-on-disk • Lub: bovine serum • Duration: 2 years test • Load = 3.45 MPa • Velocity = 50 × 106 mm/year • 28–32 °C 	Abrasion by cement particles	[40]

(continued)

Table 8.7 (continued)

Material contact	Wear rate	Wear coefficient	Tribological conditions	Wear mechanisms	References
Ti-6Al-4V Pins + UHMWPE GUR 415 plate	PE thickness change: 59 ± 12 µm	NA	<ul style="list-style-type: none"> Reciprocating pin-on-flat Sterilized with 2.5 Mrad Lub: deionized water 36 MPa Line contact stress Frequency = 2.1 Hz Stroke length = 15 mm Duration = 2 × 106 cycles Final friction = 0.112 ± 0.007 	Adhesive transfer of PE on cylinders. Oxidative wear of Ti-6Al-4V Abrasive wear of PE	[95]
Ti-6Al-4V (nitrided) + UHMWPE	0.9 mm/year	NA	<ul style="list-style-type: none"> Pin-on-disk Lub: bovine serum Duration: 2 years test Load = 3.45 MPa Velocity = 50 × 10⁶ mm/year 28–32 °C 	No scratches present	[40]
Ti-6Al-4V (passivated) + UHMWPE (HiFax 1900)	Machined UHMWPE: 0.84–2.07 in./in × 10–9	NA	<ul style="list-style-type: none"> Annular disk-on-flat pin Range of motion = 110° Sliding velocity = 43.3 in./min Stress = 500 psi Lub: Ringer's solution 	UHMWPE transfer film	[45]
Ti-6Al-4V (nitrided) + UHMWPE (HiFax 1900)	Machined UHMWPE: 1.83 in./in × 10–9	NA	<ul style="list-style-type: none"> Annular disk-on-flat pin Range of motion = 110° Sliding velocity = 43.3 in./min Stress = 500 psi Lub: Ringer's solution 	UHMWPE transfer film	[45]

Ti-6Al-4V (not passivated) + UHMWPE (Hifax 1900)	Machined UHMWPE: 1.55 in/in × 10–9	NA	<ul style="list-style-type: none"> • Annular disk-on-flat pin • Range of motion = 110° • Sliding velocity = 43.3 in./min • Stress: 500 psi • Lub: Ringer's solution • Reciprocating flat-on-flat • Load = 445 N • Velocity = 100 cycles/min • Lub: bovine serum • Duration: 4.1 × 106 cycles 	UHMWPE transfer film	[45]
Ti-6Al-4V + UHMWPE	0.04–0.11 mm ³ /106	NA	<ul style="list-style-type: none"> • Ball and socket simulator • Ra < 0.016 • Sterilized w/2.5 Mrad g rad • Lub: bovine serum w/sodium azide • Load = 2000 N • Speed = 100 mm/s 	Surface scratching	[38]
Ti-6Al-4V (implanted with nitrogen) + UHMWPE	NA	1.9 × 10–7 mm ³ /Nm	<ul style="list-style-type: none"> • Ball-and-socket simulator • Ra < 0.016 • Sterilized w/2.5 Mrad g rad • Lub: bovine serum w/sodium azide • Load = 2000 N • Speed = 100 mm/s 	Uniform superficial scratches, occasional deeper marks Metal particles, acrylic cement particles	[44]
Ti-6Al-4V (conventional) + UHMWPE	NA	1.98 × 10–7 mm ³ /Nm	<ul style="list-style-type: none"> • Pin-on-disk • Lub: bovine serum, 40–50 ml • Load = 3 MPa • Velocity = 60 mm/s • 24–26 °C 	Uniform superficial scratches, occasional deeper marks Metal particles, acrylic cement particles	[44]
Alumina + UHMWPE	NA	18.2 × 10–7 mm ³ /Nm	<ul style="list-style-type: none"> • Pin-on-disk • Lub: bovine serum, 40–50 ml • Load = 3 MPa • Velocity = 60 mm/s • 24–26 °C 	Original machine marks worn, smoother	[37]

(continued)

Table 8.7 (continued)

Material contact	Wear rate	Wear coefficient	Tribological conditions	Wear mechanisms	References
Alumina + UHMWPE	0.26 mg/106 cycles	NA	<ul style="list-style-type: none"> • Pin-on-flat • Axial load= 223 N • Duration: 250,000 cycles • Lub: bovine serum 	NA	[38]
Alumina + UHMWPE	0.04 mg/106 cycles	NA	<ul style="list-style-type: none"> • Pin-on-flat • Lub: distilled, deionized water • Contact pressure: 4.8 MPa • Frequency = 1 Hz • Sliding dist. = 50 mm • 37.1 °C 	Minimal wear	[42]
Alumina + UHMWPE	Alumina: 0.1 mg/20 h UHMWPE: 0.1 mg/20 h	NA	<ul style="list-style-type: none"> • Rolling-sliding wear and friction apparatus • Velocity = 25 m/min • Pressure = 30 N/cm² • Duration: 20 h • Dry condition • Room temperature 	NA	[46]
Zirconia + UHMWPE	0.03 mg/106 cycles	NA	<ul style="list-style-type: none"> • Pin on flat • Lub: distilled, deionized water • Contact pressure: 4.8 MPa • Frequency = 1 Hz • Sliding dist. = 50 mm • 37.1 °C 	Minimal wear	[42]

Solid yttria ZrO2 pins + UHMWPE GUR 415 plate	PE thickness change: 33±13 µm	NA	<ul style="list-style-type: none"> Reciprocating pin-on-flat Sterilized with 2.5 Mrad Lub: deionized water 36 MPa Line contact stress Frequency = 2.1 Hz Stroke length = 15 mm Duration = 2 × 106 cycles Final friction = 0.033 ± 0.005 	Abrasive wear from the surface roughness characteristic and adhesive wear	[95]
ZrO2 surface on Zr-2.5Nb pins + UHMWPE GUR 415 plate	Pe thickness change: 25±20 µm	NA	<ul style="list-style-type: none"> Reciprocating pin-on-flat Sterilized with 2.5 Mrad Lub: deionized water 36 MPa Line contact stress Frequency = 2.1 Hz Stroke length = 15 mm Duration = 2 × 106 cycles Final friction = 0.040 ± 0.008 	Abrasive wear from the surface roughness characteristics and adhesive wear	[95]
Zirconia (Y-PSZ) + UHMWPE	NA	10.7 × 10 ⁻⁷ mm ³ /Nm	<ul style="list-style-type: none"> Pin-on-disk Lub: bovine serum, 40–50 ml Load = 3 MPa Velocity = 60 mm/s 24–26 °C 	Original machine marks still visible	[37]
Co-Cr-Mo + Co-Cr-Mo	2–10 × 10 ⁻⁹ mm ³ /mm	NA	<ul style="list-style-type: none"> Disc-on-plate Lub: water 37 °C 	NA	[51]
Co-Cr-Mo (Protasul-2) + Co-Cr-Mo (Protasul-2)	Roller: 23 mg/20 h Slider: 23 mg/20 h	NA	<ul style="list-style-type: none"> Rolling-sliding wear and friction apparatus Velocity = 25 m/min Pressure = 30 N/cm² Duration: 20 h Dry condition Room temperature 	NA	[46]

(continued)

Table 8.7 (continued)

Material contact	Wear rate	Wear coefficient	Tribological conditions	Wear mechanisms	References
Co-Cr-Mo+Co-Cr-Mo (McKee-Farrar)	Max. depth of wear: 0.01 mm	NA	<ul style="list-style-type: none"> Dual-hip simulator Velocity = 30 cycles/min Load = 250 kg Duration: 1000 h Lub: serum Room temperature 	Adhesive and abrasive types of wear	[84]
Co-Cr-Mo (Protasul-2)+Co-Cr-Mo (Protasul-2)	<ul style="list-style-type: none"> initial wear: 10–20 mm linear wear: 2–4 mm/106 cycles 	NA	<ul style="list-style-type: none"> Stanmore Mk III hip simulator 37 mm diameter head Frequency = 1/2 Hz Load = 300–3500 N Duration: min. 2.5 × 106 movements/test Lub: Ringer's solution w/30 % calf serum 	Equal amount of wear on both components Preferential wear direction, with pronounced grooving	[52]
Co-Cr-Mo+Co-Cr-Mo (McKee-Farrar)	0.013 mm/1.8 × 106 cycles	NA	<ul style="list-style-type: none"> Hip joint simulator 2.5 kN static load Lub: bovine serum Duration: 1.8 × 106 cycles Velocity = 30 cycles/min 	Abrasion, scratching. Max cup wear depth	[91]
Co-Cr-Mo (Protasul-21WF)+Co-Cr-Mo (Protasul-21WF)	<ul style="list-style-type: none"> Initial wear: 10–20 mm Linear wear: 2–4 mm/106 cycles 	NA	<ul style="list-style-type: none"> Stanmore Mk III hip simulator 28 and 32 mm heads Frequency = 1/2 Hz Load = 300–3500 N Duration: min. 2.5 × 106 movements/test Lub: Ringer's solution w/30 % calf serum 	Equal amount of wear on both components Preferential wear direction, with pronounced grooving	[56]

Alumina + alumina	1.2×10^{-7} mm/mm	NA	<ul style="list-style-type: none"> • Disc-on-plate • Lub: water • 37 °C 	NA	[46]
Stainless steel (316 S16) + PTFE	2.26 mm/year	3.4×10^{-5} mm ³ /Nm	<ul style="list-style-type: none"> • Pin-on-flat • Lub: bovine serum • Ra=0.0 mm • Load=40 n/pin • Speed=2 p rad/s • Sliding dist. = 0.24 m/s 	No creep. Particles present	[96]
Stainless steel + Delrin 500	31 mm/year	NA	<ul style="list-style-type: none"> • Pin-on-flat • Velocity = 100 mm/s • Load=6.9 N/mm² • Lub: serum • Room temperature • 4.8 years' effective use 	NA	[53]
Stainless steel + Polyester	521 mm/year	NA	<ul style="list-style-type: none"> • Pin-on-flat • Velocity = 100 mm/s • Load=6.9 N/mm² • Lub: serum • Room temperature • 4.8 years' effective use 	NA	[53]
Stainless steel + alumina (Protek)	(mg/cyc) SS: 176, 146, 212 A1203: 0.3, 2.1, 0.2	NA	<ul style="list-style-type: none"> • Five station hip simulator (Helinki) • 32 mm head • Frequency = 1.08 sH3 • Load = 35 kN • Duration: 3 × 106 cycles • Lub: distilled, deionized water • 37 °C 	Corrosion of stainless steel heads	[97]

(continued)

Table 8.7 (continued)

Material contact	Wear rate	Wear coefficient	Tribological conditions	Wear mechanisms	References
Stainless steel + alumina (Thackray)	(mg/cyc) SS: 50.9, 62.4, 46.0 A12O3: 0.8, 1.0, 0.7	NA	<ul style="list-style-type: none"> • Five-station hip simulator (Helsinki) • 22.2 mm head • Frequency = 1.08 sH3 • Load = 35 kN • Duration: 3 × 106 cycles • Lub: distilled, deionized water • 37 °C 	Corrosion of stainless steel heads	[97]
Co-Cr-Mo+alumina (Link)	(mg/cyc) CoCrMo: 39.7, 48.2, 94.0 A12O3: 1.5, 0.5, 0.0	NA	<ul style="list-style-type: none"> • Five-station hip simulator (Helsinki) • 32 mm head • Frequency = 1.08 sH3 • Load = 35 kN • Duration: 3 × 106 cycles • Lub: distilled, deionized water • 37 °C 	NA	[97]
Co-Cr-Mo + alumina (Howmedica)	(mg/cyc) CoCrMo: 2.6, 4.7, 4.3 A12O3: 0.1, 0.0, 0.0	NA	<ul style="list-style-type: none"> • Five-station hip simulator (Helsinki) • 32 mm head • Frequency = 1.08 sH3 • Load = 35 kN • Duration: 3 × 106 cycles • Lub: distilled, deionized water • 37 °C 	NA	[97]

Co-Cr-Mo+Delrin 550	37.5 mm/year	NA	<ul style="list-style-type: none"> • Disk-on-flat • Velocity = 106 mm/s • Load = 3.7 N/mm² • Lub: water • 37 °C 	NA	[53]
S13N4+UHMWPE	0.27 mg/106 cycles	NA	<ul style="list-style-type: none"> • Pin-on-flat • Lub: distilled, deionized water • Contact pressure: 4.8 MPa • Frequency = 1 Hz • Sliding dist. = 50 mm • 37.1 °C 	NA	[42]

^aLub lubricant

Baykal and collaborators have critically and systematically reviewed the literature of multi-axis pin-on-disc wear testing for the past decades with a focus on UHMWPE tribological properties and relevant wear mechanisms. Data reviewed have been extracted from 22 published studies and are presented as UHMWPE average wear rate (mg/MC), average wear rate (mm³/MC), and average wear factor (mm³/Nm) as well as contact area for bearing couples [77].

Linear Clinical Wear

Methods have been proposed by Griffith et al. [98] and Deavane et al. [99] to radiographically measure linear wear in UHMWPE acetabular cups of total hip replacements. The overall penetration of a femoral head (Tables 8.8 and 8.9) into a UHMWPE acetabular cup is a consequence of both creep and wear, where creep is

Table 8.8 Clinical penetration into UHMWPE cups for metallic femoral heads

Reference	UHMWPE penetration rate	Clinical
[98]	<ul style="list-style-type: none"> 0.07 mm/year average (range 0.06–0.24 mm/year) 	491 acetabular cups 8.3-year follow-up (range 7–9 years)
[100]	<ul style="list-style-type: none"> 0.13 mm/year average (range 0–0.39 mm/year) for 22 mm head size 0.08 mm/year average (range 0–0.3 mm/year) for 28 mm head size 0.10 mm/year average (range 0–0.32 mm/year) for 32 mm head size 	Follow-up at least 9.5 years after implantation (227 of the 22 mm femoral head size; 98 of the 28 mm size; and 60 of the 32 mm head size)
[101]	<ul style="list-style-type: none"> 0.21 mm/year (range 0.005–0.6 mm/year) 	87 acetabular cups 9-year service life (range <1–17.5 years)
[102]	<ul style="list-style-type: none"> 0.022 mm/year (range 0.010–0.034 mm/year) 	Four explained acetabular cups with no apparent deterioration of the finish of the femoral head 20 year mean service life (range 17–23 years)

Table 8.9 Clinical penetration into UHMWPE cups for alumina ceramic heads

Reference	Femoral head	Average penetration rate
[103]	Alumina	0.098 mm/year (6-year follow-up; 28 mm cups)
[103]	Alumina (g irradiated UHMWPE)	0.072 mm/year (6-year follow-up; 28 mm cups)
[104]	Alumina	0.084 mm/year
[105]	Alumina	0.080 mm/year (38 acetabular cups over a period of 6.7 years)
[106]	Alumina	0.100 mm/year

predominantly observed for the first million loading cycles [19]. Atkinson et al. [107] estimated that the total UHMWPE residual compression due to creep in total hip replacements after x can be estimated by

$$\text{Residual compression} = 94 + 33(x - 1)\mu\text{m}$$

This relationship has served as a guide to the significance of UHMWPE creep for total hip arthroplasty [19]. Another important issue in the tribological behavior of polymers used as bearing surfaces is their viscoelastic-plastic character. For example, due to this time-dependent stress-strain response, the measured hardness varies continuously as a function of indentation time. Therefore, in certain conditions the wear behavior of these materials cannot accurately be characterized in terms of wear coefficient alone and is often defined in terms of wear factor and Pv limit. The wear factor is described as $K' = V/PS = V/Pvt$ where V is the wear volume, v the sliding velocity, P the normal load, and t the sliding time. The Pv limit or factor (which is equal to load times velocity) defines the onset of failure of polymeric surfaces. Pv limits have to be specified in terms of a limiting load at a given sliding velocity or limiting velocity at a given load. These values will depend on the test conditions.

Conclusion

The wear and frictional properties of materials are dependent on tribological conditions of the tribosystem. Their investigation involves many parameters such as wear rate, wear mechanisms, transition between initial and steady-state wear, and generation and geometry of wear debris. The physical and mechanical properties of the materials, the environmental and operating conditions, and the geometry of the wearing bodies are determining factors for these parameters. Another important tribological attribute that should be reported along with wear data is the coefficient of friction. The use of different lubricants combined with the operating conditions (load, velocity) will result in different coefficients of friction and consequently different lubrication mechanisms of the tribosystem. The wear mechanisms and wear data are partly governed by the lubrication of the tribosystem.

By definition, a tribosystem is a dynamic system that can potentially change over time emphasizing the importance of wear monitoring during testing. It is of utmost importance to fully define and report the tribological conditions during testing. The confidence in the quality of the wear data is not only related to the

tribological conditions, material properties, material combinations, and experimental method including device used for testing, but also to the number of tests conducted and number of specimens evaluated, level of statistical significance, and duration of the test. When these parameters are not reported, it is difficult to compare wear data obtained with different protocols. This often leads to an inconclusive analysis and disagreements. In this respect, the standardization of testing protocols for wear of biomaterials and devices as well as how they are reported can significantly improve the wear literature. This literature review clearly indicates that there is no convention for wear-testing systems as well as for reporting wear data.

Additional Reading and Selected Review Papers

1. Clarke, I.C. and McKellop, H.A. (1986) Wear Testing in *Handbook of Biomaterials Evaluation* (A.F. von Recum, Ed.) Macmillan Publishing Co., New York. pp. 114–130. A concise review of testing protocols used for wear testing of cardiovascular, orthopaedic, and dental implants. Introduces some of the technical parameters involved in the understanding and measurement of wear performance.
2. Dumbleton, J.H. (1981) *Tribology of natural and artificial joints*. Elsevier, New York. An excellent critical review of testing parameters and conditions for wear and friction of orthopaedic materials.
3. Baykal, D., Siskey, R.S., Haider, H., Saikko, V., Ahlroos, T., Kurtz, S.M. (2014) Advances in tribological testing of artificial joint biomaterials using multidirectional pin-on-disk testers. *Journal of the Mechanical Behavior of Biomedical Materials*, **31**, 117–134.
4. Sedel, L. (2000). Evolution of alumina-on-alumina implants: a review. *Clinical orthopaedics and related research*, **379**, 48–54.
5. Lewis, G. (1997). Polyethylene wear in total hip and knee arthroplasties. *Journal of biomedical materials research*, **38(1)**, 55–75.
6. Bracco, P., & Oral, E. (2011). Vitamin E-stabilized UHMWPE for total joint implants: a review. *Clinical Orthopaedics and Related Research*[®], **469(8)**, 2286–2293.
7. Brown, S. S., & Clarke, I. C. (2006). A review of lubrication conditions for wear simulation in artificial hip replacements. *Tribology transactions*, **49(1)**, 72–78.
8. Goel, V. K., Panjabi, M. M., Patwardhan, A. G., Dooris, A. P., & Serhan, H. (2006). Test protocols for evaluation of spinal implants. *The Journal of Bone & Joint Surgery*, **88 (suppl 2)**, 103–109.
9. Hoepfner, D. W., & Chandrasekaran, V. (1994). Fretting in orthopaedic implants: a review. *Wear*, **173(1)**, 189–197.

References

1. Jacobs JJ, Shanbhag A, Giant TT, Black J, Galante JO (1994) Wear debris in total joint replacements. *J Am Acad Orthop Surg* 2:212–220
2. Mittlmeier T, Walter A (1987) The influence of prosthesis design on wear and loosening phenomena. *CRC Critical Reviews in Biocompatibility*, 3(4): 319–419
3. Dowson D, Wright V (1981) An Introduction to the Bio-mechanics of Joints and Joint Replacement. Dowson D. and Wright V. Editors. Mechanical Engineering Publications, Ltd, London, England, pp. 49–60
4. Suh NP (1986) Tribophysics. Prentice-Hall, Inc., Englewood Cliffs, NJ, pp 3–11, 195–222
5. Jahanmir S, Suh NP (1977) Mechanics of subsurface void nucleation in delamination wear. *Wear* 44:17–38
6. Rowe CN (1980) Lubricated Wear, in *CRC Handbook of Lubrication. Theory and Practice of Tribology Volume II*. Booser, R.E. Editor. Boca Raton, FL: CRC Press; pp. 209–225
7. Waterhouse RB (1992) Fretting wear. *Frict Lubr Wear Technol* 18:242–256
8. Black J (1988) Orthopaedic biomaterials in research and practice. Churchill Livingstone, NY, p 255
9. Stachowiak G, Batchelor AW (2014) Engineering tribology, 4th edn. Elsevier, Amsterdam, 852 pp
10. Unsworth A, Dowson D, Wright V (1971) Cracking joints: a bioengineering study of cavitation in the metacarpophalangeal joint. *Ann Rheum Dis* 30:348–358
11. Williams JA (2005) Wear and wear particles—some fundamentals. *Tribol Int* 38:863–870
12. Archard JF (1980) Wear theory and mechanisms. In: Peterson MB, Winer WO (eds) *Wear control handbook*. ASME, New York, pp 35–80
13. Hornbogen E (1975) The role of fracture toughness in the wear of metals. *Wear* 33:251–259
14. Zum Gahr K-H (1982) Abrasive Wear of ductile materials. *Z Metallkd* 73:267–276
15. Hailing JA (1975) A contribution to the theory of mechanical wear. *Wear* 34:239–249
16. Quinn TFJ (1983) A review of oxidational wear. Parts I and II. *Tribol Int* 16(257–271): 305–315
17. Quinn TFJ, Rowson D, Sullivan JL (1980) Application of the oxidational theory of mild wear to the sliding wear of low-alloy steel. *Wear* 65:1–20
18. Wang A (2001) A unified theory of wear for ultra-high molecular weight polyethylene in multi-directional sliding. *Wear* 248:38–47
19. Dowson D (1995) A comparative study of the performance of metallic and ceramic femoral head components in total replacement hip joints. *Wear* 90:171–183
20. Dowson D, El-Hady Diab MM, Gillis BJ, Atkinson JR (1985) Influence of counterface topography on the wear of ultra high molecular weight polyethylene under wet conditions. In: LeeAm L-H (ed) *Polymer wear and its control*. Chem. soc. symposium series no. 287, Chapter 12, pp. 171–187
21. Dumbleton JH (1981) Tribology of natural and artificial joints. Elsevier, New York, pp 94–103, 110–148, 183–214
22. Gevaert MR, LaBerge M, Gordon JM, DesJardins JD (2005) The quantification of physiologically relevant cross shear wear phenomena on orthopaedic bearing materials using a novel wear testing machine. *J Tribol* 127:740–749
23. Bragdon CR, O'Connor DO, Lowenstein JD, Jasty M, Syniuta WD (1996) The importance of multi-directional motion on the wear of polyethylene. *Proc Inst Mech Eng H* 210:157–165
24. Wang A, Stark C, Dumbleton JH (1996) Mechanistic and morphological origins of UHMWPE wear debris in total joint replacement prostheses. *Proc Inst Mech Eng H* 210:141–155
25. Sambasivan S, Fischer DA, Shen MC, Hsu SM (2004) Molecular orientation of ultrahigh molecular weight polyethylene induced by various sliding motions. *J Biomed Mater Res B Appl Biomater* 70:278–285

26. Bragdon CR, O'Connor DO, Lowenstein JD, Jasty M, Biggs SA, Harris WH (2001) A new pin-on-disk wear testing method for simulating wear of polyethylene on cobalt-chrome alloy in total hip arthroplasty. *J Arthroplasty* 16:658–665
27. Hua Z, Zhang H, Fana Y, Jin Z (2014) Development of a BiotriboPOD testing methodology for the wear evaluation of orthopaedic biomaterials. *RSC Adv* 4:19987–19991
28. Joyce TJ, Vandelli C, Cartwright T, Unsworth A (2001) A comparison of the wear of cross-linked polyethylene against itself under reciprocating and multi-directional motion with different lubricants. *Wear* 250:206–211
29. Saikko V (1998) A multidirectional motion pin-on-disk wear test method for prosthetic joint materials. *J Biomed Mater Res* 41:58–64
30. Saikko V (2014) In vitro wear simulation on the RandomPOD wear testing system as a screening method for bearing materials intended for total knee arthroplasty. *J Biomech* 47(11):2774–2778
31. Toohey KS, Blanchet TA, Heckelman DD (2003) Effect of accelerated aging conditions on resultant depth-dependent oxidation and wear resistance of UHMWPE joint replacement bearing materials. *Wear* 255:1076–1084
32. Turell M, Wang A, Bellare A (2003) Quantification of the effect of cross-path motion on the wear rate of ultra-high molecular weight polyethylene. *Wear* 255:1034–1039
33. Yao JQ, Blanchet TA, Murphy DJ, Laurent MP (2003) Effect of fluid absorption on the wear resistance of UHMWPE orthopedic bearing surfaces. *Wear* 255:1113–1120
34. McGloughlin TM, Kavanagh AG (2000) Wear of ultra-high molecular weight polyethylene (UHMWPE) in total knee prostheses: a review of key influences. *Proc InstMech Eng H* 214:349–359
35. Walker PS, Blunn GW, Lilley PA (1996) Wear testing of materials and surfaces for total knee replacement. *J Biomed Mater Res* 33:159–175
36. Dowson DB, Jobbins B (1988) Design and development of a versatile hip joint simulator and a preliminary assessment of wear and creep in Charnley total replacement hip joints. *Eng Med* 17:111–117
37. Kumar P, Oka M, Ikeuchi K, Shimizu K, Yamamuro T, Okumura H, Kotoura Y (1991) Low wear rate of UHMWPE against zirconia ceramic (Y-PSZ) in comparison to alumina ceramic and SUS 316L alloy. *J Biomed Mater Res* 25:813–828
38. McKellop H, Clarke I, Markolf K, Amstutz H (1981) Friction and wear properties of polymer, metal, and ceramic prosthetic joint materials evaluated on a multichannel screening device. *J Biomed Mater Res* 15:619–653
39. DesJardins I, Aurora A, Tanner SL, Pace TB, Acampora KB, LaBerge M (2006) Increased total knee arthroplasty ultra-high molecular weight polyethylene wear using a clinically relevant hyaluronic acid simulator lubricant. *Proc Inst Mech Eng H* 220:609–623
40. McKellop HA, Clarke IC, Markolf KL, Amstutz HC (1978) Wear characteristics of UHMW polyethylene: a method for accurately measuring extremely low wear rates. *J Biomed Mater Res* 12:895–927
41. Rose RM, Ries MD, Paul IL, Crugnola AM, Ellis E (1984) On the true wear rate of ultrahigh molecular weight polyethylene in the total knee prosthesis. *J Biomed Mater Res* 18:207–224
42. Saikko V (1993) Wear and friction properties of prosthetic joint materials evaluated on a pin on flat apparatus. *Wear* 166:169–178
43. Saikko V, Ahlroos T, Calonius O, Keränen J (2001) Wear simulation of total hip prostheses with polyethylene against CoCr, alumina and diamond-like carbon. *Biomaterials* 22(12):1507–1514
44. McKellop HA, Rostlund TV (1990) The wear behavior of ion-implanted Ti-6Al-4V against UHMW polyethylene. *J Biomed Mater Res* 24:1413–1425
45. Miller DA, Ainsworth RD, Dumbleton JH, Page D, Miller EH, Shen C (1974) A comparative evaluation of the wear of ultra-high-molecular weight polyethylene abraded by Ti-6Al-4V. *Wear* 28:207–216

46. Semlitsch M, Lehmann M, Weber H, Doerre E, Willert HG (1977) New prospects for a prolonged functional life-span of artificial hip joints by using the material combination polyethylene/aluminium oxide ceramic/metal. *J Biomed Mater Res* 11:537–552
47. Desjardins JD, Burnikel B, LaBerge M (2008) UHMWPE wear against roughened oxidized zirconium and CoCr femoral knee components during force-controlled simulation. *Wear* 264:245–256
48. Medley JB, Krygier JJ, Bobyn JD, Chan FW, Tanzer M (1995) Metal-metal bearing surfaces in the hip: investigation of factors influencing wear. *Trans Orthop Res Soc* 20(2):765
49. Chan FW, Medley JB, Krygier JJ, Bobyn JD, Podgorsak GK, Tanzer M (1996) Wear performance of cobalt–chromium metal–metal bearing surfaces for total hip arthroplasty. In: *Trans. 42nd annual meeting of the orthopaedic research society*, vol 21, no. 2, p. 464
50. Chan FW, Bobyn JD, Medley JB, Krygier JJ, Tanzer M (1999) Wear and lubrication of metal-on-metal hip implants. *Clin Orthop Relat Res* 369:10–24
51. Galante J, Rostoker W (1973) Wear in total hip prostheses. *Acta Orthop Scand Suppl* 145:1–46
52. Streicher RM, Schon R, Semlitsch M (1990) Investigation of the tribological behaviour of metal-on-metal combinations for artificial hip joints. *Biomed Tech* 35(5):3–7
53. Clarke IC (1982) Wear-screening and joint simulation studies vs. materials selection and prosthesis design. *CRC Crit Rev Biomed Eng* 8:29–91
54. Scholes SC, Unsworth A (2009) Wear studies on the likely performance of CFR-PEEK/CoCrMo for use as artificial joint bearing materials. *J Mater Sci Mater Med* 20(1):163–170
55. Scholes SC, Unsworth A (2010) The wear performance of PEEK-OPTIMA based self-mating couples. *Wear* 268:380–387
56. Boutin P (1972) Arthroplastie total de la hanche par prothèse en alumina frittée. *Rev Chir Orthop* 58:229
57. Nevelos J, Ingham E, Doyle C, Streicher R, Nevelos A, Walter W, Fisher J (2000) Microseparation of the centers of alumina-alumina artificial hip joints during simulator testing produces clinically relevant wear rates and patterns. *J Arthroplasty* 15:793–795
58. Oonishi H, Clarke IC, Good V, Amino H, Ueno M (2004) Alumina hip joints characterized by run-in wear and steady-state wear to 14 million cycles in hip-simulator model. *J Biomed Mater Res A* 70A:523–532
59. Wroblewski BM, Siney PD, Dowson D, Collins SN (1996) Prospective clinical and joint simulator studies of a new total hip arthroplasty using alumina ceramic heads and cross-linked polyethylene cups. *J Bone Joint Surg* 78(2):280–285, British volume
60. Jin ZM, Dowson D, Fisher J (1993) Wear and friction of medical grade polyurethane sliding on smooth metal counterfaces. *Wear* 162–164:627–630
61. Auger DD, Dowson D, Fisher J, Jin MZ (1993) Friction and lubrication in cushion form bearings for artificial hip joints. *Proc Inst Mech Eng* 207:25–33
62. Auger DD, Dowson D, Fisher J (1995) Cushion form bearings for total knee joint replacement. Part 1: Design, friction, and lubrication. *Proc Inst Mech Eng* 209:73–81
63. Caravia L, Dowson D, Fisher J (1993) Start up and steady state friction of thin polyurethane layers. *Wear* 160:191–197
64. Chow AB, Medley JB, LaBerge M (1994) Mechanical and tribological analyses of elastomeric surface layers in load bearing implants. In: *Trans of 20th annual meeting of the society for biomaterials*, Boston, MA, p. 434
65. Graham RM, Joseph PF, Dooley RL, LaBerge M (1995) Effect of lubricant viscosity and bearing surface stiffness on the lubrication mechanism of a point contact as a total hip arthroplasty model. *Trans Soc Biomater* 23:124
66. LaBerge M, Kirkley S, Chow A, Medley JB, Brox WT (1991) Biotribological study of the contact elastomer-cartilage. In: *Proceedings of the combined meeting of orthopaedic research societies (USA, Japan, Canada)*, Banff, Alberta, Canada, June 1991
67. Pylios T, Shepherd DET (2008) Wear of medical grade silicone rubber against titanium and ultrahigh molecular weight polyethylene. *J Biomed Mater Res Part B Appl Biomater* 84B:520–523

68. Teoh SH, Tang ZG, Ramakrishna S (1999) Development of thin elastomeric composite membranes for biomedical applications. *J Mater Sci Mater Med* 10:343–352
69. Suzuki S, Suzuki SH, Cox CF (1996) Evaluating the antagonistic wear of restorative materials. *J Am Dent Assoc* 127:74–80
70. Deng M, Shalaby SW (1997) Properties of self-reinforced ultra-high-molecular-weight polyethylene composites. *Biomaterials* 18:645–655
71. Roeder RK, Sproul MM, Turner CH (2003) Hydroxyapatite whiskers provide improved mechanical properties in reinforced polymer composites. *J Biomed Mater Res A* 67A:801–812
72. Wang M, Chandrasekaran M, Bonfield W (2002) Friction and wear of hydroxyapatite reinforced high density polyethylene against the stainless steel counterface. *J Mater Sci Mater Med* 13:607–611
73. Harsha AP, Joyce TJ (2013) Comparative wear tests of ultra-high molecular weight polyethylene and cross-linked polyethylene. *Proc IMechE Part H J Eng Med* 227:600–608
74. Kyomoto M, Moro T, Miyaji F, Hashimoto M, Kawaguchi H, Takatori Y, Nakamura K, Ishihara K (2009) Effects of mobility/immobility of surface modification by 2-methacryloyloxyethyl phosphorylcholine polymer on the durability of polyethylene for artificial joints. *J Biomed Mater Res A* 90A:362–371
75. Oral E, Christensen SD, Malhi AS, Wannomae KK, Muratoglu OK (2006) Wear resistance and mechanical properties of highly cross-linked, ultrahigh-molecular weight polyethylene doped with vitamin E. *J Arthroplasty* 21:580–591
76. Agrawal CM, Micallef DM, Wirth MA, Lankford J, Dearnaley G, McCabe AR (1993) The effects of diamond-like-carbon coatings on the friction and wear of enhanced UHMWPE-metal couples. In: *Trans 21st annual meet of the society for biomaterials, Birmingham, AL, vol 26, p. 10*
77. Baykal D, Siskey RS, Haider H, Saikko V, Ahlroos T, Kurtz SM (2014) Advances in tribological testing of artificial joint biomaterials using multidirectional pin-on-disk testers. *J Mech Behav Biomed Mater* 31:117–134
78. Brown KJ, Atkinson JR, Dowson D, Wright V (1976) The wear of ultra high molecular weight polyethylene and a preliminary study of its relation to the in vivo behaviour of replacement hip joints. *Wear* 40:255–264
79. Fisher J, Dowson D (1991) Tribology of total artificial joints. *Proc Inst Mech Eng* 205:73–79
80. Rose RM, Radin EL (1982) Wear of polyethylene in total hip prostheses. *Clin Orthop Relat Res* 170:107–115
81. Schmidt MB, Lin M, Greer KW (1995) Wear performance of UHMWPE articulated against ion implanted CoCr. In: *Trans 21st annual meeting of the society for biomaterials, San Francisco, CA, vol 28, p. 230*
82. Streicher RM (1991) Ceramic surfaces as wear partners for polyethylene. In: Bonfield W, Hastings GW, Tanner KE (eds) *Bioceramics, vol 4. Butterworth-Heinemann Ltd, London, England, p 9*
83. Gavrjushenko NS (1993) Recommendations with respect to the improvement of lubrication quality of synovial fluid in artificial joints. *Proc Inst Mech Eng* 207:111–114
84. Simon SR, Radin EL (1973) Lubrication and wear of the Charnley, Charnley-Muller, and McKee-Farrar prostheses with special regard to their clinical behavior. In: *Proc. 1st scient. meet. hip society, Saint Louis, Chapter 5, pp. 33–45*
85. Saikko V (1992) Simulator study of friction in total replacement hip joints. *Proc Inst Mech Eng H* 206:201–211
86. McKellop H (1981) Wear of artificial joint materials. II. Twelve-channel wear-screening device: correlation of experimental and clinical results. *Eng Med* 10(3):123–136
87. Tateishi T, Terui A, Yunoki H (1990) Friction and wear properties for biomaterials for artificial joint. *Bioceramics* 2:145–151

88. Ruger LM, Love BJ, Drews MJ, Hutton WC, LaBerge M (1996) Effect of antioxidant on the tribological properties of gamma sterilized ultra high molecular weight polyethylene. In: Proc. fifth world biomaterials congress, Toronto, Canada, 29 May–2 June
89. Unsworth A, Pearcy MJ, White EFT, White G (1988) Frictional properties of artificial hip joints. *Eng Med* 17:101–104
90. Walker PS, Bullough PG (1973) The effects of friction and wear in artificial joints. *Orthop Clin North Am* 4:275–293
91. Weightman B, Simon S, Paul LI, Rose R, Radin EL (1972) Lubrication mechanisms of hip joint replacement prostheses. *J Lubr Technol (Trans Am Soc Mech Eng)* 94:131
92. Weightman B, Paul IL, Rose RM, Simon SR, Radin EL (1973) A comparative study of total hip replacement prostheses. *J Biomech* 6:299
93. Ungethum M, Refior HJ (1974) 1st Aluminiumoxidkeramik als Gleitlagerwerkstoff für Totalendoprothesen geeignet? *Arch Orthop Unfallchir* 79:97
94. Eyerer P, Kurth M, McKellop HA, Mittlmeier T (1987) Characterization of UHMWPE Hip cups run on joint simulators. *J Biomed Mater Res* 21:275–291
95. Poggie RA, Wert JJ, Mishra AK, Davidson JA (1992) Friction and wear characterization of UHMWPE in reciprocating sliding contact with Co–Cr, Ti-6AlV, and zirconia implant bearing surfaces. In: Denton R, Keshavan MK (eds) *Wear and friction of elastomers*. ASTM STP 1145. American Society For Testing and Materials, Philadelphia, pp 65–81
96. Dowson D, Wallbridge NC (1985) Laboratory wear tests and clinical observations of the penetration of femoral heads into acetabular cups in total replacement hip joints. I: Charnley prosthesis with polytetrafluoroethylene acetabular cups. *Wear* 104:203–215
97. Saikko V, Paavolainen P, Kleimola M, Slati P (1992) A five-station hip joint simulator for wear rate studies. *Proc Inst Mech Eng H* 206:195–200
98. Griffith MJ, Seidenstein MK, Williams D, Charnley J (1978) Socket wear in Charnley low friction arthroplasty of the hip. *Clin Orthop Relat Res* 137:36–47
99. Deavane PA, Bourne RB, Rorabeck CH, Hardie RM, Home JG (1995) Measurement of polyethylene wear in metal-backed acetabular cups. *Clin Orthop Relat Res* 319:303–316
100. Livermore J, Ilstrup D, Morrey B (1990) Effect of femoral head size on wear of the polyethylene acetabular component. *J Bone Joint Surg* 72A:518–528
101. Isaac GI, Wroblewski PJ, Atkinson JR, Dowson D (1992) Tribological study of retrieved hip prostheses. *Clin Orthop Relat Res* 276:115–125
102. Wroblewski BM, McCullagh PJ, Siney PD (1992) Quality of the surface finish of the head of the femoral component and the wear of the socket in long-term results of the Charnley low-friction arthroplasty. *Eng Med* 20:181–183
103. Oonishi H, Takayama Y (1989) Comparisons of wear of UHMW polyethylene sliding against metal and alumina in total hip prostheses. *Bioceramics* 1:272–277
104. Okumara H, Yamamuro P, Kumar T, Nakamura T, Oka M (1989) Socket wear in total hip prosthesis with alumina ceramic head. *Bioceramics* 1:284–189
105. Egli A, Weber BG, Sieber H, Semlitsch M, Dörre E (1990) Experience with the pairing of polyethylene/ceramic materials in hip endoprotheses. In: Willert H-G, Bucchorn GH, Eyerer P (eds) *Ultra-high molecular weight polyethylene as biomaterial in orthopaedic surgery*. Hoffrefe and Huber, Gottingen, pp 154–158
106. Zichner LP, Willert HG (1992) Comparison of alumina-polyethylene and metal-polyethylene in clinical trials. *Clin Orthop Relat Res* 282:86–94
107. Atkinson JR, Dowling JM, Cicek RZ (1980) Materials for internal prostheses: the present position and possible future developments. *Biomaterials* 1:89–96

Chapter 9

Degradation/resorption in Bioactive Ceramics in Orthopaedics

H. Oonishi and H. Oomamiuda

9.1 Introduction

Bioceramics have now been widely used as bone replacement materials in orthopaedic surgery. In particular, calcium phosphate ceramics have been applied as bioactive ceramics with bone bonding capacities.

Biological responses such as bone bonding and the biodegradation properties of these materials are very important in clinical applications. Any convincing conclusion has not yet been reached as to whether these materials are biodegradable or not, although it has been discussed for a long time.

Degradation is an important characteristic for biomaterials, and it is considered to have a large influence on the bone bonding properties. This degradation characteristic must be considered from the following two view points. These are the solution mediated dissolution process and the cellmediated process (phagocytosis).

This chapter overviews the literature regarding the biodegradation processes of bioactive calcium phosphate ceramics from the viewpoint of *in vitro* physico-chemical dissolution processes and *in vivo/in vitro* biological degradation processes.

H. Oonishi (✉) • H. Oomamiuda
Department of Orthopaedic Surgery, Artificial Joint Section and Biomaterial Research
Laboratory Osaka-Minami National Hospital,
677-2 Kido-Cho, Kawachinagano-shi, Osaka, Japan

DCPD ;	Dicalcium phosphate dihydrate [CaHPO ₄ ·2H ₂ O]
DCPA ;	Dicalcium phosphate anhydrate [CaHPO ₄]
OCP ;	Octacalcium phosphate [Ca ₈ H ₂ (PO ₄) ₆ ·5H ₂ O]
TCP ;	Tricalcium phosphate [Ca ₃ (PO ₄) ₂]
HAp ;	Hydroxyapatite [Ca ₁₀ (PO ₄) ₆ (OH) ₂]
TTCP ;	Tetracalcium phosphate [Ca ₄ (PO ₄) ₂ O]

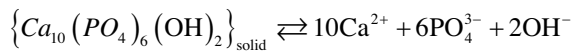
In this chapter, each calcium phosphate material is abbreviated as follows:

9.2 In Vitro Physico-chemical Dissolution Processes

Dissolution of a solid material continues until an equilibrium condition is reached, followed by a saturated condition where a solid and a liquid remain in equilibrium. Solubility is defined as the maximum concentration of solute *in the solution under the equilibrium condition*. This concept of solubility is very convenient to know how much the material has actually dissolved. However, it is not convenient for showing general solubility of the material since its value depends on the pH of the solution.

Therefore, a thermodynamic equilibrium constant known as the solubility product constant K_{sp} is used for slightly soluble salts. This solubility product constant is useful for understanding the dissolution characteristics, because its value does not change in either acid or basic solutions under the same conditions of temperature, pressure and ionic strength.

For example, HAp dissolves in water as follows;



Therefore, its solubility product constant K_{sp} is calculated as follows;

$$K_{SP(HAp)} = [Ca^{2+}]^{10} [PO_4^{3-}]^6 [OH^{-}]^2$$

where values in brackets represent ionic activities.

There are many reports on solubility product constants of calcium phosphate compounds obtained by the above equation, and these values are shown in Table 9.1.

Chow [18] calculated, based on these data, the solubility isotherms at 37 °C over a wide pH range (Figure 9.1). These solubility isotherms were shown as the function of the concentration of calcium and phosphate ions in a saturated solution of each calcium phosphate salt. The relative stability of calcium phosphate salts at various values of pH can be obtained by these solubility isotherms. At a given pH, a salt with its isotherm lying below that of another salt is less soluble and more

Table 9.1 Solubility product constants of calcium phosphate compounds at 25°C

Compound	Abbreviation	Formula	p K _{sp}	Reference
Dicalcium phosphate dihydrate	DCPD	CaHPO ₄ · 2H ₂ O	6.59	1,2
			6.63	3
Dicalcium phosphate anhydrous	DCPA	CaHPO ₄	6.90	2, 4
Octacalcium phosphate	OCP	Ca ₈ H ₂ (PO ₄) ₆ · 5H ₂ O	96.6	5
			98.6	6
α-Tricalcium phosphate	α-TCP	α-Ca ₃ (PO ₄) ₂	25.5	7
β-Tricalcium phosphate	β-TCP	β-Ca ₃ (PO ₄) ₂	28.9	2, 8
			29.7	3
			115.5	2, 9, 10
Hydroxyapatite	HAp	Ca ₁₀ (PO ₄) ₆ (OH) ₂	115–117	11
			117	12–15
			122	16
			125	17
Tetracalcium phosphate	TTCP	Ca ₄ (PO ₄) ₂ O	38	15

pK_{sp}: the negative logarithm of K_s.

stable than the other. Therefore, HAp is the most stable and least soluble salt among these salts in the range of pH below approximately 4.2 where DCPA is the least soluble. Similarly, TTCP is the least stable and most soluble salt in the range of pH below 8.5, above which pH DCPD is the most soluble.

Newesely [19] and Monma and Kanazawa [20] reported that α-TCP was converted to HAp by hydration as follows;



However, this phase diagram can apply only in a thermodynamic equilibrium for the ternary system of Ca(OH)₂–H₃PO₄–H₂O, and it shows only a general tendency under *in vivo* conditions where various different ions are involved. Furthermore, this relation is also considered to be influenced by the experimental conditions and the characteristics of the material used in the experiments.

Most of the implanted materials used in the investigations were TCP and HAp. It has been reported in earlier investigations that TCP dissolves more rapidly than HAp in various solutions [21].

Jarcho [22] compared the relative dissolution rates of dense HAp and TCP. The dissolution rate of TCP was 12.3 times higher than that of HAp in buffered lactic acid solution (0.4 M, pH 5.2), and was 22.3 times higher than that of HAp in buffered EDTA solution (0.05 M, pH 8.2). Klein *et al.* [23] carried out dissolution tests on HAp and β-TCP with various values of porosity in buffered lactic acid solution. The dissolution rate of β-TCP was three times higher than that of HAp. And it was

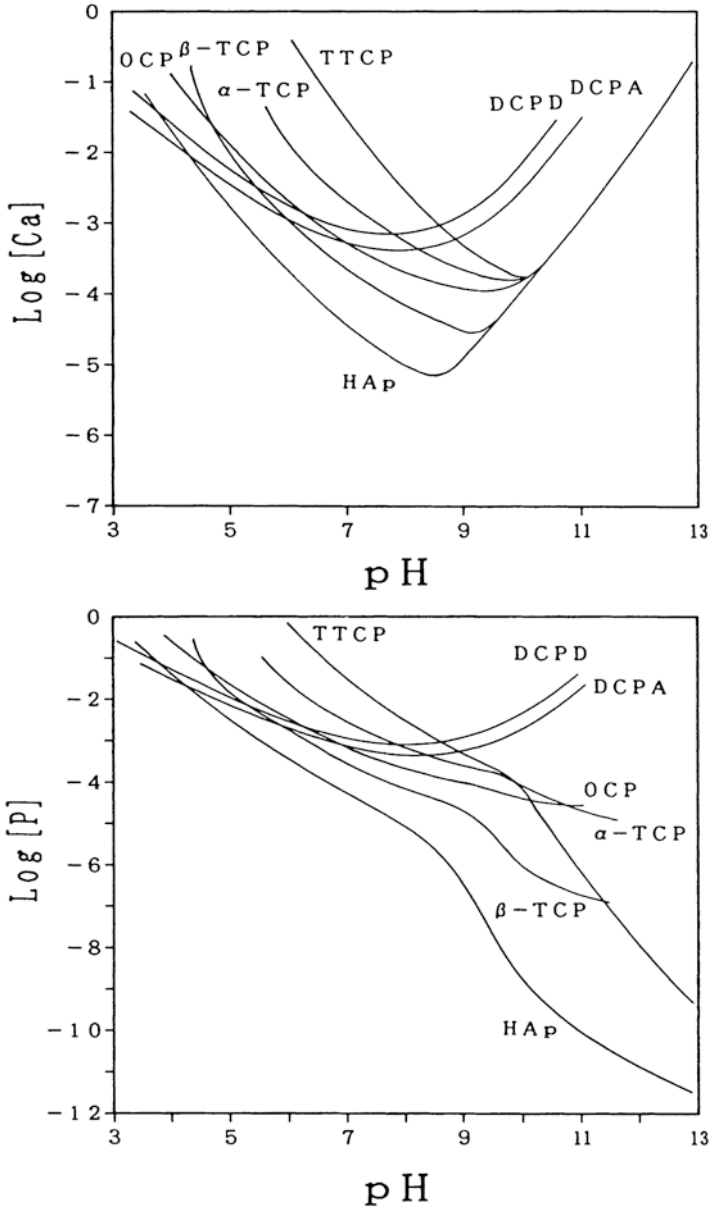


Figure 9.1 Solubility phase diagram for the ternary system $\text{Ca}(\text{OH})_2\text{-H}_3\text{PO}_4\text{-H}_2\text{O}$ at 37°C [18].

concluded that the degradation rates of these materials were determined by neck dissolution rate and neck geometry, the latter factor being dependent on the crystallography and stoichiometry of the material and of the sintering conditions. Ducheyne *et al.* [15] compared the dissolution rate and the precipitation rate of the following six calcium phosphates in calcium and phosphate free solution with pH 7.3. The dissolution rate increased in the following order:

$$\text{HAp} < \text{CDAp} < \text{OHAp} < \beta \text{ TCP} < \alpha \text{ TCP} < \text{TTCP}$$

and the precipitation rate increased as follows:

$$\beta \text{ TCP} < (\text{HAP and } \alpha \text{ TCP}) < \text{CDAp}$$

(CDAp; Ca-deficient HAp, OHAp; dehydroxylated HAp)

The precipitate that formed on CDAp was apatitic; on the other hand, the precipitates on HAp and β -TCP had a much lower Ca/P. In TTCP, the precipitate was calcium deficient carbonate containing hydroxyapatite. Niwa *et al.* [24] evaluated the concentration of calcium and phosphate ions being slightly dissolved in saline solution from HAp sintered at the temperature range from 250 to 1250 °C. It was concluded that the sintering temperature was closely related to the crystallinity and the amount of dissolution of the material. Maximan *et al.* [25] compared the dissolution rate of plasma spray coated amorphous HAp and poorly crystallized HAp by exposure to Hank's physiological solutions (pH 7.2 and 5.2). The poorly crystallized HAp coating showed faster resorption, greater surface film precipitation and greater chemical changes than amorphous HAp coating.

9.3 In Vivo/in Vitro Biological Degradation Processes

Biological degradation processes have been investigated either by animal experiments *in vivo* and clinical applications or by cell cultures *in vitro*. These results were obtained by observing the remaining implanted materials and the behavior of each cell around the materials.

9.3.1 Animal experiments and clinical applications

Most of the implanted calcium phosphate materials that were used in animal experiments and clinical applications were TCP, HAp and calcium phosphate glasses. Table 9.2 shows major reports of these investigations.

Most of the reports on TCP have concluded that TCP is biodegradable although there are some differences depending on the characteristics of the materials used. Bhaskar *et al.* [26] concluded that this biodegradation of TCP was caused by the

Table 9.2 Biodegradation of calcium phosphate compounds *in vivo*.

Implanted material (sintering temp., porosity or density)	Implantation	Duration	Biodegradation	Reference
• TCP (plug)	Tibia of rats	14 weeks	Progressive decrease	26
• TCP (pellet)	Tibia of rats	48 days	95% of implant was degraded	27
• β -TCP (porous plug) [36%]	Femur of dogs	4 months	Considerable resorption	28
• TCP and TTCP (porous cylinder) [45%]	Tibia of dogs	10 months	TCP; resorbed TTCP; unchanged	29
• TCP (block)	Vertebrae cervicales of dogs	22 weeks	Partially resorbed (implants were crushed)	30
• HAp and β -TCP (ten types of micro and macro porous cylinder)	Tibia of rabbits	9 months	HAp: no resorption TCP: more or less degradable	31
• β -TCP (seven types of micro and macro porous cylinder)	Tibia of rabbit	12 months	Microporous>macroporous porous cylinder) reduced by addition of Mg ²⁺ , F-	32,33
• HAp and TCP (porous block) [HAp: 1300 °C – 56%, TCP: 1150 °C – 50%]	Femur of dogs	50 weeks	HAp: no resorption TCP: 25–30% (in 22 weeks)	34
• Coral (porites) – HAp (porous block)	Mandible of dogs	1 year	29% of implant	35
• Coral (goniopora) – HAp (porous block)	Tibia of dogs	1 year	No bioresorption	36
• Coral (porites and goniopora) – HAp (porous block)	Animal studies	12 months	Minimal	37,38
• Coral (goniopora) – HAp and TCP [36%]	Clinical application	15 months	No degradation	
	Animal experiments	1 year	Coral-HAp: not apparent	39
	Clinical application	4 years	TCP: observed in many cases	
• HAp (three types of dense block) [900°C – 97%, 1200 °C – 97 and 99.9%]	Dorsal muscle and tibia of rats	6 months	No degradation (no difference in three types)	40
• HAp (porous blocks) [1300°C, 56%]	Femur of dogs	3.5 years	Negligible	41
• HAp (porous blocks) [900 and 1200°C, 86%]	Tibia of dogs	2 years	Slow bioresorption (900°C> 1200 °C)	42
• HAp (macro and micro porous blocks) [macroporosity: 26%, microporosity: 5%]	Middle ear of rats	1 year	Resorption by 15–20 μ m during the first yr.	43,44

Implanted material (sintering temp., porosity or density)	Implantation	Duration	Biodegradation	Reference
<ul style="list-style-type: none"> • DCPD, DCPA, OCP, α- and β-TCP; HAp, amorphous HAp Bioglass (granule sizes of 100–300 and 10 μm) 	Femur of rabbits	12 weeks	(α - and β -TCP) < (DCPD, DCPA, TTCP) < (amorphous HAp, OCP)	45
<ul style="list-style-type: none"> • MBCP (macroporous blocks) [40–50%] (60% HAp + 40% β-TCP) 	Animal experiments Clinical application	18 weeks 16 months	Initially fast (~1 month)	46
<ul style="list-style-type: none"> • Plasma sprayed HAp (cylindrical plug) 	Tibia of rabbits	3 months	Loss of coating thickness	47
<ul style="list-style-type: none"> • Plasma sprayed HAp, TTCP, MWL (cylindrical rod) (crystallinity of HAp: 10, 60, 95%) 	Femur of rats	4 weeks	60%-HAp and TTCP: distinct bulk degradation, 10%-HAp: gradual surface degradation 95%-HAp and MWL: negligible	48
<ul style="list-style-type: none"> • Plasma sprayed HAp, F Ap, MWL (cylindrical plug) 	Femur and humerus of goats	25 weeks	HAp: considerable and progressive reduction, MWL: considerable reduction in thickness, FAp: no degradation or dissolution	49
<ul style="list-style-type: none"> • Bioglass (SiO₂-P₂O₅-CaO-Na₂O system) 	Femur of rats	6 weeks	Silica-rich layer and Ca-P rich layer formation	51
<ul style="list-style-type: none"> • A-W glass-ceramics (MgO-CaO-SiO₂-P₂O₅-CaF₂ system) 	Tibia of rabbits	25 weeks	Ca-P rich layer formation	53

Table 9.3 Biodegradation of calcium phosphate compounds *in vitro*

Substrate (sintering temp., porosity or density)	Strain	Incubation	Biodegradation	Reference
HAp and β -TCP (granule, <50 μ m)	Human bone cell	7 days	Human bone cell are capable of ingesting HAp and TCP granules	54
HAp (dense disc; three types of surface rugosities) [1130°C]	Rat bone marrow cell	8 days	Osteoclast-like cells are capable of resorbing HAp	55
HAp (dense disc; three types of porosity [dried at 200°C, unsintered])	Rat bone marrow cell	7 days	Osteoclast-like cells are capable of resorbing HAp	56
Plasma sprayed HAp (crystallinity; 15,43,69%)	Rat bone marrow cell	18 days	15 & 43%: rapidly degraded 69%; degradation rate was reduced	58
Plasma sprayed HAp, FAp, TCP, TTCP, MWL	Rat bone marrow cell	2 weeks	Different bone-bonding and biodegradation properties	59

phagocytosis of the mesenchymal cells. Cameron *et al.* [28] stated that the ingestion by giant cells did play a significant role in the degradation of TCP although passive dissolution occurred. Klein *et al.* [32, 33] stated that the micro-pores played an important role in the biodegradation rate of TCP. The degradation of TCP started mostly from the medulla by solution mediated disintegration processes, and fine particles released were phagocytosed and removed by macrophages in the medulla to the lymph nodes. Renooij *et al.* [35] reported that HAp was not affected by biodegradation processes, while TCP was subject to extensive bioresorption. Resorption debris from TCP was found in mononuclear phagocytes and multinuclear osteoclastlike cells. Although multinuclear cells were occasionally seen near the surface of HAp, cells carrying HAp debris were never observed. And it was supposed that TCP was transformed into HAp in a physiologic environment.

Concerning the biodegradation of HAp, there are reports in the case of no degradation, slow or partial degradation and for the degradable case. The differences in these results are dependent on the experimental conditions such as the characteristics of the materials, animal species, implanted sites and methods of observation.

Holmes *et al.* [35–39] carried out investigations using HAp which was derived from marine coral and reported the results as follows. Significant biodegradation occurred when implanted in load bearing sites such as mandibles, while minimal biodegradation was observed in cortical bone of radius and no apparent evidence of biodegradation was observed in cancellous bone of tibia. In clinical applications, radiographic observations did not show any irrefutable evidence of biodegradation and history of biopsies showed no conclusive evidence of biodegradation, while osteoclasts were occasionally seen along the implant surface. In contrast to these results, degradation of TCP appeared to occur by passive dissolution and osteoclas-

tic resorption, and in many cases it was radiographically observed in clinical trials, especially where the implant was applied in a diaphyseal onlay fashion. Denissen *et al.* [40] reported no degradation of three different dense HAp varying in its density. Similarly, Hoogendoorn *et al.* [41] reported through their long-term study that porous HAp did not undergo biodegradation during 3.5 years of implantation, while giant multinucleated cells were occasionally seen in pores near the bone and ceramic surface.

On the other hand, Kurosawa *et al.* [42] observed the degradation of highly porous HAp in their experiments, and concluded that this degradation was caused in two ways; the mechanical collapse of the material and the ingestion of fine particles released from the HAp surface by multinuclear giant cells. Similarly, Blitterswijk *et al.* [43, 44] observed in their implantation experiments with dense and macroporous HAp that the deposition of calcium, partially in the form of calcium phosphate, was found on the implant surface, and the resorption of the implant occurred as the result of phagocytosis by mono- and multi-nuclear cells. Oonishi *et al.* [45] compared bioactivity for bone formation in several kinds of bioceramics. These materials were divided into three groups; bioinert ceramics (alumina), surface bioactive ceramics (HAp and Bioglass), and resorbable bioactive ceramics (DCPD, DCPA, OCP, α -TCP, β -TCP, TTCP and amorphous HAp). In resorbable bioactive ceramics, bioactivity or bioresorbability might increased in the following order:

$$(\alpha - \text{ and } \beta - \text{TCP}) < (\text{DCPD, DCPA and TTCP}) \\ < (\text{amorphous HAP and OCP})$$

Daculsi *et al.* [46] stated that the bioresorption of macroporous biphasic calcium phosphate consisting of HAp and β -TCP was conducted by multinucleated cells (osteoclastlike cells) and was related to the β -TCP content of this material. Bruijn *et al.* [48] and Dhert *et al.* [49] compared the degradation of plasma spray coated TTCP, MWL (magnesium whitlockite) and three types of HAp with various degrees of crystallinity. It was revealed that both TTCP and semi-crystalline HAp underwent distinct bulk degradation and amorphous HAp showed a gradual surface degradation, while the degradation was negligible with the highly crystalline HAp and MWL. Biodegradation appeared to be related to bone apposition, since more bone seemed to be present on amorphous HAp and TTCP, as compared to highly crystalline HAp and MWL. The degrading surface of TTCP and amorphous HAp coatings was most likely a dynamic zone in which dissolution and reprecipitation occurs. This zone was therefore thought to be favourable for rapid bone formation and bonding. At the interface between bone and MWL, a seam of unmineralized bone-like tissue was frequently seen, and a substantial amount of aluminum was detected in the MWL coating and the unmineralized bone-like tissue, which might cause the impaired mineralization.

Since the discovery of Bioglass by Hench *et al.* [50], various kinds of bioactive glasses and glass ceramics have been developed and applied clinically. Hench *et al.* [51] summarized their study on Bioglasses which were based on the $\text{SiO}_2\text{-P}_2\text{O}_5\text{-}$

CaO–Na₂O system. When a bioactive glass was immersed in an aqueous solution, three general processes occurred; leaching, dissolution and precipitation. In these reactions, hydrated silica was formed on the glass surface, resulting in a silica-rich gel layer, and then a calcia-phosphate-rich layer was formed on or within the gel layer. This layer was initially amorphous and later crystallized to a hydroxycarbonate apatite structure to which bone could bond. Kokubo *et al.* [52] developed A-W glass-ceramics which was based on the MgO–CaO–SiO₂–P₂O₅–CaF₂ system. In this material, oxyfluorapatite [Ca₁₀(PO₄)₆(O,F₂)] and β-wollastonite [CaO · SiO₂] both in the form of rice grain-like particles were dispersed in an MgO–CaO–SiO₂ glass matrix. In their experiments [53] it was shown that a thin layer, rich in Ca and P, was formed on the surface of this material. This Ca, P-rich layer was identified as a layer of apatite, and this material was observed to be closely connected to the surrounding bone through this apatite layer without any distinct boundary. The same type of apatite layer was formed on the surface of this material exposed to the simulated body fluid, and consisted of carbonate-containing hydroxyapatite of defective structure and small crystallites. It was concluded that this apatite layer played an essential role in forming the chemical bond of all bioactive materials which bonded to bone.

9.3.2 Cell cultures

To study biodegradation and interfacial bonding phenomena, *in vitro* cell culture systems have been developed. Gregoire *et al.* [54] investigated the influence of calcium phosphate on human bone cell activities and demonstrated that the isolated human bone cells were capable of ingesting HAp and β-TCP granules. And the capacity for ingesting a synthetic mineral component clearly suggested that bone cells were able to participate in the degradation of calcium phosphates. Gomi *et al.* [55] showed that osteoclasts are capable of resorbing sintered HAp *in vitro* and that the fusion of osteoclast mononuclear precursors was influenced by substratum rugosity. Similarly, Ogura *et al.* [56] demonstrated that osteoclast-like cells were capable of resorbing unsintered calcium phosphate substrata *in vitro*. Bruijn *et al.* [57–59] carried out a series of cell culture tests on various plasma sprayed calcium phosphate compounds and reported the results as follows. Rat bone marrow cells were cultured on plasma sprayed HAp. The cells formed a mineralized extracellular matrix that exhibited several characteristics of bone tissue. Two distinctly different interfacial structures were observed on HAp. An electron-dense layer which was rich in glycosaminoglycans was regularly present. A collagen-free amorphous zone was frequently seen interposed between the electron-dense layer and HAp. In cell culture tests on three types of plasma sprayed HAp varying in degree of crystallinity, an electron-dense layer was clearly visible on a stable, nondegrading crystalline HAp and was frequently observed at the interface of semi-crystalline HAp. An amorphous zone was regularly seen at degrading surfaces of semi-crystalline and poorly crystallized HAp. It was concluded that the crystallinity of plasma sprayed HAp was an important parameter which influenced the establishment of the bony

interface and might, as a result, have an effect on the bone formation rate and bonding strength between HAp and bone tissue. Similarly, rat bone marrow cells were cultured on various plasma sprayed calcium phosphate coatings. Mineralized extracellular matrix was formed on HAp, TCP and TTCP in 2 weeks, and was formed on FAp (fluorapatite) in 8 weeks. It was only occasionally observed in some area on MWL, which phenomenon might have been due to aluminium impurities in the coating. It was concluded that plasma sprayed calcium phosphates would display different bone-bonding and biodegradation properties, depending on their chemical composition and crystal structures.

9.4 Summary

No convincing conclusion has been reached as to the biodegradation mechanisms of bioactive ceramics. Many researchers have reported different results, as described above. These discrepancies are considered to be caused by the fact that materials used for the experiments were different, and that experimental methods and analytical methods were also different. Therefore, when these reported results are compared, it is important to consider the characteristics of the material used (chemical compositions, impurity, crystallinity, dense or porous, micro- or macro-porous, porosity), experimental methods used (*in vivo* or *in vitro*, animal species, implanted duration, implanted sites, load bearing or not), and analytical methods used (radiographic, optical microscopic, electron microscopic). Furthermore, a good understanding of the characteristics of the materials to be used becomes important when bioactive ceramics are used clinically.

References

1. L.C. Chow and W.E. Brown, *J. Dent. Res.*, **54**, 65–16, 1975.
2. F.C.M. Driessens, J.W.E. van Dijk and J.M.P.M. Borggreven, *Calcif. Tissue Res.*, **26**, 127–136, 1978.
3. J.L. Meyer, and, E.D. Eanes, *Calcif. Tissue Res.*, **25**, 59–68, 1978.
4. H. McDowell, W.E. Brown and J.R. Sutter, *Inorg. Chem.*, **10**, 1638–1643, 1971.
5. M.S. Tung, N. Eidelman, B. Sieck and W.E. Brown, *J. Res. Nat. Bur. Stand.*, **93**, 613–624, 1988.
6. J.L. Shyu, L. Perez, S.J. Zawacki, J.C. Heughebaert and G.H. Nancollas, *J. Dent. Res.*, **62**, 398–400, 1983.
7. B.O. Fowler and S. Kuroda, *Calcif. Tissue Int.*, **38**, 197–208, 1986.
8. T.M. Gregory, E.C. Moreno, J.M. Patel and W.E. Brown, *J. Res. Nat. Bur. Stand.*, **78(A)**, 667–674, 1974.
9. E.C. Moreno, T.M. Gregory and W.E. Brown, *J. Res. Nat. Bur. Stand.*, **72(A)**, 773–782, 1968.
10. J.S. Clark, *Can. J. Chem.*, **33**, 1696–1700, 1955.
11. R.M.H. Verbeek, H. Steyaer, H.P. Thun and F. Verbeek, *J. Chem. Soc. Faraday Trans. 1*, **76**, 209–219, 1980.

12. R. Chuong, *J. Dent. Res.*, **52**, 911–914, 1973.
13. A.N. Smith, A.M. Posner and J.P. Quirk, *J. Coll. Inter. Sci.*, **54**, 176–183, 1976.
14. H.McDowell, T.M. Gregory and W.E. Brown, *J. Res. Nat. Bur. Stand.*, **81(A)**, 273–281, 1977.
15. P. Ducheyne, S. Radin, L. King, K. Ishikawa and C.S. Kim, *Bioceramics* vol.4, eds W. Bonfield, G. W. Hastings and K.E. Tanner, Butterworth-Heinemann, London, UK, pp. 135–144, 1991.
16. M.B. Fawzi, J.L. Fox, M.G. Dedhiya, W.I. Higuchi and J.J. Hefferren, *J. Coll. Inter. Sci.*, **67**, 304–311, 1978.
17. M.S. Wu, W.I. Higuchi, J.L. Fox and M. Friedman, *J. Dent. Res.*, **55**, 496–505, 1976
18. L.C. Chow, *J. Ceram. Soc. Japan*, **99**, 954–964, 1991.
19. H. Newesely, *J. Oral Rehab.*, **4**, 97–104, 1977.
20. H. Monma and T. Kanazawa, *Yogyo-Kyokai-Shi*, **84**, 209–213, 1976.
21. R.W. Mooney and M.A. Aia, *Chem. Rev.*, **61**, 433–462, 1961.
22. M. Jarcho, *Cli Orthop. Rel. Res.* **157**, 259–278, 1981.
23. C.P.A.T. Klein, A. A. Driessen and K. de Groot, *Biomaterials*, **5**, 157–160, 1984.
24. J. Niwa, S. Takahasi and M. Sohmiya, *Fineceramics*, **2**, 25–32, 1981.
25. S.H. Maximan, J.P. Zawadsky and M.G. Dunn, *J. Biomed. Mater. Res.*, **27**, 111–117, 1993.
26. S.N. Bhaskar, J.M. Brady, L. Getter, M.F. Grower and T. Driskell, *Oral Surg.*, **32**, 336–346, 1971.
27. D.E. Cutright, S.N. Bhaskar, J.M. Brady, L. Getter and W.R. Posey, *Oral Surg.*, **33**, 850–856, 1972.
28. H.U. Cameron, I. Macnab and R.M. Pilliar, *J. Biomed. Mater. Res.*, **11**, 179–186, 1977.
29. K. Köster, H. Heide and R. König, *Langenbecks Arch. Chir.*, **343**, 173–181,
30. T. Shima, J.T. Keller, M.M. Alvira, F.H. Mayfield and S.B. Dunsker, *J. Neurosurg.*, **51**, 533–538, 1979.
31. C.P.A.T. Klein, A.A. Driessen and K. de Groot, *J. Biomed. Mater. Res.*, **17**, 769–784, 1983.
32. C.P.A.T. Klein, K. de Groot, A.A. Driessen and H.B.M. van der Lubbe, *Biomaterials*, **6**, 189–192, 1985.
33. D.C.P.A.T. Klein, K. de Groot, A.A. Driessen and H.B.M. van der Lubbe, *Biomaterials*, **7**, 144–146, 1986.
34. W. Renooij, H.A. Hoogendoorn, W.J. Visser, R.H.F. Lentferink, M.G.J. Schmitz, H.V. Ieperen, S.J. Oldenburg, W.M. Janssen, L.M.A. Akkermans and P. Wittebol, *Cli. Orthop. Rel. Res.*, **197**, 272–285, 1985.
35. R.E. Holmes, *Plast. & Reconstr. Surg.*, **63**, 626–633, 1979.
36. R.E. Holmes, R.W. Bucholz and V. Mooney, *J. Bone and Joint Surg.*, **68-A**, 904–911, 1986.
37. R.E. Holmes, V. Mooney, R. Bucholz and A. Tencer, *Cli. Orthop. Rel. Res.*, **188**, 252–262, 1984.
38. D.J. Sartoris, D.H. Gershuni, W.H. Akeson, R.E. Holmes and D. Resnick, *Radiology*, **159**, 133–137, 1986.
39. R.W. Bucholz, A. Carlton and R.E. Holmes, *Orthop. Cli. North America*, **18**, 323–334, 1987.
40. H.W. Denissen, K. de Groot, P.Ch. Makkes, A. van den Hooff and P.J. Klopper, *J. Biomed. Mater. Res.*, **14**, 713–721, 1980.
41. H.A. Hoogendoorn, W. Renooij, L.M.A. Akkermans, W. Visser and P. Wittebol, *Cli. Orthop. Rel. Res.*, **187**, 281–288, 1984.
42. H. Kurosawa, T. Iwata, I. Shibuya, K. Murase and Takeuchi, *J. Joint Surg.*, **8**, 1761–1769, 1989.
43. C.A. van Blitterswijk, J.J. Grote, W. Kuijpers, C.J.G. Blok-van Hoek and W. Th. Daems, *Biomaterials*, **6**, 243–251, 1985.
44. C.A. van Blitterswijk, J.J. Grote, W. Kuijpers, W. Th. Daems and K. de Groot, *Biomaterials*, **7**, 137–143, 1986.
45. H. Oonishi, S. Kushitani, T. Sugihara, H. Iwaki, H. Ohashi and E. Tsuji, *Bioceramics* vol. **8**, eds L.L. Hench and J. Wilson, ELSEVIER, New York, 1995.
46. G. Daculsi, N. Passuti, S. Martin, C. Deudon, R.Z. Legeros and S. Raheer, *J. Biomed. Mater. Res.*, **24**, 379–396, 1990.

47. J.A. Jansen, J.P.C.M. van de Waerden, J.G.C. Wolke and K. de Groot, *J. Biomed. Mater. Res.*, **25**, 973–989, 1991.
48. J.D. de Bruijn, Y.P. Bovell and C.A. van Blitterswijk, *Calcium Phosphate Biomaterials: Bone-bonding and Biodegradation Properties*, ed. J.D. de Bruijn, Offsetdrukkerij Haveka B.V., Alblasterdam, pp. 79–92, 1993.
49. W.J.A. Dhert, C.P.A.T. Klein, J.A. Jansen, E.A. van der Velde, R.C. Vriesde, P.M. Rozing and K. de Groot, *J. Biomed. Mater. Res.*, **27**, 127–138, 1993.
50. L.L. Hench, R.J. Splinter, W.C. Allen and T.K. Greenlee, *J. Biomed. Mater. Res. Symp.*, **2**, 117–141, 1971.
51. L.L. Hench and B. Andersson, *Advanced Series in Ceramic – Vol. 1 An Introduction to Bioceramics* eds L.L. Hench and J. Wilson, World Scientific, Singapore, pp. 41–62, 1993.
52. T. Kokubo, S. Ito, S. Sasaki and T. Yamamuro, *J. Mater. Sci.*, **21**, 536–540, 1986.
53. T. Kokubo, *Advanced Series in Ceramics – Vol. 1 An Introduction to Bioceramics*, eds L.L. Hench and J. Wilson, World Scientific, Singapore, pp. 75–88, 1993.
54. M. Gregoire, I. Orly and J. Menanteau, *J. Biomed. Mater. Res.*, **24**, 165–177, 1990.
55. K. Gomi, B. Lowenberg, G. Shapiro and J.E. Davies, *Biomaterials*, **14**, 91–96, 1993.
56. M. Ogura, T. Sakae and J.D. Davies, *Bioceramics* vol. 4, eds W. Bonfield, G.W. Hastings and K.E. Tanner, Butterworth-Heinemann, London, UK, pp. 121–126, 1991.
57. J.D. de Bruijn, C.P.A.T. Klein, K. de Groot and C.A. van Blitterswijk, *J. Biomed. Mater. Res.*, **26**, 1365–1382, 1992.
58. J.D. de Bruijn, J.S. Flachl, K. de Groot, C.A. van Blitterswijk and J.E. Davies, *Calcium Phosphate Biomaterials: Bone-bonding and Biodegradation Properties*, ed. J.D. de Bruijn, Offsetdrukkerij Haveka B.V., Alblasterdam, pp. 45–62, 1993.
59. J.D. de Bruijn, C.P.A.T. Klein, K. de Groot and C.A. van Blitterswijk, *Calcium Phosphate Biomaterials: Bone-bonding and Biodegradation Properties*, ed. J.D. de Bruijn, Offsetdrukkerij Haveka B.V., Alblasterdam, pp. 63–78, 1993.

Chapter 10

Corrosion of Metallic Implants

M.A. Barbosa

10.1 General Aspects

10.1.1 Incidence of corrosion

The surfaces of passive metals are normally attacked at specific points where the oxide film has been destroyed and massive quantities of metal ions are released. Depending on the magnification with which surfaces are observed, various degrees of localized attack can be detected. Sometimes, however, corrosion may not be easily distinguishable from mechanical imperfections associated with manufacturing or handling. Even under the scanning electron microscope (SEM) it is often difficult to distinguish between mechanical indentations and pitting or crevice attack.

After determining the existence of corrosion, the next step is to assess its magnitude. This can be done, by corrosion scores, such as those given in Table 10.1 (Thomas *et al.*, 1988). In this table the ‘no surface degradation’ score is obtained with a magnification of 60x. If a higher magnification was used some ‘non-degraded’ surfaces might fall in one of the ‘surface degradation’ categories. The borderline between ‘corroded’ and ‘non-corroded’) surfaces is therefore very much dependent on magnification, as well as on surface preparation, as explained above. With these limitations in mind, it is useful to have an idea of the incidence of corrosion, i.e. of the percentage of implants that suffer some degree of attack. Table 10.2 compares the data obtained by several authors. Vacuum melting (VM) significantly reduces the susceptibility of 316L stainless steel to attack, while titanium is practically immune. Corrosion, apart from affecting the mechanical performance of the implants, also results in contamination of the tissues with metallic ions.

The detection of ions released from metallic implants is dependent on the technique used. Very minute amounts of ions can be detected by electrothermal atomic

M.A. Barbosa (✉)
INEB-Ma, Rua do Campo Alegre 823, 4150 Porto, Portugal

Table 10.1 Grading scale used to evaluate the degree of interface and surface corrosion (*Thomas et al.*, 1988)

0 = no surface degradation visible at 60x magnification
1 = very mild surface degradation visible at 60x magnification
2 = mild surface degradation visible at 60x magnification
3 = moderate surface degradation visible without magnification
4 = heavy surface degradation visible without magnification
5 = very heavy severe surface degradation visible without magnification

Table 10.2 Incidence of corrosion

Implant/material	Corroded implants	Ref
38 fixation devices/AISI 316L	95%; crevice corrosion	Thomas <i>et al.</i> , 88
43 miniplates/AISI 316LVM*	19%; only at the countersinks	Torgersen and Gjerdet, 94
19 miniplates/c.p Ti	0%	Torgersen and Gjerdet, 94

* VM – Vacuum melted

absorption spectroscopy (ET-AAS), which goes down to concentrations of the order of ng/g. Electrochemical methods enable the detection of extremely low corrosion current densities, below $1 \mu\text{A}/\text{cm}^2$ corresponding to dissolution in the passive state. These rates of corrosion do not modify the aspect of the surface and are not normally considered as surface attack.

10.1.2 Potential-pH (Pourbaix) diagrams

These diagrams indicate the regions of immunity, passivation and corrosion of pure metallic elements in pure water at 25°C. Fig. 10.1 (a, b) gives the potential-pH diagrams of Cr and Ti. Cr is the element responsible for the passive behaviour of stainless steels and Co-Cr-Mo alloys. In Fig. 10.1a passivation by a Cr(OH)₃ film is assumed. The film is thermodynamically stable over a wide range of pH and potential values. Below pH 4 the film is unstable and Cr is corroded. Ti is responsible for the excellent corrosion resistance of Ti-Al-V alloys. In Fig. 10.1b passivation by a hydrated TiO₂ · nH₂O oxide has been assumed. The passivation region extends to much higher potentials than in the case of Cr. The passive film is unstable below pH 2.5. In both diagrams the dotted lines give the region of stability of water: below line *a* hydrogen is evolved, whereas above line *b* oxygen is released. Normally, the corrosion potentials of implant materials do not reach such extreme values.

In spite of their usefulness in predicting the stability of metals and their oxides, potential-pH diagrams suffer from a number of limitations. They refer to pure metals, not to alloys, and to pure water, not to environments normally found in practical situations. For example, the diversity of chemical species, and particularly the presence of chloride ions in physiological media, is responsible for substantial differences between practical and predicted behaviour. Localized attack, in the form of crevice, pitting and corrosion fatigue, is due to the presence of chloride. Furthermore, the kinetics of metal

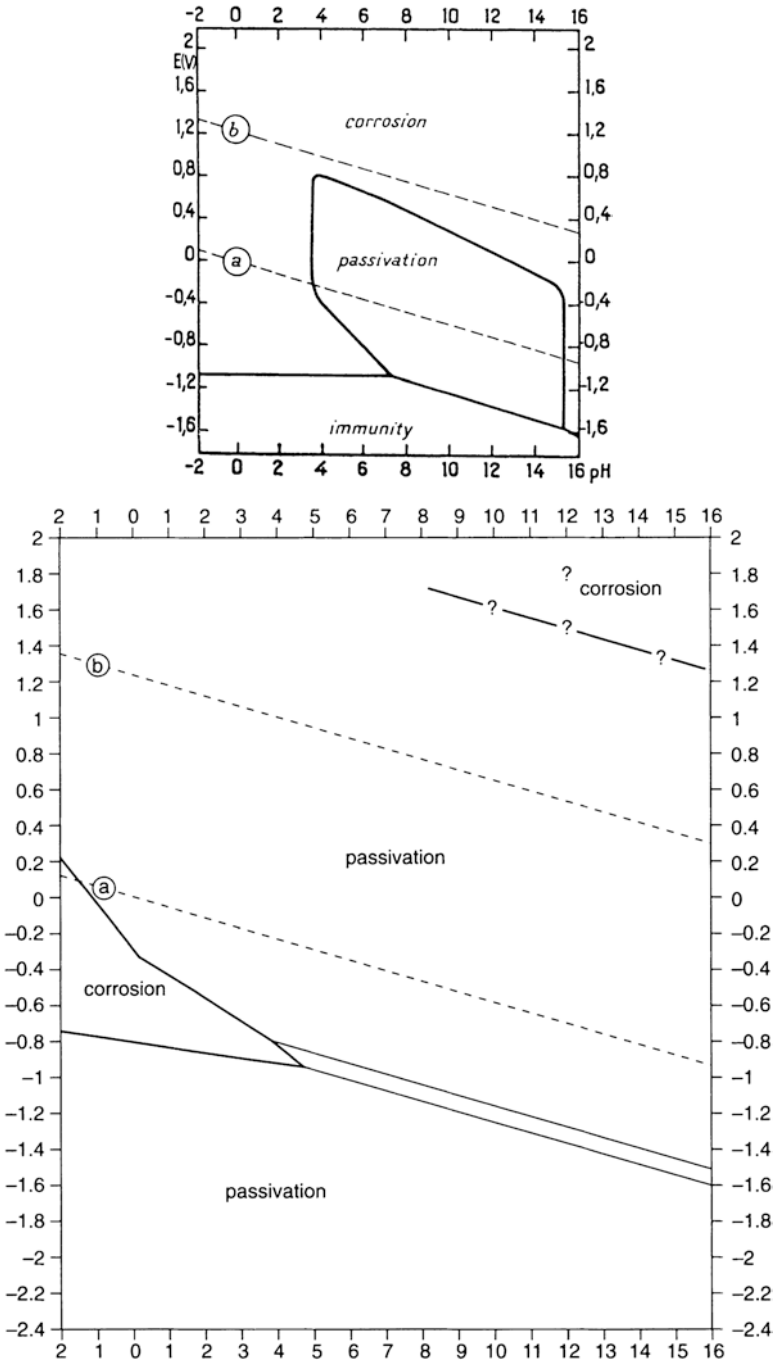


Fig. 10.1 (a) (b) Theoretical domains of corrosion, immunity and passivation of titanium, at 25°C, considering Tiltz (Pourbaix, 1971).

dissolution or passivation cannot be assessed by these diagrams, which are purely thermodynamic. However, if not misused, potential-pH diagrams can give useful information which must be complemented by other type of data, namely of kinetic nature.

10.2 Aspects Related to the Metal Composition

10.2.1 Importance of materials purity in improving the corrosion resistance

The evolution of stainless steel composition can be used to illustrate the importance of materials purity in reducing corrosion susceptibility. Chromium and molybdenum are the key elements in promoting resistance to pitting and crevice attack of stainless steels, but high chromium and molybdenum concentrations are not sufficient to ensure an adequate corrosion resistance. Low concentrations of impurities, like carbon, silicon, phosphorous and sulphur, are required. Type 316L and 316LVM stainless steels are commonly employed to fabricate a variety of fracture fixation devices. They both have low carbon concentration, below 0.03 wt%, which is indicated by the letter L. VM stands for vacuum-melted, a technique that enables the production of metals with very low concentrations of impurities.

A retrieval analysis of Kuntscher intramedullary rods (Cook *et al.* 1990) has shown that significant surface corrosion, inclusion content and carbon content occurred on early materials, which had remained *in situ* for 10 years or longer (maximum 23 years). Significant relationships were obtained for surface corrosion score vs. thin globular oxide inclusion content, and for surface corrosion score vs. sulphide inclusion content. Fig. 10.2 shows the data obtained for the former correlation.

10.2.2. Type of metallic material and influence of alloying

Due to the presence of a thin oxide film, titanium has a very high corrosion resistance. However, its low resistance under wear conditions may lead to enormously high titanium concentrations in tissues adjacent to titanium implants (section 9.3.1). Rapid film formation after surface damage is therefore of critical importance to guarantee low levels of titanium ions.

The current density (c.d.) required to form a passive film is called the critical c.d. for passivation, i_c . The lower i_c the better. Fig. 10.3 shows that Zr, Nb, Ta and Pd decrease i_c , whereas Sn increases it. It has been found (Okazaki *et al.* 1994) that i_c can be related to the percentages of Pd, Ta, Nb, Zr and Sn by the following expression

$$i_c(\text{A.m}^{-2}) = 10^{-2}\{98-89.5[\%Pd] - 9.5[\%Ta] - 3.4[\%Nb] - 0.67[\%Zr] + 8[\%Sn]\}$$

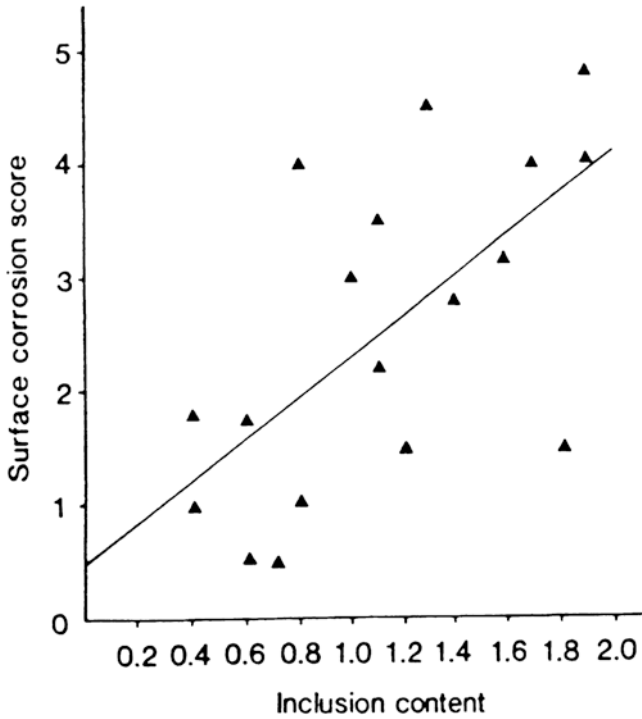


Fig. 10.2 Relationship between surface corrosion and thin globular oxide inclusion content. Regression line $y = 1.78x + 0.52$, $r = 0.65$, $n = 18$, $p < 0.05$. (Cook *et al.*, 1990.)

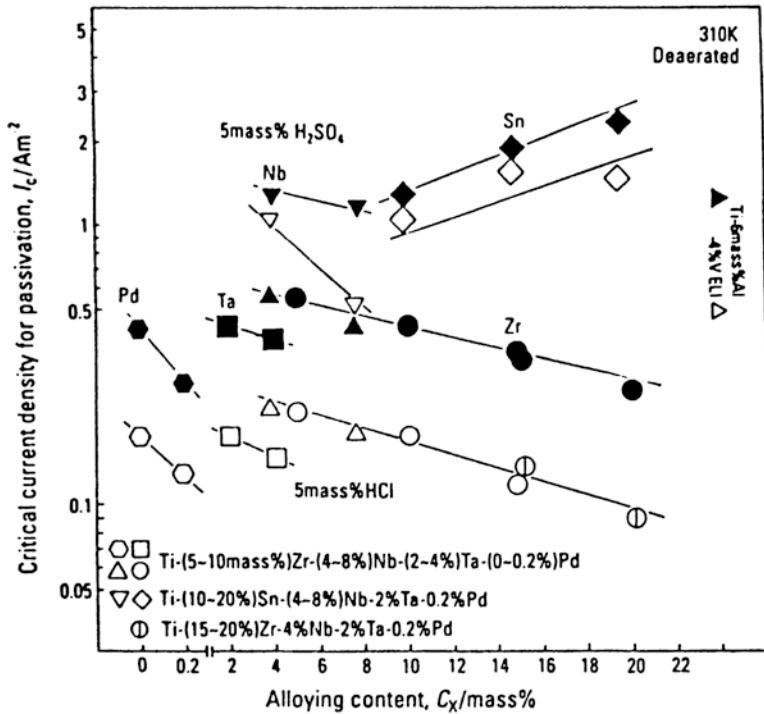


Fig. 10.3 Effects of Zr, Nb, Ta, Pd and Sn contents critical current density for passivation in 15% H₂SO₄ and 5% HCl solutions at 310 K. (Okazaki *et al.*, 1994.)

A new alloy, Ti-15Zr-4Nb-2Ta-0.2Pd, with better corrosion resistance than the conventional Ti-6Al-4V, was proposed by the same authors.

Replacement of Nb for V, in order to eliminate the possible toxic effects of the latter, has been carried out (Semlitsch *et al.*, 1992). Ti-6Al-7Nb showed a corrosion resistance similar to that of Ti-6Al-4V, as concluded from anodic polarization curves (Fig. 10.4).

Although not as widely used as titanium, tantalum has found a number of applications, e.g. in vascular clips, as a suture and to fabricate flexible stents to prevent arterial collapse. The reader is referred to a paper by J. Black (1994), where the material properties are reviewed, together with the host response and clinical applications. In terms of corrosion resistance, tantalum is at least equivalent to titanium. Its oxide, Ta₂O₅, is very stable over very wide pH and potential ranges, thus explaining the excellent corrosion resistance. According to Black, high cost and difficulties of fabrication are some of the reasons for its limited usage.

Cr and Mo are the major alloying elements responsible for the corrosion resistance of stainless steels. These alloys are also very sensitive to inclusion content, which has led to continuous attempts to reduce impurity concentrations. F138 and F139 are variations of the AISI 316L stainless steel with a lower content of non-metallic inclusions. A duplex stainless steel, 25Cr-7Ni-4Mo-0.25N, shows a better corrosion resistance than conventional austenitic stainless steels (Cigada *et al.*, 1989). The authors have established the following ranking: 23Cr-4Ni < AISI 316L < ASTM F138 < 22Cr-SNi-3Mo < 27Cr-31Ni-3.5Mo < 25Cr-7Ni-4Mo-N.

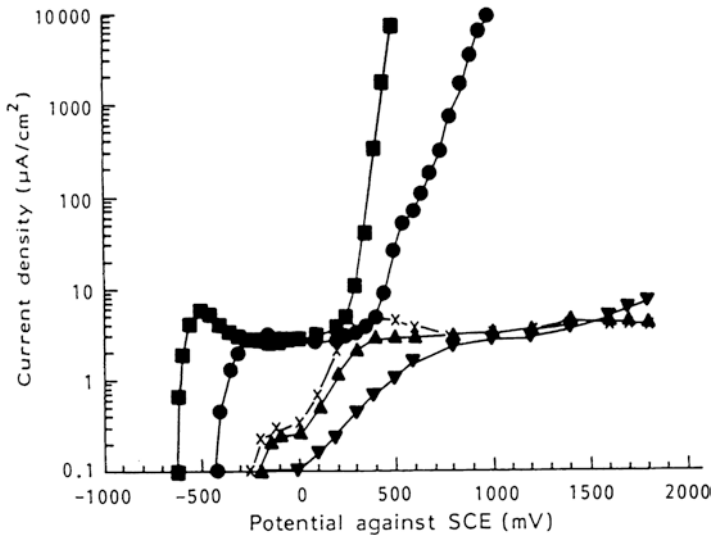


Fig. 10.4 Current density/potential curves of five different implant materials in Ringer's solution bubbled through with nitrogen. ■ AISI 316L; ● CoNiCrMo; ▲ Ti6Al-7Nb; ▼ CP-titanium; x Ti-6Al-7Nb/ODH. (Semlitsch *et al.*, 1992.)

10.2.3 *Site for attack*

Normally, pitting initiates at non-metallic inclusions. In stainless steels sulphides are particularly prone to attack. Oxide inclusions may also give origin to attack, but they are less active than sulphides. Carbides may also nucleate pitting attack and when they are numerous at grain boundaries they may give rise to intergranular corrosion. However, with surgical grades of stainless steels this type of attack should not occur. Crevice corrosion is also common with stainless steels and less frequent with Co-Cr alloys. Sintered beads of Co-Cr-Mo alloy have been studied by scanning electrochemical microscopy (Gilbert *et al.*, 1993a). At any time, some grains were more active than others, whereas at later stages shifting of the active regions occurred. Titanium is immune to both types of corrosion under static conditions. Sliding between titanium and another material (e.g. cement, polyethylene or bone) may originate severe degradation by corrosive wear.

10.2.4 *Combinations of different materials*

The need to combine different materials may sometimes arise. An example is the use of hard materials for the head of hip joints in combination with a titanium stem. Titanium has a very high corrosion resistance, but a very poor wear resistance. Therefore, either surface hardening treatments (e.g. ion implantation of nitrogen or surface alloying) or a harder material, e.g. a ceramic, are employed for the femoral head. Ceramics, like alumina or zirconia, do not cause enhanced electrochemical dissolution of the titanium stem because of their low electronic conductivity. However, when another metal (e.g. Co-Cr-Mo alloy) is used instead, the possibility of a galvanic couple between the stem and the head being formed exists. The situation illustrated by this example can be extended to other couples, including those involving carbon. Even in the case of hard coatings galvanic couples between the coating and the substrate may form.

In a first approximation, the safety of couples involving different materials can be predicted by a number of experimental techniques. Table 10.3 summarizes the data obtained by several authors. Notice that the couples between stainless steel and other materials is unsafe. On the contrary, TiAlV/CoCrMo, CoCrMo/C and TiAlV/C combinations may be considered safe. However, repeated fracture of the oxide film at the conical taper region between head and stem of Ti6Al4V/CoCr combinations has been associated with corrosion. Attack also occurred in CoCr/CoCr combinations and was proportional to the duration of implantation, as seen in Fig. 10.5 (Gilbert *et al.*, 1993b). A larger percentage (34.5%) of cases of corrosion was found with mixed CoCrffiAlV systems than with CoCr/CoCr systems (7%) (Cook *et al.*, 1994). Corrosion occurred at the interface between head and neck of modular components. No correlation between the presence or extent of corrosion with the time *in situ* was found. In another study the percentage of corroded tapered

Table 10.3 Predicted behaviour of galvanic couples (Barbosa, 1991)

Couple	Behaviour
TiAlV/C	Safe
CoCrMo/C	Safe
TiAlV/CoCrMo	Safe
316L S.S./C	Unsafe
316L S.S./TiAlV	Unsafe
316L S.S./CoCrMo	Unsafe

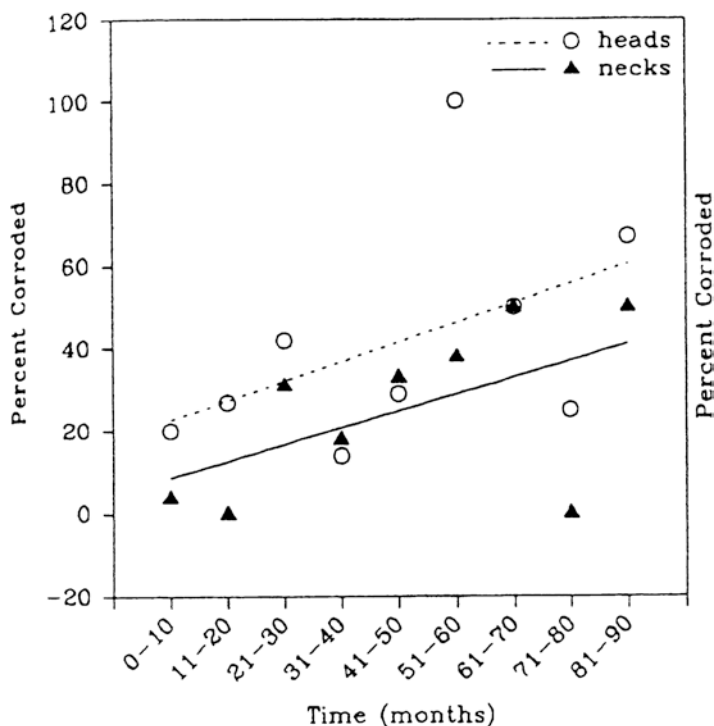


Fig. 10.5 Graphs summarizing the percentage of mixed metal components which show signs of moderate to severe corrosion as a function of duration of implantation. The dotted regression line was fit to the data for the heads (O) and the solid line was fit to the data for the necks (▲). (Gilbert *et al.*, 1993b.)

connections between titanium-alloy stems and cobalt-alloy heads was found to be about 57% (Collier *et al.*, 1991). Titanium-titanium and cobalt-cobalt alloy combinations did not result in interfacial corrosion. 85% of prostheses made of dissimilar materials exhibited corrosion 24 months or more postoperatively. The data indicate that a correlation exists between corrosion and time of implantation.

In view of the above clinical data it is advisable to avoid using dissimilar metals for modular hip prostheses. The occurrence of fretting corrosion at the taper region is responsible for the release of metallic ions that may have cytotoxic effects.

Laboratory galvanic current measurements can be very useful in the pre-screening of materials. For instance, in a study on dental implant bridges it has been reported that silver-palladium, when brazed to titanium, corrodes *in vitro* (Ravnholt and Jensen, 1991), thus eliminating the need to carry out *in vivo* tests.

As a final note it must be stressed that laboratory static tests should only be used to eliminate dangerous metal-metal combinations, and not as an acceptance criterion. Fretting may substantially alter the properties of the interface, by continuously removing the passive oxide film, thereby inducing severe attack of a metal which, otherwise, would remain unaffected.

10.3 Aspects Related to The Physiological Environment

10.3.1 Contamination of tissues by corrosion products

Contaminations of tissue with metals may have two origins. The first is the release of ionic species resulting from the process of electrochemical dissolution of the implant. This is normally associated with static corrosion. Under dynamic conditions, and particularly when fretting occurs, small metallic particles detach from the surface, and become embedded in the soft tissue around the implant. The fate of these particles may vary, depending on their size and chemical nature. They may, for instance, undergo a process of corrosion, with the consequent release of metal ions. This process may take place both in the extracellular matrix or as a result of macrophage activity. Table 10.4 gives the concentration of Cr, Ni, Fe and Co in biological samples. It shows that tissues around implants may be orders of magnitude richer in these metallic elements than normal blood or normal bone.

Titanium has a tendency to accumulate in tissues. The concentrations can be very high, as indicated in Table 10.5. Titanium was not excreted in the urine of hamsters

Table 10.4 Concentration of metallic elements in biological samples (Barbosa, 1992)

Sample		Cr	Ni	Fe	Co
Normal blood*		2-6	3-7	200-680	0.1-0.2
		ppb	ppb	ppm	ppb
Normal bone*		460	900	91	
		ppb	ppb	ppm	
Tissue around	316SS	10000	1400	20000	
Implants (max)**		ppm	ppm	ppm	
	Co-Cr-Mo	10200	1500	3650	22000
		ppm	ppm	ppm	ppm

* Wet weight; data from Tsalev and Zaprianov, 1983.

** Concentrations in dry tissue; data from Pohler, 1983.

ppm: Parts per million.

ppb: Parts per billion

Table 10.5 Concentration of titanium in tissues surrounding titanium implants

Tissue	Concentrations (ppm)	Ref.
Bone	<2100	Ducheyne, 1984
Soft tissue	2000	Meachim, 1973
Soft tissue	56–3700	Agins, 1988

injected with metal salts (Merritt *et al.*, 1992). Small concentrations were found in the serum, red blood cells and organs. Only 5.5% of the injected titanium was found in the kidneys, liver, lung and spleen tissues. The authors suggest that titanium accumulates at the injection site due to the high stability of the titanium dioxide that is formed at physiological conditions. In the same study nearly all the injected vanadium was recovered in the urine. This behaviour is similar to that of nickel and cobalt, and is related to the formation of highly soluble compounds.

High concentrations of metals were found in capsule and fibrous membranes of loose titanium and Co-Cr stems of total hip prostheses (Dorr *et al.*, 1990). The same work reports elevated metal ion concentrations in synovial fluid and blood whenever cemented and uncemented stems are loose, but no increase when they are fixed. The average values are given in Table 10.6. The standard deviations (not shown) were often very large, of the order of magnitude of the averages.

Polyethylene wear debris may artefactually contribute to high ion readings in periprosthetic tissues, as indicated in Tables 10.7 and 10.8 (Meldrum *et al.*, 1993). The high concentrations found in UHMWPE are due to the manufacturing processes. These tables show that there are statistically significant increases in Co, Al and Ti in the nonarticulated inserts with respect to bar stock. In retrieved implants, large increases with respect to bar stock were found for Cr, Mo, Ti and V. The role of UHMWPE wear debris would be twofold: irritant to tissues and source of metal ions.

The accumulation of metal ions in periprosthetic tissue is a combination of two sources: the extracellular matrix and the cells themselves. The ability of fibroblasts to incorporate metal cations is a linear function of concentration, up to 50% toxicity concentrations, for Ag⁺, Au⁴⁺, Cd²⁺, Cu²⁺, In³⁺, Ni²⁺, Pd²⁺ and Zn²⁺ (Wataha *et al.*, 1993), as illustrated in Fig. 10.6 for Cu²⁺, Ni²⁺ and Pd²⁺. By measuring the slope of the lines in this figure it is possible to estimate the uptake efficiency (Table 10.9). The efficiency is highest for In³⁺ and lowest for Pd²⁺. Two years after implantation of femoral components made of Ti-6Al-4V, the titanium and aluminium concentrations measured in the synovial fluid were higher for cemented components than for the uncemented (200 µm HA, or porous Ti coatings) components (Karrholm *et al.*, 1994). Table 10.10 gives the data for the synovial fluid and the aluminium concentrations in serum and urine. No significant concentrations of vanadium were found in any of the samples, which was also the case for titanium in serum and urine. Fast clearance of vanadium from the synovial fluid, due to high solubility of vanadium complexes, and formation of stable titanium compounds,

Table 10.6 Concentration ($\mu\text{g/l}$) of metals in tissues and blood retrieved during total arthroplasty of cementless stems (Dorr *et al.*, 1990)

Sample	TiAlV stems			CoCr stems			
	Ti	Al	V	Co	Cr	Mo	Ni
SF	556	654	62	588	385	58	32
SF (control)	13	109	5	5	3	21	5
CAP	1540	2053	288	821	3329	447	5789
CAP (control)	723	951	122	25	133	17	3996
FM	20813	10581	1027	2229	12554	1524	13234
Blood	67	218	23	20	110	1524	29
Blood (control)	17	12.5	5.8	0.1–1.2	2–6	0.5–1.8	2.9–7.0

SF – synovial fluid; CAP – capsule; FM – fibrous membrane.

Table 10.7 Cobalt-chrome alloy ion concentrations in UHMWPE *et al.* material and manufactured and retrieved inserts (Meldrum *et al.*, 1993)

	Co	Cr	Mo	Ni
Bar stock, n=3	55 \pm 5	330 \pm 5	5*	650 \pm 5
Manufactured inserts, n=9	440 \pm 250	520 \pm 440	5*	490 \pm 600
Retrieved, n=18(all cemented inserts)	54 \pm 42	1,500 \pm 1,400	87 \pm 120	1,360 \pm 1,300

All concentrations are in parts per billion (nanograms/gram).

* This is the minimum detection limit of the spectrometer.

Table 10.8 Titanium alloy ion concentrations in UHMWPE material and manufactured and retrieved inserts (Meldrum, *et al.* 1993)

	AL	Ti	Va
Bar Stock n=3	5*	5*	5*
Manufactured inserts, n=9	800 \pm 200	2300 \pm 980	60 \pm 95
Retrieved, n=21 (all metal backed)	5*	6700 \pm 4500	220 \pm 410

All concentrations are in parts per billion (nanograms/gram).

* This is the minimum detection limit of the spectrophotometer.

e.g. titanium phosphates (Ribeiro *et al.*, 1995), might be reasonable explanations for these findings.

Experiments with metal salts and with stainless steel and Co–Cr–Mo electrodes corroded *in vivo* by applying anodic potentials showed that all the nickel and most of the cobalt were rapidly excreted (Brown *et al.*, 1988). Acceleration of corrosion by the use of anodic potentials obeys similar mechanisms both *in vivo* and in saline when a potential of 500 mV vs. SCE is applied. This is illustrated by the single straight line in Fig. 10.7 (weight loss vs. total charge). In particular, this implies that the valency of the released cations is no different in both media, according to Faraday's law.

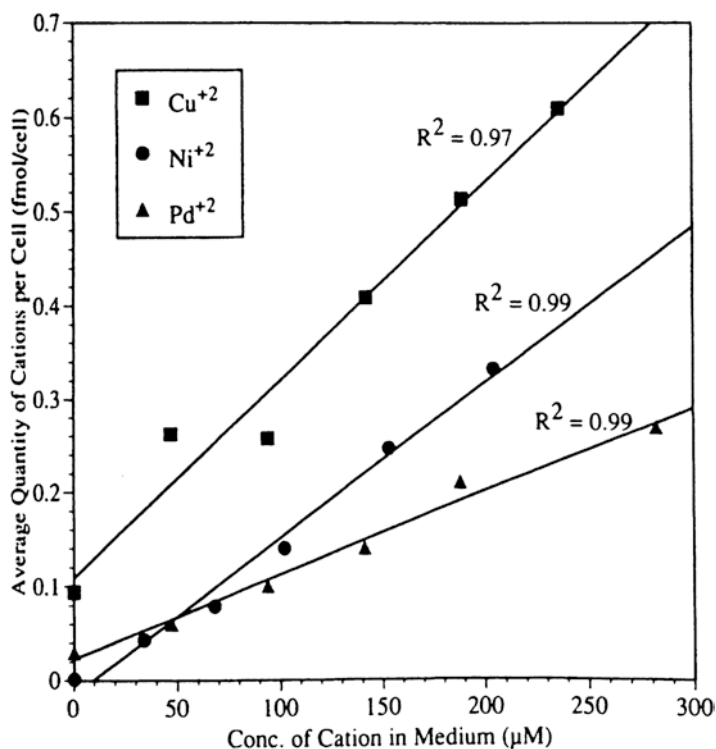


Fig. 10.6 Plots of the average uptake of metal cation per cell vs. concentration of the metal cation in the medium for Cu^{2+} , Ni^{2+} , and Pd^{2+} . The least-squares method was used to fit linear curves to the points. (Wataha *et al.*, 1993.)

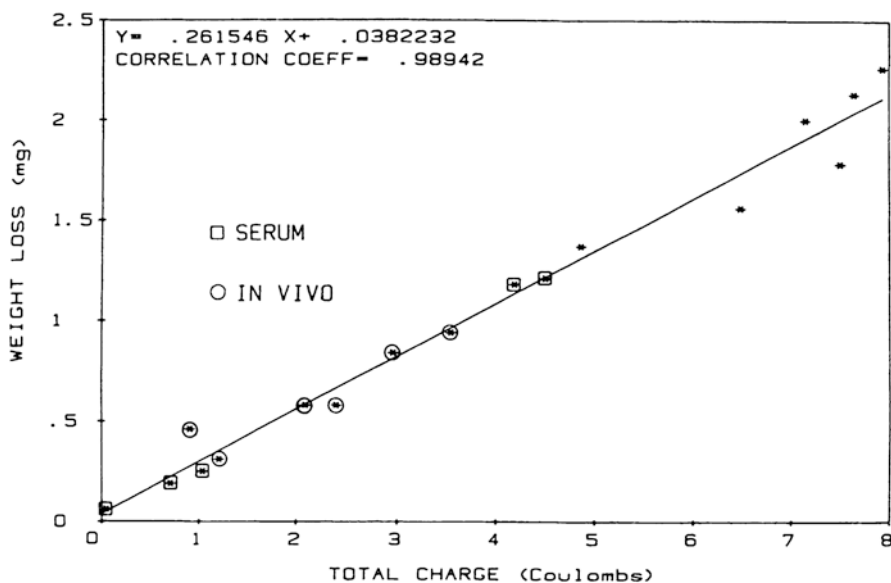
Table 10.9 Uptake efficiencies of metal cations by fibroblasts (Wataha *et al.*, 1993)

Metal cation	Uptake efficiency ((fmol/cell)/µM)/h)*
Ag^+	23.8
Au^{4+}	1.0
Cd^{2+}	38.0
Cu^{2+}	0.26
In^{3+}	45.3
Ni^{2+}	0.21
Pd^{2+}	0.11
Zn^{2+}	0.73

* fmol = femtomoles (10⁻¹⁵ moles).

Table 10.10 Metal concentrations (ng/g) in synovial fluid, serum and urine. Median (range) (Karrholm *et al.*, 1994)

	Cemented	HA-coated	Porous	Controls
Ti/synovial fluid	37 (12-56)	3.5 (0-14)	6.4 (0-7.8)	0 (0-7.5)
Al/synovial fluid	12 (6.7-28)	5.2 (2.6-13)	3.8 (2.9-9.1)	7.3 (1.9-19)
Al/serum	2.1 (0-11)	1.4 (0-5.9)	5.7 (2.1-16)	3.7 (0-17)
Al/urine	6.2 (1.7-17)	4.9 (1.7-7.0)	4.2 (3.7-4.6)	4.6 (2.1-14)

**Fig. 10.7** Linear regression analysis of weight loss as a function of total charge for stainless steel rods at 500 mV (SCE) for 30 min. Symbols: * = in saline, box = in 10% serum, circle = *in vivo*. (Brown *et al.* 1988.)

10.3.2 Problems associated with the chemical analysis of metallic elements in tissues

Accurate analysis of trace elements in tissues is essential to assess the degree of contamination. This is not an easy task, mainly because we are dealing with normal levels of the order of $\mu\text{g/litre}$. Sampling and sample preparation are steps prone to serious contaminations, if the necessary precautions are not taken. As indicated in a review by Lugowski *et al.* (1990), reported 'normal' levels of Cr in blood span over four orders of magnitude. Contamination during sampling can be avoided by using PTFE or polyethylene materials for blood collection and sample storage. For cutting tissues a blade made of a material free from the elements to be analysed should be used. For example, in our laboratory we have been using pure titanium blades to

cut soft tissues for Cr and Ni analysis. Contamination during sample preparation can be minimized by: (i) adopting a very strict protocol of labware cleaning; (ii) chemical treatment with ultrapure reagents, preferably in a microwave oven to reduce the time necessary for digesting tissues; (iii) use a laminar flow hood to prepare the samples, in order to avoid airborne contamination.

Lugowski has published a number of excellent works where the reader can find very detailed information on the above and other aspects. The degree of precision and accuracy to be expected when adequate experimental methods are used is indicated in Table 10.11. This table refers to an 'internal' lab blood standard and to a Standard Reference Material (SRM) with vanadium concentration certification. The relative standard deviation (RSD) ranges from ca. 10% for Ni and Co, to ca. 29% for V.

10.3.3 Corrosion in sweat

The main constituents of sweat are chlorides (0.3–3.0 g/l), urea (0.12–0.57 g/l) and lactic acid (0.45–4.5 g/l). When metallic objects come in contact with skin corrosion may occur, and if the corrosion products are toxic or irritating they may originate contact dermatitis. The most common example is dermatitis caused by nickel-containing jewelry. In North America ca. 10% of men and women have a history of nickel dermatitis (Randin, 1988). Although the degree of sensitization may not be directly related to the amount of metal ions released from an object, due to variability of response from person to person, it is generally considered that a high corrosion resistance gives rise to fewer allergies.

The corrosion resistance of several materials in artificial sweat is given in Table 10.12 (Randin, 1988). The composition (g/l) of the medium used was: 20 NaCl, 17.5 NH₄Cl, 5 urea, 2.5 acetic acid, 15 lactic acid, pH 4.7. The table gives the corrosion potential, E_{corr} , in O₂ and N₂-saturated medium, the pitting potential,

Table 10.11 Precision of laboratory standard and precision and accuracy of SRM 909 human serum (Lugowski et al., 1990)

Element	X (µg/litre)	n	SD	RSD (%)
Al	1.88	10	0.35	18.8
Co	2.37	9	0.26	10.9
Cr	0.71	8	0.14	19.6
Ni	2.95	8	0.30	10.1
Ti	4.20	7	0.41	9.8
V	0.28	8	0.08	29.4
V in SRM 909 certified value = 2.70±0.56 µg/litre	2.73	13	0.14	5.0

x – concentration; n – number of measurements; SD – Standard deviation; RSD – Relative SD.

Table 10.12 Main Electrochemical Parameters in ISO Sweat (Randin, 1988)

Materials	$E_{corr}(V_{SHE})$		E_{pit}	$i_{corr}O_2$	$i_{corr}N_2$
	N_2	O_2	V_{SHE}	($\mu A/cm^2$)	($\mu A/cm^2$)
Ni200	-0.16	0.06	—	22	0.18
CuNi25	-0.09	0.06	—	24	<0.1
Ni ₅₀ Al ₅₀	-0.17	0.04	1.1		
Ni ₆₀ Al ₄₀	-0.20	-0.09	—	3.6	
Ni ₇₀ Al ₃₀	-0.07	-0.02	—	2.2	
WC+Ni	-0.11	0.23	—	19	<<0.1
TiC+Mo ₂ C+Ni	0.25	0.31	0.43		
White gold	-0.01	0.23	—	0.6	<<0.1
FN 42	-0.24	0.07	0.08	~10	2.4
Nilo Alby K	-0.24	-0.09	—	190	0.32
NiTi	0.03	0.12	0.60–1.05		
AISI 303			0.43		
12/12			0.32		
AISI 304	} -0.04	} 0.21	0.32		
AISI 316F			0.50		
316 PX	} ± 0.09	} ± 0.08	0.53		
AISI 316L				0.53	
Hastelloy X	-0.06	0.17	>0.89		
Phydur	0.26	0.29	0.46		
NiP	-0.19	-0.02	—	40	-0.1
NiP/450 °C	-0.15	0.09	—	18	
PdNi	0.33	0.45	0.46		
SnNi	0.07	0.08	0.2		
Cr	0.21–0.36	0.26	0.85		
Sandvik 1802	-0.02	0.22	0.61		
Shomac	0.15	0.26	>0.75		
Co	-0.24	-0.15	—	340	~0.1
Co ₅₀ Al ₅₀	-0.29	-0.26	—	18	
WC+7% Co	-0.24	-0.10	—	200	~0.1
WC+10% Co	-0.25	-0.12	—	480	~0.1
Stellite 20			>0.75		
Ni			>3.0		

E_{pit} , and the corrosion rate, i_{corr} , measured by the Tafel extrapolation method. i_{corr} , is given only for those alloys which are in the active state. For the other alloys E_{pit} , is given. The following materials were found to corrode in the active state: Ni, CuNi25, NiAl (50:50, 60:40 and 70:30), WC+Ni, white gold, FN42, Nilo Alby K, NiP. Alloys such as stainless steels, TiC+Mo₂C+Ni, NiTi, Hastelloy X, Phydur, PdNi, and SnNi are in the passive state and may pit under exceptional circumstances. Titanium has an extremely high E_{pit} and therefore cannot pit under normal use.

10.3.4 Influence of proteins on the corrosion resistance

Albumin has a detrimental effect on the corrosion resistance of cast Co–Cr–Mo alloy (Tomás *et al.*, 1994). The breakdown potential in 0.15 M NaCl is 0.40 ± 0.02 V vs. SCE, whereas in 0.15 M NaCl+albumin it is 0.25 ± 0.06 V vs. SCE.

The presence of 5% bovine serum in lactated Ringer's solution (pH=6.5) increases the corrosion rate of Ti–6Al–4V alloy, as shown in the last two columns of Table 10.13 (Lewis and Daigle, 1993b). This table gives data obtained by direct current (d.c.) and alternating current (a.c.) methods. The difference between d.c. and a.c. corrosion rates found in this system is not unusual. The same table also shows that decreasing the pH of lactated Ringer's solution to 1 has a dramatic effect on corrosion rate.

Table 10.14 summarizes data obtained for Co–Cr, 316L stainless steel and titanium. The type of electrochemical technique used has an important influence on the results, which might indicate that the electrode potential determines the beneficial or detrimental effect of proteins on corrosion.

10.3.5 Antibiotic-metal interactions

The interaction between a number of antibiotics (oxytetracycline, tetracycline, tobramycin, clindamycin, cefamandole, bacitracin and chloramphenicol) and surgical metallic materials (316L stainless steel, Co-Cr and commercially pure Ti) has shown that only oxytetracycline exerts an effect on the electrochemical response. For all the materials this antibiotic shifted the corrosion potential of abraded surfaces in the noble direction, as seen in Fig. 10.8.

Table 10.13 Electrochemical characteristics of Ti6Al4V alloy in three biosimulating solutions (Lewis, 1993b)

Solution	E _{corr} ^a (mv)	β a ^b	β ca ^c	R _p ^d	R _c ^e	idc ^f	iac ^g
		(m V per decade)		(M Ω /cm ²)	(nA/cm ²)		
Lactated Ringer's (pH = 6.5)	185	210	301	2.57	1.00	21	54
Lactated Ringer's (pH = 6.5) + 5% bovine serum	336	187	234	1.45	0.70	31	65
Lactated Ringer's (pH = 1)	147	306	1650	0.33	0.22	340	510

a Corrosion potential.

b Anodic Tafel slope.

c Cathodic Tafel slope.

d Polarization resistance; obtained from d.c. results.

e Polarization resistance; obtained from a.c. results.

f Corrosion current density; obtained from the values for R_p.

g Corrosion current density; obtained from the values for R_c.

Table 10.14 The influence of proteins on the corrosion resistance of metals

Material	Effect	Remarks
F75 Co-Cr-Mo alloy with porous coating of F75 beads	Increased corrosion rate	Accelerated anodic corrosion method: 10% serum (Hughes <i>et al.</i> , 1990)
316L stainless steel	Marginal increase in pitting potential	Anodic polarization curves; 10% serum (Chawla <i>et al.</i> , 1990)
316L stainless steel	Increased corrosion rate*	Polarization resistance method; static conditions 10% serum (Williams <i>et al.</i> , 1988)
cp titanium	Increased corrosion rate	idem
Ti-6Al-4V	Insignificant effect	idem
c.p. titanium	Dual role	Beneficial effect in the absence of breakdown and detrimental when attack takes place; potentiodynamic and galvanostatic experiments; 10% serum (Sousa and Barbosa, 1993)
316L stainless steel	Increased pitting potential	Potentiodynamic and galvanostatic experiments; 10% serum (Sousa and Barbara, 1991)
F75 Co-Cr-Mo alloy	Increased Co and Cr release	Constant potential (500mV vs. SCE); 10% serum (Brown <i>et al.</i> , 1988)
316L stainless steel	Decreased weight loss	Constant potential (500mV vs. SCE); 10% serum (Brown <i>et al.</i> , 1988)

* Under fretting conditions the corrosion rate decreases.

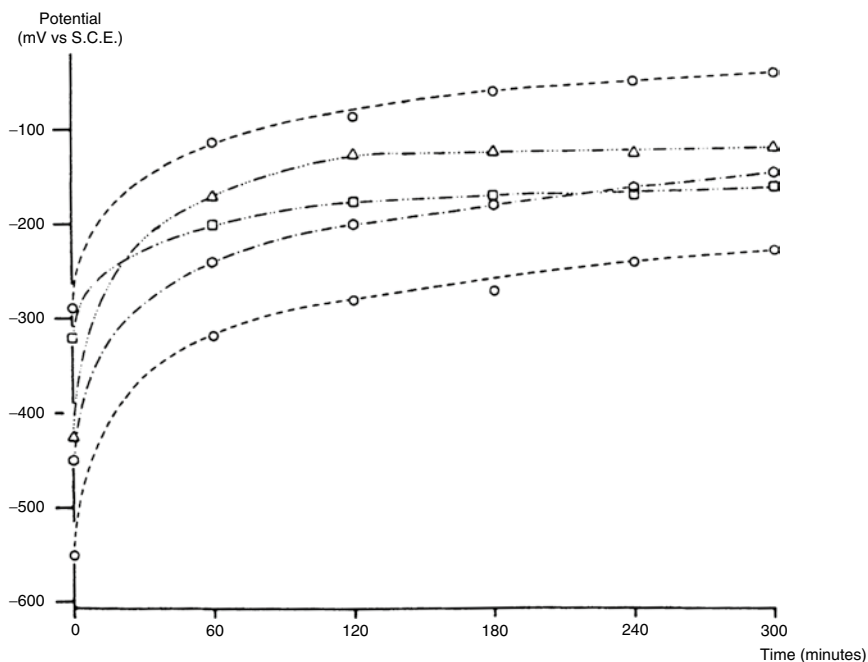


Fig. 10.8 Potential-time curves for pure titanium in 0.9% saline with and without additions of oxytetracycline: ○(upper line), as received; ○](lower line), abraded; ◇ 0.01 mg ml⁻¹; □0.1 mg ml⁻¹; Δ 1.0 mg ml⁻¹. (von Fraunhofer *et al.*, 1989.)

10.4 Aspects Related to the Oxide and Other Surface Layers

10.4.1 Effect of anodizing and passivation treatments on the corrosion resistance of titanium

For a detailed description of anodic oxidation of titanium and its alloys the reader may refer to a review by Aladjem (1973).

The oxide on titanium can grow to thicknesses of the order of 100 nm or more by applying anodic currents in suitable electrolytes. H_3PO_4 and NaOH baths have been used for this purpose. The colour of the oxide changes with thickness due to light interference. A gold colour corresponds to a thickness of the order of 10–25 nm whereas a blue colour is normally associated with thicknesses of 30–60 nm. The corrosion resistance of anodized titanium increases as the oxide becomes thicker. This is illustrated in Fig. 10.9 (Cigada *et al.* 1992), which shows that films formed in H_3PO_4 are thicker than those formed in air. They are also more protective, since the passive current density in a buffered physiological solution at 38°C is ca. 10% that measured for specimens oxidized in air. The same figure shows that anodizing in NaOH is not so effective in reducing the current density as doing it in H_3PO_4 .

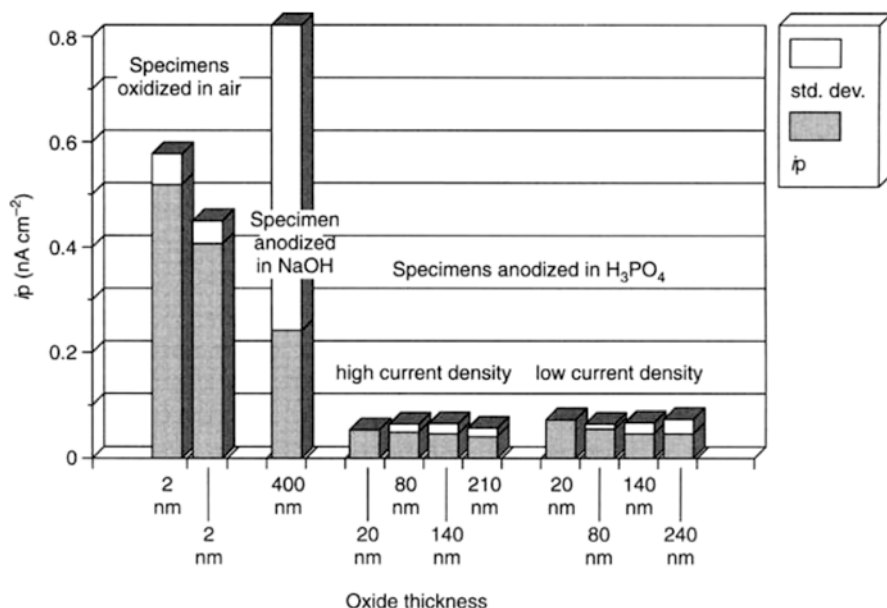


Fig. 10.9 Average passivity currents (between 600 and 500 h) and standard deviations in physiological solution of Ti6Al4V specimens, oxidized and anodized in different conditions. (Cigada *et al.* 1992.)

The corrosion rate of anodized titanium (solution: 60 ml ethanol, 35 ml water, 10 ml lactic acid, 5 ml phosphoric acid, 5 mg citric acid and 5 mg oxalic acid; 45V, 45s) is much lower than that of passivated titanium (40% volume nitric acid, room temperature, 30 min.), as indicated in Table 10.15 (Ong *et al.*, 1993). The corrosion potential of the former is also more noble, as indicated in the same table. The average thicknesses are given in Table 10.16. The anodized film is ca. 10 times thicker than the passivated film.

There have recently been reports (Lowenberg *et al.*, 1994| Callen *et al.*, 1995) indicating that passivation of Ti-6Al-4V in HNO₃ increases the release of all three constituent elements in a culture medium (α -Minimal Essential Medium with 15% foetal bovine serum and 10% antibiotics). Table 10.17 exemplifies the results obtained for titanium ions, for three periods of immersion of three days each. The level of Ti is significantly reduced throughout the 9-day experimental period.

Table 10.15 Corrosion results (Ong *et al.*, 1993)

Treatment	Average $E_{\text{corr}} \pm 1 \text{ SD}$ (mV)	Average $I_{\text{corr}} \pm 1 \text{ SD}$ ($\mu\text{A}/\text{cm}^2$)
Non-passivated	-138.4 \pm 25.9	0.015 \pm 0.01
Passivated	-104.7 \pm 22.8	0.003 \pm 0.001
Anodized	34.4 \pm 17.4	90.0006 \pm 0.0001

Table 10.16 Titanium oxide thickness (nm), relative to tantalum pentoxide (Ong *et al.*, 1993)

Treatment	Mean	SD	Sample size
Non-passivated	3.1	0.6	1.8
Passivated	4.1	1.8	1.8
Anodized	43.6	4.9	1.5

Table 10.17 Trace Levels of Ti, Al, and V in culture medium (Callen *et al.*, 1995)

Time points	cpTi Wells		Ti6Al4V Wells		Control Values
	Not Passivated	Passivated	Not Passivated	Passivated	
Ti					
1st	23.696 \pm 12.892	15.735 \pm 3.354	12.599 \pm 3.850	23.338 \pm 8.497	4.983 \pm 0.977
2nd	12.650 \pm 5.275	16.640 \pm 4.940	11.050 \pm 1.601	24.645 \pm 8.419	
3rd	6.444 \pm 2.495	8.738 \pm 2.983	5.513 \pm 1.943	10.486 \pm 3.674	
Al					
1st	4.091 \pm 0.677	4.133 \pm 0.523	8.933 \pm 1.187	16.878 \pm 4.574	3.476 \pm 0.392
2nd	4.694 \pm 1.039	5.523 \pm 2.784	5.703 \pm 0.707	9.656 \pm 2.750	
3rd	5.215 \pm 1.096	4.149 \pm 0.397	4.516 \pm 0.384	6.614 \pm 1.407	
V					
1st	0.508 \pm 0.199	0.366 \pm 0.167	6.195 \pm 2.191	21.104 \pm 8.828	0.246 \pm 0.082
2nd	0.255 \pm 0.018	0.171 \pm 0.051	2.789 \pm 1.129	10.096 \pm 5.697	
3rd	0	0.330 \pm 0.213	0.588 \pm 0.334	4.218 \pm 2.003	

10.4.2 Effect of coatings and surface treatments on the corrosion resistance of stainless steel and titanium

When metals are used as coatings the possibility of occurrence of galvanic corrosion exists, since cracks or pores in the coating enable the corrosive medium to contact the substrate. Mainly for this reason metallic coatings have not been used in internal implants. However, surface treatments with inert materials have been widely applied and are now in clinical practice. The effect of these and other surface treatments will be addressed in this section.

With the development of ion implantation the plating of practically any element on any substrate opened new perspectives to surface modification of biomaterials. Carbon and nitrogen have been the species most widely employed to modify the corrosion and wear behaviour of stainless steels and titanium alloys. However, the plating of metallic elements, with a view to modifying either the corrosion performance and/or the biological behaviour of metallic implants, is an interesting possibility. This would be particularly valuable in the case of stainless steel substrates. Very little has been reported in this area. Titanium, niobium and tantalum coatings on stainless steel act as anodes, therefore indicating that they may retard the transfer of chromium and nickel into the environment (Gluszek and Masalski, 1992). In the same medium (Ringer's solution) the oxide layers formed on titanium, niobium and tantalum by prolonged (100h) exposure to air are not very stable. Fig. 10.10 shows this effect (dotted line). The galvanic current first increases, corresponding to modification/destruction of the original oxide layer, and then decreases, corresponding to increased stability of the film formed in solution. When freshly ground specimens are used (solid line) the galvanic current decreases with time, due to film growth, which follows a logarithmic law [$\log i \propto (-\log t)$].

Laser surface alloying (LSA) of Ti6Al4V with Nb, Mo and Zr, in order to increase surface hardness, has shown that the latter element is the most promising (Akgun and Inal, 1994). The hardness increase is almost threefold in comparison to the substrate and identical to that obtained by laser surface melting (LSM). Since a nitrogen atmosphere was used in LSA and LSM, TiN formed during melting appears to be the main reason for the high hardnesses obtained. The hardened zone extends to a depth of over 0.5 mm. Wear and fretting corrosion could be considerably reduced with such surface treatments, but no experimental data are yet available.

Radio-frequency (RF) plasma treatments in air (1.0 torr) produced enhanced ionic release from Co–Cr–Mo and Ti–6Al–4V alloys, without any improvement in biological behaviour (Kummer *et al.*, 1992). Table 10.18 gives the Cr, Co and Ti concentrations obtained after 10 days exposure to cell culture fluid (DMEM with 10% FBS). The RF plasma-treated Ti–Al–V alloy shows a 3-fold increase after the plasma-treatment.

Depassivation of Ti–6Al–4V occurs during planar-planar rubbing against PMMA in Ringer's solution (Rabbe *et al.*, 1994). The free corrosion potential drops to values below -650 mV vs. SCE. This potential is substantially lower than those obtained for nitrogen ion-implanted and ion-nitrided Ti–6Al–4V, which are of the

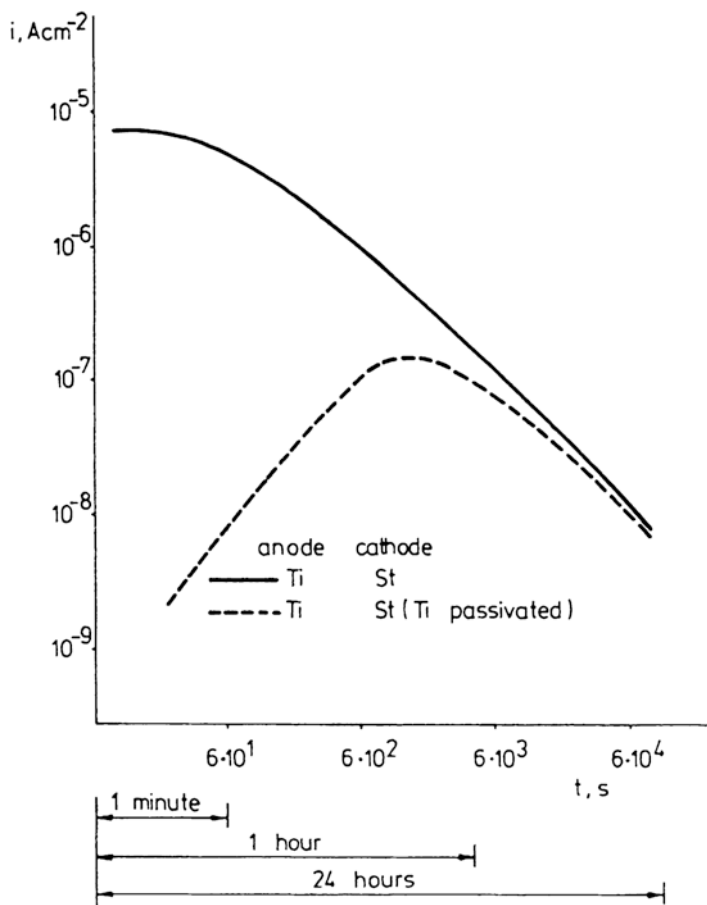


Fig. 10.10 Galvanic current density-time relationship for 316L/titanium couple in Ringer's solution. (Gluszek and Masalski, 1992.)

Table 10.18 Concentration of Cr, Co and Ti in cell culture fluid after 10 days (Kummer *et al.*, 1992)

Sample	concentration (μmL)		
	Cr	Cr	Ti
Control	1.1	<2	-
Co-Cr-Mo	96.5	720	-
Co-Cr-Mo/RF	120.5	960	-
Ti-Al-V	-	-	35.6
Ti-Al-V/RF	-	-	102.0

RF = Radio-frequency plasma treated.

order of , -100 mV vs. SCE. At high doses ($\sim 2 \times 10^{18}$ ions/cm²) a TiN layer is formed on ion-implanted surfaces, whereas TiN and Ti₂N form as a result of ion nitriding, thus increasing the hardness of the alloy surface.

Superalloy MA 956 (Fe–20Cr–4.5Al–0.5Ti–0.5Y₂O₃, wt%) possesses the interesting ability of developing a fine α -alumina scale on the surface upon isothermal treatment at 110 °C (Escudero and González-Carrasco, 1994). This layer acts as a coating, being responsible for an improved corrosion resistance of the alloy, as indicated by the anodic polarization curves given in Fig. 10.11. No pitting corrosion occurs for potentials up to 700 mV vs. SCE.

Hard ceramic coatings (Al₂O₃ and SiC) deposited by radio-frequency (RF) sputtering on Ti and Co–Cr–Mo alloy resulted in significant corrosion resistance improvement, as seen in Table 10.19 (Sella *et al.*, 1990). The data in this table were obtained by applying a constant potential of 1.4 V vs. SCE and measuring the corrosion current density (c.d.) in artificial saliva. SiC coatings deposited on Ti caused a decrease of c.d. of ca. 300 times. The same coating applied to Co–Cr–Mo was only effective when an intermediate Ti sublayer was used to avoid cracking. An Al–Al₂O₃ cermet sublayer was also very effective in improving the corrosion resistance of Al₂O₃-coated Co–Cr–Mo alloy; the c.d. decreased 200 times when both layers were used. The authors indicate that Al₂O₃ and SiC coatings gave better biocompatibility than Ti and that no signs of corrosion were observed on Al₂O₃-coated dental implants removed after several years of implantation.

Modification of Ti–6Al–4V alloy surfaces by ion implantation with iridium, at fluences of 0.74×10^{16} and 1.48×10^{16} ions/cm², corresponding to 2.5 and 5.0 at% Ir peak concentrations, has been reported (Buchanan and Lee, 1990). After pre-treatment of the implanted surfaces in 1N H₂SO₄ the surfaces become enriched in Ir

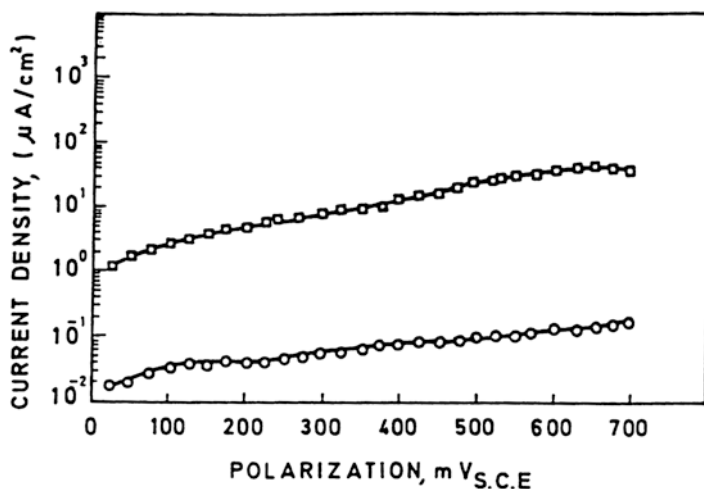


Fig. 10.11 Anodic polarization curves for MA956 in the as-received and oxidized conditions after nine months of immersion in Hank's solution. ○ Oxidized; □ as-received. (Escudero and Gonzalez-Carrasco, 1994.)

Table 10.19 Comparison of the corrosion currents of coated and uncoated metals (*Sella et al., 1990*)

	Corrosion current at E=1.4V/SCE ($\mu\text{A}/\text{cm}^2$)
Uncoated metal or alloy	
Ni-Cr	6000-8000
Co-Cr-Mo	8000
Ti	260
Experimental coatings	
SiC (1 μm) on Ti	0.8
SiC (1 μm) on Co-Cr	10000
Ti (1 μm) on Co-Cr	500
SiC (1 μm) + Ti (1 μm) on Co-Cr	28
Al ₂ O ₃ (0.5 μm) on Co-Cr	1800
Al ₂ O ₃ (0.5 μm) + Al-Al ₂ O ₃ cerment on Co-Cr	40

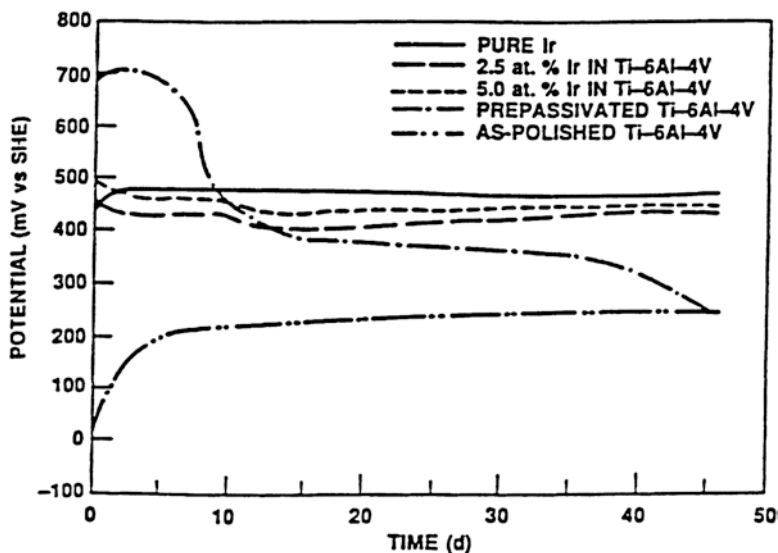


Fig. 10.12 Corrosion potential vs. time in aerated isotonic saline. (*Buchanan and Lee, 1990.*)

(the concentrations are over 60% and may approach 100%), as a consequence of alloy dissolution. The result is a corrosion potential in isotonic saline very close to that of pure Ir, as depicted in Fig. 10.12. Owing to the very high corrosion resistance of Ir, its implantation onto titanium is of potential interest, particularly if it becomes significantly enriched on the surface. Galvanic couples formed between Ir and Ti is a possibility that justifies further research.

In an attempt to reduce the release of potentially harmful metal ions from Co-Cr-Mo surgical implants, a thin coating of TiN has been applied via physical vapour deposition (PVD) (Wisbey *et al.*, 1987). *In vitro* corrosion performance has been investigated using electrochemical techniques. The release of Co and Cr ions is reduced by the presence of the TiN coating. Data concerning this study are shown in Fig. 10.13.

Thermal heating of titanium at 400 °C or immersion in 30% HN03, followed by aging in boiling distilled water for times in the range 6–14 h, greatly reduced the amount of Ti and Al released from Ti–6Al–4V, as shown in Table 10.20 (Browne and Gregson, 1994). The corrosive medium was bovine serum at 37 °C. The table also gives the ion release for two other treatments: immersion in 30% HN03, for 10 min., which is the conventional commercial treatment, and immersion for 16h in the same solution followed by rinsing in distilled water (N). The beneficial effect of the first two treatments is attributed to formation of rutile, which is more dense and has a closer packed structure, with fewer paths for ion diffusion, than the oxide formed upon passivation in nitric acid.

Commercially pure titanium and Ti–6Al–4V implants ion implanted with nitrogen heal as well as non-treated samples in cortical bone (Johansson *et al.*, 1993), as indicated by the existence of no statistically significant differences in total bone-metal contact.

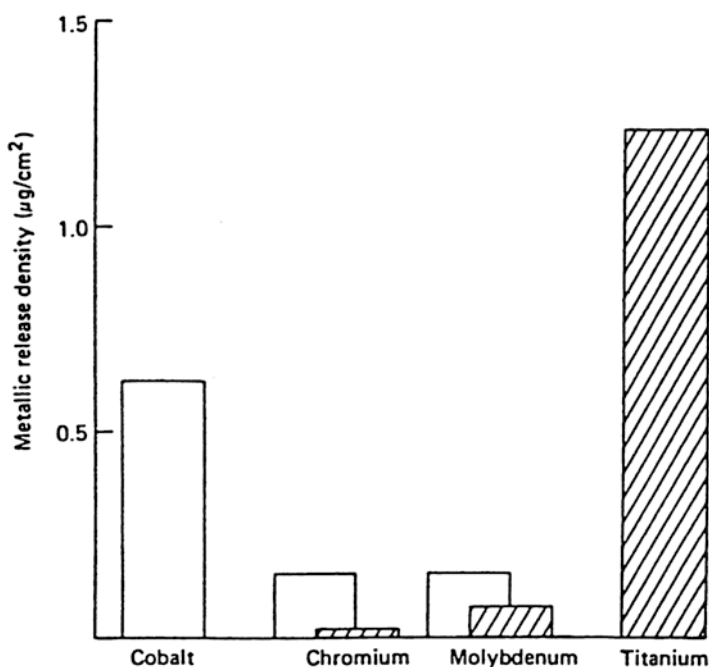


Fig. 10.13 Metallic dissolution products released from a polished Co-Cr-Mo alloy after 550 h in 0.17 M NaCl+2.7×10⁻³ M EDTA solution at 37°C. □ uncoated; ■ TiN coated. (Wisbey *et al.*, 1987.)

Table 10.20 Effect of various surface treatments on the dissolution of titanium and aluminium from Ti-6Al-4V alloy (Browne and Gregson, 1994)

	Total ion release ($\mu\text{g}/\text{cm}^2$)	
	Titanium 700 h	Aluminium 700 h
30% HNO_3 (C)	0.1	0.25
30% HNO_3 (N)	0.11	0.06
400°C (T)	0.03	0.026
Aged 10 h (A)	0.03	0.023

C - Conventional treatment (10 min. immersion).

A - Aging treatment (immersion in distilled water).

N - Immersion in HNO_3 for 16 h.

T - Thermal heating.

10.4.3 Effect of hydroxyapatite coatings on the corrosion resistance of titanium and stainless steels

Most of the data available on this topic refer to hydroxyapatite deposited by plasma spraying. Although compounds may form at the metal/hydroxyapatite interface, particularly in the case of titanium, their existence has not been unequivocally demonstrated. Titanium phosphates and phosphides, as well as calcium titanates, may exist, but they probably form very thin layers. The large surface roughness, caused by grit blasting of the substrate prior to hydroxyapatite deposition, is another factor that renders identification of any interfacial compounds by surface analysis techniques difficult.

Table 10.21 shows that the corrosion resistance of stainless steel increases upon coating with hydroxyapatite. The presence of calcium phosphate in solution, due to dissolution of hydroxyapatite, seems to be the cause for these changes. The same table indicates that calcium phosphate is detrimental to the corrosion resistance of titanium, both in terms of film breakdown potential and corrosion rate under passive conditions.

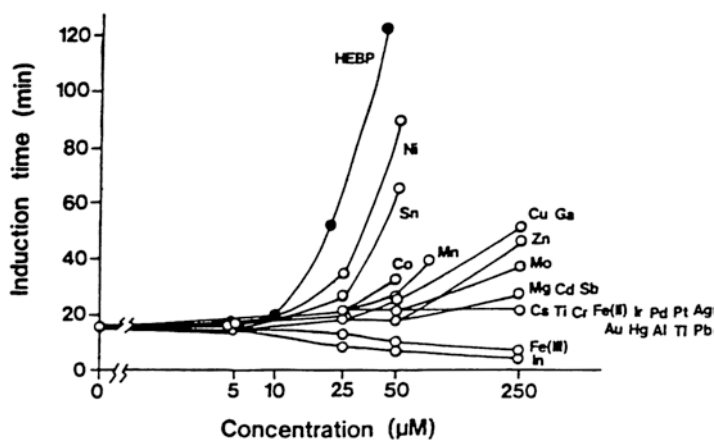
10.4.4 Interaction between metal ions and calcium phosphates

Metallic ions may influence the formation of calcium phosphates in different ways. Some inhibit (nickel, tin, cobalt, manganese, copper, zinc, gallium, thalium, molybdenum, cadmium, antimony, magnesium, and mercury), a few stimulate (iron [ferric] and iridium) whereas others have no effect (cerium, titanium, chromium, iron [ferrous], iridium, palladium, platinum, silver, gold, aluminum, and lead) (Okamoto and Hidaka, 1994). Fig. 10.14 gives the induction time for calcium phosphate formation vs. concentration for the above metal ions.

Heat treatment of Ti-6Al-4V at 280 °C for 3 h produced a high accumulation of Ca deposited next to screws implanted in rats (Hazan *et al.*, 1993), as indicated in Table 10.22. The oxide was twice as thick as that formed on non-treated screws.

Table 10.21 Effect of hydroxyapatite coatings and calcium phosphate solutions on the corrosion resistance of titanium and stainless steel

Material	Solution	Effect	Ref
316L ss/HA	Saline	Increase in breakdown potential	Hayashi <i>et al.</i> , 1990
Ti-6Al-4V/HA	Saline	Decrease in breakdown potential	Hayashi <i>et al.</i> , 1990
316L ss	Saline+ Ca phosphate	Increase in breakdown potential	Sousa and Barbosa, 1991
316L ss	Saline+ Ca phosphate	Decrease in corrosion rate (passive state)	Barbosa, 1991 b
Ti cp	Saline+ Ca phosphate	Decrease in breakdown potential	Sousa and Barbosa, 1991
Ti cp	Saline+ Ca phosphate	Increase in corrosion rate (passive state)	Barbosa, 1991 b

**Fig. 10.14** The induction time (min) versus concentration of various metal ions (open circle) and HEBP: 1-hydroxyethylidene-1, 1-biphosphonate (closed circle). (Okamoto and Hidaka, 1994.)**Table 10.22** Calcium deposition (mg) next to control and heat-treated Ti-6Al-4V implants (Hazan *et al.* 1993)

Time after immersion (days)	Control	Heat treated
4	–	–
5	–	–
6	2.0±0.2	4.5±6.5
10	3.1±0.5	7.4±1.1
35	4.0±1.0	9.6±1.0

The presence of Ca on the surface of titanium implants after a period *in vivo* is now well established. Ca deposition may be important in influencing protein adsorption, since it has been suggested that glycosaminoglycans adhere to the surface by a Ca-O link rather than via a Ti-N bond (Sutherland *et al.*, 1993).

Aluminium induces demineralization of previously formed bone (Frayssinet *et al.*, 1994), which can be ascribed to formation of stable complex aluminium phosphate compounds (Ribeiro *et al.*, 1995). Aluminium ions may be produced either as a result of dissolution of Ti-6Al-4V alloy or of corrosion of alumina coatings. In pH 4 buffer the release of aluminium ions from alumina is much more significant than at pH 7 (Frayssinet, 1994). V and Ti retard apatite formation and the growth of apatite seeds, as illustrated respectively in Figs. 10.15 and 10.16 for V (Blumenthal and Cosma, 1989). The action of V appears to be related to the formation of V-PO₄ complexes, whereas that of Ti may be due to poisoning of active growth sites, as in the case of Al.

Hydroxyapatite coatings applied to porous titanium alloys significantly reduced the titanium and aluminium releases, but had no important effect on vanadium release, as shown in Fig. 10.17 (Ducheyne and Healy, 1988). No major change was produced in the ion release kinetics from Co-Cr alloys.

Fig. 10.15 The action of V ions in affecting direct HA precipitation, V as VCl₅ in solution at pH 7.4, 0.15 M NaCl, 37°C in a pH-stat. The quantity of HA precipitated is proportional to the extent of OH uptake. Ca concentration is 2.79 mM; PO₄ concentration is 1.87 mM, A= control (no V); B=0.50 mM V; C=1.00 mM V; D=2.00 mM V. (Blumenthal and Cosma, 1989.)

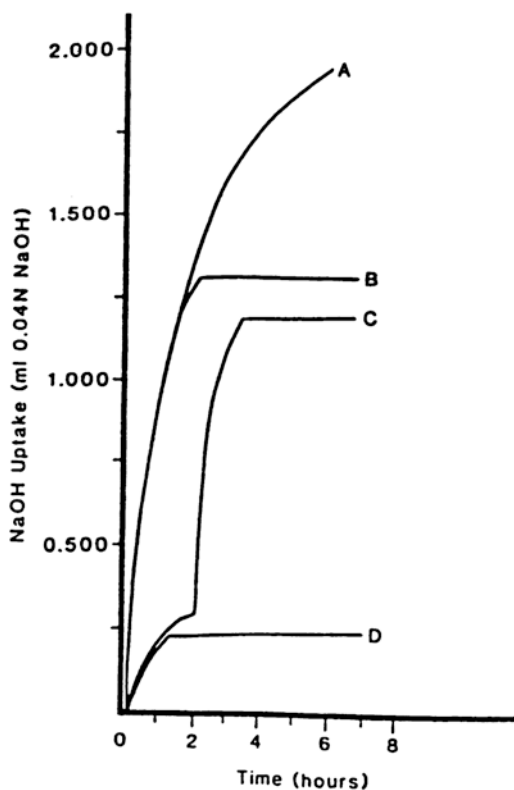
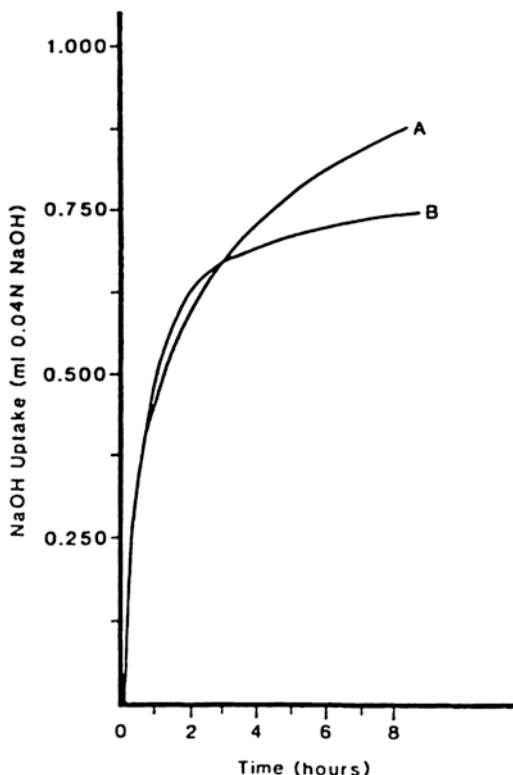


Fig. 10.16 The action of V ions on the growth of HA seeds. V as VCl_5 in solution at pH 7.4, 0.15 M NaCl, 37°C in a pH-stat. The amount of HA seeded growth is proportional to the OH uptake. Ca concentration is 1.55 mM; PO_4 concentration is 1.07 mM, Seed crystals were 0.15 mg/mL, and the seeds had a surface area of 110 m^2/g . A = control (no V); B = 1.00 mM V. (Blumenthal and Cosma, 1989.)



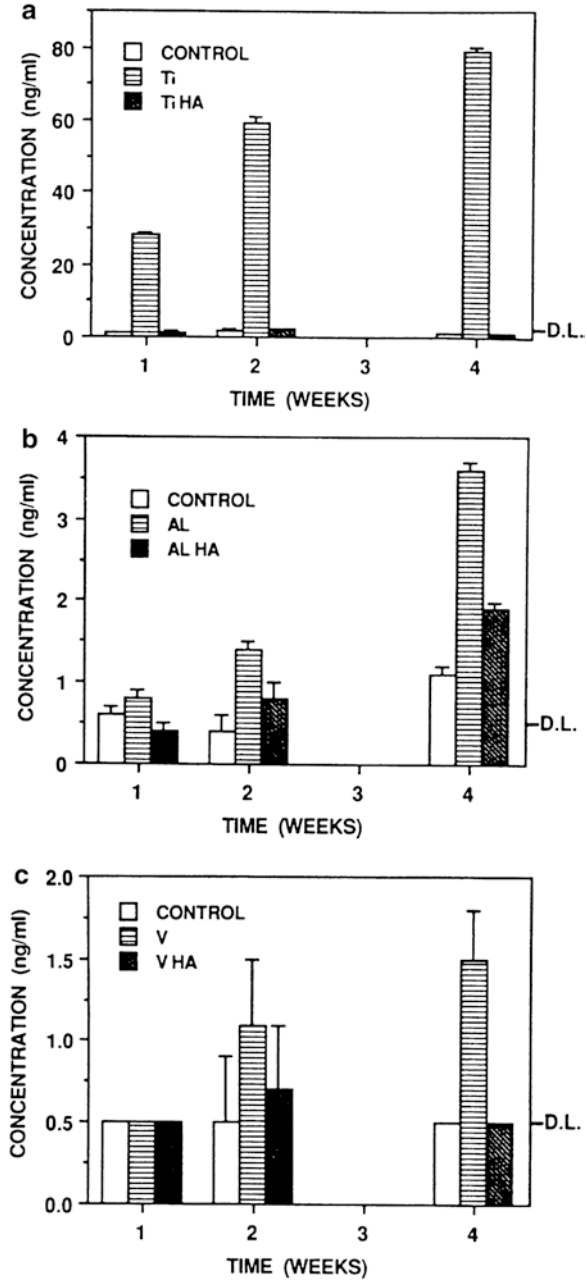
10.4.5 Physico-chemical properties of metal oxides

The corrosion resistance of some metals ultimately depends on the presence of a thin oxide film formed by the reaction of the metal with the environment. This is the case of titanium, tantalum, zirconium, molybdenum, aluminium, cobalt, chromium, etc. Table 10.23 gives the physicochemical properties of the oxides formed on some metals. A low oxide solubility is important to guarantee a low rate of corrosion, since any loss in oxide thickness, due to chemical dissolution, will tend to be balanced by oxidation of the metallic substrate. The oxides should also possess low ionic conductivity.

10.4.6 Passive films on metallic implants

The oxide film on metallic implants is usually very thin (5–10 nm). It is formed as a result of a spontaneous reaction between the metal and the environment. In spite of the common use of immersion treatments in nitric acid solutions, usually known as passivation treatments, they are not necessary to form an oxide. They are often

Fig. 10.17 (a, b, c) The release of Ti, Al and V from the Ti alloy after 1, 2 and 4 weeks of immersion; D.L. indicates the detection limit of each element. Error bars represent the 95% confidence interval on the means. (Ducheyne and Healy, 1988.)



responsible for an increase in corrosion resistance due to removal of surface contaminations or inclusions, as in the case of stainless steels. As indicated in section 9.4.1, there have been reports suggesting that this acid treatment may decrease the corrosion resistance of titanium.

Table 10.23 Selected physico-chemico properties of metal oxides in water (Tengvall and Lundstrom, 1992)

Order of practical mobility	Element	Water corrosion product	pK _s of hydrolysis	Solubility at pH 7 (M)	Isoelectric point	Charge at pH 7	Dielectric constant for oxide	0,996 Na(FeCN ₆ ⁴⁻ FeCN ₆ ³⁻) polarization resistance, R _p (KΩcm ²)	Essential	Soft tissue reaction	Corroded in H2O2 at pH7	Corrosion product
2	Nb	Nb ₂ O ₅	>20	-10 ⁻⁵	-		280	455	No	Inert?	No	
3	Ta	Ta ₂ O ₅	>20	-10 ⁻⁵	-		12	1430	No	Inert?	No	
4	Au	Au ₂ O ₃ Au(OH) ₃	-(pH7)	7x10 ⁻² 5x10 ⁶	>10 (calc.)	++		0.28	No	Sequestration	Yes	AU ₂ O ₃
7	Ti	TiO ₂ , amat. brook. rutile	+18	3x10 ⁶	6.2	--	48 78 110	714	No	No	Yes	TiO ₂ ²⁻ TiO ₂ , TiO ₂
14	Ag	Ag ₂ O AgOH	+10 Ag ⁺ +0.7	10 ⁴ >1	(Ag ⁺)12	++	9		No	Sequestration	Yes	AgO
19	Al	Al ₂ O ₃ α Al(OH) ₃ am.	14.6 -	10 ⁶ 10 ⁻³	-9	+	5-10		No	Sequestration	?	?
21	Cr	Cr ₂ O ₃ , CrO ₃ Cr(OH) ₃	-1.8(Cr(OH) ₂ ⁺) 18.6(CrO ₂)	10 ⁻¹¹ >10 ⁻¹³	8.4 (Cr ³⁺)	+	12		Yes	Toxicity	Yes Yes	CO ₂ HCO ₄
28	Fe	Fe ₂ O ₃ Fe(OH) ₂ Fe(OH) ₃	-13.3 (Fe ²⁺) (pH 9.1)	>10 ⁻¹⁰ 10 ⁻¹ 10 ⁻⁹	12.4 (Fe ²⁺) 8.0 (Fe ³⁺)	+	100 30-38	Stainless steel 316 4,38	Yes	Sequestration	Yes	FeO ₄ ²⁻ ?
29	Ni	Ni ²⁺ , NiO	12.2 (Ni ²⁺) (pH 8.9)	10 ⁻¹⁵ 10 ⁻¹¹	9.5	+			Yes	Toxicity	Yes	NiO ₄ ²⁻ ?
30	Co	Co ³⁺ , CoO	-12.6	10 ⁻¹¹ 10 ⁻¹²	10.8	+	CoCrNi 3,32	Yes	Toxicity	Yes	CoO ₂	NiO ₂
40	V	V ₂ O ₅ , V ₂ O ₄	+10.3 (HV ₂ O)	>1 10 ⁻⁴	1-2.5 (V ⁵⁺)	-			Yes	Toxicity	Yes	HVO ₄ HVO ₄

Generally, the oxide film grows according to a logarithmic law (log thickness proportional to log time), reaching a quasi-stationary thickness very rapidly. Under stationary conditions, film dissolution and film formation rates should be the same. Normally, film thickness increases slowly with time, after an initial period of rapid growth. This is illustrated in Fig. 10.18, which depicts film thickening with implantation time (Kasemo and Lausmaa, 1994).

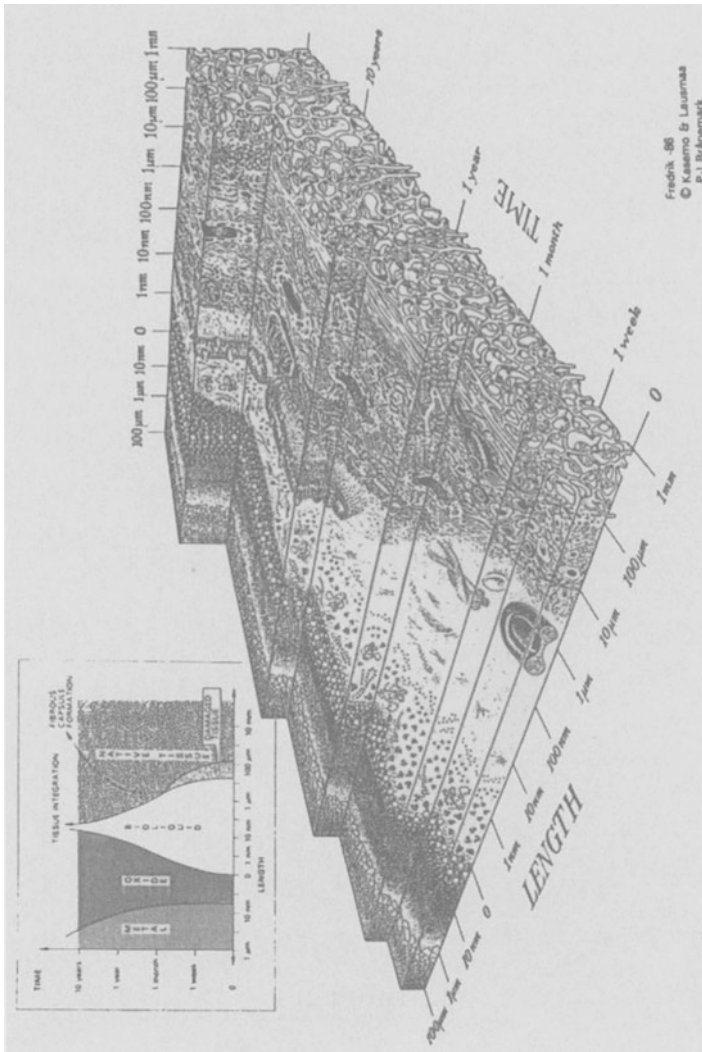
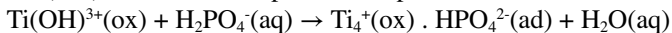


Fig. 10.18 An artist’s attempt to capture some of the complexity involved in the interaction between a material and living tissue, exemplified here by a titanium implant in bone. Note the wide range of dimensions and time scales that are relevant. (Kasemo and Lausmaa, 1994.)

The dissolution kinetics of titanium follows a two-phase logarithmic model (Healy and Ducheyne, 1992, 1993). In the first phase the concentration of OH groups increases. The second phase coincides with the adsorption of P-containing species. Fig. 10.19 clearly indicates the presence of a second phase after 400h of immersion. In the initial phase titanium is released either in the form of $Ti(OH)_n^{(4-n)+}$ or $TiO(OH)_2$. In the second phase adsorption of $H_2PO_4^-$



followed by desorption into the concentration boundary layer

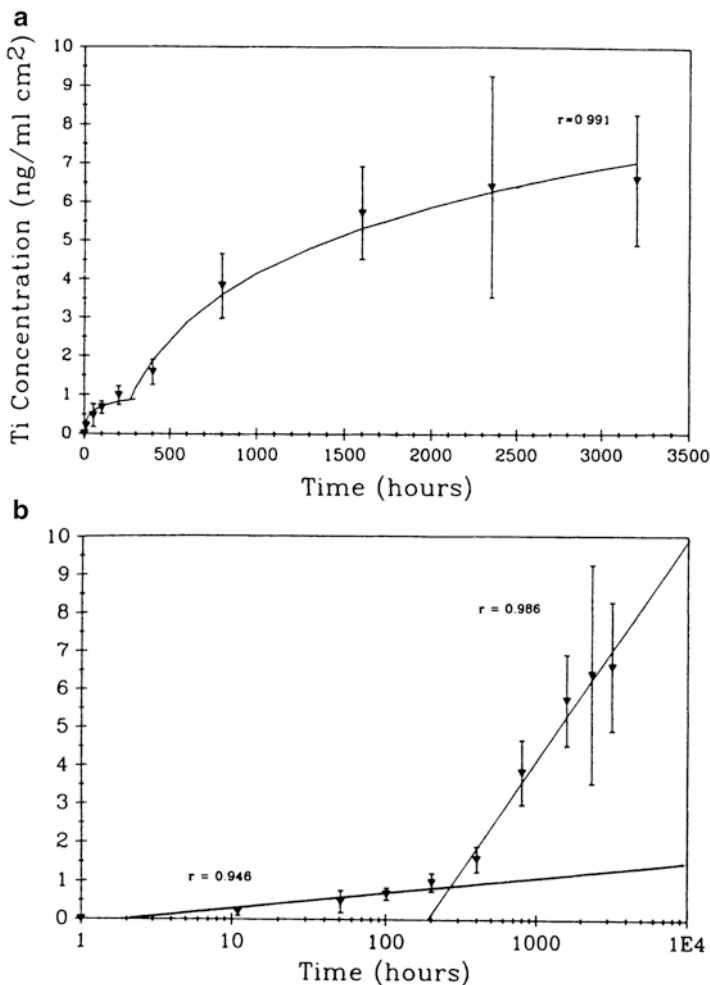
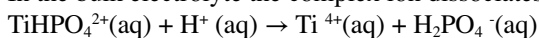
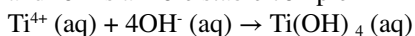


Fig. 10.19 Normalized integral passive dissolution kinetics for titanium thin films immersed in EDTA/SIE (simulated interstitial electrolyte): (a) real time data empirically fitted with two-phase logarithmic law relationship; (b) a semilogarithmic plot of the data demonstrating the two-phase logarithm relationship. The correlation coefficient for the least-squares fit of the linear functions are given. (Healy and Ducheyne, 1992.)

In the bulk electrolyte the complex ion dissociates



and forms a more stable complex



In these reactions (ox) represents O_2^{+} in TiO_2 .

This mechanism is consistent with the hypothesis that in the second stage dissolution kinetics is dependent on diffusion within the concentration boundary layer. It is conceivable that in the first stage field assisted dissolution may be the controlling step. In this stage formation of $\text{Ti}(\text{OH})_4$ or of hydroxy-cations, e.g. $\text{Ti}(\text{OH})_3^+$, has different effects on titanium transport. While $\text{Ti}(\text{OH})_4$ does not react with organic molecules, $\text{Ti}(\text{OH})_3^+$ can form organometallic complexes which may be transported systemically.

Airborne titanium oxide, TiO_{2-x} , is oxygen deficient but upon immersion in simulated interstitial electrolyte with EDTA (a metal chelating agent) changes to nearly stoichiometric TiO_2 (Healy and Ducheyne, 1993). TiO_2 is also reported to exist on the surface of a new Ti-15Zr-4Nb-2Ta-0.2Pd alloy (Okazaki *et al.*, 1994). The other oxides present were ZrO_2 , Nb_2O_5 and Ta_2O_5 .

Sterilization by various methods (conventional steam autoclaving, dry heat sterilization in air at 160–180°C, and packaging and sterilization in sealed glass ampoules) originates films with the composition TiO_2 . Their thickness is 2–6 nm, depending on the method of sterilization. Heat sterilization increased the thickness of the original oxide by a factor of ca. 2 (Lausmaa and Kasemo, 1990).

Films formed on metallic materials oxidized in pure oxygen at 300°C for 30 min. have the composition shown in Table 10.24 (Oshida, 1992). Strong oxidative conditions may exist *in vivo*, for example due to presence of the superoxide anion, O_2^- , formed by inflammatory cells. The possibility of O_2^- originating hydrogen peroxide, H_2O_2 , has led Tengvall *et al.*, (1989) to suggest that hydrogen peroxide may be of great importance to the biological behaviour of titanium. Hydrogen peroxide is responsible for the appearance of an outer layer, formed on top of a TiO_2 layer, composed of titanium oxi-hydroxide or hydrates, non-stoichiometric and rich in water (Pan *et al.*, 1994). The oxide thickness for wet-ground specimens is ca. 3 times that for dry-polished specimens, as shown in Table 10.25. Hydrogen peroxide reduces the oxide thickness and results in enhanced dissolution of titanium, according to the same authors. It is not certain whether titanium acts as a catalyst in the oxidative deterioration of biological

Table 10.24 Type of oxide formed on biomaterials (pure oxygen, 300°C, 30 min.) (Oshida *et al.*, 1992)

Material	Type of oxide
Pure Ti	TiO_2 (rutile)
Ti-6Al-4V	TiO_2 with traces of Al_2TiO_5
Ni-Ti, austenitic and martensitic	Mixture of TiO_2 and NiTiO_3
316L stainless steel	spinel-type $[(\text{Fe},\text{Ni})\text{O} \cdot (\text{Fe},\text{Cr})_2\text{O}_3]^a$ and corundum-type oxides $[(\text{Fe},\text{Cr})_2\text{O}_3]^a$

a Possible composition.

Table 10.25 Thickness (nm) of titanium oxide films (Pan *et al.*, 1994)

Source H ₂ O ₂ in the PBS (mM)	Dry-polished	Wet-ground	Polarized at 0.4 V/SCE		
			0	1	10
XPS measurements	1.5	4.6	6.3	6.2	5.8
Capacitance measurements			6.7	5.5	6.0
Literature data	1.2-1.6	4-5	6.6		

molecules, a property which has been established for other metals, e.g. iron, copper, cadmium, chromium, lead, mercury, nickel and vanadium (Stohs and Bagchi, 1995). These metals produce reactive oxygen species, leading to lipid peroxidation, DNA damage, depletion of sulphhydryls, apart from modifying calcium homeostasis. Since large concentrations of titanium debris may be found around Ti and Ti-alloy implants (section 9.3.1) the oxidative deterioration of biological molecules induced by the presence of Ti ions is a process that deserves to be studied.

The oxide formed on titanium upon passivation in HNO₃ is composed of regions of mixed titanium oxides (anatase and rutile), together with areas of amorphous titanium oxide (Browne and Gregson, 1994). Films formed on anodized titanium may be one order of magnitude thicker than those formed by passivation (section 9.4.1). The film is predominantly constituted by TiO₂, with the presence of carboxyl groups (Ong, 1993). It appears that upon passivation of cp Ti and Ti-6Al-4V alloy the film on the former is thinner (3.2 ± 0.8 nm) than that on the latter (8.3 ± 1.2 nm) (Keller *et al.*, 1994). TiO₂ films are generally amorphous, except in the case of thick films produced by thermal oxidation or anodizing. Table 10.26 summarizes the characteristics (composition, oxide thickness, surface topography/roughness, and substrate microstructure/oxide crystallinity) of titanium samples subjected to various treatments (Larsson *et al.*, 1994). Electropolished + anodized (1M acetic acid, room temperature) films are thicker than those formed by electropolishing and on 'clinical reference' (machined) surfaces. For 80V the oxide is crystalline.

Table 10.27 summarizes the composition and thickness of oxides formed on a Co-Cr-Mo alloy exposed to 'dry air' and 'wet steam' for 1 h (Lewis, 1993a).

10.4.7 Contact angles of oxide-covered surfaces

When a metallic surface covered by an oxide (either formed naturally or by an appropriate treatment) is placed in contact with the body or a culture medium adsorption of various species, namely proteins, is the prime event. Contact angle, θ , measurements can be used to ascertain the affinity of a liquid to a biomaterial surface, in particular when adsorption occurs, which is revealed by a decrease in θ . Generally speaking, θ is governed by the intermolecular forces between solid and liquid, and in the case of passive metals by the forces between metal oxide and liquid. is a complex function of surface roughness, oxide crystallinity and composition, liquid composition and time. Normally, wettability tends to progress from hydrophobic to hydrophilic. Table 10.28 gives the initial contact angles and the

Table 10.26 Summary of surface characteristics of the four different types of Ti samples (Larsson *et al.*, 1994)

Preparation	Composition	Oxide thickness	Surface topography Surface roughness	Substrate microstructure Oxide crystallinity
Clinical reference	TiO ₂ +45-80% C, traces of Ca, S, Si, P, Cl and Na	4nm	Rough, with Rough, with and protrusions, ≤ 10 μm R _{rms} =29±4 nm	Plastically deformed, amorphous metal surface Non-crystalline oxide
Electropolished	TiO ₂ +55-90% C, traces of Ca, S, Si, P, Cl and Na	4-5nm	Smooth, with occasional pits, ≤ 1 μm R _{rms} =2.7±0.9 nm	Polycrystalline metal surface Non-crystalline oxide
Electropolished + anodized, 10 V	TiO ₂ +55-70 %C, traces of Ca, S, Si, and Cl	21 nm	Smooth, with pits and porous regions, ~10 μm R _{rms} =1.5±1 nm	Polycrystalline metal surface Non-crystalline oxide
Electropolished + anodized, 10 V +	TiO ₂ +~34-40% C, traces of Ca and Cl	180nm	Heterogeneous, with smooth or porous regions, - 10 μm R _{rms} =16±2 nm	Polycrystalline metal surface. Crystalline oxide (anatase)

Table 10.27 Composition of oxides formed on a Co-Cr-Mo alloy (Lewis, 1993a)

Medium	Composition	Thickness	Remarks
Dry air	Co ₁₄ Cr ₅ MoO ₂₁	4 nm	May disaggregate into Co, Cr, Mo, CoO, CrO ₂ and Mo _x (OH) _y and suboxides of Co, Cr and Mo
Wet steam	Co ₃ Cr ₆ MoO ₂₀	3 nm	May dis aggregate into Co, Cr, Mo, Co(OH) ₂ , CrO ₃ , CoOOH, CoMoO ₄ , Mo _x (OH) _y and suboxides and hydrated species of Co, Cr and Mo

Table 10.28 Initial contact angles and changes in contact angles as function of time of oxidized surfaces of biomaterials after mechanical and buff polishing (Oshida *et al.*, 1992)

	Mechanical polish-oxidizing		Buff polish-oxidizing	
	θ _i (deg)	δθ/δt	θ _i (deg)	δθ/δt
Pure Ti	54.24	-0.0046		
Ti6A14V	32.08	-0.0010	30.85	-0.0015
NiTi (m)	69.88	-0.0055	68.92	-0.0053
NiTi (a)	71.88	-0.0048		
316L s.s.	56.46	-0.0024	55.73	-0.0025
Pure Ni	35.72	-0.0016		
Co-Cr alloy	62.04	-0.0023	61.85	-0.0021
α-alumina	60.87	-0.0044		

m – martensite; a – austenite.

changes in contact angle as a function of time, $d\theta/dt$, for a number of materials (Oshida *et al.*, 1992). Pure Ni and Ti-6Al-4V have the lowest initial contact angle, θ_0 , with low $d\theta/dt$; 316L stainless steel and Co-Cr alloy have high θ_0 with low $d\theta/dt$; and pure Ti, Ni-Ti alloys and α -alumina have high θ and high $d\theta/dt$. Shot-peening and pre-oxidation (300° C, 30 min.) of the above materials reduced the standard deviation of contact-angle measurements, probably as a result of minimization of microscopic irregularities (Oshida *et al.*, 1993). In this work pure Ti exhibited the highest initial contact angle θ_0 , and also the most noble corrosion potential. Both are related to the characteristics of the TiO₂ oxide that covers the metal surface. Note that the value of θ for Al₂O₃ is also high (Table 10.28).

The critical surface tension (CST), which is the highest surface tension of a liquid that completely wets a given surface, is given in Table 10.29 (Kilpadi and Lemons, 1994) for titanium subjected to various surface treatments. Polar (double-distilled water, glycerol and thiodoethanol) and dispersive (diiodomethane, bromonaphthalene, dicyclohexyl and decane) liquids were used in the study. Radio frequency glow

Table 10.29 Critical surface tension of Ti surfaces (Kilpadi and Lemons 1994)

Specimen	Plot	Critical Surface Tension, τ_c (dyn/cm)	Comments
I	C	–	No liquids were appropriate
	P	46.0±1.08	
	P	42.5±1.08	Only diiodomethane and bromonaphthalene were used
II	C	31.6±0.48	Water was not used in these analyses, as it did not fit with Good's criterion and also did not fall in line with the other liquids
	P	35.4±0.48	Only glycerol and thiodoethanol were used
	D	34.9±0.48	Only diiodomethane and bromonaphthalene were used
III	C	40.0±0.41	
		41.4±0.59	
	D	40.7±0.59	Only diiodomethane and bromonaphthalene were used
IV	C	41.9±0.79	
	P	41.5±1.05D	
	D	42.5±1.05	Only diiodomethane and bromonaphthalene were used
V	C	37.4±0.51	
	P	31.0±0.30	Water was not included
	D	41.8±0.51	Only diiodomethane and bromonaphthalene were used

I – Non-passivated, TFGD-treated, polished machined flats; II – Non-passivated, unsterilized, polished machined flats; III – Passivated, dry-heat-sterilized, polished machined flats; IV – Passivated, dry-heat-sterilized, polished coined flats; V – Passivated, dry-heat-sterilized, unpolished flats; C – Composite (includes all liquids); P – only polar liquids; D – only dispersive liquids. RFGD – Radio Frequency Glow Discharge.

discharge (RFGD) treated samples showed the higher CST. Grain size (70 vs. 23 μm) did not affect the CST of polished, passivated, and dry-heat-sterilized titanium surfaces.

The equilibrium contact angles of cp Ti and Ti-6Al-4V, both passivated in nitric acid, were $52\pm 2^\circ$ and $56\pm 4^\circ$, respectively (Keller *et al.*, 1994). Wettability was measured employing water drops. This similarity in contact angles reflects the similarity in oxide film composition found in the same work. However, the film on the alloy surface was significantly thicker (8.3 ± 1.2 nm) than that on the cp Ti (3.2 ± 0.8 nm).

Reference

- O.V. Akgun and O.T. Inal, 'Laser surface modification of Ti-6Al-4V alloy', *Journal of Materials Science*, **29**, 1159-1168 (1994).
- A. Aladjem, 'Review Anodic oxidation of titanium and its alloys', *Journal of Materials Science*, **8**, 688-704 (1973).
- M.A. Barbosa, 'Corrosion mechanisms of metallic biomaterials', Biomaterials Degradation-Fundamental Aspects and Related Clinical Phenomena, European Materials Research Society Monographs, Vol. **1** (eds. M.A. Barbosa, F. Burny, J. Cordey, E. Dorre, G. Hastings, D. Muster and P. Tranquilli-Leali), pp. 227-257, Elsevier Science Publishers, Amsterdam (1991 a).
- M.A. Barbosa, 'Electrochemical impedance studies on calcium phosphate-metal interfaces', Bioceramics, Vol. **4** (eds. W. Bonfield, G.W. Hastings and K.E. Tanner), pp. 326-333, Butterworth-Heinemann (1991 b).
- M.A. Barbosa, 'Surface layers and the reactivity of metallic implants', High-Tech Biomaterials, European Materials Research Society Monographs, Vol. **3** (eds. D. Muster, M.A. Barbosa, F. Burny, J. Cordey, E. Dorre, G. Hastings, and P. Tranquilli-Leali), pp. 257-283, Elsevier Science Publishers B.V., Amsterdam (1992).
- J. Black, 'Biological Performance of Tantalum', *Clinical Materials*, **16**, 167-173 (1994)
- N.C. Blumenthal and V. Cosma, 'Inhibition of apatite formation by titanium and vanadium ions', *Journal of Biomedical Materials Research: Applied Biomaterials*, **23**, 13-22 (1989).
- M. Browne and P.J. Gregson, 'Surface modification of titanium alloy implants', *Biomaterials*, **15**, 894-898 (1994).
- S.A. Brown, L.J. Farnsworth, K. Merritt, and T.D. Crowe, 'In vitro and in vivo metal ion release', *Journal of Biomedical Materials Research*, **22**, 321-338 (1988).
- R.A. Buchanan and I.S. Lee, 'Surface modification of biomaterials through noble metal ion implantation', *Journal of Biomedical Materials Research*, **24**, 309-318 (1990).
- B.W. Callen, B.F. Lowenberg, S. Lugowski, R.N.S. Sodhi, and J.E. Davies, 'Nitric acid passivation of Ti6Al4V reduces thickness of surface oxide layer and increases trace element release', *Journal of Biomedical Materials Research*, **29**, 279-290 (1995).
- S.K. Chawla, S.A. Brown, K. Merritt, and J.H. Payer, 'Serum protein effects on polarization behavior of 316L stainless steel', *Corrosion* **46**, 147-152 (1990).
- A. Cigada, G. Rondelli, B. Vicentini, M. Giacomazzi, and A. Roos, 'Duplex stainless steels for osteosynthesis devices', *Journal of Biomedical Materials Research*, **23**, 1087-1095 (1989).
- A. Cigada, M. Cabrini, and P. Pedferri, 'Increasing of the corrosion resistance of the Ti6Al4V alloy by high thickness anodic oxidation', *Journal of Materials Science: Materials in Medicine*, **3**, 408-412 (1992).
- J.P. Collier, V.A. Surprenant, R.E. Jensen, and M.B. Mayor, 'Corrosion at the interface of cobalt-alloy heads on titanium-alloy stems', *Clinical Orthopaedics*, **271**, 305-312 (1991).
- S.D. Cook, M.R. Brinker, R.C. Anderson, R.J. Tomlinson and J.C. Butler, 'Performance of retrieved Kuntscher intramedullary rods: improved corrosion resistance with contemporary material design', *Clinical Materials*, **5**, 53-71 (1990).

- S.D. Cook, R.L. Barrack, G.C. Baffes, A.J.T. Clemow, P. Serekian, N. Dong and M.A. Kester, 'Wear and corrosion of modular interfaces in total hip replacements', *Clinical Orthopaedics*, **298**, 80-88 (1994).
- S.D. Cook, R.L. Barrack, A.J.T. Clemow, 'Corrosion and wear at the modular interface of uncemented femoral stems', *The Journal of Bone and Joint Surgery [Br]*, **76-B**, 68-72 (1994).
- L.D. Dorr, R. Bloebaum, J. Emmanuel and R. Meldrum, 'Histologic, biochemical, and ion analysis of tissue and fluids retrieved during total hip arthroplasty', *Clinical Orthopaedics and Related Research*, nr. 261, 82-95 (1990).
- P. Ducheyne and K.E. Healy, 'The effect of plasma-sprayed calcium phosphate ceramic coatings on the metal ion release from porous titanium and cobalt chromium alloys', *Journal of Biomedical Materials Research*, **22**, 1137-1163 (1988).
- M.L. Escudero and J.L. Gonzalez-Carrasco, *In vitro* corrosion behaviour of MA956 superalloy *Biomaterials*, **15**, 1175-1180 (1994).
- P. Frayssinet, F. Tourenne, N. Rouquet, G. Bonel, and P. Conte, Biological effects of aluminium diffusion from plasma-sprayed alumina coatings, *Journal of Materials Science: Materials in Medicine*, **5**, 491-494 (1994).
- J.L. Gilbert, S.M. Smith and E.P. Lautenschlager, Scanning electrochemical microscopy of metallic biomaterials: reaction rate and ion release imaging modes, *Journal of Biomedical Materials Research*, **27**, 1357-1366 (1993a).
- J.L. Gilbert, C.A. Buckley, and J.J. Jacobs, *In vivo* corrosion of modular hip prosthesis components in mixed and similar metal combinations. The effect of crevice, stress, motion, and alloy coupling, *Journal of Biomedical Materials Research*, **27**, 1533-1544 (1993b).
- J. Gluszek and J. Masalski, Galvanic coupling of 316L steel with titanium, niobium, and tantalum in Ringer's solution, *British Corrosion Journal*, **27**, 135-138 (1992).
- K. Hayashi, I. Noda, K. Uenoyama, and Y. Sugioka, Breakdown corrosion potential of ceramic coated metal implants, *Journal of Biomedical Materials Research*, **24**, 1111-1113 (1990).
- R. Hazan, R. Brener and U. Oron, Bone growth to metal implants is regulated by their surface chemical properties, *Biomaterials*, **14**, 570-574 (1993).
- K.E. Healy and P. Ducheyne, The mechanisms of passive dissolution of titanium in a model physiological environment, *Journal of Biomedical Materials Research*, **26**, 319-338 (1992).
- K.E. Healy, and P. Ducheyne, Passive dissolution kinetics of titanium *in vitro*, *Journal of Materials Science: Materials in Medicine*, **4**, 117-126 (1993).
- P.J. Hughes, S.A. Brown, J.H. Payer, and K. Merritt, The effect of heat treatments and bead size on the corrosion of porous F75 in saline and serum, *Journal of Biomedical Materials Research*, **24**, 79-94 (1990).
- C.B. Johansson, J. Lausmaa, T. Rostlund, and P. Thomsen, Commercially pure titanium and Ti6Al4V implants with and without nitrogen-ion implantation: surface characterization and quantitative studies in rabbit cortical bone, *Journal of Materials Science: Materials in Medicine*, **4**, 132-141 (1993).
- J. Karrholm, W. Frech, K.-G. Nilsson and F. Snorrason, Increased metal release from cemented femoral components made of titanium alloy, *Acta Orthop. Scand.*, **65**, 599-604 (1994).
- B. Kasemo and J. Lausmaa, Material-tissue Interfaces: the role of surface properties and processes, *Environmental Health Perspectives*, **102**, 41-45 (1994).
- J.C. Keller, C.M. Stanford, J.P. Wightman, R.A. Draughn and R. Zaharias, Characterizations of titanium implant surfaces. III, *Journal of Biomedical Materials Research*, **28**, 939-946 (1994).
- D.V. Kilpadi and J.E. Lemons, Surface energy characterization of unalloyed titanium implants, *Journal of Biomedical Materials Research*, **28**, 1419-1425 (1994).
- F.J. Kummer, J.L. Ricci, and N.C. Blumenthal, RF plasma treatment of metallic implant surfaces, *Journal of Applied Biomaterials*, **3**, 39-44 (1992).
- C. Larsson, P. Thomsen, J. Lausmaa, M. Rodahl, B. Kasemo and L.E. Ericson, Bone response to surface modified titanium implants: studies on electropolished implants with different oxide thickness and morphology, *Biomaterials*, **15**, 1062-1074 (1994).
- J. Lausmaa and B. Kasemo, Surface spectroscopic characterization of titanium implant materials, *Applied Surface Science*, **44**, 133-146 (1990).

- G. Lewis, X-ray photoelectron spectroscopy study of surface layers on orthopaedic alloys. II. Co-Cr-Mo (ASTM F-75) alloy, *Journal of Vacuum Science Technology A*, **11**, 168-174 (1993a).
- G. Lewis and K. Daigle, Electrochemical behavior of Ti-6Al-4V alloy in static biosimulating solutions, *Journal of Applied Biomaterials*, **4**, 47-54 (1993b).
- B.F. Lowenberg, S. Lugowski, M. Chipman, and J.E. Davies, ASTM-F86 passivation increases trace element release from Ti6Al4V into culture medium, *Journal of Materials Science: Materials in Medicine*, **5**, 467-472 (1994).
- S. Lugowski, D.C. Smith, and J.C. VanLoon, Critical aspects of trace element analysis of tissue samples: a review, *Clinical Materials*, **6**, 91-104 (1990).
- R.D. Meldrum, R.D. Bloebaum, and L.D. Dorr, Metal ion concentrations in retrieved polyethylene total hip inserts and implications for artifactually high readings in tissue, *Journal of Biomedical Materials Research*, **27**, 1349-1355 (1993).
- K. Merritt, R.W. Margevicius, and S.A. Brown, Storage and elimination of titanium, aluminium, and vanadium salts, *in vivo*, *Journal of Biomedical Materials Research*, **26**, 1503-1515 (1992).
- Y. Okamoto and S. Hidaka, Studies on calcium phosphate precipitation: effects of metal ions used in dental materials, *Journal of Biomedical Materials Research*, **28**, 1403-1410 (1994).
- Y. Okazaki, A. Ito, T. Tateishi, and Y. Ito, Effect of alloying elements on anodic polarization properties of titanium alloys in acid solution, *Materials Transactions, JIM*, **35**, 58-66 (1994).
- J.L. Ong, L.C. Lucas, G.N. Raikar, and J.C. Gregory, Electrochemical corrosion analyses and characterization of surface-modified titanium, *Applied Surface Science*, **72**, 7-13 (1993).
- Y. Oshida, R. Sachdeva, and S. Miyazaki, Changes in contact angles as a function of time on some pre-oxidized biomaterials, *Journal of Materials Science: Materials in Medicine*, **3**, 306-312 (1992).
- Y. Oshida, R. Sachdeva, S. Miyazaki, and J. Daly, Effects of shot-peening on surface contact angles of biomaterials, *Journal of Materials Science: Materials in Medicine*, **4**, 443-447 (1993).
- J. Pan, D. Thierry, and C. Leygraf, Electrochemical and XPS studies of titanium for biomaterial applications with respect to the effect of hydrogen peroxide, *Journal of Biomedical Materials Research*, **28**, 113-122 (1994).
- O.E.M. Pohler, Degradation of metallic orthopaedic implants, in *Biomaterials in reconstructive surgery* (ed. L.R. Rubin), Chap. 15, The CV Mosby Co., 1983, pp. 158-228.
- M. Pourbaix, Atlas of electrochemical equilibria, NACE/CEBELCOR, 1974.
- A. Pourbaix, M. Marek and R.F. Hochman, Comportement électrochimique du titane à bas pH et bas potentiel d'électrode. *Rapports Techniques CEBELCOR*, **118**, RT 197, (1971).
- L.M. Rabbe, J. Rieu, A. Lopez and P. Combrade, Fretting deterioration of orthopaedic implant materials: search for solutions, *Clinical Materials*, **15**, 221-226 (1994).
- J. -P. Randin, Corrosion behavior of nickel-containing alloys in artificial sweat, *Journal of Biomedical Materials Research*, **22**, 649-666 (1988).
- G. Ravnholt and J. Jensen, Corrosion investigation of two materials for implant supraconstructions coupled to a titanium implant, *Scandinavian Journal of Dental Research*, **99**, 181-186 (1991).
- C.C. Ribeiro, M.A. Barbosa, A.A.S.C. Machado, A. Tudor, and M.C. Davies, Modifications in the molecular structure of hydroxyapatite induced by titanium ions, *Journal of Materials Science: Materials in Medicine*, **6**, 829-834 (1995).
- C. Sella, J.C. Martin, J. Lecoeur, J.P. Bellier, M.F. Harmand, A. Nadji, J.P. Davidas, and A. Le Chanu, Corrosion protection of metal implants by hard biocompatible ceramic coatings deposited by radio-frequency sputtering, *Clinical Materials*, **5**, 297-307 (1990).
- M.F. Semlitsch, H. Weber, R. Streicher and R. Schon, Joint replacement components made of hot-forged and surface-treated Ti-6Al-7Nb alloy, *Biomaterials*, **13**, 781-788 (1992).
- S.R. Sousa and M.A. Barbosa, Electrochemistry of AISI 316L stainless steel in calcium phosphate and protein solutions, *Journal of Materials Science: Materials in Medicine*, **2**, 19-26 (1991).
- S.R. Sousa and M.A. Barbosa, Corrosion resistance of titanium cp in saline physiological solutions with calcium phosphate and proteins, *Clinical Materials*, **14**, 287-294 (1993).

- S.J. Stohs and D. Bagchi, Oxidative mechanisms in the toxicity of metal ions, *Free Radical Biology and Medicine*, **18**, 321-336 (1995).
- D.S. Sutherland, P.O. Forshaw, G.C. Allen, I.T. Brown and K.R. Williams, Surface analysis of titanium implants, *Biomaterials*, **14**, 893-899 (1993).
- P. Tengvall, L. Lundstrom, L. Sjokvist, H. Elwing, and L.M. Bjurstein, Titanium hydrogen peroxide interaction: model studies of the influence of the inflammatory response on titanium implants, *Biomaterials*, **10**, 166-175 (1989).
- P. Tengvall and I. Lundstrom, Physico-chemical considerations of titanium as a biomaterial, *Clinical Materials*, **9**, 115-134 (1992).
- K.A. Thomas, S.D. Cook, A.F. Harding, and R.J. Haddad Jr., Tissue reaction to implant. corrosion in 38 internal fixation devices, *Orthopedics*, **11**, 441-451 (1988).
- H. Tomás, A.P. Freire, and L.M. Abrantes, Cast Co-Cr alloy and pure chromium in proteinaceous media: an electrochemical characterization, *Journal of Materials Science: Materials in Medicine*, **5**, 446-451 (1994).
- S. Torgersen and N.R. Gjerdet, Retrieval study of stainless steel and titanium mini plates and screws used in maxillofacial surgery, *Journal of Materials Science: Materials in Medicine*, **5**, 256-262 (1994).
- D.L. Tsalev and Z.K. Zaprianov, Atomic absorption spectrometry in occupational and environmental health practice, Vol. I, CRC Press, Boca Raton, 1983.
- J.A. von Fraunhofer, N. Berberich, and D. Seligson, Antibiotic-metal interactions in saline medium, *Biomaterials*, **10**, 136-138 (1989).
- J.C. Wataha, C.T. Hanks, and R.G. Craig, Uptake of metal cations by fibroblasts *in vitro*, *Journal of Biomedical Materials Research*, **27**, 227-232 (1993).
- A. Wisbey, P.J. Gregson, and M. Tuke Application of PVD TiN coating to Co Cr-Mo based surgical implants, *Biomaterials*, **8**, 477-480 (1987).
- R.L. Williams, S.A. Brown, and K. Merritt, Electrochemical studies on the influence of proteins on the corrosion of implant alloys, *Biomaterials*, **9**, 181-186 (1988).

Chapter 11

Carbons

A.D. Haubold, R.B. More, and J.C. Bokros

11.1 Introduction

The biocompatibility of carbon has long been appreciated: ancient man, for example, knew that pulverized charcoal could be placed under the skin without any apparent ill effects (Benson, 1969). The charcoal particles visibly remained indefinitely and thus allowed ancient man the means to decorate himself permanently with tattoos. However, it was not until the mid-1960s that carbon was first considered for use as a structural material in implantable prosthetic devices. During this period, a specific, imperfectly crystalline, man-made, pyrolytic form of carbon was found to be well suited for application in prosthetic heart valves. Because of the outstanding clinical success of pyrolytic carbon in long-term structural components of heart valve prostheses, carbons have assumed a prominent position in our repertoire of biomaterials and have sparked investigation of other forms of carbons for possible *in vivo* use. A number of these forms are listed in Table 11.1. This chapter will be devoted to a discussion of the background and historical uses of carbons in medical devices along with suggestions for future research.

11.1.1 Background

Although only two allotropic crystalline forms of elemental carbon, diamond and graphite occur in nature, carbon also occurs as a spectrum of imperfect crystalline forms that range from amorphous through mixed amorphous, graphite-like and diamond-like to the perfectly crystalline allotropes. Such imperfect crystalline

A.D. Haubold (✉) • R.B. More • J.C. Bokros
Medical Carbon Research Institute,
8200 Cameron Road Suite A-196, Austin, TX 78754–8323, USA

Table 11.1 Carbon Forms

Pyrolytic Carbon	Produced at low or high temperature from the thermal pyrolysis of a hydrocarbon in a fluidized bed. These materials have a laminar, isotropic, granular or columnar structure and may be pure carbon or alloyed with various carbides.
Glassy or Polymeric Carbons	Obtained from the thermal pyrolysis (~1000 °C) of selected polymers and may be monolithic, porous or reticulated.
Artificial Graphites	Produced from a variety of starting materials such as petroleum or naturally occurring cokes and yield bulk structures of varying grain size, crystallite orientation, purity, porosity, strength, and particle size.
Carbon Fibers	Formed from spun polymeric fibers which are subsequently pyrolysed to yield structures of unusual strength and stiffness. The properties are a function of polymer precursor and processing history. More recently, carbon fibers have been grown from the vapor phase.
Charcoal	These are perhaps the oldest and most diverse materials with interesting adsorptive properties and are produced from many organic material spanning the range from wood to coconut shells to animal bones.
Vapor Phase Coatings	Applied, generally at reduced pressures (<1 atm) and often at low temperatures to provide a carbonaceous surface coating that ranges from amorphous to diamond-like with accompanying wide variation in thermal, mechanical and electrical properties.
Composites	Structures have been produced that utilize all of the above materials and even some other binders. Found in this group of materials are carbon fibers infiltrated and held together with pyrolytic carbon, silicon carbide, glassy carbon, PTFE, methyl methacrylate, epoxies, and petroleum pitches as well as combinations thereof. The structures may contain randomly oriented chopped fibers or long filaments oriented in random, 2, 3 and n dimensions.

structures are termed turbostatic and give rise to considerable variability in physical and mechanical properties (Figure 11.1). Indeed, this ability of carbon to assume either perfectly crystalline or chaotic, turbostatic structures gives rise to confusion when considering physical and mechanical properties. For this reason, it is best to consider carbon as a spectrum of materials and to bear in mind that within this spectrum, a number of unique combinations of structure and physical and mechanical properties occur. This is true with respect to biocompatibility: the fact that one type of pyrolytic carbon has been used successfully in heart valves does not necessarily imply that other forms of pyrolytic carbons or indeed other forms of carbon in general will also prove useful in this or other prosthetic applications. For example, pyrolytic and glassy carbon can be finished to have identical appearances, yet the properties of glassy carbon make it unsuitable for use in prosthetic heart valves (Haubold *et al.*, 1981).

For successful use in implantable prostheses a material (1) must retain its properties required for device function in the hostile biological environment and (2) must not provoke adverse effects either locally or systemically. Most of the pure carbons are relatively inert and unlikely to provoke severe tissue reactions, however, only certain pyrolytic carbons have sufficient strength, fatigue resistance, wear resistance

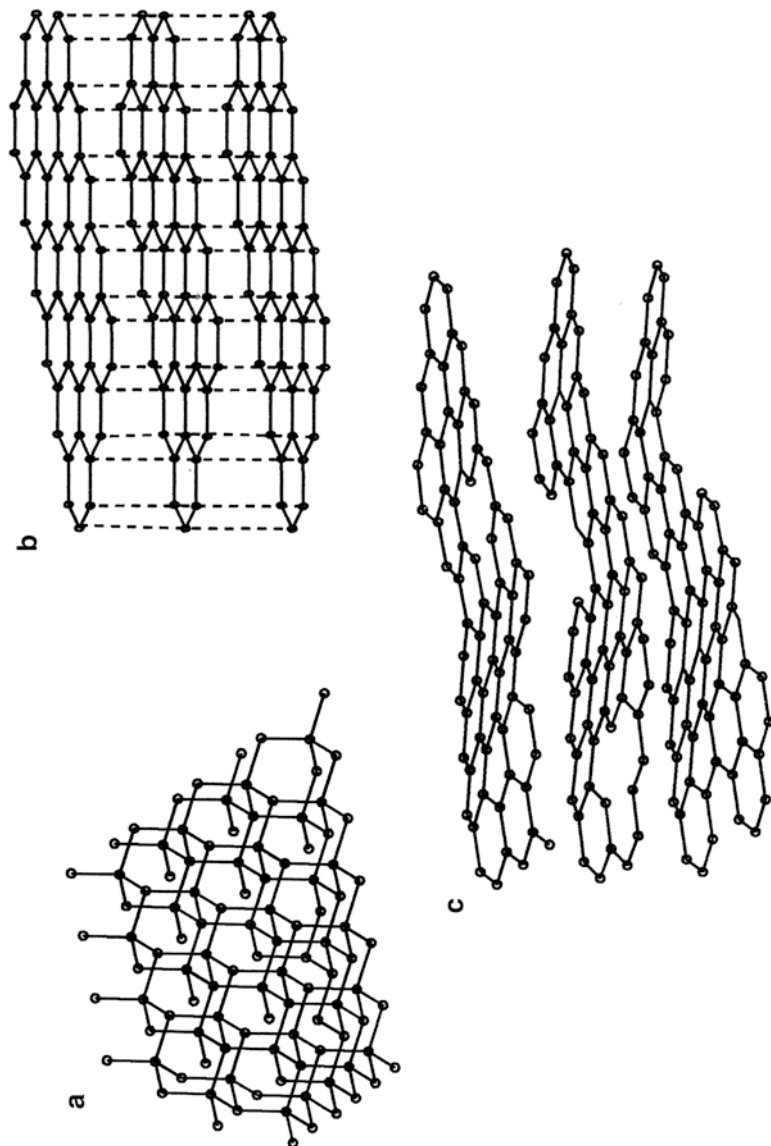


Figure 11.1 Possible atomic arrangements of crystalline carbon: (a) diamond tetrahedral, cyclohexane chair, crystalline structure, (b) graphite planar hexagonal layered structure (c) three-dimensional quasicrystalline turbostratic structure. Biomedical carbons have a turbostratic structure.

and biodegradation resistance to function as long-term implant structural components. In fact, the pyrolytic carbons were deliberately tailored to meet the specific biocompatibility requirements for heart valve component application (Bokros *et al.*, 1972; Haubold, 1977). Silicon was added in small amounts (5–12 wt%) as an alloying element in order to form silicon carbide inclusions to assure adequate wear. Furthermore, specific processing parameters were identified in order to produce suitable microstructures and densities, as well as the strength levels required. Glassy carbon, as mentioned above, could not be prepared with adequate strength and wear resistance. Thus, biocompatibility cannot be presumed *a priori* for carbon materials: each particular application has specific demands which require a unique set of properties. While the spectrum of carbon materials encompasses many such properties, the particular material must be engineered to uniquely satisfy all of the properties needed.

11.1.2 *Diamond*

Diamond, the hardest substance known, has the so called *diamond cubic structure* consisting of a network of regular tetrahedral arrays in which each carbon atom is covalently bonded to four other carbon atoms forming the corners of a regular tetrahedron (Figure 11.1). From X-ray diffraction data, there is a single value, 1.54 Å bond length and a unit cube lattice spacing of 3.56 Å. The entire crystalline array is a single covalently bonded molecule. Because many covalent bonds must be broken to break the crystal, a very large amount of energy is required, therefore, the substance is very hard (Pauling, 1964). There has been an ongoing interest in the use of diamond or diamond-like coatings (May, 1995). However, suitable manufacturing processes do not yet exist that allow economical preparation of diamond type materials in the quantity, quality, shapes and sizes required for durable long term biomedical applications. A specific application uniquely requiring diamond or diamond-like material for clinical success has not been identified as a justification to compel additional research efforts in preparation techniques.

11.1.3 *Graphites*

Graphite has a layered hexagonal crystal structure. Each atom forms two single bonds and one double bond with its three nearest in-plane neighbors to form sheet-like layers of flat six atom ring arrays (Figure 11.1). Interatomic bond distances are 1.42 Å within the layer and 3.4 Å between each layer. Within each layer, bonding is covalent and between the layers, bonding is of the much weaker van der Waals type. Consequently, the layers are easily separated giving rise to the soft, lubricating properties of graphite.

Naturally occurring graphite is generally found as a isolated small scales or imperfect single crystal precipitates in granite. These small crystals such as those

found in Madagascar, Ontario and in New York have dimensions on the order of a few millimeters. Larger graphite masses have been found in China and Korea. Natural graphites are thought to be formed by metamorphosis of sedimentary carbonaceous materials or by reaction with and precipitation from liquid magma. The naturally occurring graphite materials are useful primarily as the starting material for subsequent fabrication of some 'artificial graphites'.

Graphite was first synthesized accidentally by heating carborundum to extreme temperatures. The silicon was driven off leaving a graphite residue. A patent on this production process was granted over 100 years ago. Since then, petroleum and other types of cokes coupled with organic binders have become the major raw materials in the production of a wide variety of carbonaceous conglomerates called artificial graphite.

The manufacturing processes employed today are as varied as are the properties of the resultant materials. Bulk graphites are usually molded, extruded, hot isostatically compacted and may even be formed by combinations of these processes. They may be further reimpregnated with binder subsequent to graphitization (heat-treatment step), infiltrated isothermally or in a thermal gradient with methane or aromatic hydrocarbons. The resultant materials have widely varying properties and purity which can have a profound influence on the interaction of 'graphite' with the living environment.

Because of low strength and low wear resistance, graphite alone is not suitable as a structural member of an implant. But, investigations of colloidal graphite coatings as a blood compatible surface during the mid-1960s led investigators to examine pyrolytic carbon. Pyrolytic carbon, initially developed and used as a coating for nuclear fuel pellets, was found to have excellent blood compatibility, strength, wear resistance and durability for application in long term implants. The historical account leading to the use of LTI (low temperature-isotropic) pyrolytic carbon has been described (Bokros *et al.*, 1972, 1975). Graphite is widely used as a substrate for pyrolytic carbon coatings in heart valve components. In prosthesis applications, graphite is entirely encased in pyrolytic carbon coatings on the order of one mm thickness. Here the stronger, more durable coating stabilizes the interior graphite structures.

11.1.4 Pyrolytic carbons

Pyrolytic carbons of the type developed at General Atomic for use in bioengineering were an off-spring of research directed at developing carbon materials that would be suitable for structural applications in the severe environment of high-temperature, gas-cooled nuclear reactors. The isotropic carbon forms called high-temperature-isotropic carbon were derived from the gas phase nucleation and condensation of droplets formed during the pyrolysis of methane at temperatures in excess of 2000°C where densification can occur by thermally activated processes. The carbons called low-temperature-pyrolytic carbons are formed by the pyrolysis

of other hydrocarbons (such as propane and propylene at lower temperatures in the range 1300–1500°C. The carbon materials so produced are not uniquely structured nor are all of them isotropic. Wide and complex variations in properties are possible ranging from weak to very strong, and in structure ranging from laminar and anisotropic, to isotropic, to columnar and granular, the latter also varying in anisotropy. A comprehensive review of the deposition and structure of pyrolytic carbon is given by Bokros (1969).

11.1.5 Glassy carbons

The preparation, structure and properties of glassy, or polymeric carbons has been described in detail by Jenkins and Kawamura (1976). These carbons are derived from a polymer by a slow pyrolysis process which results in a vitreous residue free of macroscopic bubbles.

Fabrication of glassy carbon materials is a relatively straightforward, but time consuming process. A preformed polymeric precursor such as phenol-formaldehyde, polyfurfuryl alcohol, polyvinyl alcohol or oxidized polystyrene is slowly heated in an inert atmosphere to a high temperature in excess of 2000 °C. Heating times may be as short as a day or as long as one month. It is not unusual to encounter exothermic temperature regions that must be traversed very slowly (i.e., 1 °C temperature increase per hour) to avoid the nucleation of bubbles.

There is a volumetric shrinkage of about 50% so the resultant structure formed in this process is a miniature of the precursor preform. The gases generated within the preformed structure must have time to diffuse out and not nucleate bubbles so one dimension of glassy carbon structures is limited to about seven millimeters. Hence materials or objects are limited to thin flat plates or tubes with thin walls. Massive equiaxed structures are not possible unless they are small with dimensions compatible with the diffusional requirements.

11.1.6 Carbon fibers

Carbon fibers, thought by many to be a relatively new material, actually have a long history as evidenced by the issuance of the first patent for incandescent electric lamp filaments (carbon fibers). The patent was issued to Thomas Edison in 1892. Hiram Maxim (the inventor of the machine gun, among other things) was issued a process patent for carbon fibers in 1899. Prior to the 1950s, these fibers had marginal strength and were used primarily for their electrical properties.

High strength carbon fibers were developed in the 1950s for the aerospace industry and military aircraft. The mechanical properties of rayonbased carbon fibers were enhanced using stress graphitization. Since that time, a variety of other precursors have been used including polyacrylonitrile (PAN), specific fractions of asphalt or pitch, lignin, liginosulfonates, hetero and nonheterocyclic aromatic polymers,

linear polymers and even coal. The processes for fiber manufacture are as varied as the precursors themselves. In the patent literature, hundreds of processes and variants can be found (Sittig, 1980). Nevertheless, generalizations can be made. The first step in the process is the selection and treatment of a suitable raw material which can be carbonized to a high yield. The second step generally consists of a low temperature (250–500 °C heat treatment or preoxidation followed by high temperature (up to 2800 °C) carbonization and graphitization steps.

The resultant fibers generally are of three types classified according to their structure and the degree of crystallite orientation. There are the high modulus (50 million psi or above), high strength fibers which, when incorporated into structures, give the highest stiffness per unit weight. Fibers with a lower modulus (about 30 million psi) but still of high strength are the second class of generally available fibers. The lowest modulus (less than 20 million psi) do not have structural applications.

11.1.7 Vapor phase coatings

Coatings formed at reduced pressure (<1 atm) are generally termed ‘vapor deposited’. These coatings may be formed by physical vapor deposition, chemical vapor deposition or combinations thereof. Physical vapor deposition such as evaporation is probably the oldest technique for depositing thin films and involves generating a vapor from a source material at reduced pressure. The vapor subsequently condenses on the object to be coated. This technique suffers from a number of limitations such as only line-of-sight coating is possible. In the case of a carbon source, which does not evaporate but rather only sublimates at extreme temperatures, the object to be coated is exposed to direct thermal radiation from the subliming source. Few materials can withstand the intense thermal radiation for any great length of time. Hence coating thickness is limited as is the choice of substrate material to be coated. Much has been written on physical vapor deposition such as the comprehensive text by Maissel and Glang (1970).

More versatile coating techniques are broadly termed chemical vapor deposition (CVD). Coatings are formed through chemical reactions in the vapor phase or through the thermal decomposition or reduction of gases generally at reduced pressures. It is interesting to note that the process used to form pyrolytic carbon is a CVD process but is generally carried out at ambient pressures. The low temperature CVD processes are usually assisted by means of catalysts, glow discharge plasmas, ion beams and the like to activate gas reactions. In fact, production of diamond films is now almost routine through ion beam assisted disassociation of selected hydrocarbons in the presence of excess hydrogen. On the other hand, amorphous carbon films with little or no detectable crystallinity can also be produced by CVD. Thus chemical vapor deposition techniques are extremely versatile and consequently films and coatings produced by CVD must be carefully characterized and identified. An extensive and comprehensive review of thin film deposition technologies can be found in Bunshah (1982).

11.1.8 Composites

Even more complex than the materials described above are a family broadly termed 'composites'. Three-dimensional structures can be formed by combining a filler material with an appropriate matrix. Herein lies the difficulty with composites; all too often, the starting materials are not adequately described and the resultant structure characterized.

Carbon-carbon composites can be produced with a multitude of structures. The simplest have two-dimensional order and consist of stacked plies of carbon fabric held together by a carbon matrix. The fabric fibers may be any of those described previously, prepared from the pyrolysis of polyacrylonitrile and the like. The matrix could be derived from petroleum pitch or be infiltrated pyrolytic carbon or even silicon carbide. The latter are generally referred to as SiC/C composites. From two-dimensional, the next progression in structure is three-dimensional on to n-dimensional. This terminology refers to fiber orientation within the matrix.

Filament wound carbon composites have also been developed. In this case the desired shape is, as the name implies, wound using carbon fibers onto a suitable mandrel. The fibers are bonded using an epoxy type or thermoset resin. The bonding of the matrix to the fibers and direction of fiber orientation in large part determine the mechanical properties of the composite. The biological properties are generally governed by the selection of matrix.

11.2 Historical Overview -*In Vivo* Applications

Encouraged by the success of the LTI form of pyrolytic carbon in the demanding mechanical heart valve application, other carbon materials and usages were explored. Different carbon materials have been evaluated because pyrolytic carbon was patented on the one hand and processing constraints limited its versatility on the other hand. Shown in Table 11.2 are examples that demonstrate medical and engineering ingenuity in attempts to expand the use of carbons in the biological environment. Although the attempts are numerous and varied, only the use of carbon as components for artificial heart valves has achieved widespread usage.

11.2.1 Dental

One of the earliest applications of carbon as an implant material was in restorative dentistry. The first devices were bulky posts fabricated from glassy carbon that were implanted in the maxilla or mandible to serve as artificial tooth roots. Because of the inherent lack of strength of glassy carbon, they were bulky and poorly accepted. As a further complication, the stainless steel post on which a crown was cemented formed a galvanic couple *in vivo* leading to complications caused by accelerated corrosion of the stainless steel.

Table 11.2 Applications of Carbon in Medical Devices

Active Component in Hemodetoxifier	Dental Implants
Alveolar Ridge Maintenance Particles	• Posts
Carbon Fiber Patch Fabrics	• Blades
Catheter Tips	• Coating on metallic implants
Coated Components for Membrane Oxygenators	Electrodes
Coated Emboli Filters	• Solid
Coated Mandibular Trays	• Coated
Coated Tracheal Prosthesis	<i>Ex vivo</i> Blood Filters
Coated TMJ Condyle Prosthesis	Femoral Stems
Coated Prosthetic Fabrics and Polymers	• Coated
Coated Aneurysm Clips	• Composite
Coating on Angioplasty Stents	Femoral Condyle Replacements
Coatings on Heart Valve Suture Rings	Femoral Heads
Coatings on Indwelling Catheters and Delivery Systems	• Coated
Coatings on Vortex Blood Pumps	Fracture Fixation Devices
Coatings in Vascular Grafts	Left Ventricular Apex Inlet Tubes
Components for Centrifugal Blood Pumps	Ligaments and Tendons
Composites Soft Tissue Replacement	Mechanical Heart Valve Components
	Ossicular Replacement Prosthesis
	Particles for Filling Periodontal Defects
	Percutaneous Access Devices
	Small Joint Replacements
	• Hand
	• Wrist
	• Elbow
	• Foot
	Tibial Plateau Replacements
	Vascular Attachment Prosthesis

Carbon forms

	Young's Modulus (GPa)	Flexural Strength (MPa)	Hardness (DPH 500 g)	Density (g/cm ³)	Fracture Toughness (Mpa √m)	Wear Resistance
Diamond	760–104	600–2000	5700–10400 Knoop	2.9–3.5	5–7	Potentially excellent
Pure pyrolytic carbon	28	486	>230	1.5–2.1	1.67	Excellent
Si-alloyed pyrolytic Carbon	31	389	>230	2.0–2.2	1.17	Excellent
Glassy or Polymeric Carbons	21	175	150	<1.54	0.5–0.7	Poor
Artificial Graphites	4–12	65–300	50–120	1.5–1.8	1.5	Poor
Carbon fibers	172–517	896–2585	*	1.6–1.8	*	*
Charcoal	NA	NA	NA	NA	NA	NA
Vapor phase coatings	17			1.8		
Composites	*	*	*	*	*	*

* Dependent upon matrix.

In another attempt, artificial tooth roots in the form of blades were fabricated from pyrolytic carbon. Although they were less bulky than the glassy carbon implants, they were difficult to place. Improper seating of the blade caused micro-motion after implantation that ultimately caused the prosthesis to fail. The success rate of 60% after 5 years was judged inadequate. Metal blades coated with carbon fared a similar fate.

Metallic mandibular reconstruction trays coated with a vapor deposited film of carbon generally performed well. The application was complicated by the fact that the trays were custom and many times fashioned directly in the operating room, making the logistics of coating with carbon unacceptable.

11.2.2 *Vascular*

Graft prostheses >6mm diameter are generally considered to work well and improvements in performance as a result of modifying the biochemical nature of the graft lumen with carbon coatings are difficult to quantify and not significant enough to justify the cost of carbon coating. Improvements in the patency of small diameter grafts (<4 mm) as a result of carbon coating have been reported but even with the improvement, these grafts ultimately failed as a result of intimal hyperplasia proliferation at the anastomoses. While the carbon coating may retard clotting of certain grafts, the coating does little to ameliorate intimal hyperplasia formation. Carbon vascular attachment prostheses have also been reported to perform poorly, not as a result of poor biocompatibility, but rather the result of mechanical complications.

11.2.3 *Orthopedics*

Femoral stems fabricated from carbon composites fitted with a femoral head fabricated from pyrolytic carbon have been reportedly used successfully by some for over 10 years (Chen, 1986). Others have experienced disastrous failures through a lack of attention to engineering and material property details. Such failures naturally lead to questions on the suitability of 'carbon' for use in such medical devices. Attempts are underway to design and fabricate other joint replacements.

Ligaments and tendons have been fabricated from carbon fibers (Béjui and Drouin, 1988). These fibers in the initial stage perform well as a scaffolding material that aids in the regeneration of tendons and ligaments *in vivo*; but in the long term the fibers fracture and migrate to, for example, the lymph nodes.

Fracture fixation devices that are fabricated from stainless steel are unsuitable for coating or coupling with carbon because of galvanic effects (Haubold *et al.*, 1986). Carbon composite devices have been used reportedly with good results but such usage has not become widespread presumably because of an unaccepted cost/benefit ratio.

11.2.4 Other

Many applications of devices listed in Table 11.2, while successful, are not in widespread use because, even in their non-carbon form, usage is limited. For example, left ventricular apex tubes (Haubold *et al.*, 1979) are used successfully in the construction of a prosthesis to correct idiopathic hypertrophic subaortic stenosis but fortunately in man, such a medical condition is rare.

11.3 New Directions/Future Trends

LTI pyrolytic carbons, since their introduction in the late 1960s, have become the material of choice for use in the fabrication of mechanical prosthetic heart valves. Over 90% of the mechanical valves implanted worldwide utilize such carbon components. To date, more than 2 million valves have been implanted which amounts to an accumulated experience in excess of 12 million patient years. While this material has proven to be the most successful carbon biomaterial, it can be improved. Recently, advances in process control methodologies have allowed refinements in the pyrolytic carbon coating preparation. These improvements allow the elimination of the potentially thrombogenic silicon carbide from the biomedical coatings. Furthermore, this pure pyrolytic carbon can be produced with substantially improved mechanical properties relative to the silicon alloyed material (Emken *et al.*, 1993; Ely *et al.*, 1994.). Such improvements in the material open possibilities for improvements in heart valve prosthesis design and performance.

Results from investigations on the suitability of other forms of carbon for *in vivo* use yielded mixed and often seemingly contradictory results. Some of the confusion developed because of misunderstanding of carbon structure and misunderstanding of the relationship of carbon properties to such structures. The use of the generic label 'carbon' compounded the problem. A similar situation exists with 'polyurethanes'. There are polyether urethanes, polyester urethanes, polyether urethane ureas and even polyester urethane ureas – all misappropriately called simply 'urethanes'. Thus it is not surprising that the biological responses of 'carbon' (Table 11.1) are so varied.

Biocompatibility claims for a particular form of 'carbon' based on published results for a totally different form or structure should be carefully scrutinized. For example, to claim that carbon fibers have the same biological properties as bulk pyrolytic carbons or even that all pyrolytic carbons behave similarly is unjustified. In the case of fibers, geometry plays a significant role. It is well known that bulk materials may be well tolerated when the same material in particulate form may not. The lack of characterization and standardization can be devastating.

More and more entrants are anticipated into the field of carbon biomaterials. In the past, because of technology, patent or cost constraints, there were only several sources for, for example, pyrolytic carbon. A number of the earlier constraints have now been removed. Consequently, these materials are being produced in limited but increasing

quantities in many countries, using a multiplicity of fabrication techniques. The challenge for the future is to be precise in material identification, characterization and to avoid generalization.

References

- Bejui, J. and Drouin, G. (1988). Carbon Fiber Ligaments. In *CRC Critical Reviews in Biocompatibility*, 4(2), 79–108.
- Benson, J. (1969). *Pre-Survey on the Biomedical Applications of Carbon*, North American Rockwell Corporation Report R-7855.
- Bokros, J.C. (1969). Deposition, Structure, and Properties of Pyrolytic Carbon. In *Chemistry and Physics of Carbon*, Vol. 5 (Walker, P.L., ed.). Dekker, New York, pp. 1–118.
- Bokros, J.C. LaGrange, L.D. and Schoen, F.J. (1972). Control of Structure of Carbon For Use in Bioengineering. In *Chemistry and Physics of Carbon*, Vol. 9 (Walker, P.L., ed.). Dekker, New York, 103–171.
- Bokros, J.C., Akins, R.J., Shim, H.S., Haubold, A.D. and Agarwal, N.K. (1975). Carbon in Prosthetic Devices. In *Petroleum Derived Carbons* (Deviney, M.L., and O'Grady, T.M., eds). American Chemical Society, Washington, DC, pp. 237–265.
- Bunshah, R.F. (ed.) (1982). *Deposition Technologies for Films and Coatings.*, Noyes Publications, Park Ridge.
- Chen, Lan-Tian (1986). Carbon-Titanium Combined Joints. In *Chinese Journal of Biomedical Engineering* 3, 55–61.
- Ely, J., Haubold, A., Bokros, J. and Emken, M. (1994), New Unalloyed Pyrolytic Carbon with Improved Properties for Implant Applications, *XXI Congress European Society for Artificial Organs*, Oct. 20–22, Barcelona Spain. Also US Patent 5 514 410.
- Emken, M., Bokros, J., Accuntis, J. and Wilde, D., (1993) Precise Control of Pyrolytic Carbon coating, *Extended Abstracts & Program Proceedings of the 21st Biennial Conference on Carbon*, Buffalo New York, June 13–18, pp. 531–532. Also US Patent 5 284 676.
- Haubold, A.D., Shim, H.S., and Bokros, J.C. (1979). Carbon Cardiovascular Devices. In *Assisted Circulation* (Unger, F., ed.) Springer Verlag, Berlin, Heidelberg, New York, pp. 520–532.
- Haubold, A.D. (1977). Carbon in Prosthetics. In *Annals of the New York Academy of Sciences*, Vol. 283, *The Behavior of blood and its Components at Interfaces*, (Vroman, L. and Leonard E.F., eds). New York Academy of Sciences, New York.
- Haubold, A.D., Shim, H.S., and Bokros, J.C. (1981). Carbon in Medical Devices. In *Biocompatibility of Clinical Implant Materials*, Vol II (Williams, D.F., ed.). CRC Press, Boca Raton, pp. 3–42.
- Haubold, A.D., Yapp, R.A., and Bokros, J.C. (1986). Carbons for Biomedical Applications. in *Encyclopedia of Materials Science and Engineering* (Bever, M.B., ed.) Pergamon Press, Oxford, New York, Toronto, Sydney, Frankfurt, pp. 514–520.
- Jenkins, G.M. and Kawamura, K. (1976). *Polymeric Carbons - Carbon Fibre, Glass and Char*. Cambridge University Press, Cambridge. London, New York, Melbourne.
- Lewis, J.C. and Redfern, B., and Cowland, F.B. (1963). Vitreous Carbons as Crucible Materials for Semiconductors. In *Solid State Electronics*, 6, 251.
- Maissel, L.I. and Giang, R. (1970). *Handbook of Thin Film Technology*, McGrawHill, New York.
- May, P.W. (1995), CVD Diamond - a new Technology for the Future?, *Endeavor Magazine* 19(3), 101–106.
- Pauling, L. (1964), *College Chemistry*, W.H. Freeman and Co., San Francisco.
- Pierson, H.O. (1993) *Handbook of Carbon, Graphite, Diamond and Fullerenes*, Noyes Publications, Park Ridge, New Jersey.
- Sittig, M. (1980). Carbon and Graphite Fibers. Noyes Data Corporation, Park Ridge. Mechanical Behavior of Diamond and Other Forms of Carbon, *Materials Research Society Symposium Proceedings*, Vol. 383, ed. Dory M.D. et al., Materials Research Society, Pittsburgh, Pennsylvania, 1995.

Part III

Chapter 1

General Concepts of Biocompatibility

D.F. Williams

1.1 Introduction

The host responses to biomaterials are extremely varied, involve a range of different mechanisms and are controlled by factors that involve characteristics of host, material and surgical procedure. These responses themselves constitute a significant component of the phenomenon of biocompatibility. In this section, the broad concepts of biocompatibility are critically reviewed with particular reference to the role that the human host response plays in determining the performance of the biomaterial and of the device in which it is used. Particular emphasis is given to the influence of biocompatibility in the clinical applications of devices. It should be remembered, however, that biocompatibility phenomena are extremely difficult to interrogate remotely or to study in an active way, so that accurate information of the details of biomaterial–human tissue interactions is not readily available. As Black (1) has pointed out with reference to observations on the host response in general, we are usually limited to detecting events long after they have occurred by examining end-points, usually histopathologically, after the host is dead. This is largely the case with experiments on biocompatibility in animals, but is an even more relevant observation with the human clinical experience. All comments in this section must therefore be interpreted with this in mind.

D.F. Williams (✉)

Department of Clinical Engineering, Royal Liverpool University Hospital,
147, Liverpool L69 3BX, UK

1.2 The Definition of Biocompatibility

Etymologically, the term 'biocompatibility' sounds simple to interpret since it implies compatibility, or harmony, with living systems. This concept, however, is a little too simple to be useful and the meaning of compatibility has to be explored further.

It is intuitively obvious that a biomaterial or implanted medical device should cause no harm to the recipient by intent or by accident. This is the underlying principle of biological safety but is not the totality of biocompatibility. A material may well be entirely safe in the human body but unless it actually does something useful, it is not necessarily appropriate for a medical device. For many years during the evolution of biomaterials, this was not really taken into account and the 'requirements' of biomaterials were dominated by the perceived necessity to be safe, which was interpreted as a requirement that a biomaterial should be totally inert in the physiological environment and should itself exert no effect on that environment. In other words, there should be no interaction between biomaterials and the host, in the latter case implying that the material should be non-toxic, non-irritant, non-allergenic, non-carcinogenic, non-thrombogenic and so on.

This concept of biocompatibility, which equates the quality to inertness and biological indifference, has resulted in the selection of a portfolio of acceptable or standard biomaterials which have widespread usage. These range from the passivatable alloys such as stainless steel and titanium alloys, the noble metals gold and platinum, to some oxide ceramics such as alumina and zirconia, various forms of carbon and a range of putatively stable polymeric materials including silicone elastomers (polysiloxanes), polyolefins, fluorocarbon polymers and some polyacrylates. of course, if this was all there was to biocompatibility, there would be few problems other than optimizing inertness and there would be little to write about.

In practice, biocompatibility is far more complex. There are at least four reasons for this. The first is that inertness in the physiological sense requires a great deal more than resisting degradation at the atomic or molecular level and the second is that even if it were so, this goal is extremely difficult to achieve. Indeed it is now recognized that no material is totally inert in the body. Even those very stable materials mentioned above will interact to some extent with tissues; titanium, although one of the most corrosion resistant engineering alloys, corrodes in the body, as judged by the presence of the metal in the surrounding tissues as well as serum and urine. With many materials, while the main component itself may be exceptionally inert, there are often minor components, perhaps impurities or additives which can be released under some circumstances. The leaching of plasticizers and other additives from plastics provide good examples of interactions which are not related to the molecular breakdown of the material but which confer a degree of instability to the product. Moreover, in the context of interactions which affect the overall performance of the material in the physiological environment, it is important to note that an interfacial reaction involving a physicochemical process such as protein adsorption will take place with the vast majority of materials, further emphasizing the fact

that inertness is a very relative term and there is indeed no such thing as an inert biomaterial.

The third reason why biocompatibility cannot be equated with inertness is that there are several, and indeed an increasing number, of applications which involve intentionally degradable materials. The two most widely quoted situations here are absorbable sutures and implantable drug delivery systems but many more circumstances where degradable scaffolds and matrices could form an essential component of a device are envisaged. If biocompatibility is predicated on inertness, then degradable materials cannot, by definition, be biocompatible. This clearly does not make sense and suggests that the concept of biocompatibility needs to be altered.

The fourth reason is even more compelling, especially when considering biomaterials used in devices for tissue reconstruction. If a device is made from materials which are inert and which do not interact with the body in any way, then it is unlikely that it can be truly incorporated into the body. For effective long term performance in the dynamic tissue environment, it is far more preferable for there to be functional incorporation, which implies that the device should be stimulating the tissues to be reactive to it positively rather than negatively. Thus biocompatibility should not be concerned with avoiding reactions but selecting those which are the most beneficial to device performance.

On the basis of these ideas, biocompatibility was redefined a few years ago (2), as 'the ability to perform with an appropriate host response in a specific situation.' Clearly this definition encompasses the situation where inertness is still required for the most appropriate response in some situations is indeed no response. A traditional bone fracture plate is most effective when it is attached mechanically to the bone and does not corrode; no response of the tissue to the material is normally required. Even here, however, we have to concede that a material that could actively encourage more rapid bone healing might be beneficial so that a specific osteoinductive response would be considered appropriate.

More importantly, the definition allows a material to stimulate or otherwise favour a specific response, including cell activation, where that response optimizes the performance of the device. It will be obvious that the required response will vary with the particular application, which clearly implies that the response, both desired and actual, will vary with the different types of tissue encountered by biomaterials.

The above definition also stipulates that the biocompatibility of a material has to be qualified by reference to the specific application. The response to some very common and popular biomaterials may vary quite considerably and some of the major problems of implantable medical devices have been caused by a misunderstanding about transferability of biocompatibility data. To recognize the very effective performance of a material under one set of conditions but then to assume that the same material can perform equally well under entirely different circumstances is inherently dangerous since it takes into account neither the variations one might expect to see in the host response from site to site nor the fact that what is appropriate for one situation may not be appropriate for another.

1.3 Components of Biocompatibility

The above definition of biocompatibility helps to explain the subject area but cannot describe exactly what it is. For this purpose we have to consider the various components that are involved in biocompatibility processes. Biocompatibility refers to the totality of the interfacial reactions between biomaterials and tissues and to their consequences. These reactions and consequences can be divided into four categories. These involve different mechanisms and indeed quite separate sectors of science but are, nevertheless, inter-related.

The first component is that of the protein adsorption mentioned above. This process is initiated as soon as a material comes into contact with tissue fluids such that relatively quickly the surface of the biomaterial is covered with a layer of protein. The kinetics and extent of this process will vary from material to material which will in any case be a dynamic phenomenon with adsorption and desorption processes continuously taking place. Under some circumstances, this layer is extremely important in controlling the development of the host response since cell behavior near the material may depend on interactions with these proteins. For example, thrombogenicity is controlled by a number of events including the interaction between plasma proteins and surfaces, these proteins being able to influence the attachment of platelets to the surface. In other circumstances, the effects of this protein layer are far from clear.

The second component of biocompatibility is that of material degradation. It is emphasized here that degradation is a component of biocompatibility rather than a separate phenomena. There is still confusion over this since it is often perceived that degradation, which occurs on the material side of the interface, is the counterpart to biocompatibility which is equated with the other (tissue) side. This is not correct since degradation is the counterpart to the local host response, both being contributory to the biocompatibility of the system.

Degradation phenomena are covered elsewhere in this *Handbook* and will not be discussed in detail here. It is necessary to point out, however, that descriptions of material degradation mechanisms have to take the special, and indeed unique, features of the tissue environment into account. Whatever its location, a biomaterial will continuously encounter an aqueous environment during its use. This is not simply a saline solution, however, but a complex solution containing a variety of anions and cations, a variety of large molecules some of which are very reactive chemically, and a variety of cells which again may be in passive or active states. There are occasions when a degradation process can be explained, mechanistically and qualitatively, by the presence of an electrolyte. This is the situation with most metals when they suffer from corrosion in physiological environments(3). Even here, however, it is known that the kinetics of corrosion may be influenced by the organic species present, especially the proteins, and it is even possible for the corrosion mechanism to be somewhat different to that found in non-biological situations.

With other groups of materials, however, and especially with polymers, kinetics, mechanisms and consequences of the degradation are fundamentally related to the

details of the environment. Although hydrolysis remains the substantive mechanism for degradation of most heterochain polymers, including polyurethanes, polyamides and polyesters, this hydrolysis may be profoundly influenced by the active species present in the tissue, especially in the tissue of the inflammatory response to materials. Included here are the influences of lysosomal enzymes (4). Moreover the hydrolysis may be supplemented by oxidative degradation, again occurring not only by virtue of passively dissolved oxygen in body fluids, but (and probably far more importantly) by active oxidative species such as superoxides, peroxides and free radicals, generated by activated inflammatory cells such as macrophages. It is thus possible for homochain polymers not particularly susceptible to hydrolysis and not normally oxidized at room temperature, to undergo oxidative degradation upon implantation (5). Polyolefins such as polyethylene and polypropylene come into this category.

The term 'biodegradation' is often used to describe degradation which occurs in such situations although the circumstances of and requirements for degradation to be so described have not been entirely clear. A recently agreed definition of biodegradation (6) states quite simply that it is the breakdown of a material mediated by a biological environment. The interpretation of 'biological' is left to the reader.

The purpose of explaining the role of the biological, or physiological environment in degradation phenomena, was to emphasize the crucial significance of the interaction between degradation and the host response, for not only can degradation be influenced by the host response but also it can control that response.

To explain this in a little more detail, let us consider the evolution of the local host response, which is the third component of biocompatibility, using a model that involves inflammatory and repair processes (7). Whenever a material is implanted into the tissues of the body, there has to be a degree of trauma associated with the insertion process. This will inevitably establish an acute inflammatory response, which is the body's natural defence mechanism to any injury. The inflammation is totally desirable and helpful since it is the precursor to the second phase of the response, which is that of tissue repair. The response to a surgical incision is acute inflammation followed by repair, the consequences of which are a zone of fibrous (collagenous) scar tissue. If a biomaterial is placed within the tissue, this response will be modified by its presence, but the extent to which that modification occurs depends on many factors.

Considering first the role of the material, if that material were totally inert chemically and unable to react at all with the tissues, and if the device were not able to irritate the tissues in any way, the perturbation to the inflammation/repair sequence is minimal, and the result will be the formation of a zone of fibrous tissue analogous to the scar, but oriented in such a way as to envelope the implant. The classical response to an implant is its encapsulation by soft fibrous tissue. On the other hand, if the material is able to react with the tissues, chemically, mechanically or any other way, it will act as a persistent stimulus to inflammation. While there is nothing inherently harmful about inflammation as a response to injury, persistent inflammation occurring as a response to a persistent injury is less acceptable. At the very least, this results in a continued stimulus to fibrosis such that the capsule is far more

extensive and may intervene between the material and tissue it is meant to be in contact with (for example bone in the case of joint prostheses) but perhaps more importantly it can change the immediate tissue environment from one of quiescent fibrosis to that of active chronic inflammation. This is rarely the appropriate response and, as noted above, is likely to generate an even more aggressive environment.

In the context of the definition of biocompatibility, therefore, it is important that the interaction between the material and the tissues is one which leads to an acceptable balance between inflammation and repair. A few points may serve to explain this further and qualify appropriateness. First, the nature of the host response and those features which constitute acceptability will vary very considerably from one host to another and from one location (or set of circumstances) to another within a particular host. It is often forgotten that host variables are as important as material variables in the determination of biocompatibility. This is particularly important when the wide variety of tissue characteristics is considered. Obviously bone is very different from nerve tissue or a vascular endothelium and there will be very considerable difference in the details of their responses. Not all tissues of the same variety will be able to respond in the same way and it should always be remembered that host variables such as age and overall health status will have a major effect.

Secondly, the importance of time and the sequence of events should never be underestimated. While the above model describes the sequence from surgical intervention to inflammation to repair, such that the process may undergo rapid resolution, with a resulting long lasting equilibrium, the inflammation may be restimulated at any time and rarely can we guarantee long term survival. In this context the third point becomes important, for any feature of the interaction between material and tissue and material can be responsible. In many situations it is the chemical reactivity, represented by degradation processes, which drives the inflammatory response, but it can equally well be a process by which fragments of the material are extracted by physical or mechanical means. The release of wear debris from orthopaedic prostheses is a good example here, since the presence of such particles in sufficient numbers can have a profound effect on the tissue response, which is mediated by the mechanisms of inflammation but where the clinical results, manifest by loosening of the prostheses, may not be seen for quite some time(8). As far as the response to debris is concerned, in general the effects of released fragments will be quite different to those of bulk materials, both by virtue of physical factors as well as changed chemical factors.

Thirdly, the identification of these events and their importance leads to various possibilities for the control of biocompatibility. In the balance of inflammation and repair we have the possibilities of controlling that balance by aiming to eliminate or at least minimize those events which are undesirable for one set of conditions or alternatively enhancing or optimizing those events which are most desirable. This has led to the emergence of the concept and indeed introduction of bioactive materials which have been defined as biomaterials that are designed to elicit or modulate biological activity.

As a final point about the local host response, it has to be recognized that there are significant regional and tissue-specific variations to the phenomena. These

cannot be described here, but it is important to mention the particular case with blood. When a biomaterial comes into contact with blood, there are many different mechanisms by which the blood can interact with the material, most of which are preferably avoided. The most important of these are those processes, alluded to in an earlier paragraph, that are responsible for the clotting of blood. This is a vital defense mechanism which prevents death by uncontrolled bleeding under everyday circumstances, but unfortunately in the context of biomaterials, the two processes which can, either separately or together, initiate the formation of a blood clot, that is contact phase activation of clotting proteins and platelet activation, are themselves initiated by contact with foreign surfaces. Thrombogenicity, defined as the property of a material which promotes and/or induces the formation of a thrombus, is clearly an important feature of biocompatibility.

Turning now to the last component of biocompatibility, we have to recognize that if there is an interfacial reaction, there is no reason why the products of that reaction and their effects have to be confined to the locality of that interface and the presence of a benign local response is not necessarily indicative of the absence of any systemic or remote site effects. The possibility of systemic effects arising from the presence of biomaterials has long been recognized, although extreme difficulties exist with their identification and interpretation. Indeed, at the present time, there are few systemic effects that can be readily identified with biomaterials. The transformation of a thrombus into an embolus derived from an intravascular device has obvious implications and we can imagine and often demonstrate the systemic consequences of using overtly cytotoxic materials. However, the more intriguing speculations refer to the putative implant-related carcinogenicity and even more speculative implant-related immune responses. At this stage we have to be concerned about such possibilities but have to put the subject into context. While we cannot deny that there are possible mechanisms for biomaterials to induce tumors, the evidence that they do so in human clinical experience is very sparse. While it is possible for some hypersensitivity responses to be seen to implants, the evidence for any clinically significant response from the immune system to biomaterials is even less available.

1.4 Conclusions

This review attempts to outline the main concept that currently prevail in the subject area of biocompatibility. Clearly it is a complex subject, about which we are still relatively ignorant, not least because it involves a juxtaposition between two quite different sectors of science, the materials sciences and the molecular/cellular biological sciences. Based on these concepts, however, a better understanding is now emerging so that our biomaterials can be chosen, and where necessary treated, in order to determine that the tissues of the host do indeed respond appropriately to them.

Additional Reading

Black, J. (1992) *Biological Performance of Materials – Fundamentals of Biocompatibility*, 2nd edn, Marcel Dekker, Inc., New York.

A recently updated introductory text describing the basic principles of the performance of biomaterials in biological environments and the relevance of the biomaterial-tissue interactions.

Hench, L.L. and Etheridge, E.C. (1982) *Biomaterials: An Interface Approach*, Academic Press, New York.

An early text describing concepts of biomaterials and their interactions with tissues, concentrating on the interface and based on the authors' experiences with bioceramics.

Williams, D.F. (ed.) (1981) *Fundamental Aspects of Biomaterials*, Volumes I & II, CRC Press, Boca Raton.

An edited collection of contributions dealing with the major components of biocompatibility mechanisms, including corrosion and degradation phenomena, toxicology and the local tissue response.

References

1. Black, J. (1984) Systemic effects of biomaterials. *Biomaterials*, **5**, 11–18.
2. Williams, D.F. (1987) *Definitions in Biomaterials*, Elsevier, Amsterdam, pp. 49–59.
3. Williams, D.F. (1985) Physiological and microbiological corrosion. *CRC Critical Reviews in Biocompatibility*, **1**(1), 1–24.
4. Williams, D.F., Smith, R. and Oliver, C. (1987) The enzymatic degradation of polymers *in vitro*. *Journal of Biomedical Materials Research*, **21**, 991–1003.
5. Williams, D.F. and Zhong, S.P. (1991) Are free radicals involved in the biodegradation of implanted polymers? *Advanced Materials*, **3**, 623–626.
6. Williams, D.F., Black, J. and Doherty, P.J. (1992), in Doherty, P.J., Williams, R.L., Williams, D.F. *et al.* (eds.) *Biomaterial-Tissue Interfaces, Advances in Biomaterials*, Volume 10. Elsevier, Amsterdam, pp. 525–533.
7. Williams, D.F. (1989) A model for biocompatibility and its evaluation. *Journal of Biomedical Engineering*, **11**, 185–192.
8. Williams, D.F. (1976) Biomaterials and biocompatibility. *Med. Prog. Tech.*, **4**(1/2), 31–42.

Chapter 2

Soft Tissue Response

J.M. Anderson

2.1 Introduction

Soft tissue responses to biomaterials for medical devices are generally viewed from the inflammation and wound healing perspectives and are usually considered as parts of the tissue or cellular host responses to injury. Placement of a biomaterial or medical device in the soft tissue environment involves injection, insertion, or surgical implantation, all of which injure the tissues or organs involved. Early host responses are dynamic and change with time (Table 2.1). It is important to consider this time variable in determining the host response or biocompatibility of a material.

2.2 Types of Response

Four general types of response may occur following the implantation of a biomaterial. These are a minimal response, a chemically induced response, a physically induced response, and cellular/tissue necrosis [1].

A minimal response is generally called fibrous encapsulation and the implant is encapsulated within fibrous tissue containing mainly collagen with a few fibroblasts. At the tissue/implant interface, a one to two cell layer of macrophages and foreign body giant cells is present which constitutes the foreign body reaction.

J.M. Anderson (✉)

Department of Pathology Case Western Reserve University, University Hospitals of Cleveland, 2074 Abington Road, Cleveland, OH 44106–2622, USA

Table 2.1 Sequence of Local Events Following Implantation

Injury
Acute Inflammation
Chronic Inflammation
Granulation Tissue
Foreign Body Reaction
Fibrosis

Chemically induced responses may range from an acute, mild inflammatory response to a chronic, severe inflammatory response. These responses may be the result of leaching of biomaterial additives or degradation products.

Physically induced responses are usually the result of the size, shape, porosity, and other geometric factors of the biomaterial or device. The form and topography of the surface of the biomaterial may determine the composition of the foreign body reaction. With biocompatible materials, the composition of the foreign body reaction and the implant site may be controlled by the surface properties of the biomaterial, the form of the implant, and the relationship between the surface area of the biomaterial and the volume of the implant. High surface to volume implants such as fabrics, porous materials, or particulate, will have higher ratios of macrophages and foreign body giant cells at the implant site than will smooth-surface implants, which will have fibrosis as a significant component of the implant site [2–5]. These three general types of responses are generally found with biocompatible materials.

The fourth type of response, i.e., cellular necrosis, is a toxic reaction which leads to cell death. It is generally taken as a sign of the incompatibility of a material and is generally the response to highly toxic additives, residual monomer, or degradation products released from the biomaterial [6]. The similarity between chemically induced responses leading to chronic, severe inflammatory responses and cellular/tissue necrosis should be considered in determining the biocompatibility of a biomaterial.

Mechanical factors and edge effects may modify the response to a biomaterial. Implant motion or micromotion can lead to variations in the fibrous capsule thickness and the composition of the fibrous capsule and the interfacial foreign body reaction. Edges and sharp changes in surface features may lead to a variation in fibrous capsule thickness and the presence of variable concentrations of chronic inflammatory cells, i.e., monocytes and lymphocytes.

Immune and neoplastic responses are specialized responses which are rarely seen with biomaterials and medical devices. Immune responses are generally created by the phagocytosis of particulate by macrophages which biochemically process the material and communicate with lymphocytes to produce the immune response. The metal sensitivity response is a well-known immune response to metallic corrosion products. Neoplastic, i.e., tumor formation, responses are generally considered to be an example of solid state tumorigenesis. Solid state tumorigen-

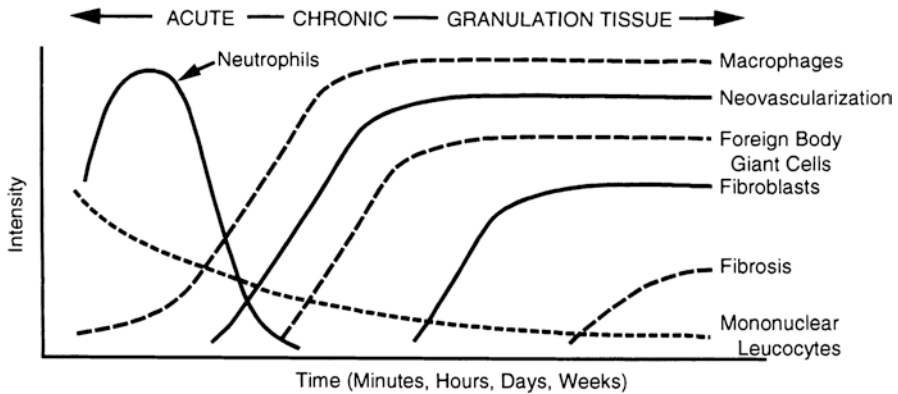


Fig. 2.1 The temporal variation in the acute inflammatory response, chronic inflammatory response, granulation tissue development, and foreign body reaction to implanted biomaterials. The intensity and time variables are dependent upon the extent of injury created in the implantation and the size, shape, topography, and chemical and physical properties of the biomaterial.

esis is generally linked to the extent or degree of fibrous capsule formation and the potential for solid state tumorigenesis is reduced with increasing foreign body reaction.

2.3 Inflammation

Inflammation is defined as the reaction of vascularized living tissue to local injury (Table 2.1) [7, 8]. The size, shape, and intended application of a biomaterial or medical device determine the implantation procedure which in turn determines the extent or degree of initial injury. The size, shape, and chemical and physical properties of the biomaterial may be responsible for variations in the intensity and time duration of the inflammatory and wound healing processes. Figure 2.1 illustrates the temporal sequence of inflammation and wound healing. The inflammatory response is a series of complex reactions involving various types of cells whose implant site concentrations (densities), activities and functions are controlled by various endogenous and autogenous mediators [9]. The predominant cell type present in the inflammatory response varies with the age of the injury, i.e., the time since the implant was inserted. Neutrophils, which are the characteristic cell type of acute inflammation, predominate during the first several days following implantation and are replaced by monocytes as the predominant cell type. Acute inflammation is of relatively short duration, lasting from minutes to days, depending on the extent of injury. The main characteristics of acute inflammation are the exudation of fluid and plasma proteins (edema) and the immigration of leukocytes (predominantly

neutrophils). Following localization of leukocytes at the implant site, phagocytosis and the release of enzymes, reactive oxygen intermediates (ROI), and other agents occur following activation of neutrophils and macrophages. Agents released from activated leukocytes, hydrogen ions (acid), enzymes, ROIs and others, may effect the biodegradation of biomaterials [10, 11]. The major role of the neutrophils in acute inflammation is to phagocytose and destroy microorganisms and foreign material.

Acute inflammation is of relatively short duration, lasting from minutes to days, and is dependent on the extent of injury. As the acute inflammatory response subsides, monocytes and lymphocytes predominate in the implant site and are the characteristic cells of chronic inflammation [7, 8]. Monocytes, migrating from the blood, in the acute and chronic inflammatory responses differentiate into macrophages within the tissue in the implant site. These macrophages will fuse or coalesce into foreign body giant cells (Figure 2.1). Macrophages and foreign body giant cells are prominent at the tissue/implant interface, even with biocompatible materials. In Figure 2.1, the intensity and time variables are dependent upon the extent of injury created in the implantation and the size, shape, topography, and chemical and physical properties of the biomaterial.

In the phagocytosis process, recognition and attachment of neutrophils and monocytes/macrophages are expedited when the biomaterial is coated by naturally occurring blood serum factors called opsonins. The two major opsonins are IgG and the complement-activated fragment C3b. Both of these plasma-derived proteins are known to adsorb to biomaterials and neutrophils and macrophages have corresponding cell membrane receptors for these opsonization proteins. These receptors may also play a role in the activation of the attached neutrophils, monocytes, macrophages, or foreign body giant cells. Small particles, of the order of 5 μm in largest dimension, may undergo the phagocytosis or engulfment process by neutrophils, monocytes/macrophages, or specialized cells in the reticuloendothelial system (liver, spleen, etc.). Medical devices with surface areas of biomaterial many times greater than the size of the cell may stimulate frustrated phagocytosis. Frustrated phagocytosis does not involve engulfment of the biomaterial but rather the extracellular release of leukocyte products in an attempt to degrade or destroy the biomaterial [12]. Macrophages and foreign body giant cells adherent to the surface of the biomaterial may undergo frustrated phagocytosis with the release of hydrogen ion (acid) enzymes, ROIs, and others. Little is known regarding the extent or time period of frustrated phagocytosis and its dependence on the chemical and physical properties of the biomaterial.

The cells and components of vascularized connective tissue (Table 2.2) are involved in the inflammatory and wound healing responses. Thus, injury to soft tissues involves the specific types of cells which constitute the organ or tissue as well as the cells and components of vascularized connective tissue. Vascularized connective tissue can be viewed as the general network which holds together specific cell types in unique three-dimensional patterns to constitute organs or tissues.

While it is convenient to consider blood-material interactions separately from tissue-material interactions, it must be emphasized that blood-material interactions

Table 2.2 Cells and Components of Vascularized Connective Tissue

Intravascular (blood) cells	Blood plasma proteins
Erythrocytes (RBC)	Coagulative Proteins
Neutrophils	Complement Proteins
Monocytes	Albumin
Eosinophils	Fibrinogen
Lymphocytes	Gamma-Globulins
Basophils	Others
Platelets	Extracellular matrix components
Connective tissue cells	Collagens
Mast Cells	Elastin
Fibroblasts	Proteoglycans
Macrophages	Fibronectin
Lymphocytes	Laminin

and the inflammatory response are intimately linked and, in fact, early responses to injury involve mainly blood and blood vessels. Therefore, both cellular and humoral elements, i.e., plasma proteins, etc., are considered as cells and components of vascularized connective tissue.

2.4 Wound Healing and Fibrosis

The wound healing response is initiated by the action of monocytes and macrophages, followed by proliferation of fibroblasts and vascular endothelial cells, i.e., capillaries, at the implant site. The proliferation of fibroblasts and the formation of capillaries constitute granulation tissue. Modified fibroblasts, i.e., myofibroblasts, which have contractile properties which assist in wound site closure are transiently present in granulation tissue. As fibroblasts predominate over macrophages in the healing response, collagens and other extracellular matrix molecules are deposited in the implant site. The extent of the wound healing response is generally dependent on the extent or degree of injury or defect created by the implantation procedure. Wound healing progresses by primary union (or first intention) if the healing is clean such as a surgical incision in which the wound edges have been approximated by surgical sutures, clips, or staples. Healing under these conditions occurs with a minimal loss of tissue. Wound healing by secondary union (or secondary intention) occurs when there is a large tissue defect that must be filled or there has been an extensive loss of cells and tissue. In wound healing by second intention, regeneration of specific organ or tissue cells cannot completely reconstitute the original architecture and more granulation tissue is formed resulting in larger areas of fibrosis or scar formation. Thus, the surgical procedure to create the implant site may influence the extent or degree of the wound healing response.

The end-stage healing response to biomaterials and medical devices is generally fibrous encapsulation by collagenous fibrous tissue. This has been previously described as the minimal response. In the minimal response, the tissue/implant interface has a layer of macrophages and foreign body giant cells, i.e., foreign body reaction, on the surface of the biomaterial and this is surrounded or encapsulated by a fibrous capsule which is composed of collagen, proteoglycans, and other extracellular matrix molecules. Fibroblasts may be present in the fibrous capsule.

2.5 Repair of Implant Sites

Repair of implant sites involves two distinct processes: regeneration, which is the replacement of injured tissue by parenchymal cells of the same type, or replacement by fibrous connective tissue that forms a capsule [7]. These processes are generally controlled by either (i) the proliferative capacity of the cells in the tissue or organ receiving the implant and the extent of injury as it relates to tissue destruction or (ii) persistence of the tissue framework of the implant site. The regenerative capacity of cells permits their classification into three groups: labile, stable (or expanding), and permanent (or static) cells. Labile cells continue to proliferate throughout life, stable cells retain this capacity but do not normally replicate, and permanent cells cannot reproduce themselves after birth of the host.

Perfect repair, with restitution of normal structure, theoretically occurs only in tissues consisting of stable and labile cells, whereas all injuries to soft tissues composed of permanent cells may give rise to fibrosis and fibrous capsule formation with very little restitution of the normal tissue or organ structure. Tissues composed of permanent cells (e.g., nerve cells, skeletal muscle cells, and cardiac muscle cells) most commonly undergo an organization of the inflammatory exudate, leading to fibrosis. Tissues composed of stable cells (e.g., parenchymal cells of the liver, kidney, and pancreas), mesenchymal cells (e.g., fibroblasts, smooth muscle cells, osteoblasts, and chondroblasts), and vascular endothelial and labile cells (e.g., epithelial cells and lymphoid and hematopoietic cells) may also follow this pathway to fibrosis or may undergo resolution of the inflammatory exudate, leading to restitution of the normal tissue structure. The condition of the underlying framework or supporting stroma of the parenchymal cells following an injury plays an important role in the restoration of normal tissue structure. Retention of the framework may lead to restitution of the normal tissue structure, whereas destruction of the framework most commonly leads to fibrosis. It is important to consider the species-dependent nature of the regenerative capacity of cells. For example, cells from the same organ or tissue but from different species may exhibit different regenerative capacities and/or connective tissue repair. An example of species differences in cell proliferation and regeneration is the endothelialization process, proliferation of endothelial cells, on the luminal surface of vascular grafts which does not occur in humans but does occur in other mammals including other primates.

Following injury, cells may undergo adaptations of growth and differentiation. Important cellular adaptations are atrophy (decrease in cell size or function), hypertrophy (increase in cell size), hyperplasia (increase in cell number), and metaplasia (change in cell type). Hyperplasia of smooth muscle cells at blood vessel/vascular graft anastomoses may lead to failure of the graft by stenosis or occlusion, i.e., narrowing of the lumen, and thrombosis. Other adaptations include a change in which cells stop producing one family of proteins and start producing another (phenotypic change) or begin a marked overproduction of protein. This may be the case in cells producing various types of collagens and extracellular matrix proteins in chronic inflammation and fibrosis. Causes of atrophy may include decreased workload (e.g., stress-shielding by implants), as well as diminished blood supply and inadequate nutrition (e.g., fibrous capsules surrounding implants).

Local and system factors may play a role in the wound healing response to biomaterials or implants. Local factors include the site (tissue or organ) of implantation, the adequacy of blood supply, and the potential for infection. Systemic factors may include nutrition, hematologic and immunologic derangements, glucocortical steroids, and pre-existing diseases such as atherosclerosis, diabetes, and infection.

2.6 Summary

Inflammation, wound healing, foreign body response, and repair of implant sites are usually considered components of the general soft tissue response to biomaterials or medical devices. The extent or degree and temporal variations in these responses are dictated by the inherent biocompatibility characteristics of the biomaterial or medical device. Factors which may play a role in the soft tissue response include the size, shape, topography, and chemical and physical properties of the biomaterial. As the implantation procedure involves injury to vascularized connective tissue, blood responses and interactions may play a role in the general soft tissue response. The extent, degree or type of soft tissue response is generally considered to be tissue-specific, organ-specific, and species-specific. Thus, a given biomaterial may be considered to be biocompatible in one shape or form but not in another and in one tissue but not in another depending on the given application.

Additional Reading

Black, J. (1992) *Biological Performance of Materials - Fundamentals of Biocompatibility*, 2nd edn, Marcel Dekker, New York.

This volume is an excellent tutorial text for the engineer/biomaterial scientist/biologist/and others who have little or no knowledge in the area of biomaterials and medical devices. The text is divided into four parts: General considerations, material response: function and degradation of materials *in vivo*, host response:

biological effects of implants, and methods of test for biological performance. The fourth part, Methods of test for biological performance, is unique to biomaterials texts and provides the reader with *in vitro* and *in vivo* test models and methods as well as perspectives on the design, selection, standardization, and regulation of implant materials.

Cohen, I.K., Diegelmann, R.F. and Lindblad, W.J. (eds) (1992) *Wound Healing: Biochemical and Clinical Aspects*, W.B. Saunders Co., Philadelphia.

This is an edited volume containing 35 chapters. The volume addresses the following areas: Biological processes involved in wound healing (6 chapters), structural and regulatory components of wound healing (7 chapters), factors affecting tissue repair (7 chapters), repair of specific tissues (7 chapters), and clinical management of healing tissues (7 chapters). This is an excellent volume which provides an up-to-date and in-depth perspective of various aspects of wound healing. The references lists provided at the end of each chapter are extensive. The strength of the volume is its biological perspective and little is provided on biomaterials. The chapter by Frederick Grinnell on cell adhesion does offer a biomaterial perspective.

Gallin, J.A., Goldstein, I.M. and Snyderman, R. (eds) (1992) *Inflammation: Basic Principles and Clinical Correlates*, 2nd ed, Raven Press, New York.

This is an edited volume containing 58 chapters by individual authors. The volume is divided in the following areas: Soluble components of inflammation (10 chapters), cytokines (5 chapters), cellular components of inflammation (21 chapters), responses to inflammation (3 chapters), clinical correlates (13 chapters), and pharmacologic modulation of inflammation (4 chapters). Each chapter is a critical, in-depth review of the indicated subject and the references are extensive. This is an excellent volume for those wanting an in-depth overview of the inflammatory process and its components. No information is provided on biomaterial/inflammation interactions.

Greco, R.S. (ed.) (1994) *Implantation Biology: The Host Response and Biomedical Devices*, CRC Press, Boca Raton.

This is an edited volume containing 23 chapters. Three chapters deal with biomaterials in general, 6 chapters address specific blood and tissue interactions with biomaterials, 10 chapters address the use of biomaterials in specific surgical disciplines, and 3 chapters address tissue engineering and genetic manipulation of cells. The reference list for each chapter is extensive. This is an excellent overview of how biomaterials interact with the host and the specific use of biomaterials in indicated applications.

Harker, L.A., Ratner, B.D. and Didisheim, P. (eds) (1993) *Cardiovascular Biomaterials and Biocompatibility: A Guide to the Study of Blood-Tissue-Material Interactions, Cardiovascular Pathology*, 2 (3 Suppl), 1S–224S.

This is the third edition of a standard National Institutes of Health reference previously entitled *Guidelines for Blood-Material Interactions - Report of the National Heart, Lung, and blood Institute Working Group*. The volume contains 20 chapters and 3 appendices. The chapters address the following areas: Pathophysiologic mechanisms, materials and their physicochemical characterization, safety testing of materials and devices, and blood-vessel-material interactions.

The appendices are entitled: NIH Primary Reference Materials, International Standards for Biological Evaluation of Medical Devices, and Blood Analog Fluid for Medical Device Evaluation. This volume provides an in-depth perspective on cardiovascular materials and state-of-the-art information is provided regarding bio-materials. This is an excellent review, however, the editors limited the length and number of references for each chapter due to space considerations.

References

1. Williams, D.F. and Roaf, R (1973) *Implants in Surgery*, W.B. Saunders Company Ltd., London, pp. 233–35.
2. Anderson, J.M. (1993) Mechanisms of inflammation and infection with implanted devices. *Cardiovascular Pathology*, **2** (3 Suppl.), M319-M321.
3. Anderson, J.M. (1994) *In vivo* biocompatibility of implantable delivery systems and biomaterials. *European Journal of Biopharmaceutics*, **40**, 1–8.
4. Anderson, J.M. (1994) Inflammation and the foreign body response. *Problems in General Surgery*, **11**(2), 147–160.
5. Black, J. (1992) The inflammatory process, in *Biological Performance of Materials -Fundamentals of Biocompatibility*, 2nd edn, Marcel Dekker, Inc., New York, pp. 125–147.
6. Marchant, R.E., Anderson, J.M. and Dillingham, E.O. (1986) *In vivo* biocompatibility studies. VII. Inflammatory response to polyethylene and to a cytotoxic polyvinylchloride. *Journal of Biomedical Materials Research*, **20**, 37–50.
7. Cotran, R.Z. et al. (1994) Inflammation and repair, in *Pathologic Basis of Disease*, 5th edn, Cotran, R.Z., Kumar, V. and Robbins, S.L. (eds), W.B. Saunders Co., Philadelphia, pp. 51–92.
8. Gallin, J.I., Goldstein, I.M. and Snyderman, R. (eds) (1992) *Inflammation. Basic Principles and Clinical Correlates*, 2nd edn, Raven Press, New York.
9. Spector, M., Cease, C. and Tong-Li, X. (1989) The local tissue response to biomaterials. *CRC Critical Reviews in Biocompatibility*, **5** (4), 269–295.
10. Weissman, G., Smolen, J.E. and Korchak, H.M. (1980) Release of inflammatory mediators from stimulated neutrophils. *New England Journal of Medicine*, **303**, 27–34.
11. Henson, P.M. (1980) Mechanisms of exocytosis in phagocytic inflammatory cells. *American Journal of Pathology*, **101**, 494–511.
12. Henson, P.M. (1971) The immunologic release of constituents from neutrophil leukocytes: II. Mechanisms of release during phagocytosis, and adherence to nonphagocytosable surfaces. *Journal of Immunology*, **107**, 1547–57.

Chapter 3

Hard Tissue Response

T.O. Albrektsson

3.1 Introduction

The initial tissue response when a biomaterial is implanted in the body is dependent on release of specific growth factors. It has been indicated by Frost [1] that the inevitable bone injury resulting from surgery and the presence of an implant will release various types of growth factors that will sensitize cells and promote cellular mitosis. This is a general healing response that will result in growth of all sorts of local connective tissues, bone as well as various types of soft tissue.

The balance between these tissue varieties is controlled by the action of chemical mediators which issue 'instructions' for the amount of bone and soft tissue to be formed as an appropriate healing response. This delicate balance can easily be disturbed inadvertently and may cause the undesirable end-result of an interfacial soft tissue embedment of the implant or, in the case of fracture healing, formation of a pseudoarthrosis. The discussion in this section will focus on various modes of implant fixation, such as cementation, ingrowth and osseointegration (Figure 3.1).

3.2 Fixation by Cementation

Bone cement, a two component acrylic, is frequently used for implant fixation in the cases of hip and knee arthroplasties. Bone cement is toxic with localized as well as general adverse tissue reactions [2]. Therefore, the good long-term results reported with cemented arthroplasties seem to be quite puzzling. However, it must be

T.O. Albrektsson (✉)
Handicap Research, Institute for Surgical Sciences, University of Gothenburg,
Medicinaregatan 8, Gothenburg S-413 90, Sweden

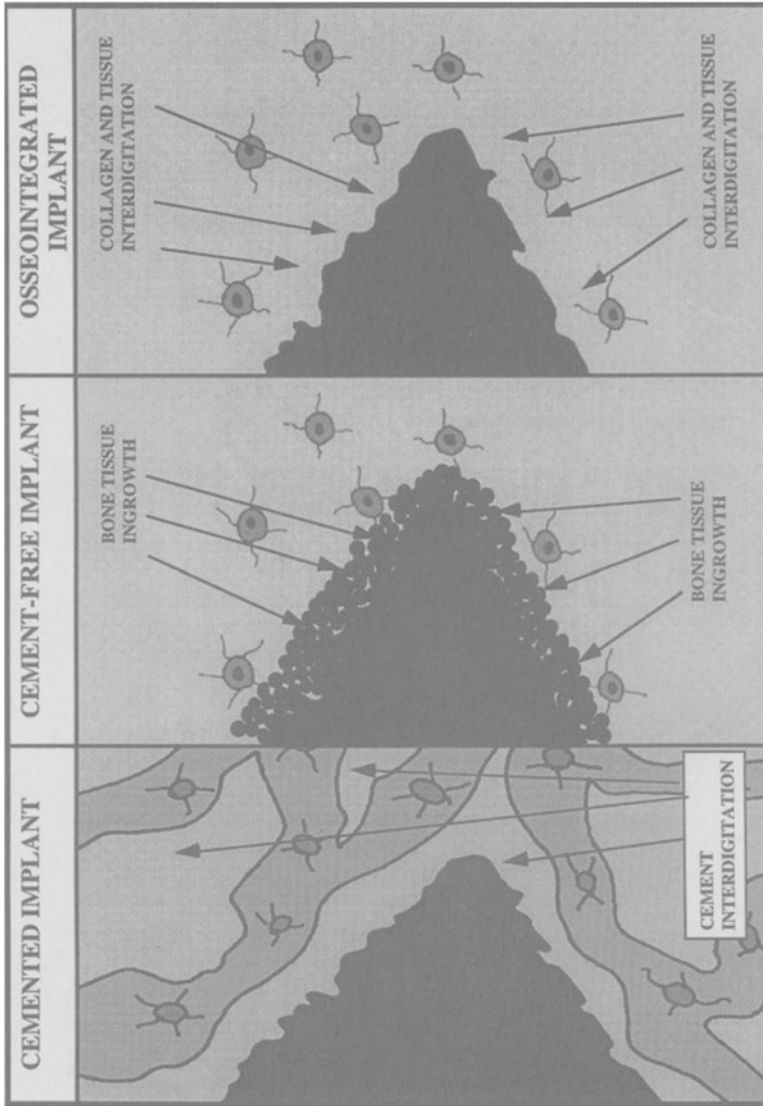


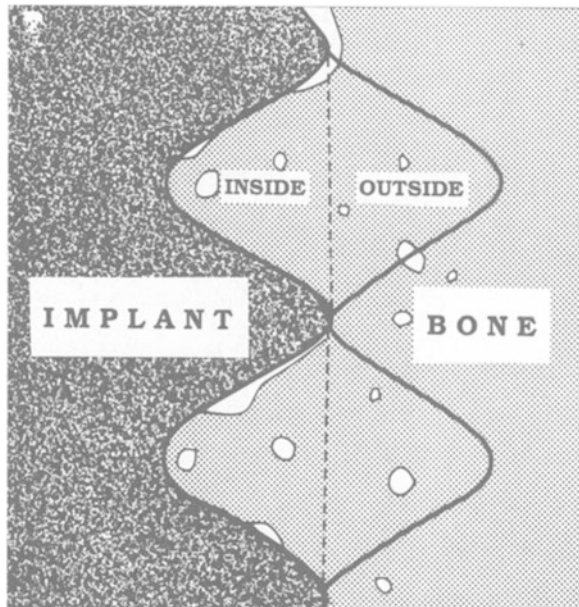
Fig. 3.1 Different classification criteria are used for implants in bone. Here we distinguish between cemented implants, which are dependent upon cure in place luting or filling agents; cement-free (ingrowth implants) which are dependent upon bone tissue growth into surface features for fixation; and osseointegrated implants, which are dependent upon collagen and cellular processes and their physicochemical interactions with the implant surface for fixation. In each case, a 'ridge' feature on the implant surface is shown in cross-section; the width of each band of the diagram is several millimeters (cells (osteocytes) are shown larger than actual size).

understood that the strength of the cemented bone interface is not related to the live state of bone tissue: in reality, the curing bone cement invading the trabecular network results in a substantial cancellous bone interdigitation (Figure 3.1). The interfacial bone usually dies from the combined trauma of heat and monomer leakage. The width of this necrotic zone varies depending on the extent of the surgical trauma and the type of bone cement used, but is at least a few millimeters [2]. Ironically, a revitalization of the interfacial bone may prove disastrous, as the bone will then run an increased risk of resorption. In examining interfacial tissues reactions to retrieved cemented orthopaedic implants, most studies have examined the tissue after removal of the implant. This leads to an uncertainty in examining the proportion of true bone to implant contact.

We have been able to investigate bone implants *in situ*, at the resolution level of light microscopy, utilizing the techniques developed by Donath *et al.* [3]. Computer assisted calculations, using custom developed software, permit determination of the proportion of bone to implant contact, the amount of bone in the region adjacent to the implant and comparisons of the bone density adjacent to and in the immediate region of the implant ('outfolded mirror image') (Figure 3.2).

These data correlate positively to biomechanical tests: the more bone in the interfacial region of the implant, the greater the torque necessary to remove the implant when we apply controlled rotational forces to the implant body. Specimens of 10 μ m thickness have been investigated at the light microscopic level of resolution [4]. Other studies using cutting and grinding techniques have investigated the implant *in*

Fig. 3.2 Computerized histomorphometric approach to evaluation of the bone-implant interface. The bone-to-implant contact percentage is the linear contact area between bone and implant in the inside zone; percent bone ingrowth is the ratio of bone 'inside' to that 'outside' in the 'mirror' zone.



situ, but ended up with sections of a final thickness of 40 μm or more leading to clear overestimates of the true bone to implant contact. In a retrieval study of cemented resurface arthroplasties, Morberg [2] was able to overcome these methodological problems and verify a very poor bone to cement contact, even though he found bone fragments with disturbed mineralization bordering the cement.

3.3 Fixation by Ingrowth (Cement-Free Implants in Bone)

In the absence of cement, fixation may be obtained by active bone tissue ingrowth into the implant surface irregularities of medullary stems (Figure 3.2). As pointed out by Black [5], one disadvantage of cement-free implants is the 3–4 week waiting time before the bone-implant interface can support significant shear loading; this is in contrast to a cemented interface which, if successful, has adequate shear strength within one hour of implantation. Osseointegrated implants have even lower interfacial shear strength at the the same 3–4 week post operative time point [6].

In the clinical experience, however, the results of cement-free joint arthroplasties utilizing ingrowth fixation have not matched those of cemented devices. The appropriate bone ingrowth is often disturbed and incomplete, leading to early failure of fixation. Cement-free knee arthroplasty components have been observed to migrate by up to 2 mm in the first post-operative year, while cemented devices of the same design migrate only half as much or less [7]. The failure rates of cement-free hip arthroplasties have been so substantial in comparison to cemented devices that the former mode of implant insertion has been restricted to young patients for whom cemented devices give poorer results at most clinics [8].

The outcome of cement-free orthopaedic implants depends, as does the outcome of craniofacial osseointegrated implants, on the more or less simultaneous control of a number of different factors including biocompatibility, design and surface conditions of the implant, the state of the host bed, the surgical technique and the loading conditions after implant insertion.

Herein is the explanation for the dubious results of many current designs of cement-free hips and knees: the implant material used, the design and surface finish have been well adapted to engineering demands, but not so well matched to the biological needs.

Ideal implant characteristics with respect to bone anchorage are quite different from those of gliding surfaces. The surgical technique utilized when inserting a cement-free hip or knee of current designs is, of necessity, traumatizing; resulting in an impaired bone healing response. Current stem-type cement-free hips migrate when loaded, as do tibial components of artificial knees, leading to a change in the chemical mediators and subsequent increase of soft tissue formation. It is, therefore, not surprising to learn from studies of retrieved cement-free hips that there is, as a rule, only sparse bony ingrowth into retrieved acetabular cups [9], femoral cups [2, 10] or femoral stems [9, 11, 12]. More modern types of cement free hip prostheses with titanium meshwork or HA-coated surfaces have had slightly better clinical

results than those implanted and retrieved during the 1980s and it may well be possible that there is more abundant bone ingrowth in some of the more recent designs. Nevertheless, from multicenter studies it seems quite clear that summed five-year failure rates for cement-free arthroplasties are greater than those for cemented devices [8]. This observation illustrates that the anchorage problems associated with cement free arthroplasties are far from solved.

3.4 Osseointegration

Osseointegration is a term introduced by Brånemark *et al.* [13] to describe a loaded, stable implant in direct contact with bone (no apparent intervening soft tissue under light microscopic examination). Osseointegrated implants differ from ingrown ones that are dependent upon bone growth into surface macroscopic features or irregularities. By contrast, osseointegration is dependent on tissue ingrowth into minute surface features, such as the fundamental asperities of a 'smooth' surface or, as postulated for surfaces of various crystalline calcium phosphates (such as calcium hydroxyapatite) or amorphous, bioactive glasses, on direct chemical bonding between tissue and implant. Irrespective of the type of interfacial contact – chemical bonding or mechanical interdigitation – an important difference is that while the former requires only limited tissue elements, the latter requires complete, mature bone elements for appropriate function. Theoretically, an ingrown interface may also be osseointegrated as well but experimental evidence for this, from examination of thin sections, is virtually nonexistent. Macroscopic features on implant surfaces designed for ingrowth fixation include sintered beads, rough plasma sprayed coatings and sintered meshes, since bone requires features of minimum dimensions of about 100 μm for successful ingrowth [14, 15].

However, surface irregularities only in the nanometer to micrometer range are necessary for osseointegration when implant stability is dependent on cellular and/or collagen ingrowth, rather than bone ingrowth. Since this ingrowth (perhaps better termed 'ongrowth') of tissue elements occurs in a three dimensional manner, the osseointegrated implant will, from a biomechanical viewpoint, be a directly bone-anchored device. In fact, Wennerberg [16] has demonstrated that implant surfaces with a CLA (center line average) roughness of $\sim 1 \mu\text{m}$ will experience more rapid bony incorporation, through osseointegration, than ones with CLAs of 0.1 or 2 μm . This observation leads to the hypothesis that too smooth surfaces (CLA ~ 0.1) may not permit proper collagen attachment while rougher ones (CLA $\geq 2 \mu\text{m}$) may release too many metal ions that disturb cellular functions necessary for anchorage.

There is no doubt that osseointegration has resulted in a clinical breakthrough in oral implants. Soft tissue embedded load-carrying devices do not function adequately in the jaw. In sharp contrast, properly osseointegrated implants do. However, this does not necessarily imply that every functioning bone implant in other parts of the body need to be osseointegrated. On the contrary, cemented hip arthroplasties with a

bone-cement interface consisting of soft tissue or mostly dead bone have demonstrated significant clinical longevity, in many cases exceeding ten to fifteen years.

Furthermore, the so called osseointegrated interface is still in need of a proper definition. First described by Brånemark [17] as a bone response that occurred everywhere around the implant circumference of c.p. titanium screws in placed in bone, osseointegration is regarded today as a more nonspecific tissue response resulting in a mix of interfacial soft and hard tissues. In reality, bone anchorage of foreign bodies is a more general type of tissue response that occurs to c.p. titanium alone [3]. The only definition of osseointegration that has stood up to a critical analysis is based on a clinical finding of implant stability: 'A process whereby clinically asymptomatic rigid fixation of alloplastic materials is achieved and maintained, in bone, during functional loading' [18]. The continued usage of a term such as osseointegration is motivated by the proven clinical results in the case of craniofacial implants and the hope to replicate these findings in the case of orthopaedic implants in the future. However, from a strict histological point of view osseointegration remains poorly defined.

Osseointegrated implants have resulted in a clinical breakthrough in two different clinical applications in the craniofacial skeleton: one of these being oral implants, irrespective of whether treating total or partial edentulousness [19, 20]; the other being skin penetrating extra-oral implants. The clinical results of screw-type, c.p. titanium oral implants in mandibles or maxillas for 5 years or more of follow up have been in the 90–99% range [21]. The results of skin penetrating implants in the temporal bone region have been similar, but not in the orbit region, where the host bed has been irradiated. Now, 20 years since their clinical introduction in 1977, permanent skin-penetrating, osseointegrated, screw-shaped titanium implants are regarded as routine clinical treatments for facial disorders or certain types of hearing impairments [22, 23].

Press-fit fixation represents one approach to the osseointegration of orthopedic implants. The design of press-fit joint replacements is based on three dimensional geometric data with the intention of fitting the implant as closely as possible to the host bone. The objective of this design approach is to transfer load across the implant-bone interface to as wide an area of the bone as possible [24]. In theory, press-fit fixation may lead to osseointegration of the implanted device. However, as it is difficult to mimic precisely the resulting intravital loading patterns, osseointegration of initially stable press-fit components is threatened by subsequent bone remodeling processes. Too stiff a device may cause 'stress shielding,' leading to bone resorption. Conversely, too high local stresses may lead to pressure necrosis and resorption prior to remodeling. Finally, bone resorption may lead to local interfacial movements: these predispose to soft-tissue formation and may cause a subsequent failure of fixation.

Polymers are not one hundred percent stable under biological conditions, leading to highly variable clinical durability. Ultrahigh molecular weight polyethylene (UHMWPE), although relatively stable, has shown poor outcomes when press-fitted in knee replacement arthroplasties [25]. The poor fixation of such devices may

relate both to intrinsic properties of the polymers involved as well as to differences in their elastic moduli from that of bone. For instance, the Young's modulus of UHMWPE is approximately 2% of that of cortical bone (0.3 GPa vs. 17 GPa). This leads to a quite different loading pattern for both the polymer and the surrounding tissue than that encountered in the case of c.p. titanium, which is approximately 7 times as stiff as cortical bone (127 GPa vs. 17 GPa).

Ceramics are still stiffer, with moduli up to 30 times that of cortical bone. Bulk ceramics, such as aluminum oxide (alumina) are well tolerated by bone but are generally insufficiently strong and tough to serve as load bearing implants, especially in the presence of tensile or bending loads. Calcium phosphates, such as calcium hydroxyapatite (CaHAP), although much weaker still, are an interesting class of biomaterials due to their assumed capability for 'bone bonding'. Søballe *et al.* [26] has observed that the addition of a CaHAP coating induces proliferating bone to bridge gaps in the bone-implant interface, in the presence of dynamic loading, which would be filled with soft tissue around uncoated metallic implants. He also suggests that such coatings enhance bone growth from osteopenic tissue, utilizing an experimental animal arthritis model with substantial pre-implantation loss of bone density.

In experimental studies, c.p. titanium has been demonstrated to induce a stronger bone response than most other pure metals or alloys, including Ti6Al4V [4, 27]. However, there is substantial evidence that CaHAP leads to a still more rapid healing response [28]. This may be due to a direct positive influence on interfacial bone from the calcium phosphate material and/or a relatively rough surface topography resulting from the manufacturing process in combination with the reduction of metal ion release by the presence of the CaHAP coating. Long term experimental and dental clinical data from CaHAP coated implants has been disappointing [29]. However, CaHAP remains a very interesting biomaterial with efforts underway to explore functional improvement through changes in crystallinity, coating thickness, method of application, etc.

Retrieval data [30–32] have contributed to our current knowledge of oral implants. Stefflik and co-workers [32] reviewed 51 retrieved oral implants of different designs. They claimed that implants inserted 10 years ago or more fail generally due to loss of bone support and other biological features while more recently placed oral implants also fail secondary to intrinsic biomaterial failure such as implant fracture. One hundred stable (uncoated) Brånemark System® 'Nobelpharma' implants were retrieved and studied at our laboratories: 33% were removed because of therapy-resistant pain or progressive bone resorption, 26% were removed after death from unrelated causes, 24% were fractured implants and 17% were removed for psychological reasons. The implants had been in situ and functioning for 1–18 years. There was on average 82% bone-to-implant contact and a similar percentage of bone within the threads of these retrieved implants (evaluated over the three best consecutive threads on both sides of the implant). Whenever possible, the entire bone to implant contact percentages were also calculated and found to be ~70%. In almost every case, there was >60% bone to implant contact. In fact, such extensive

bone to implant contact percentages may represent a histological correlate to osseointegration.

3.5 How Bone-Biomaterial Interfaces Fail

The implant-bone interface can fail for various reasons but the most common is so-called ‘aseptic loosening’: i.e. loosening not associated with infection. The causative factors for aseptic loosening may be classified as mechanical or biological. For example, early post-operative failures of cemented, cement-free (ingrown) as well as osseointegrated implants may be attributed to lack of initial fixation due to mechanical failure of the bone-cement (when present) or bone-implant interface. Such failures may relate to incidents of overload. However, early failures may also occur subsequent to overheating of the tissues during surgery, leading to bony necrosis, collapse and subsequent mechanical loosening. Overheating due to a combination of surgical trauma and polymerization heat release may occur at bone-cement interfaces; surgical trauma, with associated heating, alone may prevent bone and other tissue elements from invading cement-free implant-bone interfaces, whether designed for ingrowth or osseointegration. Biological failure is also possible in the longer term, associated with generation or release of cytotoxic products, such as cement monomer or metallic corrosion products or through induction of specific immune responses [33] (Figure 3.3).

In clinical use, cylindrical shaped oral implants which lack any additional retention features, such as threads, grooves, etc., are prone to gradual failure due to ongoing bone ‘saucerization’ (gradual loss of bone at the implant-bone-mucosal boundary) [21]. In the case of orthopaedic implants with medullary structural elements (such as a femoral stem), Willert and Semlitsch were first to propose that bone loss occurred secondary to biological response to small particles, such as wear debris. [34] Macrophages (MP) and foreign body giant cells (GC) ingest these undigestible particles of metal, polymer or ceramic and release factors which stimulate osteolytic activity by cells in membranes associated with the implant-bone interface (Figure 3.3) [35]. With modern histological staining techniques, especially the use of oil red O [33], it has now become possible to appreciate the large amounts of small and sub-micron UHMWPE particles found in the vicinity of loose orthopaedic joint replacement implants. Many investigators believe that biological response to these particles is the leading biological cause of osteolysis leading to gradual, late implant failure.

3.6 Conclusions

The major advantage of the osseointegrated interface is its remodelling capacity. Gradual adaptation to load has been verified in retrieval studies; the implants are known to have almost no bone to implant contact during the first few weeks after

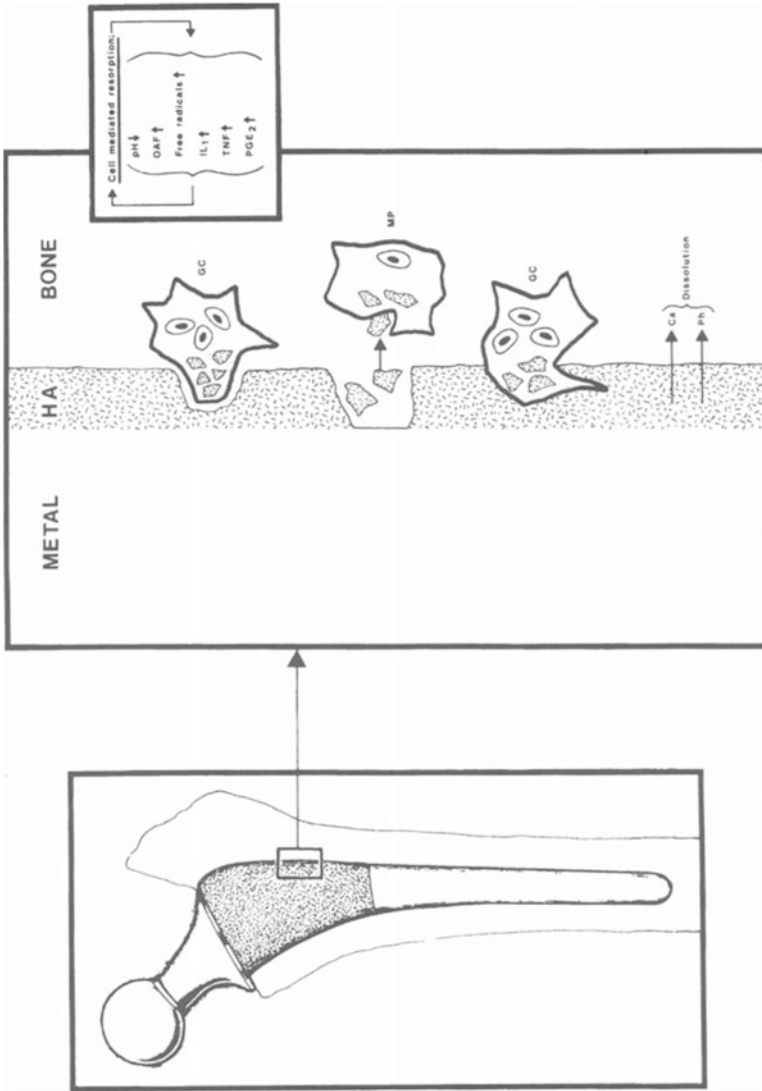


Fig. 3.3 Theoretical failure modes for an osseointegrated calcium hydroxyapatite-coated femoral stem of a total hip replacement prosthesis [29; by permission]. Key: GC: multinucleated giant cell; MP: macrophage; Ca: calcium; Ph: phosphorus; OAF: osteoclastic activating factor; IL₁: interleukin 1, TNF: tumor necrosis factor; PGE₂: prostaglandin E₂.

placement but then demonstrate an increasing amount of interfacial bone tissue. The main proportion of osseointegrated implant failures occur during the first one or two years and result from failure to achieve a proper osseointegration. This trend is quite different from most orthopaedic studies reported in the literature, which show clinical failure rates increasing with time. Cemented arthroplasties of today have resulted in a significantly better clinical outcome than cement-free ones. It must be pointed out that the results of orthopaedic implants published in the literature are generally based on the number of revisions alone. This means that the actual number of successful arthroplasties is lower than the figures quoted in the literature. Furthermore, there is a patient drop-out of more than 20% in most clinical reports. From a biological viewpoint it is important to strive for improved cement-free implants so that their clinical results will at least match those of the cemented arthroplasties. New types of osseointegrated hip and knee constructions have been designed and are presently in clinical trials. Altering prosthetic design (in comparison with current practice), and improving surgical instruments and procedures may well overcome some of the hurdles in the development of new osseointegrated arthroplasty devices.

Additional Reading

Lee, A.J.C. and Ling, R.S.M. (1984): loosening, in *Complications of Total Hip replacement*, (ed. R.S.M. Ling), Churchill-Livingstone, Edinburgh, pp. 110–145.

Still useful account of the biological and mechanical features of loosening leading to clinical failure of the various interfaces formed between rigid biomaterials and bone. Extensive bibliography.

Manley, M.T. (1993): Calcium phosphate biomaterials: A review of the literature, in *Hydroxylapatite Coatings in Orthopaedic Surgery*, (eds G.T.R. Geesink and M.T. Manley), Raven Press, New York, pp. 1–24.

The title speaks for itself. Additional chapters in the same book provide experimental and clinical results of osseointegration, specifically adhesion fixation.

Spector, M. (1987): Historical review of porous-coated implants. *J. Arthroplasty*, **2**(2), 163–177, 1987.

Historical review of experimental and clinical results of ingrowth fixation, with extensive bibliography.

References

1. Frost, H.M. (1989) The biology of fracture healing. *Clinical Orthopaedics and Related Research*, **248**, 283–293.
2. Morberg, P. (1991) On bone tissue reactions to acrylic cement. PhD Dissertation, Biomaterials Group, University of Göteborg, Sweden, pp. 1–142.

3. Donath, K., Laass, M. and Günzl, H.-J. (1992) The histopathology of different foreign body reactions in oral soft tissue and bone tissue. *Virchows Archiv A Pathologia Anatomica*, **420**, 131–137.
4. Johansson, C. (1991) On tissue reactions to metal implants. PhD Dissertation, Biomaterials/Handicap Research, University of Göteborg, Göteborg, Sweden, pp. 1–232.
5. Black, J. (1988) *Orthopaedic Biomaterials in Research and Practice*. New York, Churchill Livingstone, pp. 267–284.
6. Steinemann, S.G., Eulenberger, J., Maeusli, P.-A. *et al.* (1986) Adhesion of bone to titanium. *Adv. in Biomaterials* **6**, 40–44.
7. Ryd, L. (1986) Micromotion in knee arthroplasty. A Roentgen stereophotogrammetric analysis of tibial component fixation. *Acta Orthop. Scand.*, Suppl. **220**, 1–80.
8. Malchau, H., Herberts, P. and Anhfelt, L. (1993) Prognosis of total hip replacement in Sweden. Follow-up of 92,675 operations performed in 1978–1990, *Acta Orthop Scand.*, **64**, 497–506.
9. Collier, J.P., Mayor, M.B., Chae, J.C. *et al.* (1988) Macroscopic and microscopic evidence of prosthetic fixation with porous coated materials. *Clin. Orthop. Rel. Res.*, **235**, 173–180.
10. Willems, W.J., Eulderbrink, F., Rozing, P.M. *et al.* (1988) Histopathologic evaluation in failed Gerard double cup arthroplasty. *Clin. Orthop. Rel. Res.*, **228**, 123–133.
11. Engh, C.A., Bobyn, J.D. and Glassman, A.H. (1987) Porous coated hip replacement. The factors governing bone ingrowth, stress shielding and clinical results. *J. Bone Joint Surg.*, **69B**, 45–55.
12. Cook, S.D., Thomas, A.K. and Haddad, R.J. (1988) Histologic analysis of retrieved human porous coated joint components. *Clin. Orthop. Rel. Res.*, **234**, 90–101.
13. Brånemark, P.-I., Hansson, B.-O., Adell, R. *et al.* (1977) Osseointegrated implants in the treatment of the edentulous jaw. *Scand. J. Plastic Reconst. Surg.*, Suppl **16**, 1–116.
14. Albrektsson, T. (1979) Healing of bone grafts. *In vivo* studies of tissue reactions at autografting of bone in the rabbit tibia. PhD Dissertation, Laboratory for Experimental Biology, Göteborg University, Göteborg, Sweden, pp. 1–90.
15. Pilliar, R.M. (1986) Implant stabilization by tissue ingrowth. In *Tissue Integration in Oral and Maxillofacial Reconstruction*, D. van Steenberghe (ed.), Amsterdam, Excerpta Medica, pp. 60–76.
16. Wennerberg, A. (1995) On surface topography of implants. PhD Dissertation, Biomaterials/Handicap Research, University of Göteborg, Göteborg, Sweden, pp. 1–202.
17. Brånemark, P.-I. (1985) Introduction to osseointegration, in *Tissue Integrated Prostheses* (eds P.-I. Brånemark, G. Zarb and T. Albrektsson), Quintessence Co, Chicago, pp. 11–76.
18. Zarb, G. and Albrektsson, T. (1991) Osseointegration – A requiem for the periodontal ligament? – An editorial. *Int. J. Periodontal and Restorative Dent.*, **11**, 88–91.
19. Albrektsson, T., Dahl, E., Enbom, L. *et al.* (1988) Osseointegrated oral implants. A Swedish multicenter study of 8139 consecutively inserted Nobelpharma implants. *J. Periodont.*, **59**, 287–296.
20. Lekholm, U., vanSteenberghe, D., Herrmann, I. *et al.* (1994) Osseointegrated implants in partially edentulous jaws: A prospective 5-year multicenter study. *Inter. J. Oral & Maxillofacial Implants*, **9**, 627–635.
21. Albrektsson, T. (1993) On the long-term maintenance of the osseointegrated response. *Australian Prosthodontic J.*, **7**, 15–24.
22. Tjellström, A. and Granström, G. (1994) Long-term follow-up with the bone anchored hearing aid: A review of the first 100 patients between 1977 and 1985. *Ear Nose and Throat J.*, **2**: 138–140.
23. Jacobsson, M., Tjellström, A., Fine, L., *et al.* (1992) A retrospective study of osseointegrated skin-penetrating titanium fixtures used for retaining facial prostheses. *Int. J. Oral & Maxillofacial Implants*, **7**, 523–528.
24. Poss, R., Robertson, D.D., Walker, P.S. *et al.* (1988) Anatomic stem design for press-fit and cemented application. In *Non-cemented Total Hip Arthroplasty*, R. Fitzgerald, Jr (ed.), New York, Raven Press, pp. 343–363.
25. Freeman, M.A.R., McLoed, H.C. and Levai, J.P. (1983) Cementless fixation of prosthetic components in total arthroplasty of the knee and hip. *Clin. Orthop. Rel. Res.*, **176**, 88–94.

26. Søballe, K. (1993) Hydroxyapatite ceramic coating for bone implant fixation. *Acta Orthop. Scand.* (Suppl 225), **64**, 1–58.
27. Han, C.H., Johansson, C., Wennerberg, A. *et al.* (1995) A quantitative comparison of commercially pure titanium and titanium-6 aluminum-4 vanadium implants in rabbit bone. *Proc. Fifth Biomaterials Club Meeting*, Ischgl, Austria, Albrektsson T. and Tjellstrom, A. (eds), p. 25.
28. Søballe, K., Hansen, E.S., Rasmussen, H.B. *et al.* (1993) The effect of osteoporosis, bone deficiency, bone grafting, and micromotion on fixation of porous coated vs. hydroxyapatite-coated implants. In *Hydroxyapatite Coatings in Orthopedic Surgery*, Geesink, R.G.T. and Manley, M.T. (eds), New York, Raven Press, pp. 107–136.
29. Gottlander, M. (1994) On hard tissue reactions to hydroxyapatite-coated titanium implants. PhD Dissertation, Biomaterials/Handicap Research, University of Göteborg, Göteborg, Sweden, pp. 1–202.
30. Lemons, J.E. (1991) Bone-biomaterial interfaces in retrieved implants, in *The Bone Biomaterial Interface* (ed. J.E. Davies), University of Toronto Press, Toronto, pp. 419–424.
31. Albrektsson, T., Eriksson, A.R., Friberg, B., *et al.* (1993) Histologic investigations on 33 retrieved Nobelpharma implants. *Clinical Materials* **12** (1), 1–9.
32. Stefflik, D.E., Parr, G.R., Singh, B.B. *et al.* (1994) Light microscopic and scanning electron microscopic analyses of dental implants retrieved from humans. *J. Oral Implantol.*, **20**(1), 8–24.
33. Campbell, P. (1995) On aseptic loosening of total hip replacements: The role of UHMWPE wear particles. PhD Dissertation, Biomaterials/Handicap Research, Göteborg University, Göteborg, Sweden, pp. 1–225.
34. Willert, H., Semlitsch, M. (1976) Reactions of the articular capsule to joint prostheses. In *Biocompatibility of Implant Materials*, D.F. Williams (ed.), London, Sector Publishing, pp. 157–169.
35. Goldring, S.R., Schiller, A.L., Roelke, M., *et al.* (1983) The synovial-like membrane at the bone-cement interface in loose total hip replacements and its proposed role in bone lysis. *J. Bone Joint Surg.*, **65A**, 575–584.

Chapter 4

Immune Response

K. Merritt

4.1 Introduction

There is increasing concern about the role of specific immune response to implanted materials. This section discusses the general principles governing immune responses and outlines techniques for their measurement and evaluation. This is a necessarily brief presentation of the issues, and the reader is encouraged to pursue the topic through relevant references provided for further study.

4.2 Overview of the Specific Immune Response

The specific immune response is the normal response of vertebrates when a foreign substance is introduced into the body. This is a desirable protective response which detoxifies, neutralizes, and helps to eliminate such substances.

However, in some cases, responses to seemingly innocuous substances may cause harm to the host. Such effects are usually termed allergic or hypersensitivity responses. The responses have been classified into four types: Type I, Type II, Type III, Type IV.

These four responses share elements of a common mechanism, triggered by the presence of a foreign material termed an *antigen*. The antigen is initially processed by a cell, usually either a monocyte or macrophage, but occasionally a skin dendritic cell also referred to as an *antigen processing cell* (APC). The APC engulfs the antigen, processes it (usually by enzymatic digestion or attempted digestion), and transfers or presents it to another cell, usually a *lymphocyte* termed a *T helper cell*. The T helper cell then presents the processed antigen to another T lymphocyte,

K. Merritt (✉)
17704 Stoneridge Dr., Gaithersburg, MD 20878, USA

called the *T cytotoxic cell*, or to a B lymphocyte. The receiving cell, whether T- or B-type, initiates a response for interaction with the processed antigen, forming a less biologically active complex. In the former case, the immune response is a Type IV or cell mediated immunity while in the latter case, the final result is release of free antibody, which may lead to a humoral Type I, II, or III response. T-cell responses result in accumulation of T-cells at the site where the foreign material is present. B-cells remain at remote depots of lymphoid tissue while the antibody circulates and appears at the site of the foreign material.

The main features of the four types of responses are described in the following table:

Type:	Antibody:	Cells involved:	Mediator:	Consequences:
I	IgE	B-lymphocytes	Histamine, vasoactive amines	Itching, rhinitis, vascular collapse
II	IgG, IgM	B-lymphocytes	Histamine, vasoactive amines	Vascular collapse
III	IgG, IgM	Bclymphocytes	Vasoactive amines	Pain, swelling, some vascular plugging and collapse
IV	none	T-lymphocytes	Cytokines	Pain, swelling

Both the T- and B-cells are small lymphocytes, which circulate in the blood, and are found in lymphoid tissue. They arise from a common stem cell and then undergo processing in the thymus to become T-cells or an unknown site, probably the bone marrow, to become B-cells. They are difficult to distinguish and a great deal of work has been done to facilitate identification of these cells in order to elucidate specific immune responses. Identification of T-cells has been greatly aided by the recognition that there are unique substances on the cell surface that can be recognized by the use of monoclonal antibodies generated using murine cells. These antigens are referred to as *cluster differentiation markers* (CDs) and are given numbers. There are a large number of them, more are being identified, and the importance of each is being evaluated. However, all T-cells express CD3 which is consequently referred to as a Pan(= all) T-cell marker. CD2 may also be a Pan T-cell marker. Additionally, the T helper cell expresses CD4 while the T cytotoxic cell expresses CD8. New CDs continue to be identified and their importance evaluated.

The B-cell retains small amounts of antibody on its surface which can be used for identification. The B-cell response results in further differentiation to plasma cells which produce antibody in large quantities. Antibody is a four chain immunoglobulin which has combining sites specific for a single antigen. Antibody is soluble, circulates in the plasma, and the plasma or serum drawn from a vertebrate, or the antibody produced in cell culture for monoclonal antibodies, can be stored frozen and will last virtually forever.

There are five general classes of immunoglobulins produced as antibodies. In order of concentration in normal human blood from highest to lowest are IgG, IgM, IgA, IgE, and IgD. IgD is a surface marker on B-cells and will not be discussed further. IgE is the

antibody associated with Type I responses. IgA is a secretory immunoglobulin, found in high concentrations in saliva, GI contents, and milk and in the associated organs. IgG and IgM are present in high concentrations in blood and are excellent antibodies for immunological testing since they can participate in Type II and III responses.

Type I responses and Type II responses have the same consequences, but the mechanisms are different. Type I responses are best known as hay fever and dust allergies and are immune responses to these antigens mediated by a skin fixing antibody (IgE).

Type II responses involve the reaction of IgG, rarely IgM, antibody with a cell surface antigen. The result is lysis of the cell with release of products. If the cell contains vasoactive amines, then the consequences are signs and symptoms described here. This is commonly seen in allergies to drugs which bind to blood platelets.

Type III responses are referred to as *immune complex* reactions and occur when both antigen and antibody are present in large quantities at the same time. In the normal immune response, the antigen is processed, the immune response is initiated, and the antigen disappears shortly. However, if the antigen is persistent, then significant amounts of immune complexes can form, plug small vessels, and result in tissue or organ damage.

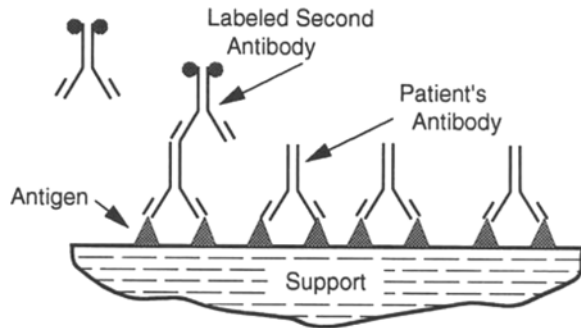
Type IV responses are those most usually associated with chronic presence of a foreign body, such as an implanted biomaterial. They are typified by the common contact dermatitis caused by poison ivy.

In each case, an antigen stimulates the immune response and the immune response in turn reacts specifically with the antigen. T-cells, B-cells and circulating antibody each recognize only one antigen. For a substance to be antigenic, it must be foreign to the host, of high molecular weight (> 3000), and processable by an APC. However, some small substances become antigenic by binding to larger carrier molecules, usually proteins, found in the host. Such a small substance is called a *hapten* and the immune response is mounted to the hapten-carrier complex.

4.3 Detection of Antibody

To evaluate whether or not a patient has produced antibody against a substance, such as an implant, a blood sample needs to be drawn, tested and the results compared to those from controls. A pre-implantation sample is an ideal control but usually this is not available. The choice of appropriate controls is a major problem. The test procedure itself requires a known positive control (often difficult to obtain for evaluating responses to biomaterials), and a known negative control (usually saline, tissue culture media, or bovine or equine serum used for tissue culture). The controls for the patient population under study are generally obtained from normal individuals without implants and without underlying disease, individuals with the disease (e.g. arthritis) but without the implant (e.g. total joint replacement), individuals with the implant and without problems, and individuals with diagnosed implant failure. The results for all of these need to be analyzed in order to ascertain

Fig. 4.1 Standard immunoassay for antibody. An antigen is fixed (attached) to a solid support and binds a specific antibody from solution. The bound antibody is detected by binding a second, labeled (enzyme, isotope, etc.) antibody.



whether or not antibody is increased in the patient population and whether or not its presence can be correlated with failure of the device.

Most current tests are based on immobilization of the antigen to a solid surface such as polystyrene. The general procedure is outlined in Figure 4.1. Detection of bound antibody involves the use of enzyme (EIA or ELISA assays) or a radioisotope labeled antibody (RIA). (The tests are simple to perform, but great care is needed to wash away excess materials and use the appropriate concentrations. Individuals wishing to initiate such testing procedures are encouraged to attend workshops (often offered by American Society for Microbiology, American Type Culture Collection, etc.) or obtain training in a clinical immunology lab, and also explore detailed manuals on procedures.) Antiserum to human antibodies, (all classes or individual types) with enzyme labels, can be purchased from several biological supply houses. Isotope labeled antibody is available to licensed laboratories.

Problems with interpretation of results:

Positive results

If negative controls are negative and patient samples are positive, then the interpretation is that the patient made antibody to that antigen. However, the question remains as to whether or not the antigen is the correct one and if contaminating antigens are contributing to the reaction. This is difficult to determine but inhibition studies with well characterized antigens are helpful.

In vivo testing

Type I sensitivity is associated with histamine and vasoactive amine release with vascular responses. Often such sensitivity is determined by 'patch' (skin) testing. The positive reaction will occur in a few minutes as a wheal and erythematous (reddening) flare response in the skin. This test is hampered by availability of antigen for testing but the biomaterial applied directly to skin or a mucosal surface may stimulate a response. Caution needs to be taken in interpreting these tests, however, since this is a short term application.

Negative results

Negative results are the desired response in evaluating biomaterials for clinical use, but they are also difficult to evaluate. If there are no responses recorded except in the positive control sample, this is indicative that patient does not produce antibody to that antigen. Again the question of appropriateness of the antigen and its concentration on the solid support remains.

In vivo testing

A negative skin test presents the same problem: Was the antigen correct and/or was it applied to a correct site?

4.4 Detection of Cell Mediated Responses (Type IV)

The procedures for detecting cell mediated responses are much more complicated and difficult than for antibody determination. Most of the assays require the use of living cells and thus tests must be done shortly after obtaining the cells. Controls may have to be done at a different time which complicates the comparisons.

The two most common *in vitro* test procedures used are lymphocyte proliferation and cell migration inhibition tests. The basic theory behind both of these is that T-cells have receptors on their surface which will each respond to a specific antigen. In the course of the response, soluble substances (cytokines or lymphokines), principally blastogenic factor and migration inhibition factor, which act on other cells, including other T-cells, are produced and released.

Blastogenic factor (lymphocyte transformation factor)

This causes other lymphocytes to transform and divide. If cell counts are done, an increased number is seen. If a radioactive cell proliferation precursor (such as tritiated thymidine) is added to the culture, the isotope is taken up by dividing cells and the 'counts' increase. This test, usually called LTT for lymphocyte transformation test, requires living cells to produce and respond to the factor. This takes several days, with 7 days being the general time for response to antigen. Some control stimulants (mitogens) such as PHA (phytohemagglutinin) act in 4–5 days. Interpretation of the tests presents the same problems as with tests for antibody: Are the appropriate controls included, what was the antigen used, were the cells viable; if the results are negative, were the culture conditions correct?

Migration inhibition factor

Migration inhibition factor (MIF) is produced by the stimulated T-cell and acts on cells that are normally motile. The two cell types are the monocyte/macrophage line and polymorphonuclear leukocytes (polys). Thus the test, usually called LIF test

(leukocyte inhibition test) requires living lymphocytes and living migrating cells which may be obtained from fresh, whole blood. The results of the LIF test are available in 18–24 hours. blood does not contain enough monocytes to evaluate inhibition of their migration and this indicator cell is usually obtained from the peritoneal cavity of other animals, typically the mouse or the guinea pig. It is possible to stimulate human lymphocytes in culture for 24–48 hours and then harvest the culture fluid and add it to the macrophages obtained from the animals. Migration (or inhibition of migration) of cells is observed by placing them into tissue culture medium solidified with purified agarose and observing them with a microscope in 18–24 hours or by packing them into capillary tubes and observing migration from the tubes in a few hours giving the appearance of ‘ice cream cones’. The factor for LIF and the one for MIF may be slightly different and thus the two separate terms remain.

Choice of test

There is no evidence that one test is better than the other. The choice is usually based on laboratory preference. This author uses blood cells and migration in agarose since it requires little equipment, is rapid, and small breaks in aseptic procedure are tolerated. The evidence is that the stimulated T-cells produce a group of cytokines. Thus detecting migration inhibition factor or lymphocyte proliferation implies the presence of the others and one is not more specific or sensitive.

Direct testing for lymphokines or cytokines

It would seem from the above studies that the ideal test would be for the lymphokines without the use of a viable indicator cell. These substances are produced in low levels, and thus the cell based assays such as LTT and LIF or MIF are required. Although ELISA based or RIA based assays can be used to detect and quantitate cytokines, reagents are not yet available for these human lymphokines (LIF, MIF, LTT) specifically.

Testing for production of cytokines

There is a current explosion of studies on production of cytokines in response to bio-materials, especially to particles produced by wear and degradation. Thus it seems pertinent to discuss these assays briefly. The assays are generally done by inhibition of ELISA or RIA based assays. This concept is shown in Figure 4.2. Many of these assays are available as complete ‘kits’ from emerging biotechnology companies. (There are many companies, each doing only a few of the cytokines; thus no specific reference will be given. A glance at the methods section in an article reporting on assays will give their source. In addition, a glance at a biotechnology based journal and *Science* will give ads, or an immunologist’s mail box will give you a plethora of choices). These tests are easy to perform, but have technical difficulties and must be done carefully. Interpretation of the results involves being sure that the control studies were done successfully. Again, as with most studies, a positive test can be evaluated but a negative test is difficult to interpret until you are confident of the laboratory doing the testing.

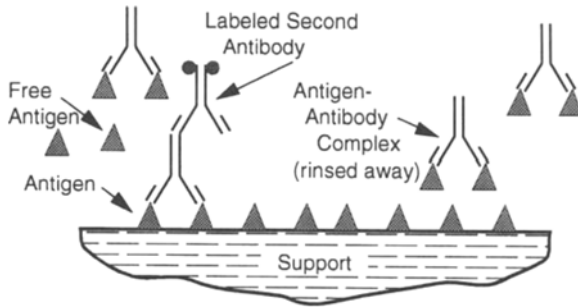


Fig. 4.2 Quantitation of antigen by competitive (inhibition) assay. An antigen is fixed (attached) and binds a specific antibody from solution. However, additional antigen is provided in solution and antibody binding to the bound antigen is reduced in direct proportion to the concentration of free antigen. The bound antibody is then detected by binding a second, labeled (enzyme, isotope, etc.) antibody.

In vivo studies

The classical test for *cell-mediated immunity* (CMI) (Type IV) in the early days of immunology was the skin test. Antigens were applied to the skin or injected under the skin and swelling was observed in 24–72 hours if there was CMI. This was differentiated from Type I, IgE mediated responses, which occur rapidly (in minutes) and usually disappears in 24 hours. CMI begins in 24 hours, has a swelling with some resemblance to the wheal but does not show a flare. This author does not advocate skin testing for responses to biomaterials since the testing is difficult to do correctly, has the potential for producing sensitivity to the test agents and the results are easily misinterpreted. In general, the use of the actual biomaterial (rather than extracts, corrosion products or constituents) is contraindicated since mechanical irritation may be read as a false positive or the biomaterial may fail to release the antigen and thus produce a false negative.

Skin testing is an excellent diagnostic procedure in patients with clinical suspicion of hypersensitivity. However, skin testing with haptens, such as metal ions, involves a risk of sensitization. For the immune response to be detected, the hapten must bind to dermal cells or proteins. However, such binding produces a complete antigen which may stimulate an immune response. Since this immune response takes time to develop, the skin test will be negative, but future tests may then be positive. Thus repeated testing increases the likelihood of inducing sensitivity and should be avoided. Bulk biomaterials will probably not give adequate release of soluble materials in the 24–48 period of testing so may produce false negative results.

Histochemical techniques

There are a number of studies now examining tissues removed from sites adjacent to implants. It is possible, using immunological techniques resembling those outlined in Figure 4.1, to identify cell types and perhaps cell products produced at the

site. The major interest is in the detection and typing of lymphocytes by use of antisera prepared against the CD markers described earlier. The same type of assay is being initiated for detection of the cytokines in the tissue. The techniques are simple but not all antisera work and thus a variety of antisera are used. The required antisera are available commercially.

Interpretation of the results is again a problem. Tests using 'home made' monoclonal antibodies are suspect until the antisera is made available to other investigators for conformation. The use of well characterized antisera from companies which supply to others is better at this stage. Since the tissue section is examined and scored by an observer, the 'data' from these studies are not really available for analysis by the reader. Computerized image analysis techniques are still not widely used. Thus, in evaluating the results, possible bias of the investigator must be taken into account.

4.5 Detection of Immune Responses to Haptens

Detection of immune responses to haptens is the same as that described above, but there are some special techniques now being used. A hapten-carrier complex can be prepared *in vitro* by combination in solution with a large protein such as albumin or a smaller molecule such as glutathione. These can then be used to coat a solid substrate. Alternatively, the protein carrier can be coated onto a substrate, the hapten added, and then the assay performed. This probably increases the amount of hapten that is available for antibody binding and minimizes that which is lost in the tertiary folding of the protein.

4.6 Human Immune Response to Materials

4.6.1 Latex

The term 'latex' actually is confusing since the name is given to some materials because of the way they are processed and not because of their source. The biomaterial latex used to fabricate gloves, condoms, etc. is a rubber (elastomer) extracted from a plant (*Hevea brasiliensis*). As such, there is a great deal of antigenic protein contamination. Allergies to latex are usually of the Type I, IgE mediated response, with an immediate reaction (in minutes) that can be life threatening. Since latex is encountered in many household objects such as household gloves, balloons, etc., sensitivity to it is a frequent pre-existing condition. Latex material cleaned of protein seems to be nonallergenic. Other types of immune response to latex have not been as frequent or of much concern. Latex is not used as a long term implanted material and thus the long term responses are not noted. The population at greatest risk are the health care workers with the increased use of examining and surgical gloves.

4.6.2 Collagen

This is another material that is an extract of material of natural origin with bovine and ovine skin or tissue the favored source. This is a foreign protein and thus capable of stimulating a variety of immune responses. Antibodies of IgE, IgM, and IgG classes have been observed. Cell mediated immune responses have also been observed. As with latex, the important precaution is to remove as much foreign material as possible. Since collagen across mammalian species has a similar structure, it is possible to remove contaminating proteins and leave a relatively nonallergenic material. Chemical treatment and cross linking of the collagen can further reduce antigenicity. Collagen products need to be carefully evaluated for their ability to initiate immune responses, but it is possible to produce safe products.

4.6.3 Synthetic polymers

The use of chemically defined synthetic polymers is associated with minimal human immune responses. These materials are based on carbon, hydrogen, nitrogen and oxygen which are basic building blocks of the biological system. Thus the generation of antigenic material would be unlikely. Nevertheless, there are some polymeric materials with additional chemical moieties that are of concern.

A. Polysiloxane (silicone elastomer)

There is abundant lay press comment and little scientific material on this topic. It is apparent that there can be binding of silicone to foreign protein with stimulation of the immune response. The use of a simple hapten test, as described in section 4.5, has added greatly to our knowledge of this. It is also apparent that silicone gel is a potent adjuvant enhancing immune responses to unrelated materials. Whether this is of relevance to the use of gel filled implants remains unknown. The possible stimulation of related and unrelated immune responses remain a major concern in the use of these materials.

B. Polyurethanes

This is a complex group of polymers. Their propensity to stimulate an immune response is very small since there are few molecular groups which would be perceived as foreign by the host, perhaps explaining why clinical immune responses to polyurethanes have not been reported.

C. Poly(methyl) methacrylate

Acrylics are in widespread use in activities of daily living. As with metals, there are documented cases of contact dermatitis from the use of these materials, especially self curing glues containing methacrylate monomer that is very skin sensitizing,

usually stimulating a Type IV response. The use of these materials for implants generally exposes the patient to the monomer for only a brief period of time as the bone cement or dental acrylic cures *in situ*. Acrylics which are fully polymerized before use will not be associated with an allergic response. Reports of sensitization responses of patients to acrylics are rare and the health care workers at most risk are the personnel, such as the surgeon and dental laboratory technician, handling the monomer frequently.

D. Metals

A number of metallic elements and alloys are used extensively in implants, external medical devices and are encountered in activities of daily living. Allergy to metals as a contact dermatitis (Type IV response) is well known in individuals in contact with metal salts, corroding metals, and jewelry or snaps and fasteners. Reactions have been seen to metals used in dental, orthopaedic, and general surgery. The contact dermatitis from topical use resolves when the device is removed. The role of the immune response in reactions to metals implanted into the deep tissue remains controversial. Cell mediated immune responses have been associated, in some studies but not in others, with pain and swelling at the implant site and loosening of the device. Antibodies to metals in patients with metallic implants have recently been reported, but again the consequences of this response remain unknown. Concern remains about the chronic use of metals that are known human sensitizers, such as chromium, nickel and cobalt.

4.7 Consequences of an Immune Response

The immune response is apparently intended to neutralize, detoxify, and help eliminate a foreign material. However, sometimes the immune response can inadvertently cause harm. This will be discussed in various categories in the next section.

1. Damage to the implant. The inflammation which is part of the initiation of the immune response is an oxidative response. Materials subject to oxidative attack, such as polyethylenes and polyurethanes, may be degraded.
2. Damage to adjacent tissues. Products, particularly from Type II and IV responses, may initiate swelling and other vascular responses at the site. This may resolve with no further harm, or it may cause tissue necrosis and/or loss of tissue mass with loosening or movement of the device.
3. Systemic responses. Immune responses of Type I and II generate vasoactive substances which may circulate and cause vascular collapse. This is seen in response to latex materials and drugs which bind to platelets, mast cells, or eosinophils, resulting in an immune response and release of these vasoactive substances.
4. Autoimmune diseases: This is the most controversial area of consequences of immune response to implants. Autoimmune diseases are technically the result

of an immune response to host tissue. Autoimmune diseases such as arthritis, glomerulonephritis, etc., occur in individuals with an unknown cause of onset although some have an association with a preceding infection (especially *streptococci*). Proving cause and effect is an epidemiological problem with surveys of large populations. It is important to refine our immunological testing techniques to prove cause and effect associated with implants and do thorough epidemiological studies.

These responses, if present in clinical populations, may arise from several mechanisms. The two most likely ones associated with the use of implants are (i) binding of the material to host tissue making it a foreign substance such as with hapten-carrier complexes or (ii) altering the host tissue through folding of proteins, degradation of cells or proteins thus making then antigenic for the host. This is the main issue now with the silicone breast implants. This is difficult to prove and massive studies as controlled as possible are needed.

4.8 Conclusions

There has been a rapid growth in our knowledge of the immune response and how to evaluate and quantitate it. As these techniques are applied to the population in contact with biomaterials, we will learn more about its importance in performance of the material. We will also learn more about how to process the materials to minimize the immune response. However, it is important to remember that the immune response is a protective response and detection of immune responses to products of biomaterials does not necessarily indicate clinical problems. On the other hand, implants are foreign material and will stimulate host responses, some of which may cause harm to the host or implant.

Thus the important issue is to distinguish between those immune responses which are normal and help to render antigens less biologically active from those which are harmful to the host. It is clear that IgE (Type I) responses are harmful. Detection of a Type I response to products of biomaterials indicates potential problems in the clinical setting. Responses of the IgG type are generally protective and may not be predictive of further problems unless there is continual release of antigenic material leading to a Type III-response. Biomaterial wear and degradation products that bind to platelets or mast cells pose a potential for adverse Type II responses.

The most commonly observed is the Type IV (cell-mediated) response. This is a protective response in walling off the stimulating agent and in killing cells which have the antigen on the surface, thus eliminating the antigen. However, the tissue reaction accompanying this response may cause harm to the host through soft and hard tissue necrosis. The difference between protection and allergy from Type IV responses is still unclear and careful evaluation of patients is required.

Additional Reading

General Immunology

- Golub, E.S. Green, D.R. (1990) *Immunology, A Synthesis*, 2nd Edition, Sinauer Associates, Inc., Sunderland: Good general text.
- Roitt, I. (1971) *Essential Immunology*, Blackwell Scientific Publications, London: Good description of types I–IV reactions.
- Annual Review of Immunology*, Annual Reviews Inc., Palo Alto, CA: Yearly publication with timely reviews.
- Immunology Today*: Elsevier Science Inc. Tarrytown, NY: Monthly: Good review articles.

Antigen Presentation

- Celada, A. and Nathan, C. (1994) Macrophage activation revisited. *Immunology Today*, **15**, 100–102: good review of macrophages.
- Chicz, R.M. and Urban, R.G. (1994). Analysis of MHC presented peptides: applications in autoimmunity and vaccine development. *Immunology Today*, **15**, 155–160: good review on a complicated subject.

CD markers

- Kemeny, D.M., Noble, A. Holmes, B.J. *et al.* (1994) Immune regulation: a new role for the CD8+ T cell. *Immunology Today*, **15**, 107–110: Good description of the function of the CD8+ T-cell which is a key cell in Type IV responses.
- Scollosman, S.F., Boumsell, L., Gilkes, L.W. *et al.* (1994) CD antigens 1993. *Immunology Today*, **15**, 98–99: good description of recently reported CDs.

Cytokines/interleukins

- Miyajima, A., Kitamura, T., Harada, N. *et al.* (1992) Cytokine receptors and Signal Transduction. *Annual Reviews of Immunology*, **10**, 295–331: Review of function and methods of stimulation.
- Mizel, S.B. (1989) The interleukins. *FASEB J.* **3**, 2379–2388: good detailed review.

Effects of cytokines/interleukins

- Goldring, M.B., and Goldring, S.R. (1990) Skeletal tissue response to cytokines. *Clin. Orthop. Rel. Res.*, **258**, 245–278: review of cytokines and orthopaedics.
- Stashenko, P., Obernesser, M.S., and Dewhirst, F.E. (1989) Effect of immune cytokines on bone. *Immuno Invest.*, **18**, 239–249: one of the few reviews focussing on bone.

Immune response to metals/metallic implants

- Agrup, G. (1968) Sensitization induced by patch testing, *Brit. J. Derm.*, **80**, 631–634: points out problem of routine skin testing in nonallergic individual.
- Benson, M.K.D., Goodwin, P.G. and Brostoff, J. (1975) Metal sensitivity in patients with joint replacement arthroplasties, *Brit. Med. J.*, **4**, 374–375: third of the original 1975 articles pointing to a possible problem. Skin test used.
- Black J. (1988) Does corrosion matter? *J. Bone Jt. Surg.*, **70B** (4), 517–520: discusses issues of importance of understanding corrosion, minimizing it, and recognizing it can be important for the patient.
- Brown, G.C., Lockshin, M.D., Salvati, E.A. *et al.*, (1977) Sensitivity to metal as a possible cause of sterile loosening after cobalt-chromium total hip-replacement arthroplasty, *J. Bone Joint Surg.*, **59A**(2), 164–168: Denies existence of metal allergy in orthopaedics. Complete misinterpretation of data. Uses negative results of an invalid test to draw conclusions. Limited patient population deliberately selected to prove lack of allergy.

- Burholm, A.; Al-Tawil, N.A.; Marcusson, J.A. *et al.* (1990): The lymphocyte response to nickel salt in patients with orthopedic implants. *Acta Orthop. Scand.*, **61**(2): 248–250: Example of use of LTT test.
- Elves, M.W., Wilson, J.N. and Kemp, H.B.S. (1975) Incidence of metal sensitivity in patients with total joint replacements. *Brit. Med. J.*, **4**, 376–378: Second one of the original 1975 articles pointing to a possible problem. Skin test used.
- Evans, E.M., Freeman, M.A.R., Miller, A.J. *et al.* (1974) Metal Sensitivity as a Cause of Bone Necrosis and loosening of the Prosthesis in Total Joint Replacement, *J. Bone and Joint Surg.*, **56B** (4), 626–642: One of the original articles pointing to a possible problem. Skin test used.
- Goh, C.L. (1986) Prevalence of contact allergy by sex, race, and age. *Contact Dermat.*, **14**, 237–240: discusses normal population
- Grimsdottir, M.R., Gjerdet, N.R. and Hensten-Petersen, A. (1992) Composition and *in vitro* corrosion of orthodontic appliances. *Am. J. Orthod. Dentofac. Orthop.*, **101**, 525–532: Discusses sensitivity and stainless steels. Release of nickel related to many metallurgical aspects and not necessarily to nickel content of the metal.
- Lalor, P.A., Revell, P.A., Gray, A.B. *et al.* (1991) Sensitivity to titanium. *J. Bone and Joint Surg.*, **73B**(1), 25–28: Description of possible titanium sensitivity. Patch test vehicle of unknown composition, larger cobalt-chromium component than titanium component in device. Of interest and important, but not conclusive.
- Menne, T.; and Maibach, H.I. (1989) Systemic contact allergy reactions. *Immunol Allergy Clin. N.A.*, **9**, 507–522: Discusses extension from contact dermatitis to systemic reactions.
- Merritt, K. (1984) Role of medical materials, both in implant and surface applications, in immune response and in resistance to infection. *Biomaterials*, **5** (1), 47–53.: Review article. Out of date now but covers literature through 1983.
- Merritt, K. (1986) Biochemistry/hypersensitivity/clinical reactions. in: Lang B, Morris, J. and Rassoog, J. (eds) *Proc. International Workshop on Biocompatibility, Toxicity, and Hypersensitivity to Alloy Systems used in Dentistry*. Ann Arbor, U. MI; pp 195–223.: Review article. Covers the literature through 1984. Good discussion of the problem in the discussion section of the symposium
- Merritt, K. (1986) Chapter 6. Immunological testing of biomaterials, *Techniques of Biocompatibility Testing*, D.F. Williams (ed.), Vol. II, CRC Press, Boca Raton: Description of possible test methods.
- Merritt, K.; and Brown, S.A. (1980): Tissue reaction and metal sensitivity: An animal study. *Acta Orthop. Scand.* **51** (3), 403–411: Example of use of LIF test.
- Rostoker, G., Robin, J., Binet, O. *et al.* (1987) Dermatitis due to orthopaedic implants. *J. Bone Joint Surg.*, **69A**, 1408–1412: Example of a reaction to implant.
- Rudner, E.J., Clendenning, W.E., Epstein, E. *et al.* (1975) The frequency of contact dermatitis in North America 1972–1974. *Contact Derm.* **1**, 277–280: Incidence of contact dermatitis.
- Shirakawa, T., Kusaka, Y. and Morimoto, K. (1992) Specific IgE antibodies to nickel in workers with known reactivity to cobalt. *Clin. Exp. Allergy*, **22** (2), 213–218: Measuring IgE and nickel cobalt interactions.
- Trobelli, L., Virgili, A., Corassa, M. *et al.* (1992) Systemic contact dermatitis from an orthodontic appliance. *Contact Dermatitis*, **27**, 259–260: Example of reaction to dental application of metals.
- Yang, J., and Merritt, K. (1994) Detection of antibodies against corrosion products in patients after Co-Cr total joint replacements. *J. Biomed. Mater. Res.*, **28**, 1249–1258: Method for measuring antibodies to metals

Immune response to latex, collagen, silicones

- Belsito, D.V. (1990) Contact urticaria caused by rubber. Analysis of seven cases. *Dermatol. Clin.* **8**, 61–66: Questions whether increased demand for latex may have decreased quality with more allergens leachable.

- Hanke, C.W., Higley, H.R., Jolivet, D.M. *et al.* (1991) Abscess formation and local necrosis after treatment with Zyderm or Zyplast collagen implant. *J. Amer. Acad. Dermatol.* **25**, 319–326: Deals with some adverse responses to collagen materials which may be related to the immune response. Points to possible problems.
- Meade, K.R., Silver, F.H. (1990) Immunogenicity of collagenous implants. *Biomaterials*, **11**, 176–180: Discusses immunogenicity problem and cross linking. Good place to begin reading.
- Naim, J.O., Lanzafame, R.J. and van Oss, C.J. (1993). The adjuvant effect of silicone gel on antibody formation in rats. *Immunol Inv.*, **22**, 151–161: Shows that the gel is better than Freund's adjuvant in stimulating the response to BSA in rats. Caution on use of gel.
- Slater, J.E. (1989) Rubber anaphylaxis. *New Eng. J. Med.* **320**, 1126–1130: Good methods. Good literature review, real cases reacting to anaesthesia mask.
- Sussman, G.L., Tarlo, S. and Dolovich, J. (1991). The spectrum of IgE responses to latex. *J. Am. Med. Assoc.* **265**, 2844–2847: Latex gloves on health workers causing allergic responses in patients. Can do skin test with latex to check patients or use non-latex gloves.
- Warpinski, J.R., Folger, J., Cohen, M. *et al.* (1991) R.K. Bush. Allergic reaction to latex: a risk factor for unsuspected anaphylaxis. *Allergy Proc.* **12**, 95–102: Clinical symptoms of Type I allergy. Identifies IgE antibodies against latex (gloves, balloons, condoms). IgE against proteins from latex.
- Wolk, L.E., Lappe, M., Peterson, R.D. *et al.* (1993) Immune response to polydimethylsiloxane (silicone): screening studies in a breast implant population. *FASEB J.*, **7**, 1265–1268: Very important study with a good technique. Hopefully more studies will be done with this technique. Valid test of antibody to silicone.

Oxidative damage of implants

- Carter, W.O., Narayanan, P.K. and Robinson, J.P. (1994). Intracellular hydrogen peroxide and superoxide anion detection in endothelial cells. *J. Leukocyte Biol.* **55**, 253–258: Good method for detecting H₂O₂ release and superoxide production. Example of biologically produced oxidizing species.
- Kao, W.J., Zhao, Q.H., Hiltner, A. *et al.* (1994) Theoretical analysis of *in vivo* macrophage adhesion and foreign body giant cell formation on polymethylsiloxane, low density polyethylene, and polyetherurethanes. *J. Biomed. Mater. Res.*, **28** (1), 73–80: Recent article on macrophages on polymers and references some articles on oxidative events.
- Kaplan, S.S., Basford, R.E., Jeong, M.H. *et al.* (1994) Mechanisms of biomaterial induced superoxide release by neutrophils. *J. Biomed. Mater. Res.*, **28**, 377–86: Discusses the release of reactive oxygen species stimulated by biomaterials. Not all materials are activating.

Consequences of immune responses to materials

- Angell, M. (1994) Do Breast implants cause systemic disease? Science in the court-room *New Eng. J. Med.*, **330** (24), 1748–1749: Editorial in response to article by Gabriel *et al.* (1994) Reiterates the necessity of doing detailed studies. Indictment of patients, manufacturers and government jumping to conclusions using inadequate data. Doesn't say how we get the adequate data though.
- Gabriel, S.E., O'Fallon, W.M., Kurland, L.T. *et al.* (1994) Risk of connective tissue diseases and other disorders after breast implantation. *New Eng. J. Med.*, **330** (24), (1697–1702): Excellent study. Shows problems of doing studies on long term consequences. Example of how it ought to be done.

Chapter 5

Cancer

M. Rock

5.1 Introduction

The widespread use of temporary and permanent implants in the post World War II era has had a dramatic impact on the practice of medicine and on the life of disabled and ill individuals. Nowhere has this been more obvious than in the frequent use of implants to stabilize fractures and replace diseased joints which has revolutionized orthopedic practice and afforded millions of patients levels of function that previously could not be achieved. Although the metal alloys used in these implants exhibit excellent resistance to corrosion, oxidation of these large components ultimately produce free ions, chlorides, oxides, and hydroxides which, in combination with particulate metal matter released by wear and fretting, are released into the surrounding environment. Efforts to improve these alloys have included compositional as well as processing changes. Additionally, modifications have been made to the plastic articulating components in efforts to produce a much more consistent ultrahigh molecular weight polyethylene. The perceived need to improve implant wear and corrosion resistance and alter design has been largely motivated by the excessive soft tissue staining noted by orthopedic surgeons at the time of removal or revision of clinically failed joint arthroplasty. The presence of particulate metal matter, polyethylene, and even fragments of polymethyl methacrylate in local tissue has been confirmed histologically and by direct analysis [1–4]. In spite of all of the modifications made in implant composition, implant fixation, and articulation, biomaterial degradation and release of these products persist [4–7].

M. Rock (✉)
Department of Orthopaedics, Mayo Clinic,
200 First Street Southwest, Rochester, MN 55905, USA

5.2 Release and Distribution of Degradation Products

The body's response to the local presence of debris is dependent on the size, amount, and composition as well as rate of accumulation. The body attempts to neutralize these foreign particles by precipitating granulomatous foreign body reactions and/or removal through local lymphatic channels. If the local accumulation of debris exceeds the body's ability to neutralize and/or transport, the debris migrates from the site to remote areas including the bone-implant interface, possibly contributing to if not initiating the phenomena of loosening and osteolysis (Figure 5.1).

Of equal or possibly even greater concern is the detection of metal ions, metallic debris, polyethylene, and even methylmethacrylate in areas remote from the implant including circulating serum, excreted urine, and regional draining lymph nodes. Elevated serum levels of metal ions consistent with the composition of the implanted alloy have been confirmed in animal models [8] and in human patients after total hip arthroplasty [9]; identifying serum levels of cobalt, chromium, nickel, and titanium that are two and three fold higher than preoperative determinations. These figures represent significant elevations both over means for contemporary control groups and for the individual patients before operation [9]. However, since they are within the widely accepted normal range for these metallic ions in the unimplanted human controls, it is assumed that toxic levels of these foreign materials do not materialize. However, when analyzing the serum to urine concentration in patients subjected to conventional total hip arthroplasty, it has become apparent that the urinary concentration of chromium in particular does not rise with the same magnitude and time course as the serum level [9]. This observation parallels that made in the accounts of industrial overexposure to Cr^{6+} and suggests that metal ions accumulate in organs and tissues remote from implantation. Such accumulation is unlike that resulting from normal systemic circulation. This was previously suggested by Steineman [10] who calculated the potential release of metallic ions of 0.15 to 0.3 micrograms per cm^2 per day which would translate to between 11 and 22 milligrams per year in patients with total hip replacement. This incidentally coincides with or exceeds the total body burden of such metallic ions in a 70 kilogram man [11].

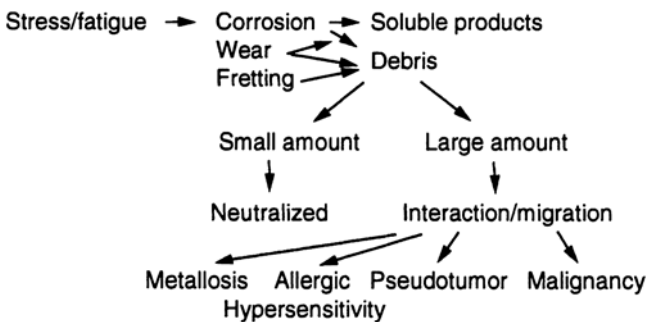


Figure 5.1 Tissue Reaction to Implant Degradation Products.

Evidence for metallic debris accumulating in distant organs has also been confirmed by Langkamer *et al.* [12] who identified wide spread dissemination of particulate wear debris from hip prosthesis to lymph nodes, liver, and spleen. He reported increases above normal levels in these organs of 30 fold for aluminum, chromium, and iron in the lymph node, and 10 fold in the spleen and liver.

These findings suggest that concentrations of metal ions and debris at remote sites may reach such proportions as to precipitate altered cellular dynamics in organs principally of the lymphoreticular system. It would only be logical to assume that local concentrations of such debris at the site of implantation would be even higher, although attempts at quantifying the effects of local concentrations have been fraught with inaccuracies mostly due to sampling error and the need to distinguish between bioavailable and non bioavailable metal species.

What is potentially more disturbing is that these figures for serum concentrations and the identification of this debris in remote organs have come primarily from patients who have received conventional polymethyl methacrylate cemented components. With the advent of using uncemented porous coated implants, particularly in younger patients, these figures would be expected to increase, creating the distinct possibility of toxic levels in the serum, tissues and organs that will respond with altered cellular dynamics and function.

5.3 Neoplasia

Perhaps one of the greatest concerns with debris dissemination locally and within the systemic circulation is the possibility of inducing malignant neoplasia. This is thought to be possible by one of two mechanisms:

- (i) A 'solid-state' mechanism has been proposed, whereby a large foreign object implanted *in vivo* possibly stimulates mutagenesis of local cells, thereby creating tumor by its mere presence. Most large foreign objects upon implantation will initiate a very marked fibrous reaction. The cells within this fibrous reaction ultimately mutate and become cancer growths.
- (ii) The other possibility is that particulate metal matter or other debris have an innate capacity, upon corrosion or dissolution, to induce cancer through a more traditional chemical route.

Cancer, the end product of carcinogenesis, is the result of transformation of a normal cells to ones which grow in an uncontrolled or malignant manner. Cancer is a genetic disease, which may result from expression of genetic pre-dispositions present from birth or from later insults to cells of many different types. In particular, the phagocytosis or pinocytosis of foreign matter (in an attempt to neutralize or eliminate it) may cause or precipitate malignant conversion. Such conversion, if not lethal to the cell, may then persist through cell duplication, creating first a cluster of cells with altered DNA and eventually a clinical malignant tumor. Malignancy is characterized by rapid, uncontrolled growth, invasion in surrounding tissues and seeding to form tumors (metastases) in other anatomical locations such as the lung.

Some of the more common malignant tumors of musculoskeletal origin are osteosarcoma (OS) of bone and malignant fibrous histiocytoma (MFA) of soft tissue.

Osteosarcoma is the most common tumor of bone: it occurs in children, adolescents and, less frequently, in adults. OS may also occur as a consequence of radiation therapy or in Paget's disease, an ostensibly benign bone embrittling disease of the elderly. It frequently appears about the knee (distal femur; proximal tibia), and in the proximal femur and proximal humerus.

MFA is the most common primary malignant tumor of soft tissues and can occur in bone in adults over the ages of 50–55. The more common soft tissue type usually involves the large muscular areas of the body, including the thigh, buttock and upper arm and shoulder.

5.4 Evidence for Carcinogenicity of Implanted Materials

Well-documented cases of carcinoma and sarcoma have developed in refinery workers who inhaled nickel and chromium and in miners who were exposed to iron or even at local injection sites of iron dextran [13]. Aluminum has been linked to a high rate of lung and bladder cancer in exposed individuals and titanium has been associated with experimental induction of lymphoreticular tumors and leukemia. Although the results have not been universally accepted, many animal experiments have shown a direct correlation between the initiation of sarcomas and the injection of particulate metal debris. This appears to be related to the concentration, as well as the physical nature, of the metal implanted [14]. Metal ions, particularly cobalt, chromium, and nickel, are known to induce infidelity of DNA synthesis by causing the pairing of non-complimentary nucleotides and thereby creating a misinterpretation of the genetic code which may lead to neoplasia.

Furthermore, it must be remembered that particulate metal matter may not be the only solid-form material that can be, and has been proven to be, carcinogenic in appropriate environments. In 1954 long before the first total hip arthroplasty was performed, Laskin [15] observed the carcinogenic capabilities of polymethylmethacrylate after subcutaneous introduction of this material in mice. His conclusions suggested that similar occurrences of tumor may appear in humans that were being treated at that time with methylmethacrylate for dental deficiencies and that this evolution of cancer may take up to 20 years of exposure given the proportional time exposure before tumors were seen in the mice. A similar conclusion was reached [16] on the use of polyethylene plastic before it was conventionally used in the management of arthritic joints. Regardless of form, whether powder or large solid segments, polyethylene plastic produced sarcomas in 25 percent and 35 percent of rats, respectively. Their conclusions also suggested a latent period, after exposure, of 20 years in humans before such an event could be expected to occur.

It is, therefore, with interest that investigators were forewarning the medical community of the carcinogenic effect of metals and polymers years before the development and introduction of joint replacement using these very same materials.

In 1961, Sir John Charnley introduced total hip arthroplasty as an alternative in the management of arthritic hips. No other orthopedic procedure has been adopted with such enthusiasm. Thirty-five years later we are still witnessing an incremental increase in the yearly utilization of this operation, attesting to the obvious success associated with it. According to some investigators, we may be coming into an era of increased tumor activity in the vicinity of or possibly remote from implantation sites of these orthopedic appliances.

5.5 Case Reports of Implant Related Tumors

In 1976, Harris *et al.* [17] were the first to describe an aggressive granulomatous lesion around a cemented femoral stem in a total hip replacement. This was a condition of localized tumor-like bone resorption that appeared radiographically as large lytic defects within the femur, approximating the cement mantle of the implant. Initially thought to be neoplastic, these lesions were surgically biopsied and found to be consistent with well-organized connective tissue containing numerous histiocytes, monocytes, and fibroblastic reactive zones. Immunohistologic evaluation revealed multinucleated giant cells and nonspecific esterase-positive monocyte macrophages. These findings suggest a foreign-body type reaction, and with the subsequent isolation of polyethylene, polymethyl methacrylate, and metal debris, it was theorized that these constituents of the construct likely migrated down around the implant cement mantle in cemented prostheses and implant-bone interface in non-circumferentially coated ingrowth implants. Such a reaction suggests an excessive accumulation of debris at the site of articulation that surpasses the body's ability to neutralize and/or transport the material resulting in migration of debris to sites remote from the source. This rapid appearance of bone loss radiographically which is often associated with a deteriorating clinical course has been termed type-II aseptic loosening [17].

In 1978, two years after the recognition of pseudo tumors of bone induced by the degradation products of total hip arthroplasty, Arden and Bywaters [20] (Table 5.1) reported a case of a 56-year-old patient who developed a high-grade fibrosarcoma of soft tissue 2.5 years after receiving a metal-on-metal McKee-Farrar hip prosthesis. The tumor apparently did not have a direct association with the underlying bone or any components of the total hip arthroplasty. No formal analysis of the tumor for debris products was performed. This case drew attention to the possibility of tumors being initiated in the presence of large orthopedic appliances. It was not until 1984 when this concept became fashionable in large part due to three articles that appeared simultaneously in the *Journal of Bone and Joint Surgery* recounting two malignant fibrous histiocytomas and one osteosarcoma at the site of a total hip arthroplasty [21–23].

This sudden and rather unexpected evolution prompted editorials [24, 25] in the same journal addressing the issue of sarcoma and total hip arthroplasty and encouraged the orthopedic community worldwide to report such cases to a central registry

Table 5.1 Malignancies Associated with Joint Replacements (published)

Author	Year	Implant	Time interval(yrs)	Tumor type
Castleman and McNeely [18]	1965	Austin-Moore	1	M.F.H.*
Rushforth [19]	1974	McKee-Farrar	0.5	Osteosarcoma
Arden and Bywaters [20]	1978	McKee-Farrar	2.5	Fibrosarcoma
Bagó-Granell <i>et al.</i> [21]	1984	Charnley-Muller	2	M.F.H.
Penman and Ring [22]	1984	Ring	5	Osteosarcoma
Swann [23]	1984	McKee-Farrar	4	M.F.H.
Weber [26]	1986	Cemented TKA	4.5	Epithelioid sarcoma
Ryu <i>et al.</i> [27]	1987	Uncemented Vitallium**	1.4	M.F.H.
Vives <i>et al.</i> [28]	1987	Charnley-Muller	2	M.F.H.
Van der List [29]	1988	Charnley-Muller	11	Angiosarcoma
Lamovec <i>et al.</i> [30]	1988	Charnley-Muller	11	Synovial sarcoma
Lamovec <i>et al.</i> [31]	1988	Charnley-Muller	10	Osteosarcoma
Tait <i>et al.</i> [32]	1988	Charnley-Muller	11	M.F.H.
Martin <i>et al.</i> [33]	1988	Charnley-Muller	10	Osteosarcoma
Haag and Adler [34]	1989	Weber-Huggler	10	M.F.H.
Mazabraud <i>et al.</i> [35]	1989	Unknown	9	Epidermoid sarcoma
Brien <i>et al.</i> [36]	1990	Charnley	8	Osteosarcoma
Troop <i>et al.</i> [37]	1990	Charnley-Muller	15	M.F.H.
Kolstad and Högstorp [38]	1990	Freeman TKA	0.25	Metastatic adenocarcinoma
Jacobs <i>et al.</i> [39]	1992	AML cementless	0.5	M.F.H.
Solomon and Sekel [40]	1992	Charnley-M uller	7	M.F.H.

* M.F.H. = malignant fibrous histiocytoma.

** Trademark, Howmedica, Inc. (Cobalt-Chromium alloy).

to obtain more accurate figures on the incidence of such a problem. These tumors occurred 2, 4, and 5 years after hip replacement that was performed with various femoral and acetabular components, some with metal-on-metal articulations and others with metal on polyethylene. In two of these cases, the proximal femur was extensively involved with tumor that was in direct contact with the component. The remaining case was a soft-tissue sarcoma not in direct approximation to the prosthesis. Two of these tumors were malignant fibrous histiocytomas, one of bone and one of soft tissue. The remaining tumor was osteosarcoma. In this particular case, there was evidence of gray-brown pigmentation both intra- and extracellularly between the tumor and femoral component. No formal metal analysis was performed. Three additional cases emerged prior to 1988 at 15 months, 4.5 years, and 2.0 years after implantation [26–28].

In 1988, five cases were reported occurring at 10 [29, 30] and 11[29, 31, 32] years after implantation. The sarcomas included two osteosarcomas, two malignant fibrous histiocytomas, and one synovial sarcoma. Two of these were soft tissue in a location with no direct association with the implant, yet in the case reported by Tait *et al.* [32] there was evidence of nickel within tumor cells. The remaining three

Table 5.2 Malignancies Associated with Joint Replacements (unpublished)[41]

Author	Year	Implant	Time interval (yrs)	Tumor type
Harris	1992	Charnley	1	Chondrosarcoma
Surin	1992	Christiansen	9	Rhabdomyosarcoma
Lightowler	1992	Charnley	10	Osteosarcoma
Rees, Thompson, Burns	1992	Thompson	3	M.F.H.*
Nelson	1992	Muller	9	M.F.H.
Rock	1992	HG ingrowth	0.8	M.F.H.
Rock	1992	PCA TKA	1.2	Osteosarcoma

* *M.F.H.* = *Malignant Fibrous Histiocytoma*.

patients all had direct contact with either the cement or implant with the tumor originating in bone.

In 1990 there were three additional reports in the literature which included an osteosarcoma developing at the site of a Charnley total hip arthroplasty 8 years [36] after implantation, malignant fibrous histiocytoma developing 15 years after a Charnley-Muller total hip arthroplasty [37], and metastatic adenocarcinoma developing at the site of a Freeman total knee arthroplasty three months after implantation [38]. In 1992, Jacobs *et al.* [39] presented a malignant fibrous histiocytoma developing one half year after implantation of a cementless AML total hip arthroplasty.

In that same journal volume, unpublished but submitted reports of five tumors occurring around implants were brought to the attention of the orthopedic community [41] (Table 5.2). These included malignant fibrous histiocytomas around a Thompson and a Muller total hip arthroplasties, an osteosarcoma around a Charnley total hip arthroplasty, a rhabdomyosarcoma of soft tissue in the vicinity of a Christiansen total hip arthroplasty, and a chondrosarcoma developing in a patient with Maffucci syndrome having a Charnley total hip arthroplasty. The intervals from implantation to tumor detection were 9, 3, 10, 9 and 1 years respectively. To this, we add two previously unreported additional patients, neither of whom had their joint replacement done at the Mayo Clinic (Table 5.2). The first is that of a 79-year-old man who nine months previously came to total hip replacement with an uncemented Harris-Galante component who was found to have a large malignant fibrous histiocytoma engulfing the proximal femur and extending to the implant. There was, however, no evidence of any particulate debris within the tumor cells removed. The second case was that of a 56-year-old man who developed a soft tissue osteosarcoma 14 months after a left total knee arthroplasty with conventional cemented components. The tumor extended down to both the femoral and patellar components.

5.6 Critical Analysis of Tumors

As such, 28 tumors have been reported in direct contact or in close proximity to joint arthroplasty. The vast majority of these appeared with total hip arthroplasty [27] with a smaller contribution from total knee arthroplasty [3]. There have been

no reported cases of malignant degeneration occurring in the vicinity of total shoulder and/or total elbow arthroplasty. Of the reported 26 cases, 8 tumors were of soft tissue origin, 19 were of primary bone pathology, and 1 metastatic gastric carcinoma. The histogenesis of the soft tissue tumor included 3 malignant fibrous histiocytomas, 1 synovial sarcoma, 1 soft tissue osteogenic sarcoma, 1 fibrosarcoma, 1 epidermoid sarcoma and 1 rhabdomyosarcoma. The histogenesis of the primary bone tumors included 10 malignant fibrous histiocytomas, 6 osteosarcomas, 1 chondrosarcoma, 1 angiosarcoma, 1 fibrosarcoma. Direct contact with the underlying tumor was noted in 15 of the 19 cases in which sufficient information is known from which to make such determinations. In three of the cases, particulate metal matter was determined to be present in the tumor including one case of a soft tissue sarcoma that appeared on image and exploration to be remote from the implant but had obvious evidence of nickel present within the tumor cells.

Many of these tumors have not had an appropriate latent interval between implantation and development to be seriously considered implant induced. Given that the interval to tumor induction from bone stimulation should be at least as long as the accepted five year interval from radiation therapy to sarcoma degeneration, 15 of the 28 patients would qualify, all of whom have had tumours around total hip arthroplasties.

Apart from tumors developing at the site of prosthetic replacement, there have been ten known malignant tumors that have developed at the site of previous internal fixation (Table 5.3). To date there have been no malignancies noted around a titanium implant. The vast majority (> 80%) of malignancies both in the prosthetic and internal fixation groups have occurred in the vicinity of Vitallium™ (cobalt-chromium alloy) implants. This is not, however, to exonerate stainless steel because tumors in the proximity of the implants made of this alloy have been reported in the animal literature [52] as well as the human experience utilizing stainless steel as fixation devices for traumatology [42, 44, 50, 51]. It is interesting to note that in 1976 veterinarians were encouraged within their own literature to report similar

Table 5.3 Malignancies Associated with Internal Fixation of Fractures

Author	Year	Implant	Time interval (yrs)	Tumor type
McDougall [42]	1956	Stainless steel	30	Ewings
Delgado [43]	1958	Unknown	3	Undifferentiated
Dube and Fisher [44]	1972	Stainless steel	36	Angiosarcoma
Tayton [45]	1980	Vitallium*	7.5	Ewings
McDonald [46]	1981	Vitallium	17	Lymphoma
Dodion <i>et al.</i> [47]	1982	Vitallium	1.2	Lymphoma
Lee <i>et al.</i> [48]	1984	Vitallium	14	M.F.H.*
Hughes <i>et al.</i> [49]	1987	Vitallium	29	M.F.H.
Ward <i>et al.</i> [50]	1990	Stainless steel	9	Osteosarcoma
Khurana <i>et al.</i> [51]	1991	Stainless steel	13	M.F.H.

* Trademark, Howmedica, Inc. (cobalt-chromium alloy).

** M.F.H. = malignant fibrous histiocytoma.

experiences of tumors around implants nearly eight years before such concern was voiced with the application of these same metallic alloys in humans [52].

5.7 Significance of Clinical Reports

As impressive as these cases may be, they must be put into perspective given the global use of internal fixation and prosthetic devices. Approximately 300 000 to 350 000 total hip joint replacements are performed worldwide on a yearly basis [53]. It can be assumed that approximately four million people will have had total hip arthroplasties performed by the end of 1995. To date, there have been 28 reports of malignant tumor arising in close proximity to these implants (25 total hip and three total knee arthroplasties). No direct contact was noted in four. If we assume a minimal latency of five years to suggest association between presence of implant and tumor, 15 of the 28 could have association. As such, the incidence of sarcomas in total joint replacement would be approximately 1 in 250 000. There are approximately 3000 new primary bone tumors and 5000 soft-tissue sarcomas in the United States per year. This would give an incidence of approximately 1 in 100 000 for the general population to develop a primary bone sarcoma and 1 in 40 000 to develop a soft tissue sarcoma a year. This is obviously not stratified for age given that many primary bone tumors develop in the second and third generation of life, yet it does afford the opportunity of putting this rather unusual event in perspective.

The prevalence of osteosarcoma among the osseous malignancies in this series is not entirely unexpected. Of the total osteosarcoma population 15 percent to 20 percent occur after the age of 50 years. Most of these cases are superimposed on Paget's disease or in previously irradiated tissue, yet *de novo* cases of osteosarcoma do occur in this age group. Malignant fibrous histiocytoma of bone is somewhat less common. A review of the Mayo Clinic files reveals 71 cases with more than half of these occurring after age 55. Malignant fibrous histiocytoma of soft tissue is the most common soft-tissue sarcoma. It is not surprising, therefore, that two of six soft-tissue tumors in the combined series are of this histogenesis. As such, the distribution of sarcomas in the combined series could have been predicted from general population data given the age of the patients and anatomical distribution.

There have been two separate reports that have critically analyzed the cancer risk after total hip arthroplast [54, 55]. The combined person years of exposure after operation between the two series was 20 015. The overall cancer incidence among total hip replacement procedure in both series did not appear to be any different than what was expected or anticipated. The cancer-observed/expected ratio was especially low for the first two years following surgery in both series, implying that patients undergoing this procedure are otherwise generally healthy. In both series, the observed/expected ratio of developing lymphoma or leukemia was two to three times higher in patients who had total hip arthroplasty. Additionally, there was a two fold decrease in breast carcinoma among patients who had total hip arthroplasty.

Of interest, Gillespie *et al.* [54] suggested a similar decrease in the incidence of rectal, colon, and lung cancer among total hip arthroplasty patients. The results suggest or are possibly compatible with the hypothesis of chronic stimulation of the immune system, thereby potentially allowing for malignancies to occur within the lymphoreticular system. We have already determined a predilection for particulate metal matter to accumulate in the reticuloendothelial system [12]. This has been further supported by studies in animals subjected to metal implants, especially those containing nickel, in which there was an increase in malignancies of the lymphoreticular systemic [52]. Additionally, due to the added immune surveillance, tumors of the breast, possibly colon, rectal, and lung may be decreased. A hyper immune state is not unexpected given the dissemination of debris locally at implantation sites as well as the well-recognized and documented capacity of this material to gain access to the systemic and possibly storage sites including the reticuloendothelial system. This trend obviously needs continued surveillance.

A recent extensive analysis of the cancer risk in a cohort of 39154 patients with at least one hip replacement operation has been performed by the Swedish Nationwide In-Patient Registry [56]. Patients were identified by means of a linkage to the Swedish Cancer Registry. The overall results, although showing a significant 3% increase in cancer, were judged by the authors not to be of clinical significance. Increases of cancer of kidney, skin and brain in women and of prostate in men were found, accompanied by a decrease in gastric cancer for women. The study showed no increase in lymphoreticular cancers as previously reported [54, 55] nor a decrease in colon, breast or rectal cancers. The authors' judgement is that the overall cancer risk associated with total hip replacement arthroplasty is negligible and should not distract from the obvious benefits of the procedure.

A similar extensive review of the relationship between metallic implants and cancer in dogs was performed by Li *et al.* [57]. This case controlled study of 1857 dogs from 22 veterinary medical centers failed to reveal significant association between stainless steel fracture fixation devices and the development of bone and soft tissue sarcomas.

5.8 Summary

In summary, careful examination of the scientific and clinical literature suggests that implant materials commonly used for fixation and joint reconstruction are not entirely inert. Accumulation of particulate debris is to some extent going to occur in all patients who have large prosthetic devices. This necessarily includes the distinct possibility of systemic and remote site exposure to these foreign objects that the body attempts to neutralize and excrete. Due to the heightened immunologic surveillance and/or possible storage of particulate metal matter in sites remote from the implantation site, patients with total hip arthroplasty may be at added risk for remote malignancies, particularly of the lymphoreticular system. The incidence of primary mesenchymal tumors in close proximity to implants appears to be consistent with

the incidence in the general public. The frequency of occurrence and the associated individual and group risks of systemic and remote site malignancy remains unresolved.

Additional Reading

Nyren, O., McLaughlin, J.K. *et al.* (1995) Cancer risk after hip replacement with metal implants: A population based study. *J. National Can. Inst.* **87**, 28–33.

An extensive review of risk of cancer in 39 154 total hip replacement patients who appeared in the Swedish National Cancer Registry between 1965 and 1983. A review of 60 cancer-specific sites showed an overall, not clinically significant increase of 3% in incidence, slight increases noted for kidney cancer, prostate cancer (in men) and melanoma accompanied by a continuous decline in gastric cancer for both sexes. This would appear to be the definitive review of the risk for developing cancers after total hip replacement arthroplasty.

Brand, K.G. and Brand, I. (1980) Risk assessment of carcinogenesis at implantation sites. *Plastic Reconst. Surg.* **66**, 591–595.

Review of possible foreign body cancer initiation in humans based upon published case reports. The authors conclude that, since the clinical use of prosthetic implants has been popular for more than twenty years and since, extrapolating from animal experience, at least 25% if not 50% of foreign body tumors should have appeared by the time of their publication, there is little risk of such non-chemically mediated tumors occurring in patients.

Gillespie, W.J., Frampton, C.M.A., Henderson, R.J. *et al.* (1988) The incidence of cancer following total hip replacement. *J. Bone Joint Surg.*, **70B**, 539–542.

A New Zealand study of 1358 patients with total hip arthroplasty, for a total of 14 286 patient years. A significant increase in tumors of the hemopoetic and lymphatic systems, accompanied by a significant decrease of cancers of breast (in women), colon and bowel was observed. The authors suggest that these data are evidence for increased immune surveillance, allowing or precipitating hemopoetic and lymphatic tumors but at the same time providing better resistance to the development of soft tissue tumors. The first large scale study of this question.

Visuri, T. and Koskenvuo, M. (1991) Cancer risk after McKee-Farrar total hip replacement. *Orthopedics*, **14**, 137–142.

A study similar to that of Gillespie *et al.* but on a Finnish patient group (433 patients; 5729 patient years) leading to the same general conclusions. Includes a historical discussion of the carcinogenic properties of various trace elements.

Jacobs, J.J., Rosenbaum, D.H., Hay, R.M. *et al.* (1992): Early sarcomatous degeneration near a cementless hip replacement. A case report and review. *J. Bone Joint Surg.*, **74B**, 740–744.

A review of a patient who developed a malignant fibrous histiocytoma at the site of a cementless total hip replacement five months after implantation and succumbed of diffuse metastases, as is typical for such patients, within one year of

presentation. Includes an extensive review of world literature on sarcomas in the vicinity of total hip replacement and suggest the need for an international registry of such case reports.

References

1. Coleman, R.R., Herrington, S. and Scales, J.T. (1973) Concentration of wear products in hair, blood, and urine after total hip arthroplasty. *Brit. Med. J.* **1** 1527–1529.
2. Lux, F. and Zeisler, R. (1974) Investigations of the corrosive deposition of components of metal implants and of the behavior of biologic trace elements in metallosis tissue by means of instrumental, multi-element activation analysis. *J. Radiol. Anal. Chem.*, **19**, 289–297.
3. Rock, M.G. and Hardie, R. (1988): Analysis of local tissue response in 50 revision total hip arthroplasty patients. *Trans. Soc. Biomater.*, **XI**, 43.
4. Agins, H.J., Alcock, N.W., Bansal, M. et al. (1988) Metallic wear in failed titanium alloy total hip replacements. A histological and quantitative analysis. *J. Bone Joint Surg.* **70A**, 347–356.
5. Buchert, B.K., Vaughn, B.K., Mallory, T.H. et al (1986): Excessive metal release due to loosening and spreading of sintered particles on porous coated hip prosthesis. Report of two cases. *J. Bone Joint Surg.*, **68A**, 606–609.
6. Jacobs, J.J., Skipor, A.K., Black, J. et al. (1991), Release in excretion of metal in patients who have a total hip replacement component made of titanium base alloy. *J. Bone Joint Surg.* **73A**, 1475–1486.
7. Witt, J.D. and Swann, M. (1991) Metal wear and tissue response in failed titanium alloy total hip replacements. *J. Bone Joint Surg.* **73B**, 559–563.
8. Woodman, J.L., Jacobs, J.J., Galante, J.O., et al. (1984), Metal ion release from titanium-based prosthetic segmental replacements of long bones in baboons. A long term study. *J. Orthop. Res.*, **1**, 421–430.
9. Bartolozzi, A. and Black, J. (1985) Chromium concentrations in serum, blood clot and urine from patients following total hip arthroplasty. *Biomaterials*, **6**, 2–8.
10. Steineman, S.G. (1985) Corrosion of Titanium and Titanium Alloys For Surgical Implant. in: Lutergering, G., Swicker, U., Bunk, W. (eds), *Titanium, Science, and Technology*, Volume 2, DG für Metal. e.V. Oberuresel, Berlin, 1373–1379.
11. Harvey, A.M., Johns, R.S., Owens, A.H. et al. (1972) *The Principles and Practice of Medicine*. New York: McGraw-Hill, pp. 68–102.
12. Langkamer, V.G., Case, C.P., Heap, P. et al. (1992) Systemic distribution of wear debris after hip replacement. A cause for concern? *J. Bone Joint Surg.*, **74B**, 831–839.
13. Doll, R. (1958) Cancer of lung and the nose. Nickel workers. *Brit. J. Indust. Med.*, **15**, 217–223.
14. Swanson, S.A.V., Freeman, M.A.R. and Heath, J.C. (1973) Laboratory tests on total joint replacement prosthesis. *J. Bone Joint Surg.*, **55B**, 759–773.
15. Laskin, D.M. (1954): Experimental production of sarcomas by methylacrylate implant. *Proc. Soc. Exper. Biol. Med.*, **87**, 329–333.
16. Carter, R.L. and Rowe, F.J.C. (1969): Induction of sarcomas in rats by solid and fragmented polyethylene: Experimental observations and clinical implications. *Brit. J. Cancer*, **23**, 401–407.
17. Harris, W.H., Schiller, A.L., Scholler, J.M. et al. (1976) Extensive localized bone resorption in the femur following total hip replacement. *J. Bone Joint Surg.* **58A**, 612–618.
18. Castleman, B., McNeely, B.U. (eds) (1965) Case 38–1965, Case records of the Massachusetts General Hospital. *New Engl. J. Med.*, **273**, 494–504.
19. Rushforth, G.F. (1947) Osteosarcoma of the pelvis following radiotherapy for carcinoma of the cervix. *Brit. J. Radiol.* **47**, 149–152.

20. Arden, G.P. and Bywaters, E.G.L. (1978), in *Surgical Management of Juvenile Chronic Poly Arthritis*. Arden, G.P., Ansel, B.M. (eds), Academic Press, London, pp. 269–270.
21. Bágo-Granel, J., Aguirre-Canyadell, M., Nardi, J. *et al.* (1984) Malignant fibrous histiocytoma of bone at the site of a total hip arthroplasty. A case report. *J. Bone Joint Surg.* **66B**, 38–40.
22. Penman, H.G. and Ring, P.A. (1984) Osteosarcoma in association with total hip replacement. *J. Bone Joint Surg.* **66B**, 632–634.
23. Swann, M. (1984) Malignant soft tissue tumor at the site of a total hip replacement. *J. Bone Joint Surg.* **66B**, 269–231.
24. Hamblen, D.L. and Carter, R.L. (1984) Sarcoma and Joint Replacement (Editorial). *J. Bone Joint Surg.* **66B**, 625–627.
25. Apley, A.G. (1989) Malignancy and joint replacement. The tip of an iceberg? (Editorial). *J. Bone Joint Surg.* **71B**, 1.
26. Weber, P.C. (1986) Epithelioid sarcoma in association with total knee replacement. *J. Bone Joint Surg.* **68B**, 824–826.
27. Ryu, R.K.N., Bovill, E.G. Jr, Skinner, H.B. *et al.* (1987) Soft tissue sarcomas associated with aluminum oxide ceramic total hip arthroplasty. A case report. *Clin. Orthop.* **216**, 207–212.
28. Vives, P., Sevestre, H., Grodet, H. *et al.* (1987) Histiocytome fibreux malin du fémur après prothèses totale de hanche (Malignant fibrous histiocytoma of the femur following total hip replacement). *Rev. Chir. Orthop.* **73**, 407–409.
29. Van der list, J.J.J. (1988) Malignant epithelioid hemangioendothelioma at the site of a hip prosthesis. *Acta Orthop. Scand.* **59**, 328–330.
- 30;31. Lamovec, J., Zidar, A., Cucek-Plenicar, M. *et al.* (1988): Synovial sarcoma associated with total hip replacement. A case report. Addendum: Osteosarcoma associated with a Charnley-Muller hip arthroplasty. *J. Bone Joint Surg.* **70A**, 1558–1560.
32. Tait, N.P., Hacking, P.M. and Malcolm, A.J. (1988) Case report, malignant fibrous histiocytoma occurring at the site of a previous total hip replacement. *Brit. J. Radiol.*, **61**, 73–76.
33. Martin, A., Bauer, T.W., Manley, M.T. *et al.* (1988) Osteosarcoma at the site of a total hip replacement. *J. Bone Joint Surg.* **70A**, 1561–1567.
34. Haag, M. and Adler, C.P. (1989) Malignant fibrous histiocytoma in association with hip replacement. *J. Bone Joint Surg. (Brit)*, **71B**, 701.
35. Mazabraud, A., Florent, J. and Laurent, M. (1989) (A case of epidermoid carcinoma developed in contact with a hip prosthesis)(Fr.)(au. transl.). *Bull. Cancer*, **76**, 573–581.
36. Brien, W.W., Salvati, E.A., Healey, J.H. *et al.* (1990) Osteogenic sarcoma arising in the area of a total hip replacement. A case report. *J. Bone Joint Surg.*, **72A**, 1097–1099.
37. Troop, J.K., Mallory, T.H., Fisher, D.A., *et al.* (1990) Malignant fibrous histiocytoma after total hip arthroplasty: A case report. *Clin. Orthop. Rel. Res.*, **253**, 297–300.
38. Kolstad, K. and Högstorp, H. (1990): Gastric carcinoma metastasis to a knee with a newly inserted prosthesis: A case report. *Acta Orthop. Scand.* **61**, 369–370.
39. Jacobs, J.J., Rosenbaum, D.H., Hay, R.M. *et al.* (1992): Early sarcomatous degeneration near a cementless hip replacement. A case report and review. *J. Bone Joint Surg.*, **74B**, 740–744.
40. Solomon, M.I. and Sekel, R. (1992) Total hip arthroplasty complicated by a malignant fibrous histiocytoma. A case report. *J. Arthroplasty*, **7**, 549–550.
41. Goodfellow, J. (1992) Malignancy and joint replacement (Editorial). *J. Bone Joint Surg.*, **74A**, 645.
42. McDougall, A. (1956) Malignant tumor at site of bone plating. *J. Bone Joint Surg.* **38B**, 709–713.
43. Delgado, E.R. (1958) Sarcoma following a surgically treated fractured tibia: A case report. *Clin. Orthop.* **12**, 315–318.
44. Dube, V.E. and Fisher, D.E. (1972) Hemangioendothelioma of the leg following metallic fixation of the tibia. *Cancer* **30**, 1260–1266.
45. Tayton, K.J.J. (1980) Ewing's sarcoma at the site of a metal plate. *Cancer* **45**, 413–415.
46. McDonald, I. (1981) Malignant lymphoma associated with internal fixation of a fractured tibia. *Cancer* **48**, 1009–1011.

47. Dodion, P., Putz, P., Amiri-Lamraski, M.H. *et al.* (1983) Immunoblastic lymphoma at the site of an infected vitallium bone plate. *Histopathol.*, **6**, 807–813.
48. Lee, Y.S., Pho, R.W.H. and Nather, A. (1984) Malignant fibrous histiocytoma at site of metal implant. *Cancer* **54**, 2286–2289
49. Hughes, A.W., Sherlock, D.A., Hamblen, D.L. *et al.* (1987) Sarcoma at the site of a single hip screw. A case report. *J. Bone Joint Surg.* **69B**, 470–472.
50. Ward, J.J., Thornbury, D.D., Lemons, J.E. *et al.* (1990) Metal-induced sarcoma: A case report and literature review. *Clin. Orthop.* **252**, 299–306.
51. Khurana, J.S., Rosenberg, A.E., Kattapuram, S.V. *et al.* (1991) Malignancy supervening on an intramedullary nail. *Clin. Orthop.* **267**, 251–254.
52. Sinibaldi, K. (1976): Tumors associated with metallic implants in animals. *Clin. Orthop. Rel. Res.*, **118**, 257–266.
53. Moss, A.J. (1991) Use of selected medical devices in the United States. *Advance Data from Vital and Health Statistics of the National Center for Health Statistics*, **191**, 1–24.
54. Gillespie, W.J., Frampton, C.M., Henderson, R.J. *et al.* (1988) The incidence of cancer following total hip replacement. *J. Bone Joint Surg.* **70B**, 539–542.
55. Visuri, T. (1992) Cancer risk after McKee-Farrar total hip replacement. *Orthopedics*, **14**, 137–142, 1992.
56. Nyren, O., McLaughlin, J.K. *et al.* (1995) Cancer risk after hip replacement with metal implants: A population based study. *J. National Can. Inst.* **87**, 28–33.
57. Li, X.Q., Stevenson, S., Hom, D.L. *et al.* (1993): Relationship between metallic implants and cancer: A case-control study in a canine population. *Vet. Comp. Orthop. Traumatol.* **6**, 70–74.

Chapter 6

Blood–material Interactions

S.R. Hanson

6.1 Introduction

The importance of understanding mechanisms of blood-material interactions is emphasized by the increasingly widespread use of cardiovascular devices; hence, this field has been the subject of intense inquiry as described in several excellent reviews [1–4]. Unfortunately, it is still not possible to simply rank or classify materials with respect to their suitability for particular blood-contacting applications. Nor is it possible to predict in any general way, based on the properties of devices and of their blood-contacting surfaces, the behavior of blood in contact with materials or the propensity of devices to produce clinically adverse events. Despite many attempts to correlate biologic responses to physicochemical property measurements, our success in understanding blood-material interactions, and the clinical application of many blood-contacting devices, has been largely empirical. It is not appropriate to discuss in detail this large and controversial literature, which has been reviewed elsewhere [1, 2]. Rather, this section will focus on the available experimental data in humans, or results which may likely be extrapolated to humans from relevant animal studies, that may guide in the development of new designs for blood-contacting devices. Cardiovascular device applications in humans have also been the subject of an excellent review [5].

6.2 Experimental Difficulties

Before summarizing relevant experimental findings, it is appropriate to review briefly the theoretical and practical limitations to our understanding of blood–material interactions.

S.R. Hanson (✉)

Division of Hematology/Oncology, Emory University, AJ, Atlanta, GA 30322, USA

There are several factors which have precluded the rational engineering design of devices based on first principles. While thousands of materials have been put forward as 'biocompatible' or non-thrombogenic, based on *in vitro* studies and animal testing, the relevance of these tests for outcomes in humans remains uncertain. Device responses *in vivo* depend upon actual device configuration and resulting flow geometry as well as upon intrinsic materials' properties. In many applications, mechanical and physical property requirements may dominate materials' selection. For example, membranes used in dialyzers and oxygenators must be both solute and gas permeable; chronic vascular grafts and heart valves must be mechanically durable and chemically stable for years; heart assist devices require flexible pumping chambers. Thus, the use of *in vitro* assays or simplified *in vivo* flow geometries, as in many animal models, has not proven adequate to predict actual device performance in patients. Furthermore, most animals and humans, as individuals, differ markedly from one another in both blood chemistry and in blood response to foreign materials [6]. It is deemed unethical to perform screening tests in humans, hence relatively few materials have undergone clinical evaluation and only limited human comparative data are available. In the case of chronic implants, devices removed at autopsy provide only a single set of observations which cannot be related to dynamic blood-material interactions prior to explantation.

Another limitation is our recognition that all blood-material interactions of clinical consequence are preceded by complex interactions between the biomaterial surface and circulating blood proteins. Plasma contains more than 100 identified proteins with specific functions and varying biologic properties [7]. These proteins interact with surfaces in a complex, interdependent and time-dependent fashion that remains poorly understood, except in low dilution, simplified model systems [8]. These reactions may vary from individual to individual depending upon coagulation status, the use antithrombotic or other drug therapies, or the administration of contrast media for fluoroscopic imaging. A partial listing of variables which may affect device outcomes following blood exposure is given in Table 6.1.

Despite these limitations, the design engineer may be guided by previous successful applications of materials in a variety of device configurations, and by certain generalizations which have resulted from these studies. Devices which are commonly used include catheters, cannulae, guide wires, stents, shunts, vascular grafts, heart valves, heart and ventricular assist devices, oxygenators, and dialyzers. With respect to these devices it is important to consider those events which can lead to serious clinical complications. These complications include: (1) thrombosis, (2) thromboembolism, (3) consumption (ongoing destruction) or activation of circulating hemostatic blood elements, and (4) activation of inflammatory and immunologic pathways. An appreciation for the biologic mechanisms of these events is essential for understanding the blood-compatibility of devices, and may be briefly described as follows. Thrombus forms as the localized accumulation of blood elements on, within, or associated with a device, and thrombus which is actively deposited can accumulate to the extent of producing device dysfunction or blood vessel occlusion. Interruption of normal blood flow may produce ischemia (relative lack of oxygen) and infarction (tissue death due to total oxygen deprivation) in distal circulatory beds leading to heart attacks and strokes. Thrombus structure may be complex, and is

Table 6.1. Variables influencing blood interactions with cardiovascular devices

Device Properties
Size and shape
Surface composition
Texture or roughness
Mechanical properties
blood Flow Phenomena
Shear forces
Convection and diffusion of reactants, products, cofactors and inhibitors
Disturbed flow and turbulence
blood Chemistry-related Effects
Coagulation status
Antithrombotic and other therapies
Contrast media
Other Variables
Duration of device blood exposure
Tissue injury
Infection

distinguished from that of whole blood clots which are often formed under static flow conditions. Thus, clots are relatively homogeneous structures containing red blood cells and platelets trapped in a mesh of polymerized protein (fibrin), while thrombus formed under arterial flow conditions and high fluid shear rates (‘white thrombus’) may be composed primarily of layers of fibrin and platelets (small procoagulant cells occupying only about 0.3% of the total blood volume). Under conditions of low fluid shear, as found in veins, thrombus may more closely resemble the structure of whole blood clots (‘red thrombus’). Thromboembolism is the dislodgement by blood flow of a thrombus which is then transported downstream, ultimately blocking vessels which are too small for the thrombus to traverse. Thromboembolism is a common cause of stroke (cerebrovascular infarction) and peripheral limb ischemia. Often the balance between dynamic processes of thrombus deposition and its removal by embolic and lytic mechanisms will produce platelet consumption (ongoing destruction) and a net reduction in circulating platelet levels. Other clotting factors may be consumed as well [9]. Finally, certain devices, particularly those having large surface areas, may activate enzyme systems (e.g., complement) leading to inflammatory or immunologic responses [10]. With these issues in mind we will now review the performance of various classes of biomaterials in actual device configurations.

6.3 Conventional Polymers

Conventional polymers, such as polyethylene (Intramedic™), poly (vinyl chloride) (Tygon™), polytetrafluoroethylene (Teflon™), and poly (dimethyl siloxane) (Silastic™), and certain polyurethanes, have been used for many decades in short-term applications including catheters, cannulas, arteriovenous shunts for

hemodialysis, and tubing components of extracorporeal circuits. When used for periods of only a few hours, and most often in patients receiving systemic anticoagulation agents, the performance of such materials has usually been clinically acceptable. For example, although thrombus on angiographic catheters can be demonstrated in about half of all cases, most thromboembolic or occlusive events are clinically silent and significant complications occur in less than 1% of procedures [5]. Even total occlusion of small peripheral veins, by short term catheters used for venous sampling or drug administration, is usually inconsequential. However, longer-term indwelling catheters in a variety of configurations and polymer compositions, particularly in infants and children, are now recognized to produce a significant risk of thrombosis which can ultimately lead to organ or limb damage, and even death [11]. Comparative, quantitative studies with different polymer formulations remain to be performed in humans.

Polyurethanes, due in part to their flexibility and toughness, are perhaps the polymer of choice for ventricular assist devices and blood pumps. Consequently, they have received considerable interest as blood-contacting materials. In non-human primates, those polyurethanes, such as Pellethane™, which exhibit the most hydrophobic surface chemistry produce the least platelet consumption [12]. In dogs, early platelet interactions with polyurethanes vary considerably although relationships to polymer surface chemistry remain unclear [13]. Thus while polyurethanes are chemically versatile and possess many desirable mechanical properties, it is generally not possible to predict their biologic responses in humans.

6.4 Hydrophilic Polymers

These materials, which preferentially adsorb or absorb water (hydrogels), were initially postulated to be blood compatible based on the view that many naturally occurring phospholipids, comprising the cell membranes of blood contacting tissues, are also hydrophilic. Thus, water, as a biomaterial, was expected to show minimal interaction with blood proteins and cells [14, 15]. Interestingly, in animal studies highly hydrophilic polymers based on acrylic and methacrylic polymers and copolymers, as well as poly(vinyl alcohol) are all found to consume platelets excessively although they accumulate little deposited thrombus [12, 16]. The materials have variable thrombogenicity, but little capacity to retain adherent thrombus, i.e., they shed deposited platelets as microemboli. Thus, while surface-grafted hydrogels (which are mechanically weak) are currently used to improve catheter lubricity and as reservoirs for drug delivery, they have not received widespread application for improving blood-compatibility.

Another hydrophilic polymer that has received considerable attention is poly(ethylene oxide) [17, 18]. While poly(ethylene oxide) surfaces have been shown (like hydrogels) to have relatively low interactions with blood proteins and cells in *in vitro* studies and in some animal models, the suitability of such poly-

mers for actual device applications and long-term implants has not been established.

6.5 Metals

Metals, as a class, tend to be thrombogenic, and are most commonly applied in situations requiring considerable mechanical strength, such as in the struts of mechanical heart valves and as endovascular stents [3, 19] or electrical conductivity, as in pacing electrodes. Stents are metallic mesh devices placed within blood vessels to preserve vessel patency after procedures to expand the vessel lumen diameter (e.g., after balloon angioplasty). Metals most commonly employed are stainless steel (316L type) and tantalum; however, both are thrombogenic [19, 20]. Catheter guide wire thrombogenicity, although readily documented, has been less of a clinical problem because of the usually short period of blood exposure involved in most procedures.

In early canine implant studies, the thrombogenicity of a wide series of metallic implants was seen to be related to the resting electrical potential of the metal which was generated upon blood contact [21]. Metals with negative potentials tend to be antithrombogenic, while stainless steel tends to be neutral. Copper, silver, and platinum are positive and extremely thrombogenic. Indeed, the use of copper coils inserted into canine arteries continues to be a widely used model for inducing a thrombotic response [22].

Theoretically, reduced thrombogenicity of metallic stents and heart valve components might be achieved by thin film polymer coatings, although the clinical effectiveness of this strategy has not been demonstrated. Thus, chronic systemic anticoagulation is generally employed in patients with prosthetic heart valves (with metallic components) and stents.

6.6 Carbons

Cardiac valves with components fabricated from low temperature isotropic carbons (pyrolytic carbon) are successfully used clinically [23]. These materials are appropriate for such applications as mechanical valves which require long-term chemical inertness, smoothness, and wear-resistance. The reasons for the marked improvement in the performance (reduced thrombosis and thromboembolic stroke rates) of these newer vs. older style heart valves are not entirely understood, but are undoubtedly multifactorial and related to improved patient management and valve design, as well as to the nature of the carbon surface. The specific benefits conferred by pyrolytic carbons with respect to blood cell and protein interactions, resulting in a very low frequency of clinical complications, remain to be defined. The use of carbon coatings has been proposed for other devices, i.e., vascular grafts, although such devices have not yet been used clinically.

6.7 Ultra-thin Film Coatings

Polymeric thin films of widely varying chemical composition may be deposited onto polymers, metals, and other surfaces using the method of plasma polymerization (also called 'glow-discharge' polymerization) [24]. This method is advantageous since very thin films (e.g., 100 nm) may selectively modify the surface chemistry of devices, but not their overall mechanical properties or surface texture. Plasma polymers form highly cross-linked, covalent, inert barrier layers which may resist the adsorption of proteins, lipids, and other blood elements. Plasma reacted coatings, based on hydrocarbon monomers such as methane, may produce durable diamond like coatings. Plasma polymer coatings have been proposed for vascular grafts and stents, based on promising animal studies [25], but are not used clinically at the present time.

6.8 Membranes

Blood contacting membranes are used for gas exchange (e.g., blood oxygenators) or solute exchange (e.g., dialyzers). The large membrane surface area, which may exceed 2 m² and the complexity of cardiopulmonary bypass circuits can produce consumption and dysfunction of circulating blood elements such as platelets, leading to an increased risk of bleeding as well as thromboembolism [26]. The activation of inflammatory and immune response pathways (complement system) by dialysis and oxygenator membranes may also produce significant complications [27]. Complement activation by dialysis membranes may be related in part to the availability of surface hydroxyl groups, particularly on cellulosic membranes. Complement activation may be greatly attenuated by the use of other membrane materials such as polysulfone and polycarbonate. Complement activation by biomaterial membranes has been reviewed [27].

6.9 Biological Surfaces

The use of biological and bioactive molecules as device surface coatings may confer thromboresistance. Such coating materials include phospholipids and heparin. Phospholipids such as phosphorylcholine, a normal constituent of cell membranes, may orient polar head groups towards the aqueous phase and locally organize water molecules, much like hydrogel surfaces. These surfaces may minimize protein and complement interactions [28]. In preliminary animal studies, phosphorylcholine coated stents, guide wires, and vascular grafts have shown improved thromboresistance. This approach is being actively developed for clinical applications.

Heparin, a naturally occurring anticoagulant glycosaminoglycan, has been considered an attractive surface coating based on its ability to directly catalyze the inactivation of procoagulant enzymes, and thus suppress thrombus development. Recently, the reduced thrombogenicity and improved biocompatibility of heparinized metallic stents has been demonstrated in animals [29]. In these studies, heparin was covalently attached to a polymer surface coating. This method has also been used clinically for the heparin coating of catheters and other devices, although it remains unclear whether the improved biocompatibility is a function of heparin's anticoagulant activity, nonspecific physicochemical properties, or both.

With biomolecule modified surfaces, there may also be important questions regarding the possible deleterious effects of sterilization procedures required before implantation.

6.10 Surface Texture

Surface 'smoothness' is a generally desirable feature of blood contacting surfaces. In this context, a smooth surface is one with irregularities with typical dimensions less than those of cells ($< 1 \mu\text{m}$). However, in certain applications, device incorporation by tissue is desirable, or the texturing of polymers may increase mechanical flexibility and durability. Thus, the sewing ring of mechanical heart valves is typically composed of poly(ethylene terephthalate) (Dacron™) fabric to permit tissue in growth and healing, which is associated with a reduction in thromboembolic events. Vascular grafts used to replace diseased blood vessels are most commonly fabricated from woven or knitted Dacron™ or textured (expanded) polytetrafluoroethylene (ePTFE) (Goretex™). In tubular form, these textured polymers remain flexible and stable for many years following implantation. Smooth-walled vascular grafts have generally not been considered attractive for long-term applications since smooth surfaces may not permit tissue ingrowth or flow surface healing. Textured flow surfaces are initially thrombogenic upon blood contact, although ePTFE appears less thrombogenic and thromboembolic than fabric Dacron™ prostheses [30]. These grafts perform acceptably in man when the graft diameter exceeds about 6 mm since the layer of thrombus that forms does not significantly restrict blood flow. Interestingly, both smoothwalled and textured ventricular assist devices have also performed successfully in clinical trials [31, 32].

6.11 Conclusion

Because the variables affecting cardiovascular device responses are sufficiently numerous and complex, those properties of blood-contacting surfaces which would be desirable to minimize adverse reactions cannot, in most instances, be predicted with confidence. The choice of material is usually constrained by mechanical property considerations and by variable requirements for material durability and chemical stability. Cardiovascular device engineering must therefore be guided by previous experience in successful clinical applications.

Acknowledgement This work was supported by Research Grant HL 31469 from the Heart, Lung and blood Institute, the National Institutes of Health.

Additional Reading

Colman, R.W., Hirsch, J., Marder, V.J. and Salzman, E.W. (eds)(1994) *Hemostasis and Thrombosis: Basic Principles and Clinical Practice*, 3rd edn, J.B. Lippincott, Philadelphia.

This book is highly recommended. This state-of-the-art text covers in detail essentially all important hematological aspects of cardiovascular device blood compatibility. In particular, Chapter 76, Interaction of blood with artificial surfaces, which considers many theoretical, experimental, and animal studies, and Chapter 77, Artificial devices in clinical practice, which describes clinical device thromboembolic complications, are of great practical value.

Harker, L.A., Ratner, B.D. and Didisheim, P. (eds)(1993) Cardiovascular Biomaterials and Biocompatibility, *Cardiovascular Pathology*, 2(3) (suppl.), 1S-224S.

In this volume, 20 chapters by expert authors treat all aspects of biomaterials and blood compatibility including pathologic mechanisms, material characterization, blood-material interactions and device performance. This volume updates an excellent earlier book *Guidelines for blood-Material Interactions*, National Institutes of Health, Washington, DC, Publication No. 85-2185 (1985).

Szycher, M. (ed.) (1983) *Biocompatible Polymers, Metals, and Composites*, Technomic Publishing Co., Lancaster, Pennsylvania.

Many of the same issues of blood-material interactions are broadly covered while selected polymer and device applications are described in additional detail. of particular interest are Section I (Fundamental Concepts in blood/Material Interactions) and Section II (Strategies for Hemocompatibility).

References

1. Salzman, E.W., Merrill, E.W. and Kent K.C. (1994) Interaction of blood with artificial surfaces, in *Hemostasis and Thrombosis: Basic Principles and Clinical Practice*, 3rd edn, R.W. Colman, J. Hirsch, V.J. Marder, and Salzman, E.W. (eds), J.B. Lippincott, Philadelphia, pp. 1469–85.
2. Harker, L.A., Ratner, B.D. and Didisheim, P. (eds) (1993) Cardiovascular Biomaterials and Biocompatibility, *Cardiovascular Pathology* **2**(3)(supplement), 1S–224S.
3. Szycher, M. (ed.) (1983) *Biocompatible Polymers, Metals, and Composites*, Technomic Publishing Co., Lancaster, Pennsylvania.
4. Williams, D.F. (ed) (1981) *Biocompatibility of Clinical Implant Materials*, CRC Press, Boca Raton, Florida.
5. Clagett, G.P. and Eberhart, R.C. (1994) Artificial Devices in Clinical Practice, in *Hemostasis and Thrombosis: Basic Principles and Clinical Practice*, 3rd edn R.W. Colman, J. Hirsch, V.J. Marder, and Salzman, E.W. (eds), J.B. Lippincott, Philadelphia, pp. 1486–1505.
6. Grabowski, E.F., Didisheim, P., Lewis, J.C. *et al.* (1977) Platelet adhesion to foreign surfaces under controlled conditions of whole blood flow: human vs. rabbit, dog, calf, sheep, pig, macaque, and baboon. *Transactions - American Society for Artificial Internal Organs*, **23**, 141–51.
7. Lentner, C. (ed.) (1984) *Geigy Scientific Tables* (vol. 3): *Physical Chemistry, Composition of blood*, Hematology, Somatometric Data, Ciba-Geigy, Basle.
8. Brash, J.L. and Horbett, T.A. (eds) (1987) *Proteins at Interfaces. Physicochemical and Biochemical Studies*, American Chemical Society, Washington, DC.
9. Harker, L.A. and Slichter, S.J. (1972) Platelet and fibrinogen consumption in man. *New England J Med.* **287**(20), 999–1005.
10. Bennett, B., Booth, N.A., Ogston D. (1987) Potential interactions between complement, coagulation, fibrinolysis, kinin-forming, and other enzyme systems, in: *Haemostasis and Thrombosis* (2nd edn), A.L. bloom and D.P. Thomas (eds), Churchill Livingstone, New York, pp. 267–82.
11. Andrew, M. (1995) Developmental hemostasis: relevance to thromboembolic complications in pediatric patients. *Thrombosis and Hemostasis*, **74**(1), 415–25.
12. Hanson, S.R., Harker, L.S., Ratner, B.D. *et al.* (1980) *In vivo* evaluation of artificial surfaces using a nonhuman primate model of arterial thrombosis. *J Laboratory Clinical Med.* **95**, 289–304.
13. Silver, J.H., Myers, C.W., Lim, F. *et al.* (1994) Effect of polyol molecular weight on the physical properties and haemocompatibility of polyurethanes containing polyethylene oxide macroglycols. *Biomaterials* **15**(9), 695–704.
14. Hoffman, A.S. (1974) Principles governing biomolecular interactions at foreign surfaces. *J. Biomedical Materials Res.* (Symp.) **5**(1), 77–83.
15. Andrade, J.D., Lee, H.B., Jhon, M.S. *et al.* (1973) Water as a biomaterial. *Transactions-American Society for Artificial Internal Organs* **19**, 1–7.
16. Strzinar, I. and Sefton, M.V. (1992) Preparation and thrombogenicity of alkylated polyvinyl alcohol coated tubing. *J. Biomedical Materials Research* **26**, 577–92.
17. Merrill, E.W. (1993) Poly(ethylene oxide) star molecules: synthesis, characterization, and applications in medicine and biology. *J. Biomaterials Science, Polymer Edition* **5**(1–2), 1–11.
18. Llanos, G.R. and Sefton, M.V. (1993) Does polyethylene oxide possess a low thrombogenicity? *J. Biomaterials Science, Polymer Edition*, **4**(4), 381–400.
19. Sigwart, U., Puel, J., Mirkovitch, V. *et al.* (1987) Intravascular stents to prevent occlusion and restenosis after transluminal angioplasty. *New England J. Med.* **316**(12), 701–6.
20. Scott, N.A., Nunes, G.L., King, S.B. *et al.* (1995) A comparison of the thrombogenicity of stainless steel and tantalum coronary stents. *American Heart J.*, **129**, 866–72.
21. Saywer, P.N., Stanczewski, B., Lucas, T.R., *et al.* (1978) Physical chemistry of the vascular interface, in *Vascular Grafts*, P.N. Sawyer and M.J. Kaplitt (eds), Appleton -Century-Crofts, New York, pp. 53–75.

22. Rapold, H.J., Stassen, T., Van de Werf, F., *et al.* (1992) Comparative copper coil-induced thrombogenicity of the internal mammary, left anterior descending coronary, and popliteal arteries in dogs. *Arteriosclerosis and Thrombosis*, **12**(5), 634–44.
23. Schoen, F.J. (1983) Carbons in heart valve prostheses: Foundations and clinical performance, in M. Szycher (ed.), *Biocompatible Polymers, Metals, and Composites*, Technomic Publishing Co., Lancaster, Pennsylvania, pp. 239–61.
24. Yasuda, H.K. (1985) *Plasma Polymerization*, Academic Press, Orlando.
25. Yeh, Y.S., Iriyama, T., Matsuzawa, Y., *et al.* (1988) blood compatibility of surfaces modified by plasma polymerization. *J. Biomedical Materials Research*, **22**, 795–818.
26. Harker, L.A., Malpass, T.W., Branson H.E., *et al.* (1980) Mechanism of abnormal bleeding in patients undergoing cardiopulmonary bypass: acquired transient platelet dysfunction associated with selective alpha-granule release. *blood*, **56**(5), 824–34.
27. Hakim, R. (1993) Complement activation by biomaterials. *Cardiovascular Pathology*, **2**(3) (suppl), 187S–198S.
28. Yu, J., Lamba, N.M., Courtney J.M., *et al.* (1994) Polymeric biomaterials: Influence of phosphorylcholine polar groups on protein adsorption and complement activation. *International Journal of Artificial Organs*, **17**(9), 499–504.
29. Hardhammer, P.A., van Beusekom H.M., Emanuelsson, H.U., *et al.* (1996) Reduction in thrombotic events with heparin-coated Palmaz-Schatz stents in normal porcine coronary arteries. *Circulation*, **93**(3), 423–30.
30. Schneider, P.A., Kotze, H.F., Heyns, A. duP., *et al.* (1989) Thromboembolic potential of synthetic vascular grafts in baboons. *J. Vascular Surgery*, **10**, 75–82.
31. Dasse, K.A., Poirier, V.L., Menconi, M.J., *et al.* (1990) Characterization of TCPS textured blood-contacting materials following long-term clinical LVAD support. In: *Cardiovascular Science and Technology: Basic and Applied: II*, JC Norman (ed.), Oxyoron Press, Boston, MA, pp. 218–220.
32. Kormos, R.L., Armitage, J.M., Borovetz, H.S., *et al.* (1990) Univentricular support with the Novocor left ventricular assist system as a bridge to cardiac transplantation: An update in *Cardiovascular Science and Technology: Basic and Applied: II*, JC Norman (Ed), Oxyoron Press, Boston, MA, pp. 322–324.

Chapter 7

Soft Tissue Response to Silicones

S.E. Gabriel

7.1 Silicones used in Medicine

Although the term 'silicone' refers to a group of organic silicone compounds, the one most commonly used in medicine is composed of a polymer known as dimethylpolysiloxane (DMPS). In silicone gel the polymer is cross-linked; the more cross-linking, the more solid is the gel. Liquid silicone consists of glucose-linked DMPS polymer chains. Silicones first became commercially available in 1943, with the first subdermal implantation of silicone occurring in the late 1940s [1–3]. Silicones have since been developed for a wide variety of medical applications, most notably in joint and breast prostheses.

There is a large body of literature attesting to the chemical and physical inertness of silicone [4–12]. Recently, there has been increasing interest in the possible adverse effects of silicones used in implantation. Much of the literature describing the adverse effects of silicone has been in reference to direct silicone injection. The following discussion will review the immunologic effects of prostheses used in breast reconstruction and augmentation.

7.2 Local immunologic reactions to silicone

Immunologic reactions to silicone can be local, regional due to silicone migration, or systemic. Local cutaneous and subcutaneous reactions to injected silicone or gel have been reported [13–18]; and it has become apparent that these reactions are not

S.E. Gabriel (✉)
Division of Rheumatology Mayo Clinic,
200 First Street Southwest, Rochester, MN 55905, USA

due to impurities in the silicone, as was originally suspected. Subcutaneous injection of silicone liquid in experimental animals provokes an acute inflammatory response characterized by a primarily polymorphonuclear reaction, followed by a chronic inflammatory response with lymphocytes, fibroblasts, and plasma cells [19]. The late response is characterized by a small amount of cellular infiltrate and an increase in extracellular material. Macrophages with clear vacuoles have been observed and are suspected to contain silicone. Occasionally, multinucleated foreign body giant cells have also been observed [16, 20–23].

In humans, liquid silicone has been injected subcutaneously for cosmetic reasons. Granulomatous reactions have been reported to occur in some instances [14–17]. Similar reactions have been noted in two case reports following the rupture of silicone gel-filled breast prostheses [24, 25]. Clinically, these reactions have the characteristics of an inflammatory response, i.e., redness, swelling, and pain. Histologic examination shows chronic inflammatory reactions, occasionally with the presence of refractile material resembling silicone [24].

Migration of silicone has been documented on numerous occasions in the literature. Following experimental intra-peritoneal injection in mice, silicone was demonstrated to be present in the liver, spleen, ovaries, and kidneys [26]. Other investigators have documented the migration of subcutaneously injected silicone to the lung, associated with an increased incidence of respiratory problems in experimental animals [27]. Pneumonitis was reported in 3 patients several days following liquid silicone injection, and silicone was demonstrated in macrophages obtained by pulmonary lavage from these patients [27]. The presence of silicone was confirmed by atomic absorption and infra-red spectrophotometry. Another case report described a patient with silicone-induced granulomatous hepatitis; analysis of liver biopsy specimens revealed quantifiable amounts of silicone [28]. Subcutaneous masses or nodules, hepatic granulomas have also been reported following injections into humans [23, 24, 28]. Regional lymphadenopathy is a frequently reported finding [29–35]. In rare cases, this has progressed to malignant lymphoma [29, 32, 33]. The relevance of these reports to silicone breast implants is uncertain.

7.3 Systemic immunologic reactions to silicone

Systemic reactions have been reported following the introduction of silicone into the body. In one instance, a severe systemic reaction consisting of a febrile illness, acute renal insufficiency, respiratory compromise, pulmonary infiltration, delirium, anemia, and thrombocytopenia has been reported following implantation of a silicone gel envelope prosthesis. Improvement followed implant removal. Silicone was identified by mass spectrophotometry in this case [36]. Another case involved the injection of a large quantity of free silicone under the breasts by an unauthorized individual. The patient expired within 10 hours of injection. Silicone was identified

by absorption spectrophotometry in large quantities in the lung, kidney, liver, brain and serum [28].

The mechanism underlying the systemic immunologic reactions to silicone has not been thoroughly investigated. A marked local granulomatous reaction to silicone has been noted in guinea pigs; however, an antibody response to silicone by Ouchterlony gel diffusion or passive cutaneous anaphylaxis was not demonstrated [37]. Other investigators have studied macrophage migration inhibition [38]. In these studies, pigs were sensitized by subcutaneous injection of silicone. Harvested macrophages demonstrated inhibition of migration in the presence of silicone, suggesting specific antigen recognition. In addition, silicone was demonstrated in the cytoplasmic bridges joining macrophages and lymphocytes. Alternatively, it has been suggested that the immune system does not respond with a specific recognition of silicone but that silicone promotes the immune response to other antigens, i.e., acts as an adjuvant. Hypergammaglobulinemia has been noted by some investigators, and silicon dioxide has been reported to have adjuvant effects [39]. A disorder which has been termed, 'human adjuvant disease', was described following injection of paraffin for breast augmentation mammoplasty [40]. In Japan, in 1973, Yoshida reviewed seven cases of human adjuvant disease in Japan following injections of paraffin or silicone for augmentation mammoplasty [41]. The symptoms included arthritis, arthralgia, lymphadenopathy, hypergammaglobulinemia, elevated erythrocyte sedimentation rates and positive rheumatoid factor. Removal of the injected materials resulted in improvement of the condition in some patients [41].

In 1979, Kumagai reported four cases of classical systemic sclerosis following cosmetic surgery [42]. Five years later, the same investigator described a series of 46 patients with signs and symptoms of connective tissue disease following injection of either silicone or paraffin [43]. Definite connective tissue diseases, based on American Rheumatism Association Criteria, were diagnosed in 24 patients. These conditions included systemic lupus erythematosus, mixed connective tissue disease, rheumatoid arthritis, Sjögren's syndrome, and systemic sclerosis. Another group of 22 patients were described as having human adjuvant disease, with signs, symptoms, and laboratory abnormalities suggestive but not diagnostic of a connective tissue disease. In 1984, three patients from Singapore were reported who developed autoimmune disease following injection augmentation mammoplasty [44]. In the same year, a 52-year-old woman who developed systemic sclerosis, primary biliary cirrhosis and Sjögren's syndrome following silicone/paraffin injection mammoplasty was reported [45].

In 1982, the first case series describing autoimmune disorders following augmentation mammoplasty with gel-filled prostheses was reported. This was followed by other reports involving both gel-filled implants and saline-filled silicone implants [46–49]. The most frequently reported connective tissue disease associated with silicone breast implants is systemic sclerosis. Table 7.1 summarizes the clinical and laboratory characteristics of 19 cases of systemic sclerosis associated with silicone breast augmentation published in the English language literature. Eleven of these cases received implantation in the United States [35]. Eleven of the 19 patients were ANA positive, 15 had Raynaud's, and 10 had diffuse systemic sclerosis. The inter-

val between augmentation to diagnosis of systemic sclerosis varied from 1 to 25 years, with a mean of 13 years. Fourteen of the 19 patients were exposed to silicone (11 silicone gel and 3 silicone injection), the remainder being exposed to paraffin injection. In two cases, histopathologic demonstration of multinucleated giant cells, vacuoles with refractile droplets, and intracytoplasmic asteroid bodies in lymph nodes draining the prostheses suggested leakage of silicone from the implants and its dissemination in lymphoid tissues. The authors used energy-dispersive X-ray analysis to confirm that the macrophage inclusions in the lymphatic tissue contain silicone.

Although systemic sclerosis is the most commonly reported disorder occurring following silicone breast implantation, there have also been reports of systemic lupus erythematosus [43, 44, 46, 50], Sjögren's syndrome [45], keratoconjunctivitis sicca [45], rheumatoid arthritis [4, 34, 43], polymyositis [43], overlap syndromes (including human adjuvant disease) [34, 43, 46, 50, 51], morphea [35, 43], Hashimoto's thyroiditis [43, 52], anticardiolipin antibody syndrome [53], primary biliary cirrhosis [45] and toxic shock syndrome [54]. Unfortunately, it is impossible to tell, on the basis of case reports, whether the frequency of these events is greater than might be expected on the basis of chance alone (Table 7.1).

7.4 Evidence for causation

It has been estimated that two million American women have undergone breast augmentation or reconstruction since the introduction of the silicone gel-filled elastomer envelope-type prosthesis in the early 1960s [60, 61]. The reported cases of systemic sclerosis among this population raise the important question of whether the association between systemic sclerosis and silicone breast implants is a real one. Unfortunately, almost all of the evidence to date is derived from case reports, which are the very weakest form of data bearing on the question of causality (Table 7.2). Indeed, the most important evidence for establishing a cause-effect relationship is the strength of the research design used to study that relationship [62]. Randomized control trials provide the strongest evidence but are seldom ethical in studies of causation because they involve randomly assigning individuals to receive or not to receive a potentially harmful intervention. In addition, the long latent periods and large numbers of subjects needed to answer most cause and effect questions in clinical medicine make it impractical to utilize this research design.

Well conducted prospective cohort studies are the next strongest design because they minimize the effects of selection bias, measurement bias, and known confounders. Such a study would involve following a large population of women, preferably for one or more decades, looking for the outcomes of interest (e.g., connective tissue disorders). A relative risk for connective tissue disorders among those women who elect to have breast implantation compared to those who do not can then be calculated. Although this is a powerful research design, it is usually impractical because of the necessary long follow-up period. This problem can be circumvented by a ret-

Table 7.1 Cases of Systemic Sclerosis after Augmentation Mammoplasty Reported in the English-Language Literature

Patient	Age at Diagnosis, y	Age at Mammoplasty, y	Type of Implant	Interval to Onset, y	Extent of Systemic Sclerosis	Raynaud Phenomenon	Systemic Involvement	Antinuclear Antibodies*	Reference
1	52	50	Silicone bag gel	2	Diffuse	No	No	-	(55)
2	41	20	Silicone bag gel	21	Diffuse	Yes	Pulmonary, gastrointestinal,	+	(55)
3	63	53	Silicone bag gel	10	Limited	Yes	Pulmonary,	+	(55)
4	37	32	Silicone bag gel	5	Diffuse	No	Pulmonary,	+	(55)
5	45	25	Paraffin injection	19	Diffuse	Yes	No	-	(42)
6	49	20	Paraffin injection	16	Diffuse	Yes	Pulmonary, gastrointestinal	-	(42)
7	51	25	Paraffin injection	17	Limited	Yes	No	-	(43)
8	36	24	Paraffin injection	9	Limited	Yes	Pulmonary	-	(43)
9	55	30	Paraffin injection	25	Limited	Yes	Pulmonary	-	(44)
10	50	31	Silicone injection	19	Limited	Yes	Pulmonary, gastrointestinal, primary biliary cirrhosis	+	(45)
11	59	34	Silicone injection	25	Diffuse	Yes	No	+	(56)
12	38	26	Silicone bag gel	7	Limited	Yes	Gastrointestinal	+	(56)
13	47	32	Silicone bag gel	15	Diffuse	Yes	Pulmonary	+	(35)
14	59	50	Silicone gel	9	Diffuse	No	Pulmonary, gastrointestinal	+	(35)
15	44	34	Silicone gel	10	Limited	Yes	Pulmonary, gastrointestinal	+	(35)
16	43	37	Silicone gel	6	Diffuse	Yes	Gastrointestinal	+	(35)
17	44	43	Silicone gel	1	Limited	Yes	Malignant hypertension	+	(57)
18	44	19	Silicone injection	25	Diffuse	Yes	Malignant hypertension/renal failure	+	(58)
19	46	34	Silicone gel	12	Limited	No	No	-	(59)

- negative.
 + positive.
 * Determined using immunofluorescence.

Table 7.2 Strength of Research Designs Used to Determine Causation

Strongest	Randomized controlled trials
↓	Prospective cohort studies
↓	Case control studies
↓	Ecological survey
Weakest	Case series

Table 7.3 Evidence that an Association is Causal[62]

<i>Characteristic</i>	<i>Definition</i>
Temporality	Cause precedes effect
Strength	Large relative risk
Dose-response	Larger exposures to cause associated with higher rates of disease
Reversibility	Reduction in exposure associated with lower rates of disease
Consistency	Repeatedly observed by different persons, in different places, circumstances, and times
Biologic plausibility	Makes sense, according to biologic knowledge of the time
Specificity	One cause leads to one effect
Analogy	Cause-and-effect relationship already established for a similar experience

rospective cohort study, which is similar with the exception that the population and the exposure (breast implantation) is identified in the past, allowing the patients to be followed to the present for the outcomes of interest. Although this is a very attractive research design, it requires that the complete exposed and unexposed populations be identifiable and that follow-up information be available on all individuals.

Case-control studies retrospectively compare the frequency of breast implantation in women with and without the outcomes of interest. If, for example, connective tissue disorders were more likely to occur among women with breast implants, this would constitute some evidence for causation. Case-control studies typically require less time and resources than cohort studies. However, they are susceptible to many more biases than cohort studies [62]. The primary reason not to perform a case-control study here, however, is that a separate case-control study would be required for each of the outcomes of interest, i.e., a case-control study of systemic sclerosis, a case-control study of rheumatoid arthritis, etc. The retrospective cohort design is much more efficient since it can evaluate multiple outcomes in a single study, as is the need here.

A set of eight criteria has been proposed as a guide to formulate decisions regarding cause and effect relationships (Table 7.3). The relationship between breast implants and connective tissue disorders does fulfill the criterion of *temporality* since, at least in the published case reports, the connective tissue disorders all followed breast implantation. There is no evidence describing the magnitude of the *relative risk* in this relationship. There is also no evidence for a *dose response* relationship, i.e., that women with bilateral implants perhaps have an increased likelihood of connective tissue disorders compared to women with unilateral

implants. The evidence regarding the *reversibility* of these disorders with removal of implants is variable. Although there have been some reports of improvement of connective tissue disorders following removal of the implants, this is not consistent and the number of patients involved is small. The relationship does appear to be consistent, i.e., it has been observed repeatedly by different persons in different places, circumstances, and times, however it has not yet been assessed using adequate study designs. Perhaps the most compelling evidence is the *biologic plausibility* of this relationship due to the hypothesis of silicone acting as an immune adjuvant. The relationship does not appear specific, as silicone implants have led to not just one effect, but several, albeit somewhat related, effects. Finally, a cause and effect relationship is strengthened if there are examples of well established causes that are analogous to the one in question. Adjuvant induced arthritis can be considered analogous [63].

In summary, in spite of the anecdotal evidence, until very recently there was a lack of evidence to either support or refute a cause-and-effect relationship between silicone breast implants and connective tissue/ autoimmune disorders.

7.5 Controlled studies examining the relationship between breast implants and connective tissue disease.

At least seven controlled studies have now been published (Table 7.4), each of which provided a quantitative assessment of the risk of connective tissue diseases among women with breast implants [64–70]. The first of these was a case-control study of augmentation mammoplasty and scleroderma [68]. The aims of this study were to compare the frequency and temporal relationship of augmentation mammoplasty among scleroderma cases and matched controls. Scleroderma patients and age stratified general practice controls were interviewed using a pretested telephone questionnaire. Self-reported dates of augmentation mammoplasty were ascertained as were dates of scleroderma symptoms and diagnoses as relevant. Frequencies of nonaugmentation mammoplasty silicone exposure between interviewed cases and controls were expressed in terms of rate ratios and 95% confidence intervals. Rate ratios were also adjusted for socioeconomic status.

A total of 315 cases and 371 controls were interviewed, of whom 251 and 289, respectively, were female. The unadjusted rates for augmentation mammoplasty among interviewed cases and controls were 4/251 (1.59%) and 5/289 (1.73%), respectively. The socioeconomic status adjusted rate of augmentation mammoplasty in scleroderma patients was 1.54% (95% CI: 0.03–3.04) which is very similar to the 1.73% rate in interviewed controls. These results indicate that augmentation mammoplasty rates were comparable in cases and controls. In addition, the rates of exposure to nonmammoplasty silicone mastectomy and breast lumpectomy were comparable in interviewed cases and controls. This study failed to demonstrate an association between silicone breast implantation and the

Table 7.4 Summary of controlled studies examining the relationship between breast implants (BI) and connective tissue diseases (CTD)

Reference	Study Design	Study Population		Outcome(s) Examined	Main Result	Conclusions
		Cases (exposed)	Controls (unexposed)			
68	Case control	315	371	Systemic sclerosis (SS, scleroderma)	Rates of BI among cases and controls were 1.59% and 1.73%	Rates of BI were similar in cases and controls.
65	Retrospective cohort	749	1498	Connective tissue and other autoimmune diseases	Relative risk (cases:controls) of developing any of these diseases was 1.06 (95% CI: 0.34–2.97).	There was no association between BI and the connective tissue and other disorders studied.
67	Case control	195	143	Systemic lupus erythematosus (SLE)	One (0.8%) of the SLE cases and 0 (0%) of the controls reported having a BI (p=0.57).	No association was shown between BI and SLE.
64	Case control	349	1456	Rheumatoid arthritis (RA)	Relative risk for a history of BI (cases:controls) was 0.41 (95% CI: 0.05–3.13).	No increased risk for RA among women with BI was demonstrated.
60	Multi-center case control	869	2061	SS (scleroderma)	Odds ratio for BI surgery (cases:controls) was 1.25 (95% CI: 0.62–2.53).	No significant causal relationship was demonstrated between BI and the development of SS.
70	Nested case control	121700		Connective tissue disease	Five cases with BI were identified among 300 patients with RA; 0 cases with BI among 123 with SLE, 20 patients with SS, 3 with Sjögren's syndrome, 13 with dermatomyositis, and 2 with mixed connective tissue disease.	No association was found between BI and CTD.
69	Case control (preliminary results)	592	1184	SS (scleroderma)	Odds ratio for BI (cases:controls) was 0.61 (95% CI: 0.14–2.68)	No significant association between BI and SS was found.

CI = confidence interval

subsequent development of scleroderma to a relative risk as low as 4.5 with 95% statistical power.

In June of 1994, a population-based retrospective cohort study was published which examined the risk of a variety of connective tissue diseases and other disorders after breast implantation [65]. In this study, all women in Olmsted County, Minnesota who received a breast implant between 1 January 1964 and 31 December 1991 (the case subjects) were studied. For each case subject, two women of the same age (within three years) from the same population who had not received a breast implant and who underwent a medical evaluation within two years of the date of the implantation in the case subject were selected as control subjects. Each woman's complete inpatient and outpatient medical records were interviewed for the occurrence of various connective tissue diseases (i.e., rheumatoid arthritis, systemic lupus erythematosus, Sjögren's syndrome, dermatomyositis, polymyositis, systemic sclerosis, ankylosing spondylitis, psoriatic arthritis, polymyalgia rheumatica, vasculitis, arthritis associated with inflammatory bowel disease, and polychondritis), certain other disorders thought to have an autoimmune pathogenesis (i.e., Hashimoto's thyroiditis), and cancer other than breast cancer. In addition, this study itemized the results of ten related symptoms and the abnormal results of four related laboratory tests. A total of 749 women who had received a breast implant were followed for a mean of 7.8 years and the corresponding 1498 community controls were followed for a mean of 8.3 years. The relative risk of developing any one of these specified connective tissue and other diseases among case subjects compared to controls was 1.06 (95% CI: 0.34–2.97). This study, therefore, found no association between breast implants and the connective tissue diseases and other disorders that were studied [65].

In the summer of 1994, Strom and colleagues published a case-control study which addressed the risk of systemic lupus erythematosus among women with breast implants [67]. A total of 219 eligible cases who met the American Rheumatism Association criteria for systemic lupus erythematosus [71] were identified from the medical practices of cooperating rheumatologists in the Philadelphia metropolitan area. One hundred ninety-five (89%) of these were enrolled in the study. Friends of the cases, matched to the cases on sex and age (± 5 years), served as controls. Using a short telephone interview, cases and controls were contacted and asked to provide information on any surgery that they had prior to the index date, i.e., the date of diagnosis of systemic lupus erythematosus, in the cases and the same year for the age-matched friend controls. Specific questions were asked about plastic surgery in general and breast implants in particular. One hundred forty-eight (75.9%) of the 195 systemic lupus erythematosus being sought and 111 (77.6%) of the 143 controls agreed to be reinterviewed for this study. Only 1 (0.8%) of the 133 female systemic lupus erythematosus cases reported having a breast implant eight years prior to the diagnosis of systemic lupus erythematosus. This compared to 0 out of the 100 female friend controls (Fisher exact one-tailed p -value=0.57). These authors concluded, based on this very large case-control study of systemic lupus erythematosus, that no association existed between silicone breast implants and the subsequent development of systemic lupus erythematosus. However, the modest statistical

power of the study was only able to provide sufficient evidence against a very large association.

Three additional controlled studies have been presented and are published in abstract form [64, 66, 70]. As part of a prospective case-control study of the risk of rheumatoid arthritis, Dugowson *et al.* recruited 349 women with new-onset rheumatoid arthritis and 1456 similarly aged control women. Information about breast implants was obtained on both cases and controls and age-adjusted risk for a history of breast implants among cases was compared to that of controls. The relative risk, i.e., comparing the rate of a history of breast implants among rheumatoid arthritis cases compared to a similar history among controls, was 0.41 (95% CI: 0.05–3.13) [64]. These data did not support an increased risk for rheumatoid arthritis among women with silicone breast implants.

A multi-center, case-controlled study was performed to examine the association between scleroderma and augmentation mammoplasty [66]. A total of 869 women with systemic sclerosis recruited from three university-affiliated rheumatology clinics and 2061 local community controls matched on age in three strata (ages 25–44, 45–64, and ≥ 65); race and sex were identified by random-digit dialing. Data on exposure and potential confounding variables were collected from cases and controls by self-administered questionnaires and telephone interviews, respectively. The frequency of breast implant surgery was compared in both groups and the odds ratio and 95% confidence intervals for the association of augmentation mammoplasty with systemic sclerosis, adjusted for age, race, marital status, and site, was 1.25 (95% CI: 0.62–2.53). These data failed to demonstrate a significant causal relationship between augmentation mammoplasty and the development of systemic sclerosis.

Using a nested case-control study, Sanchez-Guerrero *et al.* examined the association between silicone breast implants and connective tissue diseases among a cohort of 121 700 registered American nurses followed since 1976 [70]. In 1992, a questionnaire was sent to nurses who had reported any rheumatic disease from 1976 to 1990 asking about rheumatic symptoms and silicone exposure. The complete medical records were obtained on all participants who confirmed any rheumatic or musculoskeletal symptoms. Connective tissue disease cases were classified according to the American College of Rheumatology or other published criteria. Ten age-matched controls per case were randomly selected among nurses with no rheumatic or musculoskeletal complaints. Odds ratios and 95% confidence intervals were used as a measure of association. This study identified 448 cases with definite connective tissue diseases and 1209 nurses with silicone breast implants. Five patients had silicone breast implants and any connective tissue disease. The mean time since implantation was 139 ± 95.81 months among these five patients and 119.17 ± 76.64 months among all nurses with silicone breast implants. These five patients were identified among 300 patients with rheumatoid arthritis. No case with a silicone breast implant was identified among 123 patients with systemic lupus erythematosus, 20 patients with scleroderma, three with Sjögren's syndrome, 13 with dermatomyositis, and two with mixed connective tissue diseases. In

conclusion, this study found no association between silicone breast implants and connective tissue diseases.

Finally, Burns and Schottenfeld are conducting a population-based case-control study examining the relationship between this condition and prior history of breast implant surgery [69, 72]. The cases and normal population controls are being assembled from the states of Michigan and Ohio. The cases are being identified using several sources: a computerized data base of hospital discharge diagnostic listings during the period 1980–1991; a collaborative network of major medical centers; a postal survey of certified rheumatologists; and from patient members of the United Scleroderma Foundation. Although this study is still underway, preliminary results demonstrate a crude odds ratio of 0.61 (95% CI: 0.14–2.68) for breast implants among cases compared to controls. These results do not support a causal relationship between breast implants and systemic sclerosis.

In summary, although numerous anecdotal case reports have suggested an association between silicone breast implants and connective tissue diseases, all seven controlled epidemiologic studies conducted to date have failed to confirm such an association. Whether silicone breast implants cause a new and previously undescribed condition is yet to be determined.

Reference

1. Williams, D.F. (1981) *Biocompatibility of clinical implant materials*. Vol 2. Boca Raton: CRC Press, pp. 1–272.
2. Blocksma, R. and Braley, S. (1965) The silicone in plastic surgery. *Plast. Reconstr. Surg.*, **35**(4), 366–370.
3. Braley, S.A., Jr (1964) The medical silicones. *Trans. Am. Soc. Artif Int. Organs*, **10**, 240–243.
4. Weiner, S.R. and Paulus, H.E. (1986) Chronic arthropathy occurring after augmentation mammaplasty. *Plast. Reconstr. Surg.*, **77**(2), 185–192.
5. Ward, T.C. and Perry, J.T. (1981) Dynamic mechanical properties of medical grade silicone elastomer stored in simulated body fluids. *J. Biomed. Mater. Res.*, **15** 511–525.
6. Homsy, C.A. (1970). Bio-compatibility in selection of materials for implantation. *J. Biomed. Mater. Res.*, **4**, 341–356.
7. Rigdon, R.H. and Dricks, A. (1975) Reaction associated with a silicone rubber gel: An experimental study. *J. Biomed. Mater. Res.*, **9**, 645–659.
8. Robertson, G. and Braley, S. (1973) Toxicologic studies, quality control, and efficacy of the silastic mammary prosthesis. *Med. Instrum.*, **7**(2), 100–103.
9. Boone, J.L. and Braley, S.A. (1966) Resistance of silicone rubbers to body fluids. *Rubber Chern. Technol.*, **39**(4), 1293–1297.
10. Boone, J.L. (1966) Silicone rubber insulation for subdermally implanted devices. *Med. Res. Eng.*, **5**, 34–37.
11. Roggenbort, E. (1976) The biostability of silicone rubbers, a polyamide, and a polyester. *J. Biomed Mater. Res.*, **10**, 123–143.
12. Speirs, A.C. and Blocksma, R. (1963) New implantable silicone rubbers. An experimental evaluation of tissue response. *Plast. Reconstr. Surg.*, **31**(2), 166–175.
13. Symmers, W.StC. (1968) Silicone mastitis in 'topless' waitresses and some other varieties of foreign-body mastitis. *Br. Med J.*, **3**, 19–22.

14. Ortiz-Monasterio, F. and Trigos, I. (1972) Management of patients with complications from injections of foreign materials into the breasts. *Plast. Reconstr. Surg.*, **50**(1) 42–47.
15. Parsons, R.W. and Thering, H.R. (1977) Management of the silicone-injected breast. *Plast. Reconstr. Surg.*, **60**(4), 534–538.
16. Wilkie, T.F. (1977) Late development of granuloma after liquid silicone injections. *Plast. Reconstr. Surg.*, **60**(2), 179–188.
17. Pearl, R.M., Laub, D.R., and Kaplan, E.N. (1978) Complications following silicone injections for augmentation of the contours of the face. *Plast Reconstr Surg*, **61**(6): 888–891.
18. Kozeny, G.A., Barbato, A.L., Bansal, V.K. *et al.* (1984) Hypercalcemia associated with silicone-induced granulomas. *N. Engl. J. Med.*, **311**(17), 1103–1105.
19. Andrews, J.M. (1966) Cellular behavior to injected silicone fluid: A preliminary report. *Plast. Reconstr. Surg*, **38**(6), 581–583.
20. Ballantyne, D.L., Rees, T.D. and Seidman, I. (1965) Silicone fluid: Response to massive subcutaneous injections of dimethylpolysiloxane fluid in animals. *Plast. Reconstr. Surg.*, **36**(3), 330–338.
21. Ben-Hur, N. and Neuman, Z. (1965) Siliconoma - another cutaneous response to dimethylpolysiloxane. Experimental study in mice. *Plast. Reconstr. Surg.*, **36**(6), 629–631.
22. Rees, T.D., Platt, J., and Ballantyne, D.L. (1965) An investigation of cutaneous response to dimethylpolysiloxane (silicone liquid) in animals and humans - A preliminary report. *Plast. Reconstr. Surg.*, **35**(2), 131–139.
23. Travis, W.D., Balogh, K. and Abraham, J.L. (1985) Silicone granulomas: Report of three cases and review of the literature. *Hum. Pathol.*, **16**(1), 19–27.
24. Mason, J. and Apisarnthanarax, P. (1981) Migratory silicone granuloma. *Arch. Dermatol.*, **117**, 366–367.
25. Aposos, J. and Pope, T.L., Jr (1985) Silicone granuloma following closed capsulotomy of mammary prosthesis. *Ann. Plast. Surg.*, **14**(5), 403–406.
26. Rees, T.D., Ballantyne, D.L., Seidman, I. *et al.* (1967) Visceral response to subcutaneous and intraperitoneal injections of silicone in mice. *Plast. Reconstr. Surg.*, **39**(4), 402–410.
27. Chastre, J., Basset, F., Viau, F. *et al.* (1983) Acute pneumonitis after subcutaneous injections of silicone in transsexual men. *N. Engl. J. Med.*, **308**(13), 764–767.
28. Ellenbogen, R. and Rubin, L. (1975) Injectable fluid silicone therapy: Human morbidity and mortality. *J. Am. Med. Assoc.*, **234**(3), 308–309.
29. Murakata, L.A. and Rangwala, A.F. (1989) Silicone lymphadenopathy with concomitant malignant lymphoma. *J. Rheumatol.*, **16**(11), 1480–1483.
30. Christie, A.J., Weinberger, K.A. and Dietrich, M. (1977) Silicone lymphadenopathy and synovitis. Complications of silicone elastomer finger joint prostheses. *J. Am. Med. Assoc.*, **237**(14), 1463–1464.
31. Kircher, T. (1980) Silicone lymphadenopathy. A complication of silicone elastomer finger joint prostheses. *Hum. Pathol.*, **11**(3), 240–244.
32. Benjamin, E. and Ahmed, A. (1982) Silicone lymphadenopathy: A report of two cases, one with concomitant malignant lymphoma. *Diagn. Histopathol.*, **5**, 133–141.
33. Digby, J.M. (1982) Malignant lymphoma with intranodal silicone rubber particles following metacarpophalangeal joint replacements. *Hand*, **14**(3), 326–328.
34. Endo, L.P., Edwards, N.L., Longley, S. *et al.* (1987) Silicone and rheumatic diseases. *Semin. Arthritis Rheum.*, **17**(2), 112–118.
35. Varga, J., Schumacher, H.R. and Jimenez, S.A. (1989) Systemic sclerosis after augmentation mammoplasty with silicone implants. *Ann. Intern. Med.*, **111**(5), 377–383.
36. Uretsky, B.F., O'Brien, J.J., Courtiss E.H. *et al.* (1979) Augmentation mammoplasty associated with a severe systemic illness. *Ann. Plast. Surg.*, **3**(5), 445–447.
37. Nosanchuk, J.S. (1968) Injected dimethylpolysiloxane fluid: A study of antibody and histologic response. *Plast. Reconstr. Surg.*, **42**(6), 562–566.
38. Heggors, J.P., Kossovsky, N. and Parsons, R.W. *et al.* (1983) Biocompatibility of silicone implants. *Ann. Plast. Surg.*, **11**, 38–45.

39. Pernis, B. and Paronetto, F. (1962) Adjuvant effect of silica (tridymite) on antibody production. *Proc. Soc. Exp. Biol. Med.*, **110**, 390–392.
40. Miyoshi, K., Miyamura, T. and Kobayashi, Y. (1964) Hypergammaglobulinemia by prolonged advantacity in man. Disorders developed after augmentation mammoplasty. *Jpn Med. J.*, **2122**, 9.
41. Yoshida, K. (1973) Post mammoplasty disorder as an adjuvant disease of man. *Shikoku Acta Med.*, **29**, 318.
42. Kumagai, Y., Abe, C. and Shiokawa, Y. (1979) Scleroderma after cosmetic surgery. Four cases of human adjuvant disease. *Arthritis Rheum.*, **22**(5), 532–537.
43. Kumagai, Y., Shiokawa, Y. and Medsger, T.A., Jr (1984) Clinical spectrum of connective tissue disease after cosmetic surgery. *Arthritis Rheum.*, **27**(1), 1–12.
44. Fock, K.M., Feng, P.H., Tey, B.H. (1984). Autoimmune disease developing after augmentation mammoplasty: Report of 3 cases. *J. Rheumatol.*, **11**(1), 98–100.
45. Okano, Y., Nishikai, M. and Sato, A. (1984) Scleroderma, primary biliary cirrhosis, and Sjogren's syndrome after cosmetic breast augmentation with silicone injection: A case report of possible human adjuvant disease. *Ann. Rheum. Dis.*, **43**, 520–522.
46. van Nunen, S.A., Gatenby, P.A. and Basten, A. (1982) Post-mammoplasty connective tissue disease. *Arthritis Rheum.*, **25**(6), 694–697.
47. Baldwin, C.M., Jr, and Kaplan, E.N. (1983) Silicone-induced human adjuvant disease? *Ann. Plast. Surg.*, **10**, 270–273.
48. Byron, M.A., Venning, V.A. and Mowat, A.G. (1984) Post-mammoplasty human adjuvant disease. *Br. J. Rheumatol.*, **23**(3), 227–229.
49. Vargas, A. (1979) Shedding of silicone particles from inflated breast implants. *Plast. Reconstr. Surg.*, **64**(2), 252–253.
50. Walsh, F.W., Solomon, D.A., Espinoza, L.R. *et al.* (1989) Human adjuvant disease. A new cause of chylous effusions. *Arch. Intern. Med.*, **149**, 1194–1196.
51. Ziegler, V.V., Haustein, U.F., Mehlhorn, J. *et al.* (1986) Quarzinduzierte sklerodermie sklerodermie-ähnliches syndrom oder echte progressive sklerodermie? *Dermatol. Mon. Schr.*, **172**(2), 86–90.
52. Taura, N., Usa, T. and Eguchi, K. (1976) A case of human adjuvant disease. *J. Jap. Soc. Intern. Med.*, **65**, 840–841.
53. Alusik, S., Jandova, R. and Gebauerova, M. (1989) Anticardiolipin syndrome in plastic surgery of the breast. *Cor. Vasa*, **31**(2), 139–144.
54. Olesen, L.L., Ejlersen, T. and Nielsen, J. (1991) Toxic shock syndrome following insertion of breast prostheses. *Br. J. Surg.*, **78**(5), 585–586.
55. Spiera, H. (1988) Scleroderma after silicone augmentation mammoplasty. *J. Am. Med. Assoc.*, **260**(2), 236–238.
56. Brozena, S.J., Fenske, N.A., Cruse, C.W. *et al.* (1988) Human adjuvant disease following augmentation mammoplasty. *Arch. Dermatol.*, **124**, 1383–1386.
57. Gutierrez, F.J. and Espinoza, L.R. (1990) Progressive systemic sclerosis complicated by severe hypertension: Reversal after silicone implant removal. *Am. J. Med.*, **89**(3), 390–392.
58. Hitoshi, S., Ito, Y., Takehara, K. *et al.* (1991) A case of malignant hypertension and scleroderma after cosmetic surgery. *Jpn J. Med.*, **30**(1), 97–100.
59. Sahn, E.E., Garen, P.D., Silver, R.M. *et al.* (1990) Scleroderma following augmentation mammoplasty. Report of a case and review of the literature. *Arch. Dermatol.*, **126**, 1198–1202.
60. Deapen, D.M., Pike, M.C., Casagrande, J.T. *et al.* (1986) The relationship between breast cancer and augmentation mammoplasty: An epidemiologic study. *Plast. Reconstr. Surg.*, **77**(3), 361–367.
61. May, D.S. and Stroup, N.E. (1991) The incidence of sarcomas of the breast among women in the United States, 1973–1986. *Plast. Reconstr. Surg.*, **87**(1), 193–194.
62. Fletcher, R.H., Fletcher, S.W. and Wagner, E.H. (1988) Cause. In: Collins, N., Eckhart, C., Chalew, G.N., eds. *Clinical Epidemiology: The Essentials*. Baltimore: Williams & Wilkens, pp. 208–225.

63. Pearson, C.M. (1963) Experimental joint disease. Observations on adjuvant-induced arthritis. *J. Chron. Dis.*, **16**, 863–874.
64. Dugowson, C.E., Daling, J., Koepsell, T.D. *et al.* (1992) Silicone breast implants and risk for rheumatoid-arthritis. *Arthritis Rheum.*, **35**, S66. (Abstract)
65. Gabriel, S.E., O'Fallon, W.M., Kurland, L.T. *et al.* (1994) Risk of connectivetissue diseases and other disorders after breast implantation. *N. Engl. J. Med.*, **330**, 1697–1702.
66. Hochberg, M.C., Perlmutter, D.L., White, B. *et al.* (1994) The association of augmentation mammoplasty with systemic sclerosis: Results from a multi-center case-control study. *Arthritis Rheum.*, **37** (Supplement): S369 (Abstract).
67. Strom, B.L., Reidenberg, M.M., Freundlich, B. *et al.* (1994) Breast silicone implants and risk of systemic lupus erythematosus. *J. Clin. Epidemiol.* (in press).
68. Englert, H.J., Brooks, P. (1994) Scleroderma and augmentation mammoplasty - a causal relationship? *Aust. NZ J. Med.*, **24**, 74–80.
69. Burns, C.J., Laing, T.J., Gillespie, B.W. *et al.* (1996) The epidemiology of scleroderma among women: Assessment of risk from exposure to silicone and silica. *J. Rheumatol.*, **23**(11), 1904–1911.
70. Sanchez-Guerrero, J., Karlson, E.W., Colditz, G.A. *et al.* (1994) Silicone breast implants (SBI) and connective tissue disease (CTD). *Arthritis Rheum.*, **37** (Supplement): S282 (Abstract).
71. Tan, E.M., Cohen, A.S., Fries, J.F. *et al.* (1982) The 1982 revised criteria for the classification of systemic lupus erythematosus. *Arthritis Rheum.*, **25** (11), 1271–1277.
72. Schottenfeld, D., Burns, C.J., Gillespie, B.W. *et al.* (1995) The design of a population-based case-control study of systemic sclerosis (scleroderma): Commentary on the University of Michigan Study. *J. Clin. Epidemiol.* **48**(4), 583–586.

Chapter 8

Vocal Folds

Joel Gaston and Susan L. Thibeault

8.1 Introduction

Vocal folds are two infoldings of complex tissue housed in the larynx whose vibration, known as phonation, results in voice. To create voice, vocal folds are adducted, effectively closing the glottis or the space between them creating a pressure difference between the top and bottom of the tissue. This pressure difference, combined with Bernoulli forces and tissue elasticity, pushes the vocal folds apart and brings them back together again [1]. This rapid, sustained opening and closing cycle produces vocal fold vibration at various fundamental frequencies ranging from 0 to 300 Hz for normal vocal levels [2]. The vocal folds are multilayer structures that consist of muscle, lamina propria, and epithelium. Fundamental frequency is controlled by laryngeal muscles which alter vocal fold physical properties, such as length and thickness. The extracellular matrix (ECM) of the lamina propria contributes significantly to vocal quality. Disruption of vocal fold vibration and/or quality through muscular dysfunction, airflow disruption, or tissue damage results in disturbance of normal voice production. Vocal fold scarring, a prevalent vocal fold injury, is characterized by pathophysiologic changes to the lamina propria ECM, directly causing a marked decrease in voice quality [3].

J. Gaston

Department of Biomedical Engineering, University of Wisconsin–Madison,
5118 WIMR, 1111 Highland Ave., Madison, WI 53705, USA

S.L. Thibeault (✉)

Department of Surgery, University of Wisconsin–Madison,
5107 WIMR, 1111 Highland Ave., Madison, WI 53705, USA

Department of Biomedical Engineering, University of Wisconsin–Madison,
5107 WIMR, 1111 Highland Ave., Madison, WI 53705, USA

Department of Communication Sciences and Disorders, University of Wisconsin–Madison,
5107 WIMR, 1111 Highland Ave., Madison, WI 53705, USA

e-mail: THIBEAUL@surgery.wisc.edu

8.2 Composition

The vocal fold can be divided into three layers, divided primarily by tissue function. The top layer consists of squamous cell epithelium, which separates the underlying tissue from the exposed airway. Below that lies the primary vibratory region, the lamina propria. The cellular and protein composition of this layer determines the ease of phonation. The lamina propria can be further subdivided into three layers, superficial, intermediate, and deep lamina propria (Fig. 8.1). The most interior section of the vocal fold consists of the thyroarytenoid muscle (muscularis), which relaxes and shortens the vocal folds. The large majority of biomechanical characterization has been completed on the lamina propria for biomaterial applications; subsequently the remainder of this chapter concentrates on the properties of this specific layer. The most important proteins, glycosaminoglycan (GAG), and proteoglycans in the lamina propria, as well as their concentrations at different depths, can be found in Table 8.1.

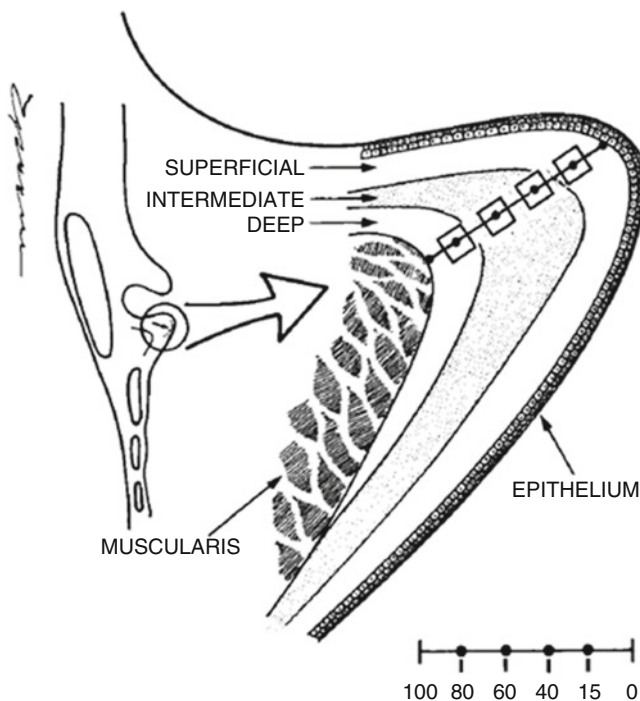


Fig. 8.1 Schematic of the divisions of the vocal fold, including lamina propria subdivisions. Reprinted with permission from [4]

Table 8.1 Lamina propria ECM components and their relative concentrations with respect to tissue depth

ECM component		Superficial lamina propria	Intermediate lamina propria	Deep lamina propria
Fibrous proteins	Collagen I	Low	High	Highest
	Collagen III	Low	High	Highest
	Elastin	Low	Highest	High
	Fibronectin	Highest	Low	Low
GAG	Hyaluronic acid	Very low	Highest	Low
Proteoglycans	Decorin	High	Very low	High
	Biglycan	Intermediate	Very low	Highest
	Versican	Very low	High	High

8.2.1 Collagen

The primary protein component of the vocal fold lamina propria is collagen, which constitutes roughly 43 % of the total tissue protein by weight [5]. Immunohistological staining shows that collagen I and collagen III are the primary collagens of the lamina propria. Both collagen types show the highest staining in the deep lamina propria, close to the thyroarytenoid muscle, with the intermediate layer having slightly lower staining intensity. The high fibrillar collagen content imparts strength and resiliency to the vocal folds. In general, the collagen fibers are spatially oriented from anterior to posterior, allowing them to support the force applied by the intrinsic laryngeal muscles [6].

8.2.2 Elastin

Elastin plays a crucial role in vocal fold vibration and the mechanical properties of the lamina propria. Accounting for approximately 8.5 % of the total lamina propria tissue protein by weight, it is mainly responsible for imparting elastic recoil to the human vocal folds [7]. Like collagen, higher concentrations of elastin are observed in the deep and intermediate layers of the lamina propria, with the concentration decreasing closer to the epithelial layer. Fibrillin, another elastic protein, appears to have deposition opposite that of elastin, with the highest concentration in the superficial lamina propria and the lowest concentration in the intermediate layer [7].

8.2.3 Hyaluronic Acid

Hyaluronic acid (HA), a linear nonsulfated glycosaminoglycan, is a major component of the vocal fold ECM. It is the most prevalent glycosaminoglycan present, consisting of roughly 6.4 μg of HA for each mg of total protein within the lamina

propria [7]. The high concentration has a significant effect on vocal fold mechanical properties. The long chain length and loosely coiled molecular structure of HA allow it to sequester large volumes of water, resulting in high tissue viscosity. The high tissue viscosity acts as a shock absorber, resisting tissue compression and damage caused during phonation.

8.2.4 Interstitial Proteins

Several other proteins play prominent roles in the vocal fold lamina propria. These small proteins contribute to ECM organization and typically are found at different levels in the lamina propria. Fibronectin plays a key role in both matrix organization and interaction with resident fibroblasts [8]. It is primarily located in the superficial layer of the lamina propria and the basement membrane that divides the epithelium from the superficial layer of the lamina propria. Decorin, a small proteoglycan, is also predominantly found in the superficial lamina propria [9]. It plays a role in collagen fibril assembly [10] and may contribute to the low density of collagen fibers in the superficial lamina propria. In addition, the ability of decorin to modulate stress transmission through the extracellular matrix is crucial for vocal fold phonation. Biglycan, a small proteoglycan with a similar role to decorin, is mainly located in the deep lamina propria. Within the deep lamina propria, it appears to be most dense near the intermediate layer [9]. Versican, a large chondroitin sulfate proteoglycan, is found primarily in the intermediate lamina propria [9]. It is often found colocalized with HA, though it is capable of binding with a variety of partners. Extracellular proteins such as fibrillin, fibronectin, and collagen I are capable of binding versican, and may affect cell adhesion to these structural proteins.

8.2.5 Voice Disorders

Scarring is the leading cause of poor voice quality after vocal fold surgery. The tissue fibrosis defined by scarring results in disorganized ECM architecture and altered mechanical properties. Controlled animal studies show that the major fibrous ECM proteins, collagen and elastin, are altered following scarring of the lamina propria (Table 8.2). To date, only one ten-patient study has analyzed the histology of scarred vocal folds [15]. Collagen deposition in the scarred lamina propria was found to be related to injury depth, with thicker fiber deposition correlated with deeper injury depth. Elastin was absent or fragmented and disorganized in all but one patient, consistent with animal studies. HA deposition followed a similar pattern, with HA being unobservable in all but one patient, where staining was barely visible. Finally, a quantitative assessment of the collagen, elastin, and HA content could not be performed, as the study did not have a normal control from the patients.

Table 8.2 Review of animal studies detailing vocal fold injury with histological and compositional changes

Animal model	Type of injury	Timeline post-injury	Collagen	Elastin	HA
Rabbit [11]	Lamina propria forceps biopsy	60 days	Disorganized fibers, less dense than normal controls	Short, compact fibers. Less dense than normal controls	Density similar to normal controls
Rabbit [13]	Lamina propria forceps biopsy	6 months	Organized fibers, thicker than normal control	Fibers fragmented and disorganized	Density similar to normal control
Canine [14]	Vocal fold stripping	2 months	Disorganized fibers, thicker than normal control	Disorganized fibers, less dense compared to normal control	Density similar to normal control
Rat [15]	Unilateral vocal fold stripping	8 weeks	Increased density compared to normal controls	N/A	Decreased density compared to normal controls
Rat [15]	Unilateral vocal fold stripping	12 weeks	Increased density compared normal to controls	N/A	Decreased density compared to normal controls

8.3 Mechanical Properties

8.3.1 General

The mechanical properties of the vocal fold are critical for normal phonation. Vocal fold tissue mechanical properties contribute to the minimum amount of air pressure needed to produce voice, also known as phonation threshold pressure. Phonation threshold pressure is the minimum subglottal pressure needed to overcome airway pressure, forcing the vocal folds open to begin oscillation. This measure is often taken as an objective indication of the energy required by an individual for vocal function. The combination of large quantities of collagen, elastin, and hyaluronic acid, and their respective mechanical properties, imparts viscoelastic properties to the vocal fold lamina propria. In normal conditions, and different disease states, the amount and organization of each protein affect the overall viscoelasticity of the tissue. In the past, the Young's modulus for the human intermediate and deep layers of the vocal fold has been calculated at 33.1 ± 10.4 kPa and 135 kPa for strains of 15 % and 25 %, respectively [16]. The wide frequency range covered during vocal fold phonation means direct measurement of the vocal fold viscoelastic properties has greater clinical application. Presently there are no methods to measure viscoelastic properties *in vivo*. For *in vitro* analysis, shear rheology is the favored method for quantifying the mechanical properties of excised lamina propria vocal fold tissue.

8.3.2 Rheology

Oscillatory shear deformation, a standard rheological technique, is used to determine the complex shear modulus of the vocal fold lamina propria [17]. Typically, a parallel plate rheometer is used to subject the tissue to precisely control sinusoidal torque, resulting in oscillatory shear stress. During testing, the controlling software measures the shear amplitudes and phase shift from the shear stress and strain functions. Measurement of these properties allows for the calculation of the elastic shear modulus, dynamic viscosity, viscous modulus, and damping ratio.

8.3.3 Elastic Shear Modulus

Elastic shear modulus quantifies the elasticity of the tissue under shear stress, and is proportional to the energy stored elastically due to strain. With rheological testing, the elastic shear modulus is a function of frequency, and only increases gradually across most of the frequency range tested (Fig. 8.2). At frequencies greater than 1 Hz, the elastic shear modulus increases with higher frequency. Shear properties are typically only measured at a frequency range of .01 to 15 Hz, as shear thinning and the small sample size prevent meaningful results at higher testing frequencies for vocal fold tissue. Rheology data published indicates that in general, the female vocal fold lamina propria had a lower elastic shear modulus compared to the male vocal fold lamina propria.

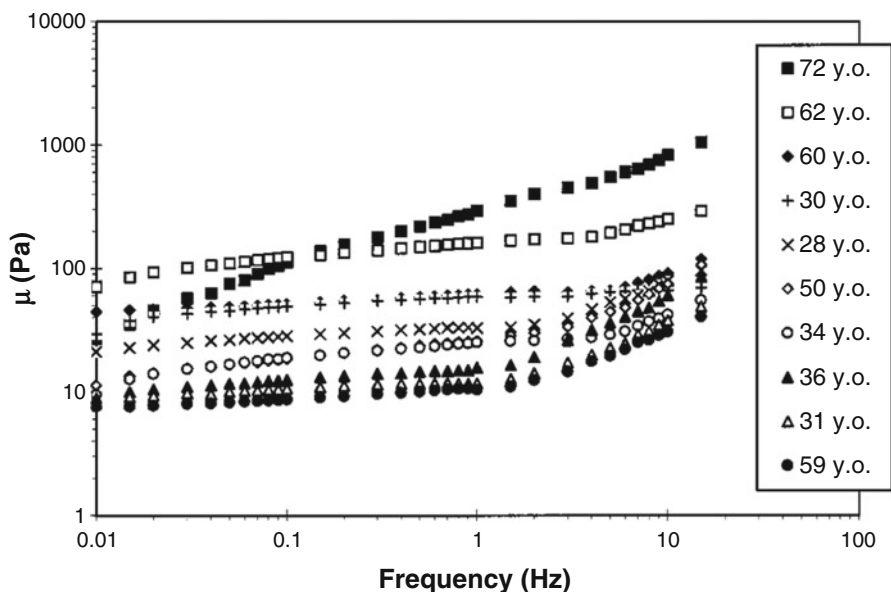


Fig. 8.2 Elastic shear modulus of male human vocal fold lamina propria. Reprinted with permission from [18]

8.3.4 Dynamic Viscosity

Dynamic viscosity characterizes the opposition of the tissue to shear flow, and is proportional to the energy lost in the viscoelastic tissue. Dynamic viscosity is related to the viscous shear modulus through the angular frequency. Rheological testing shows that the dynamic viscosity decreases as a function of frequency, and as such the vocal folds exhibit shear thinning behavior (Fig. 8.3). This behavior is fundamental to vocal fold movement—as the fundamental frequency of vibration increases, the lamina propria will shear thin providing movement of this tissue at very high frequencies.

8.3.5 Poisson's Ratio

Only one study has investigated the Poisson ratio of human vocal folds [19]. An optical method was used, where a marked vocal fold sample was illuminated, cyclically stretched at 1 Hz and 37 °C, and video recorded using a high-speed camera system. Processing of the recorded images resulted in a Poisson ratio of .392. This number should be taken with caution; several models consider the human vocal folds to be transversely isotropic [20, 21], and testing was performed at only one frequency [19].

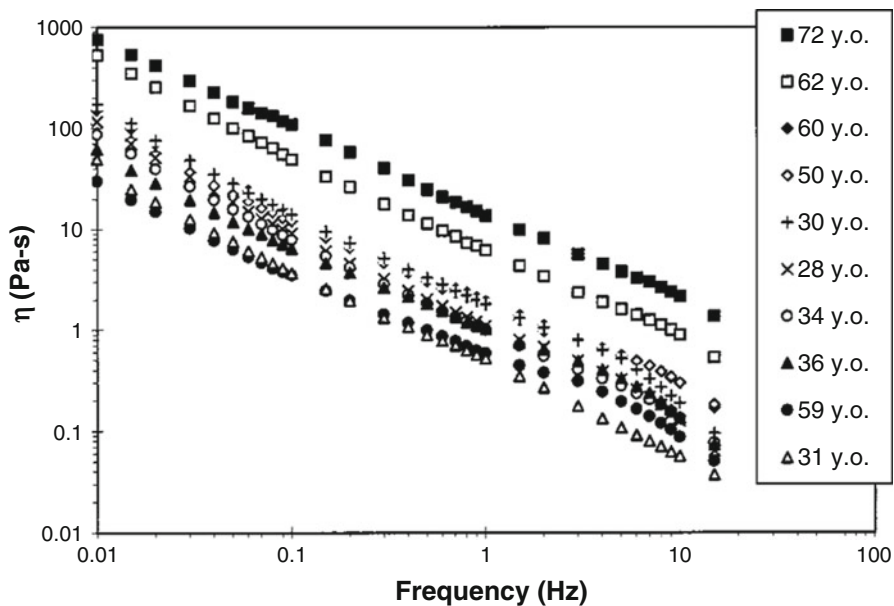


Fig. 8.3 Dynamic viscosity of male human vocal fold lamina propria. Reprinted with permission from [18]

8.3.6 Vocal Fold Scarring

Numerous studies have shown that scarring of vocal fold tissue results in tissue mechanics detrimental to normal voice function. Animal models have shown that vocal fold scarring results in permanently elevated elastic shear modulus and dynamic viscosity, making the tissue both stiffer and more viscous (Table 8.3). Rabbit models are particularly useful, as normal vocal fold viscoelastic shear properties are similar to those of human vocal fold tissue [17]. This can be visualized further when the viscoelastic moduli are plotted as a function of frequency for rabbit animal models. Elastic shear modulus of scarred vocal fold tissue is higher than the normal control tissue for all samples tested (Fig. 8.4a), indicating an increase in stiffness [22]. The same trend is seen for the dynamic viscosity, with scarred tissue having a significantly higher modulus than normal controls (Fig. 8.4b). Though no direct comparison of mechanical properties between normal and scarred human vocal folds, nearly all mammalian animal models have shown the same patterns described above [13, 14].

8.4 Biomaterial Injections

Injectable biomaterials have been developed and used to treat vocal fold lamina propria with abnormal viscoelastic properties due to ECM disruption. The most important property for consideration for a vocal fold injectable is that the biomaterial has biomechanical properties most similar to the lamina propria, so as to allow for normal tissue movement. When injected into the vocal fold lamina propria, the viscoelastic properties of injectable biomaterials should be matched as closely as possible to normal lamina propria. To this end, several natural and synthetic biomaterials have been developed to mitigate dysphonia. Upon injection, biomaterials with significantly higher viscous and elastic moduli make vocal fold oscillation, and therefore phonation, difficult. Finally, any biomaterial implanted into the vocal fold must undergo shear thinning in order to match the basic viscoelastic behavior of the lamina propria.

Table 8.3 Animal studies detailing vocal fold injury and changes in mechanical properties

Animal model	Type of injury	Timeline post-injury	Elastic shear modulus	Dynamic viscosity
Rabbit [12]	Lamina propria forceps biopsy	60 days	Stiffer tissue, higher modulus	More viscous, higher modulus
Rabbit [13]	Lamina propria forceps biopsy	6 months	Stiffer tissue, higher modulus in eight out of ten samples	More viscous, higher modulus in nine out of ten samples
Canine [14]	Vocal fold stripping	2 months	Stiffer tissue, higher modulus	More viscous, higher modulus

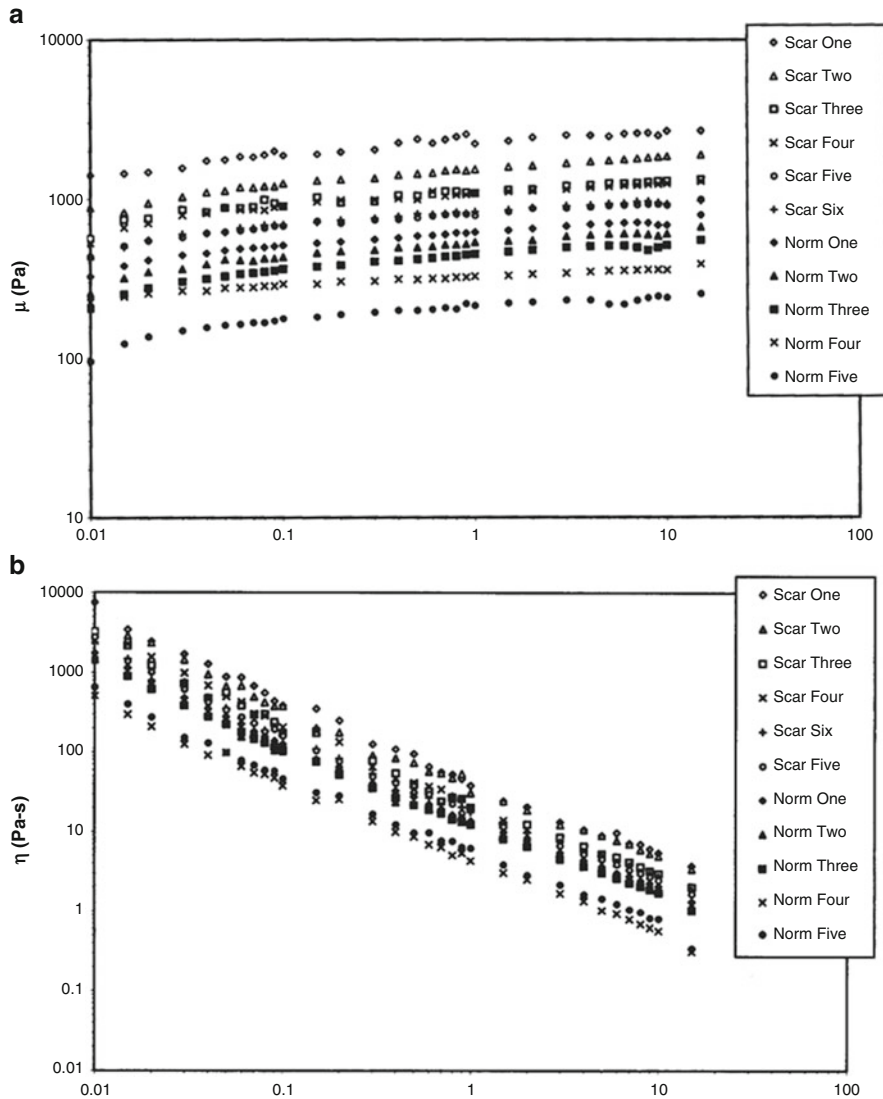


Fig. 8.4 (a) Elastic shear modulus (μ) of rabbit vocal fold. (b) Dynamic viscosity (η) of rabbit vocal fold tissue. Reprinted with permission from [22]

8.4.1 Collagen and Fat Injections

Several different collagen formulations and adipose have been tested as injectables for vocal fold scarring. A study utilized rheological testing to compare collagen and adipose tissue to normal vocal fold tissue, with a specific focus on viscosity [17]. Adipose tissue prepared as a fat graft was found to have the closest viscosity to normal vocal fold tissue, followed by uncrosslinked collagen (Fig. 8.5).

TABLE II.
Dynamic Viscosity of Implantable Biomaterials and Human Vocal Fold Mucosal Tissues
Measured at 10 Hz and Extrapolated to 100 Hz.

Material Sample	Dynamic Viscosity (Pa-s)	
	Measured at 10 Hz	Extrapolated to 100 Hz
Polytetrafluoroethylene (Teflon)	116.144	10.186
Gelatin (Gelfoam)	21.297	2.335
GAX collagen (Phonagel or Zyplast)	12.844	1.480
Noncrosslinked collagen (Zyderm)	8.563	0.980
Human abdominal subcutaneous fat (70-year-old woman)	3.026	0.296
Vocal fold mucosa (72-year-old man)	2.702	0.281
Vocal fold mucosa (62-year-old man)	0.897	0.099

Fig. 8.5 Comparison of dynamic viscosity of several biomaterial injections for the vocal fold lamina propria. Reprinted with permission from [17]

8.4.2 Modified Hyaluronic Acid

HA hydrogels show the most promise as injectable biomaterials for the vocal fold to date. However, natural HA is rapidly degraded upon injection, typically taking roughly 3–5 days to dissolve [12]. As such several different HA hydrogel formulations with differing cross-links and chemical moieties have been designed and investigated for vocal fold applications (Table 8.4).

Hylan B, a non-inflammatory divinyl sulfone cross-linked simple HA hydrogel, has been used in the past as a space-filling injection. It is no longer in the market, but has since been succeeded by the Restylane line of HA injectables. Multiple animal studies show that Hylan-B injections into rabbit vocal fold lamina propria show mechanical results similar to normal vocal fold [24, 27]. Specifically, 6 months after injection no significant difference in dynamic viscosity was observed between Hylan-B-injected tissue and normal, noninjected tissue. In the same study, vocal fold tissue injected with Hylan-B was found to have a lower dynamic viscosity than tissue injected with other biomaterials, such as collagen or Teflon. In an 83-person clinical study, Hylan-B had a more favorable effect than collagen on vocal fold function [28]. Most notable was the increase in vocal fold mucosal wave production compared to baseline, indicating positive viscoelastic mechanics. This result could not be directly corroborated, as rheology can only be performed on ex vivo tissue.

Hydrogel cross-linking is of particular interest in vocal fold applications, as different cross-linking methods and groups can alter the mechanical properties of the hydrogel. Several different HA hydrogels have been formulated that utilize a polyethylene glycol diacrylate (PEGDA) cross-linker, allowing the gelation time and swelling ration to be easily modified [29]. PEGDA cross-linking is prominent

Table 8.4 Summary of studies utilizing HA derivatives and their outcomes

HA derivative		Normal	Prophylactic	Chronic
Hylan B	Fibrotic effects	No inflammation up to 12 months post-injection [31]. Hylan B residence time of at least 6 months [23, 31]		
	Mechanical effects	No change in dynamic viscosity compared to no injection [27]		
Carbylan-S	Fibrotic effects		Decreased fibrosis compared to saline [30]	
	Mechanical effects		Lower elastic shear modulus and lower dynamic viscosity [30]	
HA-DTPH-PEGDA	Mechanical effects		No significant difference compared to saline [30]	
	Fibrotic effects		No change in elastic shear modulus. Lower dynamic viscosity [30]	
Extracel	Fibrotic effects		Decreased procollagen, fibronectin, and fibromodulin mRNA [12]	Increased collagen and procollagen [23]
	Mechanical effects		Lower elastic shear modulus and lower dynamic viscosity [12]	Lower elastic shear modulus and lower dynamic viscosity [23]

in two HA hydrogels for vocal fold applications; HA-DTPH and Carbylan-S. Both HA-DTPH and Carbylan-S are similar in composition, consisting of an HA backbone with PEGDA cross-links. The Carbylan-S backbone has additional carboxylate groups on the HA backbone, resulting in a higher elastic shear modulus than HA-DTPH [25]. To date, both hydrogel formulations have been primarily examined as a prophylactic treatment to reduce or prevent vocal fold scarring by injection at the time of injury. Excised tissue from injured rabbit vocal fold injected with Carbylan-S had a lower elastic shear modulus than injured tissue treated with saline controls or injured tissue injected with HA-DTPH-PEGDA [30]. Tissue injected with either Carbylan-S or HA-DTPH-PEGDA was significantly less viscous than the saline-treated samples as well. Trichrome staining performed on sections of the excised larynges showed that the average fibrosis levels for animals injected with the HA-DTPH-PEGDA were moderate and not significantly different from saline-treated controls.

The Carbylan-S HA backbone has also been cross-linked using thiolated gelatin to generate a hydrogel commercially designated as Extracel[®] [26]. Extracel[®] has undergone several naming changes since its first formulation, and can also be found as Gycosil[®] or HyStem[®]. Extracel[®] has been investigated as both a prophylactic treatment for vocal fold tissue injury and as a treatment for previously scarred tissue. A rabbit study showed that 6 months after injury and injection, excised vocal fold tissue injected with Extracel[®] had a lower elastic shear modulus and lower viscous modulus compared to saline controls [12]. While histology was not performed, quantitative PCR showed a decrease in mRNA transcript levels for fibronectin, fibromodulin, and procollagen [12]. A similar study was performed on rabbits where an injury was induced and allowed to scar for 3 months [23], at which time Extracel[®] or saline was injected into the vocal fold. Two months following injection, the tissue injected with Extracel[®] had a lower elastic shear modulus and viscous modulus compared to saline injections. Finally, histological staining showed that the Extracel[®]-treated vocal folds had higher procollagen and collagen than saline, a marked contrast from the prophylactic study.

Additional Reading

Miri AK. Mechanical characterization of vocal fold tissue: a review study. *J Voice* 2014; 28:657–67.

Caton T, Thibeault SL, Klemuk S, Smith ME. In reference to viscoelasticity of hyaluronan and nonhyaluronan based vocal fold injectables: Implications for mucosal versus muscle use—Reply. *Laryngoscope* 2007, 117(8): 1506–1508.

Chan RW, Titze IR. Dependence of phonation threshold pressure on vocal tract acoustics and vocal fold tissue mechanics. *Journal of the Acoustical Society of America* 2006; 119:2351–62.

References

1. Benninger MS, Alessi D, Archer S, Bastian R, Ford C, Koufman J et al (1996) Vocal fold scarring: current concepts and management. *Otolaryngol Head Neck Surg* 115:474–482
2. Titze IR (2000) Principles of voice production. National Center for Voice and Speech
3. Smith E, Gray S, Verdolini K, Lemke J (1995) Effects of voice disorders on quality of life. *Otolaryngol Head Neck Surg* 113:P121
4. Butler JE, Hammond TH, Gray SD (2001) Gender-related differences of hyaluronic acid distribution in the human vocal fold. *Laryngoscope* 111:907–911
5. Hahn MS, Kobler JB, Zeitels SM, Langer R (2006) Quantitative and comparative studies of the vocal fold extracellular matrix. II: Collagen. *Ann Otol Rhinol Laryngol* 115:225–232
6. Gray SD, Titze IR, Alipour F, Hammond TH (2000) Biomechanical and histologic observations of vocal fold fibrous proteins. *Ann Otol Rhinol Laryngol* 109:77–85
7. Hahn MS, Kobler JB, Starcher BC, Zeitels SM, Langer R (2006) Quantitative and comparative studies of the vocal fold extracellular matrix. I: Elastic fibers and hyaluronic acid. *Ann Otol Rhinol Laryngol* 115:156–164

8. Hansen JK, Thibeault SL (2006) Current understanding and review of the literature: vocal fold scarring. *J Voice* 20:110–120
9. Hahn MS, Kobler JB, Zeitels SM, Langer R (2005) Midmembranous vocal fold lamina propria proteoglycans across selected species. *Ann Otol Rhinol Laryngol* 114:451–462
10. Kalamajski S, Oldberg A (2010) The role of small leucine-rich proteoglycans in collagen fibrillogenesis. *Matrix Biol* 29:248–253
11. Hirano S, Minamiguchi S, Yamashita M, Ohno T, Kanemaru S, Kitamura M (2009) Histologic characterization of human scarred vocal folds. *J Voice* 23:399–407
12. Thibeault SL, Klemuk SA, Chen X, Johnson BHQ (2011) In vivo engineering of the vocal fold ECM with injectable HA hydrogels—late effects on tissue repair and biomechanics in a rabbit model. *J Voice* 25:249–253
13. Rousseau B, Hirano S, Chan RW, Welham NV, Thibeault SL, Ford CN et al (2004) Characterization of chronic vocal fold scarring in a rabbit model. *J Voice* 18:116–124
14. Rousseau B, Hirano S, Scheidt TD, Welham NV, Thibeault SL, Chan RW et al (2003) Characterization of vocal fold scarring in a canine model. *Laryngoscope* 113:620–627
15. Tateya T, Tateya I, Sohn JH, Bless DM (2005) Histologic characterization of rat vocal fold scarring. *Ann Otol Rhinol Laryngol* 114:183–191
16. Caton T, Thibeault SL, Klemuk S, Smith ME (2007) In reference to viscoelasticity of hyaluronan and nonhyaluronan based vocal fold injectables: implications for mucosal versus muscle use—Reply. *Laryngoscope* 117:1506–1508
17. Chan RW, Titze IR (1998) Viscosities of implantable biomaterials in vocal fold augmentation surgery. *Laryngoscope* 108:725–731
18. Chan RW, Titze IR (1999) Viscoelastic shear properties of human vocal fold mucosa: measurement methodology and empirical results. *J Acoust Soc Am* 106:2008–2021
19. Alipour F, Vigmostad S (2012) Measurement of vocal folds elastic properties for continuum modeling. *J Voice* 26:9
20. Alipour F, Berry DA, Titze IR (2000) A finite-element model of vocal-fold vibration. *J Acoust Soc Am* 108:3003–3012
21. Rosa MD, Pereira JC, Grellet M, Alwan A (2003) A contribution to simulating a three-dimensional larynx model using the finite element method. *J Acoust Soc Am* 114:2893–2905
22. Thibeault SL, Gray SD, Bless DM, Chan RW, Ford CN (2002) Histologic and rheologic characterization of vocal fold scarring. *J Voice* 16:96–104
23. Thibeault SL, Dufflo S (2008) Inflammatory cytokine responses to synthetic extracellular matrix injection to the vocal fold lamina propria. *Ann Otol Rhinol Laryngol* 117:221–226
24. Borzacchiello A, Mayol L, Garskog O, Dahlqvist A, Ambrosio L (2005) Evaluation of injection augmentation treatment of hyaluronic acid based materials on rabbit vocal folds viscoelasticity. *J Mater Sci Mater Med* 16:553–557
25. Shu XZ, Liu Y, Prestwich GD (2011) Modified macromolecules and methods of making and using thereof
26. Dufflo S, Thibeault SL, Li WH, Shu XZ, Prestwich GD (2006) Vocal fold tissue repair in vivo using a synthetic extracellular matrix. *Tissue Eng* 12:2171–2180
27. Dahlqvist A, Garskog O, Laurent C, Hertegard S, Ambrosio L, Borzacchiello A (2004) Viscoelasticity of rabbit vocal folds after injection augmentation. *Laryngoscope* 114:138–142
28. Hertegard S, Hallen L, Laurent C, Lindstrom E, Olofsson K, Testad P et al (2002) Cross-linked hyaluronan used as augmentation substance for treatment of glottal insufficiency: safety aspects and vocal fold function. *Laryngoscope* 112:2211–2219
29. Shu XZ, Liu YC, Palumbo FS, Lu Y, Prestwich GD (2004) In situ crosslinkable hyaluronan hydrogels for tissue engineering. *Biomaterials* 25:1339–1348
30. Hansen JK, Thibeault SL, Walsh JF, Shu XZ, Prestwich GD (2005) In vivo engineering of the vocal fold extracellular matrix with injectable hyaluronic acid hydrogels: early effects on tissue repair and biomechanics in a rabbit model. *Ann Otol Rhinol Laryngol* 114:662–670
31. Hallen L, Johansson C, Laurent C (1999) Cross-linked hyaluronan (hylan B gel): a new injectable remedy for treatment of vocal fold insufficiency—an animal study. *Acta Otolaryngol* 119:107–111

ERRATUM TO

Chapter 6 Ceramic Materials Testing and Fracture Mechanics

Garth Hastings, Ishbel Gair, and D. Daily

© Springer Science+Business Media New York 2016
W. Murphy et al. (eds.), *Handbook of Biomaterial Properties*,
DOI 10.1007/978-1-4939-3305-1_22

DOI 10.1007/978-1-4939-3305-1_36

The chapter was edited by Prof. Garth Hastings and Dr. Ishbel Gair. These author names were unfortunately not indicated in the chapter under the title. Now, the author names are included in the chapter under the title.

Garth Hastings
Staffordshire University (Emeritus), Lyme, Staffordshire, UK
e-mail: garth.hastings@btinternet.com

Ishbel Gair
Technical Consultant, Lucideon Ltd, Staffordshire, UK
e-mail: ishbel-@hotmail.co.uk

D. Daily (deceased)

The updated online version of the original chapter can be found at
http://dx.doi.org/10.1007/978-1-4939-3305-1_22

Index

Page numbers in bold refer to figures; those in italics refer to tables

A

Above knee tissues, elastic moduli, *64*

Adhesion

bioglass, 157

titanium alloys, 157

Age of donors, cortical bone, 5–6

Alloys, 515–7, **516**

AgPd, *197, 201*

galvanic, 515

chemical composition, *202*

NiCr, *202–13, 212–13*

properties, *202, 203*

Pd, *197, 201*

precious metal, *198–200*

bonding with ceramics, 199

brazing, 199

casting, 198

heat treatment, *198–9*

Alumina, 342–3

ceramic hip balls, 340

chemical properties, 343

clinical performance, 344

dental implants, 341

engineering properties, *342*

implants, 339–40

physical properties, 342

standards, *343*

wear resistance, 343

Aluminum/graphite, tensile

strengths, *254*

Aluminum/silicon, tensile data, *254*

Aluminum/Thornel, mechanical properties, *253*

Al₂O₃ whisker-nickel, tensile properties, *255*

Amalgamization, 192

Amalgams, *191, 191–4, 193, 194*

chemical composition, *191*

copper content, 192

corrosion, 194

and wear, *193–4*

high copper type, 194

mercury vapour release, *194*

mixed alloys, 192

one-component, 192

processing, 193

properties, *191, 191–2, 193*

Amino plastics, properties, *237*

Animal cornea, 136

Annulus fibrosus, 46, *47, 50*

Antibiotics, metal interactions, *524*

Antibodies, 594–5

antiserum, 596

detecting, *595–7, 596*

in vivo testing, 596, *597*

negative results, *597*

positive results, *596*

immunoglobins, 594–5

Antigens, 593

immobilization, 596, **606**

processing cell, 593

Antioxidants

additives, *248*

low toxicity, *245*

synergism, *248*

- Aorta
 compliance, 87–8
 hydrodynamic properties, 87
 morphometric properties, 82, 82
 pressure/cross-sectional area, 87–8
 retraction, 87–8, 89
 tapered, 78
- Apatite parameters
 dentin, 27
 enamel, 27
- Apparent density, 15
- Aramid fibers, 209
 disadvantages, 209
- Arterial tissues
 change with age, 79, 81, 83
 composition, 81
- Arterial wall, composition, 79–84, 81, 82, 83, 84
- Arteries
 coronary, tensile properties, 89
 creep, 90–2, 91
 elastic modulus, 86
 hypertension, 81, 83
 mechanical properties, 84–92, 85, 86, 87, 89, 90, 91
 morphometric properties, 78, 78
 Reynolds number, 78
 stress relaxation, 90–2, 91
 tensile properties, 88, 89
- Articular cartilage, 37
 composition, 38
 compression, 38–9, 39
 lubrication, 41–2
 mechanical properties, 38–42
 permeability, 41
 Poisson's ratio, 41
 shear properties, 40, 40
 tensile properties, 39–40, 40
 tribologic properties, 41–2
 wear tests, 42
- Artificial saliva, repassivation rates, 193
- Aseptic loosening, 588
- A-S/3501 graphite/epoxy
 aging, 249
 moisture effects, 249
- ASTM F75, 159–61
 chemical composition, 160
 investment casting, 160
 mechanical properties, 161
- ASTM F90, 161–2
 chemical composition, 161, 162
 mechanical properties, 162
- ASTM F552, 162–3
 chemical composition, 163
 mechanical properties, 163
- MP35N, 162
- ASTM F553, 164
 chemical composition, 164, 174
 mechanical properties, 164, 165
- ASTM F799, 161
 chemical composition, 161
 mechanical properties, 162
- ASTM F1058, 164
 chemical composition, 165
 mechanical properties, 165
- Atherosclerosis, 81, 84
- Autoclave molding, 221–2
- Autoimmune diseases, 602–3
- B**
- Basal ganglia, 67
- B/5505 boron/epoxy
 aging, 249
 moisture effects, 249
- Beam theory, 357–60
- Below knee tissues, 64
- Bending modulus, osteons, 8, 8
- Bioactive
 bonding, 447–8, 448, 449, 458
 ceramics, orthopaedics, 495–5
 compositions, 449–50
 glasses, 447–54
 bone bonding, 452
 clinical uses, 453
 physical properties, 450, 451, 453
- Bioactivity
 definition, 447
 index, 449
- Bioceramics, 339–51
 ASTM standards, 347
 biocompatibility, 347–8, 348, 349
 dental applications, 350
 failure loads, 448
 ISO standards, 347
 manufacturers, 350
 orthopaedic applications, 348
 trade names, 350
- Biocompatibility, 563–9
 components, 566–9
 control of, 568
 definition, 564–5
 local host response, 567–9
 material degradation, 566–7
- Biofunctionality, metallic biomaterials, 154–6
- Biological
 degradation, 499–5, 500–1, 502
 animal experiments, 499–4
 calcium phosphate, 500–1, 502
 clinical applications, 499–4

- properties
 - titanium, 185
 - Biomaterials, systemic effects, 569
 - Biospan, 294
 - Biospan-D, 294
 - Biospan-S, 294
 - Blastogenic factor, 597
 - Blood, 115–23
 - and cardiovascular devices, 623
 - coagulation, proteins, 122
 - metals in, 519
 - physiochemical properties, 116
 - velocity, 78
 - vessels, 77–97
 - atherosclerosis, 96
 - changes with age, 94–5
 - hypertension, 95
 - transport properties, 94, 95
 - Bone
 - cement, 581
 - formation, interfacial, **450**
 - Bone-biomaterial interfaces, 588, **589**
 - Bone/biomaterial interfaces, 621–7
 - Bone remodeling, 16
 - Born equation, 379
 - Boron fibers, 208, 209
 - application, 209
 - manufacturing technique, 208
 - properties, 208
 - Bovine bone, creep, 10
 - Brain tissues, 67–75
 - bulk modulus, 69
 - composition, 68
 - creep modulus, 69, 72–3
 - density, 69
 - diffusion properties, 74
 - dimensions, 68
 - elastic modulus, 69, 70–71
 - electrical conductivity, 69, 74
 - mass, 68
 - mechanical stimuli, 68
 - Poisson's ratio, 69
 - shape, 68
 - shear modulus, 69, 70–71
 - stem, 67
 - thermal properties, 74, 74
 - Breast augmentation, 633
 - scleroderma, 640
 - subsequent diseases, 632–4
 - causes, 634–7, 636
 - systemic sclerosis, 633, 635
 - Breast implants
 - and connective tissue disease, 637–41, 638
 - rheumatoid arthritis, 640
 - silicone, 640
 - systemic lupus erythematosus, 639
 - Brittle behaviour, ceramic materials, 353
 - Brittle fiber/Sic, properties, 258
 - Brittle ring test, 367
 - Bulk modulus, brain tissues, 69
- C**
- Calcium phosphates, and metallic ions, 533–6, **534, 535, 536**
 - Cancellous bone, 15–20
 - compression, 16
 - fracture toughness, 19
 - mechanical properties, 16, 17
 - microstructure, 15
 - Poisson's ratio, 18
 - stiffness and strength, 16–18
 - strain, 18
 - surface-to-volume ratio, 15
 - tissue composition, 16
 - tissue damage, 19–20
 - tissue-level mechanical properties, 20
 - and ultrastructure, 16
 - viscoelastic and fatigue properties, 18–19
 - Young's and shear modulus, 16, 18
 - Cancer, 607–17
 - and metallic implants, 616
 - Capillaries, morphometrics, 78
 - Ca/P molar ratio
 - dentin, 27
 - enamel, 27
 - Carbon fiber
 - precursors, 208
 - properties, 208
 - trade names, 208
 - Carbon prostheses, mechanical properties of, 251
 - Carbons, 551–62
 - atomic arrangement, **553**
 - biocompatibility, 551
 - charcoal, 552
 - composites, 552, 558
 - filament wound, 558
 - dental applications, 558, 560
 - fibers, 552, 556–7
 - forms, mechanical properties, 559
 - glassy, 455, 556
 - in vivo*, 558
 - medical applications, 559
 - orthopaedics, 560
 - polymeric, 552
 - pyrolytic, 552, 554, 555, 562–6
 - low-temperature, 555

- Carbons (*cont.*)
 structures, 551–2
 vapour phase coatings, 552, 557
 vascular applications, 560
- Carbon/silicon nitride, properties, 257
- Carbo thane, 308
- Cardiac valves, 625
- Cardiovascular devices, and blood, 623
- Cartilage, 37–42
 articular, 37
 composition, 38, 38
 elastic, 38
 mechanical properties, 42
 fibrocartilage, 38
 hyaline, 37
 water content, 37
- Cataractous human lenses
 hardness, 108
 water content, 105
- Catheters, 622–626
- Causal association
 analogy, 636, 646
 biologic plausibility, 636, 646
 consistency, 636, 646
 dose-response, 636, 646
 reversibility, 636, 646
 specificity, 636, 646
 strength, 636, 646
 temporality, 636, 646
- CCR₅₀, 154
- Cell
 adaptation, 576
 cultures, 504–5
 testing, 504
 mediated
 immunity, 599
 responses, 597–600
 responses: choice of test, 598
 migration inhibition, 597
- Cellular necrosis, 572
- Cementation, 581–4, **582**, **583**
- Cement-free implants, **582**, **583**, 584–5
 hip prostheses, 584–5
 knees, 584–5
 orthopaedic, 584
- Cement line, cortical bone, 4
- Central corneal thickness (CCT), 138
- Centrifugal
 casting, 220–21
 molding, 226–8
 release agents, 226
- Ceramic acetabular cup, 443
- Ceramic materials
 brittle behaviour, 353
 compliance, 387–392
 digital imaging correlation, 443–4
 double cantilever beam, 396–8, 417–20, **418**
 double torsion method, 414–7
 ductile behaviour, 353
 energy release rate, 385–7
 engines, 430
 fracture work, 392–6
 Griffith's criterion, 384–5
 Griffith's theory, 381–4
 hip joints endoprosthesis
 finite element analysis (FEA), 433–5
 Weibull equation, 435–41
 microstructure, 354–5
 porosity, 355–6
 SPT diagram, 428–30
 stem fixation problem, 442
 strength of solids, 377–81
 strength testing
 3 and 4 point bending, 360–65
 beam theory, 357–60
 ceramic machining, 357
 flexion and flexure testing, 357
 nature of test, 374–7
 processing of failure data, 369–72
 ranking, 372–4
 significance of test results, 368–9
 tensile testing, 356–7
 test configurations, 365–8
 test pieces, 357
 volume of test piece, 377
 stress concentrators and cracks,
 398–12
 stress corrosion, 426–8
 stress-volume-integral, 436
 valency type, 356
- Ceramics, 256–8, 257, 258
 calcium phosphate, 495
 flexural strength, 258
 fracture toughness, 258
 glass, 257
 hip balls, 340
 physical properties, 450, 451, 453
 processing, 347
- Cerebellum, 67
- Cerebrospinal fluid, 67, 117
 inorganic content, 117–18
 organic content, 118–19
 protein content, 118–20
- Cerebrum, 67
- C-Flex TPE, 310
- Chemical vapour deposition, 557
- Chromium
 corrosion, **511**

- immunity, **511**
- passivation, **511**
- ChronoFlex, 308
- Cluster differentiation markers, 594
- Coatings, 528–33, *529*, **530**, *531*, **532**, *533*, **539**, **541**
 - corrosion currents, *531*
 - HAp, *533*, *534*, *535*
 - hard ceramic, 530
 - metallic, 528
 - niobium, 528
 - tantalum, 528
 - titanium, 528
 - ultra-thin, 625–6
- Cobalt-chromium (CoCr) alloys, 159–66
 - ASTM F75, 159–61
 - chemical composition, *160*
 - investment casting, 160
 - mechanical properties, *161*
 - ASTM F90, 161–2
 - chemical composition, *161*, *162*
 - mechanical properties, *162*
 - ASTM F552, 162–3
 - chemical composition, *163*
 - mechanical properties, *163*
 - MP35N, 162
 - ASTM F553, 164
 - chemical composition, *164*, *174*
 - mechanical properties, *164*, *165*
 - ASTM F799, 161
 - chemical composition, *161*
 - mechanical properties, *162*
 - ASTM F1058, 164
 - chemical composition, *165*
 - mechanical properties, *165*
 - Havar
 - chemical composition, *165*
 - mechanical properties, *166*
 - UNS R30005, 164–6
- Collagen
 - content, cartilage, *37*
 - cortical bone, 3
 - immune response to, 601
 - shrinkage temperature, 3
- Collagen/elastin ratio, 82
- Collagen fibers, 55
- Combined loading, cortical bone, 9
- Composites, 205–58
 - classifying, 205
 - fabrication, 220–9
 - fibrous, 205
 - laminar, 205
 - in medicine, 250–2
 - metal matrix, 252–6
 - particulate, 205
 - radiation resistance, *246–7*
 - reinforcements, 253
- Compression
 - articular cartilage, 38–9, *39*
 - cortical bone, 8
 - modulus
 - cortical bone, 6–7
 - osteons, 8, 8
- Compressive strength
 - dentin, 29
 - enamel, 28–9
- Connective tissue disease, and breast implants, 637–41, *638*
- Contact angles, 542–5, *543*
 - equilibrium, 545
 - oxidized surfaces, *543*
- Contamination of tissues, 517–21
- Continuous sheets, 228–9
 - decorative, 228
 - glass reinforcement, 228
- Coremer, 308
- Corethane, 308
- Corhesive, 308
- Cornea, 135–6
 - animal, 136
 - biomechanics, 140
 - composition, *137*
 - diameter, *137*, *137*
 - electric properties of tissue, *141*
 - geometrical and optical properties, 139
 - keratometry, 139
 - mechanical properties of tissue, *142–3*
 - refractive index, *140*
 - stress-strain relationship, 141
 - thickness, *137–8*, *138*
 - ultraviolet and visible radiation transmission, *141*
- Corneal diameter, 137
- Corrosion, 509–45
 - contamination of tissues, 517–21
 - detection of ions, 509
 - duration of implantation, 515, **516**
 - grading scale, 510
 - incidence of, 510
 - and inertness, metallic biomaterials, 153–4
 - materials purity, 512
 - proteins, 524, 525
 - Ti-15Zr-4Nb-2Ta-O.2Pd, 514
 - and wear, *182*, *182–5*, *183*, *184*, *185*
 - noble metals, 201
- Cortical bone, 3–12
 - age of donors, 5–6
 - collagen, 3

- Cortical bone (*cont.*)
 combined loading, 9
 compression, 8
 compressive modulus, 6–7
 constituents, 3, 4
 creep, 10
 density, 4, 4
 dry testing, 5
 elastic moduli, 7
 electromechanical behaviour, 5
 fatigue, 10–11
 health of donors, 5–6
 mineral, 4
 mineralization, 6, 10
 physical properties, 4–5
 Poisson's ratios, 7, 7
 remodelling, 11, 11
 shear moduli, 7, 7
 small specimens, 7
 stiffness, 6–9
 strain rate, 6, 8–10
 effects, 10
 strength, 9, 9–11
 tensile modulus, 6
 time to failure, 10
 viscoelastic damage, 8–6
 Young's modulus, 11
 cp-titanium, chemical composition, 168
 Creep
 bovine bone, 10
 cortical bone, 10
 modulus, brain tissues, 69, 72–3
 Critical stress intensity factor, 400
 Critical surface tensions
 dentin, 33
 enamel, 33
 Curing agents
 amine, 213–4
 anhydride, 214
 accelerators, 214
 epoxide resins, 213–5
 polyamide, 214–5
 Cutting and milling titanium, 173
 Cytokines, testing for, 598–9, 599
- D**
 DAP, properties, 237
 Debris
 accumulation, 608
 metallic, 608, 609
 Definitions
 bioactivity, 447
 biocompatibility, 564–5
 elastomers, 291
 ligament, 55
 osseointegration, 585
 ply, 216
 repassivation, 153–4
 solubility, 496
 tendon, 55
 thermoplastic resins, 211
 thermoset resins, 211
 tribosystem, 487
 Degradation, 608, 618–19
 Density
 brain tissues, 69
 cortical bone, 4, 4
 Dental
 alloys
 AgPd, 197
 composition of, 195, 196
 high gold containing, 195, 200
 low gold containing, 195, 201
 Pd, 197
 precious, 198
 amalgams, 151
 implants, 151, 152, 157
 restoration, 191–203
 Dentin, 23–34
 apatite in, 27
 apatite parameters, 27
 Ca/P molar ratio, 27
 compressive strength, 29
 constituents, 24
 critical surface tensions, 33
 elastic moduli, 28
 elemental composition, 24
 flexural strength, 29
 fracture toughness, 30
 mineral density, 24
 organic density, 24
 permeability, 31
 stress, 29
 tensile strength, 29
 toughness, 30
 viscoelastic properties, 28
 water density, 24
 wettability, 33
 work of fracture, 30
 Dentino-enamel junction (DEJ), 23
 Descaling titanium and titanium alloys, 171–2
 Diamond, 557
 Diaphysis, vs. metaphysis, 7, 7, 9–10
 Diencephalon, 67
 Diffusion properties, brain tissues, 74
 Diffusion welding, titanium, 174
 Digital imaging correlation, 443–4

- Diluents, 212–3
 non reactive, 213
 reactive, 212–3
- Dimethylpolysiloxane, 631
- Dissolution, *in vitro*, 496–9
- Doppler results, 63–4, 64
- Double cantilever beam, ceramic materials,
 396–8, 417–20
- Double torsion method, 414–7
- Drag coefficients, menisci, 47–8
- Drug delivery, implantable, 565
- Dry testing, cortical bone, 5
- Ductile behaviour, ceramic, 353
- Dynamic viscosity, 651, **661**
- E**
- Ear bones, 6
- ECDEL, 293
- Elastic
 behaviour
 blood vessels, 77
 lymphatic vessels, 77
 cartilage, 38
 properties
 intervertebral discs, 48–9, 49
 menisci, 48–9, 49
- Elastic shear modulus of vocal fold, 650, **653**
- Elastin/collagen ratio, 82
- Elastomers, 291–37
 ASTM standards, 335, 336
 biocompatibility, 293, 318–31, 335
 copolyester
 manufacturers, 296
 properties, 296
 trade names, 296
 crosslinked, 310–1
 definition, 291
 dispersions
 manufacturers, 314–5
 properties, 314–5
 trade names, 314–5
 equivalent, 317
 silicone, 317, 334
- HC silicone
 manufacturers, 312
 properties, 312
 trade names, 312
- LIM silicone
 manufacturers, 313
 properties, 313
 trade names, 313
 polypropylene-based
 manufacturers, 301
 properties, 301
 trade names, 301
 polyurethane, 301–5
 polyurethane-based, 294
 manufacturers, 297–9
 properties, 297–9
 trade names, 297–9
- PVC, 309–10
- silicone, 310–1
 high consistency, 311
 LIM, 311
 silicone adhesives
 manufacturers, 316
 properties, 316
 trade names, 316
- sterilization, 335
 methods, 332–3
- styrene-based
 manufacturers, 306
 properties, 306
 trade names, 306
 thermoplastic, 292–10
 types of, 295–34
 water absorption, 333
- Electrical conductivity, brain tissues, 69, 74
- Electromechanical behaviour, cortical bone, 5
- Electron beam welding, titanium, 174
- Elemental composition
 dentin, 24
 enamel, 24
 surface enamel, 25–6
 whole enamel, 25–6
- Elgiloy, 164
- Elliptical cracks, ceramic materials, 398–400
- Enamel, 23–34
 apatite in, 27
 apatite parameters, 27
 Ca/P molar ratio, 27
 compressive strength, 28–9
 critical surface tensions, 33
 elastic moduli, 28
 elemental composition, 24
 fracture toughness, 30
 hardness of fracture, 31
 mineral density, 24
 organic density, 24
 stress, 28
 surface, elemental composition, 25–6
 tensile strength, 28
 toughness, 30
 water density, 24
 wettability, 32
 whole, elemental composition, 26
 work of fracture, 30

Endoprostheses
 hip, 151
 knee, 151
 Environmental stress cracking, 264
 Epiligament/epitenon, 55
 Epoxy resins
 curing agents, 212–5
 description, 240
 end uses, 240
 properties, 244
 Equivalence, 317–35
 Extracellular matrix (ECM) of lamina
 propria, 645

F

Face-centered cubic (FCC), 162, 167
 Fatigue, 178, 178–81, 179, 180, 181
 cortical bone, 10–11
 porosity, 11
 wear, 456, 458, 473, 475
 Young's modulus, 11
 Female, fluid volume, 120
 Femoral articulating surface, 45–6
 Fiberglass, properties, 238
 Fiber-reinforced plastic pipe,
 220–1
 Fibrocartilage, 38, 45–51
 anisotropy, 45
 composition, 45–7, 46, 47
 mechanical properties, 42
 structure, 45–7, 46, 47
 Fibrosis, 575
 Filament winding, 224
 storage tanks, 225
 Fillers
 brazing temperatures, 199
 chemical composition, 199
 Finite element analysis (FEA), ceramic
 materials, 433–5
 Flexural strength, dentin, 29
 Fluid volume
 female, 120
 male, 120
 Fractures, internal fixation
 malignancies, 614
 Fracture toughness
 dentin, 30
 enamel, 30
 Fracture toughness, cancellous bone, 19
 Fracture work, ceramic materials,
 392–6
 Friction coefficients, implants, 464–71

G

Gauge length, 357
 Glass ceramics, 447–54
 clinical uses, 453
 physical properties, 450, 451, 453
 Glass fibers, 206–7, 208–9
 advantages, 208
 chemical composition, 206
 electrical properties, 206–7
 grades, 209
 mechanical properties, 206
 optical properties, 207
 physical properties, 206
 thermal properties, 206
 Glassy carbons, 556
 fabrication, 556
 mechanical properties, 252
 shrinkage, 556
 Glycosaminoglycan (GAG), 646
 Graphite-fiber-reinforced
 thermoplastics, properties, 235
 Graphite fibers, 208, 209
 Graphites, 554–5
 colloidal, 555
 manufacturing processes, 555
 natural, 554–5
 synthesized, 555
 Griffith's theory, 381–4

H

Hand lay-up, 220
 Hanks' buffered saline solution, 154
 HAp, 496
 bioresorption, 503
 degradation, 499–505
 dissolution rate, 497
 highly porous, 503
 from marine coral, 502
 precipitation, 535
 seeds, 536
 Haptens, immune response to, 600
 Havar
 chemical composition, 165
 mechanical properties, 166
 Haversian
 remodelling, 11
 systems, 4
 HDPE, properties, 230
 Health of donors, cortical bone, 5–6
 Heart
 pacemakers, 152
 valves, 551, 552

Hip

replacement, accelerated test data, 251

Histochemical techniques, 599–600

Hooke's law, 388

Hot isotactic pressing (HIP), 160

Human

adjuvant disease, 633

calf, stress relaxation, 64

dentition, structure of, 23

Hyaline cartilage, 37

Hyaluronic acid (HA), 647–8

Hydraulic

conductivity, blood vessels, 77

permeability, menisci, 47–8

Hydrocarbon polymers, stability, 248

Hydrophilic polymers, 624

Hydrothane, 301

Hydroxyapatite. *See* HAP

Hydroxy carbonate apatite, 449

rate of formation, 449

Hydroxyl radical, 156

Hypertension, 81, 83

I

Iliac vessels, 95

Immune

complex reactions, 595

responses, 602–3

implants, 593–603

Implants

alumina, 339–40

bone, in situ, 583–4

calcium deposition, 533, 534

cancer, 607–17

carcinogenicity, 610–1

cemented, **582**

cement-free, **582**, **583**, 584–5

dental, 151, 152, 157

exposure time, 157

friction coefficient, 464–71

hard tissue response, 581–2

immune response, 593–603

metallic

corrosion, 509–45

surface roughness, 157

oral, 588

orthopaedic, 583, 584, 586, 588

penetration rates, 486

porous, 157

retrieved, 518, 519

site repairs, 576–7

tribological conditions, 464–71, 472–85

Inflammation, **573**, 583–5

characteristics, 573, **583**

chronic, 574

Ingrowth behaviour, 156–7

Injection molding, 223–4

advantages, 223

Injured (T/L) function, 60

Intervertebral discs, 45

adult

shape, 47

size, 47

annulus fibrosus, 46

elastic properties, 48–9, 49

nucleus pulposus, 46

shape, 46, 47

stiffness, 50

strength, 50

viscoelastic behaviour, 49–51, 51

Intraocular crystalline lens. *See* Intraocular

lens (IOL)

Intraocular lens (IOL), 103. *See also* Lens

Investment casting, 160

Ion implantation, 154

nitrogen in titanium, 154

Ischemia, 622, 623

J

Joint replacements

associated malignancies, 612, 613

K

Keratometry, 139

Kevlar 49, 209

electrical properties, 242

mechanical properties, 207

shear properties, 240–1

thermal properties, 207, 242

Kraton, 310

L

Lamina propria, 645, **646**

extracellular matrix (ECM), 645, 647

Laminates

angle ply, 219

properties, 216–20

Large veins, morphometric properties, 78

Latex, immune response to, 600

LDPE, properties, 242

Lead/graphite, properties, 256

Length, arteries, 78

- Lens, 103–11
 capsule, mechanical properties, 109
 cataractous, 105
 composition, 104
 density, 107
 dimensional variation with age, 107
 electrical properties, 110
 force of contraction, 109
 hardness of cataractous, 108
 inorganic ion content, 106
 normal
 inorganic ion content, 106
 water content, 105
 organic content, 106
 physicochemical characteristics, 104–10
 refractive index, 107
 shear modulus of, 108
 spring constants, 110
 tensile modulus, 108
 thickness of capsule, 107
 transmissivity, 108
 viscoelastic properties, 110
 volume, 107
 water content, 105
 weight, 107
- Ligaments, 560
- Ligaments and tendons (T/L)
 composition, 56, 56–7
 hierarchical structure, 56
 injured function, 60
 mechanical behavior, 57
 mechanical properties of, 59
 normal function, 57–9
 stiffness, 58
 structural properties, 57
 structure, 55–6
 viscoelastic behavior, 58
- Linear low density polyethylene, 263
- LTI carbon, mechanical properties, 252
- Lubrication, 487
- Lymph
 inorganic content, 117–18
 organic content, 118–19
- Lymphocyte, 593, 594
 proliferation, 597
 transformation factor, 597
- Lymphokines, testing for, 598
- M**
- Macrophage migration inhibition, 633
- Magnesium-graphite, mechanical properties, 256
- Male, fluid volume, 120
- Malignancies, osseous, 615
- Malignant fibrous histiocytoma (MFA),
 610, 615
- Mass, brain tissues, 68
- Matched die molding, 221–4
- Materials
 pre-screening, 517
 and tissue interaction, 567
- Matrix, materials, 210, 253
- Mechanical stimuli, brain tissues, 68
- Medicaflex, 301
- Membranes, 626
- Menisci, 45–51
- Mesencephalon, 67
- Metal
 cations, uptake efficiencies, 520
 oxides, physico-chemical properties, 536, 538
- Metallic
 biomaterials, 151–8, 151–2
 adhesion strength, 152
 alloys and applications, 152
 bioadhesion, 154
 biocompatibility, 152, 154
 biofunctionality, 154–6
 CoCr alloys (*see* Cobalt-chromium
 (CoCr) alloys)
 corrosion, 155
 corrosion: and inertness, 153–4
 corrosion: measurements, 153
 densities, 153
 generations of, 151
 inorganic reaction, 155
 mechanical properties, 153
 Nitinol, 152
 organic reaction, 155
 orthopedics, 153
 oxide layer, 151
 polarization resistance, 153
 primary corrosion products, 153
 repassivation, 153
 structural applications, 151
 testing, 153
 thermodynamic stability, 156
 titanium, 152
 Young's modulus, 151–2, 155
- implants
 and cancer, 616
 corrosion, 509–45
 passive films, 536–42, 539, 540,
 541, 542
 ions, and calcium phosphates, 533–6, 534,
 535, 536
 materials
 alloys, 512–4, 513, 514
 in biological samples, 517

- Metals, 625
 in blood vessels, 625
 immune response to, 602
 thrombogenic, 625
- Metaphysis, *vs.* diaphysis, 7, 7, 9–10
- Microstructure, cancellous bone, 15
- Mineral
 cortical bone, 4
 density
 dentin, 24
 enamel, 24
- Mineralization, cortical bone, 6, 10
- Morphometries
 pulmonary arteries, 79
 systemic circulation, 78
- Muscle
 mechanical properties, 63–5, 64, 65
 preservation, 63
 and skin, 63–5
 specimen preparation, 63
 tissue handling, 63
- N**
- Natural rubber, 310
- Neoplasia, 609–10
 malignant, 609–10
- Neutrophils, 573
- Niobium, 152, 153
- Nitinol, 152, 186–7
- Ni45Ti, properties, 186
- Noble metals, 194–201, 195–201
 corrosion and wear, 201
 heat treatments, 199, 200
 polarization current, 201
 polarization resistance, 201
- Non-collagenous protein (NCP), 3
- Normal (T/L) function, 57–59
- Normal human lens
 inorganic ion content, 106
 water content, 105
- Nucleus pulposus, 46
- O**
- Organic density
 dentin, 24
 enamel, 24
- Orowan–Petch relation, 354
- Orowan’s argument, 380
- Orowan value, 400
- Orthopaedics, 495–505
 bioactive ceramics, 495–505
- Orthopedic alloys, 154
- Osseointegration, 582, 584–7
 calcium phosphates, 587
 ceramics, 587
 craniofacial skeleton, 586
 definition, 585
 interfaces, 586
 oral implants, 585, 586
 polymers, 586–7
 press-fit fixation, 586
 surface irregularities, 585
- Ossicles, 6. *See also* Ear bones
- Osteocalcin, 4
- Osteolysis, 608, 618
- Osteonectin, 4
- Osteons
 bending modulus, 8, 8
 compression modulus, 8, 8
 secondary, 4, 8, 8
 strength, 9
 tension modulus, 8, 8
 torsional modulus, 8, 8
- Osteosarcoma, 610
- Oxide ceramics, 340, 341
 applications, 341
 evaluation, 340
- Oxide formation, 541
 Co-Cr-Mo alloy, 542, 543
- Oxide layer, metallic biomaterials, 151
- P**
- PBT, properties, 236
- PEEK, 272
 characteristics, 272
 chemical structure, 276
 processing conditions, 284
 properties, 230
 trade names, 289
- Pellethane, 304
- PEI, properties, 231
- Permeability
 articular cartilage, 41
 dentin, 31
- PES, 211
- PET, 271–2
 chemical structure, 276
 physical properties, 271
 processing conditions, 284
 properties, 236
 trade names, 289
- Petrosals, 6. *See also* Temporal bones
- Phagocytosis, 573–4
 frustrated, 574
- Physical properties, cortical bone, 4–5

- Physicochemical properties
 blood, 115
 cerebrospinal fluid, 115
 plasma, 115
 synovial fluid, 115
 tear fluid, 115
 whole blood, 115
- PIE, 211
- Plasma
 concentration, 121–2
 diffusion coefficient, 122
 extinction coefficient, 122
 half-life, 121–2
 inorganic content, 117–18
 molecular weight, 121–2
 organic content, 118–19
 proteins
 content, 119–20
 properties, 121–2
 sedimentation constant, 122
- Ply
 definition, 216
 orientated, 216–7
 rotated, 217
 transverse, failure, 219
- PMMA, properties, 241, 269
- Pneumonitis, 632
- Poisson's ratios
 articular cartilage, 41
 brain tissues, 69
 cancellous bone, 18
 cortical bone, 7, 7
 of human vocal folds, 651
- Polarization resistance, 182
- Polyacetal, 269–70
 chemical structure, 275
 processing conditions, 283
 solvents, 270
 trade names, 289
- Polyacrylates, 268–9
 chemical structure, 275
 processing conditions, 283
 trade names, 288
- Polyamide-imide, 210
 properties, 232
- Polyamides, 210, 268
 aliphatic, 268
 chemical structure, 275
 processing conditions, 282
 trade names, 288
- Polyarylate, properties, 232
- Polyblend, polyurethane, 304
- Polycarbonate, 210, 270–1
 chemical resistance, 270–1
 chemical structure, 275
 processing conditions, 283
 properties, 271
 sheets, properties of, 231
 trade names, 289
- Polyester
 fiberglass-reinforced, properties, 244
 properties, 238
- Polyester resins, 215–6
 accelerators, 216
 catalysts, 215–6
- Polyetheretherketones. *See* PEEK
- Polyetherimides. *See* PEI
- Polyether sulfones. *See* PES
- Polyethylene, 263–4
 chemical structure, 274
 plastic, carcinogenicity, 610
 processing conditions, 280
 trade names, 285
 wear debris, 518
- Polyfluorocarbons, properties, 241
- Polyimides, properties, 237
- Polymer/carbon, mechanical
 properties, 251
- Polymers
 manufacturer, 251
 trade names, 251
- Polymethylmethacrylate
 carcinogenicity, 610
 immune response to, 601–2
- Polyphenylene sulfides. *See* PPS
- Polypropylene, 264–5
 chemical structure, 274
 processing conditions, 280
 properties, 230
 trade names, 286
- Polysiloxane, immune response to, 601
- Polysulfone, 272–3
 characteristics, 273
 chemical structure, 276
 processing conditions, 284
 properties, 233
 trade names, 289
- Polytetrafluoroethylene. *See also* PTFE
 chemical structure, 274
 processing conditions, 281
 trade names, 287
- Polyurethane, 265–6
 blood pumps, 624
 chemical structure, 274
 elastomers, 265
 immune response to, 601
 polycarbonate-based
 manufacturers, 300

- properties, 300
 - trade names, 300
 - processing conditions, 281
 - ventricular assist devices, 624
 - trade names, 286–7
 - Polyvinylchloride. *See also* PVC
 - chemical structure, 275
 - Porosity, fatigue, 11
 - Potential-pH diagrams, 510–2, **511**
 - limitations, 510
 - PPS, 211
 - fabric reinforce, 222
 - properties, 232
 - Presbyopia, 103
 - Preservation
 - muscle, 63
 - skin, 63
 - Press-fit fixation, 586
 - knee replacement, 586
 - Prostheses, heart valves, 551
 - Proteins
 - adsorption, 566
 - coagulation, 122
 - complement system, 123
 - PTFE, 266
 - properties, 241
 - Pulmonary arteries, morphometrics, 79
 - Pultrusion, 229
 - PVC, 267
 - Elastichem, 309
 - elastomers, 309
 - Ellay, 309
 - Geon, 309
 - Multichem, 309
 - plasticized, 267
 - manufacturers, 302–4
 - properties, 302–4
 - trade names, 302–4
 - processing conditions, 282
 - Teknor Apex, 310
 - trade names, 287
 - unplasticized, 267
- R**
- Reaction bonded silicon nitride, axial
 - strength, 257
 - Refractive index of human lens, 107
 - Reinforcement filaments
 - manufacturing technique, 208
 - properties, 208
 - Remodelling
 - cortical bone, 11, 11
 - Haversian, 11
 - tensile strength, 11
 - ultimate strain, 11
 - Young's modulus, 11
 - Repassivation, definition, 153–4
 - Residual compression, UHMWPE, 486
 - Resins
 - cured polyester, properties, 239
 - epoxy, 212
 - description, 240
 - end uses, 240
 - polyester, 215–6
 - properties, 238
 - thermoplastic, 210
 - thermoset, 210
 - vinyl ester, 211–2
 - Resin system, choice of, 226, 229
 - Responses
 - allergic, 593
 - cell mediated, 597–600
 - cellular necrosis, 572
 - chemically induced, 571
 - hard tissue, 581–91
 - hypersensitivity, 593
 - immune, 572, 602–3
 - local host, 567–9
 - minimal, 571
 - neoplastic, 572
 - physically induced, 572
 - soft tissue, 571–7
 - silicone, 631–41
 - Retrieved implants, 518, 519
 - oral, 587
 - Reynolds number, 78
 - aorta, 78
 - arteries, 78
 - capillaries, 78
 - vena cava, 78
 - Rheometry, 105
 - Rheumatoid arthritis, breast implants, 640
- S**
- Santoprene, 293, 295
 - Sarlink, 308–9
 - Secondary, osteons, 4, 8, 8
 - Serum
 - levels, total hip arthroplasty, 608, **618**
 - metal concentrations, 518, 521
 - Shape
 - brain tissues, 68
 - intervertebral discs, 46, 47
 - Shear modulus
 - brain tissues, 69, 70–71
 - cortical bone, 7, 7

- Shear modulus (*cont.*)
 of human lens, 108
 trabecular bone, 16, 18
- Shear properties
 articular cartilage, 40, 40
 dentin, 29
- Shear stress, 155
- Shrinkage temperature, collagen, 3
- SiC/RBSN, axial strength, 257
- Silicones
 breast implants, 640
 cosmetic surgery, 632
 granulomatous hepatitis, 632
 immunologic reactions, 631–2
 migration, 632
 soft tissue response, 631–41
 systemic reactions, 632–4
- Silicon nitride, properties, 257
- Sintering, 515
- Skeletal reconstructions, 151
- Skin
 elastic moduli, 63–4
 forehead, indentation, 64
 mechanical properties, 63–5, 64, 65
 and muscle, 63–5
 preservation, 63
 specimen preparation, 63
 testing, 599
 tissue handling, 63
- Slip movement, 353
- Soft tissues
 indentation, 64–5
 stiffness, 64
- Soldering and brazing titanium, 172–3
- Solubility
 calcium phosphate, 497
 definition, 496
 isotherms, **498**
 product constant, 496
- Specific immune response, 593–5
- Specimen preparation
 muscle, 63
 skin, 63
- Spongy bone. *See* Cancellous bone
- Spray-up, 220
- Spring constants of human lens, 110
- Sterilization, 541
- Stiffness
 cortical bone, 6–9
 intervertebral discs, 50
- Strain
 rate, cortical bone, 8, 10
- Strength
 cortical bone, 9
 intervertebral discs, 50
 osteons, 9
 testing for ceramic material
 3 and 4 point bending, 360–5
 beam theory, 357–60
 ceramic machining, 357
 flexion and flexure testing, 357
 nature of test, 374–7
 processing of failure data, 369–72
 ranking, 372–4
 significance of test results, 368–9
 tensile, 356–7
 test configurations, 365–8
 test pieces, 357
 volume of test piece, 377
- Stress
 corrosion, ceramic materials, 426–8
 dentin, 29
 enamel, 28
 intensity factor, 381
 relaxation
 human calf, 64
- Structure, fibrocartilage, 45–7, 46, 47
- Styrene polymer, properties, 236
- Superalloy MA956, 530
 polarization curves, **530**
- Surfaces, blood contacting, 627
- Surface treatments, 528–33, 529, **530**, 531, **532**, 533, **539**, **541**
- Surgery, tissue overheating, 588
- Sutures
 absorbable, 565
 mechanical propertie, 252
- Sweat
 corrosion in, 522–3, 523
 ISO, electrochemical parameters, 523
- Synovial fluid, 116
 cellular composition, 117
 inorganic content, 117–18
 metallic concentrations, 521
 organic content, 118–19
 protein content, 119–20
- Synthetic polymers, immune response to, 601–2
- Systemic
 circulation, canine, morphometric
 properties, 80
 sclerosis, 633, 635
- T**
- Tantalum, 155, 156, 514
 corrosion resistance, 514
 pentoxide, thickness, 527
 plates, 156

- Ta-oxide, 156
- TCP, 496
 - bioresorption, 503
 - degradation, 499–505
 - dissolution rate, 497
- T cytotoxic cell, 594
- Tear
 - fluid, 116
 - inorganic content, 117–18
 - organic content, 118–19
 - protein content, 119–20
- Tecoflex, polyurethane, 304–5
- Tecothane, 305
- Teknor Apex, 310
- Temporal bones, 6
- Tendon, 55–61
 - definitions, 55
- Tendons, 560
- Tensile
 - modulus
 - annulus fibrosus, 50
 - cortical bone, 6
 - menisci, 49
 - modulus articular cartilage, 39–40, 40
 - strength
 - dentin, 29
 - enamel, 28
 - menisci, 48–9, 49
 - remodelling, 11
- Tension, modulus, osteons, 8, 8
- Texin, 305
- Thermal properties, brain tissues, 74, 74
- Thermoforming, 222–3
- Thermoplastics, 210–1, 261–89
 - amorphous, 262
 - biocompatibility, 262
 - branching, 262
 - mechanical properties, 277–8
 - molecular weight, 262
 - physical properties, 277
 - processability, 261
 - states of, 262
 - thermal properties, 278–9
 - vulcanizates, 293, 295
 - manufacturers, 295
 - properties, 295
 - trade names, 297
- Thornel/Kevlar, properties, 243
- Thromboembolism, 622, 623, 626
- Thromboresistance, 626
- Thrombus, 622, 623
- Ti-6Al-4V
 - contact angles, 543
 - depassivation, 528
 - dissolution, 533
 - electrochemical characteristics, 524
 - femoral components, 518
 - laser surface alloying, 528
 - passivity currents, 526, 536
 - and pure titanium, implants, 532
- Ti-6Al-4V-50 v/o BORSIC, properties, 255
- Ti-6Al-4V-28 v/o SiC, tensile properties, 255
- Ti6Al4V
 - ageing, 177
 - fatigue strength, 178
 - fretting corrosion, 184
 - notch factor, 178
 - plasma nitriding, 177
 - rotating bending failure, 181
 - rotating bending strength, 179
 - solution treatment, 177
 - wear properties, 185
- Time to failure, cortical bone, 10
- Tissues
 - density, 15
 - granulation, 575
 - handling
 - muscle, 63
 - skin, 63
 - metals in, 519, 521–2
 - vascularized, 574, 575
- TiTa30, 152
 - thermal coefficient, 152
- Titanium, 156, 167–87
 - accumulation, 517, 518
 - alloys, 167–87
 - biological properties, 185
 - chemical composition, 167, 168
 - corrosion and wear, 182, 192–5, 183, 184, 185
 - fatigue, 178, 178–81, 179, 180, 181
 - fracture toughness, 177
 - hip endoprostheses, 178
 - mechanical properties, 174, 175, 176
 - physical properties, 168–9, 169
 - and alloys, 152
 - anodic, electrochemical data, 183
 - anodized, corrosion rate, 527, 537
 - biological properties, 185
 - cold deformation, 175
 - corrosion, **511**
 - formation, 185
 - resistance, **526**, 526–7, 527
 - and wear, 182, 192–5, 183, 184, 185
 - cutting, 172
 - deformation temperatures, 170
 - descaling, 171–2
 - dissolution, 539, **540**

- Titanium (*cont.*)
- hot working, 169–70
 - immunity, **511**
 - implant in bone, **539**
 - international standards, 167
 - machining, 172
 - mechanical properties, 174, 174–7, 175, 176, 177
 - milling, 172
 - oxide
 - films, 542
 - sterilization, 541
 - thickness, 527
 - passivation, **511**
 - corrosion rate, 527, 537
 - physical properties, 168–9, 169
 - polarization current, 182
 - processing, 169–74, 171, 172, 173
 - pure
 - potential-time curves, **525**
 - pure
 - physical properties, 168
 - repassivation time, 182, 183
 - sheet working, 170, 170–1
 - soldering and brazing, 172–3
 - surface characteristics, 543
 - thermal heating, 532
 - welding, 173–4
- Ti-15Zr-4Nb-2Ta-0.2Pd, 514
- Torsional modulus, osteons, 8, 8
- Total hip
 - arthroplasty, 486, 608, **618**
 - cancer risk, 616
 - endoprosthesis, 340
 - replacements, 154
- Toughness
 - dentin, 30
 - enamel, 30
- Toxicity
 - additive, 244, 245
 - plasticizers, 245
 - polymer stabilizers, 244, 245
- Trabeculae, 15
- Trabecular alignment, 18
- Trabecular bone. *See* Cancellous bone
 - compression, 16
 - fracture toughness, 19
 - mechanical properties, 16, 17
 - microstructure, 15
 - Poisson's ratio, 18
 - stiffness and strength, 16–18
 - strain, 18
 - surface-to-volume ratio, 15
 - tissue composition, 16
 - tissue damage, 19–20
 - tissue-level mechanical properties, 20
 - and ultrastructure, 16
 - viscoelastic and fatigue properties, 18–19
 - Young's and shear modulus, 16, 18
- Transfer molding, 222–3
- Transmissivity of human lens, 108
- Tribologic properties
 - articular cartilage, 41–2
- Tribosystem, definition, 487
- Tricalcium phosphate. *See* TCP
- Tubing, 624
- Tumorigenesis, solid state, 572
- Tumors
 - analysis of, 613–5, 614
 - implant-related, 611–3, 614
 - prosthetic replacement, 614
 - titanium implant, 614
- U**
- UHMWPE, 263, 434
- Ultimate
 - strain, remodelling, 11
 - stress, annulus fibrosus, 50
 - tensile strength (UTS), 58, 368
- Ultra high molecular weight polyethylene. *See* UHMWPE
- UNS R30005, 164–6
- Urine, metal concentrations, 521
- Usui process, 227
- V**
- Vanadium, 152, 155
- Vapor-deposited carbon, mechanical properties, 252
- Vapour phase coatings, 552, 557
- Vascular grafts, 627
- Vascular wall, layers, 85
- Veins
 - canine jugular, 92, 93
 - human saphenous, 92, 93
 - mechanical properties, 92–3, 93, 94
 - tensile properties, 92–3, 93, 94
- Vena cava, morphometric properties, 78
- Venous tissues
 - changes with age, 84, 85
 - constituents, 84, 84
- Ventricular system, 67
- Vicker's diamond pyramid, 423, **426**
- Vicker's indenter, 425
- Vinyl ester resins, 211–2

- Viscoelastic
 behaviour
 intervertebral discs, 49–51, 51
 menisci, 49–51, 51
 properties, trabecular bone, 18–19
- Vitallium, 152, 157, 614
- Vitreous body, 125–30
 age of protein content, 129
 animal, 126
 axial length, 129
 compliance, 130
 gel and liquid volume, 130
 inorganic ions content, 128
 nature of, 125
 organic content, 128
 physical properties, 127
 radiation, 130
 rheology, 130
 viscosity, 130
 water content, 127
- Vitreous humor. *See* Vitreous body
- Vocal folds, 645
 animal studies detailing injury on, 649, 652
 biomaterial injections, 652–3
 collagen and fat injections, 653–4
 composition, 646–7
 collagen, 647
 elastin, 647
 hyaluronic acid, 647–8
 interstitial proteins, 648
 voice disorders, 648, 649
 dynamic viscosity, 651, **661**
 elastic shear modulus, 650, **653**
 mechanical properties
 dynamic viscosity, 651
 elastic shear modulus, 650
 general, 649
 Poisson's ratio, 651
 rheology, 650
 vocal fold scarring, 652
 modified hyaluronic acid, 654–6
 Young's modulus, 649
- Volume fraction, trabecular bone, 15
- von Mises criterion, 353
- W**
- Wall thickness, 78
- Water
 content, cartilage, 37
 density
 dentin, 24
 enamel, 24
 permeability, blood vessels, 77
- Wear, 455–87
 abrasive, 456
 Rabinowicz model, 457
 Zum Gahr model, 457
 adhesive, 456
 Archard equation, 457
 Hornbogen equation, 457
 artificial joints, 455
 ASTM standards, 462–3
 corrosive, 456
 Quinn model, 458
 debris, release of, 568
 delamination, 456
 fatigue, 456
 Halling model, 458
 fretting, 456
 linear clinical, 486, 486–7
 rates, 472–85
 testing
 machines, 461
 test apparatus, 461
 in vitro, 459–85
- Weibull equation, ceramic materials, 435–41
- Welding, 173–4
 diffusion, 174
 electron beam, 174
 spot, 174
- Welding titanium, 173–4
- Wetability
 dentin, 33
 enamel, 32
- Wet lay-up, 224–6
- Whole blood
 cellular composition, 117
 inorganic content, 117–18
 organic content, 118–19
- Whole enamel, elemental composition, 25–6
- Work of fracture
 dentin, 30
 enamel, 30
- Wounds, healing, 575
- Y**
- Young's modulus
 cortical bone, 7
 fatigue, 11
 metallic biomaterials, 151–2, 155
 remodelling, 11
 titanium and titanium alloys, 168, 169
 vocal folds, 649
- Young's modulus
 trabecular bone, 16, 18

Z

Zinc/graphite, mechanical properties, 256

Zinc, mechanical properties, 256

Zirconia, 344–7, **345**, 354–5

 biocompatibility, 348

 chemical stability, 346

 clinical performance, 346

 engineering properties, 342

 fracture toughness, 346

 mechanical properties, 341, 344

 partially stabilized, 344

 standards, 343

 tetragonal polycrystals, 344

 wear resistance, 346